frontiers | Research Topics

Neoadjuvant therapy in breast cancer: Biomarkers and early response prediction

Edited by
Annarita Fanizzi, Raffaella Massafra, Vito Lorusso and Nicola Amoroso

Published in
Frontiers in Oncology

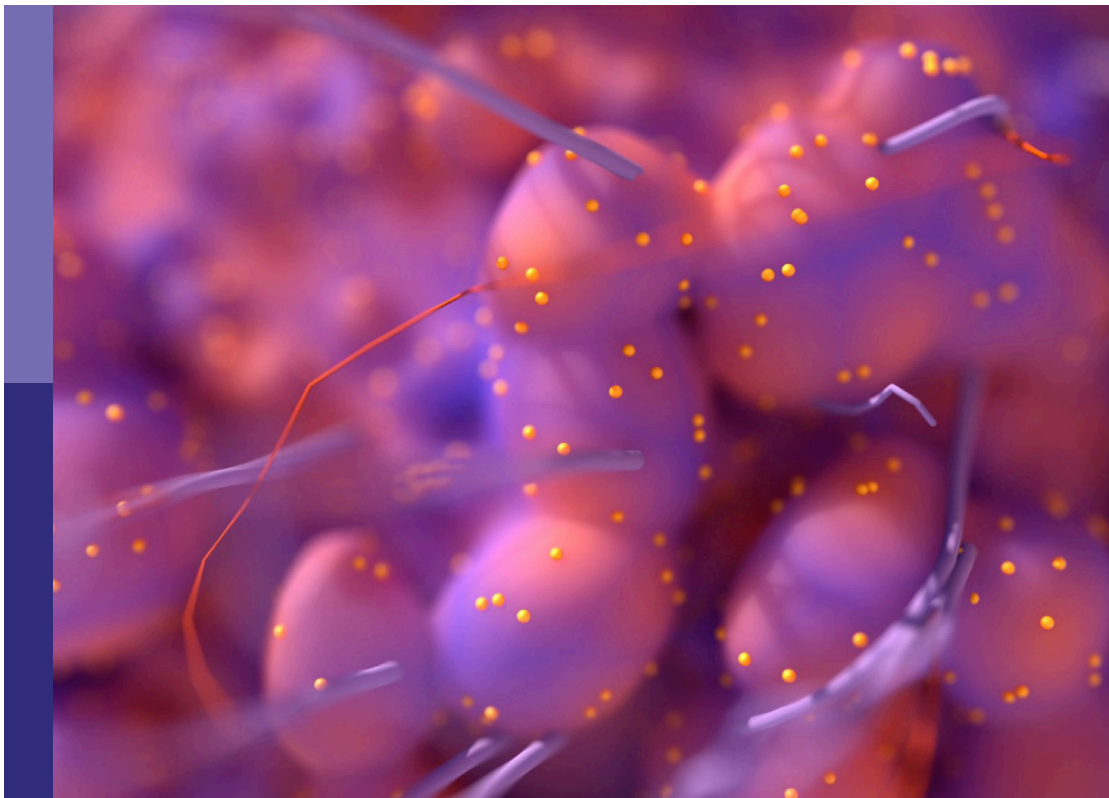

FRONTIERS EBOOK COPYRIGHT STATEMENT

The copyright in the text of individual articles in this ebook is the property of their respective authors or their respective institutions or funders. The copyright in graphics and images within each article may be subject to copyright of other parties. In both cases this is subject to a license granted to Frontiers.

The compilation of articles constituting this ebook is the property of Frontiers.

Each article within this ebook, and the ebook itself, are published under the most recent version of the Creative Commons CC-BY licence. The version current at the date of publication of this ebook is CC-BY 4.0. If the CC-BY licence is updated, the licence granted by Frontiers is automatically updated to the new version.

When exercising any right under the CC-BY licence, Frontiers must be attributed as the original publisher of the article or ebook, as applicable.

Authors have the responsibility of ensuring that any graphics or other materials which are the property of others may be included in the CC-BY licence, but this should be checked before relying on the CC-BY licence to reproduce those materials. Any copyright notices relating to those materials must be complied with.

Copyright and source acknowledgement notices may not be removed and must be displayed in any copy, derivative work or partial copy which includes the elements in question.

All copyright, and all rights therein, are protected by national and international copyright laws. The above represents a summary only. For further information please read Frontiers' Conditions for Website Use and Copyright Statement, and the applicable CC-BY licence.

ISSN 1664-8714
ISBN 978-2-8325-3595-0
DOI 10.3389/978-2-8325-3595-0

About Frontiers

Frontiers is more than just an open access publisher of scholarly articles: it is a pioneering approach to the world of academia, radically improving the way scholarly research is managed. The grand vision of Frontiers is a world where all people have an equal opportunity to seek, share and generate knowledge. Frontiers provides immediate and permanent online open access to all its publications, but this alone is not enough to realize our grand goals.

Frontiers journal series

The Frontiers journal series is a multi-tier and interdisciplinary set of open-access, online journals, promising a paradigm shift from the current review, selection and dissemination processes in academic publishing. All Frontiers journals are driven by researchers for researchers; therefore, they constitute a service to the scholarly community. At the same time, the *Frontiers journal series* operates on a revolutionary invention, the tiered publishing system, initially addressing specific communities of scholars, and gradually climbing up to broader public understanding, thus serving the interests of the lay society, too.

Dedication to quality

Each Frontiers article is a landmark of the highest quality, thanks to genuinely collaborative interactions between authors and review editors, who include some of the world's best academicians. Research must be certified by peers before entering a stream of knowledge that may eventually reach the public - and shape society; therefore, Frontiers only applies the most rigorous and unbiased reviews. Frontiers revolutionizes research publishing by freely delivering the most outstanding research, evaluated with no bias from both the academic and social point of view. By applying the most advanced information technologies, Frontiers is catapulting scholarly publishing into a new generation.

What are Frontiers Research Topics?

Frontiers Research Topics are very popular trademarks of the *Frontiers journals series*: they are collections of at least ten articles, all centered on a particular subject. With their unique mix of varied contributions from Original Research to Review Articles, Frontiers Research Topics unify the most influential researchers, the latest key findings and historical advances in a hot research area.

Find out more on how to host your own Frontiers Research Topic or contribute to one as an author by contacting the Frontiers editorial office: frontiersin.org/about/contact

Neoadjuvant therapy in breast cancer: Biomarkers and early response prediction

Topic editors

Annarita Fanizzi — Bari John Paul II Cancer Institute, National Cancer Institute Foundation (IRCCS), Italy

Raffaella Massafra — Bari John Paul II Cancer Institute, National Cancer Institute Foundation (IRCCS), Italy

Vito Lorusso — Bari John Paul II Cancer Institute, National Cancer Institute Foundation (IRCCS), Italy

Nicola Amoroso — University of Bari Aldo Moro, Italy

Citation

Fanizzi, A., Massafra, R., Lorusso, V., Amoroso, N., eds. (2023). *Neoadjuvant therapy in breast cancer: Biomarkers and early response prediction*. Lausanne: Frontiers Media SA. doi: 10.3389/978-2-8325-3595-0

Table of contents

frontiers | Frontiers in Oncology

ORIGINAL RESEARCH
published: 01 April 2022
doi: 10.3389/fonc.2022.865121

Metagenomic Analyses Reveal Distinct Gut Microbiota Signature for Predicting the Neoadjuvant Chemotherapy Responsiveness in Breast Cancer Patients

Yuanyuan Li[1,2,3†], *Bingbin Dong*[1,3†], *Wei Wu*[1,3†], *Jiawei Wang*[1,2,3†], *Hao Jin*[1,2,3], *Kangmei Chen*[1,3], *Kangling Huang*[1,2,3], *Songyin Huang*[3,4*] *and Yandan Yao*[1,2,3*]

[1] Breast Tumor Center, Sun Yat-sen Memorial Hospital, Sun Yat-sen University, Guangzhou, China, [2] Shenshan Medical Center, Sun Yat-sen Memorial Hospital, Sun Yat-sen University, Shanwei, China, [3] Guangdong Provincial Key Laboratory of Malignant Tumor Epigenetics and Gene Regulation, Sun Yat-sen Memorial Hospital, Sun Yat-sen University, Guangzhou, China, [4] Biotherapy Center, Sun Yat-Sen Memorial Hospital, Sun Yat-Sen University, Guangzhou, China

Background: Growing evidence supports the modulatory role of human gut microbiome on neoadjuvant chemotherapy (NAC) efficacy. However, the relationships among the gut microbiome, tumor-infiltrating lymphocytes (TILs), and NAC response for breast cancer (BC) patients remain unclear. We thus proposed this preliminary study to investigate the relationship between gut microbiome and BC patients' responses to NAC treatment as well as underlying mechanisms.

Methods: Prior to receiving NAC, the fecal metagenome collected from 23 patients with invasive BC was analyzed. Patients were subsequently assigned to the NAC non-effectual group and the NAC effectual group based on their response to NAC. The peripheral T lymphocyte subset counts were examined by flow cytometry methods. CellMinor analysis was employed to explore the relationship between CD4 mRNA expression and the reaction of tumor cells to NAC drugs.

Results: The gut microbiomes of the NAC non-effectual group showed characteristics of low diversity with low abundances, distinct metagenomic composition with decreased butyrate-producing and indolepropionic acid-producing bacteria, and increased potential pathobionts compared with the NAC effectual group. The combination of *Coprococcus, Dorea*, and uncultured *Ruminococcus* sp. serves as signature bacteria for distinguishing NAC non-effectual group patients from the NAC effectual group. The absolute numbers of $CD4^+$ and $CD8^+$ TIL infiltration in tumors in the NAC non-effectual group were significantly lower than those in the effectual group. Similar findings were reported for the $CD4^+$ T lymphocytes in the peripheral blood (p's < 0.05). NAC effectual-related signature bacteria were proportional to these patients' $CD4^+$ T lymphocyte counts in peripheral blood and tumors (p's < 0.05). CellMinor analysis showed that the CD4 mRNA expression level

OPEN ACCESS

Edited by:
Annarita Fanizzi, National Cancer Institute Foundation (IRCCS), Italy

Reviewed by:
Maria Magdalena Montt-Guevara, University of Pisa, Italy
Alessandro Rizzo, National Cancer Institute Foundation (IRCCS), Italy

***Correspondence:**
Songyin Huang
huangsy@mail.sysu.edu.cn
Yandan Yao
yaoyand@mail.sysu.edu.cn

†*These authors have contributed equally to this work*

Specialty section:
This article was submitted to Breast Cancer, a section of the journal Frontiers in Oncology

Received: *29 January 2022*
Accepted: *28 February 2022*
Published: *01 April 2022*

Citation:
Li Y, Dong B, Wu W, Wang J, Jin H, Chen K, Huang K, Huang S and Yao Y (2022) Metagenomic Analyses Reveal Distinct Gut Microbiota Signature for Predicting the Neoadjuvant Chemotherapy Responsiveness in Breast Cancer Patients. Front. Oncol. 12:865121. doi: 10.3389/fonc.2022.865121

dramatically climbed with increased sensitivity of tumor cells to NAC drugs such as cyclophosphamide, cisplatin, and carboplatin (p's < 0.05).

Conclusions: The composition of the gut microbial community differs between BC patients for whom NAC is effective to those that are treatment resistant. The modulation of the gut microbiota on host $CD4^+$ T lymphocytes may be one critical mechanism underlying chemosensitivity and NAC pathologic response. Taken together, gut microbiota may serve as a potential biomarker for NAC response, which sheds light on novel intervention targets in the treatment of NAC non-effectual BC patients.

Keywords: gut microbiota, breast cancer, neoadjuvant chemotherapy, pathologic response, $CD4^+$ T lymphocytes

INTRODUCTION

Breast cancer (BC) has the highest incidence rate among all malignant tumors and is ranked the second cause of mortality in women (1). Patients with locally advanced breast cancer were often treated with neoadjuvant chemotherapy (NAC) (2), which is evident to reduce the primary tumor size in the breast prior to surgery to allow for breast conservation, thereby limiting the metastatic axillary lymph node, and increasing the surgical resection rate. However, some patients with breast cancer respond poorly to chemotherapy, the adoption of which not only pose little benefits but also can lead to potential chemotherapy toxicity, side effects, and disease progression in such population. Therefore, explorations in the influencing factors on the efficacy of NAC in such patients, in order to propose a predictive model for the patients' responses to NAC, will be practically beneficial for planning better differential treatments for breast cancer.

Recent findings revealed that BC is related to microbial dysbiosis in both the gut microenvironment and breast tissue (3, 4). Multiple previous studies also reported that gut microbial composition modulates the chemotherapy efficacy and toxicity through key mechanisms including regulation of the translocation, steroid-hormone metabolism, and immune response to NAC drugs (5–8). More recently, it was reported that NAC could modulate the microbiome in the breast tumor tissue, as well as specific microbes, which are associated with tumor relapses through breast cancer signaling (9). Evidence from these human, animal, and *in vitro* studies together suggested that gut microbiota can be a promising biomarker for predicting the therapeutic outcome such as NAC efficacy in BC. Therefore, the multidimensional role of gut microbiota on cancer and treatment progress implies that gut microbiota can be a target for the development of personalized cancer therapeutics.

Much evidence has highlighted the prognostic value of tumor immune landscape and its role as therapeutic targets. The differential tumor immune landscape may contribute to the variations in clinical outcomes (10). Tumor infiltrating lymphocytes (TILs), commonly recognized as an immunological parameter and a morphological manifestation of anticancer immune response, represent a major infiltrating immune cell subpopulation, which consist of $CD3^+$, $CD4^+$, and $CD8^+$ TILs. Much research has shown that TILs, which are known for their antitumor activities, also play a key role in modulating responses to NAC, with significant predictive values for the prognosis across breast cancer subtypes (11). For example, one study that assessed 3,771 BC patients reported that triple negative breast cancers (TNBCs), as well as HER2-positive ($HER2^+$) breast cancer, were found with a significant increase in disease-free survival when TIL concentrations showed 10% escalation (12). However, the exact mechanism through which TILs regulate the responses to NAC in BC patients is still not clear.

Specific TILs are involved in the regulation of the microbiota, including $CD3^+$, $CD4^+$, and $CD8^+$ TILs (13). Their functions range from providing help for regulation of intestinal barrier function, immunity, and metabolism to avoiding systemic and chronic inflammation, which have been proposed to underlie the impact of gut microbiota on carcinogenesis (14). For example, *Lactobacillus acidophilus* was reported to be able to modulate the immune response against breast cancer in murine models (15). *Bifidobacteria* also modify the induction of tumor–specific T cell and promote the entrances of circulating T cells into the tumor microenvironment in patients who received immunomodulator treatment (16). It is evidenced that lymphocytes-associated immune responses may affect tumorigenesis in breast tissue (17). At the same time, lymphocytes are regulated by microbes (18). For example, *Sphingomonas* was reported to engage in the effector maturation of CD8+ T cells, which are the most important immune cells that inhibit the growth of breast tumor cells (19). Altogether, it is reasonable to hypothesize that microbiomes may modulate the BC patients' response to NAC by regulating their TIL induction.

Although logically reasonable, the impact of microbiome composition on BC patients' responses to NAC and the role of TILs during this progress have remained unstudied. In addition, most previous studies focused on sequencing 16S rRNA or investigating biochemical interactions, which fail to comprehensively examine the entire taxonomies of the microbiota in BC. We thus conducted metagenomic analysis to explore the composition of gut microbiota and T lymphocyte subsets between NAC effectual patients and NAC non-effectual patients to fill such gaps. As in the literature, microbiota modulates the host response to chemotherapies, and immunity is implicated in the impact of microbiota on the development and progression of BC. By utilizing the machine-learning approach, this study also proposes a microbial signature for predicting the efficacy of

NAC for BC and untangling the association between microbial signature, T lymphocyte subsets, as well as patients' responses to NAC.

MATERIALS AND METHODS

Patients

A total of 26 patients newly diagnosed with BC were recruited from the Sun Yat-Sen Memorial Hospital during half a year. Two of these 26 patients were excluded because they had used antibiotics, probiotics, prebiotics, or symbiotic drugs during NAC, and one was excluded because of a personal history of ulcerative colitis. All patients were female and between 18 and 70 years. Their clinical demographics (age, gender, BMI, menopause) and the histopathology of tumor (size, histologic grade, lymph node metastasis, the status of estrogen (ER), progesterone (PR), and human epidermal growth factor (HER2) receptors) were recorded along with the primary treatments they received (e.g., previous surgery, radiotherapy, or chemotherapy) (**Table 1**), since these indicators will have impacts on their responsiveness to NAC based on previous studies (20). The processes of participant recruitment and sample collection are depicted in **Figure 1**. To ensure the homogeneity of the patients in the different groups, detailed exclusion criteria included the following: (1) patients have received any chemotherapy, radiotherapy, endocrine therapy, or surgery prior to fecal sample collection; (2) patients who have used antibiotics, probiotics, prebiotics, or symbiotic drugs within 3 months prior to recruitment; (3) patients with concurrent malignant tumors; (4) patients with distant metastasis at initial presentation; (5) patients with comorbidities including severe heart, lung, liver, or kidney diseases; and (6) patients who were pregnant or lactating. Signed informed consents were obtained from all

TABLE 1 | Comparison of clinical indices and pathological data between NAC non-effectual group and NAC effectual group.

Characteristics		NAC non-effectual group n = 5	NAC effectual group n = 18	*p*-value
Age (years, mean ± SD)		52.80 ± 7.16	50.50 ± 10.41	0.58
BMI (kg/m^2, mean ± SD)		21.99 ± 3.10	22.74 ± 3.20	0.65
Menopausal status	Premenopausal	2	10	0.64
	Postmenopausal	3	8	
Pathological Type (tumor size)	IDC	5	17	1.00
	LDC	0	1	
T stage	T1-T2	3	13	0.62
	T3-T4	2	5	
N stage	N0-N1	4	16	0.54
	N2-N3	1	2	
Histologic grade	Period II A-II B	3	11	1.00
	Period III A-III C	2	7	
ER expression	Positive	4	12	1.00
	Negative	1	6	
PR expression	Positive	3	6	0.34
	Negative	2	12	
HER2 expression	0-2+	5	10	0.12
	3+	0	8	
Ki-67 expression	≥20%	3	13	0.62
	<20%	2	5	
Blood TILs ratio (%, mean ± SD)				
CD3$^+$TILs		69.34 ± 9.25	73.78 ± 8.63	0.23
CD4$^+$TILs		**36.12 ± 3.95**	**41.39 ± 6.94**	**0.04**
CD8$^+$TILs		23.92 ± 3.39	24.60 ± 6.37	1.00
CD4$^+$/CD8$^+$TILs		1.54 ± 0.35	1.77 ± 0.42	0.22
Therapy				
Cyclophosphamide-containing chemotherapy regimen	Yes	5	18	/
	No	0	0	
Anthracycline-containing chemotherapy	Yes	3	12	1.000
	No	2	6	
Taxol-containing chemotherapy	Yes	4	14	1.000
	No	1	4	
Herceptin targeted therapy	Yes	5	10	0.12
	No	0	8	
Chemotherapy cycle	≤6 cycles	4	14	1.000
	>6 cycles	1	4	
Chemotherapy interval	Intensive chemotherapy	1	3	1.000
	Conventional chemotherapy	4	15	

IDC, invasive ductal carcinoma; LDC, invasive lobular carcinoma; TILs, tumor infiltrating lymphocytes.

Tumors were categorized as ER, PR, HER2, and Ki-67 based on immunohistochemical testing results. If HER2 immunohistochemical testing result is 2+, two-probe method FISH is required. Bolded values indicate the significant results.

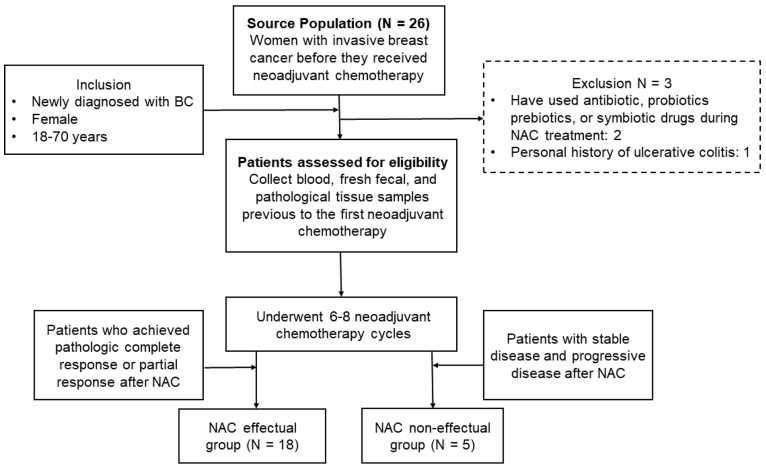

FIGURE 1 | The recruitment of participants and the process of sample collection.

participants before sample collection. Ethic approval has been granted by the Ethics Committee of Sun Yat-Sen Memorial Hospital of Sun Yat-Sen University.

Blood and fresh fecal samples were collected from the patients the day before the first neoadjuvant chemotherapy. Reserved on ice, they were guaranteed to be transported within 2 h and immediately stored at −80°C until usage.

Metagenomic DNA Sequencing and Annotation

Bacteria was investigated in 200 mg feces (7), and bacterial DNA was extracted with the stool sample DNA extraction kit (Guangzhou meiji biotechnology co., Ltd, China) following the manufacturer's directions. We used the PE150 assay to sequence all the samples on the Illumina Hiseq 3000 platform. After removing contaminant distractions and the readings from human DNA (based on alignment with the SOAPdenovo aligner) in the raw data, clean reads for subsequent analysis were obtained. The qualified reads from each sample were aligned using SPAdes-v3.10.1 to satisfy the taxonomic assignments. By comparing the DIAMOND gene set with the NR database, we aligned our data to the NR database and completed the profile of taxonomic relative abundance. The estimation of its abundance was performed *via* evaluating the accumulation of all relative genes belonging to this feature.

Blood Sample Analysis

Blood was collected from the patients prior to treatment for BC. Flow cytometry was used to determine T lymphocyte subset ratios in peripheral blood (21). For the detection of peripheral blood T lymphocyte subsets, the following antibodies were used: CD3-FITC/CD8-PE/CD4-APC (all from Becton-Dickinson). Cytofluorimetric analysis was performed with CytomicsTM FC500 (Beckman Coulter). CXP Cytometer and FlowJo Software (Tree Star Inc.) were used to analyze flow cytometry data. T lymphocyte subsets were identified as follows: $CD3^+$ T cells, $CD4^+$ T cells, and $CD8^+$ T cells.

Tissue Samples and TIL Scoring

All tissue samples were obtained from participants using core needle biopsies before the start of their NAC treatment. At the end of the clinical trial, TIL analysis was done by retrospectively reviewing the medical records. Clinicopathologic information was obtained using hematoxylin and eosin (H&E) stained slides and immunohistochemical slides for the standard biomarkers. Primary antibodies (Cell Signaling Technology, USA) specific for CD4 (1:400) and CD8 (1:400) were utilized for slide incubation overnight at 4°C. The secondary antibody (Cell Signaling Technology, USA) was incubated for 30 min at 37°C the following day, and the immunodetection was performed using a DAB kit (Beijing ComWin Biotech, China) following the manufacturer's instructions. Absolute numbers of $CD4^+$, $CD8^+$ T cells, and their ratios were calculated in both intratumoral and stromal areas under 400× magnification using 3DHISTECH's SlideViewer version 2.5 (3DHISTECH Ltd. Budapest, Hungary). A pathologist blinded to the purpose of our study independently examined and scored all the slides.

Neoadjuvant Chemotherapy for Breast Cancer and Surgical Treatment

We employed the anthracycline-based regimen to all patients undergoing NAC. A total of 10 patients received the TEC regimens (Taxol 75 mg/m^2+ Epirubicin 75 mg/m^2 + Cyclophosphamide 500 mg/m^2); 8 patients received the TC regimens (e.g., Cyclophosphamide 500 mg/m^2 + Taxol 75 mg/m^2); 3 patients received the EC regimens (e.g., Epirubicin 90 mg/m^2 + Cyclophosphamide 600 mg/m^2); 2 patients received the CEF regimens (e.g. Cyclophosphamide 500 mg/m^2+ Epirubicin 75 mg/m^2+ 5-Fluorouracil 500 mg/m^2). The $HER2^+$ BC patients received trastuzumab (Herceptin) triweekly for 12 months. Breast ultrasonography and breast MRI were used to assess the patients' response to NAC treatment every 2 chemotherapy cycles. If tumor remission was detected, the NAC treatment would continue, and the patients would undergo breast surgery

after 6–8 chemotherapy cycles. Meanwhile, under circumstances in which exacerbation or stable severity of disease was found, an alternative treatment plan with the chemotherapy regimen or performing breast surgery would be adopted. According to the Response Evaluation Criteria in Solid Tumors (RECIST 1.1), we categorized the subjects into two groups based on the treatment responses for tumor: the patients who achieved pathologic complete response (pCR) or partial response (PR) after NAC were assigned into the NAC effectual group, while those with stable disease (SD) and progressive disease (PD) were assigned into the NAC non-effectual group.

Using CellMiner for System Analysis of the Relationship Between CD4 mRNA, CD8 mRNA Expression, and Reaction of Tumor Cells to NAC Drugs

CellMiner Cross-Database (CellMinerCDB, http://discover.nci.nih.gov/cellminer/) is a web-based application that provides both molecular and pharmacological data, and the tools to analyze these data within and across cancer cell line datasets from the National Cancer Institute (NCI), Broad Institute, Sanger/MGH, and MD Anderson Cancer Center (MDACC), which also allows systems pharmacology analysis of the largest publicly available database of anticancer drug activity (22). To understand the role of tumor immune landscape in the chemosensitivity and pathologic responses to NAC from BC patients, CellMinor (version 2.6) was used to analyze the relationship between the CD4 mRNA and CD8mRNA expression level and NAC drugs across cancer cell lines. The NAC drugs included in this analysis were anthracyclines (Doxorubicin, Epirubicin), cyclophosphamide, taxol derivative (Taxol, Docetaxel), platinum (Cisplatin, Carboplatin), Fluorouracil, alpha Methotrexate, Gemcitabine, Vinorelbine, Eribulin, and Ixabepilone.

Statistical Analysis and Bioinformatics

Between-group comparison of clinical indices and pathological data was conducted with Student's t-test, the chi-square test, and Mann–Whitney test using the SPSS 24.0 software (IBM, Inc., Chicago, IL). R software 3.6.1 was used to perform other analyses. Significant differences in alpha diversity based on the Chao estimate, Shannon, and Simpson index were measured using Wilcoxon rank-sum test by utilizing the "picante" package in R. Beta diversity was estimated by principal coordinate analysis (PCoA) of unweighted UniFrac analysis. Significant differences in abundance of genera between two groups were identified by linear discriminant analysis effect size (LEfSe) analysis. For LEfSe, the nonparametric factorial Kruskal–Wallis sum-rank test was employed to identify features with significant differential abundance, the effect size of which was calculated by subsequent linear discriminant analysis (LDA) (23). To detect the key signature microbiota at genus and species levels, we trained and run a random forest model (v.4.6–14 package in R 3.6.1) together with the 5-fold cross-validation to detect importance scores (mean decrease accuracy, MDA) and to examine the biomarkers' importance rank ordering. The case probability was calculated using this set of species and a receiver operating characteristic (ROC) curve within the pROC package in R. Correlation analysis between T lymphocyte subsets and the signature microbiota was conducted using Spearman's rank-based correlation. Statistical significance was set at $p<0.05$.

RESULTS

Clinicopathological Characteristics in BC Patients From NAC Non-Effectual Group and NAC Effectual Group

Data from a total of 23 patients with invasive breast cancer were included in the study. According to RECIST 1.1, 18 cases were assigned into the NAC effectual group (the chemotherapy efficacy rate was 78.3%), and 5 cases were in the NAC non-effectual group. The two groups were comparable in terms of age, BMI, menopausal status, pathological type, clinical staging, ER expression, PR expression, HER2 expression, and Ki-67 expression ($p > 0.05$). Detailed patient clinical pathology data and clinical information are shown in **Table 1**.

Taxonomic Characterization of Gut Microbiota in BC Patients From NAC Non-Effectual Group and NAC Effectual Group

Considering that treatment factors may bias the predictive effect of the microbiota, we then used baseline specimens to explore the potential roles of discriminatory bacterial taxa as biomarkers. Based on the species profile, various alpha-diversity indexes (i.e., Chao1, Shannon, and Simpson index) were used to estimate gut microbiota richness and evenness in the sample. Compared with the NAC non-effectual group, the NAC effectual group exhibited highly diversified intra-individual characters, as indicated by the Chao 1 ($p = 0.012$), Shannon ($p = 0.002$), and Simpson ($p = 0.005$) index (Wilcoxon rank-sum test, **Figures 2A–C**).

Results of principal coordinate analysis based on unweighted UniFrac distance demonstrated significant differences in between-sample variability (beta-diversity) of the overall microbial composition between the NAC non-effectual group and the NAC effectual group ($p = 0.046$) (**Figure 2D**).

To further identify microbial signatures, defined by groups of bacterial taxa that were able to distinguish the NAC non-effectual group from the NAC effectual group patients, we performed LEfSe analysis on the fecal microbiota composition between the two groups. The entire abundance of genes determined the relative enrichments of gut microbiota. At the genus level, enriched levels of *Bacteroides* were found in the NAC non-effectual group patients, while 15 genera were found enriched in the NAC effectual group patients (LDA score >2.2, $p < 0.05$), 11 of which belonged to the phylum *Firmicutes* (*Clostridium, Faecalibacterium, Roseburia, Eubacterium, Ruminococcus*, *Ruminiclostridium, Butyrivibrio, Fusicatenibacter, Lactobacillus, Coprococcus, and Dorea* genera), followed by *Bacteroidetes* bacterial taxa (Odoribacter), and *Fusobacter* (*Fusobacterium* genus), *Proteobacteria* (*Bilophila* genus), and *Mycoplasma* genera. From the view of species, 25 microbes showed

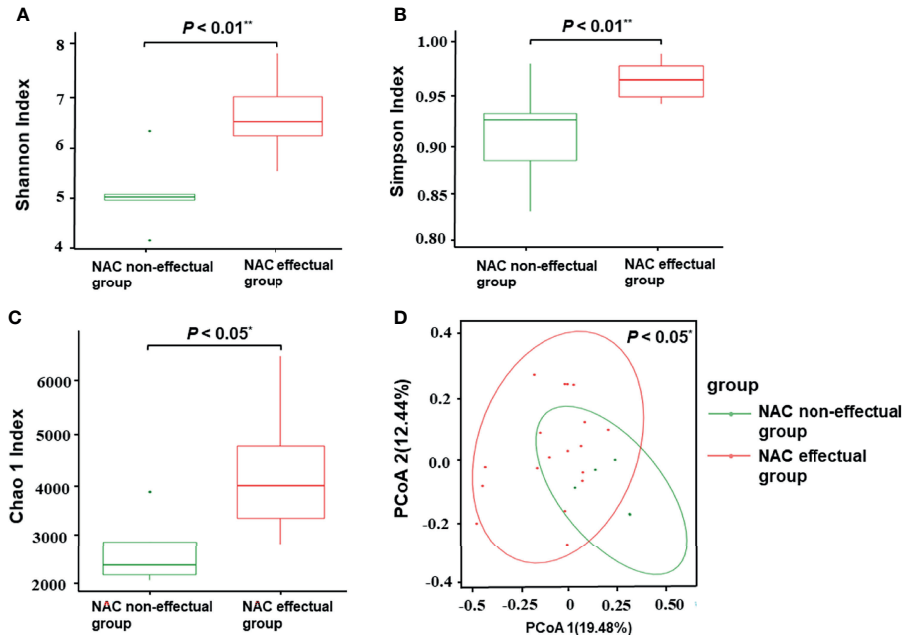

FIGURE 2 | Comparisons of alpha-diversity and beta-diversity between the NAC effectual group (n = 5) and the NAC non-effectual group (n = 18). **(A–C)** Alpha-diversity of the two groups at the species level, measured in terms of the Shannon **(A)**, Simpson **(B)**, and Chao1 index **(C)**. **(D)** PCoA of unweighted UniFrac analysis showed that the overall fecal microbiota composition was different between the NAC non-effectual group and the NAC effectual group. NAC, neoadjuvant chemotherapy; PCoA, principal coordinate analysis. Superscript symbols indicate statistically significant differences between the two groups: $^{*}p < 0.05$, $^{**}p < 0.01$.

enrichments in the NAC effectual group, while the abundance of 10 species belonging to the *Bacteroides* genus was increased in the NAC non-effectual group (**Figure 3**). Hence, our analysis revealed that there are significant intergroup differences between NAC non-effectual patients and the NAC effectual group in their gut microbial composition.

Gut Microbiome-Based Signature Discriminated the Therapeutic Response to NAC in BC Patients

To identify signature bacteria that could predict the BC patients' response to NAC, a random forest model with 5-fold cross-validation was performed to build a classification model with a training set consisting of 5 NAC non-effectual group patients and 18 NAC effectual group patients based on the above-mentioned 56 genera. Based on the mean decrease accuracy (**Figure 4B**), which depicts the ranked importance of signature microbial in differences between the NAC non-effectual group from the NAC effectual group patients, 9 optimal species markers were selected, including *Bacteroides, Coprococcus, Dorea, Fusicatenibacter, Ruminococcus, Butyrivibrio* sp. CAG 318, *Lactobacillus salivarius, Bacteroides xylanisolvens*, and uncultured *Ruminococcus* sp. We found that the combination of 3 signature bacteria (*Coprococcus, Dorea*, and uncultured *Ruminococcus* sp.) worked best to distinguish the NAC non-effectual group from the NAC effectual group patients with an AUC = 0.833 (95% CI: 0.678–0.989). However, employing all the 9 genera (AUC: 0.604, 95% CI: 0.499–0.71) did not significantly improve the predictive performance (**Figure 4A**).

Analysis of Tumor-Infiltrating Lymphocytes in Peripheral Blood and Tumor Tissue of BC Patients Treated by NAC

As shown in **Table 1**, after controlling for age, BMI, and menopausal status, results of the Mann–Whitney test showed that, although the NAC effectual group had increased levels of the peripheral blood T lymphocyte subset ratio than the NAC non-effectual group, the difference was only significant in $CD4^{+}$T lymphocyte between the two groups ($p < 0.05$).

As shown in **Figure 5**, infiltration of $CD4^{+}$ and $CD8^{+}$TILs was found in the intratumoral and stromal areas; infiltration of $CD4^{+}$ and $CD8^{+}$ TILs was significantly higher in the tumors of the NAC effectual group. After controlling for age, BMI, and menopausal status, results of the Mann–Whitney test showed that in the NAC effectual group, the absolute numbers of $CD4^{+}$ and $CD8^{+}$ TIL infiltration were significantly higher than those in the NAC non-effectual group ($p < 0.001$, $p < 0.01$, respectively).

Signature Bacteria Associated With T Lymphocyte Cell Subsets in BC Patients Treated by NAC

We used partial Spearman's rank-based correlation tests (controlling for age, BMI, and menopausal status) to uncover the associations between blood and tumor-infiltrating T lymphocytes and NAC effectual-related signature bacteria in BC patients treated by NAC. Two signature bacteria *Coprococcus* and uncultured *Ruminococcus* sp. were found to be significantly overrepresented

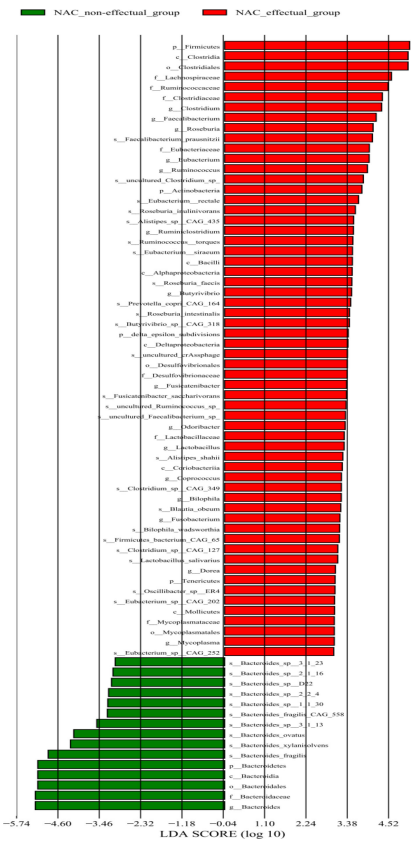

FIGURE 3 | Relative abundance of 75 species differing significantly between the NAC non-effectual group and the NAC effectual group (LDA effect size analysis).

in patients with advanced blood $CD4^+$ TIL counts compared to those with lower blood $CD4^+$ TIL counts (r = 0.44 and 0.44, respectively, all p's<0.05). All the three signature bacteria *Coprococcus, Dorea*, and uncultured *Ruminococcus* sp. were significantly and positively correlated with $CD4^+$ T lymphocyte in tumor (r = 0.49, 0.44, and 0.51, respectively, all p's<0.05). However, no significant correlation between $CD3^+$ and $CD8^+$ T lymphocyte and signature bacteria was found (**Figure 6**).

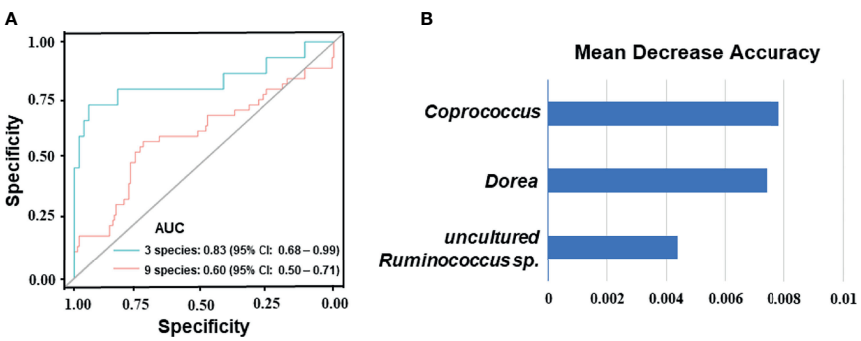

FIGURE 4 | Disease classification based on gut microbiome signature. **(A)** Classification performance of the random forest model using the relative abundance of NAC- efficacy associated genera was assessed by the area under the ROC in BC patients. The combination of 3 signature bacteria: *Coprococcus, Dorea*, and uncultured *Ruminococcus* sp. The combination of 9 optimal species markers: *Bacteroides, Coprococcus, Dorea, Fusicatenibacter, Ruminococcus, Butyrivibrio* sp. CAG 318, *Lactobacillus salivarius, Bacteroides xylanisolvens*, and uncultured *Ruminococcus* sp. **(B)** Identification of the signature gut microbiota associated with NAC- efficacy by random forest. Fivefold cross-validation together with random forest was performed to determine the signature biomarkers. Detailed signature biomarkers' random seed from the random forest is presented between the NAC non-effectual group and the NAC effectual group.

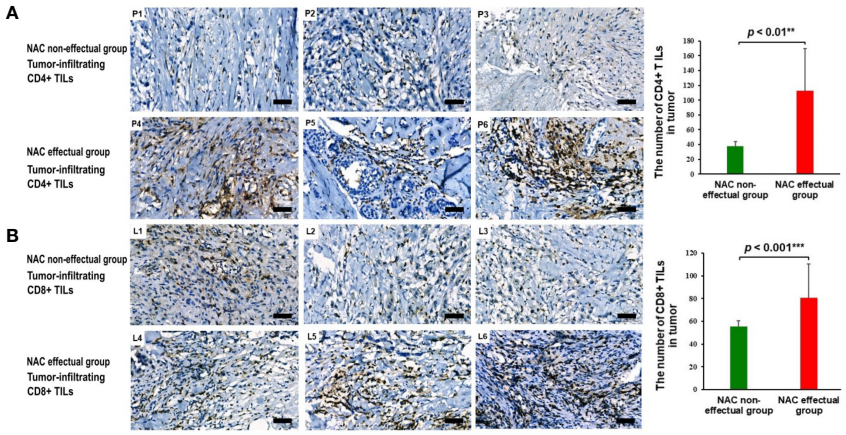

FIGURE 5 | **(A)** The presence and abundance of tumor-infiltrating $CD4^+$ TILs as assessed with IHC staining between representing NAC non-effectual patients (P1, P2, P3) and NAC effectual patients (P4, P5, P6). Scale bars, 50 μm. **(B)** The presence and abundance of tumor-infiltrating $CD8^+$ TILs as assessed with IHC staining between representing NAC non-effectual patients (L1, L2, L3) and NAC effectual patients (L4, L5, L6). Scale bars, 50 μm. IHC, immunohistochemistry. Data show means ± s.d. ** denotes $p < 0.01$ by Student's *t*-test. *** denotes $p < 0.001$ by Student's *t* test.

Correlations Between CD4, CD8 mRNA Expression Level, and the Sensitivity of Tumor Cells to NAC Drugs

As shown in **Figure 7**, the result of CellMiner Cross-Database analysis showed that a higher level of CD4 mRNA expression was significantly associated with higher sensitivity of cancer cell lines to cyclophosphamide ($r = 0.81$, $p< 0.001$, **Figure 7A**), cisplatin ($r = 0.30$, $p< 0.05$, **Figure 7B**), and carboplatin ($r = 0.47$, $p< 0.001$, **Figure 7C**). As for CD8 mRNA expression, it was only found significantly and positively correlated with cyclophosphamide ($r = 0.41$, $p< 0.01$, **Figure 7D**) but not with cisplatin ($r = 0.18$, p = 0.18, **Figure 7E**) or carboplatin ($r = 0.18$, $p = 0.17$, **Figure 7F**).

DISCUSSION

NAC has been routinely prescribed for patients with locally advanced breast cancer, which can relieve local tumor burden and create favorable conditions for surgery. However, not all breast cancer patients can benefit significantly from NAC. Therefore, it is of great clinical significance to identify effective predictive markers for BC patients' responses to NAC treatment. There is growing evidence that altered gut microbiome correlates with the development of multiple tumor types and modulates the host response to chemotherapeutic drugs. In this study, we performed a comprehensive metagenomic comparison of gut microbiota in highly homogenous breast cancer patients treated

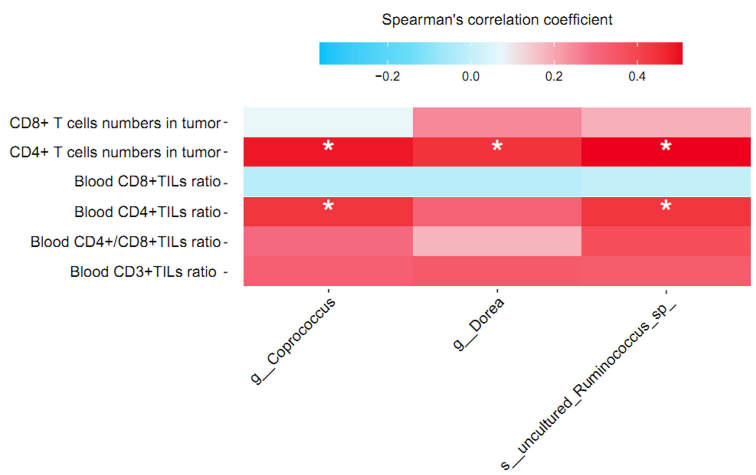

FIGURE 6 | Correlation between relative abundance of signature gut microbiota and T lymphocyte cell subsets in breast cancer patients treated by NAC. Partial Spearman's rank correlation coefficient is indicated using a color gradient: red indicates positive correlation; blue, negative correlation. TIL, tumor infiltrating lymphocyte. * denotes $p < 0.05$.

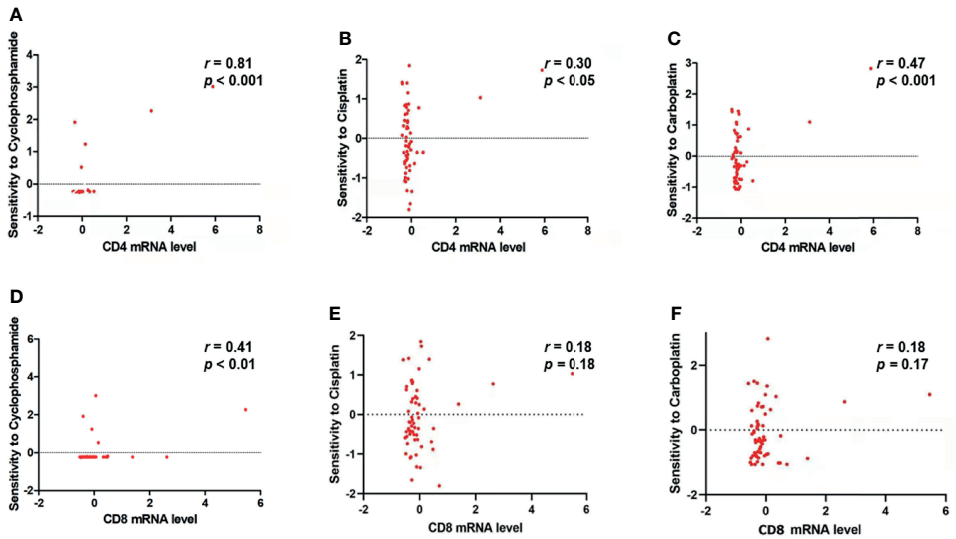

FIGURE 7 | CD4 mRNA and CD8 mRNA expression level is related to the sensitivity of tumor cells to NAC drugs. **(A–C)** CD4 mRNA expression level is significantly and positively correlated with the sensitivity of tumor cells to **(A)** cyclophosphamide ($r = 0.81$, $p < 0.0001$), **(B)** cisplatin ($r = 0.30$, $p < 0.05$), and **(C)** carboplatin ($r = 0.47$, $p < 0.001$). **(D)** CD8 mRNA expression level is significantly and positively correlated with the sensitivity of tumor cells to cyclophosphamide ($r = 0.41$, $p < 0.01$). **(E, F)** CD8 mRNA expression level is not significantly correlated with the sensitivity of tumor cells to **(E)** cisplatin ($r = 0.18$, $p = 0.18$) and **(F)** carboplatin ($r = 0.18$, $p = 0.17$).

by NAC. We also investigated the association between gut microbiome and BC patients' responses to NAC treatment, as well as the related mechanism. The results highlighted the characteristics of the NAC effectual group defined as abundant bacterial diversity and variation in microbial community. Given the necessity of predicting BC patients' responses to NAC treatment, a model with discriminatory diagnostic power was exploratorily trained. The most notable finding was that 3 signature bacteria were associated with TIL concentrations and NAC response in BC patients.

The fecal microbiome in patients in the NAC non-effectual group showed decreased species richness and distinct within-sample diversity compared with patients in the NAC effectual group. Researchers had reached consensus that low bacterial diversity, as one of the major types of gut dysbiosis, was involved in a variety of diseases (4). The Goedert team published a series of case-control studies on the relationship between gut microbiota and breast cancer, which indicated that BC patients had decreased α and β diversity of gut microbiota compared to healthy controls, and they also had gut microbiome dysbiosis that was characterized by an increase in the abundance of *Clostridium* (24–26). Moreover, highly diverse fecal microbiome endorsed significantly longer progression-free survival in contrast to low or moderate diversities of microbiota (4). These studies, together with the current findings, imply that lowered bacterial diversity may increase the possibility of resistance to NAC treatment and a lowered NAC efficacy, which can thus be an important predictive index.

Regarding relative abundances in microbiota composition, the NAC non-effectual group and the NAC effectual group showed differences in the abundance of 56 bacteria species. The levels of the major component of the adult fecal microbiota, phylum Firmicutes (including *Clostridium, Faecalibacterium, Roseburia, Eubacterium, Ruminococcus, Ruminiclostridium, Butyrivibrio, Fusicatenibacter, Lactobacillus, Coprococcus*, and *Dorea* genera), were decreased while *Bacteroides*, that of the core genus of the phylum Bacteroidetes, were increased in the NAC non-effectual group relative to the NAC effectual group. The pro-inflammatory bacteria *Bacteroides* showed the most effective association with the NAC non-effectual group patients, which is in line with the previous findings that *Bacteroides* were positively associated with breast tumors and the severity of cancer (8, 27). In addition, a significant decrease in the Firmicutes phylum and an increase in the Bacteroidetes phylum were reported to be indicative of poorer cancer outcomes. Interestingly, an increased relative abundance of *Bacteroides* was also reported, which might cause increased intestinal barrier permeability and inflammation in women diagnosed with invasive breast cancer, which might influence their fear for cancer recurrence (28). Further study compared the differences in gut microbiota between before and after chemotherapy and found that chemotherapy induced gastrointestinal mucositis and gastrointestinal reaction, which was associated with severe gut microbiome dysbiosis such as a decrease in Firmicutes (29). Remarkably, in the NAC non-effectual group, we also identified a decrease in antioxidant indolepropionic acid producers (e.g., *Clostridium, Fusobacterium, Fusicatenibacter*), which could maintain or promote intestinal permeability and systemic immunity (30). While no study, to date, has documented the impact of microbiota populations on the NAC response in breast cancer, our results, as well as the aforementioned findings, indicate that BC patients' microbial signatures such as a decreased ratio of Firmicutes/Bacteroidetes may influence their

therapeutic outcome. In addition, the microbial community in the NAC non-effectual group patients may shift toward the depletion of butyrate-producing and indolepropionic acid-producing bacteria, which may modulate the activity and efficacy of NAC treatment for them.

Our results from the random forest model found that three bacteria, *Coprococcus, Dorea*, and uncultured *Ruminococcus* sp., were most useful for distinguishing the NAC non-effectual group patients from the NAC effectual group patients. The accumulation of numerous metabolites from human gut microbiota rendered systemic influences on the host. An increase in butyrate-producing bacteria (e.g., *Coprococcus* and uncultured *Ruminococcus* sp.) was observed in the NAC effectual group patients. In addition, *Dorea*, which was found to be an acetate and lactate producer, and may serve as a substrate for butyrate production, was also overrepresented in NAC responders. Besides its anti-inflammatory roles, butyrate also works to immune cells *via* specific G-protein-coupled receptors expressed on the surface (31). In addition, the heightened levels of these butyrate-producing bacteria promote the production of short-chain fatty acids (SCFAs) and contribute to a more favoring microbial profile (31). Increased production of SCFA by microbiota was suggested to pose health benefits through anti-inflammatory effects (23) and to play an important role in protecting the intestinal barrier function and ameliorating mucosal inflammation (28, 32). Interestingly, higher abundance of butyrate-producing bacteria was also significantly associated with a better response to immunotherapy (33–35). However, consistent with some of the findings from immunotherapy and chemotherapy research, no direct association between enrichment of the butyrate-producing microbes in responders and treatment responses was found in our study. Fortunately, published experimental studies have provided some mechanistic insights into this issue.

$CD4^+$ and $CD8^+$ T cells as immunological parameters were well known to assist the activation of the antigen-presenting cells *via* cytokine secretion, which favored the prognosis of breast cancer (10, 36). Within the result of the CellMiner Cross-Database for system analysis of the relationship between NAC drugs and CD4 mRNA expression across cancer cell lines, we found that the CD4 mRNA expression level was significantly associated with the sensitivity of tumor cells to NAC drugs such as cyclophosphamide, cisplatin, and carboplatin. Moreover, the CD8 mRNA expression level was also significantly and positively correlated with the sensitivity of tumor cells to cyclophosphamide. This is in line with past studies (36) and also correlated evidence that CD4+ and CD8+ TILs may serve as biomarkers for the clinical outcome of NAC in BC patients.

Substantial data supported that the regulations of the immune system by composed gut microbiota could lead to huge impacts to the efficacy and toxicity of antitumor therapy (37, 38). Nevertheless, the underlying physiological mechanisms in the antitumor-related immune response remained unclear. Research suggested that gut microbiota may participate in the plasticity of CD4+ T cells in the tumor microenvironment and cause antitumor or tumor-promoting immune responses, thereby exerting anticancer or tumor-promoting effects (39), but the specific signature bacteria that related to the immune function in the breast cancer patients are rarely reported. In this study, we found that the NAC effectual group showed a higher level of peripheral blood $CD4^+$T cells and higher absolute numbers of $CD4^+$ and $CD8^+$ TIL infiltration in tumor tissues than the NAC non-effectual group, which suggest that the NAC effectual group patients may have better immune functions compared with the NAC non-effectual group. Likewise, we also found that a higher abundance of *Coprococcus, Dorea*, and uncultured *Ruminococcus* sp. may contribute to the higher levels of peripheral blood and tumor-infiltrating $CD4^+$TILs in BC patients. These findings suggest that enhanced antigen presentation or $CD4^+$T cell recruitment in the local tumor environment by microbiota holds their momentousness in the NAC treatment responders. This is consistent with the previous studies (40, 41) and in support of our research hypothesis that gut microbiota may regulate the efficacy of the NAC *via* its interactions with immune cells.

Many studies have documented the beneficial role of *Coprococcus* in promoting healthy immune function, and decreased *Coprococcus* representation has been linked with several diseases including lung cancer (42), psoriatic arthritis (43), and immune-mediated inflammatory disease (44). As for uncultured *Ruminococcus* sp., it was found to have an anti-inflammatory effect (45) and was involved in immunomodulatory and promoting glucose homeostasis (46). Previous studies have also reported that the genus *Dorea* is positively correlated with the response to NAC in rectal cancer patients (47). However, there is no previous research that has examined the relationship between $CD4^+$ T cells and gut microbiota in BC patients. Our findings echoed with one existing study conducted in patients with metastatic melanoma, where before receiving anti-PD-1 immunotherapy, patients who later responded to immunotherapy were found with more abundant baseline *Bifidobacterium* and *Enterococcus* in their gut microbiota (48). Taken together, these results provide suggestive evidence that *Coprococcus, Dorea*, and uncultured *Ruminococcus* sp. may be closely linked to TILs such as $CD4^+$ T cells; therefore, modulating these three bacteria may further affect NAC treatment outcomes in BC patients by regulating their immune function. *Coprococcus, Dorea*, and uncultured *Ruminococcus* sp. may serve as novel bacterial biomarkers in predicting the activity and efficacy of NAC treatment in BC patients. This implication is worthy of further verification in a larger sample. In the future, developing a novel therapeutic approach using bacteriophages to target the specific signature bacteria identified to be related to NAC efficacy in this study, which will precisely edit the intestinal microbiota, should be a promising intervention strategy to alter the intestinal microbiomes of and improve the therapeutic effect in breast cancer patients.

The advantages of the current study mainly lie in the following areas: i) methodology, such as a collection of highly homogeneous samples prior to NAC treatment; ii) utilization of the metagenomic analyses; and iii) the adoption of database analysis such as CellMiner Cross-Database analysis. Yet, there are still limitations that need to be addressed. First, this study is preliminary. The sample size is small and therefore the findings should be considered with caution, and repetition of bacteria

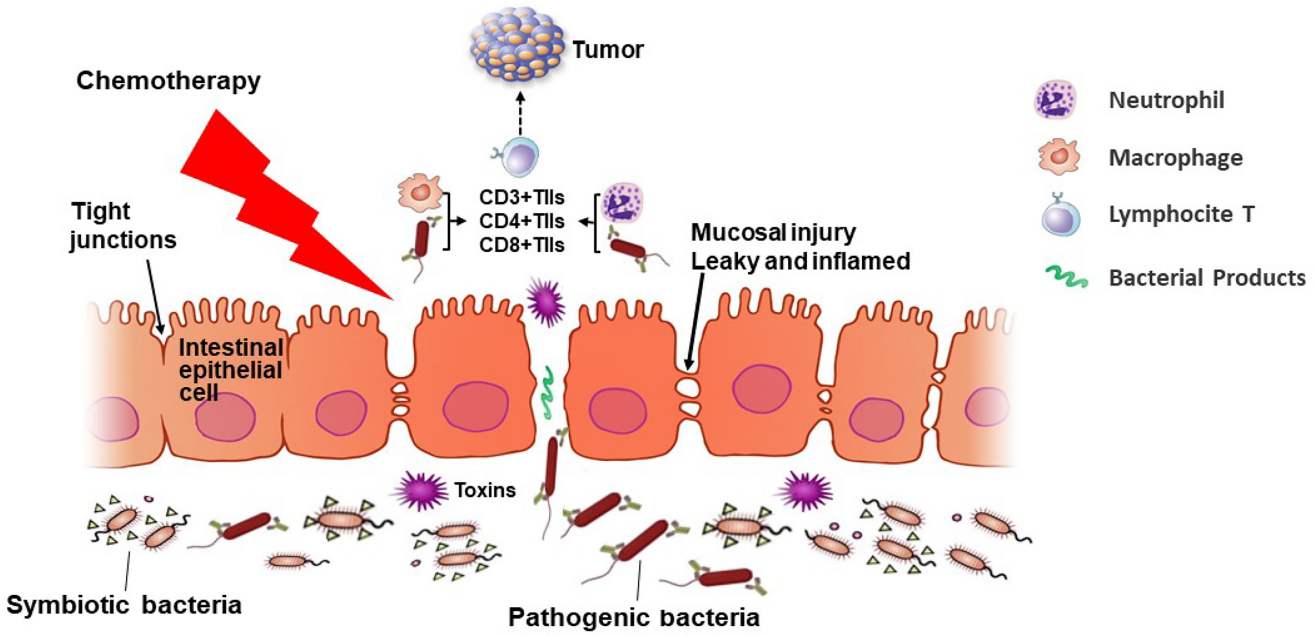

FIGURE 8 | An overview of the microbiota–T lymphocyte (TILs) interactions that modulate neoadjuvant chemotherapy (NAC) efficacy. NAC treatment induces changes in the gut microbiota diversity, causing inflammation and damage to the mucosal barrier of cancer patients, permitting pathogenic bacteria to cross the intestinal barrier and enter lymphoid organs. Then the intestinal microbiota may mediate the induction of TILs such as $CD3^+$, $CD4^+$, and $CD8^+$ cells in patients undergoing NAC. When the tight junctions between epithelial cells are broken and the intestinal permeability reduces, pathogenic bacteria interact with immune cells, regulating the response rate of the NAC treatment.

signature related to the response rate to NAC *in vivo* is desired to further establish the causal relationships between gut microbiota changes, immune activation, and neoadjuvant chemotherapy efficacy. Multicenter studies involving diverse populations across different ages and breast cancer types would also provide further definite evidence to ensure the predictive role of signature bacteria on NAC response. Second, despite strict criteria applied to the inclusion/exclusion of participants, they were recruited from the same region (i.e., similar dietary habits existed among the subjects), and patients' dietary habits and lifestyles were not controlled, which might induce confounding bias to our results. Third, this study was not able to indicate the possible functional relevance of these microbes in the patients. The possible mechanisms such as immunoregulation, which may elucidate the relationships between signature bacteria, TILs, and NAC efficacy, were not examined in this study without measuring the serum inflammatory biomarkers and related microbial metabolomics, such as interleukin-6, interleukin-1 receptor antagonist, tumor necrosis factor-α, and the tryptophan's metabolites (49). Future studies should adopt these inflammatory biomarkers as well as the microbial metabolite to examine these mechanisms. Fourth, this research is a cross-sectional study, which cannot provide the dynamics between gut microbiota and NAC efficacy. A prospective cohort trial to show the longitudinal changes in the NAC efficacy-associated microbiota is needed in the future.

CONCLUSION

This study contributes to identifying the differential composition of the gut microbiota community between the NAC non-effectual group and NAC effectual group patients. We developed a prediction model for neoadjuvant chemotherapy response based on the relative abundance of gut microbiota. The bacteria signature related to the response rate to NAC and cancer outcome also links to TIL levels, especially $CD4^+$ T cells (as **Figure 8** proposes). The findings raise the possibility of using novel microbiota biomarkers in the evaluation of the responsiveness to NAC treatment for BC patients and put forward new strategies for regulating gut microbiota as potential therapeutic targets. Future understanding about the possible role of microbiota, especially *Coprococcus, Dorea*, and uncultured *Ruminococcus* sp., and their interaction with TILs in improving breast cancer outcome is warranted.

DATA AVAILABILITY STATEMENT

The datasets presented in this study can be found in online repositories. The names of the repository/repositories and accession number(s) can be found below: Zenodo under accession number 10.5281/zenodo.5939855 (https://zenodo.org/record/5939855#.YfkzK5pBxPY).

ETHICS STATEMENT

Permission has been granted by the Ethics Committee of Sun Yat-Sen Memorial Hospital of Sun Yat-Sen University. The patients/participants provided their written informed consent to participate in this study.

AUTHOR CONTRIBUTIONS

Each author contributed substantially to the paper. YL conceived the study hypothesis, performed data analysis, and drafted the manuscript. BD, WW, and JW had made contributions to the conception, design of the work, sample collection, and data analysis. HJ contributed to data analysis and validation. KC and KH contributed to reviewing the literature and sample collection. SH and YY conceived the study hypothesis, revised it critically for important intellectual content, and supervised the writing of the manuscript. All the authors read and approved the final manuscript.

FUNDING

This work was supported by grants from the Fundamental Research Funds for the Central Universities (20ykjc03), the National Science Foundation of China (82071859, 81772837, 82071860, 82003176), Guangdong Natural Science Foundation (2018A0303130322), the Science and Technology Foundation of the Guangdong Province (2019A050510016), and Guangdong Innovation and Entrepreneurship Team Projects (2019BT02Y198).

ACKNOWLEDGMENTS

We are grateful to all the subjects who participated in the study.

REFERENCES

1. Bray F, Ferlay J, Soerjomataram I, Siegel RL, Torre LA, Jemal A. Global Cancer Statistics 2018: GLOBOCAN Estimates of Incidence and Mortality Worldwide for 36 Cancers in 185 Countries. *CA Cancer J Clin* (2018) 68 (6):394–424. doi: 10.3322/caac.21492
2. Mieog JS, van der Hage JA, van de Velde CJ. Preoperative Chemotherapy for Women With Operable Breast Cancer. *Cochrane Database Syst Rev* (2007) 2007(2):CD005002. doi: 10.1002/14651858
3. Nejman D, Livyatan I, Fuks G, Gavert N, Zwang Y, Geller LT, et al. The Human Tumor Microbiome Is Composed of Tumor Type-Specific Intracellular Bacteria. *Science* (2020) 368(6494):973–80. doi: 10.1126/science.aay9189
4. Chen J, Douglass J, Prasath V, Neace M, Atrchian S, Manjili MH, et al. The Microbiome and Breast Cancer: A Review. *Breast Cancer Res Treat* (2019) 178 (3):493–6. doi: 10.1007/s10549-019-05407-5
5. Goedert JJ, Jones G, Hua X, Xu X, Yu G, Flores R, et al. Investigation of the Association Between the Fecal Microbiota and Breast Cancer in Postmenopausal Women: A Population-Based Case-Control Pilot Study. *J Natl Cancer Institute* (2015) 107(8):djv147. doi: 10.1093/jnci/djv147
6. Fuhrman BJ, Feigelson HS, Flores R, Gail MH, Xu X, Ravel J, et al. Associations of the Fecal Microbiome With Urinary Estrogens and Estrogen Metabolites in Postmenopausal Women. *J Clin Endocrinol Metab* (2014) 99(12):4632–40. doi: 10.1210/jc.2014-2222
7. Zhu J, Liao M, Yao Z, Liang W, Li Q, Liu J, et al. Breast Cancer in Postmenopausal Women Is Associated With an Altered Gut Metagenome. *Microbiome* (2018) 6(1):136. doi: 10.1186/s40168-018-0515-3
8. Laborda-Illanes A, Sanchez-AlcoholadoL, Dominguez-Recio ME, Jimenez-Rodriguez B, Lavado R, Comino-Méndez I, et al. Breast and Gut Microbiota Action Mechanisms in Breast Cancer Pathogenesis and Treatment. *Cancers (Basel)* (2020) 12(9):2465. doi: 10.3390/cancers12092465
9. Chiba A, BawanehA, Velazquez C, Clear KYJ, Wilson AS, Howard-McNatt M, et al. Neoadjuvant Chemotherapy Shifts Breast Tumor Microbiota Populations to Regulate Drug Responsiveness and the Development of Metastasis. *Mol Cancer Res* (2020) 18(1):130–9. doi: 10.1158/1541-7786.MCR-19-0451
10. Jin YW, Hu P. Tumor-Infiltrating CD8 T Cells Predict Clinical Breast Cancer Outcomes in Young Women. *Cancers (Basel)* (2020) 12(5):1076. doi: 10.3390/cancers12051076
11. Lee KH, Kim E, Yun JS, Park YL, Do SI, Chae SW, et al. The Prognostic and Predictive Value of Tumor-Infiltrating Lymphocytes and Hematologic Parameters in Patients With Breast Cancer. *BMC Cancer* (2018) 18(1):938. doi: 10.1186/s12885-018-4832-5
12. Denkert C, von MinckwitzG, Darb-Esfahani S, Lederer B, Heppner BI, Weber KE, et al. Tumour-Infiltrating Lymphocytes and Prognosis in Different Subtypes of Breast Cancer: A Pooled Analysis of 3771 Patients Treated With Neoadjuvant Therapy. *Lancet Oncol* (2018) 19(1):40–50. doi: 10.1016/S1470-2045(17)30904-X
13. Brown EM, SadaranganiM, Finlay BB. The Role of the Immune System in Governing Host-Microbe Interactions in the Intestine. *Nat Immunol* (2013) 14(7):660–7. Sadarangani. doi: 10.1038/ni.2611
14. Plaza-Díaz J, Álvarez-MercadoA, Ruiz-Marín CM, Reina-Pérez I, Pérez-Alonso AJ, Sánchez-Andujar MB, et al. Association of Breast and Gut Microbiota Dysbiosis and the Risk of Breast Cancer: A Case-Control Clinical Study. *BMC Cancer* (2019) 19(1):495. doi: 10.1186/s12885-019-5660-y
15. Maroof H, HassanZ, Mobarez AM, Mohamadabadi MA. Lactobacillus Acidophilus Could Modulate the Immune Response Against Breast Cancer in Murine Model. *J Clin Immunol* (2012) 32(6):1353–9. doi: 10.1007/s10875-012-9708-x
16. Alexander JL, Wilson I, Teare J, Marchesi JR, Nicholson JK, Kinross JM. Gut Microbiota Modulation of Chemotherapy Efficacy and Toxicity. *Nat Rev Gastroenterol Hepatol* (2017) 14(6):356–65. doi: 10.1038/nrgastro.2017.20
17. Erdman SE, Poutahidis T, Tomczak M, Rogers AB, Cormier K, Plank B, et al. CD4+ CD25+ Regulatory T Lymphocytes Inhibit Microbially Induced Colon Cancer in Rag2-Deficient Mice. *Am J Pathol* (2003) 162(2):691–702. doi: 10.1016/S0002-9440(10)63863-1
18. Shapira I, Sultan K, Lee A, Taioli E. Evolving Concepts: How Diet and the Intestinal Microbiome Act as Modulators of Breast Malignancy. *ISRN Oncol* (2013) 2013:693920. doi: 10.1155/2013/693920
19. Franchi L, Warner N, Viani K, Nunez G. Function of Nod-Like Receptors in Microbial Recognition and Host Defense. *Immunol Rev* (2009) 227(1):106–28. doi: 10.1111/j.1600-065X.2008.00734.x
20. Shui L, Yang X, Li J, Yi C, Sun Q, Zhu H. Gut Microbiome as a Potential Factor for Modulating Resistance to Cancer Immunotherapy. *Front Immunol* (2020) 17(10):2989. doi: 10.3389/fimmu.2019.02989
21. Flynn J, Gorry P. Flow Cytometry Analysis to Identify Human CD4+ T Cell Subsets. *Methods Mol Biol* (2019) 2048:15–25. doi: 10.1007/978-1-4939-9728-2_2
22. Reinhold WC, Sunshine M, Varma S, Doroshow JH, Pommier Y. Using CellMiner 1.6 for Systems Pharmacology and Genomic Analysis of the NCI-60. *Clin Cancer Res an Off J Am Assoc Cancer Res* (2015) 21(17):3841–52. doi: 10.1158/1078-0432.CCR-15-0335
23. Wei Y, Li Y, Yan L, Sun C, Miao Q, Wang Q, et al. Alterations of Gut Microbiome in Autoimmune Hepatitis. *Gut* (2020) 69(3):569–77. doi: 10.1136/gutjnl-2018-317836
24. Goedert JJ, Jones G, Hua X, Xu X, Yu G, Flores R, et al. Investigation of the Association Between the Fecal Microbiota and Breast Cancer in Postmenopausal Women: A Population-Based Case-Control Pilot Study. *J Natl Cancer Inst* (2015) 107(8):djv147. doi: 10.1093/jnci/djv147

25. Flores R, Shi J, Fuhrman B, Xu X, Veenstra TD, Gail MH, et al. Fecal Microbial Determinants of Fecal and Systemic Estrogens and Estrogen Metabolites: A Cross-Sectional Study. *J Transl Med* (2012) 10:253. doi: 10.1186/1479-5876-10-253
26. Goedert JJ, Hua X, Bielecka A, Okayasu I, Milne GL, Jones GS, et al. Feigelson HS Postmenopausal Breast Cancer and Oestrogen Associations With the IgA-Coated and IgA-Noncoated Faecal Microbiota. *Br J Cancer* (2018) 118 (4):471–9. doi: 10.1038/bjc.2017.435
27. Urbaniak C, GloorG, Brackstone M, Scott L, Tangney M, Reid G. The Microbiota of Breast Tissue and Its Association With Breast Cancer. *Appl Environ Microbiol* (2016) 82(16):5039–48. doi: 10.1128/AEM.01235-16
28. Okubo R , KinoshitaT, Katsumata N, Uezono Y, Xiao J, Matsuoka YJ. Impact of Chemotherapy on the Association Between Fear of Cancer Recurrence and the Gut Microbiota in Breast Cancer Survivors. *Brain Behav Immun* (2020) 85:186–91. doi: 10.1016/j.bbi.2019.02.025
29. Zhang M, Zhou H, Xu S, Liu D, Cheng Y, Gao B, et al. The Gut Microbiome can be Used to Predict the Gastrointestinal Response and Efficacy of Lung Cancer Patients Undergoing Chemotherapy. *Ann Palliat Med* (2020) 9 (6):4211–27. doi: 10.21037/apm-20-2183
30. Dodd D, Spitzer M, Van Treuren W, Merrill BD, Hryckowian AJ, Higginbottom SK, et al. A Gut Bacterial Pathway Metabolizes Aromatic Amino Acids Into Nine Circulating Metabolites. *Nature* (2017) 551 (7682):648–52. doi: 10.1038/nature24661
31. Ryan PM, Patterson E, Carafa I, Mandal R, Wishart DS, Dinan TG, et al. Metformin and Dipeptidyl Peptidase-4 Inhibitor Differentially Modulate the Intestinal Microbiota and Plasma Metabolome of Metabolically Dysfunctional Mice. *Can J Diabetes* (2020) 44(2):146–55.e2. doi: 10.1016/j.jcjd.2019.05.008
32. Loman BR, Jordan K, Haynes B, Bailey MT, Pyter LM. Chemotherapy-Induced Neuroinflammation Is Associated With Disrupted Colonic and Bacterial Homeostasis in Female Mice. *Sci Rep* (2019) 9(1):16490. doi: 10.1038/s41598-019-52893-0
33. Chaput N, Lepage P, Coutzac C, Soularue E, Le Roux K, Monot C, et al. Baseline Gut Microbiota Predicts Clinical Response and Colitis in Metastatic Melanoma Patients Treated With Ipilimumab. *Ann Oncol* (2017) 28(6):1368–79. doi: 10.1093/annonc/mdx108
34. Frankel AE, Coughlin LA, Kim J, Froehlich TW, Xie Y, Frenkel EP, et al. Metagenomic Shotgun Sequencing and Unbiased Metabolomic Profiling Identify Specific Human Gut Microbiota and Metabolites Associated With Immune Checkpoint Therapy Efficacy in Melanoma Patients. *Neoplasia* (2017) 19(10):848–55. doi: 10.1016/j.neo.2017.08.004
35. Gopalakrishnan V, Spencer CN, Nezi L, Reuben A, Andrews MC, Karpinets TV, et al. Gut Microbiome Modulates Response to Anti-PD-1 Immunotherapy in Melanoma Patients. *Science* (2018) 359(6371):97–103. doi: 10.1126/science.aan4236
36. Stanton SE, Disis M. Clinical Significance of Tumor-Infiltrating Lymphocytes in Breast Cancer. *J Immunother Cancer* (2016) 4:59. doi: 10.1186/s40425-016-0165-6
37. Gori S, Inno A, Belluomini L, Bocus P, Bisoffi Z, Russo A, et al. Gut Microbiota and Cancer: How Gut Microbiota Modulates Activity, Efficacy and Toxicity of Antitumoral Therapy. *Crit Rev Oncol Hematol* (2019) 143:139–47. doi: 10.1016/j.critrevonc.2019.09.003
38. Byrne A, Savas P, Sant S, Li R, Virassamy B, Luen SJ, et al. Tissue-Resident Memory T Cells in Breast Cancer Control and Immunotherapy Responses. *Nat Rev Clin Oncol* (2020) 17(6):341–8. doi: 10.1038/s41571-020-0333-y
39. Chiba T, Seno H. Indigenous Clostridium Species Regulate Systemic Immune Responses by Induction of Colonic Regulatory T Cells. *Gastroenterology* (2011) 141(3):1114–6. doi: 10.1053/j.gastro.2011.07.013
40. York A. Microbiome: Gut Microbiota Sways Response to Cancer Immunotherapy. *Nat Rev Microbiol* (2018) 16(3):121. doi: 10.1038/nrmicro.2018.12
41. Atarashi K, Tanoue T, Shima T, Imaoka A, Kuwahara T, Momose Y, et al. Induction of Colonic Regulatory T Cells by Indigenous Clostridium Species. *Science* (2011) 331(6015):337–41. doi: 10.1126/science.1198469
42. Liu F, Li J, Guan Y, Lou Y, Chen H, Xu M, et al. Dysbiosis of the Gut Microbiome Is Associated With Tumor Biomarkers in Lung Cancer. *Int J Biol Sci* (2019) 15(11):2381–92. doi: 10.7150/ijbs.35980
43. Scher JU, UbedaC, Artacho A, Attur M, Isaac S, Reddy SM, et al. Decreased Bacterial Diversity Characterizes the Altered Gut Microbiota in Patients With Psoriatic Arthritis, Resembling Dysbiosis in Inflammatory Bowel Disease. *Arthritis Rheumatol* (2015) 67(1):128–39. doi: 10.1002/art.38892
44. Forbes JD, ChenC, Knox NC, Marrie RA, El-Gabalawy H, de Kievit T, et al. A Comparative Study of the Gut Microbiota in Immune-Mediated Inflammatory Diseases-Does a Common Dysbiosis Exist? *Microbiome* (2018) 6(1):221. doi: 10.1186/s40168-018-0603-4
45. van den Munckhof ICL, KurilshikovA, Ter Horst R, Riksen NP, Joosten LAB, Zhernakova A, et al. Role of Gut Microbiota in Chronic Low-Grade Inflammation as Potential Driver for Atherosclerotic Cardiovascular Disease: A Systematic Review of Human Studies. *Obes Rev* (2018) 19 (12):1719–34. doi: 10.1111/obr.12750
46. Blanco-Míguez A, Fdez-Riverola F, Lourenço A, Sánchez B. In Silico Prediction Reveals the Existence of Potential Bioactive Neuropeptides Produced by the Human Gut Microbiota. *Food Res Int* (2019) 119:221–6. doi: 10.1016/j.foodres.2019.01.069
47. Yi Y, Shen L, Shi W, Xia F, Zhang H, Wang Y, et al. Gut Microbiome Components Predict Response to Neoadjuvant Chemoradiotherapy in Patients With Locally Advanced Rectal Cancer: A Prospective, Longitudinal Study. *Clin Cancer Res* (2021) 27(5):1329–40. doi: 10.1158/1078-0432.CCR-20-3445
48. Matson V, Fessler J, Bao R, Chongsuwat T, Zha Y, Alegre ML, et al. The Commensal Microbiome Is Associated With Anti-PD-1 Efficacy in Metastatic Melanoma Patients. *Science* (2018) 359(6371):104–8. doi: 10.1126/science.aao3290
49. Alpuim Costa D, Nobre J, Batista MV, Ribeiro C, Calle C, Cortes A, et al. Human Microbiota and Breast Cancer-Is There Any Relevant Link?-A Literature Review and New Horizons Toward Personalised Medicine. *Front Microbiol* (2021) 12:584332. doi: 10.3389/fmicb.2021.584332

Conflict of Interest: The authors declare that the research was conducted in the absence of any commercial or financial relationships that could be construed as a potential conflict of interest.

Publisher's Note: All claims expressed in this article are solely those of the authors and do not necessarily represent those of their affiliated organizations, or those of the publisher, the editors and the reviewers. Any product that may be evaluated in this article, or claim that may be made by its manufacturer, is not guaranteed or endorsed by the publisher.

Copyright © 2022 Li, Dong, Wu, Wang, Jin, Chen, Huang, Huang and Yao. This is an open-access article distributed under the terms of the Creative Commons Attribution License (CC BY). The use, distribution or reproduction in other forums is permitted, provided the original author(s) and the copyright owner(s) are credited and that the original publication in this journal is cited, in accordance with accepted academic practice. No use, distribution or reproduction is permitted which does not comply with these terms.

frontiers | Frontiers in Oncology

ORIGINAL RESEARCH
published: 02 June 2022
doi: 10.3389/fonc.2022.877219

High DNMT1 Expression in Stromal Fibroblasts Promotes Angiogenesis and Unfavorable Outcome in Locally Advanced Breast Cancer Patients

*Layla A. Al-Kharashi[1,2], Asma Tulbah[3], Maria Arafah[4], Abdelmonneim M. Eldali[5], Taher Al-Tweigeri[6] and Abdelilah Aboussekhra[1]**

[1] Department of Molecular Oncology, King Faisal Specialist Hospital and Research Center, Riyadh, Saudi Arabia, [2] Department of Pharmacology and Toxicology, Faculty of Pharmacy, King Saud University, Riyadh, Saudi Arabia, [3] Department of Pathology, King Faisal Specialist Hospital and Research Center, Riyadh, Saudi Arabia, [4] Department of Pathology, King Saud University, Riyadh, Saudi Arabia, [5] Department of Biostatistics, Epidemiology and Scientific Computing, King Faisal Specialist Hospital and Research Center, Riyadh, Saudi Arabia, [6] Department of Oncology, King Faisal Specialist Hospital and Research Center, Riyadh, Saudi Arabia

OPEN ACCESS

Edited by:
Raffaella Massafra,
National Cancer Institute Foundation (IRCCS), Italy

Reviewed by:
Sandra Donnini,
University of Siena, Italy
Madhuri Wadehra,
University of California, Los Angeles, United States
Christopher Gerner,
University of Vienna, Austria

***Correspondence:**
Abdelilah Aboussekhra
aboussekhra@kfshrc.edu.sa

Specialty section:
This article was submitted to Breast Cancer, a section of the journal Frontiers in Oncology

Received: 16 February 2022
Accepted: 05 May 2022
Published: 02 June 2022

Citation:
Al-Kharashi LA, Tulbah A, Arafah M, Eldali AM, Al-Tweigeri T and Aboussekhra A (2022) High DNMT1 Expression in Stromal Fibroblasts Promotes Angiogenesis and Unfavorable Outcome in Locally Advanced Breast Cancer Patients. Front. Oncol. 12:877219. doi: 10.3389/fonc.2022.877219

Background: Active breast cancer-associated fibroblasts (CAFs) play a leading role in breast carcinogenesis through promoting angiogenesis and resistance to therapy. Consequently, these active stromal cells have significant influence on patient outcome. Therefore, we explored here the role of the DNA methyltransferase 1 (DNMT1) protein in CAF-dependent promotion of angiogenesis as well as the prognostic power of DNMT1 level in both cancer cells and their adjacent CAFs in locally advanced breast cancer patients.

Methods: We applied immunohistochemistry to evaluate the level of DNMT1 in breast cancer tissues and their adjacent normal counterparts. Quantitative RT-PCR and immunoblotting were performed to investigate the role of DNMT1 in regulating the expression of pro-angiogenic genes in active CAFs and also their response to the DNMT1 inhibitors decitabine (DAC) as well as eugenol.

Results: We have shown that DNMT1 controls the pro-angiogenic potential of CAFs both *in vitro* and *in vivo* through positive regulation of the expression/secretion of 2 important pro-angiogenic factors VEGF-A and IL-8 as well as their upstream effectors mTOR and HIF-1α. To confirm this, we have shown that these DNMT1-related pro-angiogenic effects were suppressed by 2 DNMT1 inhibitors decitabine and eugenol. Interestingly, in a cohort of 100 tumors from locally advanced breast cancer patients (LABC), we have shown that high expression of DNMT1 in tumor cells and their adjacent stromal fibroblasts is correlated with poor survival of these patients.

Conclusion: DNMT1 upregulation in breast stromal fibroblasts promotes angiogenesis *via* IL-8/VEGF-A upregulation, and correlates well with poor survival of LABC patients.

Keywords: DNMT-1, breast cancer, cancer-associated fibroblasts, VEGF-A, prognosis

INTRODUCTION

Breast cancer (BC) is a high-burden malignancy and a serious threat for women's health world-wide (1). Despite important advances in BC biology and therapeutic approaches, locally advanced breast cancer (LABC) remains a major clinical issue with unfavorable prognosis and increased risk of locoregional recurrence as well as distant metastasis (2). Unfortunately, the use of neoadjuvant chemotherapy, the standard management therapy for LABC, allows disappearance of the tumor (pathological complete response: PCR) in only 20–30% of cases (3, 4). Therefore, efforts have been made to identify molecular biomarkers and therapeutic targets to predict and improve the response to the various neoadjuvant therapeutic protocols.

Tumor cells reside in a highly complex and heterogeneous tumor microenvironment (TME), which contains several types of cells with various functions and tumorigenic capacities. Among the components of the TME, cancer-associated fibroblasts (CAFs) play important roles in tumor onset and spread. Most of these cells are highly active with strong capacity to enhance breast carcinogenesis through promoting cancer cells stemness and angiogenesis (5, 6). This CAF-related promotion of neo-vascularization is mediated through secretion of various pro-angiogenic factors such as SDF-1, VEGF-A and IL-8 (7–10). Neovascularization allows tumor growth and facilitates the dissemination of tumor cells, which are escorted and supported by CAFs all over the metastatic process from the primary site to the metastatic site (5, 9, 11, 12). Additionally, recent findings have highlighted the important role of CAFs in modulating the response to various types of therapies, and also their valuable role as prognostic tool (13–15). The prognostic function of CAFs depends on the variation in the expression of many important cancer-related genes. We have recently shown that the DNA methyl-transferase gene (DNMT1) is highly expressed in CAF cells as compared to their adjacent counterpart cells, and that DNMT1 upregulation activates breast stromal fibroblasts (16).

Furthermore, several studies have shown that the expression of DNMT1 is higher in various types of breast cancers compared with paired normal breast tissues, and that DNMT1 upregulation is associated with higher grades of the disease and poor survival (17–22). Therefore, it has become clear that CAF-related biomarkers have powerful prognostic value and can also guide the next-generation therapeutic approaches.

In the present report we have shown that DNMT1 controls the pro-angiogenic role of active breast stromal fibroblasts (BSFs) through positive regulation of two key angiogenic factors VEGF-A and IL-8. In addition, we provide clear information on the prognostic value of CAF-DNMT1 for LABC patients.

MATERIALS AND METHODS

Cells and Cell Culture

Breast fibroblast cells (CAF-64 and TCF-64) were obtained and used as previously described (23). HUVEC cells were purchased from ATCC. Cells were regularly screened for mycoplasma contamination using MycoAlert Mycoplasma Detection Kits (Lonza). All supplements were obtained from Sigma (Saint Louis, MO, USA) except for antibiotic and antimycotic solutions, which were obtained from Gibco (Grand Island, NY, USA). Cells were maintained at 37°C in humidified incubator with 5% CO_2.

Cellular Lysate Preparation and Immunoblotting

This has been performed as previously described (24). Antibodies directed against DNMT1 (ab19905), IL-8 (ab52612) and VEGF-A (ab46154) were purchased from Abcam (Cambridge, MA), mTOR (7C10)/p.mTOR (Ser2448, D9C2), HIF-1α and Glyceraldehydes-3-phosphate dehydrogenase (GAPDH, FL-335) from Cell Signaling (Danvers, MA). The immunoblotting experiments were repeated at least 2 times.

RNA Purification and qRT-PCR

Total RNA was purified using the miRNeasy mini kit (Qiagen, UK) according to the manufacturer's instructions and was treated with RNase-free DNase. One (1) µg RNA was used to synthesize cDNA utilizing Advantage RT-PCR kit (Clontech Laboratories, Mountain View, CA, US). Quantitative RT-PCR was performed in triplicate using 4 µl cDNA mixed with 2x FastStart Essential DNA Green qPCR mastermix (Roche, New York, NY, US) and 0.3 µM forward and reverse primers. Amplifications were performed utilizing the LightCycler 96 Real-time PCR detection system (Roche) using the following cycle conditions: 95°C for 10 min (1 cycle); 95°C for 10 sec, 59°C for 20 sec, 72°C for 30 sec (45 cycles). GAPDH expression levels were used for normalization, and gene expression differences were calculated using the threshold cycle (Ct). Three independent experiments were performed for each reaction, and the obtained values were plotted as mean ± SD. The respective primers are:

GAPDH: 5'-GAGTCCACTGGCGTCTTC-3' and 5'-GGGG TGCTAAGCAGTTGGT-3'

VEGF-A:5'- CCCACTGAGGAG TCCAACAT -3' and 5'-TGGATGGTGGTACAGTCAGAG C -3'

IL-8: 5'- GAT CCACAAGTCCTTGTTCCA -3' and 5'- GCT TCCACATGTCCTCACAA -3'

SiRNA Transfection

The transfections using DNMT1-siRNA (Origene, SR301244A) and control–siRNA were carried out using the RNAi Fect reagent (Qiagen) as recommended by the manufacturer.

Viral Infection

Lentivirus-based vector bearing *DNMT1*–ORF as well as its corresponding control (GeneCopoeia) were used to prepare the lentiviral supernatant from 293FT cells. Lentiviral supernatants were collected 48 h post-transfection, filtered and used for infection. 48 h later, media were replaced with complete media and cells were grown for 3 days.

DNMT1-ORF Transfection

Lentivirus-based vectors bearing *DNMT1*-ORF, and the corresponding control were used to carry out transfection of BSF cells using human dermal fibroblast nucleofector 2000 transfection kit (Invitrogen) following the manufacturer's recommendations. After 2 weeks, transfected cells were selected by puromycin (1μg/mL).

ELISA Assays

Supernatants from 24 h fibroblast cell cultures were harvested, and ELISA was performed according to the manufacturer's instructions (R&D Systems). The OD was used at 450-nm on a standard ELISA plate-reader. These experiments were performed in triplicates, and were repeated three times.

Conditioned Media

Log phase cells (80% confluent) were cultured in medium without serum for 24 h, and then media were collected, briefly centrifuged and filtered, and then cells were counted. The resulting supernatants were used either immediately (taking into account the number of cells) or were frozen at -80 °C until needed.

HUVEC Endothelial Tube Formation Assay

The formation of capillary-like structures was assessed in a 96-well plate coated with ice-cold growth factor-reduced Matrigel (in vitro angiogenesis assay, Millipore). After solidification of the matrix at 37°C, 1x104 HUVEC cells were seeded onto the polymerized matrix in the presence of 200 μl of conditioned medium. Formation of capillary-like structure was photographed after 5 h of incubation and their number was counted. The total tube area was obtained from five random microscopic fields and expressed as a mean of three different experiments.

Patients and Archived Clinical Materials

Formalin-fixed paraffin-embedded tissues were obtained from the Pathology Department at KFSH&RC with institutional review board approval (RAC#2160005). The study cohort consisted of 100 locally advanced breast cancer patients who were diagnosed between 2006 and 2013, with a median fellow up time of 52. 6 months. Written informed consent was not required and a waiver was granted since samples were anonymized to the research team.

Immunohistochemistry Staining on FFPE Tissues

Immunohistochemistry for DNMT1 done on formalin-fixed, paraffin-embedded tissue using anti-DNMT1 antibody from Abcam (Cambridge, MA) overnight at a dilution of 1:500 and were stained using automated staining platform (Ventana). Envision + polymer (ready to use; Dako) was used as a secondary antibody. Color was developed with 3,3′-diaminobenzidine (DAB) and instant hematoxylin (Shandon) was used for counterstaining. The DNMT1 level was evaluated and verified by two qualified pathologists, who scored both the proportion of positive cells as well as the intensity of DNMT1 expression in both cancer cells and their stromal fibroblasts.

For CD31, the number of CD31-positive vessels was counted in five different highest fields of microvessel density (40x objective lens and 10x ocular lens). CD31[P2B1] (ab24590) was purchased from Abcam.

Quantification of Protein Expression Level

The protein signal intensity of each band was determined using ImageQuant TL software (GE Healthcare). Next, dividing the obtained value of each band by the value of the corresponding internal control allowed a correction of the loading differences. The fold change in the protein levels was determined by dividing the corrected values by that of the control.

Statistical Analysis

Statistical analysis was performed by the software package SAS version 9.4 (SAS Institute Inc., Cary, NC, USA). Continuous variables were compared by Student's t-test and *P* values of 0.05 and less were considered as statistically significant. Kaplan-Meyer method was used in survival tables and curves, and the different subgroups were compared by the log-rank test.

RESULTS

DNMT1 Positively Regulates VEGF-A and IL-8 in Breast Stromal Fibroblasts

We have recently shown that DNMT1 plays important role in the activation of breast stromal fibroblasts, which are known to promote angiogenesis in a paracrine manner (7, 16). Therefore, we sought to investigate the role of this methylation promoting gene in enhancing the pro-angiogenic effect of active fibroblasts. To this end, we have first investigated the implication of DNMT1 in regulating the expression of the pro-angiogenic factors VEGF-A and IL-8 within breast stromal fibroblasts (BSFs). To achieve this, DNMT1 was first ectopically expressed using a vector bearing DNMT1-ORF into TCF-64 cells (tumor counterpart fibroblasts present in a histologically normal part of the breast), while an empty vector was used as a control (TCF64-ORF and TCF64-c, respectively). **Figures 1A, B** show that DNMT1 upregulation increased the level of the VEGF-A and IL-8 proteins in TCF64-ORF cells compared to their corresponding control TCF64-c cells. This result was confirmed at the mRNA level for both genes (**Figure 1C**). Likewise, the secreted level of VEGF-A and IL-8 were also increased upon ectopic expression of DNMT1 in TCF-64 cells (**Figure 1D**). This indicates that DNMT1 positively controls the expression of both VEGF-A and IL-8. To confirm this, we decided to test the effect of DNMT1 down-regulation on the expression of both genes. Therefore, CAF-64 cells (cancer-associated fibroblasts present in the tumor) were transfected with either DNMT1 siRNA or a scrambled sequence that was used as a control, and then the levels of the VEGF-A and IL-8 proteins were assessed. **Figures 1A, B** show DNMT1 down-regulation accompanied by clear decrease in the protein level of

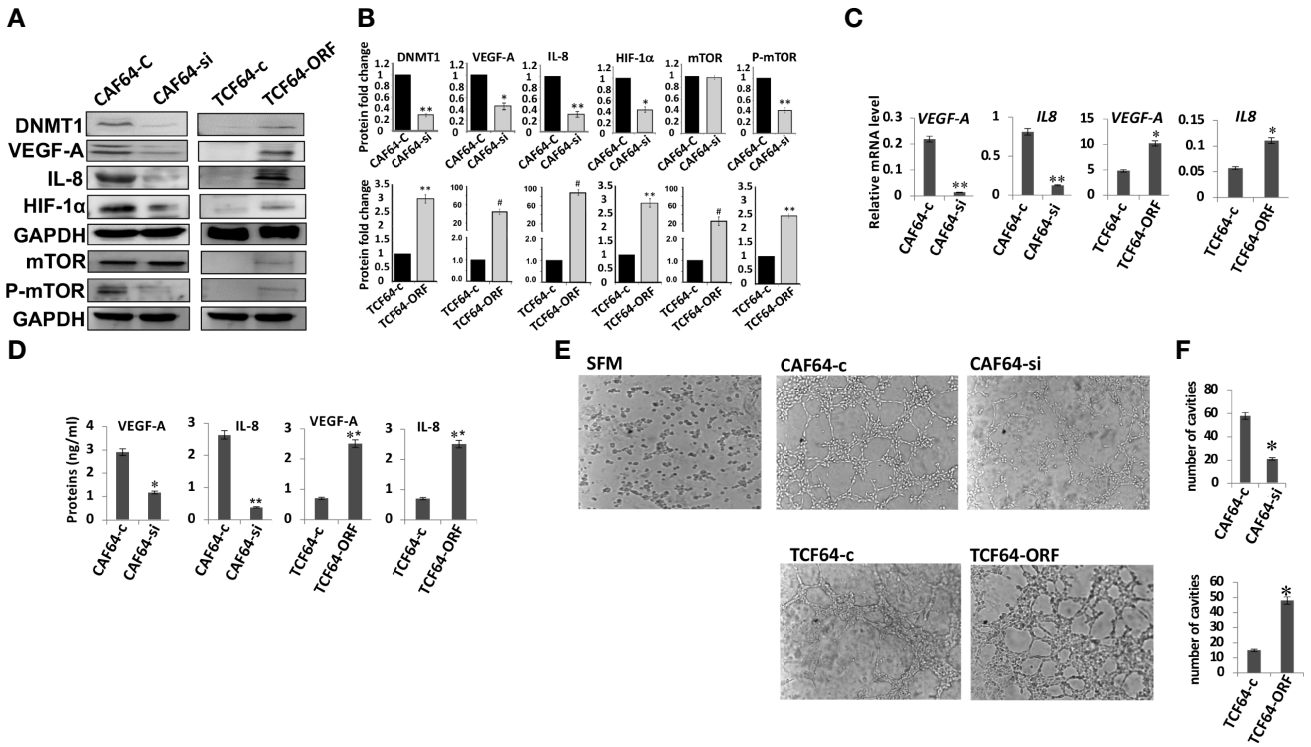

FIGURE 1 | DNMTl controls the expression of VEGF-A and IL-8 in breast stromal fibroblasts and promotes their pro-angiogenic effects *in vitro*. CAF-64 cells were transfected with *DNMT1-siRNA* (CAF64-si) or with a plasmid bearing the *DNMT1* ORF (TCF64-orf). A scrambled sequence (CAF64-c) and an empty vector (TCF64-c) were used as controls, respectively. Whole-cell lysates were prepared, and then were used for immunoblotting analysis using specific antibodies against the indicated proteins. **(A)** Immunoblotting analysis **(B)** The histograms show the averaged protein level fold changes relative to the respective controls after normalization against the internal control GAPDH, while the level of the phospho-protein was further normalized to the level of the total protein. Error bars represent mean ± S.D (n=3). *P<0.05, **P<0.01 and $^{\#}$P<0.0001. **(C)** Total RNA was extracted from the indicated cells and the mRNA levels of the indicated genes were assessed using qRT-PCR. Error bars represent mean ± S.D (n=3). *P<0.05 and **P<0.01. **(D)** SFCM from the indicated cells were collected after 24 h and the levels of the indicated proteins were determined by ELISA. Error bars indicate mean ± S.D (n=3). *P<0.05 and **P<0.01. **(E)** SFCM from the indicated cells were collected and used to treat HUVEC cells previously plated on matrigel (96-well plate), then incubated at 37°C for 8 hr. **(F)** Histograms show the average number of formed cavities. Error bars represent means ± S.D (n=3). *p<0.05.

VEGF-A and IL-8 in DNMT1-deficient cells compared to control cells. Similarly, the mRNA levels of both genes were significantly reduced in DNMT-1 deficient cells compared to controls (**Figure 1C**). Furthermore, the secreted levels of VEGF-A and IL-8 were also significantly reduced upon DNMT1 knockdown (**Figure 1D**). These results confirm the role of DNMT1 in the positive regulation of VEGF-A and IL-8, most likely at the mRNA level.

DNMT1 Activates mTOR and Up-Regulates HIF-1α in Breast Stromal Fibroblasts

Next, we sought to delineate the molecular mechanism responsible for DNMT1-dependent regulation of VEGF-A and IL-8, which are both transcriptionally regulated by HIF-1α, a transcription factor at the heart of the angiogenic response (25, 26). Therefore, we checked the role of DNMT1 in controlling the expression of this transcription factor in breast stromal fibroblasts. **Figure 1A** shows that while the DNMT1 ectopic expression increased the level of HIF-1α in TCF-64 cells, DNMT1 down-regulation decreased the level of HIF-1α in CAF-64 cells, compared to the respective control cells. This suggests that DNMT1 positively regulates the expression of VEGF-A and IL-8 through positive regulation of their major transactivator gene HIF-1α. Since this gene is an important target of mTOR, we also checked the effect of DNMT1 on the expression of this protein kinase. Interestingly, DNMT1 upregulation in TCF-64 cells increased the level of the basal as well as the phosphorylated form of mTOR relative to control cells (**Figures 1A, B**). However, DNMT1 down-regulation reduced only the active form of the protein (P-mTOR) with only slight effect on the basal level of the protein (**Figures 1A, B**). This indicates that DNMT1 can activate mTOR and its downstream proangiogenic effector HIF-1α in breast fibroblasts.

DNMT1 Promotes the Paracrine Pro-Angiogenic Effect of Active CAFs *In Vitro*

The fact that DNMT1 enhances the expression and the secretion of 2 major angiogenesis factors, prompted us to investigate the possible involvement of DNMT1 in promoting the paracrine

pro-angiogenic effect of active breast fibroblasts. To this end, serum-free conditioned media (SFCM) collected from TCF64-ORF/TCF64-c and CAF64-si/CAF64-c cells were added separately to 96-well plates seeded with 2×10^4 human umbilical vein endothelial cells (HUVECs) in matrigel and used for *in vitro* angiogenic assay, serum-free medium (SFM) was also added as negative control. After 5 h of incubation, the number of closed cavity constructions was significantly lower in the presence of SFCM from CAF64-si cells compared to SFCM from CAF64-c cells (**Figure 1E**). However, SFCM from TCF64-ORF significantly increased the number of meshs compared to SFCM from TCF64-c or SFM (**Figures 1E, F**). These results demonstrate the role of the stromal fibroblast DNMT1 protein in stimulating endothelial cell differentiation into capillary-like structures through a paracrine effect.

Ectopic Expression of DNMT1 Enhances the Paracrine Pro-Angiogenic Effects of Breast Stromal Fibroblasts *In Vivo*

To study the paracrine effect of DNMT1-expressing BSFs on vascular formation *in vivo*, we made use of previously created orthotopic BC xenografts by co-injecting MDA-MB-231 cells with TCF64-ORF (TCTorf) or TCF64-c (TCTC) cells in nude mice (16). Tumors were excised and a significant difference in tumor size and microvascular density were observed between tumors bearing TCF64-ORF and their controls (**Figure 2A**). To further confirm this, the level of CD31, an endothelial cell marker, was assessed in the orthotopic tumor xenografts by immunohistochemistry using anti-CD31 antibody. **Figure 2B** shows a higher density of $CD31^+$ cells in tumors containing TCF64-ORF cells compared to tumors mixed with TCF64-c cells. To explore the molecular mechanism(s) that underlies the proangiogenic effect of TCF64-ORF cells, we assessed the level of the proangiogenic proteins in the two tumors by immunoblotting. **Figures 2C, D** show that the levels of VEGF-A, IL-8 as well as their upstream regulators mTOR and HIF-1α, were increased in TCTorf compared to TCTC tumors. These results show the role of DNMT1 in promoting the paracrine proangiogenic effect of breast stromal fibroblasts *in vivo*.

Eugenol and Decitabine Suppress the Proangiogenic Effects of Breast Myofibroblasts by Inhibiting DNMT1 Expression

We have recently shown that the DNMT inhibitor decitabine (5-Aza-2'-deoxycytidine, DAC) and eugenol suppress the pro-carcinogenic effects of active fibroblasts through targeting DNMT1 (27). Therefore, we decided to investigate the role of these two DNMT1 inhibitors on the proangiogenic process of active fibroblasts. To this end, CAF-64 cells were treated for 24 h with eugenol (1μM) or DAC (5μM), while DMSO was utilized as

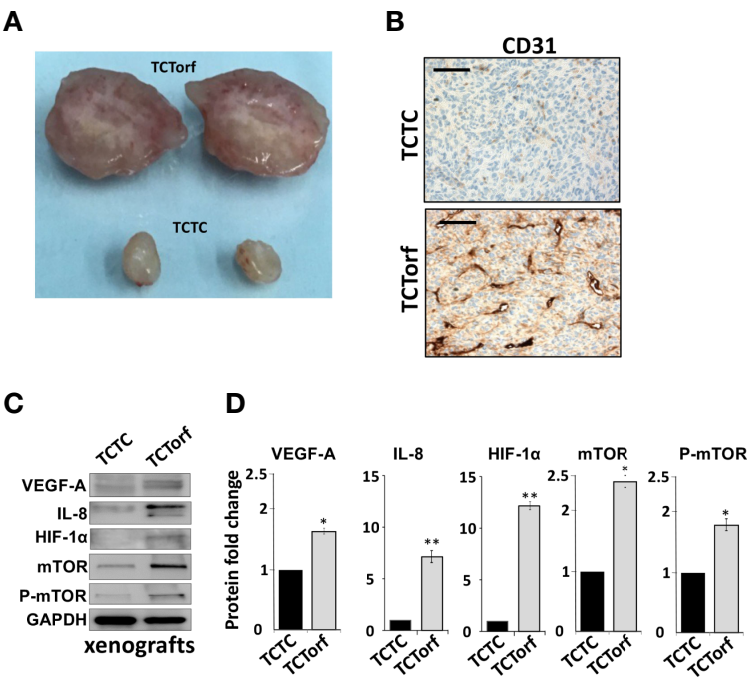

FIGURE 2 | Ectopic expression of DNMT1 enhances the paracrine pro-angiogenic effects of breast stromal fibroblasts *in vivo*. Orthotopic BC xenografts were created by co-injecting MDA-MB-231 cells with TCF64-orf or TCF64-c cells under the nipple of nude mice as previously described (16). **(A)** Picture of excised tumors **(B)** Immunohistochemical staining was carried out on FFPE sections using an anti–CD-31 antibody. Scale bars represent 200 μM. **(C)** Whole-cell lysates were prepared from the excised tumors, and then were used for immunoblotting analysis using specific antibodies against the indicated proteins. **(D)** The histograms show the averaged protein level fold changes relative to the control (TCTC) after normalization against the internal control GAPDH, while the level of the phospho-protein was further normalized to the level of the total protein. Error bars represent mean ± S.D (n=3). *P<0.05 and **P<0.01.

a negative control, and then whole cell lysates were prepared. The immunoblotting analysis showed that DNMT1 protein level declined along with reduction in the protein level of VEGF-A and IL-8 in cells treated with DAC or eugenol as compared to controls (**Figures 3A, B**). Similarly, DAC and eugenol significantly reduced the mRNA levels of both VEGF-A and IL-8 (**Figure 3C**). Since DNMT1 controls the expression of HIF-1α and mTOR, we decided to check the effect of DNMT1 inhibition on such angiogenesis regulatory factors. Indeed, eugenol and DAC strongly inhibited the expression of both mTOR/P-mTOR and HIF1α (**Figures 3A, B**). This indicates that eugenol and DAC are strong suppressors of the major angiogenesis effectors and regulators, probably through controlling DNMT1.

To confirm this, we have shown that eugenol and DAC significantly reduced more than 5 fold the levels of secreted VEGF-A and IL-8 from CAF cells as compared to control cells (**Figure 3D**). This shows that eugenol and DAC could suppress the paracrine proangiogenic effect of CAF cells through DNMT1 inhibition. To verify this, we investigated the effect of eugenol- and DAC -treated CAF cells on the differentiation of endothelial cells *in vitro*. Therefore, CAF-64 cells were either DMSO-treated or challenged with either eugenol (1μM) or DAC (5μM) in SFM for 24 h to generate SFCM that have been used to treat HUVEC cells (0.5×10^5) on matrigel pre-coated 96-well plate for 16 h at 37°C. **Figures 3E, F** show that while HUVEC cells were differentiated into mech structures in the presence of DMSO-SFCM, only marginal differentiation occurred in the presence of eugenol- and DAC-SFCM. Together, these results indicate that eugenol and decitabine suppress the paracrine pro-angiogenic effect of CAF cells through inhibiting DNMT1 and its downstream angiogenic effectors VEGF-A and IL-8.

Correlation of DNMT1 Expression in Cancer and Stromal Fibroblasts With Clinicopathological Parameters

Next, we sought to investigate the predictive value of DNMT1 expression levels in cancer cells as well as their stromal fibroblasts as a candidate biomarker for clinical outcome of patients with LABC. Remarkably, 69% of the patients were less than 50 years old and 60% of patients had tumor sizes more than 5 cm (**Table 1**). Thirty-three (33) patients developed recurrence and 13 died (**Table 1**). Furthermore, 70% of the patients had high tumor stage, while 48% of the tumors were of grade 3 (**Table 1**). Estrogen receptor positive (ER+)/Her2+ patients represented

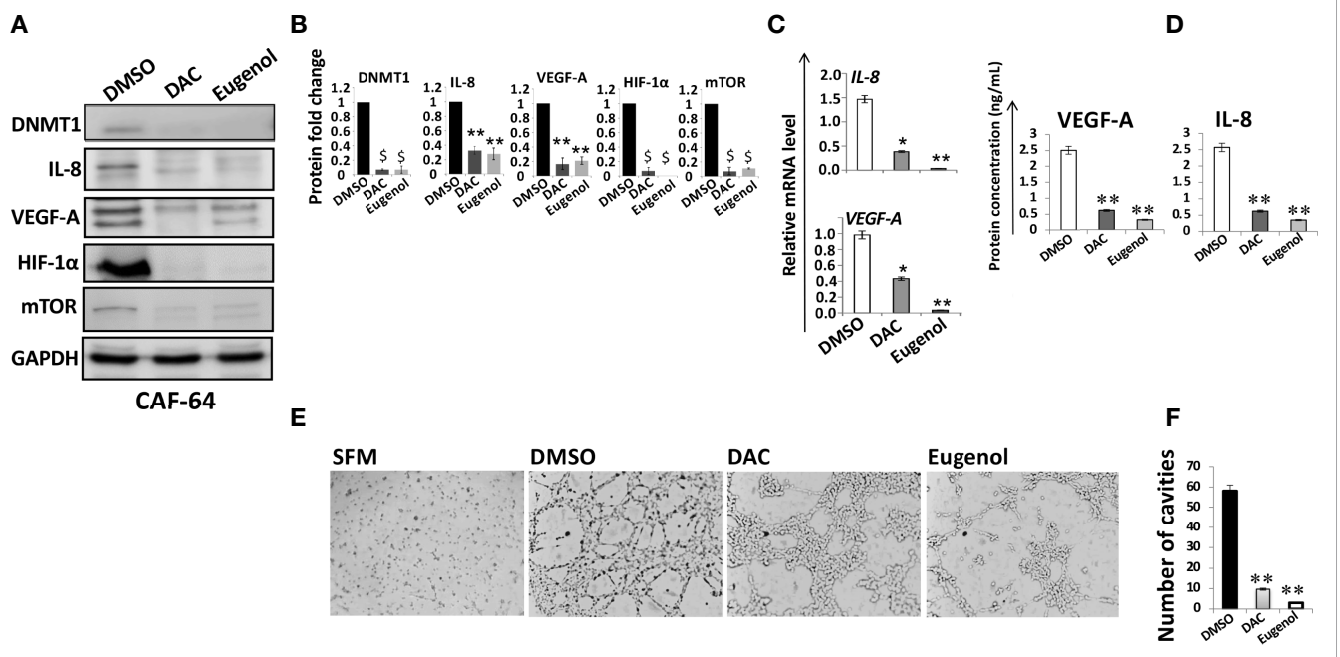

FIGURE 3 | Eugenol and DAC suppress the proangiogenic effects of breast myofibroblasts by inhibiting DNMT1 expression. **(A)** CAF-64 cells were treated with the indicated concentrations of DAC and eugenol while DMSO was used as control, and then whole-cell lysates were prepared and utilized for immunoblotting analysis using specific antibodies against the indicated proteins. The numbers under the bands represent fold changes relative to the control (DMSO) after normalization against the internal control GAPDH. **(B)** The histograms show the averaged protein level fold changes relative to the control after normalization against the internal control GAPDH. Error bars represent mean ± S.D (n=3). ** P<0.01 and $P<0.001. **(C)** Total RNA was extracted from CAF-64 cells treated as shown, and the mRNA levels of the indicated genes were assessed using qRT–PCR. Error bars represent mean± S.D (n=3).*$P \le 0.05$, **$P \le 0.01$ **(D)** CAF-64 cells were treated as indicated in SFM for 24 h, and then SFCM were collected, and the levels of the indicated proteins were determined by ELISA. Error bars indicate mean ± S.D (n=3). **$P \le 0.01$. **(E)** HUVEC cells previously plated on matrigel (96-well plate) were treated with SFCM collected as described in **(D)**, while SFM was used as negative control, and then cells were incubated at 37°C for 8 hr. **(F)** Histogram shows the average number of formed cavities. Error bars represent means ± S.D (n=3). **$P \le 0.01$.

TABLE 1 | Correlations between DNMT1 expression and clinicopathological features in breast cancer patients.

Parameter	Total n=100 (%)	DNMT1 in cancer cells		*P* value
		>10%	≤10%	
Age				
≤50	69 (69.00)	35 (35.00)	34 (34.00)	0.6068
>50	31 (31.00)	14 (14.00)	17 (17.00)	
Survival status				
Alive	87 (87.00)	39 (39.00)	48 (48.00)	**0.0014**
Died	13 (13.00)	12 (12.00)	1 (1.00)	
HIS-Subtype				
Invasive Ductal Ca	83 (83.00)	39 (39.00)	44 (44.00)	0.3712
1,4	3 (3.00)	1 (1.00)	2 (2.00)	
Invasive Ductal Ca with DCIS	11 (11.00	7 (7.00)	4 (4.00)	
Infiltrating Lobular Ca	2 (2.00)	2 (2.00)	0 (0.00)	
Other	1 (1.00)	0 (0.00)	1 (1.00)	
Tumor stage				
T2	29 (29.00)	14 (14.00)	15 (15.00)	0.8909
T3	31 (31.00)	14 (14.00)	17 (17.00)	
T4	39 (39.00)	20 (20.00)	19 (19.00)	
Tx	1 (1.00)	1 (1.00)	0 (0.00)	
Grade				
G1	2 (2.00)	2 (2.00)	0 (0.00)	0.0676
G2	48 (48.00)	26 (26.00)	22 (22.00)	
G3	48 (48.00)	19 (19.00)	29 (29.00)	
Gx	2 (2.00)	2 (2.00)	0 (0.00)	
Recurrence				
No	67 (67.00)	34 (34.00)	33 (33.00)	0.6187
Yes	33 (33.00)	15 (15.00)	18 (18.00)	
Progression				
No	17 (17.00)	9 (9.00)	8 (8.00)	0.7212
Yes	83 (83.00)	40 (40.00)	43 (43.00)	
Tumor size				0.9108
≤2cm	1 (1.16)	0 (0.00)	1 (1.16)	
2-5cm	33 (38.37)	17 (19.77)	16 (18.60)	
> 5cm	52 (60.47)	27 (31.40)	25 (29.07)	
Parameter	**Total n=100 (%)**	**DNMT1 in fibroblasts**		***P* value**
		>10%	**≤10%**	
Age				
≤50	69 (69.00)	44 (44.00)	25 (25.00)	0.1759
>50	31 (31.00)	24 (24.00)	7 (7.00)	
Survival status				
Alive	87 (87.00)	25 (25.00)	62(62.00)	**0.01081**
Died	13 (13.00)	10 (10.00)	3 (3.00)	
HIS-Subtype				
Invasive Ductal Ca	83 (83.00)	55 (55.00)	28 (28.00)	0.4853
1,4	3 (3.00)	1 (1.00)	2 (2.00)	
Invasive Ductal Ca with DCIS	11 (11.00) 2 (2.00) 1 (1.00)	9 (9.00)	2 (2.00)	
Infiltrating Lobular Ca		2 (2.00)	0 (0.00)	
Other		1 (1.00)	0 (0.00)	
Tumor stage				
T2	29 (29.00)	22 (22.00)	7 (7.00)	0.8909
T3	31 (31.00)	21 (21.00)	10 (10.00) 19 (19.00)	
T4	39 (39.00)	20 (20.00)	0 (0.00)	
Tx	1 (1.00)	1 (1.00)		
Grade				
G1	2 (2.00)	2 (2.00)	0 (0.00)	0.0676
G2	48 (48.00)	26 (26.00)	22 (22.00)	
G3	48 (48.00)	19 (19.00)	29 (29.00)	
Gx	2 (2.00)	2 (2.00)	0 (0.00)	
Recurrence				
No	67 (67.00)	34 (34.00) 15 (15.00)	33 (33.00) 18 (18.00)	0.6187
Yes	33 (33.00)			

(Continued)

TABLE 1 | Continued

Parameter	Total n=100 (%)	DNMT1 in cancer cells		*P* value
		>10%	≤10%	
Progression				
No	17 (17.00)	9 (9.00)	8 (8.00)	0.7212
Yes	83 (83.00)	40 (40.00)	43 (43.00)	
Tumor size				
≤ 2cm	1 (1.16)	0 (0.00)	1 (1.16)	0.9108
2-5cm	33 (38.37)	17 (19.77)	16 (18.60)	
> 5cm	52 (60.47)	27 (31.40)	25 (29.07)	

26%, ER+/Her2- represented 31%, ER-/Her2+ represented 25%, while ER-/Her2- represented 18% (**Table 1**).

In order to study the role of DNMT1 in the prognosis of LABC patients, a total of 100 breast pretreatment tumor tissues were assessed for the expression of the DNMT1 protein in cancer cells and their adjacent stromal fibroblasts. **Figure 4A** shows the immunostaining of DNMT1 in both tumor as well as stromal cells from breast cancer tissues. The level of DNMT1 immunostaining in both cancer and stromal cells was classified into 2 subgroups: low (≤10% DNMT1-positive cells) and high (>10% DNMT1-positive cells). DNMT1 expression was low in 51% epithelial and 32% fibroblast cells, while DNMT1 was highly expressed in 49% epithelial and 68% fibroblast cells (**Table 2**). The level of DNMT1 in fibroblasts in the different breast cancer subtypes showed association with ER/Her2 status. Indeed, significant correlation (P = 0.0121) was observed between low DNMT1 level in fibroblasts and lack of ER/PR (**Table 2**). However, no correlation was observed between DNMT1 level in cancer cells and ER/Her2 expression levels (**Table 2**). Interestingly, the level of DNMT1 was highly correlated with patient survival in both breast cancer cells (P=0.0014) and fibroblasts (P=0.01081) (**Table 2**). Indeed, high DNMT1 expression levels were highly correlated with poor patient survival (**Table 2**). However, no significant correlation was observed between the level of DNMT1 in tumor or stromal cells and the other clinicopathological parameters (**Table 2**).

DNMT1 Expression in Both Breast Cancer Cells and Their Stromal Fibroblasts Predicts Survival

Kaplan-Meier plots indicate significant association between DNMT1 expression levels in cancer cells and their stromal fibroblasts and patient's overall survival (OS) (P = 0.0029 and P = 0.01091, respectively) (**Figure 4B**). Indeed, patients with tumors expressing high level of DNMT1 in stromal fibroblasts or cancer cells had significantly poorer OS rates (**Figure 4B**). In contrast, low

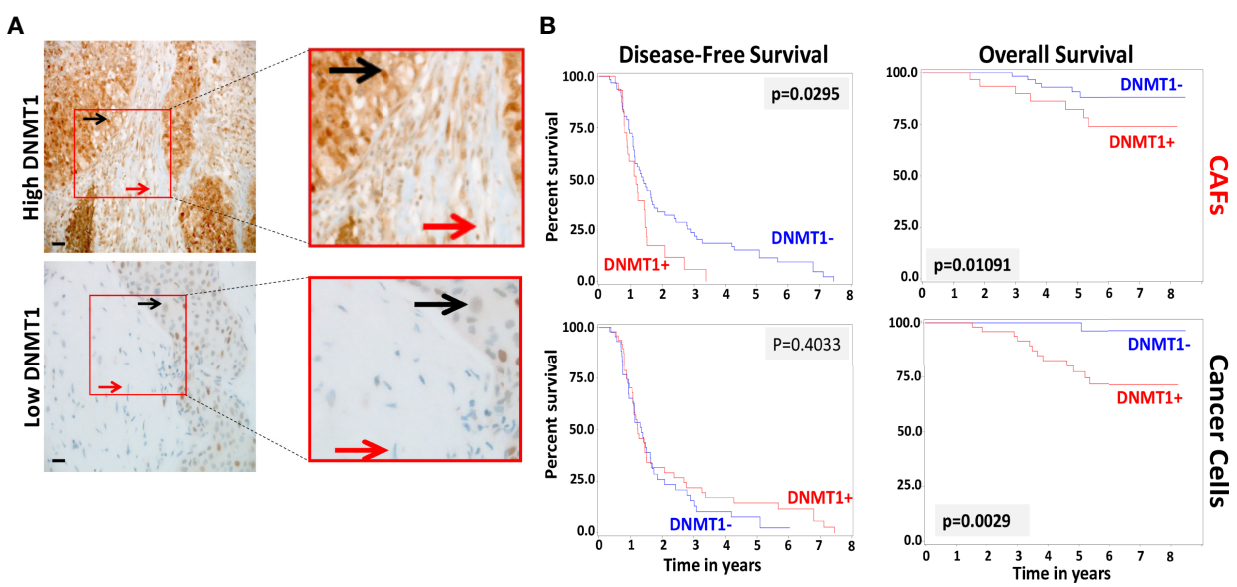

FIGURE 4 | Loss of DNMT1 in stromal and tumoral cells is predictive of poor disease-free and overall survival. **(A)** Tissue sections cut from formalin-fixed paraffin embedded breast tumors were immunostained with an anti-DNMT1 antibody. Red arrows indicate stromal fibroblasts, black arrows indicate cancer cells. (Envision 60x). **(B)** Kaplan-Meier analysis of overall survival (OS) and disease-free survival (DFS).

TABLE 2 | Expression of DNMT1 in cancer cells and stromal fibroblasts by breast cancer ER/Her2 subtypes.

Cancer cells		Total n=100 (%)	ER(+ve)/Her2(+ve)	ER(+ve)/Her2(-ve)	ER(-ve)/Her2(+ve)	ER(-ve)/Her2(-ve)	*P value*
DNMT1	>10%	49 (49.00)	12 (12.00)	20 (20.00)	9 (9.00)	8 (8.00)	0.1784
	≤10%	51 (51.00)	14 (14.00)	11 (11.00)	16 (16.00)	10(10.00)	
Fibroblasts		Total n=100 (%)	ER(+ve)/Her2(+ve)	ER(+ve)/Her2(-ve)	ER(-ve)/Her2(+ve)	ER(-ve)/Her2(-ve)	***P value***
DNMT1	>10%	68 (68.00)	16 (16.00)	28 (28.00)	13 (13.00)	11 (11.00)	0.0121
	≤10%	32 (32.00)	10 (10.00)	3 (3.00)	12 (12.00)	7 (7.00)	

DNMT1 levels were significantly associated with better OS (**Figure 4B**). However, while high DNMT1 levels in fibroblasts correlated significantly with poorer disease-free survival (DFS) (P = 0.0295), DNMT1 expression level in cancer cells did not significantly correlate with patient DFS (*P* = 0.4033) (**Figure 4B**).

The poor outcome of patients with high DNMT1 expression in stromal fibroblasts (*P* = 0.01204) and cancer cells (*P* = 0.0187) was confirmed by univariate Cox regression analysis (**Table 3**). Furthermore, multivariate Cox regression analysis was conducted to investigate the link between the prognostic power of DNMT1 expression level and other well-known breast cancer risk factors. **Table 4** shows that the DNMT1 level in cancer cells and their stromal fibroblasts is a strong independent predictor of OS (*P* = 0.011) and (*P* = 0.0360), respectively. Furthermore, DNMT1 level in fibroblasts was also an independent prognostic factor for DFS (*P* = 0.0492) (**Table 4**).

DISCUSSION

When active, CAFs boost breast carcinogenesis through promoting several pro-carcinogenic processes such as angiogenesis (5, 6). Our recent findings indicate that DNMT1 is highly expressed in CAFs and that when upregulated it enables the activation of breast stromal fibroblasts (16). The present findings indicate that DNMT1 controls the paracrine pro-angiogenic potential of BSFs through positive regulation of both pro-angiogenic factors VEGF-A and IL-8. Indeed, while DNMT1 knock-down reduced the expression level of both genes and consequently the pro-angiogenic capacity of CAFs, ectopic expression of DNMT1 up-regulated VEGF-A and IL-8 and enhanced the pro-angiogenic ability of BSFs both *in vitro* and *in vivo*. In a previous study, Achour et al., have shown that DNMT1 forms a heterocomplex with ICBP90, which positively controls the expression of VEGF (28). To elucidate the molecular pathway underlying the DNMT1-dependent induction of the VEGF-A and IL-8 genes, we have shown that DNMT1 is an activator of HIF-1α and mTOR two upstream activators of VEGF-A (29). Since DNMT1 positively regulates the expression of these genes, DNMT1 may not directly control their expression through methylation, which is a gene repressor process. In fact, approximately 30% of the upregulated genes in DNMT1 knockout cells do not contain dense CpG islands (30), confirming DNMT1-dependent gene expression regulation in a methylation-independent manner. This suggests that DNMT1 may indirectly regulate these genes through controlling their

TABLE 3 | Univariate Cox proportional regression analysis on 5-year overall and disease-free survival of 100 LABC patients.

Parameter	Overall survival			Disease-free survival		
	Hazard Ratio	95% Hazard Ratio Confidence Limits	*P value*	Hazard Ratio	95% Hazard Ratio Confidence Limits	*P value*
DNMT1 (Fibroblasts)						
≤10%	1	0.141-1.255	0.01204	1	0.353-0.955	**0.0322**
>10%	0.421			0.581		
DNMT1 (Cancer cells)	1	0.011-0.666	**0.0187**	1	0.635-0.997	0.4068
≤10%	0.087			1.207		
>10%						
Clinical_Tumor_Stage						
T2	1	0.834-1.762	0.3139	1	0.635-0.997	0.0469
T3, T4, Tx	1.212			0.796		
Grade						
G1, G2	1	0.577-1.771	0.9686	1	0.817-1.155	0.7446
G3, Gx	1.011			0.972		
Tumor size						
≤ 5cm	1	0.754-9.972	0.1255	1	0.615-1.559	0.9308
> 5cm	2.743			0.980		
AGE						
≤50	1	0.952-1.058	0.8979	1	0.980-1.025	0.8626
>50	1.003			1.002		

TABLE 4 | Multivariate Cox Regression analysis on 5-year overall and disease-free survival.

Parameter	OS			DFS		
	Hazard Ratio	95% Hazard Ratio Confidence Limits	*P value*	Hazard Ratio	95% Hazard Ratio Confidence Limits	*P value*
DNMT1 (Cancer cells)	0.014	0.000-0.375	**0.011**	1.385	0.830-2.312	0.212
ER-PR-Status						
ER(+ve)/PR(-ve)	2.559	0.277-23.675	0.4079	1.001	0.354-2.830	0.9982
ER(-ve)/PR(-ve)	0.935	0.109-8.054	0.9512	1.001	0.347-1.789	0.5694
Tumor-Stage	10.207	1.830-56.943	0.0081	0.953	0.626-1.450	0.8213
Grade	0.048	0.006-0.378	0.0040	1.048	0.764-1.437	0.7701
Tumor size	2.576	0.341-19.482	0.3594	0.893	0.464-1.717	0.7338
HIS-Subtype						
ER(+ve)/Her2(-ve)	0.862	0.074-10. 045	0.905	0.535	0.254-1.129	0.1007
ER(-ve)/Her2(+ve)	7.318	0.716-74.791	0.093	1.328	0.362-2.031	0.7261
ER(-ve)/Her2(-ve)	52.729	2.055-1353.196	0.016	0.800	0.367-1.898	0.6657
AGE	0.871	0.764-0.993	0.0392	0.999	0.966-1.034	0.9507
DNMT1 (Fibroblasts)	0.661	0.119-3.673	0.0360	0.426	0.308-0.998	0.0492
ER-PR-Status						
ER(+ve)/PR(-ve)	1.388	1.167-11.522	0.7612	0.852	0.291-2.497	0.7706
ER(-ve)/PR(-ve)	0.552	0.064-4.753	0.5886	0.9	0.385-2.104	0.8084
Tumor-Stage	7.898	1.606-38.836	0.0110	0.936	0.608-1.442	0.7642
Grade	0.163	0.018-1.461	0.1049	0.998	0.709-1.407	0.9929
Tumor size	1.598	0.242-10.555	0.6268	0.765	0.394-1.484	0.4276
HIS-Subtype						
ER(+ve)/Her2(-ve)	0.563	0.045-7.012	0.6551	0.574	0.272-1.208	0.1436
ER(-ve)/Her2(+ve)	12.537	1.715-91.654	0.0127	0.711	0.293-1.724	0.4506
ER(-ve)/Her2(-ve)	34.608	2.105-569.059	0.0131	0.778	0.324-1.834	0.5557
AGE	0.886	0.789-0.995	0.0416	1.005	0.970-1.040	0.7893

upstream transactivators. Indeed, we have recently shown that DNMT1 positively controls the expression of AUF1, which is part of the IL-6/STAT3/NF-κB positive feedback loop in breast fibroblasts (16, 31). This indicates that DNMT1 is involved in the regulation of a plethora of genes involved in various physiological processes including angiogenesis.

In recent years natural products showed promising ability to repress the procarcinogenic effects of active CAFs through multiple mechanisms. Thereby, agents that can normalize CAFs may improve the efficiency of traditional tumor cell-directed therapy. Consequently, we tested the effect of the nontoxic and pharmacologically safe dietary compound eugenol, and we compared its effects with the well-known DNMTs inhibitor decitabine, on the expression of HIF-1α/mTOR as well as VEGF-A and IL-8 and the related pro-angiogenic effect of active BSFs. We have shown that both eugenol and DAC repress VEGF-A and IL-8 expression and secretion as well as the expression and activation of HIF-1α/mTOR in CAFs, and consequently suppress their pro-angiogenic paracrine effect *in vivo* and *in vitro*. Several studies reveal the therapeutic potential of eugenol in cancer prevention and treatment. Indeed, administration of eugenol inhibits angiogenesis as evidenced by changes in the activities of VEGF-A and VEGFR1 in a rat model of gastric carcinogenesis (32). Additionally, a recent study reported that eugenol promotes cisplatin cytotoxicity against TNBC by inhibiting the NF-κB signaling pathway (33). Notably, the present report shows that eugenol possesses anti-angiogenic effect indirectly through inhibition of the pro-angiogenic effect of CAFs. This suggests that eugenol could be of great value for cancer prevention and/or treatment by preventing the pro-vascularization potential of active stromal myofibroblasts.

Additionally, these findings suggest that high levels of DNMT1 could be associated with poor patient survival. Thereby, we investigated the link between the level of DNMT1 in breast cancer cells and their stromal fibroblasts with the survival of patients with LABC treated with neoadjuvant chemotherapy ± Trastuzumab. We have found significant association between high tumor expression of DNMT1 and shorter OS of LABC patients. Similar association has been previously reported in breast cancer (34), malignant lymphoma (35), renal cell carcinoma (36), bladder cancer (37) and pancreatic cancer (38). Furthermore, we have shown here that high level of DNMT1 in stromal fibroblasts is also associated with significantly shorter OS and DFS of LABC patients. This shows that the importance of DNMT1 as prognostic

biomarker for LABC patients may not be restricted to malignant cells but also their stromal adjacent fibroblasts. This suggests that high DNMT1 level in breast malignant cells or their adjacent CAFs can significantly predict high risk or recurrence. This points to DNMT1 as promising therapeutic target in the neoadjuvant treatment of LABC patients. In fact, this possibility has been explored for several tumors (39–42).

CONCLUSIONS

The present findings show that DNMT1 positively controls two major angiogenesis factors VEGF-A and IL-8 in breast stromal fibroblasts, and consequently DNMT1 upregulation in these cells promotes angiogenesis in a paracrine manner. Interestingly, these DNMT1-related pro-angiogenic effects can be suppressed by 2 DNMT1 inhibitors decitabine and eugenol. Furthermore, we present clear indication that high levels of DNMT1 in tumor cells as well as their adjacent stromal fibroblasts predict poor survival post-neoadjuvant treatment of locally advanced breast cancer patients. Thereby, DNMT1 level in both cancer cells and their adjacent stromal fibroblasts could constitute a powerful prognostic biomarker for these high-risk patients who need downstaging tumors to facilitate breast conservation therapy.

DATA AVAILABILITY STATEMENT

The original contributions presented in the study are included in the article/supplementary material. Further inquiries can be directed to the corresponding author.

ETHICS STATEMENT

Written informed consent was not required and a waiver was granted since the study was retrospective and samples were anonymized to the research team. This was granted by the institutional review board approval (RAC#2160005).

AUTHOR CONTRIBUTIONS

All authors contributed to the article and approved the submitted version. Conception and design: AA; Development of methodology and acquisition of data: LA-K, AE, AT, and MA; Analysis and interpretation of data: LA-K, TA-T, and AA; Writing of the manuscript: LA-K, and AA.

FUNDING

This work was solely supported by the King Faisal Specialist Hospital and Research Centre.

ACKNOWLEDGMENTS

We are grateful to Dr. Falah Al-Mohanna for his help with animal work. We also appreciate the continuous support of the Research Center administration.

REFERENCES

1. Ferlay J, Colombet M, Soerjomataram I, Parkin DM, Pineros M, Znaor A, et al. Cancer Statistics for the Year 2020: An Overview. *Int J Cancer* (2021). doi: 10.1002/ijc.33588
2. Tryfonidis K, Senkus E, Cardoso MJ, Cardoso F. Management of Locally Advanced Breast Cancer-Perspectives and Future Directions. *Nat Rev Clin Oncol* (2015) 12(3):147–62. doi: 10.1038/nrclinonc.2015.13
3. Guarneri V, Broglio K, Kau SW, Cristofanilli M, Buzdar AU, Valero V, et al. Prognostic Value of Pathologic Complete Response After Primary Chemotherapy in Relation to Hormone Receptor Status and Other Factors. *J Clin Oncol* (2006) 24(7):1037–44. doi: 10.1200/JCO.2005.02.6914
4. Haque W, Verma V, Hatch S, Suzanne Klimberg V, Brian Butler E, Teh BS. Response Rates and Pathologic Complete Response by Breast Cancer Molecular Subtype Following Neoadjuvant Chemotherapy. *Breast Cancer Res Treat* (2018) 170(3):559–67. doi: 10.1007/s10549-018-4801-3
5. Chen X, Song E. Turning Foes to Friends: Targeting Cancer-Associated Fibroblasts. *Nat Rev Drug Discov* (2018) 18:99–115. doi: 10.1038/s41573-018-0004-1
6. Sahai E, Astsaturov I, Cukierman E, DeNardo DG, Egeblad M, Evans RM, et al. A Framework for Advancing Our Understanding of Cancer-Associated Fibroblasts. *Nat Rev Cancer* (2020) 20(3):174–86. doi: 10.1038/s41568-019-0238-1
7. Orimo A, Gupta PB, Sgroi DC, Arenzana-Seisdedos F, Delaunay T, Naeem R, et al. Stromal Fibroblasts Present in Invasive Human Breast Carcinomas Promote Tumor Growth and Angiogenesis Through Elevated SDF-1/CXCL12 Secretion. *Cell* (2005) 121(3):335–48. doi: 10.1016/j.cell.2005.02.034
8. De Palma M, Biziato D, Petrova TV. Microenvironmental Regulation of Tumour Angiogenesis. *Nat Rev Cancer* (2017) 17(8):457–74. doi: 10.1038/nrc.2017.51
9. O'Connell JT, Sugimoto H, Cooke VG, MacDonald BA, Mehta AI, LeBleu VS, et al. VEGF-A and Tenascin-C Produced by S100A4+ Stromal Cells are Important for Metastatic Colonization. *Proc Natl Acad Sci USA* (2011) 108 (38):16002–7. doi: 10.1073/pnas.1109493108
10. Buchsbaum RJ, Oh SY. Breast Cancer-Associated Fibroblasts: Where We Are and Where We Need to Go. *Cancers (Basel)* (2016) 8(2):19. doi: 10.3390/cancers8020019
11. Kaplan RN, Riba RD, Zacharoulis S, Bramley AH, Vincent L, Costa C, et al. VEGFR1-Positive Haematopoietic Bone Marrow Progenitors Initiate the Pre-Metastatic Niche. *Nature* (2005) 438(7069):820–7. doi: 10.1038/nature04186
12. Ao Z, Shah SH, Machlin LM, Parajuli R, Miller PC, Rawal S, et al. Identification of Cancer-Associated Fibroblasts in Circulating Blood From Patients With Metastatic Breast Cancer. *Cancer Res* (2015) 75(22):4681–7. doi: 10.1158/0008-5472.CAN-15-1633
13. Su S, Chen J, Yao H, Liu J, Yu S, Lao L, et al. CD10(+)GPR77(+) Cancer-Associated Fibroblasts Promote Cancer Formation and Chemoresistance by Sustaining Cancer Stemness. *Cell* (2018) 172(4):841–56.e16. doi: 10.1016/j.cell.2018.01.009
14. Paulsson J, Micke P. Prognostic Relevance of Cancer-Associated Fibroblasts in Human Cancer. *Semin Cancer Biol* (2014) 25:61–8. doi: 10.1016/j.semcancer.2014.02.006
15. Kalluri R. The Biology and Function of Fibroblasts in Cancer. *Nat Rev Cancer* (2016) 16(9):582–98. doi: 10.1038/nrc.2016.73
16. Al-Kharashi LA, Al-Mohanna FH, Tulbah A, Aboussekhra A. The DNA Methyl-Transferase Protein DNMT1 Enhances Tumor-Promoting Properties of Breast Stromal Fibroblasts. *Oncotarget* (2018) 9(2):2329–43. doi: 10.18632/oncotarget.23411
17. Girault I, Tozlu S, Lidereau R, Bieche I. Expression Analysis of DNA Methyltransferases 1, 3A, and 3B in Sporadic Breast Carcinomas. *Clin Cancer Res* (2003) 9(12):4415–22.

18. Mirza S, Sharma G, Parshad R, Gupta SD, Pandya P, Ralhan R. Expression of DNA Methyltransferases in Breast Cancer Patients and to Analyze the Effect of Natural Compounds on DNA Methyltransferases and Associated Proteins. *J Breast Cancer* (2013) 16(1):23–31. doi: 10.4048/jbc.2013.16.1.23
19. Jahangiri R, Jamialahmadi K, Gharib M, Emami Razavi A, Mosaffa F. Expression and Clinicopathological Significance of DNA Methyltransferase 1, 3A and 3B in Tamoxifen-Treated Breast Cancer Patients. *Gene* (2019) 685:24–31. doi: 10.1016/j.gene.2018.10.060
20. Jahangiri R, Mosaffa F, Emami Razavi A, Teimoori-Toolabi L, Jamialahmadi K. Altered DNA Methyltransferases Promoter Methylation and mRNA Expression are Associated With Tamoxifen Response in Breast Tumors. *J Cell Physiol* (2018) 233(9):7305–19. doi: 10.1002/jcp.26562
21. Ben Gacem R, Hachana M, Ziadi S, Ben Abdelkarim S, Hidar S, Trimeche M. Clinicopathologic Significance of DNA Methyltransferase 1, 3a, and 3b Overexpression in Tunisian Breast Cancers. *Hum Pathol* (2012) 43 (10):1731–8. doi: 10.1016/j.humpath.2011.12.022
22. Yu Z, Xiao Q, Zhao L, Ren J, Bai X, Sun M, et al. DNA Methyltransferase 1/3a Overexpression in Sporadic Breast Cancer Is Associated With Reduced Expression of Estrogen Receptor-Alpha/Breast Cancer Susceptibility Gene 1 and Poor Prognosis. *Mol Carcinog* (2015) 54(9):707–19. doi: 10.1002/mc.22133
23. Hawsawi NM, Ghebeh H, Hendrayani SF, Tulbah A, Al-Eid M, Al-Tweigeri T, et al. Breast Carcinoma-Associated Fibroblasts and Their Counterparts Display Neoplastic-Specific Changes. *Cancer Res* (2008) 68(8):2717–25. doi: 10.1158/0008-5472.CAN-08-0192
24. Al-Mohanna MA, Al-Khalaf HH, Al-Yousef N, Aboussekhra A. The P16ink4a Tumor Suppressor Controls P21waf1 Induction in Response to Ultraviolet Light. *Nucleic Acids Res* (2007) 35(1):223–33. doi: 10.1093/nar/gkl1075
25. Semenza GL. HIF-1: Using Two Hands to Flip the Angiogenic Switch. *Cancer Metastasis Rev* (2000) 19(1-2):59–65. doi: 10.1023/A:1026544214667
26. Kim KS, Rajagopal V, Gonsalves C, Johnson C, Kalra VK. A Novel Role of Hypoxia-Inducible Factor in Cobalt Chloride- and Hypoxia-Mediated Expression of IL-8 Chemokine in Human Endothelial Cells. *J Immunol* (2006) 177(10):7211–24. doi: 10.4049/jimmunol.177.10.7211
27. Al-Kharashi LA, Bakheet T, AlHarbi WA, Al-Moghrabi N, Aboussekhra A. Eugenol Modulates Genomic Methylation and Inactivates Breast Cancer-Associated Fibroblasts Through E2F1-Dependent Downregulation of DNMT1/DNMT3A. *Mol Carcinog* (2021) 60(11):784-95. doi: 10.1002/mc.23344
28. Achour M, Jacq X, Ronde P, Alhosin M, Charlot C, Chataigneau T, et al. The Interaction of the SRA Domain of ICBP90 With a Novel Domain of DNMT1 is Involved in the Regulation of VEGF Gene Expression. *Oncogene* (2008) 27 (15):2187–97. doi: 10.1038/sj.onc.1210855
29. Feinman R, Deitch EA, Watkins AC, Abungu B, Colorado I, Kannan KB, et al. HIF-1 Mediates Pathogenic Inflammatory Responses to Intestinal Ischemia-Reperfusion Injury. *Am J Physiol Gastrointest Liver Physiol* (2010) 299(4): G833–43. doi: 10.1152/ajpgi.00065.2010
30. Schuebel KE, Chen W, Cope L, Glockner SC, Suzuki H, Yi JM, et al. Comparing the DNA Hypermethylome With Gene Mutations in Human Colorectal Cancer. *PloS Genet* (2007) 3(9):1709–23. doi: 10.1371/journal.pgen.0030157
31. Hendrayani SF, Al-Harbi B, Al-Ansari MM, Silva G, Aboussekhra A. The Inflammatory/Cancer-Related IL-6/STAT3/NF-kappaB Positive Feedback Loop Includes AUF1 and Maintains the Active State of Breast Myofibroblasts. *Oncotarget* (2016) 7(27):41974–85. doi: 10.18632/oncotarget.9633
32. Manikandan P, Murugan RS, Priyadarsini RV, Vinothini G, Nagini S. Eugenol Induces Apoptosis and Inhibits Invasion and Angiogenesis in a Rat Model of Gastric Carcinogenesis Induced by MNNG. *Life Sci* (2010) 86(25-26):936–41. doi: 10.1016/j.lfs.2010.04.010
33. Herrera M, Islam AB, Herrera A, Martin P, Garcia V, Silva J, et al. Functional Heterogeneity of Cancer-Associated Fibroblasts From Human Colon Tumors Shows Specific Prognostic Gene Expression Signature. *Clin Cancer Res* (2013) 19(21):5914–26. doi: 10.1158/1078-0432.CCR-13-0694
34. Shin E, Lee Y, Koo JS. Differential Expression of the Epigenetic Methylation-Related Protein DNMT1 by Breast Cancer Molecular Subtype and Stromal Histology. *J Transl Med* (2016) 14:87. doi: 10.1186/s12967-016-0840-x
35. Zhao H, Zhang LE, Guo S, Yuan T, Xia B, Zhang L, et al. Overexpression of DNA Methyltransferase 1 as a Negative Independent Prognostic Factor in Primary Gastrointestinal Diffuse Large B-Cell Lymphoma Treated With CHOP-Like Regimen and Rituximab. *Oncol Lett* (2015) 9(5):2307–12. doi: 10.3892/ol.2015.3038
36. Li M, Wang Y, Song Y, Bu R, Yin B, Fei X, et al. Aberrant DNA Methyltransferase 1 Expression in Clear Cell Renal Cell Carcinoma Development and Progression. *Chin J Cancer Res* (2014) 26(4):371–81. doi: 10.3978/j.issn.1000-9604.2014.08.03
37. Wu CT, Wu CF, Lu CH, Lin CC, Chen WC, Lin PY, et al. Expression and Function Role of DNA Methyltransferase 1 in Human Bladder Cancer. *Cancer* (2011) 117(22):5221–33. doi: 10.1002/cncr.26150
38. Zhang JJ, Zhu Y, Zhu Y, Wu JL, Liang WB, Zhu R, et al. Association of Increased DNA Methyltransferase Expression With Carcinogenesis and Poor Prognosis in Pancreatic Ductal Adenocarcinoma. *Clin Transl Oncol* (2012) 14 (2):116–24. doi: 10.1007/s12094-012-0770-x
39. Amato RJ, Stephenson J, Hotte S, Nemunaitis J, Belanger K, Reid G, et al. MG98, a Second-Generation DNMT1 Inhibitor, in the Treatment of Advanced Renal Cell Carcinoma. *Cancer Invest* (2012) 30(5):415–21. doi: 10.3109/07357907.2012.675381
40. Mutze K, Langer R, Schumacher F, Becker K, Ott K, Novotny A, et al. DNA Methyltransferase 1 as a Predictive Biomarker and Potential Therapeutic Target for Chemotherapy in Gastric Cancer. *Eur J Cancer* (2011) 47(12):1817–25. doi: 10.1016/j.ejca.2011.02.024
41. Subramaniam D, Thombre R, Dhar A, Anant S. DNA Methyltransferases: A Novel Target for Prevention and Therapy. *Front Oncol* (2014) 4:80. doi: 10.3389/fonc.2014.00080
42. Sohal D, Krishnamurthi S, Tohme R, Gu X, Lindner D, Landowski TH, et al. A Pilot Clinical Trial of the Cytidine Deaminase Inhibitor Tetrahydrouridine Combined With Decitabine to Target DNMT1 in Advanced, Chemorefractory Pancreatic Cancer. *Am J Cancer Res* (2020) 10(9):3047–60.

Conflict of Interest: The authors declare that the research was conducted in the absence of any commercial or financial relationships that could be construed as a potential conflict of interest.

Publisher's Note: All claims expressed in this article are solely those of the authors and do not necessarily represent those of their affiliated organizations, or those of the publisher, the editors and the reviewers. Any product that may be evaluated in this article, or claim that may be made by its manufacturer, is not guaranteed or endorsed by the publisher.

Copyright © 2022 Al-Kharashi, Tulbah, Arafah, Eldali, Al-Tweigeri and Aboussekhra. This is an open-access article distributed under the terms of the Creative Commons Attribution License (CC BY). The use, distribution or reproduction in other forums is permitted, provided the original author(s) and the copyright owner(s) are credited and that the original publication in this journal is cited, in accordance with accepted academic practice. No use, distribution or reproduction is permitted which does not comply with these terms.

frontiers | Frontiers in Oncology

ORIGINAL RESEARCH
published: 06 June 2022
doi: 10.3389/fonc.2022.916526

A Novel Combined Nomogram Model for Predicting the Pathological Complete Response to Neoadjuvant Chemotherapy in Invasive Breast Carcinoma of No Specific Type: Real-World Study

Xuelin Zhu[1,2,3†], Jing Shen[1,2†], Huanlei Zhang[4], Xiulin Wang[2,5], Huihui Zhang[2], Jing Yu[2], Qing Zhang[2], Dongdong Song[2], Liping Guo[6], Dianlong Zhang[7], Ruiping Zhu[8] and Jianlin Wu[2]*

[1] Graduate School, Tianjin Medical University, Tianjin, China, [2] Department of Radiology, Affiliated Zhongshan Hospital of Dalian University, Dalian, China, [3] Department of Ultrasound, Qingzhou People's Hospital, Weifang, China, [4] Department of Radiology, Yidu Central Hospital of Weifang, Weifang, China, [5] School of Biomedical Engineering, Faculty of Electronic Information and Electrical Engineering, Dalian University of Technology, Dalian, China, [6] Department of Ultrasound, Affiliated Zhongshan Hospital of Dalian University, Dalian, China, [7] Department of Breast and Thyroid Surgery, Affiliated Zhongshan Hospital of Dalian University, Dalian, China, [8] Department of Pathology, Affiliated Zhongshan Hospital of Dalian University, Dalian, China

OPEN ACCESS

Edited by:
Annarita Fanizzi, National Cancer Institute Foundation (IRCCS), Italy

Reviewed by:
Cheng Dong, The Affiliated Hospital of Qingdao University, China
Alessandro Rizzo, National Cancer Institute Foundation (IRCCS), Italy

***Correspondence:**
Jianlin Wu
cjr.wujianlin@vip.163.com

†These authors share first authorship

Specialty section:
This article was submitted to Breast Cancer, a section of the journal Frontiers in Oncology

Received: *09 April 2022*
Accepted: *02 May 2022*
Published: *06 June 2022*

Citation:
Zhu X, Shen J, Zhang H, Wang X, Zhang H, Yu J, Zhang Q, Song D, Guo L, Zhang D, Zhu R and Wu J (2022) A Novel Combined Nomogram Model for Predicting the Pathological Complete Response to Neoadjuvant Chemotherapy in Invasive Breast Carcinoma of No Specific Type: Real-World Study. Front. Oncol. 12:916526. doi: 10.3389/fonc.2022.916526

Objective: To explore the value of a predictive model combining the multiparametric magnetic resonance imaging (mpMRI) radiomics score (RAD-score), clinicopathologic features, and morphologic features for the pathological complete response (pCR) to neoadjuvant chemotherapy (NAC) in invasive breast carcinoma of no specific type (IBC-NST).

Methods: We enrolled, retrospectively and consecutively, 206 women with IBC-NST who underwent surgery after NAC and obtained pathological results from August 2018 to October 2021. Four RAD-scores were constructed for predicting the pCR based on fat-suppression T2-weighted imaging (FS-T2WI), diffusion-weighted imaging (DWI), contrast-enhanced T1-weighted imaging (T1WI+C) and their combination, which was called mpMRI. The best RAD-score was combined with clinicopathologic and morphologic features to establish a nomogram model through binary logistic regression. The predictive performance of the nomogram was evaluated using the area under receiver operator characteristic (ROC) curve (AUC) and calibration curve. The clinical net benefit of the model was evaluated using decision curve analysis (DCA).

Results: The mpMRI RAD-score had the highest diagnostic performance, with AUC of 0.848 among the four RAD-scores. T stage, human epidermal growth factor receptor-2 (HER2) status, RAD-score, and roundness were independent factors for predicting the pCR ($P < 0.05$ for all). The combined nomogram model based on these factors achieved AUCs of 0.930 and 0.895 in the training cohort and validation cohort, respectively, higher than other models ($P < 0.05$ for all). The calibration curve showed that the predicted probabilities of the nomogram were in good agreement with the actual probabilities, and

DCA indicated that it provided more net benefit than the treat-none or treat-all scheme by decision curve analysis in both training and validation datasets.

Conclusion: The combined nomogram model based on the mpMRI RAD-score combined with clinicopathologic and morphologic features may improve the predictive performance for the pCR of NAC in patients with IBC-NST.

Keywords: multiparametric MRI, radiomics, neoadjuvant chemotherapy, invasive breast carcinoma of no specific type, pathologic complete response

INTRODUCTION

For females, breast cancer (BC) is the leading cause of cancer in 157 countries and the leading cause of death in 119 countries (1). Neoadjuvant chemotherapy (NAC) for BC is a systemic therapy using a cytotoxic drug administered before definitive surgical treatment (2). As a personalized precision treatment approach, the purpose of NAC is to: (i) reduce tumor stage; (ii) treat potential metastatic lesions in a timely manner; (iii) observe the sensitivity of tumors to chemotherapy regimens to provide a basis for the selection of subsequent treatment regimens (3, 4). However, about 20% of BC patients are not sensitive to NAC, and a few even experience disease progression during treatment (5). Meanwhile, chemotherapeutic drugs can also lead to adverse effects (e.g., bone-marrow suppression, liver and kidney impairment, heart failure) in some patients (6, 7). Therefore, evaluating BC patients before chemotherapy and predicting if they will benefit from NAC are crucial. pCR is the most widely used surrogate endpoint for NAC efficacy assessment, and patients achieving pCR may have higher disease-free survival and overall survival (8). Hence, early prediction of pCR may help to improve personalized treatment plans and even avoid surgery in the future.

Conventional imaging medicine obtains the morphological characteristics of tumor phenotypes through visual assessment by radiologists, which can provide an overall image of the tumor phenotype and its environment. These morphological features (e.g., shape, border, lobing) observed originally by the naked eye are dichotomous variables based on two-dimensional (2D) sections. Some scholars have suggested that they can be characterized by quantitative data using mathematical formulae in which "roundness" can indicate the shape of the lesion, "concavity" reflects the irregularity of the lesion border, and "curvature" describes the morphologic changes of breast-tumor lesions (9). They are all based on quantitative measurements, so refining dichotomous variables into digital variables would be advantageous compared with using conventional morphologic qualitative features assessed by the naked eye.

Dynamic contrast enhanced magnetic resonance imaging (DCE-MRI) is one of the most sensitive methods for early prediction of pCR, which can reflect changes in tissue pathophysiology before morphological changes (10). In addition, T2 weighted imaging (T2WI), diffusion weighted imaging (DWI) and other sequences have also been used in the prediction of NAC for BC (11, 12).

Multiparametric magnetic resonance imaging (mpMRI) involves combined application of several MRI imaging sequences. mpMRI can be employed to quantify the evolution of cancer development at multiple levels and dimensions, and provide specific quantitative information about tumor characteristics. Compared with single-sequence MRI models, mpMRI improves the diagnostic accuracy of BC and the evaluation and prediction performance of NAC efficacy (13).

Radiomics uses automated algorithms to convert the image data of the region of interest in medical images into high-dimensional spatial data, and then extracts the key information that really works from a large amount of information through a variety of statistical analysis and data mining methods. Then, the obtained information is applied to support systems for clinical decision-making to aid disease characterization, tumor staging, efficacy assessment, and prognosis prediction (14). Compared with conventional imaging, radiomics fully reflects the most essential characteristics of the underlying medical images. In recent years, radiomics based on mpMRI has developed rapidly and become a "hotspot" for basic research and clinical applications, and has made great progress in BC and other research fields (15–19).

Invasive breast carcinoma of no specific type (IBC-NST) is the most common type of pathologic staging for BC. It accounts for about 70–80% of cases, and is characterized by low differentiation and a poor prognosis (20, 21). Few studies have been conducted to predict the pathologic complete response (pCR) of NAC based on mpMRI radiomics for people with IBC-NST.

We aimed to establish and validate a nomogram model based on mpMRI radiomics, clinicopathologic features, and morphologic features for early prediction of pCR in IBC-NST.

MATERIALS AND METHODS

Ethical Approval of the Study Protocol

The protocol for this retrospective study was approved (2018068) by the Ethics Committee of Zhongshan Hospital Affiliated to Dalian University (Dalian, China). The requirement for written informed consent from study participants was waived.

Patients

The inclusion criteria were: (i) female BC patients over 18 years old who came to our hospital for treatment; (ii) MRI was performed and immunohistochemical results were obtained by

ultrasound-guided needle biopsy before NAC; (iii) surgery was performed after NAC, and pCR was confirmed by postoperative pathologic examination. The exclusion criteria were: (i) a specific type of invasive breast cancer; (ii) MRI findings were obtained >1 week before NAC; (iii) not receiving a standardized and complete NAC regimen or other related treatment previously; (iv) lesions were combined with other sites of primary cancer; (v) lesions were combined with distant metastases; (vi) the quality of the MR image was insufficient to obtain measurements; (vii) the correlation between the tumor and assessment of the pathologic response in MR images was uncertain; (viii) incomplete clinical or pathologic data.

Patients suffering from BC who underwent NAC and a surgical procedure at Zhongshan Hospital from August 2018 to October 2021 were included retrospectively and consecutively. Patients were divided into a pCR group and non-pathologic complete response (NpCR) group according to whether pCR was achieved after NAC. Enrolled patients were assigned randomly to a training cohort and a validation cohort at a ratio of 7:3. The training cohort is used for model establishment, and the validation cohort is used for model performance verification. A flowchart showing the study population is presented as **Figure 1**.

Baseline clinical data were obtained from medical records. The age, body mass index (BMI), menopause status, fibrinogen, T stage, and N status of patients before NAC were collected. Treatment regimens and treatment cycles followed the National Comprehensive Cancer Network guideline (22). All BC patients completed ≥4 cycles of NAC with: (i) paclitaxel-based chemotherapy (4.4%, 9/206); (ii) anthracycline-based chemotherapy (21.8%, 45/206); (iii) anthracycline-based chemotherapy combined with paclitaxel-based chemotherapy (73.8%, 152/206). Human epidermal growth factor receptor 2 (HER2)-positive patients also received trastuzumab or/and pertuzumab (35.4%, 73/206). All patients underwent surgery at our hospital within 2 weeks of completing a full cycle of NAC. Analyses of pathologic histologic sections and diagnosis were undertaken by two pathologists with 12 years and 10 years of experience in the diagnosis of breast disease, respectively, who were blinded to the study protocol. Pre-NAC status of the estrogen receptor (ER), progesterone receptor (PR), HER2, and Ki-67 expression were obtained from immunohistochemical analyses of the puncture specimen (for assessment criteria see **Supplemental Data 1**). pCR was confirmed by postoperative pathological examination. The "pCR" was defined as an absence of residual invasive carcinoma in the specimen (residual ductal carcinoma *in situ* can be present), ipsilateral anterior sentinel lymph node or no lymph node infiltration in lymph nodes removed during axillary dissection (23).

MRI Protocol

All MR images were acquired on a 3.0-T Magnetom Verio superconducting MRI scanner equipped with a 16-channel breast-specific coil (Siemens, Hamburg, Germany) within one week prior to NAC. Imaging sequences were fat-suppression T2-weighted imaging (FS-T2WI), diffusion-weighted imaging (DWI, contrast-enhanced T1-weighted imaging (T1WI+C). Scan parameters are shown in **Supplemental Data 2**.

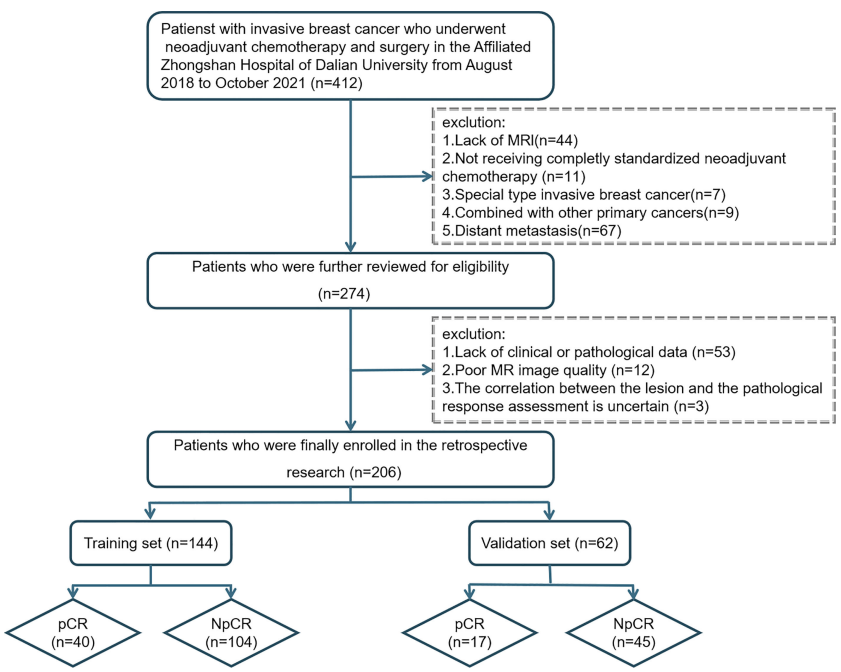

FIGURE 1 | Flowchart revealing the study population based on exclusion criteria.

Extraction and Selection of Morphologic Features

MR images were evaluated independently by two radiologists, A and B, with 11 years and 14 years of experience of diagnosing BC using MRI, respectively. Measurements were made using a double-blind method (neither radiologist was aware of clinicopathologic findings or the other radiologist's interpretation of images). Morphologic features were measured using 3D Slicer (version 4.11, www.slicer.org/). The maximum cross-section of the T1WI +C sequence was used for measurement, and the following values measured under the "Markups" module: vertical diameter, transverse diameter, perimeter, surface area, convex closure area, curvature maximum, and curvature mean (**Figure 2**). Roundness was calculated using the formula: $4\pi \times$ surface area/perimeter^2. Concavity was calculated indirectly from the measured convex closure area: (convex closure area – surface area)/convex closure area (24). Thirty cases were randomly selected from the enrolled population before assignment, and the repeatability of feature extraction was assessed using intra-observer and inter-observer intraclass correlation coefficients (ICCs). Each parameter was measured twice, and the mean value calculated: this was used as the final measurement. Multicollinearity was used to reduce morphologic features, and parameters with a variance inflation factor (VIF) <10 were selected for subsequent analyses.

Tumor Segmentation and Radiomics Feature Extraction

The region of interest (ROI) was delineated manually *via* 3D Slicer (version 4.11, www.slicer.org/) on each slice of the FS-T2WI, DWI (b-value of 800s/mm^2), and T1+C (second period after contrast agent injection) image sets (DICOM format) of all cases. On each slice of the images, necrotic, air, and calcified regions were excluded.

Two radiologists (A and B) were responsible for the evaluation of tumor segmentation. Inter- and intra-observer reproducibility of radiomic feature extraction were initially analyzed with the data of 30 randomly selected patients from each sequence in a double-blinded fashion by these 2 radiologists. The ICCs were used to evaluate the agreement of radiomics features.

Prior to feature extraction, all images were resampled to a common voxel spacing of 1mm × 1mm × 1mm by using the Resize method, to resample the images into an isotropic dataset to allow comparison between image data from different sequences.

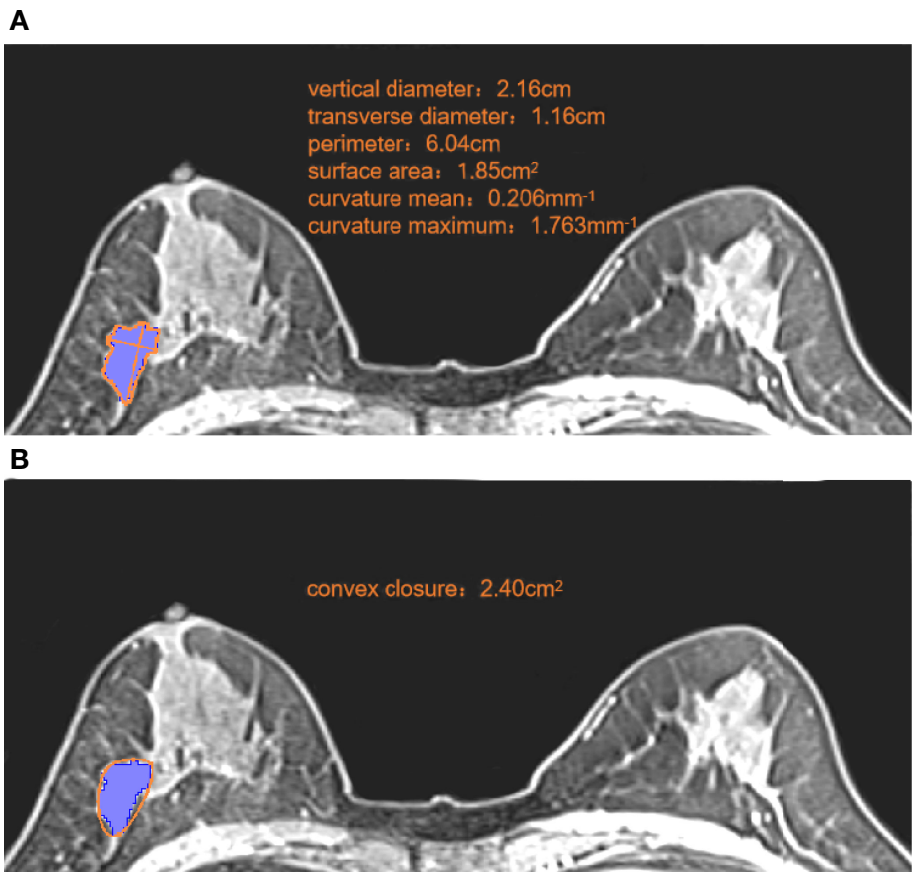

FIGURE 2 | Measurement of morphologic parameters. **(A)** We measured the vertical diameter and transverse diameter at the largest cross-section. We drew along the edge of the lesion, and obtained the perimeter, surface area, curvature mean, and curvature maximum. Roundness $=4\pi \times 1.85/6.04^2 = 0.64$ **(B)** We made a small convex polygon along the line connecting the edge of the lesion to obtain the convex closure area. Concavity= (2.40-1.85)/2.40 = 0.23.

The "Radiomics" module in the 3D Slicer (version 4.11, www.slicer.org/) was used to extract 1223 radiomics features from each sequence of FS-T2WI, DWI, and T1WI+C. One hundred and seven radiomic features were extracted from the original images, including 18 first-order features, 14 shape features, and 75 texture features derived from the gray level co-occurrence matrix (GLCM, 24), gray level dependence matrix(GLDM, 14), gray level run length matrix (GLRLM, 16), gray level size zone matrix (GLSZM, 16) and neighbourhood gray-tone difference matrix (NGTDM, 5). With a Laplacian of Gaussian filter, 372 features with four sigma levels (0.5, 1, 1.5, 2) were obtained. A total of 744 features were obtained from 8 derived images by wavelet transform.

Selection of Radiomics Features and Construction of a "RAD-Score"

All extracted features were normalized by z-score in the training cohort before selecting radiomic features. First, features with ICC >0.75 within the training cohort were retained. Second, *t*-tests or *u*-tests were carried out on the retained features, and we targeted those with discriminatory ability ($P < 0.05$) for further analyses. Third, we applied the least absolute shrinkage and selection operator (LASSO) regression for selecting the key radiomics features with nonzero coefficients, and a 10-fold cross-validation with a maximum area under the receiver operator characteristic (ROC) curve (AUC) criterion was conducted to determine an optimal regulation weight (lambada). After the steps stated above, the remaining features were subjected to RAD-score construction. The above-mentioned RAD-scores were constructed for FS-T2WI, DWI, T1WI+C sequences and mpMRI, respectively. The sequence with the best diagnostic efficacy RAD-score was selected for entry into subsequent analyses. The RAD-score of each patient is linear combinations of selected features weighted by their coefficients, which are mathematically represented as follows:

$$RAD - score = \sum_{i=1}^{n} C_i \times X_i + b$$

where b is the intercept, X_i is the ith selected feature, and C_i is the coefficient of the ith selected feature. Feature selection and RAD-score construction were performed using the "glmnet" package of R software (version 4.1.4, www.r-project.org/).

Development of Prediction Models

Prediction models were developed using univariate and multifactorial logistic regression based on clinicopathologic, morphologic, and radiomics features. Clinicopathologic features included age, menopausal status, fibrinogen level, BMI, T stage, N stage, receptor status (ER, PR, HER2), and Ki-67 expression. Features with $P < 0.05$ after univariate analysis were included in the multifactorial analysis. Next, we development 3 models based on features of different categories. Model A was established based on clinicopathologic features. Model B was established based on clinicopathologic and radiomics features. Model C was established based on clinicopathologic, radiomics, and morphologic features.

Comparison of the Performance of Prediction Models

Accuracy, specificity, sensitivity, and the area under receiver operator characteristic curve (AUC) were used to estimate the predictive performance of the three models in the training cohort and validation cohort. The model with the best performance was presented as a nomogram. Then, a calibration curve was used to evaluate the consistency between the estimated probability and actual probability of the pCR. Decision curve analysis (DCA) was used to assess the clinical usefulness by estimating the net benefit within threshold probabilities. A flowchart of extraction of radiomics features and model establishment is shown as **Figure 3**.

Statistical Analyses

Differences between pCR and NpCR groups were analyzed using the *t*-test, *u*-test, or chi-square test. Statistical analyses were undertaken using R software (version 4.1.4, www.r-project.org/). Within R software, the packages "performance" and "see" were employed for multicollinearity analyses. "glmnet" were used for feature selection and RAD-score construction, and "pROC", "rms", "Hmisc" and "ggDCA" were employed for model construction and performance evaluation. $P < 0.05$ was considered significant.

RESULTS

Patient Characteristics

A total of 206 BC patients formed the study cohort. They had a median age of 52 (range, 42–60) years. Among them, 57 (27.7%) were in the pCR group and 149 (72.3%) were in the NpCR group. There was no significant difference in age, menopausal status, fibrinogen level, body mass index, or lymph-node metastasis between pCR and NpCR groups ($P > 0.05$ for all). T stage, ER status, PR status, HER2 status, and Ki-67 expression were significantly different between the groups ($P < 0.05$ for all) (**Table 1**).

All patients were divided randomly into a training cohort (144) and a validation cohort (62) at a ratio of 7:3. In the training cohort, 41 cases had a pCR and 103 had a NpCR. In the validation cohort, 16 patients had a pCR and 46 had a NpCR. There was no significant differences pCR ratio between the training cohort and validation cohort ($P > 0.05$) (**Table 1**).

Morphologic Features

Table S1 shows that all eight morphologic variables have ICCs >0.9 (i.e., showed good agreement). Multicollinearity analysis (**Figure S1**) meant that the final remaining two variables (roundness and concavity) entered the next step of analysis.

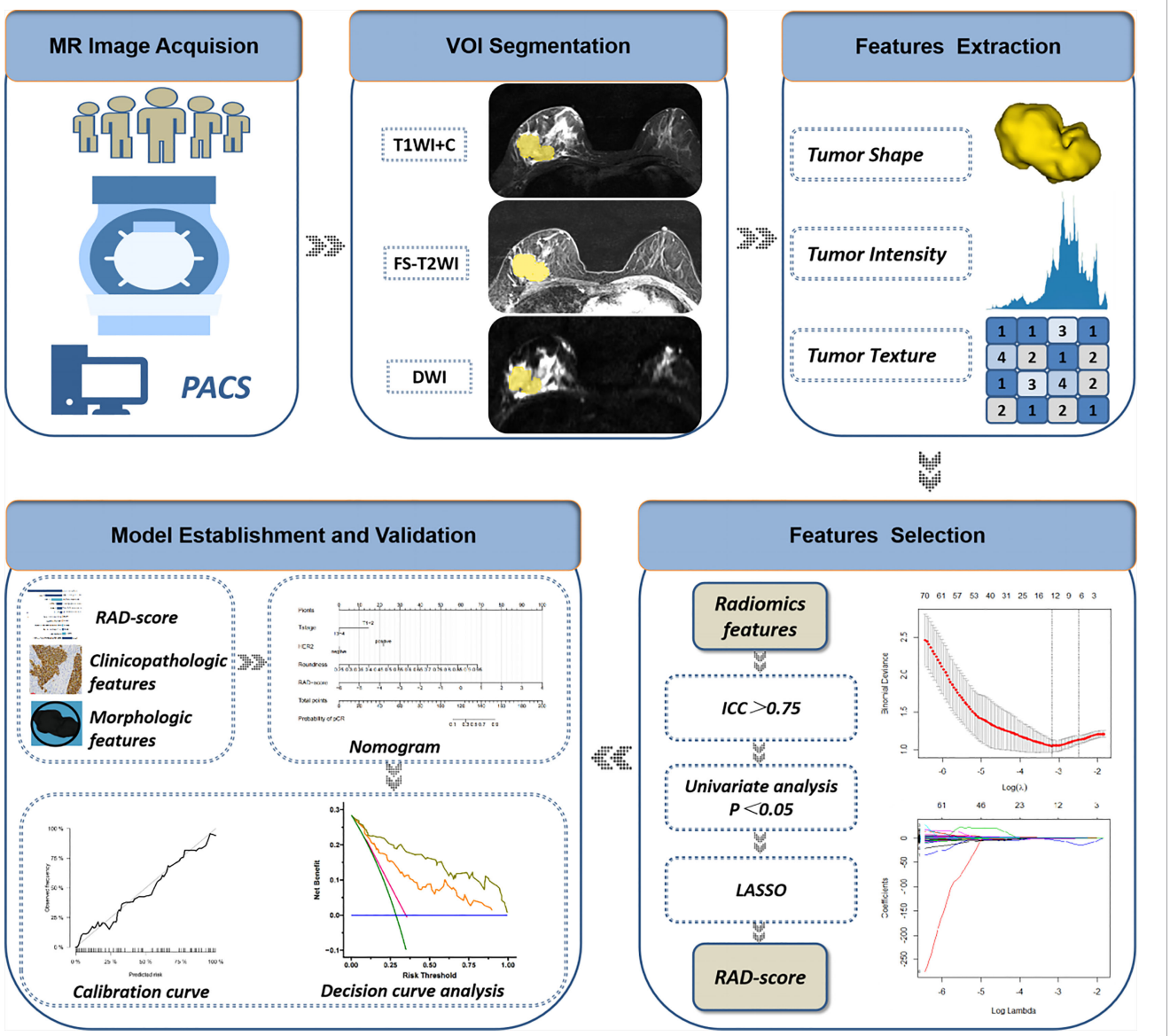

FIGURE 3 | Flowchart of extraction of radiomics features, model establishment and performance evaluation. ICC, intraclass correlation coefficient; LASSO, least absolute shrinkage and selection operator; RAD-score, radiomics score.

Selection of Radiomics Features and Establishment of the RAD-Score

After screening, the mpMRI sequence has 12 remaining features, including 1 shape feature, 2 original texture features, 5 Gaussian filter transformation features and 4 wavelet features. Texture features, Gaussian filter features and wavelet features are based mainly on the GLCM, GLDM, NGTDM, and GLSZM.The selection process operated by LASSO is represented in **Figure 4**. Reduction of feature dimensionality and the display of each sequence feature are shown in **Figure S2** and **Table S2**, respectively. The RAD-score was calculated as follows:

RAD-score= (T1WI+C/Log-sigma-0-5-mm-3D/ngtdm/Strength×0.12370077) -(T1WI+C/Original/shape/Maximum2DDiameterSlice×0.17457776) -(T1WI+C/Log-sigma-1-0mm-3D/glcm/Correlation×1.59333848) -(T1WI+C/Log-sigma-0-5-mm-3D/glcm/Idn×3.24587525) +(T1WI+C/Log-sigma-2-0-mm-3D/glrlm/ShortRunLowGrayLevel Emphasis×0.94972916) -(T1WI+C/Wavelet-LHL/gldm/DependenceVariance×0.479 87897) -(T1WI+C/Wavelet-HLL/gldm/DependenceVariance×0.53138627) -(DWI/Original/gldm/DependenceVariance×1.03259897) +(DWI/Original/ngtdm/Contrast×0.35 02368) +(DWI/Wavelet-LHL/glszm/LargeAreaLowGrayLevelEmphasis×0.1019391 2) +(FS-T2WI/Log-sigma-1-5-mm-3D/ngtdm/Strength×0.04867799) +(FS-T2WI/Wavelet-LHL/ngtdm/Coarseness×0.05095310) +4.59154672

The features shown by mpMRI had the highest diagnostic performance in the training cohort (AUC=0.848) and validation

TABLE 1 | Demographic and clinical characteristics of the study cohort.

Variable	All patients (n = 206)	NpCR group (n = 149)	pCR group (n = 57)	*P*-value
Age, median	52 (42, 60)	52 (42, 59)	51 (42, 61)	0.889
Menopausal status, n (%)				0.640
Pre	103 (50.0)	76 (51.0)	27 (47.4)	
Post	103 (50.0)	73 (49.0)	30 (52.6)	
BMI, median	24.65 (22.28, 26.64)	24.65 (22.6, 26.29)	24.58 (20.7, 26.81)	0.181
FIB, median	2.69 (2.42, 3.07)	2.69 (2.46, 3.1)	2.65 (2.37, 3.02)	0.387
T Stage, n (%)				0.019
T1–2	114 (55.3)	65 (49.2)	49 (66.2)	
T3–4	92 (44.7)	67 (50.8)	25 (33.8)	
N Status, n (%)				0.631
Negative	33 (16.0)	25 (16.8)	8 (14.0)	
Positive	173 (84.0)	124 (83.2)	49 (86.0)	
ER Status, n (%)				<0.001
Negative	79 (38.4)	39 (26.2)	40 (70.0)	
Positive	127 (61.6)	110 (73.8)	17 (29.8)	
PR Status, n (%)				<0.001
Negative	95 (46.1)	52 (34.9)	43 (75.4)	
Positive	111 (53.9)	97 (65.1)	14 (24.6)	
HER2 Status, n (%)				<0.001
Negative	133 (64.6)	111 (74.5)	22 (38.6)	
Positive	73 (35.4)	38 (25.5)	35 (61.4)	
Ki-67 Status, n (%)				0.010
Low expression	42 (20.4)	37 (24.8)	5 (8.8)	
High expression	164 (79.6)	112 (75.2)	52 (91.2)	
Cohort, n (%)				0.695
Training cohort	144 (69.9)	103 (69.1)	41 (71.9)	
Validation cohort	62 (30.1)	46 (30.9)	16 (28.1)	

pCR, pathologic complete response; NpCR, non-pathologic complete response; BMI, body mass index; FIB, fibrinogen; ER, estrogen receptor; PR, progesterone receptor; HER2, human epidermal growth factor receptor 2.

cohort (AUC =0.742), followed by T1WI+C sequence, with an AUC of 0.799 in the training cohort and 0.741 in validation cohort. For the FS-T2WI sequence, the AUC of training cohort was 0.737 and the AUC of validation cohort was 0.635, while DWI sequence yielded an AUC of 0.750 in training cohort and 0.626 in validation cohort. (**Figure S3**).

Construction of Predictive Models

In the training cohort, univariate logistic regression analysis showed that T stage, HER2 status, roundness, and RAD-score were potential predictors ($P < 0.05$) which were associated with pCR status. Then, the variables stated above were included in the multivariate logistic regression analysis for the construction of the 3 models: model A (T stage + HER2 status), model B (Model A + RAD-score), and model C (Model B + roundness) (**Table 2**). The AUC of model A in the training cohort was 0.612 (95% CI, 0.528-0.692) and in the validation cohort was 0.626 (95% CI, 0.493-0.760). Model B yielded an AUC of 0.869 (95% CI, 0.802-0.919) and an AUC of 0.775 (95% CI, 0.642-0.907). Compared to the other 2 models, model C exhibited the highest discrimination performance in the training cohort (AUC, 0.930; 95% CI, 0.875-0.966) and validation cohort (AUC, 0.895; 95% CI, 0.808-0.983) (**Figure 5**). Accuracy, sensitivity, specificity, and AUC of each model are shown in **Table 3**. Model C is shown in a nomogram (**Figure 6**).

The calibration curve of the nomogram showed that the predicted results were in good agreement with the actual results (**Figure 7**). The result of the DCA indicated that the prediction of pCR using model C could give more net benefit than by treating none or all patients in both training and validation datasets (**Figure 8**).

DISCUSSION

Using an IBC-NST population, we developed a nomogram model based on the RAD-score of mpMRI combined with clinicopathologic and morphologic features. This combined model had high value for predicting the pCR prior to NAC. The performance of this model was better than that of the clinical model, or the model combining clinical features with radiomics features.

We established RAD-score models for FS-T2WI, DWI, T1WI+C, and mpMRI to predict the pCR before NAC, respectively. The mpMRI RAD-score model had the highest diagnostic performance in the training cohort (AUC=0.848) and validation cohort (AUC =0.742). Among the other three single-sequence models, the T1WI+C model performed the best with AUCs of 0.799 and 0.741 in the training and validation cohorts, respectively. This indicates that T1WI+C is one of the most sensitive methods for predicting pCR in the single MRI sequence, which is also consistent with many previous studies (25, 26). Whereas in studies comparing mpMRI with single sequence, Chen et al. (27) evaluated 91 patients and found that in the pCR prediction models, the radiomics signature of mpMRI exhibited higher predictive power (AUC = 0.848) compared to DCE(AUC=0.750) and ADC(AUC=0.785). Bian et al. (28) also found that the mpMRI model had the highest predictive power for

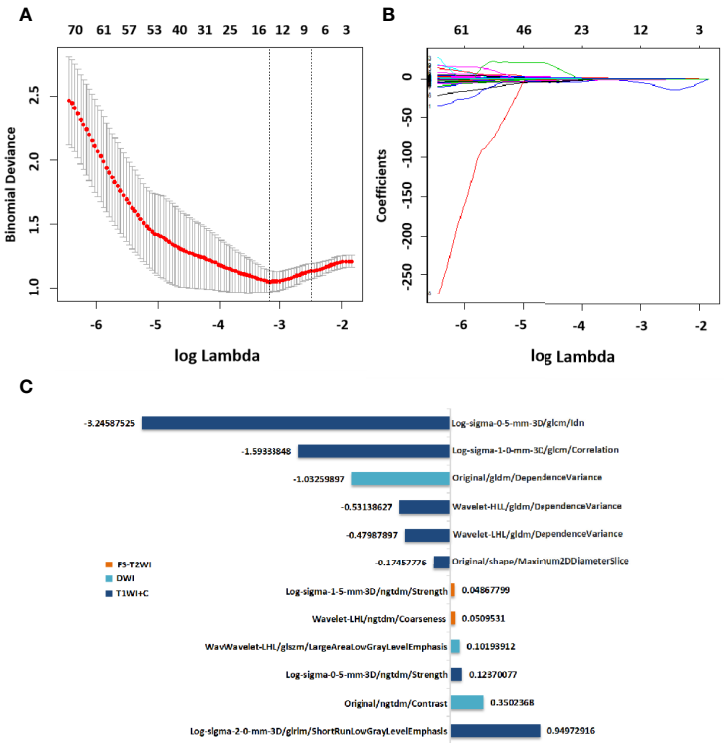

FIGURE 4 | Selection of radiomics features *via* LASSO algorithm to establish a RAD-score. **(A)** Tuning parameter selection by 10-fold cross-validation with minimum criteria. Mean square error (y-axis) was plotted as a function of log(lambda) (x-axis). **(B)** LASSO coefficient profiles for the whole features. **(C)**12 radiomics features corresponding to the selected optimal values for establishment of a RAD-score. LASSO, least absolute shrinkage and selection operator; RAD-score, radiomics score.

TABLE 2 | Multivariate logistic analysis.

Variable	Model A		Model B		Model C	
	OR (95%CI)	*P*-value	OR (95%CI)	*P*-value	OR (95%CI)	*P*-value
T stage	4.47 (2.33–9.59)	0.035	2.266 (1.132–5.397)	0.044	2.354 (1.023–5.236)	0.036
HER2 status	2.56 (1.83–7.89)	0.012	3.713 (1.677–8.291)	0.009	1.947 (1.320–4.321)	0.024
RAD-score			5.057 (2.031–11.851)	0.026	3.911 (1.591–9.642)	0.003
Roundness					7.554 (3.2151–7.664)	<0.001

HER2, human epidermal growth factor receptor. RAD-score, radiomics score; OR, odds ratio; CI, confidence interval.

the pCR in a study of 152 patients, with AUC of 0.91 and 0.93 in the training and validation cohort. Using a larger cohort, we demonstrated that combined application of different imaging sequences was superior to that using a single sequence. Under a logistic algorithm model, *t*-test, *U*-test, and LASSO regression were employed to select the optimal number of features. Within the range of standard deviation of the highest AUC value, 12 features were selected for the mpMRI RAD-score (T1WI+C7, DWI 3, FS-T2WI 2). These features included one shape feature, four wavelet features, and seven texture features. Among them, the only shape feature was the maximum 2D diameter slice of the T1WI+C sequence, which reflected the tumor diameter. The smaller the tumor, the easier the pCR could be achieved.

Texture features, Gaussian filter features and wavelet features are based mainly on the GLCM, GLDM, NGDTM, and GLSZM. The GLCM provides comprehensive information about the direction, adjacent interval, and variation range of the gray level of the image. The GLCM is the basis for analyzing the local patterns of the image and their arrangement rules, and is used to describe the texture distribution and characteristics within the tumor. The NGTDM describes the visual characteristics of texture based on a voxel and its neighborhood. The GLSZM can aid characterization of texture consistency, a periodic texture, or speckle texture (29). These are high-order features and cannot be identified by the naked eye. However, they can capture information on the spatial heterogeneity of intratumoral cells and tumor perfusion, thereby making them sensitive for treatment evaluation (30). Therefore, the RAD-score could serve as a non-invasive imaging marker for pCR prediction.

We found that the T stage and HER2 status, as clinicopathologic features, were independent influencing factors of the pCR. The T stage represents the diameter of tumor tissue and the extent of

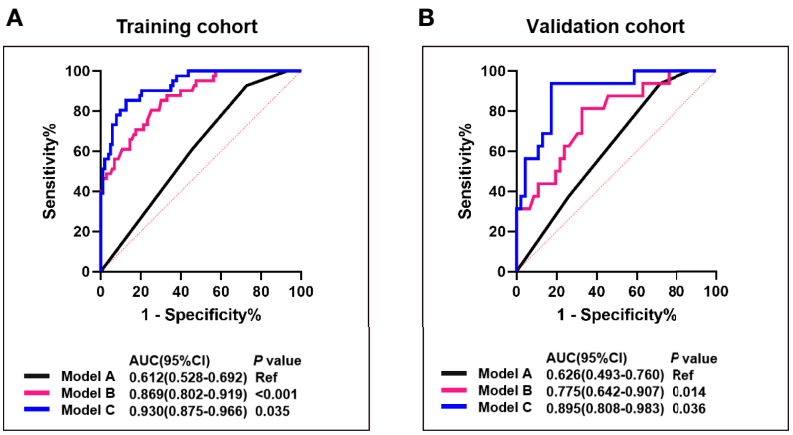

FIGURE 5 | Comparison of the predictive performance between model A, B and (C) ROC curves and AUCs for predicting pCR of model A (blue curve), model B (pink curve), and model C (black curve) in the training **(A)** and the validation cohort **(B)**. Model A, T stage + HER2 status; Model B, model A + RAD-score; Model C, model B + roundness.

TABLE 3 | Performance of prediction models in the training cohort and validation cohort.

Model	Cohort	AUC (95%CI)	*P**	SE	SP	ACC
Model A	Training cohort	0.612 (0.528-0.692)	Ref	0.927	0.272	0.458
	Validation cohort	0.626 (0.493-0.760)	Ref	0.626	0.261	0.355
Model B	Training cohort	0.869 (0.802-0.919)	<0.001	0.854	0.699	0.743
	Validation cohort	0.775 (0.642-0.907)	0.014	0.813	0.674	0.710
Model C	Training cohort	0.930 (0.875-0.966)	0.035	0.854	0.874	0.868
	Validation cohort	0.895 (0.808-0.983)	0.036	0.938	0.826	0.855

Model A, T stage + HER2; Model B, Model A + RAD-score; Model C, Model B + roundness; AUC, the area under receiver operator characteristic curve; CI, confidence interval; P, Delong test; SE, sensitivity; SP, specificity; ACC, accuracy.*

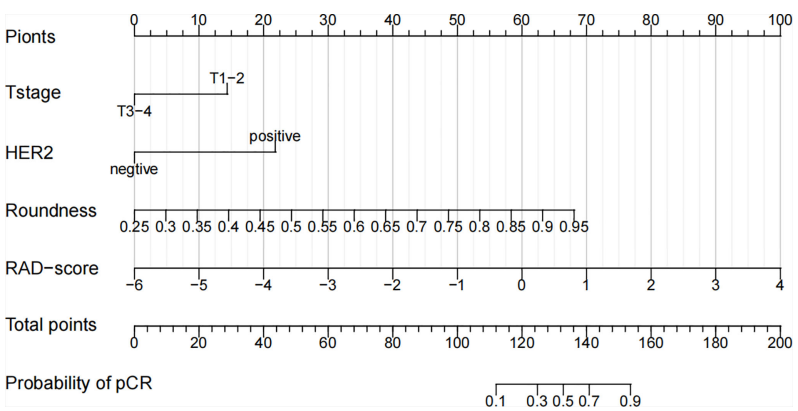

FIGURE 6 | A nomogram for the prediction of the pathological complete response of neoadjuvant chemotherapy in invasive breast carcinoma of no specific type.

tumor invasion. Briete et al. (31) postulated clinical tumor stage to be the most important predictor of a pCR in BC patients after NAC. We further confirmed that a lower T stage (T1–2 and T3-4) is an important independent predictor of a higher prevalence of a pCR.

HER2 is a prognostic indicator for monitoring of clinical treatment and an important target for selection of tumor-targeting drugs. Several studies (5, 32, 33) have suggested that HER2-positivity can lead to a higher prevalence of the pCR: we reached the same conclusion. Also, we found roundness to be an independent predictor of the pCR after NAC. The roundness of a tumor represents the shape of the lesion. The value of roundness is between 0 and 1. The closer the value is to 1, the closer is the shape to a circle (34). Based on the most intuitive impression by radiologists, roundness quantifies shape features and is accepted

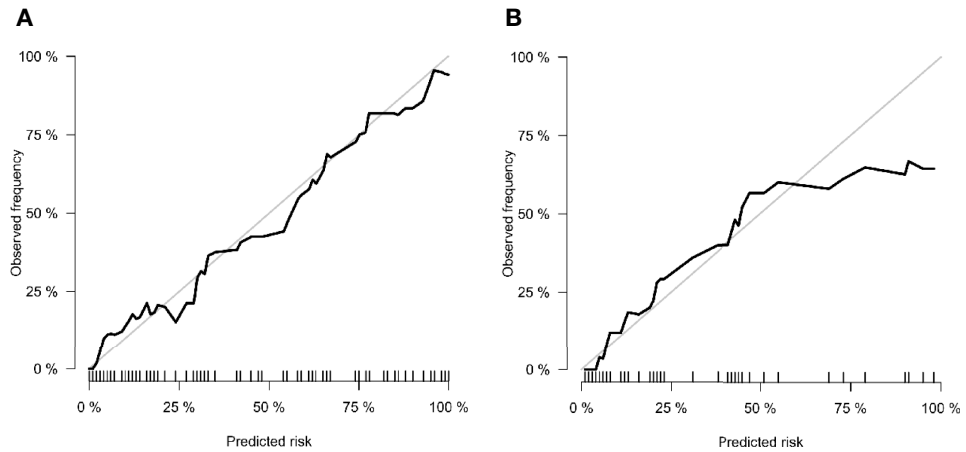

FIGURE 7 | Calibration curves of **(A)** training cohort and **(B)** validation cohort. The x-axis is the nomogram-predicted probability. The y-axis is the observed probability. The closer fit of the diagonal curved line to the ideal straight line indicates the predictive accuracy of the nomogram from the best model.

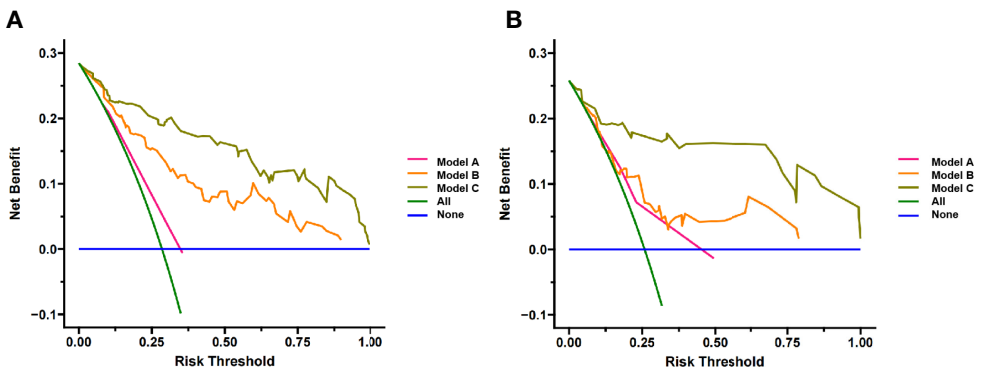

FIGURE 8 | Decision Curve analysis for three models in **(A)** training cohort and **(B)** validation cohort. The y-axis measures the net benefit. The pink line represents model A, the orange line represents model B and the brown line represents model C. The green line represents the assumption that all patients gained substantial benefit after NAC. The horizontal blue line represents the assumption that no patients gained substantial benefit after NAC.

readily by clinicians. Few studies have shown the relationship between roundness and the pCR. However, Zhang et al. (35) concluded, in a retrospective analysis of 120 BC patients, that the roundness observed in triple-negative BC patients was higher than that observed in non-triple-negative BC patients whereas, in general, triple-negative BC responded better to NAC than other molecular subtypes. Their data supported our findings indirectly. In a multicenter study by Liu et al. (36), the radiomics signature of mpMRI achieved an AUC of 0.79 (the highest of the four radiomics signatures), whereas a prediction model combining the RAD-score and clinicopathologic characteristics before NAC had higher predictive value for the pCR (AUC = 0.86). A study by Zhang et al. (37) obtained similar results (AUC = 0.84). On the basis of the radiomics features of mpMRI combined with clinicopathologic features, we also added roundness (a quantitative morphologic feature) and narrowed the study cohort to IBC-NST patients: the AUC of the combined prediction model reached 0.930. The clinical value must be validated further, but addition of quantitative morphologic factors aids improvement of the predictive power of the model.

Our study had four main limitations. First, this was a retrospective, single-center study, and a selection bias was inevitable. Second, the heterogeneity of molecular subtypes included in our study led to the use of different chemotherapy regimens, this scenario is in accordance with clinical practice, but may lead simultaneously to an imbalance in the pathologic response of NAC. Third, we carried out comprehensive internal verification, which demonstrated the reliability and repeatability of the constructed model to a certain extent, and reduced the risk of a confounding bias. However, the conclusions of our study are based only on a particular population. Verification in multicenter studies is needed to improve the universality of our model. Fourth, the sequences used in the mpMRI radiomics were FS-T2WI, DWI, and T1WI+C. Whether combination with other sequences or even other imaging modalities (e.g., ultrasound, computed tomography, positron emission tomography) can help improve the prediction

performance must be explored further. Meanwhile, the comparison of multiple classifiers and the application of deep learning will also become our future research directions.

CONCLUSIONS

We developed a combined nomogram model based on mpMRI radiomics, clinicopathologic features, and morphologic features for early prediction of pCR to NAC in IBC-NST. Compared with models based on clinicopathologic features alone or combining clinicopathologic and radiomic features, this model has higher predictive performance and is expected to provide more references for making decisions on clinical treatment in the future.

DATA AVAILABILITY STATEMENT

The original contributions presented in the study are included in the article/**Supplementary Material**. Further inquiries can be directed to the corresponding author.

ETHICS STATEMENT

This study was reviewed and approved by the Ethics Committee of Affiliated Zhongshan Hospital of Dalian University, and patient informed consent was waived.

AUTHOR CONTRIBUTIONS

XZ, JS, HLZ, and JW conceived the study. XZ, JS, and HHZ collected the data. HLZ, XW, and DS analyzed the data. XZ wrote the manuscript. JW, JY, QZ, and LG provided study supervision. DZ and RZ conducted the histological assessments. All authors contributed to the article and approved the submitted version.

FUNDING

This study is supported by Scientific Research Project Plan of Weifang Health Commission (WFWSJK–2021–071).

ACKNOWLEDGMENTS

The authors thank all the staff from the Departments of Breast and thyroid surgery, Radiology and Pathology, Affiliated Zhongshan Hospital of Dalian University, for their help in collecting the clinical data.

SUPPLEMENTARY MATERIAL

The Supplementary Material for this article can be found online at: https://www.frontiersin.org/articles/10.3389/fonc.2022.916526/full#supplementary-material

REFERENCES

1. Kocarnik JM, Compton K, Dean FE, Fu W, Gaw BL, Harvey JD, et al. Cancer Incidence, Mortality, Years of Life Lost, Years Lived With Disability, and Disability-Adjusted Life Years for 29 Cancer Groups From 2010 to 2019: A Systematic Analysis for the Global Burden of Disease Study 2019. *JAMA Oncol* (2021) 8:420–44. doi: 10.1001/jamaoncol.2021.6987
2. Sutton EJ, Onishi N, Fehr DA, Dashevsky BZ, Sadinski M, Pinker K, et al. A Machine Learning Model That Classifies Breast Cancer Pathologic Complete Response on MRI Post-Neoadjuvant Chemotherapy. *Breast Cancer Res* (2020) 22(1):57. doi: 10.1186/s13058-020-01291-w
3. Slanetz PJ, Moy L, Baron P, diFlorio RM, Green ED, Heller SL, et al. ACR Appropriateness Criteria(®) Monitoring Response to Neoadjuvant Systemic Therapy For Breast Cancer. *J Am Coll Radiol* (2017) 14(11s):S462^{TM}75. doi: 10.1016/j.jacr.2017.08.037
4. Valdés-Ferrada J, Muñoz-Durango N, Pérez-Sepulveda A, Muñiz S, Coronado-Arrázola I, Acevedo F, et al. Peripheral Blood Classical Monocytes and Plasma Interleukin 10 Are Associated to Neoadjuvant Chemotherapy Response in Breast Cancer Patients. *Front Immunol* (2020) 11:1413. doi: 10.3389/fimmu.2020.01413
5. Xiong Q, Zhou X, Liu Z, Lei C, Yang C, Yang M, et al. Multiparametric MRI-Based Radiomics Analysis for Prediction of Breast Cancers Insensitive to Neoadjuvant Chemotherapy. *Clin Transl Oncol* (2020) 22(1):50–9. doi: 10.1007/s12094-019-02109-8
6. Liu W, Chen W, Zhang X, Zhao P, Fan Z, Bi L, et al. Higher Efficacy and Reduced Adverse Reactions in Neoadjuvant Chemotherapy for Breast Cancer by Using Pegylated Liposomal Doxorubicin Compared With Pirarubicin. *Sci Rep* (2021) 11(1):199. doi: 10.1038/s41598-020-80415-w
7. Wang BC, Fu C, Xie LK, Kuang BH, Zhao YX. Comparative Toxicities of Neoadjuvant Chemotherapy With or Without Bevacizumab in HER2-Negative Breast Cancer Patients: A Meta-Analysis. *Ann Pharmacother* (2020) 54(6):517–25. doi: 10.1177/1060028019895783
8. Spring LM, Fell G, Arfe A, Sharma C, Greenup R, Reynolds KL, et al. Pathologic Complete Response After Neoadjuvant Chemotherapy and Impact on Breast Cancer Recurrence and Survival: A Comprehensive Meta-Analysis. *Clin Cancer Res* (2020) 26(12):2838–48. doi: 10.1158/1078-0432.Ccr-19-3492
9. Fusco R, Sansone M, Granata V, Di Bonito M, Avino F, Catalano O, et al. Use of Quantitative Morphological and Functional Features for Assessment of Axillary Lymph Node in Breast Dynamic Contrast-Enhanced Magnetic Resonance Imaging. *BioMed Res Int* (2018) 2018:2610801. doi: 10.1155/2018/2610801
10. La Forgia D, Vestito A, Lasciarrea M, Comes MC, Diotaiuti S, Giotta F, et al. Response Predictivity to Neoadjuvant Therapies in Breast Cancer: A Qualitative Analysis of Background Parenchymal Enhancement in DCE-MRI. *J Pers Med* (2021) 11(4):256. doi: 10.3390/jpm11040256
11. Harada TL, Uematsu T, Nakashima K, Kawabata T, Nishimura S, Takahashi K, et al. Evaluation of Breast Edema Findings at T2-Weighted Breast MRI Is Useful for Diagnosing Occult Inflammatory Breast Cancer and Can Predict Prognosis After Neoadjuvant Chemotherapy. *Radiology* (2021) 299(1):53–62. doi: 10.1148/radiol.2021202604
12. Partridge SC, Zhang Z, Newitt DC, Gibbs JE, Chenevert TL, Rosen MA, et al. Diffusion-Weighted Mri Findings Predict Pathologic Response in Neoadjuvant Treatment of Breast Cancer: The Acrin 6698 Multicenter Trial. *Radiology* (2018) 289(3):618–27. doi: 10.1148/radiol.2018180273
13. Marino MA, Helbich T, Baltzer P, Pinker-Domenig K. Multiparametric MRI of the Breast: A Review. *J Magn Reson Imaging* (2018) 47(2):301–15. doi: 10.1002/jmri.25790
14. Conti A, Duggento A, Indovina I, Guerrisi M, Toschi N. Radiomics in Breast Cancer Classification and Prediction. *Semin Cancer Biol* (2021) 72:238–50. doi: 10.1016/j.semcancer.2020.04.002
15. Kim JY, Park JE, Jo Y, Shim WH, Nam SJ, Kim JH, et al. Incorporating Diffusion- and Perfusion-Weighted MRI Into a Radiomics Model Improves Diagnostic Performance for Pseudoprogression in Glioblastoma Patients. *Neuro Oncol* (2019) 21(3):404–14. doi: 10.1093/neuonc/noy133

16. Horvat N, Veeraraghavan H, Khan M, Blazic I, Zheng J, Capanu M, et al. MR Imaging of Rectal Cancer: Radiomics Analysis to Assess Treatment Response After Neoadjuvant Therapy. *Radiology* (2018) 287(3):833–43. doi: 10.1148/radiol.2018172300
17. Fang J, Zhang B, Wang S, Jin Y, Wang F, Ding Y, et al. Association of MRI-Derived Radiomic Biomarker With Disease-Free Survival in Patients With Early-Stage Cervical Cancer. *Theranostics* (2020) 10(5):2284–92. doi: 10.7150/thno.37429
18. Leech M, Osman S, Jain S, Marignol L. Mini Review: Personalization of the Radiation Therapy Management of Prostate Cancer Using MRI-Based Radiomics. *Cancer Lett* (2021) 498:210–16. doi: 10.1016/j.canlet.2020.10.033
19. Kim SY, Cho N, Choi Y, Lee SH, Ha SM, Kim ES, et al. Factors Affecting Pathologic Complete Response Following Neoadjuvant Chemotherapy in Breast Cancer: Development and Validation of a Predictive Nomogram. *Radiology* (2021) 299(2):290–300. doi: 10.1148/radiol.2021203871
20. Budzik MP, Fudalej MM, Badowska-Kozakiewicz AM. Histopathological Analysis of Mucinous Breast Cancer Subtypes and Comparison With Invasive Carcinoma of No Special Type. *Sci Rep* (2021) 11(1):5770. doi: 10.1038/s41598-021-85309-z
21. Kim J, Kim JY, Lee HB, Lee YJ, Seong MK, Paik N, et al. Characteristics and Prognosis of 17 Special Histologic Subtypes of Invasive Breast Cancers According to World Health Organization Classification: Comparative Analysis to Invasive Carcinoma of No Special Type. *Breast Cancer Res Treat* (2020) 184(2):527–42. doi: 10.1007/s10549-020-05861-6
22. Gradishar WJ, Anderson BO, Abraham J, Aft R, Agnese D, Allison KH, et al. Breast Cancer, Version 3.2020, NCCN Clinical Practice Guidelines in Oncology. *J Natl Compr Canc Netw* (2020) 18(4):452–78. doi: 10.6004/jnccn.2020.0016
23. Chen S, Shu Z, Li Y, Chen B, Tang L, Mo W, et al. Machine Learning-Based Radiomics Nomogram Using Magnetic Resonance Images for Prediction of Neoadjuvant Chemotherapy Efficacy in Breast Cancer Patients. *Front Oncol* (2020) 10:1410. doi: 10.3389/fonc.2020.01410
24. Gómez-Flores W, Hernández-López J. Assessment of the Invariance and Discriminant Power of Morphological Features Under Geometric Transformations for Breast Tumor Classification. *Comput Methods Programs BioMed* (2020) 185:105173. doi: 10.1016/j.cmpb.2019.105173
25. Comes MC, Fanizzi A, Bove S, Didonna V, Diotaiuti S, La Forgia D, et al. Early Prediction of Neoadjuvant Chemotherapy Response by Exploiting a Transfer Learning Approach on Breast DCE-MRIs. *Sci Rep* (2021) 11(1):14123. doi: 10.1038/s41598-021-93592-z
26. Braman NM, Etesami M, Prasanna P, Dubchuk C, Gilmore H, Tiwari P, et al. Intratumoral and Peritumoral Radiomics for the Pretreatment Prediction of Pathological Complete Response to Neoadjuvant Chemotherapy Based on Breast DCE-MRI. *Breast Cancer Res* (2017) 19(1):57. doi: 10.1186/s13058-017-0846-1
27. Chen X, Chen X, Yang J, Li Y, Fan W, Yang Z. Combining Dynamic Contrast-Enhanced Magnetic Resonance Imaging and Apparent Diffusion Coefficient Maps for a Radiomics Nomogram to Predict Pathological Complete Response to Neoadjuvant Chemotherapy in Breast Cancer Patients. *J Comput Assist Tomogr* (2020) 44(2):275–83. doi: 10.1097/rct.0000000000000978
28. Bian T, Wu Z, Lin Q, Wang H, Ge Y, Duan S, et al. Radiomic Signatures Derived From Multiparametric MRI for the Pretreatment Prediction of Response to Neoadjuvant Chemotherapy in Breast Cancer. *Br J Radiol* (2020) 93(1115):20200287. doi: 10.1259/bjr.20200287
29. Hu C, Zheng D, Cao X, Pang P, Fang Y, Lu T, et al. Application Value of Magnetic Resonance Radiomics and Clinical Nomograms in Evaluating the Sensitivity of Neoadjuvant Chemotherapy for Nasopharyngeal Carcinoma. *Front Oncol* (2021) 11:740776. doi: 10.3389/fonc.2021.740776
30. Zhou J, Lu J, Gao C, Zeng J, Zhou C, Lai X, et al. Predicting the Response to Neoadjuvant Chemotherapy for Breast Cancer: Wavelet Transforming Radiomics in MRI. *BMC Cancer* (2020) 20(1):100. doi: 10.1186/s12885-020-6523-2
31. Goorts B, van Nijnatten TJ, de Munck L, Moossdorff M, Heuts EM, de Boer M, et al. Clinical Tumor Stage Is the Most Important Predictor of Pathological Complete Response Rate After Neoadjuvant Chemotherapy in Breast Cancer Patients. *Breast Cancer Res Treat* (2017) 163(1):83–91. doi: 10.1007/s10549-017-4155-2
32. Şahin AB, Cubukcu E, Ocak B, Deligonul A, Oyucu Orhan S, Tolunay S, et al. Low Pan-Immune-Inflammation-Value Predicts Better Chemotherapy Response and Survival in Breast Cancer Patients Treated With Neoadjuvant Chemotherapy. *Sci Rep* (2021) 11(1):14662. doi: 10.1038/s41598-021-94184-7
33. Baumgartner A, Tausch C, Hosch S, Papassotiropoulos B, Varga Z, Rageth C, et al. Ultrasound-Based Prediction of Pathologic Response to Neoadjuvant Chemotherapy in Breast Cancer Patients. *Breast* (2018) 39:19–23. doi: 10.1016/j.breast.2018.02.028
34. Ma W, Zhao Y, Ji Y, Guo X, Jian X, Liu P, et al. Breast Cancer Molecular Subtype Prediction by Mammographic Radiomic Features. *Acad Radiol* (2019) 26(2):196–201. doi: 10.1016/j.acra.2018.01.023
35. Zhang HX, Sun ZQ, Cheng YG, Mao GQ. A Pilot Study of Radiomics Technology Based on X-Ray Mammography in Patients With Triple-Negative Breast Cancer. *J Xray Sci Technol* (2019) 27(3):485–92. doi: 10.3233/xst-180488
36. Liu Z, Li Z, Qu J, Zhang R, Zhou X, Li L, et al. Radiomics of Multiparametric MRI for Pretreatment Prediction of Pathologic Complete Response to Neoadjuvant Chemotherapy in Breast Cancer: A Multicenter Study. *Clin Cancer Res* (2019) 25(12):3538–47. doi: 10.1158/1078-0432.Ccr-18-3190
37. Zhang L, Jiang X, Xie X, Wu Y, Zheng S, Tian W, et al. The Impact of Preoperative Radiomics Signature on the Survival of Breast Cancer Patients With Residual Tumors After NAC. *Front Oncol* (2020) 10:523327. doi: 10.3389/fonc.2020.523327

Conflict of Interest: The authors declare that the research was conducted in the absence of any commercial or financial relationships that could be construed as a potential conflict of interest.

Publisher's Note: All claims expressed in this article are solely those of the authors and do not necessarily represent those of their affiliated organizations, or those of the publisher, the editors and the reviewers. Any product that may be evaluated in this article, or claim that may be made by its manufacturer, is not guaranteed or endorsed by the publisher.

Copyright © 2022 Zhu, Shen, Zhang, Wang, Zhang, Yu, Zhang, Song, Guo, Zhang, Zhu and Wu. This is an open-access article distributed under the terms of the Creative Commons Attribution License (CC BY). The use, distribution or reproduction in other forums is permitted, provided the original author(s) and the copyright owner(s) are credited and that the original publication in this journal is cited, in accordance with accepted academic practice. No use, distribution or reproduction is permitted which does not comply with these terms.

frontiers | Frontiers in Oncology

ORIGINAL RESEARCH
published: 07 June 2022
doi: 10.3389/fonc.2022.903372

Improved Prediction of Survival Outcomes Using Residual Cancer Burden in Combination With Ki-67 in Breast Cancer Patients Underwent Neoadjuvant Chemotherapy

*Ji-Yeon Kim[1,2], Jung Min Oh[2], Se Kyung Lee[3], Jonghan Yu[3], Jeong Eon Lee[3,4], Seok Won Kim[3], Seok Jin Nam[3], Yeon Hee Park[1,2,4], Jin Seok Ahn[1], Kyunga Kim[5,6,7] and Young-Hyuck Im[1,2,4]**

[1] Division of Hematology–Oncology, Department of Medicine, Samsung Medical Center, Sungkyunkwan University School of Medicine, Seoul, South Korea, [2] Biomedical Research Institute, Samsung Medical Center, Sungkyunkwan University School of Medicine, Seoul, South Korea, [3] Department of Surgery, Samsung Medical Center, Sungkyunkwan University School of Medicine, Seoul, South Korea, [4] Department of Health Sciences and Technology, Samsung Advanced Institute for Health Sciences & Technology, Sungkyunkwan University, Seoul, South Korea, [5] Department of Data Convergence and Future Medicine, Samsung Medical Center, Sungkyunkwan University School of Medicine, Seoul, South Korea, [6] Department of Digital Health, Samsung Advanced Institute for Health Sciences & Technology, Sungkyunkwan University, Seoul, South Korea, [7] Biomedical Statistics Center, Research Institute for Future Medicine, Samsung Medical Center, Seoul, South Korea

OPEN ACCESS

Edited by:
Raffaella Massafra, National Cancer Institute Foundation (IRCCS), Italy

Reviewed by:
Shuo Zhang, ShengJing Hospital of China Medical University, China
Rui Chen, Affiliated Hospital of Zunyi Medical University, China

***Correspondence:**
Young-Hyuck Im
imyh00@skku.edu

Specialty section:
This article was submitted to Breast Cancer, a section of the journal Frontiers in Oncology

Received: *24 March 2022*
Accepted: *09 May 2022*
Published: *07 June 2022*

Citation:
Kim J-Y, Oh JM, Lee SK, Yu J, Lee JE, Kim SW, Nam SJ, Park YH, Ahn JS, Kim K and Im Y-H (2022) Improved Prediction of Survival Outcomes Using Residual Cancer Burden in Combination With Ki-67 in Breast Cancer Patients Underwent Neoadjuvant Chemotherapy. Front. Oncol. 12:903372. doi: 10.3389/fonc.2022.903372

We developed a model for improving the prediction of survival outcome using postoperative Ki-67 value in combination with residual cancer burden (RCB) in patients with breast cancer (BC) who underwent neoadjuvant chemotherapy (NAC). We analyzed the data from BC patients who underwent NAC between 2010 and 2019 at Samsung Medical Center and developed our residual proliferative cancer burden (RPCB) model using semi-quantitative Ki-67 value and RCB class. The Cox proportional hazard model was used to develop our RPCB model according to disease free survival (DFS) and overall survival (OS). In total, 1,959 patients were included in this analysis. Of 1,959 patients, 905 patients were excluded due to RCB class 0, and 32 were due to a lack of Ki-67 data. Finally, an RPCB model was developed using data from 1,022 patients. The RPCB score was calculated for DFS and OS outcomes, respectively (RPCB-DFS and RPCB-OS). For further survival analysis, we divided the population into 3 classes according to the RPCB score. In the prediction of DFS, C-indices were 0.751 vs 0.670 and time-dependent areas under the receiver operating characteristic curves (AUCs) at 3-year were 0.740 vs 0.669 for RPCB-DFS and RCB models, respectively. In the prediction of OS, C-indices were 0.819 vs 0.720 and time-dependent AUCs at 3-year were 0.875 vs 0.747 for RPCB-OS and RCB models, respectively. The RPCB model developed using RCB class and semi-quantitative Ki-67 had superior predictive value for DFS and OS compared with that of RCB class. This prediction model could provide the basis to decide risk-stratified treatment plan for BC patients who had residual disease after NAC.

Keywords: neoadjuvant chemotherapy, Ki-67, residual cancer burden, prediction model, breast cancer, residual proliferative cancer burden

INTRODUCTION

Neoadjuvant chemotherapy (NAC) is a standard therapeutic strategy for patients with locally advanced breast cancer (BC) (1). NAC can reduce tumor burden and downsize tumor mass, resulting in increasing the possibility of breast conservation and avoiding axillary dissection and rendering inoperable tumors operable ones (2–5). More importantly, NAC provides the rationale for de-escalation of surgery in both the breast and axilla and for risk-stratified treatment after curative surgery in BC patients who undergo NAC (1, 6, 7).

A large number of studies have shown that patients who achieve a pathological complete response (pCR) to NAC in both primary breast tissue and ipsilateral axillary lymph nodes have significantly longer overall survival (OS) and disease-free survival (DFS) (8). Additionally, residual cancer burden (RCB) was a significant long-term predictor of DFS and OS in all subtypes of BC (9, 10). In the I-SPY 2 trial, it was suggested that the RCB score could be used to assess the outcomes of novel agents in combination with a standard NAC backbone (11, 12).

However, some patients who achieved pCR have undergone BC recurrence, and the others with RCB III class have had long DFS and OS.

Ki-67 is a nuclear protein expressed in the G1, S, and G2 phases of the cell cycle and not in the resting G0 phase, and it is one of the proliferation markers in many cancers (13). High expression of Ki-67 in tumor cells is associated with tumor growth, higher tumor grades, and poorer survival in breast cancer. Since Ki-67 indicates tumor biology such as tumor growth activity, assessment of Ki-67 can be used to estimate the tumor response to therapies that specifically target dividing cells, such as chemotherapy in particular (14).

Several studies have evaluated the prognostic and/or predictive values of Ki-67. According to these previous studies, a high pCR rate was associated with a high Ki-67 level with statistical significance (15). Additionally, the post-chemotherapeutic Ki-67 value was a strong predictor of survival for BC patients not achieving a pCR (16).

We hypothesized the combination of the biological index of Ki67 with the anatomic index of RCB would provide more prognostic information than either alone. In this study, we developed a prognostic model of BC treated with NAC using an anatomic index of RCB in combination with a biological index of Ki-67. We evaluated the prognostic values of the clinical and pathological characteristics of BC at baseline and curative surgery and made a prognostic model that cooperated with these clinical factors.

METHODS

Patients

We retrospectively analyzed BC patients diagnosed with clinical stages II to IIIC BC who underwent NAC followed by curative surgery at the Samsung Medical Center between January 2010 and December 2019. Among these patients, patients who received the second operation for ipsilateral or contralateral BC due to local recurrence after initial curative surgery or palliative operation with stage IV disease were excluded. We also excluded patients who underwent surgery for bilateral BC. This study was reviewed and approved by the Institutional Review Board (IRB) of Samsung Medical Center, Seoul, Korea (IRB No. 2019-04-021) with an informed consent waiver due to the use of medical records with retrospective clinical data. This study was conducted in accordance with the Declaration of Helsinki.

Breast Cancer Pathology

All pathological specimens were reviewed by experienced pathologists who determined primary tumor characteristics based on biopsy specimens obtained for BC diagnosis. Pathologists determined BC histology and receptor status (estrogen receptor [ER], progesterone receptor [PgR], and human epidermal growth factor receptor-2 [HER2]) according to hematoxylin and eosin (H&E) and immunohistochemical (IHC) staining (17). In terms of Ki-67, pathologists assessed it by IHC on the Ventana Discovery autostainer using the antibody MIB-1 as previously described (18). For semiquantitative analysis, signals for Ki-67 were graded by two expert pathologists as follows: 0–25%, 1+; more than 25–50%, 2+; more than 50–75%, 3+; more than 75%, 4+. Histologic grade and nuclear grade were also evaluated by Bloom–Ricardson grading and the World Health Organization grading system (19).

Pathologists determined the pathological response to NAC using surgical specimens. Pathologic complete response was defined as no residual invasive tumor in both the primary tumor bed and ipsilateral axillary lymph nodes (ypT0/Tis, N0) (20). An RCB class was also calculated based on pathological characteristics at surgery (9).

Statistical Analysis

Disease-free survival (DFS) was defined as the elapsed time from the date of curative surgery to detect any recurrences, including loco-regional and distant metastases. Overall survival (OS) was defined as the duration between curative surgery and death. DFS and OS were analyzed using the Kaplan–Meier method. Differences among the groups with different characteristics were estimated using the t-test in univariate analysis. In multivariate analysis, Cox proportional-hazards regression was used to estimate hazard ratios (HRs), concordance indexes (c-indexes), and 95% confidence intervals (CIs). Statistical analyses were executed with R version 4.0.1 (R Foundation for Statistical Computing, Vienna, Austria; http://cran.r-project.org). Two-tailed p-values of <0.05 were considered statistically significant in all analyses.

Prediction Model Development

A prediction model for DFS and OS was developed on the basis of semi-quantitative Ki-67 grade (range 1–4) and RCB class (range 1–3). We developed RPCB, which was calculated as the sum across all parameters of the Cox-coefficient for the particular parameter, multiplied by the parameter value of the patient.

*b1*and *b2* were coefficients from the Cox model of RCB class and semi-quantitative Ki-67 grade.

RPCB = *b1*(RCB class) +*b2*(ln[semi-quantitative Ki67 grade + 0.1]) (21)

Performance comparison of the RPCB score system, RCB class, and Ki-67 grade was performed using Cox proportional-hazards regression. The binary logistic regression method was used for the 3-year survival prediction model development. We calculated the area under the curve (AUC) of the receiver operating characteristic (ROC) curve.

For data validation, we performed internal validation with 500 bootstrap resampling datasets (out of bag data used for testing sets).

RESULTS

Clinical and Pathological Characteristics

In all, 2,851 patients with BC who received NAC at the Samsung Medical Center from 2010 to 2019 were analyzed (**Figure 1**). Among 2,851 patients, 73 with bilateral BC and 42 with no pathologic information were excluded from further analysis. We further excluded 777 patients because their RCB score could not be calculated due to a lack of pathological information at the operation. Therefore, 1,959 BC patients were included in our analysis. We have described the pathological and clinical characteristics of the patients in **Supplementary Table 1**.

Clinical Characteristics and Survival Outcome

We performed multivariate analysis to evaluate the relationship between clinical characteristics and survival outcome. We observed 220 cases of distant recurrence of BC and 81 cases of BC-related death. The median follow-up duration was 37 months (InterQuartile Range [IQR]: 18.9–48.3). Advanced clinical stage (HR of stage IIIC vs. IIA: 3.053; p <0.001), high expression of Ki-67 at curative surgery (HR of Ki-67 4+ vs. 1+: 4.080; p <0.001) and high score of the RCB class (HR of class III vs. I: 2.749; p <0.001) were associated with poor DFS (**Table 1**). In OS, high expression of Ki-67 at curative surgery (HR of Ki-67 4+ vs. 1+: 7.624, p = 0.015) and high score of RCB class (HR of class III vs. I: 2.749, p <0.001) affected to a poor survival outcome (**Supplementary Table 2**).

Survival Model According to Expression of Postop. Ki-67 in RCB Class

We performed survival analysis according to Ki-67 grade in each RCB class. In DFS, postop Ki-67 at curative surgery had a prognostic value in RCB class I (p = 0.011), class II (p = 0.001), and class III (p <0.001) (**Supplementary Figures 1A–C**). In OS, postop. Ki-67 did not have prognostic value in RCB class I (p = 0.378) but did in class II (p = 0.012) and class III (p <0.001) (**Supplementary Figures 1D–F**). These findings suggest the possibility that the addition of Ki-67 to the RCB class might improve the accuracy of prediction for DFS and OS in patients who are undergoing NAC with BC.

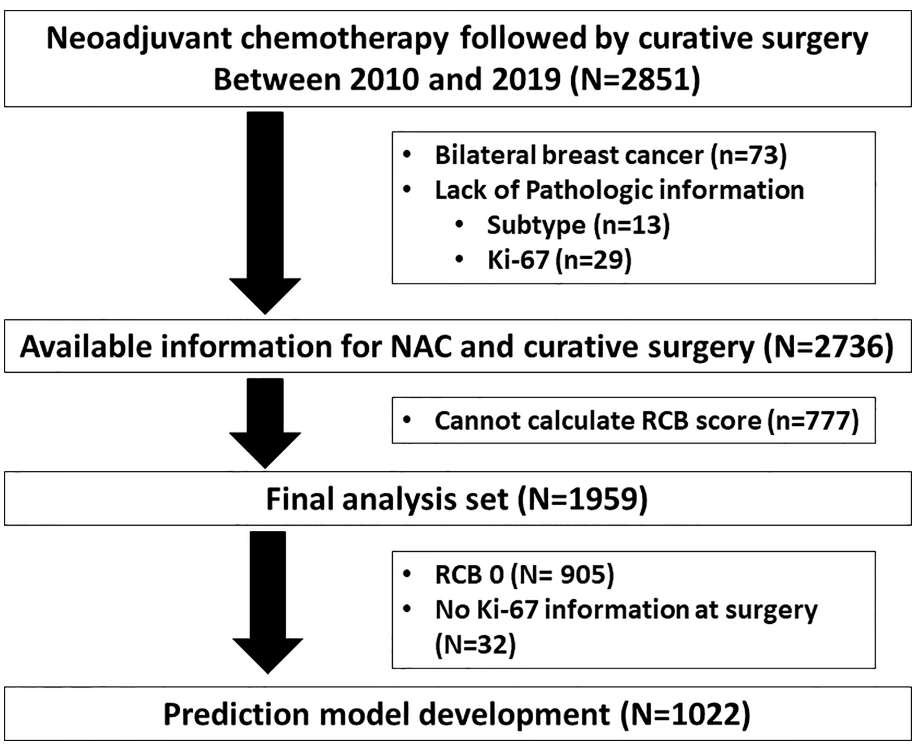

FIGURE 1 | Consort diagram.

TABLE 1 | Disease free survival prediction according to RCB class, Ki-67 and RPCB model.

Model 1		coef	Se(coef)	z	Pr(>|z|)	Type III p-value	Hazard ratio	95% CI[1] of HR[2]		C-index	95% CI of C-index	
RCB[3]	2 vs 1	0.715	0.291	2.456	0.014	<.001	2.045	1.155	3.619	0.670	0.632	0.708
	3 vs 1	1.818	0.291	6.253	<.001		6.161	3.485	10.894			
Model 2		**coef**	**Se (coef)**	**z**	**Pr(>|z|)**	**Type III p-value**	**Hazard ratio**	**95% CI of HR**		**C-index**	**95% CI of C-index**	
Ki-67	2 vs 1	1.010	0.240	4.213	<.001	<.001	2.746	1.716	4.393	0.699	0.661	0.736
	3 vs 1	1.024	0.225	4.545	<.001		2.785	1.790	4.330			
	4 vs 1	1.511	0.192	7.855	<.001		4.530	3.107	6.603			
Model 3		**coef**	**Se (coef)**	**z**	**Pr(>|z|)**	**Type III p-value**	**Hazard ratio**	**95% CI of HR**		**C-index**	**95% CI of C-index**	
RPCB[4]-DFS[5]		1.000	0.089	11.290	<.001		2.718	2.285	3.233	0.751	0.710	0.792
RCB	2 vs 1	0.411	0.294	1.398	0.162	<.001	1.509	0.848	2.685			
	3 vs 1	1.602	0.292	5.485	<.001		4.964	2.800	8.800			
Ki-67	2 vs 1	0.927	0.240	3.860	<.001	<.001	2.526	1.578	4.043			
	3 vs 1	1.007	0.226	4.455	<.001		2.736	1.757	4.260			
	4 vs 1	1.497	0.195	7.670	<.001		4.467	3.047	6.547			

[1]Confidence interval; [2]Hazard ratio; [3]Residual cancer burden; [4]Residual proliferative cancer burden; [5]Disease free survival.

Residual Proliferative Cancer Burden Model for DFS and OS

For development of the RPCB model for DFS and OS, we excluded cases of RCB 0 and those of the absence of Ki-67 value at curative surgery (**Figure 1**). In 1,022 cases, disease recurrence from BC was 170 (16.6%) and BC related death was 68 (6.7%) (**Supplementary Table 3**).

RPCB model had 2.718 in HR (95% of CI: 2.285, 3.233) and 0.751 in c-index (95% CI: 0.710, 0.792) (**Table 1**). In the RPCB model, RCB class and Ki-67 maintained their predictive capacities (HR of RCB class II vs. I: 1.509, III vs. I: 4.964, p <0.001; HR of Ki-67 4+ vs. 1+: 4.467, 3+ vs. 1+: 2.736, 2+ vs. 1+: 2.526, p <0.001). Compared with the prediction model of the RCB class and that of Ki-67, the RPCB model had superior predictive capacity (c-index of RCB model: 0.670, 95% CI: 0.632, 0.708; c-index of Ki-67: 0.699, 95% CI: 0.661, 0.736).

RPCB model for OS had 2.718 in HR (95% of CI: 2.169, 3.407) and 0.819 in c-index (95% CI: 0.755, 0.883) (**Table 2**). RPCB model had more precisely predicted OS compared with the RCB class and Ki-67 (c-index of the RCB model: 0.720, [95% of CI: 0.660, 0.779]; c-index of Ki-67: 0.750, [95% of CI: 0.695, 0.805]).

Three Year DFS Prediction According to RPCB Model

We divided them into three classes of the RPCB model according to their value. After making the RPCB class, we performed survival analysis in terms of 3-year DFS. In the RPCB model, there were 94.5% of 3-year DFS in RCB 0, 90.6% in RPCB class I, 77.3% in class II, and 38.9% in class III (p <0.001) (**Figures 2A-B**). HR of RPCB class I was 1.75 (95% CI: 1.14, 2.68), 4.04 of RPCB class II (95% CI: 2.78, 5.86), and 18.24 of RPCB class III (95% CI: 12.48, 26.65) compared with RCB 0.

In the RCB class model, the 3-year DFS of RCB 0 was 94.5%, 93.4% in RCB class I, 82.3% in class II, and 58.5% in class III (p <0.001) (**Supplementary Figure 2A**). HR of RCB class I vs. pCR was 1.41 (95% CI: 0.79, 2.52), 3.08 of RCB class II (95% CI: 2.14, 4.43), and 9.45 of RCB class II (95% CI: 6.58, 13.58). Additionally, Ki-67 model had 88.6% of 3-year DFS in 1+, 71.2% in 2+, 72.7% in 3+, and 61.6% in 4+ (p <0.001) (**Supplementary Figure 2B**). HR of 1.98 in the Ki-67 1+ group (95% CI: 1.33, 2.95), 5.43 of Ki-67 2+ (95% CI: 3.38, 9.71), 5.54 of Ki-67 3+ (3.55, 8.64), and 9.01 of Ki-67 4+ (95% CI: 6.15, 13.18).

TABLE 2 | Overall survival prediction according to RCB class, Ki-67 and RPCB model.

Model 1		coef	Se(coef)	z	Pr(>|z|)	Type IIIp-value	Hazard ratio	95% CI[1] of HR[2]		C-index	95% CI of C-index	
RCB[3]	2 vs 1	1.783	0.743	2.401	0.016	<.001	5.949	1.388	25.501	0.720	0.660	0.779
	3 vs 1	3.070	0.741	4.142	<.001		21.534	5.039	92.035			
Model 2		**coef**	**Se (coef)**	**z**	**Pr(>|z|)**	**Type III p-value**	**Hazard ratio**	**95% CI of HR**		**C-index**	**95% CI of C-index**	
Ki-67	2 vs 1	1.848	0.484	3.818	<.001	<.001	6.345	2.458	16.382	0.750	0.695	0.805
	3 vs 1	2.297	0.442	5.194	<.001		9.949	4.181	23.675			
	4 vs 1	2.663	0.419	6.359	<.001		14.344	6.312	32.598			
Model 3		**coef**	**Se (coef)**	**z**	**Pr(>|z|)**	**Type III p-value**	**Hazard ratio**	**95% CI of HR**		**C-index**	**95% CI of C-index**	
RPCB[4]-OS[5]		1.000	0.115	8.677	<.001		2.718	2.169	3.407	0.819	0.755	0.883
RCB	2 vs 1	1.185	0.739	1.604	0.109	<.001	3.272	0.769	13.919			
	3 vs 1	2.575	0.733	3.511	<.001		13.133	3.119	55.300			
Ki-67	2 vs 1	1.606	0.485	3.308	0.001	<.001	4.983	1.924	12.904			
	3 vs 1	2.166	0.443	4.888	<.001		8.719	3.659	20.777			
	4 vs 1	2.579	0.422	6.115	<.001		13.184	5.768	30.135			

[1]Confidence interval; [2]Hazard ratio; [3]Residual cancer burden; [4]Residual proliferative cancer burden; [5]Overall survival.

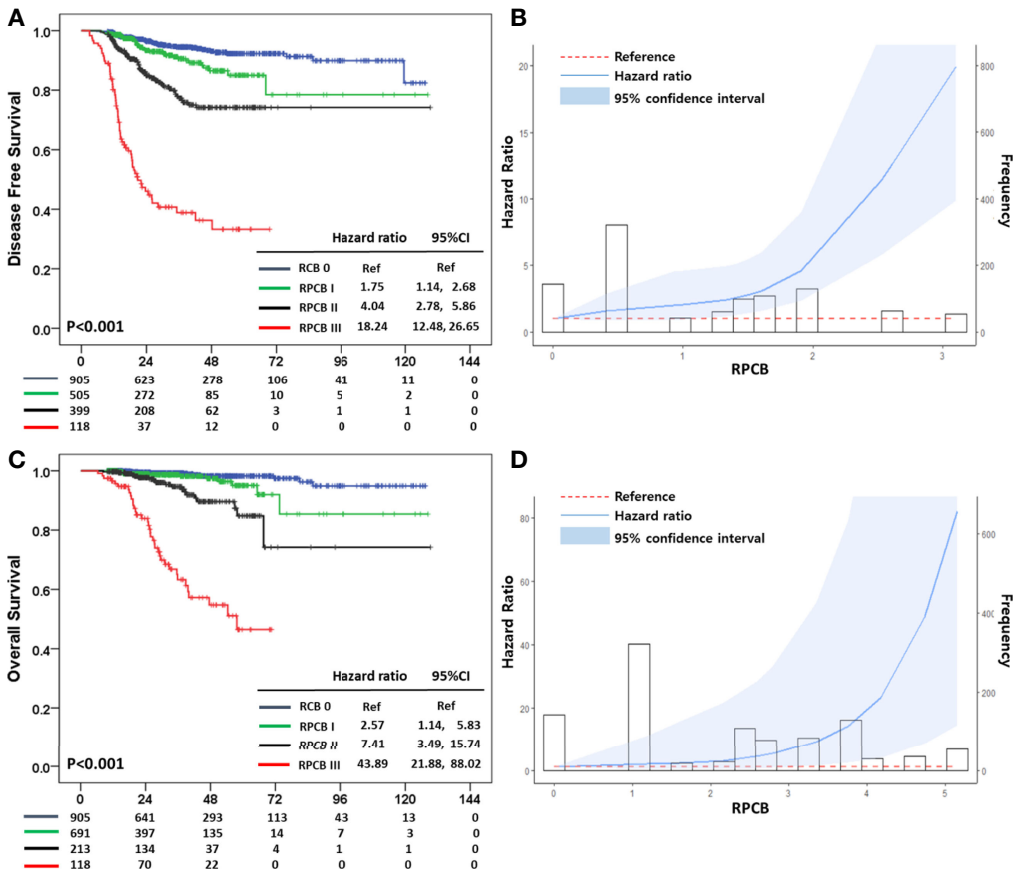

FIGURE 2 | **(A)** Disease Free Survival (DFS) according to Residual Proliferative Cancer Burden (RPCB) class after neoadjuvant chemotherapy (NAC), **(B)** Hazard ratio (HR) according to RPCB score for DFS, **(C)** Overall Survival (OS) according to RPCB after NAC, **(D)** HR according to RPCB score for OS.

In the 3-year DFS prediction model, the AUC of the RPCB model was 0.740 (95% CI: 0.691, 0.789) compared with 0.669 of the RCB model (95% CI: 0.621, 0.716), and 0.673 of Ki-67 (95% CI: 0.621, 0.726) (**Supplementary Figures 3A–C**).

We performed internal validation with 500 bootstrap resampling datasets. In DFS, the c-index of internal validation of the RPCB model was 0.751 (95% CI: 0.710, 0.792) and the AUC of the 3-year DFS model was 0.741 (95% CI: 0.692, 0.789) (**Table 3**).

Three Year OS Prediction According to RPCB Model

In terms of 3-year OS, RCB 0 was 99.3%, 98.6% in RPCB class I, 94.6% in class II, and 63.3% in class III (p <0.001) (**Figures 2C, D**). In OS, the HR of RPCB class I was 2.57 (95% CI: 1.14, 5.83), 7.41 of RPCB class II (95% CI: 3.49, 15.74), and 43.89 of RPCB class III (95% CI: 21.88, 88.02) compared with RCB 0.

The RCB class model had 99.4% of 3-year OS in RCB class I, 95.8% in class II, and 79.5% in class III (**Supplementary Figure 2C**).

TABLE 3 | Internal validation of RPCB_OS and RPCB_DFS model.

	HR[1]	95% CI[2] of HR		C-index	95% CI of C-index		AUC[3] at 3Y[4]	95% CI of AUC	
RPCB[5]_OS[6]									
Original	2.718	2.169	3.407	0.819	0.755	0.883	0.875	0.822	0.928
Validation	2.822	1.884	3.761	0.818	0.752	0.884	0.873	0.819	0.928
RPCB_DFS[7]									
Original	2.718	2.285	3.233	0.751	0.710	0.792	0.740	0.691	0.789
Validation	2.764	2.092	3.437	0.751	0.710	0.792	0.741	0.692	0.789

[1]Hazard ratio; [2]Confidence interval; [3]Area under curve; [4]Year; [5]Residual proliferative cancer burden; [6]Overall survival; 7: Disease free survival.

The HR of RCB I was 1.36 (95% CI: 0.38, 4.81), 6.17 of RCB II (95% CI: 3.03, 12.53), and 22.83 of RCB III (95% CI: 11.39, 45.76). According to Ki-67 grade, 98.6% in 1+, 93.9% in 2+, 86.3% in 3+, and 77.6% in 4+ (p<0.001) for 3-year OS, and we observed 1.49 of Ki-67 1+ in HR (95% CI: 0.58, 3.84), 9.42 of Ki-67 2+ (95% CI: 4.11, 21.58), 14.88 of Ki-67 3+ (95% CI: 7.11, 31.12), and 21.52 of Ki-67 4+ (95% CI: 10.85, 42.72) (**Supplementary Figure 2D**). In the 3-year OS of the RPCB model, 0.875 in AUC was observed (95% CI: 0.822, 0.928) compared with 0.747 in RCB class (95% CI: 0.684, 0.810) and 0.811 in Ki-67 grade (95% CI: 0.758, 0.862) (**Supplementary Figures 3D-F**).

Internal validation for OS presented that the c-index of internal validation was 0.818 (95% CI: 0.752, 0.884) and the AUC of the 3-year OS model was 0.873 (95% CI: 0.819, 0.928) (**Table 3**).

RPCB Prediction Model According to BC Subtypes

The prediction value of the RPCB prediction model according to BC subtypes was analyzed. In DFS, RPCB class I in hormone receptor+HER2− BC had an HR of 6.38 (95% CI: 1.14, 28.91), 13.71 in class II (95% CI: 3.06, 61.42), and 36.75 in class III (95% CI: 7.91, 170.67) compared with RCB 0 (p <0.001) (**Figure 3A**). In TNBC, RPCB class I had an HR of 1.72 (95% CI: 0.90, 4.12), 4.51 in class II (95% CI: 2.49, 8.18), and 19.90 in class III (95% CI: 11.10, 35.67) compared with pCR (p <0.001) (**Figure 3B**). In HER2+ BC, HR of 2.17 in RPCB class I (95% CI: 1.14, 5.83), 7.41 of class II (95% CI: 3.49, 15.74), and 43.89 of class III (95% CI: 21.88, 88.02) (p <0.001) (**Figure 3C**).

In OS, the pCR group in hormone receptor +HER2− BC did not experience any death events, and therefore we calculated HR compared with RPCB class I. In hormone receptor+HER2− BC, the HR of RPCB class II was 1.81 (95% CI: 0.16, 20.04) and 43.89 of RPCB class III (95% CI: 4.69, 242.42) (p <0.001) (**Figure 4A**). The RPCB model also well predicted OS in TNBC as well as HER2+ BC. RPCB class I had HR of 3.74 (95% CI: 1.24, 11.33), 7.31 of class II (95% CI: 2.68, 19.94), and 37.31 of class III (95% CI: 14.49, 96.11) compared with pCR group (p <0.001) (**Figure 4B**). Additionally, HR was 1.19 of class I (95% CI: 0.24, 5.97), 2.26 of class II (95% CI: 0.27, 18.86), and 27.30 of class III (95% CI: 6.36, 117.27) compared with pCR group in HER2+ BC (p <0.001) (**Figure 4C**).

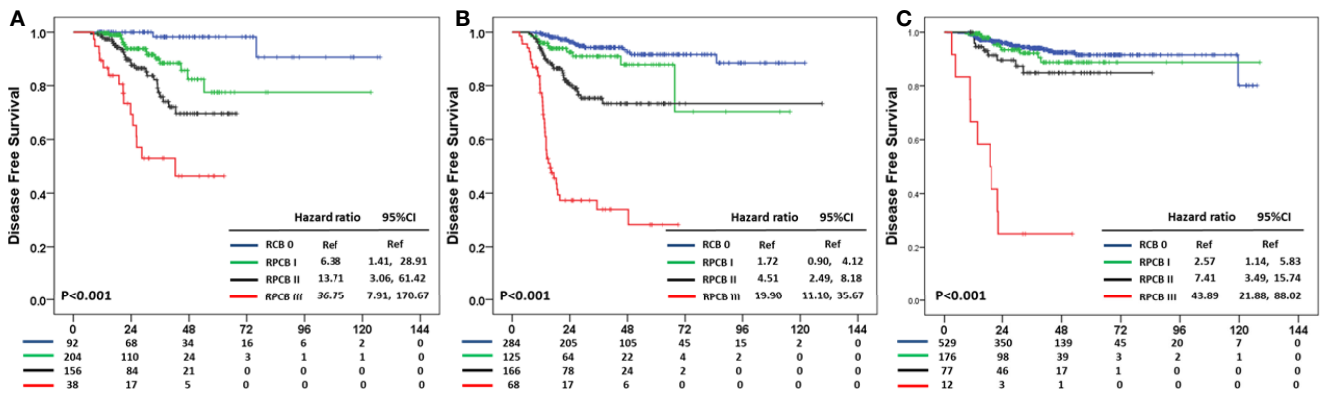

FIGURE 3 | Residual Proliferative Cancer Burden prediction model according to BC subtypes in DFS **(A)** HR+HER2− subtype **(B)** TNBC subtype **(C)** HER2+ subtype.

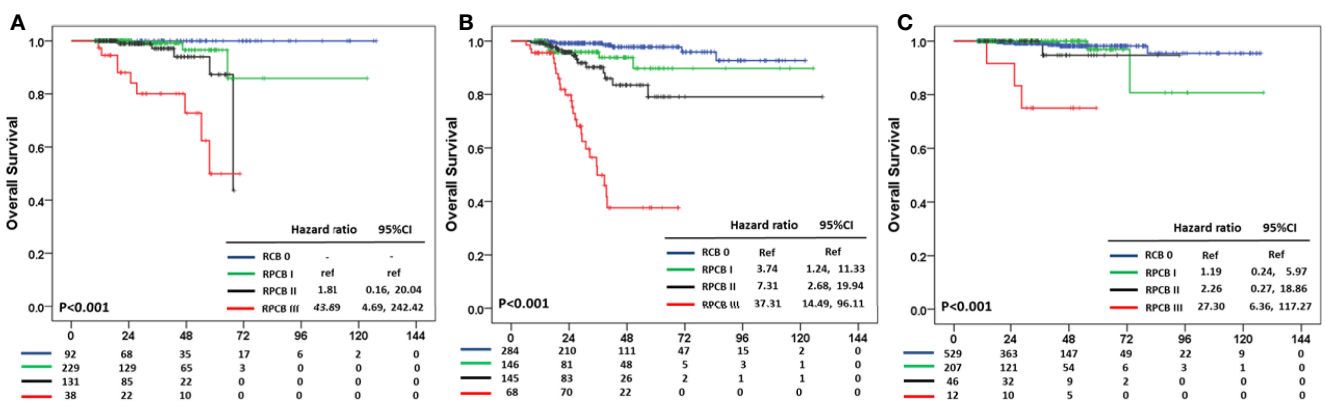

FIGURE 4 | Residual Proliferative Cancer Burden prediction model according to BC subtypes in OS. **(A)** HR+HER2− subtype. **(B)** TNBC subtype. **(C)** HER2+ subtype.

Disease Free Survival and Overall Survival According to RCB Class and Post-Op Ki-67

We also evaluated DFS and OS according to RCB class and post-op Ki-67, respectively. The RCB class well predicted DFS in all BC subtypes with statistical significance (ps <0.001) (**Supplementary Figure 4**). However, we did not find the DFS difference between RCB class 0 and I in all BC subtypes. The OS predictive value of the RCB class decreased in hormone receptor+HER2− BC (p = 0.580) (**Supplementary Figure 5**). In HER+ BC, only RCB class III predicted different OS and RCB class relatively well predicted OS in TNBC (p <0.001), but RCB class I did not predict different OS compared with RCB class 0.

Post-op Ki-67 predicted DFS and OS according to BC subtypes (**Supplementary Figure 5**). Post-op Ki-67 well predicted DFS in hormone receptor +HER2− and TNBC subtypes, whereas DFS of HER2+ BC did not correlate with post-op Ki-67. OS in hormone receptor +HER2− BC and TNBC were well predicted by post-op Ki-67 (p = 0.001 and p <0.001), but only RCB class III had a different OS compared with RCB 0 in HER2+ BC.

DISCUSSION

We evaluated the role of Ki-67 as a prognostic value in combination with RCB class, which is the strongest prognostic factor of BC specific survival in patients who received NAC followed by curative surgery. For predicting both DFS and OS, residual proliferative cancer burden (RPCB) consisting of grade of post-op Ki-67 expression and score of RCB class had superior prognostic value compared with that of RCB class. Moreover, like the RCB class, our model of the RPCB class had a predictive value regardless of BC subtypes. Therefore, the RPCB class was easy to use and precisely predicted BC prognosis.

Ki-67 has been considered the prognostic marker and predictive marker for response to NAC (22–24). BC with high Ki-67 had a higher pCR rate but shorter survival compared with that with low Ki-67 in case of TNBC (24–26). Additionally, Ki-67 change during NAC was associated with NAC response and prognosis (24). We analyzed the prognostic value of Ki-67 expression at BC diagnosis and curative surgery after NAC and the change of Ki-67 expression during NAC in our NAC cohort. In multivariate analysis, Ki-67 at BC diagnosis did not impact on DFS and OS. Change of Ki-67 during NAC and postoperative Ki-67 at curative surgery impacted BC survival (data not shown).

During the last decade, treatment strategies for BC have been greatly updated. However, neoadjuvant chemotherapeutic regimens have not been changed greatly, except for HER2 targeting agents. In a neoadjuvant setting, doxorubicin plus cyclophosphamide followed by taxane has been the standard chemotherapeutic regimen for HER2− BC subtypes (2). In HER2+ BC, adding pertuzumab to trastuzumab has become a new standard since 2016 (2). A previous study for NAC suggested that the NAC regimen affected RCB and/or the pathologic complete response rate in BC (27, 28). But RCB was the independent prognostic factor for survival outcome regardless of the NAC regimen (29). Besides, the NAC regimen did not impact on the long-term survival outcome. Therefore, we suggested that the NAC regimen would not be associated with our RPCB prediction model.

A previous report investigating the role of Ki-67 as a prognostic factor suggested that adding Ki-67 to the RCB class improved their predictive value (21). Moreover, they incorporated other values, including ER expression and histological grade, to improve the prediction of long-term outcome. However, the benefits of adding ER expression and histological grade were not clear in terms of predicting DFS and/or OS. In our study, histological grade and BC subtype were not associated with DFS and OS, and we excluded these two factors.

In contrast to a previous study, we used semi-quantitative Ki-67 as a categorical variable, not a continuous variable. We could create our prediction model with two categorical variables; three classes of RCB and four grades of Ki-67; and an RPCB class was created based on the combination of these two categorical variables. In total, 12 scores from two categorical variables were used in our analysis, and we converted 12 scores into 3 categories of the RPCB class (**Supplementary Table 4**). This meant our RPCB prediction model would be replicable and easily adapted in a real clinic compared with a previous model (21).

Moreover, we would like to develop a prediction model that can be operated regardless of BC subtype, such as the RCB class. Each RCB class and the value of Ki-67 at curative surgery also had their own predictive values for BC prognosis in DFS and OS. However, they did not precisely predict BC prognosis in either BC subtypes or all categories. However, all categories of our model work very well in all BC subtypes of both DFS and OS.

Our model had a superior outcome in predicting OS than DFS. This trend was also observed in other prediction models, the RCB and Ki-67 models. Furthermore, the RCB class and Ki-67 models had similar predictive power in DFS, whereas the Ki-67 model had a higher value of AUC compared with the RCB model in predicting OS. This result would suggest that post-Ki-67 was more associated with DFS than OS, even though both DFS and OS were related to Ki-67. Therefore, the prediction ability of our model increased more in OS than in DFS.

In conclusion, our RPCB model, in cooperation with the anatomical RCB class and biological post-op Ki-67, more precisely predicts BC prognosis compared with the RCB class. Both DFS and OS were well estimated by our model regardless of BC subtypes. This information is helpful for decision-making regarding BC patients who had residual disease after NAC followed by curative surgery.

DATA AVAILABILITY STATEMENT

The original contributions presented in the study are included in the article/**Supplementary Material**. Further inquiries can be directed to the corresponding author.

ETHICS STATEMENT

This study was reviewed and approved by the Institutional Review Board (IRB) of Samsung Medical Center, Seoul, Korea (IRB No. 2019-04-021) with an informed consent waiver due to the use of medical records with retrospective clinical data. This study was performed in accordance with the Declaration of Helsinki. Written informed consent for participation was not required for this study in accordance with the national legislation and the institutional requirements.

AUTHOR CONTRIBUTIONS

Conception/design: Y-HI and J-YK. Provision of patient data: J-YK, SL, JY, JL, SK, SN, YP, JA, and Y-HI. Collection and/or assembly of data: J-YK, JO. Statistical analysis: J-YK and KK. Manuscript writing: J-YK and Y-HI. Final approval of manuscript: J-YK, SL, JY, JL, SK, SN, YP, JA, KK, and Y-HI. All authors listed have made a substantial, direct, and intellectual contribution to the work and approved it for publication.

FUNDING

This work was supported by an Institute for Information and Communications Technology Promotion grant funded by the Korean government (2018-0-00861, Intelligent SW Technology Development for Medical Data Analysis), a grant from the Korea Health Technology R&D Project through the Korea Health Industry Development Institute (KHIDI) funded by the Ministry of Health & Welfare, Republic of Korea (grant number: HR20C0025), and grants from the National Research Foundation of Korea (NRF-2017R1D1A1B03028446, NRF-2020R1F1A1072616).

SUPPLEMENTARY MATERIAL

The Supplementary Material for this article can be found online at: https://www.frontiersin.org/articles/10.3389/fonc.2022.903372/full#supplementary-material

Supplementary Figure 1 | Disease free survival according to Ki-67 in **(A)** RCB class I, **(B)** RCB class II and **(C)** RCB class III and overall survival according to Ki-67 in **(D)** RCB class I, **(E)** RCB class II and **(F)** RCB class III.

Supplementary Figure 2 | Disease free survival according to **(A)** RCB class and **(B)** Ki-67 grade and overall survival according to **(C)** RCB class and **(D)** Ki-67 grade.

Supplementary Figure 3 | AUC according to 3year's disease free survival in **(A)** RPCB class **(B)** RCB class and **(C)** Ki-67 grade and AUC according to 3 year's overall survival in **(D)** RPCB class **(E)** RCB class and **(F)** Ki-67 grade.

Supplementary Figure 4 | DFS according to RCB class in **(A)** HR+HER2- BC **(B)** TNBC **(C)** HER2+ BC and OS according to RCB class in **(D)** HR+HER2- BC **(E)** TNBC **(F)** HER2+ BC.

Supplementary Figure 5 | DFS according to post op Ki-67 in **(A)** HR+HER2- BC **(B)** TNBC **(C)** HER2+ BC and OS according to post op Ki-67 in **(D)** HR+HER2- BC **(E)** TNBC **(F)** HER2+ BC.

REFERENCES

1. Loibl S, Poortmans P, Morrow M, Denkert C, Curigliano G. Breast Cancer. *Lancet* (2021) 397:1750–69. doi: 10.1016/S0140-6736(20)32381-3
2. Giordano SH, Elias AD, Gradishar WJ. NCCN Guidelines Updates: Breast Cancer. *J Natl Compr Canc Netw* (2018) 16:605–10. doi: 10.6004/jnccn.2018.0043
3. Mauri D, Pavlidis N, Ioannidis JP. Neoadjuvant Versus Adjuvant Systemic Treatment in Breast Cancer: A Meta-Analysis. *J Natl Cancer Inst* (2005) 97:188–94. doi: 10.1093/jnci/dji021
4. Rastogi P, Anderson SJ, Bear HD, Geyer CE, Kahlenberg MS, Robidoux A, et al. Preoperative Chemotherapy: Updates of National Surgical Adjuvant Breast and Bowel Project Protocols B-18 and B-27. *J Clin Oncol* (2008) 26:778–85. doi: 10.1200/JCO.2007.15.0235
5. Early Breast Cancer Trialists' Collaborative G. Long-Term Outcomes for Neoadjuvant Versus Adjuvant Chemotherapy in Early Breast Cancer: Meta-Analysis of Individual Patient Data From Ten Randomised Trials. *Lancet Oncol* (2018) 19:27–39. doi: 10.1016/S1470-2045(17)30777-5
6. Masuda N, Lee SJ, Ohtani S, Im YH, Lee ES, Yokota I, et al. Adjuvant Capecitabine for Breast Cancer After Preoperative Chemotherapy. *N Engl J Med* (2017) 376:2147–59. doi: 10.1056/NEJMoa1612645
7. von Minckwitz G, Huang CS, Mano MS, Loibl S, Mamounas EP, Untch M, et al. Trastuzumab Emtansine for Residual Invasive HER2-Positive Breast Cancer. *N Engl J Med* (2019) 380:617–28. doi: 10.1056/NEJMoa1814017
8. Cortazar P, Zhang L, Untch M, Mehta K, Costantino JP, Wolmark N, et al. Pathological Complete Response and Long-Term Clinical Benefit in Breast Cancer: The CTNeoBC Pooled Analysis. *Lancet* (2014) 384:164–72. doi: 10.1016/S0140-6736(13)62422-8
9. Symmans WF, Peintinger F, Hatzis C, Rajan R, Kuerer H, Valero V, et al. Measurement of Residual Breast Cancer Burden to Predict Survival After Neoadjuvant Chemotherapy. *J Clin Oncol* (2007) 25:4414–22. doi: 10.1200/JCO.2007.10.6823
10. Symmans WF, Wei C, Gould R, Yu X, Zhang Y, Liu M, et al. Long-Term Prognostic Risk After Neoadjuvant Chemotherapy Associated With Residual Cancer Burden and Breast Cancer Subtype. *J Clin Oncol* (2017) 35:1049–60. doi: 10.1200/JCO.2015.63.1010
11. Pusztai L, Foldi J, Dhawan A, DiGiovanna MP, Mamounas EP. Changing Frameworks in Treatment Sequencing of Triple-Negative and HER2-Positive, Early-Stage Breast Cancers. *Lancet Oncol* (2019) 20:e390–e6. doi: 10.1016/S1470-2045(19)30158-5
12. Campbell JI, Yau C, Krass P, Moore D, Carey LA, Au A, et al. Comparison of Residual Cancer Burden, American Joint Committee on Cancer Staging and Pathologic Complete Response in Breast Cancer After Neoadjuvant Chemotherapy: Results From the I-SPY 1 TRIAL (CALGB 150007/150012; ACRIN 6657). *Breast Cancer Res Treat* (2017) 165:181–91. doi: 10.1007/s10549-017-4303-8
13. Scholzen T, Gerdes J. The Ki-67 Protein: From the Known and the Unknown. *J Cell Physiol* (2000) 182:311–22. doi: 10.1002/(SICI)1097-4652(200003)182:3<311::AID-JCP1>3.0.CO;2-9
14. Urruticoechea A, Smith IE, Dowsett M. Proliferation Marker Ki-67 in Early Breast Cancer. *J Clin Oncol* (2005) 23:7212–20. doi: 10.1200/JCO.2005.07.501
15. Chen X, He C, Han D, Zhou M, Wang Q, Tian J, et al. The Predictive Value of Ki-67 Before Neoadjuvant Chemotherapy for Breast Cancer: A Systematic Review and Meta-Analysis. *Future Oncol* (2017) 13:843–57. doi: 10.2217/fon-2016-0420
16. von Minckwitz G, Schmitt WD, Loibl S, Muller BM, Blohmer JU, Sinn BV, et al. Ki67 Measured After Neoadjuvant Chemotherapy for Primary Breast Cancer. *Clin Cancer Res* (2013) 19:4521–31. doi: 10.1158/1078-0432.CCR-12-3628
17. Kim JY, Jung HH, Sohn I, Woo SY, Cho H, Cho EY, et al. Prognostication of a 13-Immune-Related-Gene Signature in Patients With Early Triple-Negative

Breast Cancer. *Breast Cancer Res Treat* (2020) 184:325–34. doi: 10.1007/s10549-020-05874-1
18. Denkert C, Loibl S, Muller BM, Eidtmann H, Schmitt WD, Eiermann W, et al. Ki67 Levels as Predictive and Prognostic Parameters in Pretherapeutic Breast Cancer Core Biopsies: A Translational Investigation in the Neoadjuvant GeparTrio Trial. *Ann Oncol* (2013) 24:2786–93. doi: 10.1093/annonc/mdt350
19. Bloom HJ, Richardson WW. Histological Grading and Prognosis in Breast Cancer; a Study of 1409 Cases of Which 359 Have Been Followed for 15 Years. *Br J Cancer* (1957) 11:359–77. doi: 10.1038/bjc.1957.43
20. Cortazar P, Geyer CEJr. Pathological Complete Response in Neoadjuvant Treatment of Breast Cancer. *Ann Surg Oncol* (2015) 22:1441–6. doi: 10.1245/s10434-015-4404-8
21. Sheri A, Smith IE, Johnston SR, A'Hern R, Nerurkar A, Jones RL, et al. Residual Proliferative Cancer Burden to Predict Long-Term Outcome Following Neoadjuvant Chemotherapy. *Ann Oncol* (2015) 26:75–80. doi: 10.1093/annonc/mdu508
22. Fasching PA, Heusinger K, Haeberle L, Niklos M, Hein A, Bayer CM, et al. Ki67, Chemotherapy Response, and Prognosis in Breast Cancer Patients Receiving Neoadjuvant Treatment. *BMC Cancer* (2011) 11:486. doi: 10.1186/1471-2407-11-486
23. Kanyilmaz G, Yavuz BB, Aktan M, Karaagac M, Uyar M, Findik S. Prognostic Importance of Ki-67 in Breast Cancer and Its Relationship With Other Prognostic Factors. *Eur J Breast Health* (2019) 15:256–61. doi: 10.5152/ejbh.2019.4778
24. Nishimura R, Osako T, Okumura Y, Hayashi M, Arima N. Clinical Significance of Ki-67 in Neoadjuvant Chemotherapy for Primary Breast Cancer as a Predictor for Chemosensitivity and for Prognosis. *Breast Cancer* (2010) 17:269–75. doi: 10.1007/s12282-009-0161-5
25. Keam B, Im SA, Lee KH, Han SW, Oh DY, Kim JH, et al. Ki-67 can be Used for Further Classification of Triple Negative Breast Cancer Into Two Subtypes With Different Response and Prognosis. *Breast Cancer Res* (2011) 13:R22. doi: 10.1186/bcr2834
26. Keam B, Im SA, Kim HJ, Oh DY, Kim JH, Lee SH, et al. Prognostic Impact of Clinicopathologic Parameters in Stage II/III Breast Cancer Treated With Neoadjuvant Docetaxel and Doxorubicin Chemotherapy: Paradoxical Features of the Triple Negative Breast Cancer. *BMC Cancer* (2007) 7:203. doi: 10.1186/1471-2407-7-203
27. Schneeweiss A, Chia S, Hickish T, Harvey V, Eniu A, Hegg R, et al. Pertuzumab Plus Trastuzumab in Combination With Standard Neoadjuvant Anthracycline-Containing and Anthracycline-Free Chemotherapy Regimens in Patients With HER2-Positive Early Breast Cancer: A Randomized Phase II Cardiac Safety Study (TRYPHAENA). *Ann Oncol* (2013) 24:2278–84. doi: 10.1093/annonc/mdt182
28. Gianni L, Pienkowski T, Im YH, Roman L, Tseng LM, Liu MC, et al. Efficacy and Safety of Neoadjuvant Pertuzumab and Trastuzumab in Women With Locally Advanced, Inflammatory, or Early HER2-Positive Breast Cancer (NeoSphere): A Randomised Multicentre, Open-Label, Phase 2 Trial. *Lancet Oncol* (2012) 13:25–32. doi: 10.1016/S1470-2045(11)70336-9
29. Muller HD, Posch F, Suppan C, Bargfrieder U, Gumpoldsberger M, Hammer R, et al. Validation of Residual Cancer Burden as Prognostic Factor for Breast Cancer Patients After Neoadjuvant Therapy. *Ann Surg Oncol* (2019) 26:4274–83. doi: 10.1245/s10434-019-07741-w

Conflict of Interest: The authors declare that the research was conducted in the absence of any commercial or financial relationships that could be construed as a potential conflict of interest.

Publisher's Note: All claims expressed in this article are solely those of the authors and do not necessarily represent those of their affiliated organizations, or those of the publisher, the editors and the reviewers. Any product that may be evaluated in this article, or claim that may be made by its manufacturer, is not guaranteed or endorsed by the publisher.

Copyright © 2022 Kim, Oh, Lee, Yu, Lee, Kim, Nam, Park, Ahn, Kim and Im. This is an open-access article distributed under the terms of the Creative Commons Attribution License (CC BY). The use, distribution or reproduction in other forums is permitted, provided the original author(s) and the copyright owner(s) are credited and that the original publication in this journal is cited, in accordance with accepted academic practice. No use, distribution or reproduction is permitted which does not comply with these terms.

frontiers | Frontiers in Oncology

ORIGINAL RESEARCH
published: 01 July 2022
doi: 10.3389/fonc.2022.899335

Metabolic Syndrome Predicts Response to Neoadjuvant Chemotherapy in Breast Cancer

*Ying Lu[1], Pinxiu Wang[1], Ning Lan[1], Fei Kong[1], Awaguli Abdumijit[1], Shiyan Tu[1], Yanting Li[1] and Wenzhen Yuan[2]**

[1] The First School of Clinical Medicine, Lanzhou University, Lanzhou, China, [2] The Department of Oncology, The First Hospital of Lanzhou University, Lanzhou, China

Purpose: This research investigated the predictive role of metabolic syndrome (MetS) in breast cancer neoadjuvant chemotherapy (BCNACT) response.

Methods: One hundred fifty primary breast cancer (BC) patients who underwent neoadjuvant chemotherapy (NACT) were included retrospectively. MetS, MetS components [waist circumference (WC), fasting blood glucose (FBG), blood pressure, triglycerides (TG), and high-density lipoprotein cholesterol (HDL-C)], serum lipid, and other MetS-related laboratory indicators within two weeks before BCNACT were evaluated. Univariate, multivariate, and subgroup analyses were performed to determine the predictors of BCNACT pathologic complete response (pCR), clinical response, and pathologic response. The effectiveness of the model was evaluated *via* receiver operating characteristic curve (ROC) and calibration curve. External validation was performed through 135 patients.

Results: Univariate analysis revealed that MetS before BCNACT predicted poor BCNACT response (pCR, P = 0.003; clinical response, P = 0.033; pathologic response, P < 0.001). Multivariate analysis confirmed that MetS before BCNACT predicted lower pCR rate (P = 0.041). Subgroup analysis showed that this relationship was significant in estrogen receptor (ER) (–) (RR = 0.266; 95% CI, 0.074–0.954), human epidermal growth factor 2 (HER2) (–) (RR = 0.833; 95% CI, 0.740–0.939) and TNBC (RR = 0.833; 95% CI, 0.636–0.995). Multivariate analysis of external validation confirmed that pretreatment MetS was associated with a lower pCR rate (P = 0.003), and subgroup analysis also confirmed that this relationship had significant statistical differences in ER (–), HER2 (–), and TNBC subgroups.

Conclusions: MetS before BCNACT predicted a lower pCR rate. Intervention on MetS status, especially in ER (–), HER2 (–), and TNBC subgroups, is expected to improve the response rate of BCNACT further.

Keywords: breast cancer, metabolic syndrome, neoadjuvant chemotherapy, efficacy prediction, MP grading, RECIST criteria

OPEN ACCESS

Edited by:
Raffaella Massafra, National Cancer Institute Foundation (IRCCS), Italy

Reviewed by:
Maria Colomba Comes, National Cancer Institute (IRCCS), Italy
Shengchun Liu, First Affiliated Hospital of Chongqing Medical University, China

***Correspondence:**
Wenzhen Yuan
yuanwzh@lzu.edu.cn

Specialty section:
This article was submitted to Breast Cancer, a section of the journal Frontiers in Oncology

Received: *18 March 2022*
Accepted: *30 May 2022*
Published: *01 July 2022*

Citation:
Lu Y, Wang P, Lan N, Kong F, Abdumijit A, Tu S, Li Y and Yuan W (2022) Metabolic Syndrome Predicts Response to Neoadjuvant Chemotherapy in Breast Cancer. Front. Oncol. 12:899335. doi: 10.3389/fonc.2022.899335

INTRODUCTION

Breast cancer (BC) is the most common type of female malignant tumor. Despite the overall incidence of cancer decreasing every year, the incidence of BC continues to increase, and rise in obesity is one of the key factors (1). Neoadjuvant chemotherapy (NACT) is known to shrinkage even eliminate tiny lesions, reduce the chances of distant metastasis, and improve clinical and pathologic response rates. NACT is also an excellent model for evaluating efficacy and looking for potential clinical or biological factors associated with efficacy. With the widespread implementation of breast cancer neoadjuvant chemotherapy (BCNACT), NACT is considered as the standard treatment for locally advanced BC, which has improved the overall survival rate of BC (2). Hence, predicting the response of NACT is helpful to evaluate the prognosis of patients. Moreover, some patients still could not benefit from NACT, subject to the risk of adverse reactions and death risk from chemotherapy, and even show cancer progression while undergoing NACT. Therefore, it is needed to determine predictive indicators which could prejudge whether a BC patient will benefit from NACT (3). These indicators help to achieve individualized treatment, avoid unnecessary chemotherapy-related side effects and death, and indirectly promote the development of new drugs. Furthermore, accurate intervention on predictors could further improve chemotherapy efficiency and survival time (4).

Metabolic syndrome (MetS) is a set of complex metabolic disorder syndromes, which describes a pathologic state in protein, fat, carbohydrate, and other metabolic components. The main causes of MetS are obesity (especially centripetal obesity) and insulin resistance. With an increase in the number of obese patients worldwide, the MetS population has also raised (5). Multiple studies have indicated that MetS and related indicators such as obesity, hyperinsulinemia, insulin resistance, inflammation, and adipocytokine secretion disorders are associated with the occurrence, recurrence, and all-cause mortality of BC (6–8). Stebbing et al. confirmed that MetS before adjuvant chemotherapy (ACT) can predict poor clinical response of BC patients with metastasis (P = 0.030) (9). Moreover, studies found that insulin was relevant to the efficiency of BCNACT (10, 11). However, obesity (12, 13), diabetes, high fasting blood glucose (FBG) (14, 15), and blood lipid (16, 17) were not consistent in predicting the efficiency of BCNACT. Furthermore, the research on the relationship between MetS and the efficiency of BCNACT is still very limited. To this end, we evaluated the potential contribution of MetS and relevant indicators in predicting the response of BCNACT. The correlation between the two and the predict ability can be determined by the traditional statistical and machine learning (logistic regression) approaches. In addition, studies have found that, in the estrogen receptor (ER) (+) subgroup, blood glucose (18) and lipid (17) are related to the efficacy of BC chemotherapy; therefore, we also investigated this relationship under different ER states.

MetS was observed to have hyperuricemia and vascular endothelial dysfunction, and vascular endothelial dysfunction could lead to microalbuminuria and mild renal injury (19). Furthermore, oxidative stress was considered as a pathogenesis mechanism of MetS. Lactate dehydrogenase (LDH) was observed to induce conditions of oxidative stress (20). Oxidative stress could disrupt the secretion of adipocytokines (adipose-derived hormones) including adiponectin, plasminogen activator inhibitor 1, interleukin-6, and monocyte chemoattractant protein 1 (21). These adipocytokines mediated the development of MetS by participating in the regulation of insulin sensitivity and glucose metabolism (22); thus, MetS might be accompanied by low-grade inflammatory reaction. Therefore, apart from MetS and its components, uric acid (UA), creatinine (Cr), LDH, neutrophil-lymphocyte ratio (NLR), lymphocyte-monocyte ratio (LMR), and platelet-lymphocyte ratio (PLR) were also considered as potential predictors of BCNACT. In addition, studies have found that, in the postmenopausal subgroup, MetS is related to stage and lymph node metastasis of BC patients, so we also studied the relationship between MetS and clinical characteristics of BC under different menstrual states (23).

PATIENTS AND METHODS

Population Study

In this study, patients diagnosed with BC in The First Hospital of Lanzhou University between 1 July, 2018 and 31 July, 2021 were retrieved through the electronic medical record system (n = 2,152) and the pathologic registration system (n = 2,361). A total of 1,246 patients were retained after duplicates were removed, and 348 of them underwent NACT. Patients who not yet received surgery (n = 31) did not receive whole course NACT in The First Hospital of Lanzhou University (n = 4), had no biochemical experiment (n = 2), lost to follow up and unable to obtain waist circumference (WC) (n = 5), participated in clinical trials (NACT regimen: albumin paclitaxel + perlotinib maleate) (n = 6), and underwent neoadjuvant endocrine therapy (n = 2). Patients with bilateral BC (n = 3) or whose chemotherapy cycle ≤3 (n = 10) were excluded. Finally, a total of 285 primary BC patients were evaluated. Study model was built with 150 patients (1 July, 2020 to 31 July, 2021), and 135 patients (1 July, 2018 to 30 June, 2020) were used for external validation (**Figure 1**). Patients included in this study did not receive any antitumor treatment before diagnosis and underwent surgery after four to eight cycles of standard NACT. They had no infectious diseases, hematological diseases, or severe liver or kidney dysfunction and did not take glucocorticoids and other drugs that might affect laboratory indicators within 3 months before diagnosis. The study was approved by the ethics committee of The First Hospital of Lanzhou University (No. LDYYLL2021-265). Written informed consent has been remitted in this study.

Medical Record Collection

Clinical data were obtained through the electronic medical record system of The First Hospital of Lanzhou University and

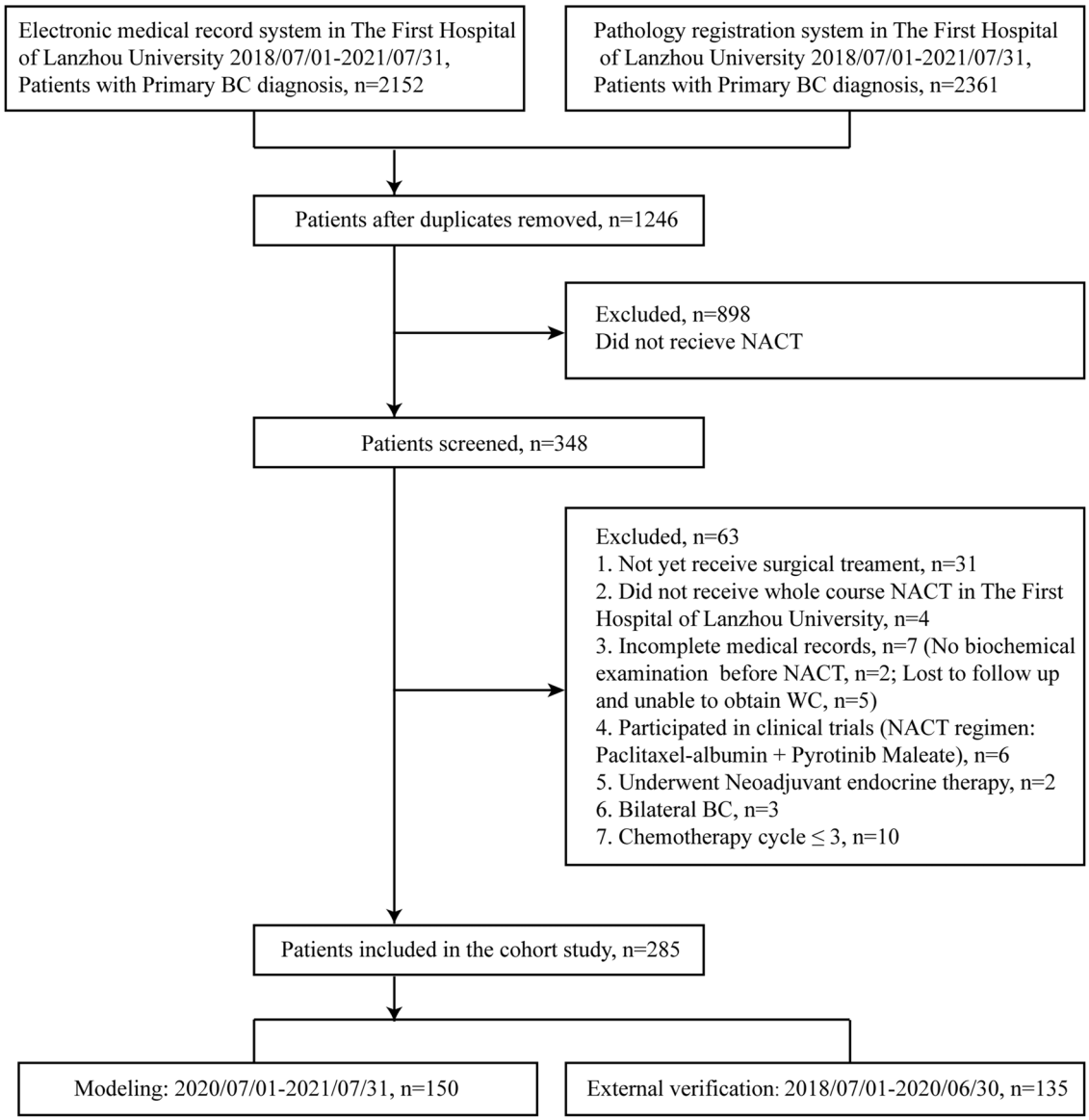

FIGURE 1 | Selection of patients for present study. BC, breast cancer; NACT, neoadjuvant chemotherapy; WC, waist circumference.

via telephone follow up. WC was measured at the navel level (24). The weight and height were measured using a digital scale while patients were not wearing heavy clothes and shoes. Body mass index (BMI) was calculated according to the standard formula of weight (kg)/height (m^2). Blood pressure was measured using the same electronic sphygmomanometer. Blood and biochemical indicators were tested through blood samples from patients within 2 weeks before NACT. All patients underwent clinical staging through breast ultrasound, computed tomography (CT) scans or magnetic resonance imaging (MRI) before NACT. Ultrasound-guided breast puncture (lymph node puncture if necessary) was also performed in patients to clarify the pathology type and molecular classification of BC. Pathological data were independently evaluated by two experienced pathologists from The First Hospital of Lanzhou University. If the results of the two pathologists were inconsistent, a second evaluation was conducted until reaching a consensus.

MetS Definition

The, 2006 criteria of IDF (International Diabetes Federation) were adopted to diagnose MetS (5, 25). For a person to be defined as having MetS, they must have WC >80 cm, with the presence of two or more of the following conditions: 1. FBG > 5.6 mmol/L

(100 mg/dl) or diagnosed with diabetes; 2. high-density lipoprotein cholesterol (HDL-C) <1.3 mmol/L (50 mg/dl) or drug therapy for low HDL-C; 3. blood triglycerides (TG) >1.7 mmol/L (150 mg/dl) or undergoing medical treatment for elevated TG; 4. blood pressure >130/85 mmHg or drug treatment for hypertension.

Treatment

Patients with human epidermal growth factor 2 (HER2) (–) received AC-T, AC, or TAC regimens. Most of patients with HER2 (+) received TCbHP, THP, AC-TH, TCbH, AC-THP, or TH regimens (T: taxane, including docetaxel, albumin paclitaxel or paclitaxel; A: anthracycline, C: cyclophosphamide; including epirubicin, pyridoxorubicin or doxorubicin; Cb: carboplatin; H: trastuzumab; P: pertuzumab). The NACT protocol used for the patients is shown in **Supplementary Tables 1**, **2**. It was reported that taxanes can improve the response of BCNACT (26), so the chemotherapy regimens were grouped into categories that either included or excluded taxanes (12). The chemotherapy dose was provided according to the body surface area, and an individualized treatment plan was formulated according to the Chinese Society of Clinical Oncology guidelines and patient's conditions.

NACT Response Evaluation

Pathologic complete response (pCR) was defined as no residual cancer lesions in any excised breast tissue or lymph nodes. Clinical response was evaluated according to the response evaluation criteria in solid tumors criteria (RECIST) version 1.1 (27). Partial response (PR) and complete response (CR) were defined as a good clinical response; progressive disease (PD) and stable lesions (SD) were defined as a poor clinical response. Pathologic response was assessed according to the Miller and Payne grading (MP grading) (28, 29). G1–G3 were defined as poor pathologic response and G4–G5 were defined as good pathologic response (30).

Statistical Analysis

The SPSS 26.0 software was utilized to conduct statistical analysis, and the GraphPad Prism 9 and R 4.1.2 software were used to draw pictures. Dichotomous variables were defined by the optimal cutoff value of the receiver operating characteristic curve (ROC). Measurement data were analyzed by *t*-test and counting data were analyzed by Chi-square ($\chi 2$) test, Fisher's exact test, or non-parametric test. Univariate, multivariate logistics regression and subgroup (log-linear regression) analyses were made to assess possible predictors on pCR, clinical, and pathologic response. Predictors related to MetS [age at initiation of treatment, BMI, menstrual status, WC, FBG, systolic blood pressure (SBP), diastolic blood pressure (DBP), TG, HDL-C, and UA] and predictors with $P < 0.05$ on univariate analysis were included in multivariate analysis. The confidence interval (CI) of the risk ratio (RR) is 95% and p-value < 0.05 is considered statistically significant.

RESULTS

Patient Characteristics

This study included 104 non-MetS (69.30%) and 46 MetS patients (30.70%). The average age was 49.43 ± 10.314 years old (26–76 years old). The average chemotherapy cycle was 6.69 ± 1.589. BCNACT scheme was shown in **Supplementary Table 1**. The age, BMI, WC, FBG, SBP, DBP, TG, and UA levels of MetS patients were significantly higher than those without MetS, and the HDL-C level was significantly lower than those without MetS. Postmenopausal patients were more prone to have MetS. These two groups were comparable in tumor size, lymph node status, stage, histological type, NACT regimen, molecular subtype, ER, progesterone receptor (PR), HER2, and Ki-67 expression levels (**Table 1**). In addition, regardless of menstrual status, the status of MetS was not related to clinical characteristics (**Supplementary Table 3**).

Relationship Between MetS and BCNACT Response

The overall pCR rate of BCNACT was 31.33%, of which the pCR rate of HER2 (+) patients was 55.88% and that of HER2 (–) patients was 10.98%. Compared with non-MetS patients, MetS patients had lower pCR rate ($P = 0.003$), poorer clinical response ($P = 0.033$), and poorer pathological response ($P < 0.001$) (**Figure 2A**). Mass shrinkage (RECIST criteria 1.1) was more obvious ($P = 0.004$) (**Figure 2B**), and the pathological grade was lower ($P < 0.001$) (**Figure 2C**) in non-MetS patients.

When taking pCR as the outcome, multivariate analysis found that non-MetS patients had a higher probability of pCR ($P = 0.003$) (**Table 2**). According to ROC curve, the C index of this model was 0.895 (95% CI, 0.841–0.948; $P < 0.001$), and the sensitivity and specificity were 0.957 and 0.728 respectively (**Figure 3A**). The calibration curve shows that the predicted probability of the model is in good agreement with ideal probability (**Figure 3B**).

When taking clinical remission as the outcome, multivariate analysis found that, compared with patients with BMI ≥25 and <30 kg/m^2, patients with BMI <25 kg/m^2 were less likely to have good clinical response ($P = 0.006$). Compared with patients with TG ≤1.3, patients with TG >1.3 were less likely to obtain good clinical response ($P = 0.036$) (**Supplementary Table 4**). When pathological remission was used as the outcome, multivariate analysis found that patients with TG >0.865 were less likely to obtain clinical remission than patients with TG ≤0.865 ($P = 0.007$) (**Supplementary Table 5**). MetS was not found to be associated with clinical and pathological response of BCNACT. Analysis according to ER status found that the relationship between fast blood glucose, serum lipid, and BCNACT response was not affected by ER expression status (**Supplementary Table 6**).

Subgroup Analysis of MetS and BCNACT pCR

Interaction analysis showed that MetS had no interaction with ER, PR, HER2, triple negative BC (TNBC), molecular subtype,

TABLE 1 | Population and clinicopathologic characteristics.

Characteristics	Non-MetS (%/ ± SD)	MetS (%/ ± SD)	Total	p-value
	104(69.30%)	46(30.70%)	150	
Mean age, year				
<50	52	13	65	**0.010**
≥50	52	33	85	
BMI, kg/m^2				
<25	78	16	94	**<0.001**
25<T ≤ 30	25	24	49	
T>30	1	6	7	
Menopausal status				
Premenopausal	59	17	76	**0.020**
Postmenopausal	45	29	74	
WC, cm				
≤80	65	0	65	**<0.001**
>80	39	46	85	
FBG, mmol/L				
≤5.6	91	23	114	**<0.001**
>5.6	13	23	36	
Blood pressure				
SBP, mmHg				
≤130	65	19	84	**0.013**
>13	39	27	66	
DBP, mmHg				
≤85	78	26	104	**0.020**
>85	26	20	46	
Lipid profile				
TG, mmol/L				
≤1.7	89	22	111	**<0.001**
>1.7	15	24	39	
HDL-C, mmol/L				
<1.3	60	8	68	**<0.001**
≥ 1.3	44	38	82	
TC, mmol/L	4.46 ± 0.93	4.60 ± 1.07		0.436
LDL-C, mmol/L	2.92 ± 0.74	3.07 ± 0.82		0.268
UA, μmol/L	261.02 ± 60.56	287.48 ± 79.62		**0.027**
Cr, μmol/L	57.88 ± 8.04	57.70 ± 8.86		0.905
LDH, U/L	179.66 ± 38.74	186.20 ± 43.53		0.361
Inflammation				
NLR	3.07 ± 2.11	3.13 ± 2.86		0.900
LMR	7.89 ± 14.99	6.30 ± 2.92		0.476
PLR	168.02 ± 86.31	145.00 ± 62.23		0.105
Tumor size				0.070
T ≤ 2 cm	19	5	24	
2 cm<T ≤ 5 cm	78	35	113	
T>5 cm	7	6	13	
Lymph node				0.271
Negative	34	12	46	
Positive	70	34	104	
Clinical stage				0.065
I	4	0	4	
IIA	44	16	60	
IIB	49	25	74	
III	7	5	12	
Pathogenic type				0.338
Invasive carcinoma	71	31	102	
Invasive carcinoma with ductal carcinoma	28	10	38	
Others	5	5	10	
Molecular subtype				0.383
HER2+/HR+	19	10	29	
HER2+/HR–	31	8	39	
Luminal	43	24	67	
TNBC	11	4	15	
ER				0.461
Negative	41	17	58	

(Continued)

TABLE 1 | Continued

Characteristics	Non-MetS (%/ ± SD)	MetS (%/ ± SD)	Total	p-value
Positive	63	29	92	
PR				0.462
Negative	59	25	84	
Positive	45	21	66	
HER2				0.202
Negative	54	28	82	
Positive	50	18	68	
Ki-67				0.072
Negative	2	4	6	
Positive	102	42	144	
TNBC				0.489
Yes	11	4	15	
No	93	42	135	
NACT regimen				0.281
Non-taxane based	5	4	9	
Taxane based	99	42	141	

MetS, metabolic syndrome; SD, standard deviation; BMI, body mass index; WC, waist circumference; FBG, fasting blood glucose; SBP, systolic blood pressure; DBP, diastolic blood pressure; TG, triglycerides; HDL-C, high-density lipoprotein cholesterol; TC, total cholesterol; LDL-C; low-density lipoprotein cholesterol; UA, uric acid; Cr, creatinine; LDH, lactate dehydrogenase; NLR, neutrophil-lymphocyte ratio; LMR, lymphocyte-monocyte ratio; PLR, platelet-lymphocyte ratio; HER2, human epidermal growth factor 2; HR, hormone receptor; TNBC, triple negative breast cancer; ER, estrogen receptor; PR, progesterone receptor; NACT, neoadjuvant chemotherapy. Bold means p-value < 0.05.

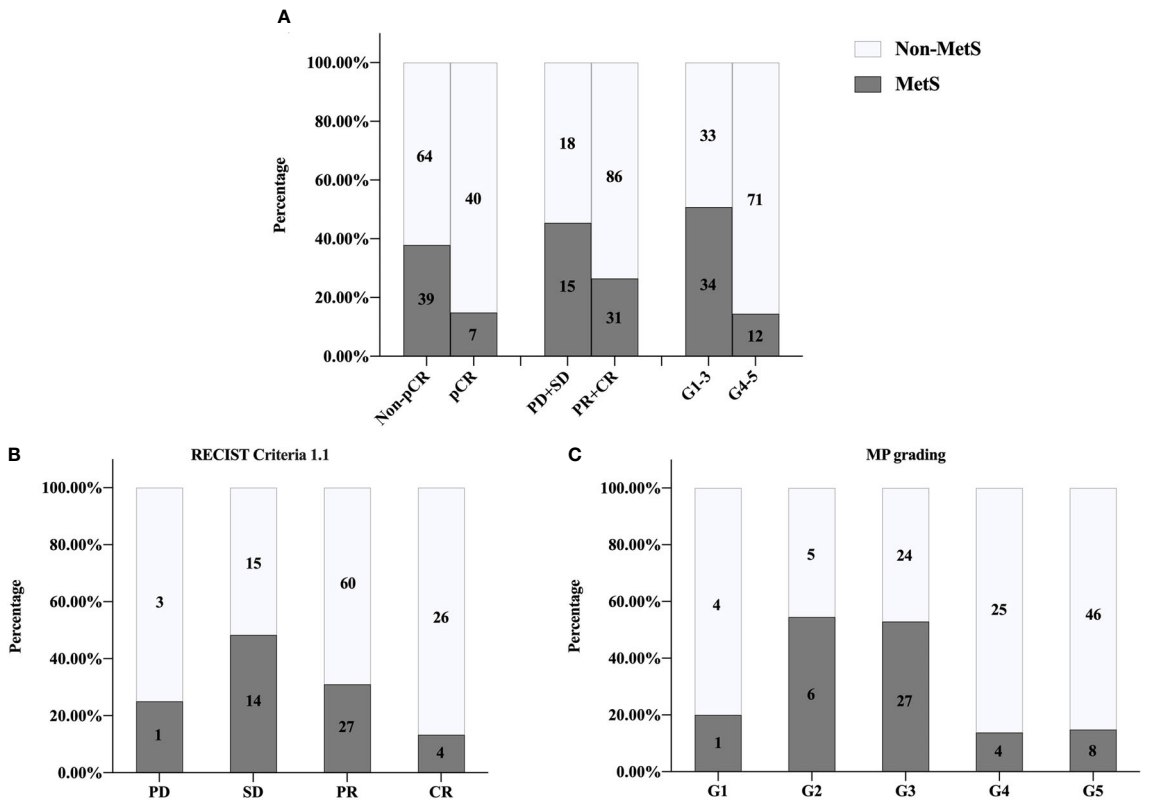

FIGURE 2 | Univariate analysis of relationship between MetS and NACT response. **(A)** pCR, P = 0.003; clinical responses, P = 0.033; pathologic responses, P <0.001. **(B)** RECIST1.1 criteria P = 0.004. **(C)** MP grading P < 0.001. MetS, metabolic syndrome; pCR, pathologic complete response; PD, progressive disease; SD, stable lesions; PR, partial response; CR, complete response; MP, Miller-Payne; RECIST, response evaluation criteria in solid tumors.

TABLE 2 | Univariate and multivariate analysis of laboratory and clinical indicators with BCNACT pathologic complete response.

Indicators	Total	pCR		Univariate analysis	Multivariate analysis (Hosmer–Lemeshow test, P = 0.250)	
		No	Yes	p-value	RR (95% CI)	p-value
	150	103	47			
Age, year				**0.018**		0.064
<50	65	51	14		1 (reference)	
≥50	85	52	33		0.278 (0.072–1.076)	
BMI, kg/m^2				0.420		0.357
<25	94	66	28		1 (reference)	
25 ≤BMI <30	49	30	19		4.189*10^8 (0.000–~)	0.999
≥30	7	7	0		1.010*10^9 (0.000–~)	0.999
Menopausal status				0.122		0.541
Premenopausal	76	56	20		1 (reference)	
Postmenopausal	74	47	27		1.511 (0.403–5.672)	
WC, cm				0.204		0.539
≤93.665	131	92	39		1 (reference)	
>93.665	19	11	8		0.596 (0.115–3.102)	
FBG, mmol/L				0.097		0.059
≤5.415	102	74	28		1 (reference)	
>5.415	48	29	19		0.312 (0.103–1.046)	
Blood pressure						
SBP, mmHg				0.060		0.470
≤137.5	95	70	25		1 (reference)	
>137.5	55	33	22		0.617 (0.166–2.289)	
DBP, mmHg				0.233		0.897
≤83.5	91	65	26		1 (reference)	
>83.5	59	38	21		1.087 (0.304–3.887)	
Lipid profile						
TG, mmol/L				0.242		0.868
≤1.525	97	69	28		1 (reference)	
>1.525	53	34	19		1.107 (0.332–3.687)	
HDL-C, mmol/L				**0.027**		0.980
≤1.465	121	88	33		1 (reference)	
>1.465	29	15	14		0.984 (0.296–3.274)	
TC, mmol/L				**0.021**		0.786
≤4.720	90	68	22		1 (reference)	
>4.720	60	35	25		0.665 (0.035–12.761)	
LDL-C, mmol/L				**0.047**		0.822
≤3.225	93	69	24		1 (reference)	
>3.225	57	34	23		1.419 (0.067–29.963)	
UA, μmol/L				0.234		0.442
≤221.5	36	27	9		1 (reference)	
>221.5	114	76	38		1.613 (0.477–5.451)	
Cr, μmol/L				0.169		
≤53.9	48	36	12			
>53.9	102	67	35			
LDH, U/L				0.151		
≤162	52	39	13			
>162	98	64	34			
Inflammation						
NLR				0.142		
≤1.925	49	37	12			
>1.925	101	66	35			
LMR				0.320		
≤6.585	95	67	28			
>6.585	55	36	19			
PLR				0.065		
≤114.085	39	31	8			
>114.085	111	72	39			
Tumor size				0.327		
T ≤ 2 cm	24	16	8			
2 cm <T ≤ 5 cm	113	77	36			
T > 5 cm	13	10	3			
Lymph node				0.336		

(Continued)

TABLE 2 | Continued

Indicators	Total	pCR		Univariate analysis	Multivariate analysis (Hosmer–Lemeshow test, P = 0.250)	
		No	Yes	p-value	RR (95% CI)	p-value
Negative	46	30	16			
Positive	104	73	31			
Clinical stage				0.252		
I	4	1	3			
IIA	60	42	18			
IIB	74	51	23			
III	12	9	3			
Pathogenic type				**0.014**		0.941
Invasive carcinoma	102	172	30		1 (reference)	
Invasive carcinoma with ductal carcinoma	38	21	17		$8.763*10^{8}$ (0.000–~)	0.999
Others	10	10	0		$1.061*10^{9}$ (0.000-–~)	0.999
Molecular subtype				**<0.001**		
HER2+/HR+	29	15	14			
HER2+/HR–	39	16	23			
Luminal	67	61	6			
TNBC	15	11	4			
ER				**0.004**		0.610
Negative	58	32	26		1 (reference)	
Positive	92	71	21		0.716 (0.198–2.584)	
PR				**0.002**		0.096
Negative	84	49	35		1 (reference)	
Positive	66	54	12		3.177 (0.814–12.398)	
HER2				**<0.001**		**<0.001**
Negative	82	73	9		1 (reference)	
Positive	68	30	38		0.123 (0.038–0.396)	
Ki-67				0.278		
Negative	6	3	3			
Positive	144	100	44			
TNBC				0.465		
Yes	15	11	4			
No	135	92	43			
NACT regimen				0.165		
Non-taxane based	9	8	1			
Taxane based	141	95	46			
MetS				**0.003**		**0.003**
No	104	64	40		1 (reference)	
Yes	46	39	7		10.765 (2.256–51.361)	

*pCR, pathologic complete response; RR, risk ratio; CI, confidence interval; BMI, body mass index; WC, waist circumference; FBG, fasting blood glucose; SBP, systolic blood pressure; DBP, diastolic blood pressure; TG, triglycerides; HDL-C, high-density lipoprotein cholesterol; TC, total cholesterol; LDL-C; low-density lipoprotein cholesterol; UA, uric acid; Cr, creatinine; LDH, lactate dehydrogenase; NLR, neutrophil-lymphocyte ratio; LMR, lymphocyte-monocyte ratio; PLR, platelet-lymphocyte ratio; HER2, human epidermal growth factor 2; HR, hormone receptor; TNBC, triple negative breast cancer; ER, estrogen receptor; PR, progesterone receptor; NACT, neoadjuvant chemotherapy. Bold means p-value < 0.05. * means multiplication.*

and NACT regimen. Subgroup analysis showed that the relationship between MetS and BCNACT pCR was more significant in ER (–), PR (–), HER2 (–), TNBC (–), TNBC, luminal subgroup, and NACT regimen based on taxane (**Figure 4**).

External Validation of Relationship Between MetS and BCNACT Response

Patient characteristics of external validation group were showed in **Supplementary Table 7**. There was no relationship between MetS and clinical characteristics of BC patients regardless of menstrual status (**Supplementary Table 8**). BCNACT scheme was shown in **Supplementary Table 2**. Univariate analysis confirmed that MetS was associated with BCNACT response (pCR, P = 0.011; clinical response, P = 0.004; pathological response; P = 0.014; RECIST criteria 1.1, P < 0.001; MP grade, P = 0.048) (**Figure 5**).

Multivariate analysis confirmed that MetS was associated with BCNACT pCR (P = 0.046). Multivariate analysis also found that patients with FBG ≤5.415 were more likely to get obtain pCR than patients with FBG >5.415 (P = 0.023) (**Table 3**). The C index of the model was 0.917 (95% CI, 0.862–0.973; P < 0.001), and the sensitivity and specificity were 0.983 and 0.714, respectively (**Supplementary Figure 1**). Multivariate analysis did not find indicators related to clinical and pathological response (**Supplementary Tables 9, 10**). Subgroup analysis confirmed that the relationship between MetS and BCNACT pCR was more significant in ER (–), HER2 (–), and TNBC subgroups (**Figure 6**). It was not found that the relationship between blood lipid, blood glucose, and response was affected by ER expression status (**Supplementary Table 11**).

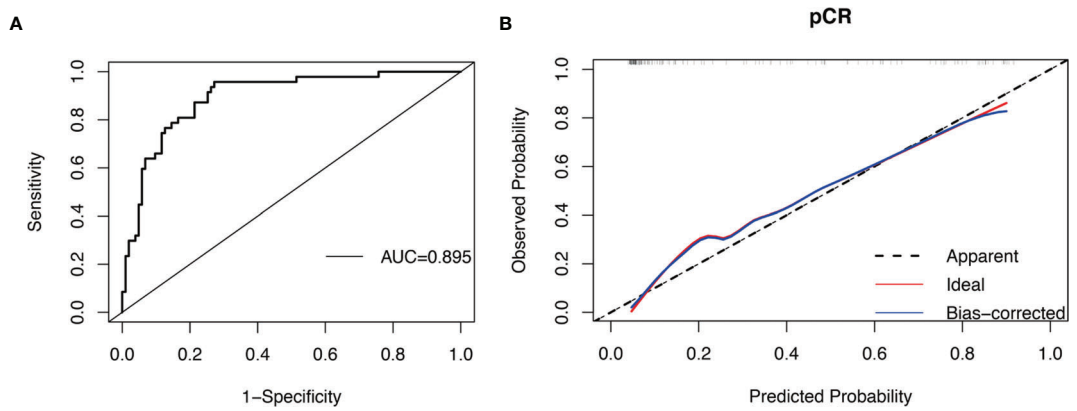

FIGURE 3 | ROC curve and calibration curve of BCNACT pCR prediction model: **(A)** ROC curve. **(B)** calibration curve.

DISCUSSION

NACT is an indispensable treatment for locally advanced BC, which can shrink the tumor volume, increase the opportunity of operation and breast preservation, lessen the surgical trauma, eliminate the minor subclinical cancer focus, reduce the activity of tumor cells, so as to decrease the risk of distant metastasis, and provide the basis of drug sensitivity for preoperative ACT. Furthermore, predicting the response of BCNACT is helpful to evaluate the prognosis of patients, promote individualized treatment, and further improve the BCNACT response rate. To the best of our knowledge, this study is the first research, which specifically explores the relationship between the response of BCNACT and MetS. Previously, only the relationship between MetS components and BCNACT response was studied. MetS can be diagnosed merely through routine examination, without the need for new technology or equipment. Thus, it has the advantages of low cost, high efficiency, and ease to generalize

	Mets n/N	pCR (Mets vs. non-Mets) n/N	%	RR (95% CI)	P Value for Interaction
Overall	46/150	7/46 vs. 40/104	15.20% vs. 38.50%	0.287 (0.117-0.704)	
ER					
Negative	17/58	4/17 vs. 22/41	23.50% vs. 53.70%	0.266 (0.074-0.954)	0.696
Positive	29/92	3/29 vs. 18/63	10.30% vs. 28.60%	0.288 (0.078-1.074)	
PR					
Negative	25/84	6/25 vs. 29/59	24.00% vs. 49.20%	0.327 (0.114-0.934)	0.645
Positive	21/66	1/21 vs. 11/45	4.80% vs. 24.40%	0.155 (0.019-1.288)	
HER2					
Negative	28/82	0/28 vs. 9/54	0.00% vs. 16.70%	0.833 (0.740-0.939)	0.687
Positive	18/68	7/18 vs. 31/50	38.90% vs. 62.00%	0.390 (0.129-1.179)	
TNBC					
No	42/135	7/42 vs. 36/93	16.70% vs. 38.70%	0.317 (0.127-0.789)	0.644
Yes	4/15	0/4 vs. 4/11	0.00% vs. 36.40%	0.833 (0.636-0.995)	
Molecular subtype					
HER2+/HR+	10/29	3/10 vs. 11/19	30.00% vs. 57.90%	0.312 (0.061-1.592)	0.698
HER2+/HR-	8/39	4/8 vs. 19/31	50.00% vs. 61.30%	0.632 (0.132-3.015)	
Luminal	24/67	0/24 vs. 6/43	0.00% vs. 14.00%	0.860 (0.763-0.971)	
TNBC	4/15	0/4 vs. 4/11	0.00% vs. 36.40%	0.833 (0.636-0.995)	
NAC regimen					
Nontaxane based	4/9	0/4 vs. 1/5	0.00% vs. 20.00%	0.800 (0.516-1.240)	0.552
Taxane based	42/141	7/42 vs. 39/99	16.70% vs. 39.40%	0.308 (0.124-0.761)	

FIGURE 4 | Subgroup analysis of MetS and BCNACT pCR. MetS, metabolic syndrome; pCR, pathologic complete response; RR, risk ratio; CI, confidence interval; ER, estrogen receptor; PR, progesterone receptor; HER2, human epidermal growth factor 2; TNBC, triple negative breast cancer; NACT, neoadjuvant chemotherapy.

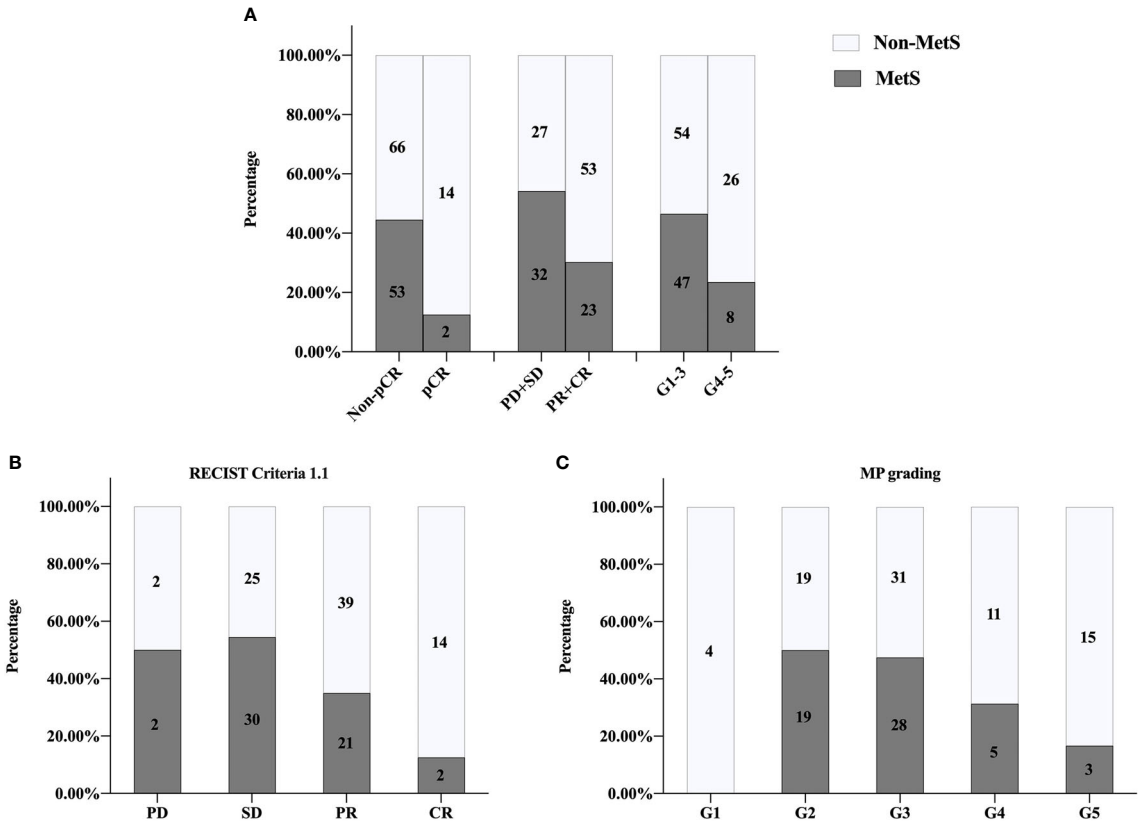

FIGURE 5 | External validation of univariate analysis on relationship between MetS and NACT response. **(A)** pCR, P = 0.011; clinical responses, P = 0.004; pathologic responses, P = 0.014. **(B)** RECIST1.1 criteria P < 0.001. **(C)** MP grading P = 0.048. MetS, metabolic syndrome; pCR, pathologic complete response; PD, progressive disease; SD, stable lesions; PR, partial response; CR, complete response; MP, Miller-Payne; RECIST, response evaluation criteria in solid tumors.

in predicting the efficiency of BCNACT. Studies have shown that MetS is associated with later staging (P = 0.022) and lymph node metastasis (P = 0.028) in postmenopausal BC (23). Our study did not find this link (**Supplementary Tables 3**, **8**), which may be due to the different clinical characteristics of the population participating in BCNACT from the whole BC population with postmenopausal. MetS patients are also accompanied by hyperuricemia, persistent low-grade inflammatory reaction, oxidative stress, and mild renal injury. Our study found that MetS patients had higher UA levels (**Table 1**), which was consistent with other study (31). In addition, external validation found higher LDH levels in MetS patients (**Supplementary Table 7**), suggesting that MetS patients were easily predisposed to oxidative stress than non-MetS patients. This research has not yet found a direct link between MetS and mild renal injury (Cr) or persistent low inflammatory reaction (NLR, LMR, and PLR) (**Table 1** and **Supplementary Table 7**), perhaps MetS did not participate in the pathogenesis of BC through these mechanisms.

In our study, univariate analysis found that patients with MetS before chemotherapy were more difficult to achieve pCR, clinical, and pathological response than non-MetS (**Figures 2**, **5**). Multivariate analysis found that MetS was associated with BCNACT pCR (**Tables 2**, **3**). A study demonstrated that, among BC patients with metastasis, non-MetS patients before ACT were easier to achieve clinical response than MetS patients (9); this study is a good complement in predicting the response of BC chemotherapy *via* MetS. Alan et al. did not find the relationship between MetS and BCNACT pCR in the study of 55 patients (33% vs. 23%, P = 0.200) (11), but the sample size of this study is small and the diagnostic criteria of MetS are different from this study (32).

Regarding the relationship between obesity and BCNACT response, studies have discovered that obese patients have a lower pCR rate (OR = 0.59; 95% CI, 0.37–0.95) (12), and similar studies have confirmed it. Maybe insufficient dose of obese patients led to poor response (33). However, a meta-analysis concluded that BMI is not associated with BCNACT response (34). Our study found that overweight patients were more likely to achieve clinical response than patients with normal weight (**Supplementary Table 4**). This conclusion is contrary to previous studies, and the external validation group did not find this association.

As for the relationship between serum lipids and BCNACT response, Hilvo et al. found that lower-level TG suggests BCNACT pCR (16). Our study found that low-level TG was

TABLE 3 | Univariate and multivariate analyses of laboratory and clinical indicators with BCNACT pathologic complete response on external validation patients.

Indicators	Total	pCR		Univariate analysis	Multivariate analysis (Hosmer–Lemeshow test, P = 0.853)	
		No	Yes	p-value	RR (95% CI)	p-value
	135	119	16			
Age, year				0.517		0.226
<50	64	56	8		1 (reference)	
≥50	71	63	8		0.277 (0.035–2.207)	
BMI, kg/m^2				0.435		0.259
<25	83	73	10		1 (reference)	
25 ≤ BMI <30	44	38	6		3.388*10^6 (0.000–~)	0.999
≥30	8	8	0		1.615*10^7 (0.000–~)	0.999
Menopausal status				0.450		0.092
Premenopausal	78	68	10		1 (reference)	
Postmenopausal	57	51	6		6.419 (0.737–55.916)	
WC, cm				**0.048**		0.998
≤93.665	113	97	16		1 (reference)	
>93.665	22	22	0		3.883*10^8 (0.000–~)	
FBG, mmol/L				**0.012**		**0.023**
≤5.415	91	76	15		1 (reference)	
>5.415	44	43	1		79.074 (1.809–3456.590)	
Blood pressure						
SBP, mmHg				0.430		0.060
≤137.5(没变)	99	88	11		1 (reference)	
>137.5	36	31	5		0.038 (0.002–1.093)	
DBP, mmHg				0.262		0.603
≤83.5	96	83	13		1 (reference)	
>83.5	39	36	3		1.788(0.200–15.958)	
Lipid profile						
TG, mmol/L				0.240		0.666
≤1.525	95	82	13		1 (reference)	
>1.525	40	37	3		1.528 (0.223–10.452)	
HDL-C, mmol/L				0.337		0.997
≤1.465	27	25	2		1 (reference)	
>1.465	108	94	14		0.996 (0.111–8.955)	
TC, mmol/L				0.195		
≤4.720	75	64	11			
>4.720	60	55	5			
LDL-C, mmol/L				0.467		
≤3.225	87	76	11			
>3.225	48	43	5			
UA, μmol/L				0.295		0.081
≤221.5	39	33	6		1 (reference)	
>221.5	96	86	10		4.788 (0.827–27.734)	
Cr, μmol/L				0.567		
≤53.9	28	25	3			
>53.9	107	94	13			
LDH, U/L				0.142		
≤162	36	34	2			
>162	99	85	14			
Inflammation						
NLR				0.240		
≤1.925	40	37	3			
>1.925	95	82	13			
LMR				0.309		
≤6.585	98	85	13			
>6.585	37	34	3			
PLR				0.415		
≤114.085	33	30	3			
>114.085	102	89	13			
Tumor size				0.346		
T ≤ 2 cm	25	22	3			
2 cm < T≤ 5 cm	100	87	13			
T > 5 cm	10	10	0			
Lymph node				0.102		

(Continued)

TABLE 3 | Continued

Indicators	Total	pCR		Univariate analysis	Multivariate analysis (Hosmer–Lemeshow test, P = 0.853)	
		No	Yes	p-value	RR (95% CI)	p-value
Negative	52	43	9			
Positive	83	76	7			
Clinical stage				0.076		
I	10	8	2			
IIA	57	49	8			
IIB	55	49	6			
III	13	13	0			
Pathogenic type				1.000		
Invasive carcinoma	125	109	16			
Invasive carcinoma with ductal carcinoma	6	6	0			
Others	0	8	8			
Molecular subtype				**<0.001**		
HER2+/HR+	27	23	4			
HER2+/HR–	14	9	5			
Luminal	73	71	2			
TNBC	21	16	5			
ER				**0.003**		0.552
Negative	39	29	10		1 (reference)	
Positive	96	90	6		1.764 (0.272–11.413)	
PR				**0.002**		0.093
Negative	53	41	12		1 (reference)	
Positive	82	78	4		7.208 (0.719–72.297)	
HER2				**0.020**		**0.023**
Negative	94	87	7		1 (reference)	
Positive	41	32	9		0.157 (0.063–0.519)	
Ki-67				0.219		
Negative	14	11	3			
Positive	121	108	13			
TNBC				0.077		
Yes	21	16	5			
No	114	103	11			
NACT regimen				0.176		
Non-taxane based	34	32	2			
Taxane based	101	87	14			
MetS				**0.011**		**0.046**
No	80	66	14		1 (reference)	
Yes	55	53	2		9.416 (1.038–85.443)	

*pCR, pathologic complete response; RR, risk ratio; CI, confidence interval; BMI, body mass index; WC, waist circumference; FBG, fasting blood glucose; SBP, systolic blood pressure; DBP, diastolic blood pressure; TG, triglycerides; HDL-C, high-density lipoprotein cholesterol; TC, total cholesterol; LDL-C; low-density lipoprotein cholesterol; UA, uric acid; Cr, creatinine; LDH, lactate dehydrogenase; NLR, neutrophil-lymphocyte ratio; LMR, lymphocyte-monocyte ratio; PLR, platelet-lymphocyte ratio; HER2, human epidermal growth factor 2; HR, hormone receptor; TNBC, triple negative breast cancer; ER, estrogen receptor; PR, progesterone receptor; NACT, neoadjuvant chemotherapy. Bold means p-value < 0.05. * means multiplication.*

easy to obtain better clinical and pathological response (**Supplementary Tables 4, 5**), but the external validation group did not confirm this relationship (**Supplementary Tables 9, 10**). A study has found that the lower HDL-C in the ER (+) subgroup suggests better clinical response (17), which may be due to, in different ER subgroups, the activation of different signal pathways during chemotherapy or tumor heterogeneity was different. However, our research did not discover an association between HDL-C and BCNACT response in ER (+) subgroup (**Supplementary Tables 6, 11**). In general, blood lipids can indicate the efficacy of BCNACT, but it is still necessary to use unified standards to further evaluate its predictive value in a larger scale.

With regard to the relationship between blood glucose and BCNACT response, Arici et al. suggested that diabetes and high FBG levels predicted poor pathological response (14). Alan et al. found that insulin resistance had an adverse relationship on BCNACT pCR (11). Our study did not find this relationship (**Table 2**), although external validation found higher FBG indicated lower PCR rate (**Table 3**). The study of Cao et al. also showed that FBG could not predict clinical response of BCNACT (15). Additionally, studies have found that hyperglycemia participated in ER (+) chemotherapy resistance. When hyperglycemia occurs, insulin-like growth factor 1 (IGF-1) concentration increases. IGF-1 can specifically induce FASN (fatty acid synthase) to activate the mitogen-activated protein kinase pathway of BC and increase ERα phosphorylation levels, which up-regulated nuclear localization of ERα. Nuclear ERα could raise the expression of CCND1 (cell cycle–related protein), which will weaken the inhibition of anticancer drugs on the proliferation of tumor cells (18, 35). However, our study did not consider that the relationship between blood glucose and

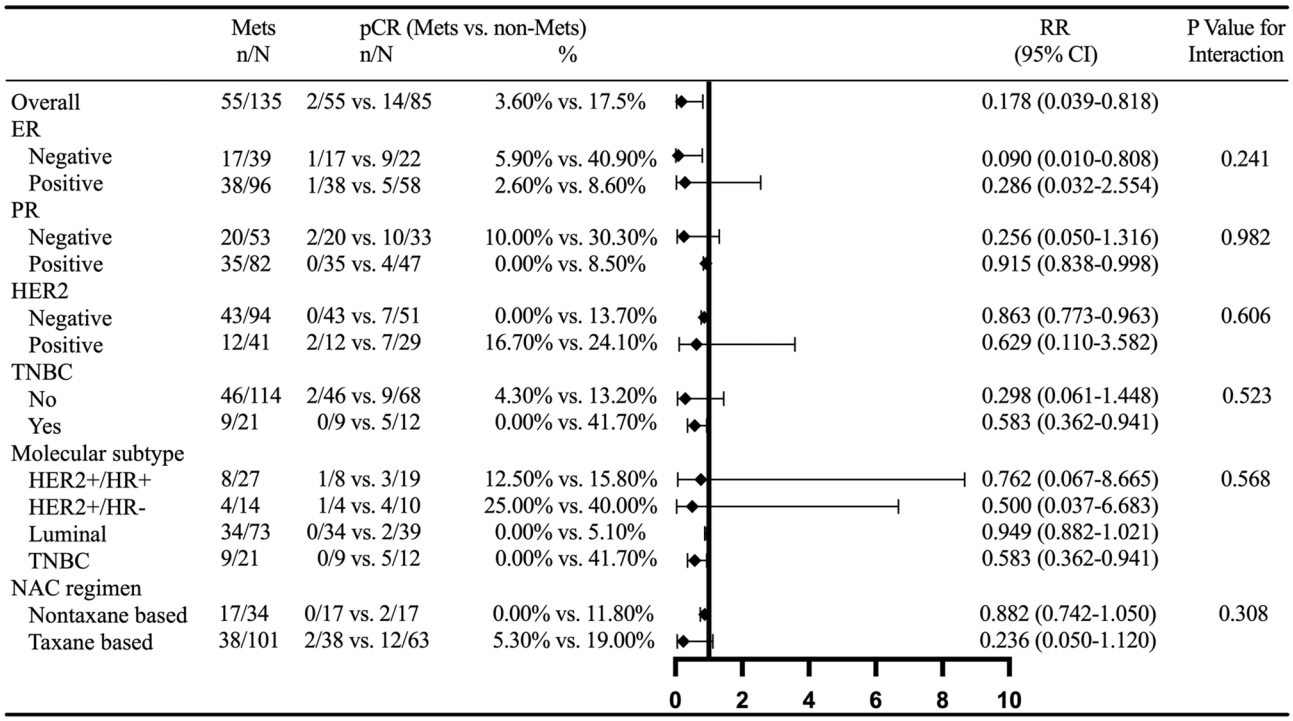

FIGURE 6 | External validation of subgroup analysis on the relationship between MetS and BCNACT pCR. MetS, metabolic syndrome; pCR, pathologic complete response; RR, risk ratio; CI, confidence interval; ER, estrogen receptor; PR, progesterone receptor; HER2, human epidermal growth factor 2; TNBC, triple negative breast cancer; NACT, neoadjuvant chemotherapy.

BCNACT response related to ER status (**Supplementary Tables 6, 11**). In conclusion, we believe that this link between FBG and BCNACT response still needs to be verified in more rigorous research.

The relationship between MetS-related indicators UA, LDH, Cr, and BCNACT response was analyzed, but there is no predictor on response. Dennison et al. found that high LDH-B can predict BCNACT pCR on hormone receptor (HR) (+)/HER2 (–) (OR = 4.1, P < 0.001) and TNBC (OR = 3.0, P = 0.003) subtype (36). Therefore, it is necessary to further study the relationship among LDH subunits in various molecular subtypes and BCNACT response. In addition, studies have shown that NLR, LMR, and PLR predicted BCNACT response (37). However, our multivariate analysis did not confirm this conclusion, and the research conclusions of Alan et al. and Şahin et al. were consistent with ours (11, 38). In summary, we speculated that, as a comprehensive indicator, MetS could be a more precise indicator in predicting BCNACT response than MetS components. Multicenter studies are required to confirm the predictive role of blood lipids, blood glucose, and inflammatory parameters in BCNACT response.

In order to guide clinical practice better and verify the reliability of the conclusion, we conducted subgroup analysis on MetS and BCNACT pCR (**Figures 4**, **6**). The study of Tong et al. found that MetS was not indictor for BCNACT pCR in HER2 (+) (17.24% vs. 82.76%, P = 0.106) (39), which is consistent with our conclusion. However, we found significant differences in ER (–), HER2 (–), and TNBC subgroups. It is suggested that the intervention of MetS status in the above subgroups can improve BCNACT pCR rate more effectively.

This study has some limitations: 1. As a single-center study, only Chinese patients were included, the incidence of MetS varied greatly between China and other countries (40). Due to the small sample size and excessive fitting, reliable conclusions cannot be obtained *via* machine learning. The universality of conclusions from this study still needs to be verified in a larger population. 2. As a retrospective study, recall bias of patient data may exist. The diet and exercise status of patients before diagnosis had not been evaluated, which may be confounding factors (41). 3. This study did not rule out the interference of chemotherapy dose in the assessment of BCNACT response. During the NACT process, physicians appropriately adjusted the dose according to the degree of the patient's tolerance or adverse reaction, and the dosages of some patients have also changed accordingly with the weight fluctuation. 4. In terms of protocol and dose, the guidelines referenced by external validation patients are not as good as those in modeling patients, which resulted in worse response than modeling group and cause inconsistencies on several secondary conclusions between modeling and external validation group.

Finally, our study suggests that it is necessary to conduct an in-depth study to find out the mechanism of BCNACT resistance in MetS patients, especially in ER (–), HER2 (–), and TNBC subgroups. Furthermore, a variety of methods to improve the metabolism of cancer patients can ameliorate the prognosis to a

greater extent. For example, appropriate nutritional intervention and psychological support were observed to significantly prolong the survival rate for cancer patients (4). Heys et al. considered that supplementing L-arginine to BC patients could improve the NACT response (42). Adams et al. confirmed that resistance exercise training improved the life quality of BCNACT (43).

CONCLUSION

MetS before NACT predicted BCNACT pCR, especially in ER (−), HER2 (−), and TNBC subgroups. Developing appropriate intervention strategies to rectify MetS status was speculated to improve the BCNACT response further.

DATA AVAILABILITY STATEMENT

The original contributions presented in the study are included in the article/**Supplementary Material**. Further inquiries can be directed to the corresponding author.

ETHICS STATEMENT

The studies involving human participants were reviewed and approved by The First Hospital of Lanzhou University Ethics Committee. Written informed consent for participation was not required for this study in accordance with the national legislation and the institutional requirements.

AUTHOR CONTRIBUTIONS

WYZ and YL conceived the study. YL, PWX, NL, and FK designed the methods, analyzed the data and wrote the article. YL, PWX, AA, STY, and YLT collected the data. WY, PWX, NL, and FK revised the article. All authors contributed to the article and approved the submitted version.

ACKNOWLEDGMENTS

We thank the patients who volunteered their time and effort to participate in this study, all the reviewers who participated in the review, and MJEditor (www.mjeditor.com) for its linguistic assistance during the preparation of this manuscript.

SUPPLEMENTARY MATERIAL

The Supplementary Material for this article can be found online at: https://www.frontiersin.org/articles/10.3389/fonc.2022.899335/full#supplementary-material

REFERENCES

1. Siegel RL, Miller KD, Fuchs HE, Jemal A. Cancer Statistics, 2021. *CA Cancer J Clin* (2021) 71(1):7–33. doi: 10.3322/caac.21654
2. Kaufmann M, von Minckwitz G, Bear HD, Buzdar A, McGale P, Bonnefoi H, et al. Recommendations From an International Expert Panel on the Use of Neoadjuvant (Primary) Systemic Treatment of Operable Breast Cancer: New Perspectives 2006. *Ann Oncol* (2007) 18(12):1927–34. doi: 10.1093/annonc/mdm201
3. Hu D, Peng F, Lin X, Chen G, Zhang H, Liang B, et al. Preoperative Metabolic Syndrome Is Predictive of Significant Gastric Cancer Mortality After Gastrectomy: The Fujian Prospective Investigation of Cancer (FIESTA) Study. *EBioMedicine* (2017) 15:73–80. doi: 10.1016/j.ebiom.2016.12.004
4. Lu Z, Fang Y, Liu C, Zhang X, Xin X, He Y, et al. Early Interdisciplinary Supportive Care in Patients With Previously Untreated Metastatic Esophagogastric Cancer: A Phase III Randomized Controlled Trial. *J Clin Oncol* (2021) 39(7):748–56. doi: 10.1200/jco.20.01254
5. Alberti KG, Eckel RH, Grundy SM, Zimmet PZ, Cleeman JI, Donato KA, et al. Harmonizing the Metabolic Syndrome: A Joint Interim Statement of the International Diabetes Federation Task Force on Epidemiology and Prevention; National Heart, Lung, and Blood Institute; American Heart Association; World Heart Federation; International Atherosclerosis Society; and International Association for the Study of Obesity. *Circulation* (2009) 120 (16):1640–5. doi: 10.1161/CIRCULATIONAHA.109.192644
6. Goodwin PJ, Ennis M, Pritchard KI, Trudeau ME, Koo J, Taylor SK, et al. Insulin- and Obesity-Related Variables in Early-Stage Breast Cancer: Correlations and Time Course of Prognostic Associations. *J Clin Oncol* (2012) 30(2):164–71. doi: 10.1200/jco.2011.36.2723
7. Duggan C, Irwin ML, Xiao L, Henderson KD, Smith AW, Baumgartner RN, et al. Associations of Insulin Resistance and Adiponectin With Mortality in Women With Breast Cancer. *J Clin Oncol* (2011) 29(1):32–9. doi: 10.1200/jco.2009.26.4473
8. Dong S, Wang Z, Shen K, Chen X. Metabolic Syndrome and Breast Cancer: Prevalence, Treatment Response, and Prognosis. *Front Oncol* (2021) 11:629666. doi: 10.3389/fonc.2021.629666
9. Stebbing J, Sharma A, North B, Athersuch TJ, Zebrowski A, Pchejetski D, et al. A Metabolic Phenotyping Approach to Understanding Relationships Between Metabolic Syndrome and Breast Tumour Responses to Chemotherapy. *Ann Oncol* (2012) 23(4):860–6. doi: 10.1093/annonc/mdr347
10. de Groot S, Charehbili A, van Laarhoven HW, Mooyaart AL, Dekker-Ensink NG, van de Ven S, et al. Insulin-Like Growth Factor 1 Receptor Expression and IGF1R 3129g > T Polymorphism are Associated With Response to Neoadjuvant Chemotherapy in Breast Cancer Patients: Results From the NEOZOTAC Trial (BOOG 2010-01). *Breast Cancer Res* (2016) 18(1):3. doi: 10.1186/s13058-015-0663-3
11. Alan O, Akin Telli T, Aktas B, Koca S, Okten IN, Hasanov R, et al. Is Insulin Resistance a Predictor for Complete Response in Breast Cancer Patients Who Underwent Neoadjuvant Treatment? *World J Surg Oncol* (2020) 18(1):242. doi: 10.1186/s12957-020-02019-y
12. Litton JK, Gonzalez-Angulo AM, Warneke CL, Buzdar AU, Kau SW, Bondy M, et al. Relationship Between Obesity and Pathologic Response to Neoadjuvant Chemotherapy Among Women With Operable Breast Cancer. *J Clin Oncol* (2008) 26(25):4072–7. doi: 10.1200/JCO.2007.14.4527
13. Protani M, Coory M, Martin J. Effect of Obesity on Survival of Women With Breast Cancer: Systematic Review and Meta-Analysis. *Breast Cancer Res Treat* (2010) 123(3):627–35. doi: 10.1007/s10549-010-0990-0
14. Arici S, Geredeli C, Secmeler S, Cekin R, Sakin A, Cihan S. The Effects of Diabetes and Fasting Plasma Glucose on Treatment of Breast Cancer With Neoadjuvant Chemotherapy. *Curr Probl Cancer* (2020) 44(1):100485. doi: 10.1016/j.currproblcancer.2019.05.007
15. Cao MD, Giskeodegard GF, Bathen TF, Sitter B, Bofin A, Lonning PE, et al. Prognostic Value of Metabolic Response in Breast Cancer Patients Receiving Neoadjuvant Chemotherapy. *BMC Cancer* (2012) 12:39. doi: 10.1186/1471-2407-12-39

16. Hilvo M, Gade S, Hyotylainen T, Nekljudova V, Seppanen-Laakso T, Sysi-Aho M, et al. Monounsaturated Fatty Acids in Serum Triacylglycerols are Associated With Response to Neoadjuvant Chemotherapy in Breast Cancer Patients. *Int J Cancer* (2014) 134(7):1725–33. doi: 10.1002/ijc.28491
17. Qu F, Chen R, Peng Y, Ye Y, Tang Z, Wang Y, et al. Assessment of the Predictive Role of Serum Lipid Profiles in Breast Cancer Patients Receiving Neoadjuvant Chemotherapy. *J Breast Cancer* (2020) 23(3):246–58. doi: 10.4048/jbc.2020.23.e32
18. Zeng L, Zielinska H, Arshad A, Shield J, Bahl A, Holly J, et al. Hyperglycaemia-Induced Chemoresistance in Breast Cancer Cells: Role of the Estrogen Receptor. *Endocrine-related Cancer* (2016) 23(2):125–34. doi: 10.1530/erc-15-0507
19. Johnson RJ, Segal MS, Srinivas T, Ejaz A, Mu W, Roncal C, et al. Essential Hypertension, Progressive Renal Disease, and Uric Acid: A Pathogenetic Link? *J Am Soc Nephrol* (2005) 16(7):1909–19. doi: 10.1681/asn.2005010063
20. Le A, Cooper CR, Gouw AM, Dinavahi R, Maitra A, Deck LM, et al. Inhibition of Lactate Dehydrogenase A Induces Oxidative Stress and Inhibits Tumor Progression. *Proc Natl Acad Sci U S A* (2010) 107(5):2037–42. doi: 10.1073/pnas.0914433107
21. Furukawa S, Fujita T, Shimabukuro M, Iwaki M, Yamada Y, Nakajima Y, et al. Increased Oxidative Stress in Obesity and its Impact on Metabolic Syndrome. *J Clin Invest* (2004) 114(12):1752–61. doi: 10.1172/jci21625
22. Fasshauer M, Paschke R. Regulation of Adipocytokines and Insulin Resistance. *Diabetologia* (2003) 46(12):1594–603. doi: 10.1007/s00125-003-1228-z
23. Healy L, Ryan A, Carroll P, Ennis D, Crowley V, Boyle T, et al. Metabolic Syndrome, Central Obesity and Insulin Resistance are Associated With Adverse Pathological Features in Postmenopausal Breast Cancer. *Clin Oncol (Royal Coll Radiol (Great Britain))* (2010) 22(4):281–8. doi: 10.1016/j.clon.2010.02.001
24. Dieli-Conwright CM, Wong L, Waliany S, Bernstein L, Salehian B, Mortimer JE. An Observational Study to Examine Changes in Metabolic Syndrome Components in Patients With Breast Cancer Receiving Neoadjuvant or Adjuvant Chemotherapy. *Cancer* (2016) 122(17):2646–53. doi: 10.1002/cncr.30104
25. Xiang Y, Zhou W, Duan X, Fan Z, Wang S, Liu S, et al. Metabolic Syndrome, and Particularly the Hypertriglyceridemic-Waist Phenotype, Increases Breast Cancer Risk, and Adiponectin Is a Potential Mechanism: A Case-Control Study in Chinese Women. *Front Endocrinol (Lausanne)* (2019) 10:905. doi: 10.3389/fendo.2019.00905
26. Bear HD, Anderson S, Smith RE, Geyer CEJr., Mamounas EP, Fisher B, et al. Sequential Preoperative or Postoperative Docetaxel Added to Preoperative Doxorubicin Plus Cyclophosphamide for Operable Breast Cancer:National Surgical Adjuvant Breast and Bowel Project Protocol B-27. *J Clin Oncol* (2006) 24(13):2019–27. doi: 10.1200/jco.2005.04.1665
27. Eisenhauer EA, Therasse P, Bogaerts J, Schwartz LH, Sargent D, Ford R, et al. New Response Evaluation Criteria in Solid Tumours: Revised RECIST Guideline (Version 1.1). *Eur J Cancer* (2009) 45(2):228–47. doi: 10.1016/j.ejca.2008.10.026
28. Romero A, García-Sáenz JA, Fuentes-Ferrer M, López Garcia-Asenjo JA, Furió V, Román JM, et al. Correlation Between Response to Neoadjuvant Chemotherapy and Survival in Locally Advanced Breast Cancer Patients. *Ann Oncol* (2013) 24(3):655–61. doi: 10.1093/annonc/mds493
29. Ogston KN, Miller ID, Payne S, Hutcheon AW, Sarkar TK, Smith I, et al. A New Histological Grading System to Assess Response of Breast Cancers to Primary Chemotherapy: Prognostic Significance and Survival. *Breast* (2003) 12(5):320–7. doi: 10.1016/s0960-9776(03)00106-1
30. Zhu Q, Ademuyiwa F, Young C, Appleton C, Covington M, Ma C, et al. Early Assessment Window for Predicting Breast Cancer Neoadjuvant Therapy Using Biomarkers, Ultrasound, and Diffuse Optical Tomography. *Breast Cancer Res Treat* (2021) 188(3):615–30. doi: 10.1007/s10549-021-06239-y
31. Johnson RJ, Nakagawa T, Sanchez-Lozada LG, Shafiu M, Sundaram S, Le M, et al. Sugar, Uric Acid, and the Etiology of Diabetes and Obesity. *Diabetes* (2013) 62(10):3307–15. doi: 10.2337/db12-1814
32. Grundy SM, Cleeman JI, Daniels SR, Donato KA, Eckel RH, Franklin BA, et al. Diagnosis and Management of the Metabolic Syndrome: An American Heart Association/National Heart, Lung, and Blood Institute Scientific Statement. *Circulation* (2005) 112(17):2735–52. doi: 10.1161/circulationaha.105.169404
33. Fontanella C, Lederer B, Gade S, Vanoppen M, Blohmer J, Costa S, et al. Impact of Body Mass Index on Neoadjuvant Treatment Outcome: A Pooled Analysis of Eight Prospective Neoadjuvant Breast Cancer Trials. *Breast Cancer Res Treat* (2015) 150(1):127–39. doi: 10.1007/s10549-015-3287-5
34. Erbes T, Stickeler E, Rücker G, Buroh S, Asberger J, Dany N, et al. BMI and Pathologic Complete Response to Neoadjuvant Chemotherapy in Breast Cancer: A Study and Meta-Analysis. *Clin Breast Cancer* (2016) 16(4):e119–32. doi: 10.1016/j.clbc.2016.02.018
35. Zeng L, Biernacka K, Holly J, Jarrett C, Morrison A, Morgan A, et al. Hyperglycaemia Confers Resistance to Chemotherapy on Breast Cancer Cells: The Role of Fatty Acid Synthase. *Endocrine-related Cancer* (2010) 17(2):539–51. doi: 10.1677/erc-09-0221
36. Dennison JB, Molina JR, Mitra S, Gonzalez-Angulo AM, Balko JM, Kuba MG, et al. Lactate Dehydrogenase B: A Metabolic Marker of Response to Neoadjuvant Chemotherapy in Breast Cancer. *Clin Cancer Res* (2013) 19(13):3703–13. doi: 10.1158/1078-0432.CCR-13-0623
37. Graziano V, Grassadonia A, Iezzi L, Vici P, Pizzuti L, Barba M, et al. Combination of Peripheral Neutrophil-to-Lymphocyte Ratio and Platelet-to-Lymphocyte Ratio is Predictive of Pathological Complete Response After Neoadjuvant Chemotherapy in Breast Cancer Patients. *Breast (Edinburgh Scotland)* (2019) 44:33–8. doi: 10.1016/j.breast.2018.12.014
38. Şahin A, Cubukcu E, Ocak B, Deligonul A, Oyucu Orhan S, Tolunay S, et al. Low Pan-Immune-Inflammation-Value Predicts Better Chemotherapy Response and Survival in Breast Cancer Patients Treated With Neoadjuvant Chemotherapy. *Sci Rep* (2021) 11(1):14662. doi: 10.1038/s41598-021-94184-7
39. Tong YW, Wang G, Wu JY, Huang O, He JR, Zhu L, et al. Insulin-Like Growth Factor-1, Metabolic Abnormalities, and Pathological Complete Remission Rate in HER2-Positive Breast Cancer Patients Receiving Neoadjuvant Therapy. *Onco Targets Ther* (2019) 12:3977–89. doi: 10.2147/OTT.S194981
40. Hirode G, Wong R. Trends in the Prevalence of Metabolic Syndrome in the United States, 2011-2016. *JAMA* (2020) 323(24):2526–8. doi: 10.1001/jama.2020.4501
41. de Groot S, Lugtenberg R, Cohen D, Welters M, Ehsan I, Vreeswijk M, et al. Fasting Mimicking Diet as an Adjunct to Neoadjuvant Chemotherapy for Breast Cancer in the Multicentre Randomized Phase 2 DIRECT Trial. *Nat Commun* (2020) 11(1):3083. doi: 10.1038/s41467-020-16138-3
42. Heys SD, Ogston K, Miller I, Hutcheon AW, Walker LG, Sarker TK, et al. Potentiation of the Response to Chemotherapy in Patients With Breast Cancer by Dietary Supplementation With L-Arginine: Results of a Randomised Controlled Trial. *Int J Oncol* (1998) 12(1):221–5. doi: 10.3892/ijo.12.1.221
43. Adams S, Segal R, McKenzie D, Vallerand J, Morielli A, Mackey J, et al. Impact of Resistance and Aerobic Exercise on Sarcopenia and Dynapenia in Breast Cancer Patients Receiving Adjuvant Chemotherapy: A Multicenter Randomized Controlled Trial. *Breast Cancer Res Treat* (2016) 158(3):497–507. doi: 10.1007/s10549-016-3900-2

Conflict of Interest: The authors declare that the research was conducted in the absence of any commercial or financial relationships that could be construed as a potential conflict of interest.

Publisher's Note: All claims expressed in this article are solely those of the authors and do not necessarily represent those of their affiliated organizations, or those of the publisher, the editors and the reviewers. Any product that may be evaluated in this article, or claim that may be made by its manufacturer, is not guaranteed or endorsed by the publisher.

Copyright © 2022 Lu, Wang, Lan, Kong, Abdumijit, Tu, Li and Yuan. This is an open-access article distributed under the terms of the Creative Commons Attribution License (CC BY). The use, distribution or reproduction in other forums is permitted, provided the original author(s) and the copyright owner(s) are credited and that the original publication in this journal is cited, in accordance with accepted academic practice. No use, distribution or reproduction is permitted which does not comply with these terms.

frontiers | Frontiers in Oncology

ORIGINAL RESEARCH
published: 08 July 2022
doi: 10.3389/fonc.2022.909426

Pegylated Liposomal Doxorubicin, Docetaxel, and Trastuzumab as Neoadjuvant Treatment for HER2-Positive Breast Cancer Patients: A Phase II and Biomarker Study

Haoqi Wang[1], Yuntao Li[1], Yixin Qi[1], Erbao Zhao[2], Xiangshun Kong[3], Chao Yang[1], Qiqi Yang[1], Chengyuan Zhang[1], Yueping Liu[4] and Zhenchuan Song[1]**

[1] Breast Center, Fourth Hospital of Hebei Medical University, Key Laboratory for Breast Cancer Molecular Medicine of Hebei Province, Shijiazhuang, China, [2] Department of Breast Center, Shanxi Cancer Hospital, Taiyuan, China, [3] Department of Breast Surgery, Xingtai People's Hospital, Xingtai, China, [4] Pathology Department, Fourth Hospital of Hebei Medical University, Hebei Province Key Laboratory of Breast Cancer Molecular Medicine, Shijiazhuang, China

OPEN ACCESS

Edited by:
Sonia Pernas,
Catalan Institute of Oncology, Spain

Reviewed by:
Erica Quaquarini,
Scientific Clinical Institute Maugeri (ICS Maugeri), Italy
Takahiro Kogawa,
Cancer Institute Hospital of Japanese Foundation for Cancer Research, Japan

***Correspondence:**
Zhenchuan Song
songzhch@hotmail.com
Yueping Liu
annama@163.com

Specialty section:
This article was submitted to Breast Cancer, a section of the journal Frontiers in Oncology

Received: *31 March 2022*
Accepted: *30 May 2022*
Published: *08 July 2022*

Citation:
Wang H, Li Y, Qi Y, Zhao E, Kong X, Yang C, Yang Q, Zhang C, Liu Y and Song Z (2022) Pegylated Liposomal Doxorubicin, Docetaxel, and Trastuzumab as Neoadjuvant Treatment for HER2-Positive Breast Cancer Patients: A Phase II and Biomarker Study. Front. Oncol. 12:909426. doi: 10.3389/fonc.2022.909426

Background: Combined neoadjuvant chemotherapy with trastuzumab and pertuzumab is the standard regimen for human epidermal growth receptor 2 (HER2)-positive breast cancer (BC). However, pertuzumab is not available because it is not on the market or covered by medicare in some regions or poor economy. Anthracyclines and taxanes are cornerstones in BC chemotherapy, and their combination contributes to satisfactory efficiency in neoadjuvant settings. Nonetheless, concomitant administration of trastuzumab and an anthracycline is generally avoided clinically due to cardiotoxicity. Pegylated liposomal doxorubicin (PLD) is less cardiotoxic compared with traditional anthracyclines. Here, we conducted this prospective study to evaluate the efficacy, safety, and potential biomarkers for PLD plus trastuzumab and docetaxel as neoadjuvant treatment in HER2-positive BC.

Patients and Methods: Patients with stage II or III HER2-positive BC were recruited in this multicenter, open-label, single-arm, phase II study. Eligible patients were given 6 cycles of PLD plus docetaxel and trastuzumab. Primary endpoint was total pathological complete response (tpCR, ypT0/is ypN0). Secondary endpoints were breast pathological complete response (bpCR, ypT0/is), objective response rate (ORR), operation rate, breast-conserving surgery rate, and safety. Metadherin (MTDH), glutaminyl-peptide cyclotransferase (QPCT), topoisomerase II alpha (TOP2A), programmed death ligand 1 (PD-L1), and tumor-infiltrating lymphocytes (TILs) were evaluated in BC tissues pre-neoadjuvant for potential biomarkers.

Results: Between March 2019 and February 2021, 54 patients were enrolled, 50 were included in the analysis, and 35 (70.0%) completed 6 cycles of neoadjuvant treatment. Forty-nine (98.0%) patients underwent surgery with a breast-conserving rate of 44.0%. The tpCR rate, bpCR rate, and ORR were 48.0% (95% CI, 33.7%–62.6%), 60.0% (95% CI, 45.2%–73.6%), and 84.0% (95% CI, 70.9%–92.8%), respectively. tpCR was

associated with MTDH (p = 0.002) and QPCT (p = 0.036) expression but not with TOP2A (p = 0.75), PD-L1 (p = 0.155), or TILs (p = 0.76). Patients with HR-negative status were more likely to achieve bpCR compared with those with HR-positive status (76.2% vs. 48.3%, p = 0.047). Grade ≥3 adverse events occurred in 38.0% of patients. Left ventricular ejection fraction decline by ≥10% was reported in 18.0% of patients, and no patient experienced congestive heart failure.

Conclusions: PLD plus docetaxel and trastuzumab might be a potential neoadjuvant regimen for HER2-positive BC with a high tpCR rate and manageable tolerability. MTDH and QPCT are potential predictive markers for tpCR.

Keywords: HER2-positive breast cancer, neoadjuvant treatment, pegylated liposomal doxorubicin, trastuzumab, efficacy, safety, biomarker

INTRODUCTION

Breast cancer (BC) has been the most common malignancy for women worldwide in terms of both morbidity and mortality (1). As a kind of systemic treatment before surgery, neoadjuvant chemotherapy (NAC) has become the preferred treatment for patients with locally advanced BC (2). Human epidermal growth receptor 2 (HER2) is positive in about 20%–25% of breast tumors (3). Although HER2-positive breast tumors are associated with aggressive phenotypes and poor prognosis, they are highly sensitive to some chemotherapeutic agents such as anthracyclines or taxanes (4–6). Previous studies have displayed a high pathological complete response (pCR) rate in neoadjuvant treatment with combined application of anthracyclines and taxane (7). Therefore, anthracycline and taxane-based combination chemotherapy is currently considered to be the standard neoadjuvant regimen for HER2-positive BC (8). However, long-term follow-up data showed that around 15%–24% of patients with BC will still experience disease recurrence—even death (9). In this regard, exploring optimal regimens is crucial for patients with BC to obtain longer survival.

Trastuzumab, the first anti-HER2 monoclonal antibody, was approved by the Food and Drug Administration for HER2-positive BC in 1998 (10). Since the advent of trastuzumab, the outcomes of patients with HER2-positive BC have been greatly improved (11–13). Trastuzumab combined with pertuzumab is the preferred treatment in the HER2-positive neoadjuvant setting. However, pertuzumab is not available because it is not on the market or covered by Medicare in some regions or poor economy. A preclinical study has shown that there are additive interactions between trastuzumab and doxorubicin and synergistic interaction between trastuzumab and docetaxel (14). However, the concurrent use of trastuzumab and an anthracycline is clinically avoided on account of synergetic cardiotoxicity (15).

To overcome the cardiotoxicity and improve the penetration of doxorubicin, liposomal doxorubicin (LD) has been developed (16). Compared with conventional doxorubicin, LD offers a significant reduction in cardiotoxicity while preserving its antitumor efficacy for metastatic BC (17, 18). Therefore, LD can serve as an alternative for traditional anthracyclines in the neoadjuvant setting for HER2-positive BC. Several phase II clinical trials have confirmed that LD plus docetaxel and trastuzumab as neoadjuvant treatment is active in HER2-positive BC and entails a favorable cardiotoxicity profile (19, 20). Pegylated liposomal doxorubicin (PLD) is a formulation of doxorubicin encapsulated in about 100-nm vesicles with a lipophilic surface that is coated with hydrophilic polyethylene glycol (21). Although both LD and PLD show a preferential uptake in tumor tissue, mononuclear phagocytic system uptake is avoided by PLD, resulting in increased circulation time (22, 23). Thus far, no studies have assessed the combination of PLD plus trastuzumab and docetaxel as neoadjuvant treatment for patients with HER2-positive BC. For this purpose, a multicenter, open-label, single-arm, phase II study was designed to assess the efficacy and safety of PLD plus trastuzumab and docetaxel for the neoadjuvant treatment of patients with stage II or III HER2-positive BC for the first time.

METHODS

Study Design

This study was a multicenter, open-label, single-arm, phase II study conducted in 3 hospitals in China. Patients with stage II or III HER2-positive BC were recruited between March 2019 and February 2021. This trial was registered in the Chinese Clinical Trial Registry (number ChiCTR1900021473) and was done in conformance with Good Clinical Practice guidelines and the Declaration of Helsinki. The implementation and modification of the protocol were approved by the ethics committee of the Fourth Hospital of Hebei Medical University. All patients provided written informed consents.

Patient Eligibility

Treatment-naive cases aged 18–70 years with histologically verified invasive HER2-positive BC staging II–III were eligible. Patients were required to have a Karnofsky performance status (KPS) score of 80–100, at least one assessable target lesion based on Response Evaluation Criteria in Solid Tumours (RECIST) 1.1, and left ventricular ejection fraction (LVEF) ≥55%. Patients with

adequate organ function according to local laboratory examination were also included. Patients who had a history of other malignancies within 5 years (other than cured cervix carcinoma *in situ* or basal cell carcinoma of the skin), with involved supraclavicular or internal mammary lymph nodes, or other conditions that researchers considered inappropriate for participation were ineligible for this study. Pregnant or lactating women were also excluded.

Procedures

Eligible patients were scheduled for six cycles (every 3 weeks per cycle) of PLD (40 mg/m^2; CSPC Ouyi Pharmaceutical Co., Ltd., Shijiazhuang, China) plus docetaxel (75 mg/m^2) and trastuzumab (loading dose 8 mg/kg, maintenance dose 6 mg/kg) intravenously for neoadjuvant treatment. Dose adjustment of PLD from 40 to 35 mg/m^2 would be performed once grade ≥3 adverse events (AEs) occurred. In addition, discontinuation and suspension of neoadjuvant treatment were allowed when patients experienced disease progression or unacceptable toxicity. Breast-conserving operation or modified radical mastectomy was scheduled within 3–4 weeks after the final dose of chemotherapy based on the condition of patients and their own choice. The decision of postoperative therapy was based on physician preference.

Based on RECIST 1.1, tumor response was assessed by the investigator using magnetic resonance imaging (MRI) every two NAC cycles. Toxicity was assessed by laboratory tests, electrocardiogram (ECG) examination, and intracoronary Doppler ultrasound every one chemotherapy cycle. All eligible patients were followed up until the withdrawal of consent or death.

Before neoadjuvant treatment, ultrasound-guided needle biopsy of the primary tumor in both breast and abnormal lymph nodes was performed for histological diagnosis, including an evaluation of hormone receptors (HRs), HER2, Ki-67, *metadherin (MTDH), glutaminyl-peptide cyclotransferase (QPCT), topoisomerase II alpha (TOP2A)*, and *programmed death ligand 1 (PD-L1). Tumors with estrogen receptor (ER)* or *progesterone receptor (PR)* expression ≥1% were considered as HR-positive. HER2 positivity was defined as immunohistochemistry (IHC) 3+ or 2+ with fluorescence *in situ* hybridization (FISH) positivity. HR, HER2, and Ki-67 status were confirmed at the local pathology department in each research center. The expression of MTDH was assessed based on the staining intensity (0, negative; 1, weak; 2, moderate; 3, strong) and percentage of positively stained tumor cells (0, none; 1, 1%–20%; 2, 21%–50%; 3, 51%–70%; 4, >70%). The immunoreactive score (IRS) was calculated by multiplying the percentage of positively stained tumor cells and staining intensity score. IRS exhibiting ≤4 was regarded as low expression and >4 as high expression. The evaluation criteria for QPCT expression were in accordance with MTDH, except for IRS ≤3 representing low expression. TOP2A expression ≥10% was defined as TOP2A-positive. PD-L1 expression (22C3 antibody) was assessed as the combined positive score (CPS), which was defined as the number of PD-L1-positive cells (tumor cells, lymphocytes, and macrophages) of any type divided by the total number of tumor cells (24). CPS ≥1 was defined as PD-L1-positive. Infiltration status of tumor-infiltrating lymphocytes (TILs) was analyzed by hematoxylin–eosin (HE) staining and was scored as low (0%–10%), moderate (11%–59%), and high (>60%) (25).

Endpoints

The primary endpoint was total pathological complete response (tpCR), which was defined as the absence of invasive lesions in the breast and axillary lymph nodes (ypT0/is ypN0). Pathological response status was assessed according to Miller–Payne (MP) grading system. The secondary endpoints were breast pathological complete response (bpCR; ypT0/is, defined as no invasive carcinoma in the breast), objective response rate [ORR; calculated as the proportion of patients achieving a complete response (CR) and a partial response (PR) after the last neoadjuvant treatment], operation rate, breast-conserving surgery rate, and safety. Safety was assessed using the Common Terminology Criteria for Adverse Events (CTCAE) version 5.0. Cardiotoxicity was defined as a resting LVEF less than 50%, LVEF that decreased by ≥10% from baseline, or occurrence of congestive heart failure (CHF). Exploratory endpoint was the tpCR according to MTDH, QPCT, TOP2A, and PD-L1 expressions, as well as infiltration status of TILs.

Statistical Analysis

Sample size of this study was not statistically calculated but was expected to provide sufficient data to support the research purposes. All statistical analyses were performed using IBM SPSS 25.0 (IBM Corp., Armonk, NY, USA). Efficacy analysis was carried out according to full analysis set (FAS), which was defined as all participants who received at least one cycle of neoadjuvant treatment and without serious violation of the eligibility criteria. Safety was evaluated based on safety analysis set (SAS), which was defined as all participants who received at least one cycle of neoadjuvant treatment and at least one assessment of safety data. Categorical variables were presented as percentages and numbers. The proportion of patients with tpCR, bpCR, and ORR was tested and recorded with 95% confidence interval (CI) obtained by the Clopper–Pearson method. Differences between the groups were estimated using chi-square test. A $p < 0.05$ was considered to be statistically significant.

RESULTS

Patient Characteristics

Between March 2019 and February 2021, 54 patients from 3 centers in China were assessed for eligibility, and 53 were eligible for this trial (one did not meet inclusion criteria). Of the 53 eligible patients, 51 received neoadjuvant treatment (two withdrew consent before treatment), and 50 were finally included in the FAS and SAS (**Figure 1**). The reason for not being included in the FAS and SAS was protocol violation (n = 1).

Baseline characteristics of the 50 patients are listed in **Table 1**. The median age of the 50 patients was 50.5 years (range, 44.0–56.0 years). The majority of patients were premenopausal (27/50, 54.0%), older than 50 years of age (26/50, 52.0%), had T2 tumors (34/50, 68.0%), and had axillary lymph node involvement (48/50, 96.0%). HR was positive in 58.0% (29/50) of patients, and Ki-67 was >30% in 66.0% (33/50) of patients.

Clinical Activity

In total, 35 patients (70.0%) completed 6 cycles of neoadjuvant treatment, and 41 patients (82.0%) completed 4–6 cycles of neoadjuvant treatment. Reasons for 15 cases that did not complete 6 cycles of neoadjuvant treatment included intolerable AEs (n = 13), death due to interstitial pneumonia without standardized treatment for the AE (n = 1), and patient withdrawal because of allergy to granulocyte colony-stimulating factor (n = 1). Of these, the AEs that led to incompletion of the full course regimen were grade 2–4 hand–foot syndrome (HFS) (6 cases, 12%), grade 3 interstitial pneumonia (4 cases, 8%), grade 2 stomatitis (2 cases, 4%), and intolerable grade 2 malaise (2 cases, 4%).

Forty-nine (98.0%) of 50 patients received surgery after neoadjuvant treatment finally, of which 22 (44.0%) underwent breast-conserving surgery and 27 (54.0%) underwent modified radical mastectomy. The reason for one surgery cancelation was death due to interstitial pneumonia without standardized treatment. The median interval from the completion of neoadjuvant therapy to surgery was 3.1 weeks (interquartile range, 2.9–4.9 weeks).

Twenty-four (48.0%; 95% CI, 33.7%–62.6%) of 50 patients achieved a tpCR, and 30 (60.0%; 95% CI, 45.2%–73.6%) had a bpCR. The univariate analyses revealed that age, menopausal state, tumor size stage, axillary lymph node involvement, clinical stage, or Ki-67 level was not associated with tpCR (all $p > 0.05$; **Table 2**) or bpCR (all $p > 0.05$). HR status was associated with

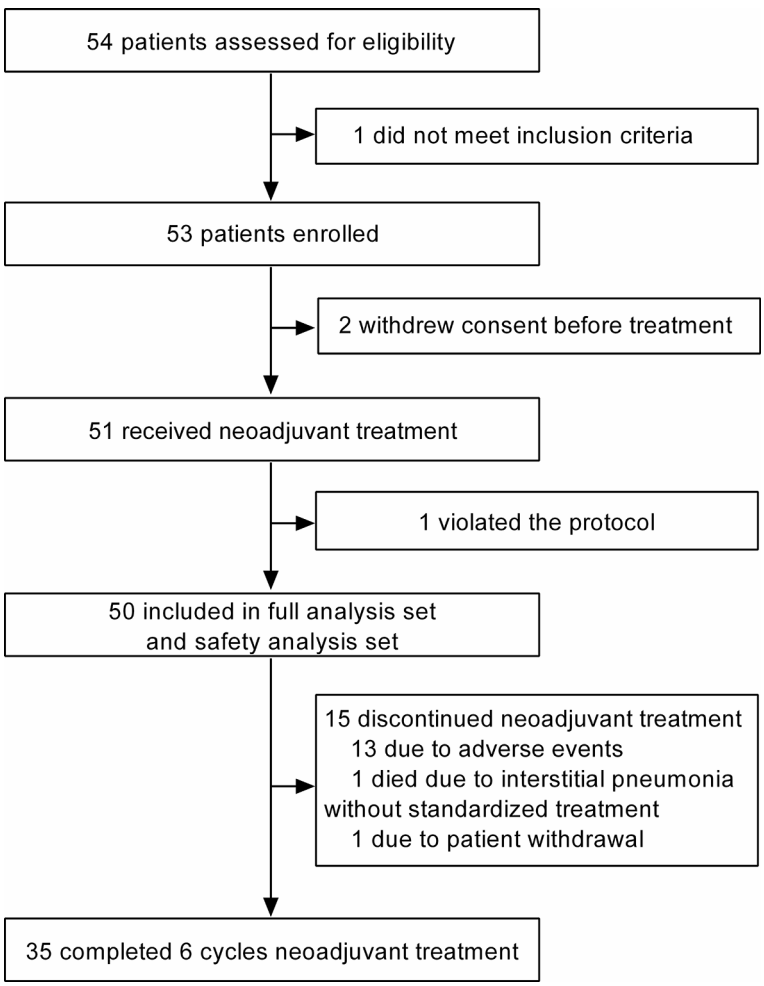

FIGURE 1 | Trial profile.

TABLE 1 | Baseline characteristics of patients.

	Patients (n = 50)
Age (years), median (range)	50.5 (44.0–56.0)
Age (years; n, %)	
≤50	24 (48.0)
>50	26 (52.0)
Axillary lymph nodes involvement (n, %)	
Positive	48 (96.0)
Negative	2 (4.0)
Menopausal state (n, %)	
Postmenopausal	23 (46.0)
Premenopausal	27 (54.0)
Clinical stage (n, %)	
II	25 (50.0)
III	25 (50.0)
Ki-67 (n, %)	
≤30%	17 (34.0)
>30%	33 (66.0)
Hormone receptor status (n, %)	
Positive	29 (58.0)
Negative	21 (42.0)
Karnofsky performance status (n, %)	
100	36 (72.0)
90	12 (24.0)
80	2 (4.0)
Tumor size stage (n, %)	
T1	5 (10.0)
T2	34 (68.0)
T3	5 (10.0)
T4	6 (12.0)
Surgery (n, %)	
Modified radical mastectomy	27 (54.0)
Breast-conserving surgery	22 (44.0)
Surgery not performed	1 (2.0)

bpCR (HR-negative vs. HR-positive: 76.2% vs. 48.3%, $p = 0.047$) but not tpCR ($p > 0.05$).

Of the 50 patients, 19 (38.0%) achieved a CR, 23 (46.0%) achieved a PR, and 6 (12.0%) had stable disease (SD) as their best response, for an ORR of 84.0% (95% CI, 70.9%–92.8%). No patient experienced disease progression.

Exploratory Endpoint

The IHC results of MTDH, QPCT, and TOP2A were available in 37 cases. High expression of MTDH and QPCT was detected in 28 (75.7%) and 26 (70.3%) patients, respectively. The incidence of negative and positive expression for TOP2A was exhibited similarly (48.6% vs. 51.4%). Both MTDH and QPCT were highly expressed in 59.5% (22/37) of 37 cases. Patients who carried a high level of MTDH (60.7%, $p = 0.002$; **Figures 2A, D**) or QPCT (57.7%, $p = 0.036$; **Figures 2A, E**) or both ($MTDH_{high}QPCT_{high}$, 68.2%; $p = 0.002$) were inclined to achieve a tpCR. There was no significant difference in tpCR between patients with TOP2A negativity and TOP2A positivity ($p = 0.75$; **Figures 2B, F**).

The PD-L1 expression was assessed in 41 cases. Although patients with PD-L1 positivity (12/21, 57.1%) tended to show a higher tpCR proportion compared to those with PD-L1 negativity (7/20, 35.0%), there was no significant difference ($p = 0.155$; **Figures 2B, G**).

Due to the limited amount of puncture tissue, 44 cases had available TIL results. Among them, 26 (59.1%) exhibited low infiltration, 17 (38.6%) displayed moderate infiltration, and 1 (2.3%) showed high infiltration. The tpCR of patients with low infiltration status of TILs (46.2%) was lower than those with moderate and high infiltration status (55.6%), although without statistical significance ($p = 0.76$; **Figures 2C, H**).

Safety

Treatment-related AEs (**Table 3**) of any grade occurred in 88.0% (44/50) of all patients, and most AEs were grades 1–2. In this study, 38.0% (19/50) of cases experienced grade ≥3 AEs. The most common AEs were oral mucositis (68.0%), followed by HFS (56.0%) and watery eyes (40.0%). Nineteen patients (38.0%) experienced dose reduction of PLD due to grade 3 AEs including oral mucositis and HFS. One patient died of neoadjuvant treatment-related interstitial pneumonia without standardized treatment for the AE.

From baseline to surgery, LVEF decline by ≥10% was noted in 9 patients (18%), but none of them was <50%. The changes of LVEF in all assessable patients are displayed in **Figure 3**. LVEF decline was observed initially after 1 cycle of NAC in one case, while most of the LVEF reduction events occurred after 3 cycles of chemotherapy. Six of the 9 decreased LVEF were recoverable, and 2 of them ultimately recovered to baseline level after a full course of neoadjuvant therapy. CHF was not noted in this study. Apart from LVEF reduction, palpitation (grade 1 or 2) was observed in 10.0% (5/50) of patients. Grade 1 ventricular

TABLE 2 | The effect of clinical characteristic variables on the tpCR.

	tpCR (n = 50)		*p* value
	Yes (n = 24)	No (n = 26)	
Age			0.402
≤50	13 (54.2)	11 (45.8)	
>50	11 (42.3)	15 (57.7)	
Menopausal state			0.982
Postmenopausal	11 (47.8)	12 (52.2)	
Premenopausal	13 (48.1)	14 (51.9)	
Axillary lymph nodes involvement			0.506
Positive	24 (50.0)	24 (50.0)	
Negative	0 (0.0)	2 (100.0)	
Clinical stage			0.571
II	11 (44.0)	14 (56.0)	
III	13 (52.0)	12 (48.0)	
Ki-67			0.402
≤30%	7 (41.2)	10 (58.8)	
>30%	17 (51.5)	16 (48.5)	
Hormone receptor status			0.271
Positive	12 (41.4)	17 (58.6)	
Negative	12 (57.1)	9 (42.9)	
Tumor size stage			0.459
T1	2 (40.0)	3 (60.0)	
T2	17 (50.0)	17 (50.0)	
T3	1 (20.0)	4 (80.0)	
T4	4 (66.7)	2 (33.3)	

tpCR, total pathological complete response.

premature contraction was reported in only 1 case before the second cycle of neoadjuvant treatment.

DISCUSSION

To the best of our knowledge, this multicenter, open-label, single-arm, phase II study provided the first analysis of the combination of PLD, trastuzumab, and docetaxel for the neoadjuvant treatment of patients with HER2-positive BC. In general, most of the patients (70.0%) completed the full course (6 cycles) of NAC, and relatively high tpCR (48%) and bpCR (60%) were attained in the present study, which demonstrated that PLD plus docetaxel and trastuzumab might be a potential neoadjuvant regimen for HER2-positive BC.

The achievement of pCR after neoadjuvant treatment has been confirmed to be associated with better long-term outcomes in terms of progression-free survival and overall survival (26–28). Accordingly, tpCR and bpCR were defined as efficacy endpoints in our study. PLD plus docetaxel and trastuzumab in the neoadjuvant setting for stage II or III HER2-positive BC showed good antitumor activity, with a tpCR rate of 48.0% and a bpCR rate of 60.0%. The tpCR obtained in our study was higher than that observed in other studies (6, 19, 20). Uriarte-Pinto et al. (6) demonstrated that the tpCR rate of patients with HER2-positive BC managed with LD plus trastuzumab and paclitaxel was 40%. Besides, two phase II clinical trials evaluated the efficacy of LD in combination with trastuzumab and docetaxel as neoadjuvant treatment for patients with HER2-positive BC and reported tpCR rates of 27% (19) and 38.3% (20). The patient characteristics including clinical stage, Ki-67 level, and HR status, as well as different chemotherapeutic regimens, might contribute to this discrepancy in pCR. It was worth noting that the pCR observed in our study was even comparable to double anti-HER2 therapy (29). The Opti-HER HEART trial documented a tpCR rate of 56.6% following neoadjuvant LD, paclitaxel, trastuzumab, and pertuzumab in HER2-positive BC (29). In addition, patients with early-stage HER2-positive BC in a real-world study presented a tpCR rate of 54% after neoadjuvant pertuzumab and trastuzumab with chemotherapy (30). However, pertuzumab is not available in some regions for a variety of reasons; thus, single trastuzumab plus chemotherapy remains to be the preferred regimen. In addition, the ORR and breast-conserving surgery rates observed in our study were 84.0% and 44.0%, respectively. Taken together, the neoadjuvant regimen containing PLD plus docetaxel and trastuzumab was active for patients with HER2-positive BC. However, further follow-up should be conducted to verify whether the high pCR rate could contribute to the survival benefit.

Accumulating evidence had illustrated that HR-negative cases had the advantage of achieving pCR (31, 32). Our data did not observe the variance between HR-positive and HR-negative subsets as for tpCR. However, patients who had HR-negative status were more likely to achieve bpCR compared with those who had HR-positive status (76.2% vs. 48.3%, $p = 0.047$). Prior findings discovered that patients with high Ki-67 level, small tumor size, or low clinical stage have better access to get pCR (33–35). Due to the limited sample size, this study failed to confirm the correlation between tpCR and other clinicopathological indicators. Thus, studies with large sample sizes are necessary to further investigate predictions of pCR and prognosis.

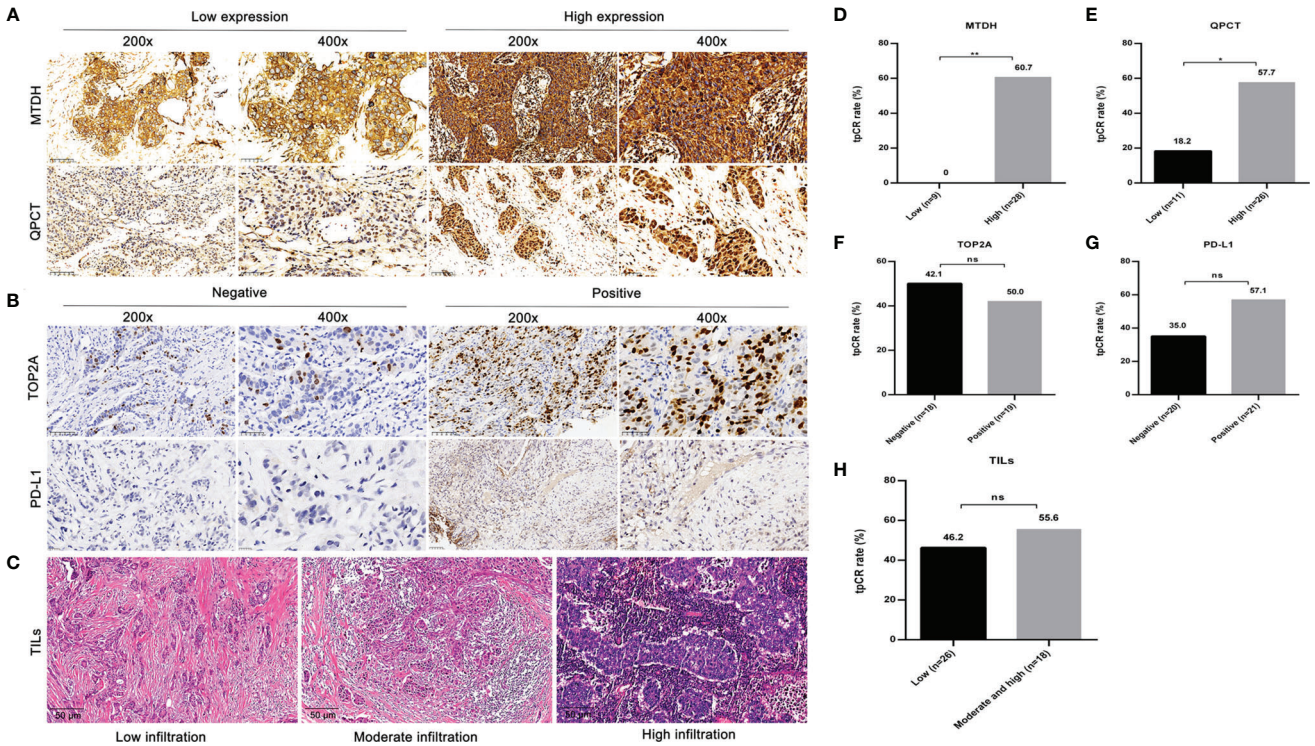

FIGURE 2 | The representative images and effect of MTDH, QPCT, TOP2A, and PD-L1 expressions, as well as infiltration status of TILs on tpCR. **(A)** Representative IHC images of MTDH and QPCT (low and high expressions). **(B)** Representative IHC images of TOP2A and PD-L1 (positive and negative). **(C)** Representative HE staining images of TILs. **(D)** The tpCR according to MTDH expressions. **(E)** The tpCR according to QPCT expressions. **(F)** The tpCR according to TOP2A expressions. **(G)** The tpCR according to PD-L1 expressions. **(H)** The tpCR according to infiltration status of TILs. tpCR, total pathological complete response; MTDH, metadherin; QPCT, glutaminyl-peptide cyclotransferase; TOP2A, topoisomerase II alpha; PD-L1, programmed death ligand 1; TILs, tumor-infiltrating lymphocytes; IHC, immunohistochemistry; HE, hematoxylin–eosin. * $p < 0.05$; ** $p < 0.01$.; ns, no significance.

MTDH acting as an oncogene can promote tumor cell proliferation and inhibit apoptosis (36). Overexpression of MTDH is noted in aggressive BC subsets, such as triple-negative BC and HER2-overexpressed tumors (37). QPCT, a secreted protein implicated in the biosynthesis of pyroglutamyl peptides, is found to contribute to angiogenesis (38). Our preceding experiment suggested that MTDH and QPCT were intensively expressed in local advanced breast tumors and positively correlated with poor disease-free survival. The current study showed that patients who carried a high level of MTDH, QPCT, or both were more liable to attain tpCR. Interestingly, published studies demonstrated that a high expression of MTDH was associated with drug resistance (39), but our cases with a high expression of MTDH showed a sensitive response to neoadjuvant treatment. Of note, we only examined the MTDH level at baseline, not after neoadjuvant therapy, which may be not enough to explain the relationship between MTDH and drug resistance. The changes of MTDH after neoadjuvant treatment should be probably taken into consideration to evaluate its correlation with chemoresistance. Although pCR after preoperative therapy is considered to be a powerful surrogate of survival, in view of the influence of MTDH on chemoresistance and trastuzumab resistance, follow-up should be continued to further assess the influence of MTDH on long-term efficiency.

TOP2A is a proliferation marker associated with Ki-67 index and tumor grade (40). Considering that tumors with TOP2A positivity were more sensitive to anthracyclines (41), the expression TOP2A was tested in our study. However, there was no trend to obtain pCR in cases with TOP2A positivity, which might be attributed to the limited sample size and different interpretation criteria for TOP2A. Evidence has shown that PD-L1 positivity is correlated with a high proportion of pCR rate in patients with HER2-positive BC (42). In our study, patients with PD-L1 positivity tended to show a higher tpCR proportion compared to those with PD-L1 negativity, but statistical significance was not reached in tpCR due to the small sample size. It is documented that the high infiltration status of TILs before neoadjuvant treatment can significantly predict a high pCR rate of HER2-positive BC (25). Nevertheless, only 1 (2.3%) case exhibited high infiltration of TILs in our study due to the small sample size. Thus, we failed to observe a significant trend to achieve pCR in patients with a high infiltration status of TILs.

Although our studied treatment attained excellent efficiency, the safety issues related to treatment deserve attention. First of all, some patients did not complete the full course

TABLE 3 | Treatment-related adverse events in all patients (n = 50).

Adverse events (n, %)	Grade 1–2	Grade 3–4	Any grade
Hematological toxicity			
Leukopenia	7 (14.0)	6 (12.0)	13 (26.0)
Neutrocytopenia	1 (2.0)	3 (6.0)	4 (8.0)
Non-hematological toxicity			
Oral mucositis	30 (60.0)	4 (8.0)	34 (68.0)
Hand–foot syndrome	22 (44.0)	6 (12.0)	28 (56.0)
Watery eyes	20 (40.0)	0 (0.0)	20 (40.0)
Diarrhea	16 (32.0)	3 (6.0)	19 (38.0)
Alopecia	18 (36.0)	0 (0)	18 (36.0)
Nausea	17 (34.0)	0 (0)	17 (34.0)
Vomiting	13 (26.0)	0 (0)	13 (26.0)
Anorexia	12 (24.0)	0 (0)	12 (24.0)
Fever	11(22.0)	0 (0)	11 (22.0)
Malaise	11 (22.0)	0 (0)	11 (22.0)
LVEF reduction	9 (18.0)	0 (0.0)	9 (18.0)
Bloating	9 (18.0)	0 (0)	9 (18.0)
Insomnia	6 (12.0)	2 (4.0)	8 (16.0)
Headache	8 (16.0)	0 (0)	8 (16.0)
Cough	6 (12.0)	1 (2.0)	7 (14.0)
Dysphagia	5 (10.0)	1 (2.0)	6 (12.0)
Alanine aminotransferase elevation	6 (12.0)	0 (0)	6 (12.0)
Interstitial pneumonia	0 (0)	5 (10.0)	5 (10.0)
Constipation	5 (10.0)	0 (0)	5 (10.0)
Palpitations	5 (10.0)	0 (0)	5 (10.0)
Oropharyngeal pain	3 (6.0)	0 (0)	3 (6.0)
Aspartate aminotransferase elevation	4 (8.0)	0 (0)	4 (8.0)
Cutaneous pigmentation	3 (6.0)	0 (0)	3 (6.0)
Sore throat	3 (6.0)	0 (0)	3 (6.0)
Ventricular premature contraction	1 (2.0)	0 (0)	1 (2.0)

LVEF, left ventricular ejection fraction.

of chemotherapy due to poor tolerance. The completion rate of NAC in terms of concomitant use of anthracyclines, taxanes, and trastuzumab in published clinical trials differs. In the GEICAM 2003-03 study (43), only 4 patients (6%) did not finish the full course of NAC schedule containing liposome-encapsulated doxorubicin (50 mg/m^2) and docetaxel (60 mg/m^2) on day 1 every 3 weeks combined with trastuzumab (4 mg/kg loading dose on day 1, followed by 2 mg/kg weekly). Gavilá et al. (44) reported that 72.6% of the NAC settings completed a full course of study treatment with six cycles of non-pegylated liposome-encapsulated doxorubicin (50 mg/m^2 every 3 weeks), paclitaxel (80 mg/m^2 weekly), and trastuzumab (loading dose 4 mg/kg, maintenance dose 2 mg/kg weekly). In another observational study (6), 66.7% of the studied patients finished six cycles of the combination of non-pegylated liposome-encapsulated doxorubicin (50 mg/m^2 on day 1 every 3 weeks), paclitaxel (80 mg/m^2 on days 1, 7, and 14), and trastuzumab (loading dose 8 mg/kg, maintenance dose 6 mg/kg every 3 weeks). Accordingly, considering the variation in drug type and initial drug dosage, our therapeutic regimen has been relatively well tolerated. Secondly, consistent with previous reports (45, 46), the most frequent PLD-related AEs of any grade in our study were oral mucositis (68.0%) and HFS (56.0%), and most AEs were grades 1–2. These AEs were the main cause for the incompleted full course of chemotherapy, which may result from the high dosage of PLD (40 mg/m^2–35 mg/m^2) relative to that of other studies (35 mg/m^2–30 mg/m^2). In one of our published studies (47), four cycles of PLD (40 mg/m^2) plus cyclophosphamide (600 mg/m^2) on day 1 of a 21-day schedule, followed by four cycles of docetaxel (85 mg/m^2) on day 1 of a 21-day schedule, were tested in NAC populations whatever the molecular typing. Although 86.6% of all cohorts completed the full course of chemo, the pCR was lower than that of the current data. Even if the incidence of HFS (45.53%) and oral mucositis (39.28%) was

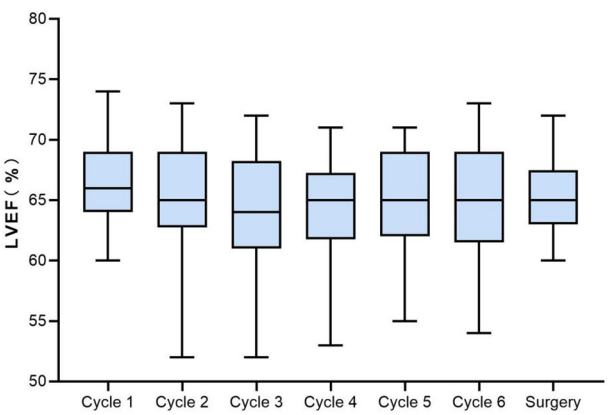

FIGURE 3 | Boxplots of LVEF from baseline to surgery in the assessable population. LVEF, left ventricular ejection fraction.

relatively low, nausea/vomiting (81.25%) and fatigue (74.11%) were the most common events. The mechanism underlying skin and mucous injury induced by PLD was not fully elucidated, but it might be related to increased vascular permeability caused by PLD (48). Our team is dedicating to explore potential approaches to cope with HFS caused by PLD, and we have reported that calcium dobesilate (CaD) could alleviate HFS in the Sprague–Dawley rat model treated by PLD (49). The clinical trial on the prevention of HFS by CaD conducted in PLD-treated BC settings is undergoing, and the result will be published in the future. In the present study, only one case died of interstitial pneumonia after 3 cycles of neoadjuvant treatment, which mainly resulted from the lack of standardized treatment for the AE.

It has been reported that traditional anthracyclines (doxorubicin and epirubicin) combined with trastuzumab might cause cardiotoxicity (11). To avoid potential heart problems, PLD was used as a substitute for traditional anthracycline. In a series of studies assessing concurrent use of trastuzumab and PLD for metastatic HER2-positive BC, around 4.5%–23% of LVEF decline was noted (50–52). The diversity may be on account of different therapeutic regimens and characteristics of patients. In the present study, PLD in combination with trastuzumab showed good cardiac safety, with 9 (18.0%) cases that experienced LVEF decline by ≥10%, 2 of which recovered to baseline before surgery. No case of CHF was observed, and no death from cardiotoxicity occurred in our study. Follow-up will be carried out to monitor long-term effects of PLD plus trastuzumab on cardiac function. To sum up, PLD in combination with docetaxel and trastuzumab was generally well tolerated for HER2-positive BC in the neoadjuvant setting.

In consideration of the overlap in cardiotoxicity of anthracyclines and trastuzumab, clinical trials have attempted therapeutic protocols in the absence of anthracyclines. However, there is no unified conclusion until now. In terms of efficacy, the PH-FECH (paclitaxel 80 mg/m2 weekly for 12 weeks or paclitaxel 225 mg/m2 every 3 weeks, followed by 4 cycles of FEC (fluorouracil 500 mg/m2, epirubicin 75 mg/m2, and cyclophosphamide 500 mg/m2) on day 1, and trastuzumab loading dose 8 mg/kg, maintenance dose 6 mg/ kg, every 3 weeks regimen showed a higher pCR rate (60.6% vs. 43.3%) and relapse-free survival (RFS) advantage (93% vs. 71%) compared with TCH (docetaxel 75 mg/m2 IV on day 1, carboplatin at an area under the concentration curve (AUC) of 6 IV on day1, and trastuzumab loading dose 8 mg/kg, maintenance dose 6 mg/ kg, administered at 3-week intervals for 6 cycles in a retrospective study (53). Even when the dual HER2 blockade was applied, the pCR did not differ significantly [TRYPHAENA (54): anthracycline group vs. non-anthracycline: 61.6% vs. 66.2%, TRAIN-2 (55): anthracycline group vs. non-anthracycline: 67% vs. 68%]. As for the safety, the combination of trastuzumab and anthracycline did not result in significant difference in cardiotoxicity (53–55). However, grade 3 or worse febrile neutropenia was the most common AE in anthracycline-included regimens (53–55). Consequently, we selected PLD in our study to alleviate the cardiotoxicity and hematologic toxicity. Although in the era of optimized HER2-directed therapies trastuzumab concurrent with anthracycline and taxanes (ATH) is not the preferred strategy in the guidelines, ATH might be an alternative option in HER2-positive NAC setting if dual blockade with pertuzumab and trastuzumab is not available.

There were some limitations in the study. Firstly, this trial was limited by the small sample size of patients who were only recruited from 3 hospitals in China. The results might not be generalized to BC cases from other geographic regions or other racial or ethnic backgrounds. Secondly, due to the combination of PLD plus trastuzumab and docetaxel, it was impossible to ascertain the respective contribution of each drug to the overall therapeutic effect. Nonetheless, our results showed that this drug combination appeared to be active for patients with HER2-positive BC with acceptable safety. Thirdly, the open-label, single-arm study design precluded the comparison of clinical benefits with traditional anthracyclines. Finally, due to the relatively short follow-up period, the long-term efficacy as progression-free survival and overall survival was not mature. Thus, randomized controlled trials with larger sample sizes and longer follow-up time are necessary in the future to continue to validate the efficacy and safety of PLD plus docetaxel and trastuzumab for the neoadjuvant treatment of patients with HER2-positive BC.

CONCLUSIONS

In conclusion, the first published phase II study demonstrated that the neoadjuvant regimen containing PLD plus docetaxel and trastuzumab showed good antitumor activity for patients with stage II or III HER2-positive BC, with a relatively high tpCR and bpCR rate. The majority of AEs related to this regimen were mild and controllable, with an acceptable cardiotoxicity profile. These findings suggest that this neoadjuvant regimen might offer a potential therapeutic option for HER2-positive BC. Further follow-up is still needed to confirm the long-term benefit of the neoadjuvant regimen for this population. MTDH and QPCT in BC tissues pre-neoadjuvant are potential predictive markers for tpCR.

DATA AVAILABILITY STATEMENT

The original contributions presented in the study are included in the article/**Supplementary Material**. Further inquiries can be directed to the corresponding authors.

ETHICS STATEMENT

The studies involving human participants were reviewed and approved by the ethics committee of the Fourth Hospital of

Hebei Medical University. The patients/participants provided their written informed consent to participate in this study.

AUTHOR CONTRIBUTIONS

ZS conceived and designed the study. YTL, YQ, EZ, XK, and CY provided study materials and performed data collection. HW, QY, and CZ were involved in data analysis and interpretation and article writing. YPL examined the pathology and immunohistochemistry. All authors were involved in final approval of the article.

FUNDING

This study was supported by the Natural Science Foundation of Hebei Province (H2020206365, H2021206071), Special Fund for Clinical Research of Wu Jieping Medical Foundation (320.6750.2020-07-17), and Beijing Xisike Clinical Oncology Research Foundation (Y-SY201901-0021).

REFERENCES

1. Sung H, Ferlay J, Siegel RL, Laversanne M, Soerjomataram I, Jemal A, et al. Global Cancer Statistics 2020: GLOBOCAN Estimates of Incidence and Mortality Worldwide for 36 Cancers in 185 Countries. *CA Cancer J Clin* (2021) 71(3):209–49. doi: 10.3322/caac.21660
2. Rauch GM, Adrada BE, Kuerer HM, van la Parra RF, Leung JW, Yang WT. Multimodality Imaging for Evaluating Response to Neoadjuvant Chemotherapy in Breast Cancer. *AJR Am J Roentgenol* (2017) 208(2):290–9. doi: 10.2214/AJR.16.17223
3. Schlam I, Swain SM. HER2-Positive Breast Cancer and Tyrosine Kinase Inhibitors: The Time Is Now. *NPJ Breast Cancer* (2021) 7(1):56. doi: 10.1038/s41523-021-00265-1
4. Perrier A, Gligorov J, Lefèvre G, Boissan M. The Extracellular Domain of Her2 in Serum as a Biomarker of Breast Cancer. *Lab Invest* (2018) 98(6):696–707. doi: 10.1038/s41374-018-0033-8
5. Pritchard KI, Messersmith H, Elavathil L, Trudeau M, O'Malley F, Dhesy-Thind B. HER-2 and Topoisomerase II as Predictors of Response to Chemotherapy. *J Clin Oncol* (2008) 26(5):736–44. doi: 10.1200/JCO.2007.15.4716
6. Uriarte-Pinto M, Escolano-Pueyo Á, Gimeno-Ballester V, Pascual-Martínez O, Abad-Sazatornil MR, Agustín-Ferrández MJ. Trastuzumab, non-Pegylated Liposomal-Encapsulated Doxorubicin and Paclitaxel in the Neoadjuvant Setting of HER-2 Positive Breast Cancer. *Int J Clin Pharm* (2016) 38 (2):446–53. doi: 10.1007/s11096-016-0278-5
7. Bines J, Earl H, Buzaid AC, Saad ED. Anthracyclines and Taxanes in the Neo/Adjuvant Treatment of Breast Cancer: Does the Sequence Matter? *Ann Oncol* (2014) 25(6):1079–85. doi: 10.1093/annonc/mdu007
8. Tuxen MK, Cold S, Tange UB, Balslev E, Nielsen DL. Phase II Study of Neoadjuvant Pegylated Liposomal Doxorubicin and Cyclophosphamide ± Trastuzumab Followed by Docetaxel in Locally Advanced Breast Cancer. *Acta Oncol* (2014) 53(10):1440–5. doi: 10.3109/0284186X
9. Pernas S, Barroso-Sousa R, Tolaney SM. Optimal Treatment of Early Stage HER2-Positive Breast Cancer. *Cancer* (2018) 124(23):4455–66. doi: 10.1002/cncr.31657
10. Nami B, Maadi H, Wang Z. Mechanisms Underlying the Action and Synergism of Trastuzumab and Pertuzumab in Targeting HER2-Positive Breast Cancer. *Cancers (Basel)* (2018) 10(10):342. doi: 10.3390/cancers10100342
11. Slamon DJ, Leyland-Jones B, Shak S, Fuchs H, Paton V, Bajamonde A, et al. Use of Chemotherapy Plus a Monoclonal Antibody Against HER2 for Metastatic Breast Cancer That Overexpresses HER2. *N Engl J Med* (2001) 344(11):783–92. doi: 10.1056/NEJM200103153441101
12. Romond EH, Perez EA, Bryant J, Suman VJ, Geyer CEJr, Davidson NE, et al. Trastuzumab Plus Adjuvant Chemotherapy for Operable HER2-Positive Breast Cancer. *N Engl J Med* (2005) 353(16):1673–84. doi: 10.1056/NEJMoa052122
13. Gianni L, Eiermann W, Semiglazov V, Lluch A, Tjulandin S, Zambetti M, et al. Neoadjuvant and Adjuvant Trastuzumab in Patients With HER2-Positive Locally Advanced Breast Cancer (NOAH): Follow-Up of a Randomised Controlled Superiority Trial With a Parallel HER2-Negative Cohort. *Lancet Oncol* (2014) 15(6):640–7. doi: 10.1016/S1470-2045(14)70080-4
14. Pegram MD, Konecny GE, O'Callaghan C, Beryt M, Pietras R, Slamon DJ. Rational Combinations of Trastuzumab With Chemotherapeutic Drugs Used in the Treatment of Breast Cancer. *J Natl Cancer Inst* (2004) 96(10):739–49. doi: 10.1093/jnci/djh131
15. Nicolazzi MA, Carnicelli A, Fuorlo M, Scaldaferri A, Masetti R, Landolfi R, et al. Anthracycline and Trastuzumab-Induced Cardiotoxicity in Breast Cancer. *Eur Rev Med Pharmacol Sci* (2018) 22(7):2175–85. doi: 10.26355/eurrev_201804_14752
16. Chastagner P, Sudour H, Mriouah J, Barberi-Heyob M, Bernier-Chastagner V, Pinel S. Preclinical Studies of Pegylated- and Non-Pegylated Liposomal Forms of Doxorubicin as Radiosensitizer on Orthotopic High-Grade Glioma Xenografts. *Pharm Res* (2015) 32(1):158–66. doi: 10.1007/s11095-014-1452-x
17. Harris L, Batist G, Belt R, Rovira D, Navari R, Azarnia N, et al. Liposome-Encapsulated Doxorubicin Compared With Conventional Doxorubicin in a Randomized Multicenter Trial as First-Line Therapy of Metastatic Breast Carcinoma. *Cancer* (2002) 94(1):25–36. doi: 10.1002/cncr.10201
18. Batist G, Ramakrishnan G, Rao CS, Chandrasekharan A, Gutheil J, Guthrie T, et al. Reduced Cardiotoxicity and Preserved Antitumor Efficacy of Liposome-Encapsulated Doxorubicin and Cyclophosphamide Compared With Conventional Doxorubicin and Cyclophosphamide in a Randomized, Multicenter Trial of Metastatic Breast Cancer. *J Clin Oncol* (2001) 19 (5):1444–54. doi: 10.1200/JCO.2001.19.5.1444
19. Antón A, Ruiz A, Plazaola A, Calvo L, Seguí MA, Santaballa A, et al. Phase II Clinical Trial of Liposomal-Encapsulated Doxorubicin Citrate and Docetaxel, Associated With Trastuzumab, as Neoadjuvant Treatment in Stages II and IIIA HER2-Overexpressing Breast Cancer Patients. *GEICAM 2003-03 Stud Ann Oncol* (2011) 22(1):74–9. doi: 10.1093/annonc/mdq317
20. Rocca A, Cortesi P, Cortesi L, Gianni L, Matteucci F, Fantini L, et al. Phase II Study of Liposomal Doxorubicin, Docetaxel and Trastuzumab in Combination With Metformin as Neoadjuvant Therapy for HER2-Positive Breast Cancer. *Ther Adv Med Oncol* (2021) 13:1758835920985632. doi: 10.1177/1758835920985632
21. Barenholz Y. Doxil®–the First FDA-Approved Nano-Drug: Lessons Learned. *J Control Release* (2012) 160(2):117–34. doi: 10.1016/j.jconrel.2012.03.020
22. Waterhouse DN, Tardi PG, Mayer LD, Bally MB. A Comparison of Liposomal Formulations of Doxorubicin With Drug Administered in Free Form: Changing Toxicity Profiles. *Drug Saf* (2001) 24(12):903–20. doi: 10.2165/00002018-200124120-00004
23. Shafei A, El-Bakly W, Sobhy A, Wagdy O, Reda A, Aboelenin O, et al. A Review on the Efficacy and Toxicity of Different Doxorubicin Nanoparticles for Targeted Therapy in Metastatic Breast Cancer. *BioMed Pharmacother* (2017) 95:1209–18. doi: 10.1016/j.biopha.2017.09.059
24. Adams S, Loi S, Toppmeyer D, Cescon DW, De Laurentiis M, Nanda R, et al. Pembrolizumab Monotherapy for Previously Untreated, PD-L1-Positive, Metastatic Triple-Negative Breast Cancer: Cohort B of the Phase II KEYNOTE-086 Study. *Ann Oncol* (2019) 30(3):405–11. doi: 10.1093/annonc/mdy518
25. Denkert C, von Minckwitz G, Darb-Esfahani S, Lederer B, Heppner BI, Weber KE, et al. Tumour-Infiltrating Lymphocytes and Prognosis in Different Subtypes of Breast Cancer: A Pooled Analysis of 3771 Patients Treated With Neoadjuvant Therapy. *Lancet Oncol* (2018) 19(1):40–50. doi: 10.1016/S1470-2045(17)30904-X

26. Miyashita M, Ishida T. Prospect of Immunotherapy in Neoadjuvant/Adjuvant Treatment for Early Breast Cancer. *Chin Clin Oncol* (2020) 9(3):28. doi: 10.21037/cco.2020.04.01
27. Cortazar P, Zhang L, Untch M, Mehta K, Costantino JP, Wolmark N, et al. Pathological Complete Response and Long-Term Clinical Benefit in Breast Cancer: The CTNeoBC Pooled Analysis. *Lancet* (2014) 384(9938):164–72. doi: 10.1016/S0140-6736(13)62422-8
28. Brown-Glaberman U, Dayao Z, Royce M. HER2-Targeted Therapy for Early-Stage Breast Cancer: A Comprehensive Review. *Oncol (Williston Park)* (2014) 28(4):281–9. doi: 10.1634/theoncologist.2013-0456
29. Gavilá J, Oliveira M, Pascual T, Perez-Garcia J, Gonzàlez X, Canes J, et al. Safety, Activity, and Molecular Heterogeneity Following Neoadjuvant Non-Pegylated Liposomal Doxorubicin, Paclitaxel, Trastuzumab, and Pertuzumab in HER2-Positive Breast Cancer (Opti-HER HEART): An Open-Label, Single-Group, Multicenter, Phase 2 Trial. *BMC Med* (2019) 17(1):8. doi: 10.1186/s12916-018-1233-1
30. Boér K, Kahán Z, Landherr L, Csőszi T, Máhr K, Ruzsa Á, et al. Pathologic Complete Response Rates After Neoadjuvant Pertuzumab and Trastuzumab With Chemotherapy in Early Stage HER2-Positive Breast Cancer - Increasing Rates of Breast Conserving Surgery: A Real-World Experience. *Pathol Oncol Res* (2021) 27:1609785. doi: 10.3389/pore.2021.1609785
31. Tanioka M, Sasaki M, Shimomura A, Fujishima M, Doi M, Matsuura K, et al. Pathologic Complete Response After Neoadjuvant Chemotherapy in HER2-Overexpressing Breast Cancer According to Hormonal Receptor Status. *Breast* (2014) 23(4):466–72. doi: 10.1016/j.breast.2014.03.008
32. Echavarria I, Granja M, Bueno C, Lopez-Tarruella S, Peinado P, Sotelo M, et al. Multicenter Analysis of Neoadjuvant Docetaxel, Carboplatin, and Trastuzumab in HER2-Positive Breast Cancer. *Breast Cancer Res Treat* (2017) 162(1):181–9. doi: 10.1007/s10549-016-4098-z
33. Chen X, He C, Han D, Zhou M, Wang Q, Tian J, et al. The Predictive Value of Ki-67 Before Neoadjuvant Chemotherapy for Breast Cancer: A Systematic Review and Meta-Analysis. *Future Oncol* (2017) 13(9):843–57. doi: 10.2217/fon-2016-0420
34. Rouzier R, Extra JM, Klijanienko J, Falcou MC, Asselain B, Vincent-Salomon A, et al. Incidence and Prognostic Significance of Complete Axillary Downstaging After Primary Chemotherapy in Breast Cancer Patients With T1 to T3 Tumors and Cytologically Proven Axillary Metastatic Lymph Nodes. *J Clin Oncol* (2002) 20(5):1304–10. doi: 10.1200/JCO.2002.20.5.1304
35. Dong J, Sun Q, Pan Y, Lu N, Han X, Zhou Q. Pretreatment Systemic Inflammation Response Index Is Predictive of Pathological Complete Response in Patients With Breast Cancer Receiving Neoadjuvant Chemotherapy. *BMC Cancer* (2021) 21 (1):700. doi: 10.1186/s12885-021-08458-4
36. Dhiman G, Srivastava N, Goyal M, Rakha E, Lothion-Roy J, Mongan NP, et al. Metadherin: A Therapeutic Target in Multiple Cancers. *Front Oncol* (2019) 9:349. doi: 10.3389/fonc.2019.00349
37. Tokunaga E, Nakashima Y, Yamashita N, Hisamatsu Y, Okada S, Akiyoshi S, et al. Overexpression of Metadherin/MTDH Is Associated With an Aggressive Phenotype and a Poor Prognosis in Invasive Breast Cancer. *Breast Cancer* (2014) 21(3):341–9. doi: 10.1007/s12282-012-0398-2
38. Zhao T, Zhou Y, Wang Q, Yi X, Ge S, He H, et al. QPCT Regulation by CTCF Leads to Sunitinib Resistance in Renal Cell Carcinoma by Promoting Angiogenesis. *Int J Oncol* (2021) 59(1):48. doi: 10.3892/ijo.2021.5228
39. Meng X, Thiel KW, Leslie KK. Drug Resistance Mediated by AEG-1/MTDH/LYRIC. *Adv Cancer Res* (2013) 120:135–57. doi: 10.1016/B978-0-12-401676-7.00005-X
40. An X, Xu F, Luo R, Zheng Q, Lu J, Yang Y, et al. The Prognostic Significance of Topoisomerase II Alpha Protein in Early Stage Luminal Breast Cancer. *BMC Cancer* (2018) 18(1):331. doi: 10.1186/s12885-018-4170-7
41. Norimura S, Kontani K, Kubo T, Hashimoto SI, Murazawa C, Kenzaki K, et al. Candidate Biomarkers Predictive of Anthracycline and Taxane Efficacy Against Breast Cancer. *J Cancer Res Ther* (2018) 14(2):409–15. doi: 10.4103/jcrt.JCRT_1053_16
42. Kurozumi S, Inoue K, Matsumoto H, Fujii T, Horiguchi J, Oyama T, et al. Clinicopathological Values of PD-L1 Expression in HER2-Positive Breast Cancer. *Sci Rep* (2019) 9(1):16662. doi: 10.1038/s41598-019-52944-6
43. Anto´ A, Ruiz A, Plazaola A, Calvo L, Seguı´ MA, Santaballa A, et al. Phase II Clinical Trial of Liposomal-Encapsulated Doxorubicin Citrate and Docetaxel, Associated With Trastuzumab, as Neoadjuvant Treatment in Stages II and IIIA HER2-Overexpressing Breast Cancer Patients. GEICAM 2003-03 Study. *Ann Oncol* (2011) 22(1):74–9. doi: 10.1093/annonc/mdq317
44. Gavilá J, Guerrero Á, Climent MÁ, Fernández A, Gozalbo F, Carrascosa M, et al. Efficacy and Safety of Neoadjuvant Chemotherapy With Concurrent Liposomal-Encapsulated Doxorubicin, Paclitaxel and Trastuzumab for Human Epidermal Growth Factor Receptor 2-Positive Breast Cancer in Clinical Practice. *Int J Clin Oncol* (2015) 20(3):480–9. doi: 10.1007/s10147-014-0727-x
45. Yao J, Pan S, Fan X, Jiang X, Yang Y, Jin J, et al. Pegylated Liposomal Doxorubicin as Neoadjuvant Therapy for Stage II-III Locally Advanced Breast Cancer. *J Chemother* (2020) 32(4):202–7. doi: 10.1080/1120009X.2020.1746886
46. Dong M, Luo L, Ying X, Lu X, Shen J, Jiang Z, et al. Comparable Efficacy and Less Toxicity of Pegylated Liposomal Doxorubicin Versus Epirubicin for Neoadjuvant Chemotherapy of Breast Cancer: A Case-Control Study. *Onco Targets Ther* (2018) 11:4247–52. doi: 10.2147/OTT.S162003
47. Li R, Tian F, Qi Y, Ma L, Zhou T, Li Y, et al. Pegylated Liposomal Doxorubicin Plus Cyclophosphamide Followed by Docetaxel as Neoadjuvant Chemotherapy in Locally Advanced Breast Cancer (Registration Number: Chictr1900023052). *Sci Rep* (2019) 9:18135. doi: 10.1038/s41598-019-54387-5
48. Gabizon AA. Pegylated Liposomal Doxorubicin: Metamorphosis of an Old Drug Into a New Form of Chemotherapy. *Cancer Invest* (2001) 19(4):424–36. doi: 10.1081/cnv-100103136
49. Song Z, Tian F, Feng S, Shi L, Chen X, Liu X, et al. Pegylated Liposomal Doxorubicin-Induced Hand-Foot Syndrome Predicted by Serum Metabolomic Profiling and Prevented by Calcium Dobesilate. *J Am Acad Dermatol* (2022) 86(3):688–90. doi: 10.1016/j.jaad.2021.02.079
50. Chia S, Clemons M, Martin LA, Rodgers A, Gelmon K, Pond GR, et al. Pegylated Liposomal Doxorubicin and Trastuzumab in HER-2 Overexpressing Metastatic Breast Cancer: A Multicenter Phase II Trial. *J Clin Oncol* (2006) 24(18):2773–8. doi: 10.1200/JCO.2005.03.8331
51. Stickeler E, Klar M, Watermann D, Geibel A, Földi M, Hasenburg A, et al. Pegylated Liposomal Doxorubicin and Trastuzumab as 1st and 2nd Line Therapy in Her2/Neu Positive Metastatic Breast Cancer: A Multicenter Phase II Trial. *Breast Cancer Res Treat* (2009) 117(3):591–8. doi: 10.1007/s10549-008-0306-9
52. Andreopoulou E, Gaiotti D, Kim E, Volm M, Oratz R, Freedberg R, et al. Feasibility and Cardiac Safety of Pegylated Liposomal Doxorubicin Plus Trastuzumab in Heavily Pretreated Patients With Recurrent HER2-Overexpressing Metastatic Breast Cancer. *Clin Breast Cancer* (2007) 7 (9):690–6. doi: 10.3816/CBC.2007.n.028
53. Bayraktar S, Gonzalez-Angulo AM, Lei X, Buzdar AU, Valero V, Melhem-Bertrandt A, et al. Efficacy of Neoadjuvant Therapy With Trastuzumab Concurrent With Anthracycline- and Nonanthracycline-Based Regimens for HER2-Positive Breast Cancer. *Cancer* (2012) 118(9):2385–93. doi: 10.1002/cncr.26555
54. Schneeweiss A, Chia S, Hickish T, Harvey V, Eniu A, Hegg R, et al. Pertuzumab Plus Trastuzumab in Combination With Standard Neoadjuvant Anthracycline-Containing and Anthracycline-Free Chemotherapy Regimens in Patients With HER2-Positive Early Breast Cancer: A Randomized Phase II Cardiac Safety Study (TRYPHAENA). *Ann Oncol* (2013) 24(9):2278–84. doi: 10.1093/annonc/mdt182
55. Ramshorst MS, Voort A, Werkhoven ED, Mandjes IA, Kemper I, Dezentjé VO, et al. Neoadjuvant Chemotherapy With or Without Anthracyclines in the Presence of Dual HER2 Blockade for HER2-Positive Breast Cancer (TRAIN-2): A Multicentre, Open-Label, Randomised, Phase 3 Trial. *Lancet Oncol* (2018) 19(12):1630–40. doi: 10.1016/S1470-2045(18)30570-9

Conflict of Interest: The authors declare that the research was conducted in the absence of any commercial or financial relationships that could be construed as a potential conflict of interest.

Publisher's Note: All claims expressed in this article are solely those of the authors and do not necessarily represent those of their affiliated organizations, or those of the publisher, the editors and the reviewers. Any product that may be evaluated in

this article, or claim that may be made by its manufacturer, is not guaranteed or endorsed by the publisher.

Copyright © 2022 Wang, Li, Qi, Zhao, Kong, Yang, Yang, Zhang, Liu and Song. This is an open-access article distributed under the terms of the Creative Commons Attribution License (CC BY). The use, distribution or reproduction in other forums is permitted, provided the original author(s) and the copyright owner(s) are credited and that the original publication in this journal is cited, in accordance with accepted academic practice. No use, distribution or reproduction is permitted which does not comply with these terms.

frontiers | Frontiers in Oncology

TYPE Original Research
PUBLISHED 26 August 2022
DOI 10.3389/fonc.2022.941496

Check for updates

OPEN ACCESS

EDITED BY
Raffaella Massafra,
National Cancer Institute Foundation (IRCCS), Italy

REVIEWED BY
Xiangyi Kong,
Chinese Academy of Medical Sciences and Peking Union Medical College, China
Marco Invernizzi,
University of Eastern Piedmont, Italy

*CORRESPONDENCE
Min Kyeong Jang
espoir8571mk@gmail.com

SPECIALTY SECTION
This article was submitted to Breast Cancer, a section of the journal Frontiers in Oncology

RECEIVED 11 May 2022
ACCEPTED 29 July 2022
PUBLISHED 26 August 2022

CITATION
Jang MK, Park S, Park C, Doorenbos AZ, Go J and Kim S (2022) Body composition change during neoadjuvant chemotherapy for breast cancer.
Front. Oncol. 12:941496.
doi: 10.3389/fonc.2022.941496

COPYRIGHT
© 2022 Jang, Park, Park, Doorenbos, Go and Kim. This is an open-access article distributed under the terms of the Creative Commons Attribution License (CC BY). The use, distribution or reproduction in other forums is permitted, provided the original author(s) and the copyright owner(s) are credited and that the original publication in this journal is cited, in accordance with accepted academic practice. No use, distribution or reproduction is permitted which does not comply with these terms.

Body composition change during neoadjuvant chemotherapy for breast cancer

Min Kyeong Jang[1]*, Seho Park[2], Chang Park[3], Ardith Z. Doorenbos[3,4], Jieon Go[2] and Sue Kim[1]

[1]Mo-Im Kim Nursing Research Institute, Yonsei University College of Nursing, Seoul, South Korea, [2]Division of Breast Surgery, Department of Surgery, Yonsei University College of Medicine, Seoul, South Korea, [3]Department of Biobehavioral Nursing Science, College of Nursing, University of Illinois Chicago, Chicago, IL, United States, [4]Department of Medicine, University of Illinois Cancer Center, Chicago, IL, United States

Background: Sarcopenia is receiving attention in oncology as a predictor of increased chemotherapy toxicities. Research into body composition change during neoadjuvant chemotherapy for breast cancer is both urgently needed and generally lacking. This study assessed sarcopenia prevalence before and after neoadjuvant chemotherapy using CT imaging, evaluated body composition changes during neoadjuvant chemotherapy, and determined predictors of sarcopenia status after neoadjuvant chemotherapy for breast cancer.

Materials and Methods: In this retrospective, descriptive study, we used data collected from 2017 to 2020 to measure body composition parameters on cross-sectional CT slices for 317 Korean women with breast cancer patients before and at completion of neoadjuvant chemotherapy. Changes in skeletal muscle index, visceral fat index, subcutaneous fat index, and sarcopenia were assessed and correlated, and multivariate logistic regression was conducted to identify predictive factors associated with sarcopenia status at completion of neoadjuvant chemotherapy.

Results: Of the 80 breast cancer patients (25.2%) who had sarcopenia before beginning neoadjuvant chemotherapy, 64 (80.0%) retained their sarcopenia status after chemotherapy. Weight, body mass index, body surface area, and visceral fat index showed significant increases after neoadjuvant chemotherapy; notably, only skeletal muscle index significantly decreased, showing a reduction of 0.44 cm^2/m^2 (t (316) = 2.15, p <.5). Lower skeletal muscle index at baseline was associated with greater loss of muscle mass during neoadjuvant chemotherapy (r = −.24, p <.001). Multivariate logistic regression showed that baseline sarcopenia status was the only significant predictor of sarcopenia status after neoadjuvant chemotherapy (p <.001). Specifically, the log odds of sarcopenia after neoadjuvant chemotherapy were 3.357 higher in the baseline sarcopenia group than in the group without baseline sarcopenia (β = 3.357, p <.001).

Conclusion: Sarcopenia during neoadjuvant chemotherapy can be obscured by an increasing proportion of fat in body composition if clinical assessment

focuses on only body mass index or body surface area rather than muscle mass. For breast cancer patients who have sarcopenia when they begin neoadjuvant chemotherapy, the risk of muscle mass loss during treatment is alarmingly high. To reduce masking of muscle mass loss during treatment, comprehensive evaluation of body composition, beyond body surface area assessment, is clearly needed.

KEYWORDS

body composition, breast neoplasm, muscle/skeletal, neoadjuvant chemotherapy, sarcopenia

Introduction

Breast cancer, with an estimated 2.1 million cases diagnosed globally in 2018 (1), is one of the most prevalent cancers in women. A recent trend analysis showed an increasing trend in breast cancer incidence rates, especially among younger women, but a downward trend in mortality rates (2). With increasing survival rates, the disease burden of breast cancer survivors is also increasing worldwide. In the search for effective strategies to improve long-term management of physical and psychological consequences of cancer and its treatment in this population, previous studies have emphasized the need to improve body composition. For example, one study showed that wearable technology to improve body composition (3) produced a significant reduction in body fat, weight, and BMI. Furthermore, a previous study that applied a 4-week rehabilitation protocol for breast cancer survivors showed significant reduction of fatigue and improvement of muscle mass and function (4). In addition, a previous systematic review that focused on cancer treatment-induced bone loss in patients with early breast cancer identified medicinal treatments that improved bone mass density but also called for further bone health management (5). These studies indicate that better treatment outcomes are achievable for breast cancer survivors, but to accomplish this, assessments of risk factors for poor clinical outcomes arising during cancer treatment are important.

Sarcopenia, or decreased muscle mass, has been receiving attention in oncology as a predictor of increased chemotherapy toxicities and as a sensitive early marker of treatment effectiveness (6–9). The prevalence of sarcopenia among breast cancer patients has been variously reported as 45.0% and as ranging from 15.9% to 66.9% (10). In addition, sarcopenia has been related to a significantly higher risk of mortality. In a study of 1,460 breast cancer patients in the Republic of Korea (11), half were found to have sarcopenia, a somewhat higher prevalence than has been observed in the United States and France (10). Separately, a sarcopenia prevalence of 20.2% in Korean women 50 years and older in the general population was reported by a Korean National Health and Nutrition Examination Survey (12). This suggests that breast cancer patients may be more vulnerable to sarcopenia, and that the epidemiological status of sarcopenia and its prevalence in breast cancer patients require examination.

Determination of sarcopenia status involves assessment of alterations in body composition. Changes in body composition have been reported to occur in breast cancer patients during chemotherapy and endocrine therapy (9). In addition, obesity is known to be an accelerator of breast cancer, and the interaction between obesity and sarcopenia accelerates tumor recurrence (9). However, both clinical practice and oncology research assessments tend to focus on body mass index (BMI) or body surface area (BSA) rather than muscle mass change during treatment. Traditionally, BSA has been used to calculate chemotherapy doses, while BMI, a related measure that also incorporates weight and height, has often been employed in oncology research. In the last decade, the importance of identifying specific body composition changes during chemotherapy has emerged as an issue of interest (13–16). A 2018 study involving 119 breast cancer patients found sarcopenia status to be an independent prognostic factor for disease-free survival, while BMI was not significantly related to disease-free survival (17). The 2016 study of 1,460 Korean breast cancer patients showed that muscle volume was a significant prognostic factor for overall survival regardless of BMI, whereas fat volume and BMI were not significantly related to survival (11). Previous studies (11, 17) also have indicated that, unlike BMI, muscle mass appears to be a sensitive marker of overall survival. These studies show the importance of investigating body composition change during chemotherapy.

Although urgently needed, research in the area of body composition change during neoadjuvant chemotherapy for

Abbreviations: BMI, body mass index; BSA, body surface area; L3, third lumbar spine vertebra; SFI, subcutaneous fat index; SMI, skeletal muscle index; VFI, visceral fat index.

breast cancer is generally lacking. Descriptive analyses of body composition during other forms of cancer treatment (such as surgery, radiotherapy, or adjuvant chemotherapy) have been performed, for various cancer types (18–20), but few studies have examined changes in muscle mass during neoadjuvant chemotherapy among patients with breast cancer. This study was conducted to improve understanding of the current status of sarcopenia in breast cancer patients. Specifically, we evaluated body composition changes during neoadjuvant chemotherapy using CT imaging, assessed sarcopenia prevalence before and after neoadjuvant chemotherapy, and determined predictors of sarcopenia status in breast cancer patients after neoadjuvant chemotherapy.

Materials and methods

Study design and setting

We used a retrospective, descriptive, observational study design to determine body composition change and sarcopenia prevalence among breast cancer patients who had visited the breast cancer clinic at Severance Hospital in Seoul, Korea, from January 2017 to November 2020. Eligible participants were Korean women 20 years or older who had received a diagnosis of breast cancer at the hospital, completed neoadjuvant chemotherapy, and received at least two abdominal CT scans, before and after neoadjuvant chemotherapy, that provided images of the third lumbar spine vertebra (L3). We excluded patients with stage IV breast cancer and patients with CT images that were insufficient or inappropriate for analysis of body composition. Our sample size of 317 cases was sufficient to meet the study objectives. Initially, the target sample size was determined using G*Power 3.1 software. To accommodate regression analysis and pseudo R2 (0.39), a required sample size of 265 was calculated based on an odds ratio of 1.3. a power of 0.8.

Approval for this study was obtained from the Severance Hospital Institutional Review Board (#4-2021-0452) at Yonsei University Health Systems, Seoul, Korea. The Severance Hospital Data Review Board also approved the study data set with respect to protection of patients' data and assessment of data-protection risks and tools.

Data collection

The Big Data Team in the Yonsei University Health System provided comprehensive information from the selected sample' medical records, including sociodemographic data and clinical data such as cancer- and treatment-related information. We used this information to assess age, clinical stage, TN stage, Ki-67, breast cancer subtype, chemotherapy regimen, duration of neoadjuvant chemotherapy, and BMI and BSA (both of which are calculated from weight and height). For Ki-67, we used a cutoff value based on the expressed cell ratio (<14% and ≥14%). For breast cancer subtype, we evaluated both hormone receptor and human epidermal growth factor receptor 2 (HER2); to explore HER2 gene amplification, we also assessed silver stain hybridization *in situ* findings.

We measured body composition by analyzing CT images taken before and after chemotherapy. The Yonsei University Convergence Medical Technology Center performed the body composition analysis using Aquarius iNtuition viewer version 4.4.13.P6 (TeraRecon, Durham, North Carolina). Using the analysis program provided in the software, we analyzed the CT slices at L3 as a standardized landmark. We calculated the total cross-sectional areas of skeletal muscle, subcutaneous fat, and visceral fat (in cm^2). The Hounsfield unit values used for measurement ranged from −29 to 150 for muscle, −190 to −30 for subcutaneous fat, and −150 to −50 for visceral fat. Figure 1 presents a single axial CT slice at the L3 level and shows the areas of skeletal muscle, subcutaneous fat, and visceral fat for two study participants; this figure illustrates differences in body composition between two participants with the same BMI. The skeletal muscle index (SMI, in cm^2/m^2) was calculated as skeletal muscle area (in cm^2) divided by height squared (in m^2); both subcutaneous fat area and visceral fat area were also divided by height squared to determine the associated indexes. With respect to the sarcopenia cutoff value, we applied the value introduced by Prado et al. (SMI <38.5 cm^2/m^2) as an SMI cutoff for women (21).

Our investigative focus was on secondary sarcopenia, which involves loss of muscle mass—but not necessarily muscle function—accompanying cancer and other diseases (22). A variety of sarcopenia definitions and body composition evaluation techniques have been employed to assess sarcopenia across the international research. Investigation of primary sarcopenia, which is associated with aging, typically involves measurement of a combination of muscle mass, muscle strength, and physical performance. However, given that only muscle mass data were available for our retrospective study, we elected to concentrate our efforts on secondary sarcopenia, which can be evaluated through measurement of muscle mass alone.

Statistical analysis

Data analysis was performed using Stata/IC 16 statistical software (College Station, Texas). We conducted descriptive analyses to characterize the study sample and to assess their body composition before (at baseline) and at completion of neoadjuvant chemotherapy. In addition, we used a paired *t*-test

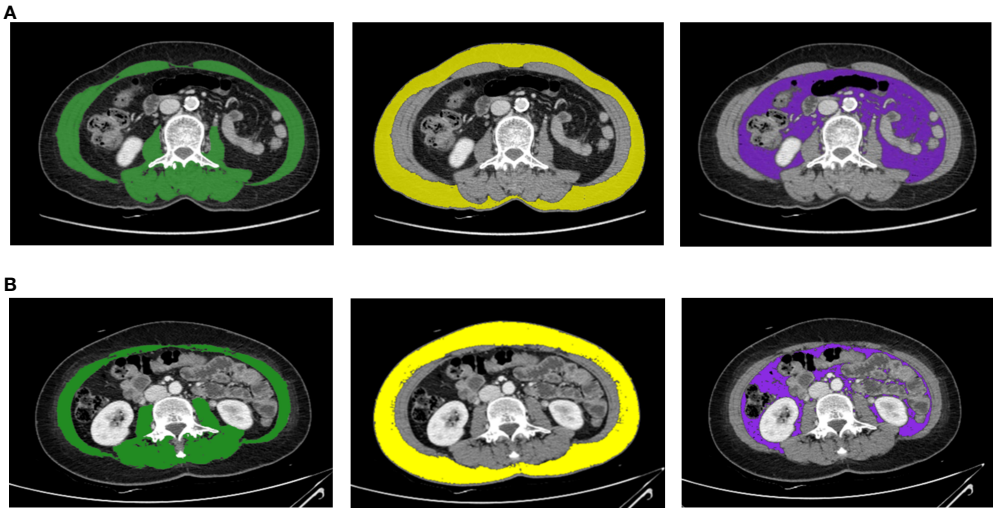

FIGURE 1
Body composition evaluation CT images for two breast cancer patients with the same BMI (23.37 kg/m^2) and weight (54.7 kg). These axial CT images of the third lumbar vertebral region show that two study participants with the same BMI can have different body compositions. Panel **(A)** is a CT image for a 69-year-old female, and panel **(B)** is a CT image for a 48-year-old female. The images illustrate the different proportions of skeletal muscle mass (green), subcutaneous fat area (yellow), and visceral fat area (purple).

to compare sarcopenia prevalence and body composition change (i.e., changes in muscle mass and fat mass) before and after neoadjuvant chemotherapy. We calculated Pearson correlation coefficients to evaluate associations among body composition parameters. Finally, we applied multivariate logistic regression to determine predictors of sarcopenia at completion of neoadjuvant chemotherapy. All p values were two-tailed, and p values <.05 were considered significant.

Results

Demographic and clinical characteristics

Table 1 presents descriptive data for the 317 women with breast cancer patients at baseline—before neoadjuvant chemotherapy. The mean age was 53 years, with ages ranging from 26 to 82 years. According to the BMI for Asia classification (23, 24), the most common weight category in the sample was normal (BMI of 18.5–22.9; n = 132, 41.6%), followed by obese (n = 94, 29.7%) and overweight (n = 82, 25.9%).

Among the combinations of chemotherapy drugs used, the combination of anthracyclines and taxanes was the most common (n = 214, 67.5%), followed by the docetaxel, carboplatin, trastuzumab, and pertuzumab regimen (n = 84, 26.5%). The mean duration of chemotherapy was 142 days, with durations ranging from 49 to 196 days. Stage II cancer was the most common in the sample (n = 224, 73.2%).

Body composition changes during neoadjuvant chemotherapy

Table 2 and Figure 2 show body composition change during neoadjuvant chemotherapy. Weight significantly increased (by an average of 0.67 kg) during neoadjuvant chemotherapy (from 59.33 to 60.00 kg, t (316) = −3.84, p = .001). Similarly, BMI and BSA (both based on weight in relation to their height) showed significant increases after neoadjuvant chemotherapy, by an average of 0.24 kg/m^2 for BMI and 0.01 m^2 for BSA.

Among the body composition changes during neoadjuvant chemotherapy, visceral fat index (VFI) significantly increased by 1.31 cm^2/m^2 (from 29.97 to 31.28 cm^2/m^2). There was no significant difference in subcutaneous fat index (SFI) before and after chemotherapy. SMI showed the only significantly decrease during neoadjuvant chemotherapy, by 0.44 cm^2/m^2 (from 42.37 to 41.93 cm^2/m^2).

Sarcopenia prevalence during neoadjuvant chemotherapy

Table 3 shows the sarcopenia prevalence before (at baseline) and at completion of neoadjuvant chemotherapy. According to Prado's sarcopenia criteria (21), at baseline, 80 patients (25.24%) had sarcopenia and 237 patients (74.76%) did not. After neoadjuvant chemotherapy, the number of patients with sarcopenia increased (n = 93, 29.34%). Of the 80 patients who

TABLE 1 Demographics and clinical characteristics of the sample (N = 317).

Characteristic	Category	Mean ± SD (range) or n (%)
Age (years)		52.78 ± 10.41 (26–82)
	20–29	3 (0.95)
	30–39	31 (9.78)
	40–49	93 (29.34)
	50–59	107 (33.75)
	≥60	83 (26.18)
Stage of tumor	I	6 (1.96)
	II	224 (73.20)
	III	76 (24.84)
Initial clinical T stage	1	30 (9.86)
	2	212 (69.74)
	3	32 (10.53)
	4	29 (9.54)
Initial clinical N stage	0	114 (37.50)
	1	148 (48.68)
	2	19 (6.25)
	3	23 (7.57)
Ki-67	Low (<14%)	34 (11.26)
	High (≥14%)	268 (88.75)
Tumor subtype	HR+/HER2−	108 (34.07)
	HR+/HER2+	49 (15.46)
	HR−/HER2+	58 (18.30)
	TNBC	102 (32.18)
Chemotherapy regimen	AC-T regimen	214 (67.51)
	TCHP regimen	84 (26.50)
	Other	19 (5.99)
Duration of neoadjuvant chemotherapy	(days)	142 ± 30.86 (49–196)
BMI at baseline	<18.5 (underweight)	9 (2.84)
	18.5–22.9 (normal)	132 (41.64)
	23–24.9 (overweight)	82 (25.87)
	≥25 (obese)	94 (29.65)

AC-T regimen, combination of an anthracycline and cyclophosphamide, followed by a taxane; BMI, body mass index; HER2−, human epidermal growth factor receptor 2-negative; HER2+, human epidermal growth factor receptor 2-positive; HR−, hormone receptor-negative; HR+, hormone receptor-positive; TCHP regimen, docetaxel, carboplatin, trastuzumab, and pertuzumab; TNBC, triple negative breast cancer.

had sarcopenia before their chemotherapy, 64 (80%) retained their sarcopenia status after chemotherapy.

Associations between body composition changes

Table 4 presents the statistically significant correlations between body composition parameters at baseline and the mean differences in these parameters after neoadjuvant chemotherapy. A lower SMI at baseline was associated with a greater loss of muscle mass during neoadjuvant chemotherapy (r = −.24, p <.001). Baseline SFI and VFI showed a similar direction of association with the mean differences in body composition parameters; lower VFI at baseline was associated with a greater loss of subcutaneous fat and visceral fat mass during neoadjuvant chemotherapy (r = −.22, p <.001 and r = −.34, p <.001, respectively). All mean differences in body composition parameters—including muscle, subcutaneous fat, and visceral fat mass—after neoadjuvant chemotherapy were positively related to one another. All significant relationships between body composition parameters were observed both at baseline and at completion of neoadjuvant chemotherapy.

TABLE 2 Body composition changes during neoadjuvant chemotherapy.

Parameter	Mean ± SD before NAC	Mean ± SD after NAC	t	p value
BMI	23.61 ± 3.17	23.85 ± 3.21	−3.315	0.001
Weight	59.33 ± 8.11	60.00 ± 8.53	−3.843	0.0001
BSA	1.61 ± 0.12	1.62 ± 0.13	−3.811	0.0002
SFI (cm^2/m^2)	66.58 ± 26.23	66.44 ± 26.57	0.190	0.849
VFI (cm^2/m^2)	29.97 ± 20.20	31.28 ± 19.15	−2.547	0.0114
SMI (cm^2/m^2)	42.37 ± 5.41	41.93 ± 5.76	2.153	0.0321

BMI, body mass index; BSA, body surface area; NAC, neoadjuvant chemotherapy; SFI, subcutaneous fat index; SMI, skeletal muscle mass index; VFI, visceral fat index.

Multivariate logistic regression analyses to predict sarcopenia after neoadjuvant chemotherapy

As shown in Table 5, we fit a multivariate logistic regression model to predict sarcopenia status after neoadjuvant chemotherapy. The regression included patient age, tumor subtype, chemotherapy duration, chemotherapy regimen, baseline SFI and VFI, and baseline sarcopenic status as independent predictors ($\chi^2[9]$ = 140.67, p = .0000, pseudo R^2 = 0.3908). Baseline sarcopenia status was the only significant predictor of sarcopenia status after neoadjuvant chemotherapy. Specifically, the sarcopenia after neoadjuvant chemotherapy increased for the group with baseline sarcopenia, with 3.357 times increasing log odds (β = 3.357, p <.001). Other variables showed no significant association with sarcopenia risk after neoadjuvant chemotherapy. Finally, no interactions of baseline sarcopenia status with other variables were observed to predict sarcopenia status after neoadjuvant chemotherapy.

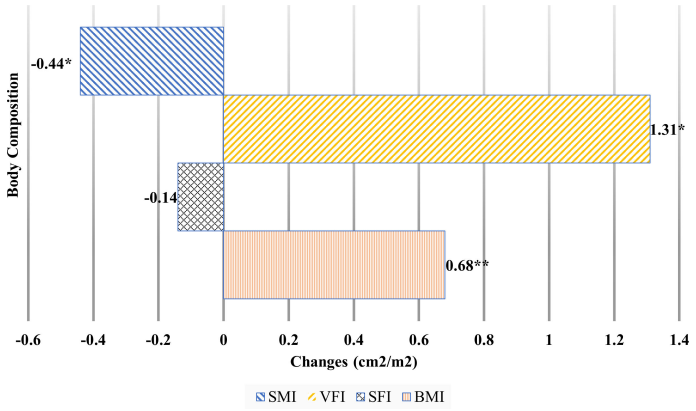

FIGURE 2
Body composition changes during neoadjuvant chemotherapy.BMI, body mass index; SFI, subcutaneous fat index; SMI, skeletal muscle mass index; VFI, visceral fat index. *p <.05, **p <.01.

TABLE 3 Sarcopenia prevalence during neoadjuvant chemotherapy.

Group		After chemotherapy		
		No sarcopenia	Sarcopenia	Total
Before chemotherapy	No sarcopenia	208 (92.86%)	29 (31.18%)	237 (74.76%)
	Sarcopenia	16 (7.14%)	64 (68.62%)	80 (25.24%)
	Total	224 (100%)	93 (100%)	317 (100%)

Pearson $\chi^2(1) = 132.48$, p = 0.000.

TABLE 4 Associations between body composition changes.

Variables		Mean differences		
		SMI	SFI	VFI
Baseline	SMI	−.2381**	−.1048	−.1244*
	SFI	−.0363	−.2283**	−.0809
	VFI	−.0948	−.2202**	−.3387**

SFI, subcutaneous fat index; SMI, skeletal muscle mass index; VFI, visceral fat index. *p <.05, **p <.001.

TABLE 5 Multivariate logistic regression analyses to predict sarcopenia after neoadjuvant chemotherapy.

Variable	Value	Coef.	95% CI		*p-value*
Baseline sarcopenia	Yes	3.357	2.565	4.149	.000
	No	1.000			
Baseline subcutaneous fat		-.007	-.027	.013	.485
Baseline visceral fat		-.027	-.056	.001	.058
Age at diagnosis		.008	-.030	.046	.675
Chemotherapy regimen	AC-T regimen	1.000			
	TCHP regimen	2.089	-.237	4.415	.078
Tumor subtype	HR+/HER2−	1.000			
	HR+/HER2+	-.204	-1.847	1.439	.808
	HR−/HER2+	-.494	-2.171	1.183	.564
	TNBC	.091	-.781	.963	.838
Chemotherapy duration		.014	-.017	.045	.368

AC-T regimen, combination of an anthracycline and cyclophosphamide, followed by a taxane; CI, confidence interval; HER2−, human epidermal growth factor receptor 2-negative; HER2+, human epidermal growth factor receptor 2-positive; HR−, hormone receptor-negative; HR+, hormone receptor-positive; TCHP regimen, docetaxel, carboplatin, trastuzumab, and pertuzumab; TNBC, triple negative breast cancer. LR $\chi^2(9) = 140.67$, p <.000, pseudo $R^2 = 0.3908$.

Discussion

We conducted this study to improve understanding of the current status of sarcopenia in breast cancer patients by evaluating body composition changes during neoadjuvant chemotherapy, using CT imaging to assess sarcopenia prevalence before and after neoadjuvant chemotherapy, and determining predictors of sarcopenia status after neoadjuvant chemotherapy in this population. To our knowledge, this is the first study to use CT imaging to comprehensively quantify body composition changes during neoadjuvant chemotherapy in Korean breast cancer patients. Determination of sarcopenia status is often complicated or obscured by obesity; sarcopenia is difficult to recognize visually without medical imaging. Therefore, this study used abdominal CT scans, which are routinely performed during treatment and are among the most accurate measures of body composition parameters, to accurately quantify body composition changes.

Our study generated meaningful findings regarding sarcopenia status and body composition changes among patients with breast cancer undergoing neoadjuvant chemotherapy. Notably, BMI and BSA increased significantly

during neoadjuvant chemotherapy. This finding is clinically significant because BSA is typically used in clinical oncology settings to calculate chemotherapy doses. Additionally, an unchanged BSA during chemotherapy can mask more specific changes to body composition, such as alterations in the proportions of fat and muscle. For example, the detailed body composition results in our study showed that although visceral fat mass significantly increased during neoadjuvant chemotherapy, SMI significantly decreased. While the observed weight gain indicates that most body composition–related variables increased or were maintained, that gain can also mask significant decreases in the actual amount of skeletal muscle mass. These findings suggest that weight maintenance and muscle mass maintenance during chemotherapy are not proportional, and thus that muscle mass loss could be easily overlooked in clinical settings.

Among the important findings of this study, 80% of the patients who had sarcopenia before neoadjuvant chemotherapy (n = 64) maintained their sarcopenia status after completing chemotherapy. Additionally, 12.2% of those who did not have sarcopenia at baseline (n = 29) were newly diagnosed with the condition after neoadjuvant chemotherapy. A similar result was reported by a systematic review and meta-analysis involving 11 studies of patients receiving neoadjuvant therapy for esophageal cancer, which found that 15.4% of participants showed new incidence of sarcopenia after neoadjuvant chemotherapy (25). Another multi-institutional analysis, involving patients with gastric cancer, showed that 14% had newly developed sarcopenia during neoadjuvant chemotherapy (26). In comparison, a previous systematic review and meta-analysis in a general population found that 10% of women aged 60 years or older had sarcopenia and that non-Asian women had a higher prevalence of sarcopenia than Asian women (20% versus 11%), as measured by bioelectric impedance analysis (27).

Considering that the overall sarcopenia prevalence in Korean women 50 years and older has been reported as about 20% (12), it is noteworthy that even before surgery, almost 30% of the breast cancer patients in our study (mean age = 53 years) were diagnosed with sarcopenia. Our findings, combined with those of previous studies, show that the prevalence of newly diagnosed sarcopenia in breast cancer patients after neoadjuvant chemotherapy is similar to that in patients with other types of cancer. However, the overall prevalence of sarcopenia in breast cancer patients is higher than that in the healthy population. Therefore, careful assessment of breast cancer patients for sarcopenia—with consideration of cancer type, cultural background, age, and treatment- and cancer-related factors—is necessary.

Among our findings, baseline sarcopenia status was the only significant predictor of sarcopenia after neoadjuvant chemotherapy. The dramatic rise in the risk of sarcopenia after neoadjuvant chemotherapy in the baseline sarcopenia group— with 3.357 times increasing log odds —is a remarkable finding that has important implications for assessment of muscle mass during treatment. Many studies have shown that preoperative sarcopenia is a risk factor for postoperative complications, severe complications, decreased overall survival, and decreased disease-free survival in patients with various cancer types (28–33). Given that preoperative sarcopenia status appears to be a significant prognostic factor for poor treatment outcomes and reduced survival, our findings indicate that ongoing assessment of sarcopenia as well as overall body composition from the beginning of cancer treatment could enhance long-term therapeutic effectiveness for breast cancer patients.

Several recent studies on sarcopenia, or muscle mass loss, have drawn the attention of the scientific community because they identified muscle mass loss as a key factor in chemotherapy toxicity and hospitalization as well as mortality for various cancer types (34–38). Previous studies have reported that BMI is not related to breast cancer progression but that muscle volume is a significant factor influencing severe laboratory adverse events (8) and overall survival (11). In clinical settings, therefore, combined assessments of sarcopenia and body composition change would be beneficial for predicting patients' chemotherapy toxicities and mortality. Such assessments would also support early intervention to prevent or reduce muscle mass loss. Thus, to fully understand breast cancer patients' condition in the oncology setting, combined interpretations of various body composition changes are called for; such interpretations can reveal patients' sarcopenia status, provide direction for personalized chemotherapy, and help to prevent chemotherapy toxicity.

Study limitations

This retrospective study had limitations that should be acknowledged. First, we focused on changes in body composition during neoadjuvant chemotherapy, which prevented us from examining the trajectory of sarcopenia during subsequent surgery and radiotherapy. Future studies should apply a repeated measures design throughout the entire process of active cancer treatment to obtain a better understanding of patients' sarcopenia status and trajectory. Second, because the data available to us were limited by our retrospective design, we could not examine potential mediators for sarcopenia (such as nutrition and exercise) during neoadjuvant chemotherapy. Furthermore, the retrospective data available to us were limited to muscle mass measurements, as muscle strength and physical performance data had not been collected. Consequently, we focused our evaluation on secondary sarcopenia, for which muscle mass data would suffice. Based on the available evidence on various factors related to sarcopenia, future studies should comprehensively investigate potential mediators, their

associations with sarcopenia, and their underlying mechanisms, with the goal of minimizing muscle mass loss during cancer treatment. Finally, as sarcopenia is more prevalent in the general population of Korea than is the case in the United States and Europe, our study sample may have been subject to selection bias.

Conclusion

Comprehensive body composition analysis can improve our understanding of subtle yet meaningful changes in muscle and fat mass among breast cancer patients undergoing neoadjuvant chemotherapy. To reduce masking of muscle mass loss during cancer treatment in clinical settings, active interpretation of body composition beyond BSA and BMI assessment is clearly needed. This is particularly true for patients who have sarcopenia when they begin neoadjuvant chemotherapy, as their risk of muscle mass loss during treatment is alarmingly high. Assessment of body composition and sarcopenia status beginning at breast cancer diagnosis and extending throughout the neoadjuvant chemotherapy period should become a cornerstone for successful completion of planned cancer treatment.

Data availability statement

The raw data supporting the conclusions of this article will be made available by the authors, without undue reservation.

Ethics statement

This study was reviewed and approved by the Severance Hospital Institutional Review Board in the Yonsei University Health Systems, Seoul, Korea (#4-2021-0452). Written informed consent for participation was not required for this study in accordance with the national legislation and the institutional requirements. Written informed consent was not obtained from the individual(s) for the publication of any potentially identifiable images or data included in this article.

Author contributions

MJ, SK, SP, and JG, study concept and design. MJ and SK, data acquisition and data quality control. MJ and CP, data analysis and interpretation, manuscript preparation. MJ, SK, SP, CP, JG, and AD, contributed to the article, reviewed the manuscript, and approved the submitted version. All authors contributed to the article and approved the submitted version.

Funding

This work was supported by a National Research Foundation of Korea (NRF) grant, which was funded by the government of the Republic of Korea through the Ministry of Science and ICT (NRF No. 2021R1C1C2004628).

Conflict of interest

The authors declare that the research was conducted in the absence of any commercial or financial relationships that could be construed as a potential conflict of interest.

Publisher's note

All claims expressed in this article are solely those of the authors and do not necessarily represent those of their affiliated organizations, or those of the publisher, the editors and the reviewers. Any product that may be evaluated in this article, or claim that may be made by its manufacturer, is not guaranteed or endorsed by the publisher.

References

1. Sharma R. Global, regional, national burden of breast cancer in 185 countries: Evidence from GLOBOCAN 2018. *Breast Cancer Res Treat* (2021) 187(2):557–67. doi: 10.1007/s10549-020-06083-6

2. Huang J, Chan PS, Lok V, Chen X, Ding H, Jin Y, et al. Global incidence and mortality of breast cancer: A trend analysis. *Aging (Albany NY)* (2021) 13(4):5748. doi: 10.18632/aging.202502

3. Zhou C, Mo M, Wang Z, Shen J, Chen J, Tang L, et al. A short-term effect of wearable technology-based lifestyle intervention on body composition in stage I–III postoperative breast cancer survivors. *Front Oncol* (2020) 10:563566. doi: 10.3389/fonc.2020.563566

4. Invernizzi M, De Sire A, Lippi L, Venetis K, Sajjadi E, Gimigliano F, et al. Impact of rehabilitation on breast cancer related fatigue: a pilot study. *Front Oncol* (2020) 10:556718. doi: 10.3389/fonc.2020.556718

5. de Sire A, Lippi L, Venetis K, Morganti S, Sajjadi E, Curci C, et al. Efficacy of antiresorptive drugs on bone mineral density in post-menopausal women with early breast cancer receiving adjuvant aromatase inhibitors: A systematic review of

randomized controlled trials. *Front Oncol* (2021) 11:829875. doi: 10.3389/fonc.2021.829875

6. Caan BJ, Feliciano EM, Prado CM, Alexeeff S, Kroenke CH, Bradshaw P, et al. Association of muscle and adiposity measured by computed tomography with survival in patients with nonmetastatic breast cancer. *JAMA Oncol* (2018) 4 (6):798–804. doi: 10.1001/jamaoncol.2018.0137

7. Aleixo GF, Williams GR, Nyrop KA, Muss HB, Shachar SS. Muscle composition and outcomes in patients with breast cancer: meta-analysis and systematic review. *Breast Cancer Res Treat* (2019) 177(3):569–79. doi: 10.1007/s10549-019-05352-3

8. Ueno A, Yamaguchi K, Sudo M, Imai S. Sarcopenia as a risk factor of severe laboratory adverse events in breast cancer patients receiving perioperative epirubicin plus cyclophosphamide therapy. *Support Care Cancer* (2020) 28 (9):4249–54. doi: 10.1007/s00520-019-05279-x

9. Iwase T, Wang X, Shrimanker TV, Kolonin MG, Ueno NT. Body composition and breast cancer risk and treatment: mechanisms and impact. *Breast Cancer Res Treat* (2021) 186(2):273–83. doi: 10.1007/s10549-020-06092-5

10. Zhang XM, Dou QL, Zeng Y, Yang Y, Cheng AS, Zhang WW. Sarcopenia as a predictor of mortality in women with breast cancer: a meta-analysis and systematic review. *BMC Cancer* (2020) 20(1):1–11. doi: 10.1186/s12885-020-6645-6

11. Song EJ, Lee CW, Jung SY, Kim BN, Lee KS, Lee S, et al. Prognostic impact of skeletal muscle volume derived from cross-sectional computed tomography images in breast cancer. *Breast Cancer Res Treat* (2018) 172(2):425–36. doi: 10.1007/s10549-018-4915-7

12. Kwon HJ, Ha YC, Park HM. Prevalence of sarcopenia in the Korean woman based on the Korean national health and nutritional examination surveys. *J Bone Metab* (2016) 23(1):23–6. doi: 10.11005/jbm.2016.23.1.23

13. Felici A, Verweij J, Sparreboom A. Dosing strategies for anticancer drugs: the good, the bad and body-surface area. *Eur J Cancer* (2002) 38(13):1677–84. doi: 10.1016/S0959-8049(02)00151-X

14. Pin F, Couch ME, Bonetto A. Preservation of muscle mass as a strategy to reduce the toxic effects of cancer chemotherapy on body composition. *Curr Opin Support Palliat Care* (2018) 12(4):420. doi: 10.1097/SPC.0000000000000382

15. Feliciano EM, Chen WY, Lee V, Albers KB, Prado CM, Alexeeff S, et al. Body composition, adherence to anthracycline and taxane-based chemotherapy, and survival after nonmetastatic breast cancer. *JAMA Oncol* (2020) 6(2):264–70. doi: 10.1001/jamaoncol.2019.4668

16. Shachar SS, Deal AM, Weinberg M, Williams GR, Nyrop KA, Popuri K, et al. Body composition as a predictor of toxicity in patients receiving anthracycline and taxane–based chemotherapy for early-stage breast cancer. *Clin Cancer Res* (2017) 23(14):3537–43. doi: 10.1158/1078-0432.CCR-16-2266

17. Deluche E, Leobon S, Desport JC, Venat-Bouvet L, Usseglio J, Tubiana-Mathieu N. Impact of body composition on outcome in patients with early breast cancer. *Support Care Cancer* (2018) 26(3):861–8. doi: 10.1007/s00520-017-3902-6

18. Pak S, Kim MS, Park EY, Kim SH, Lee KH, Joung JY. Association of body composition with survival and treatment efficacy in castration-resistant prostate cancer. *Front Oncol* (2020) 10:558. doi: 10.3389/fonc.2020.00558

19. Almada-Correia I, Neves PM, Mäkitie A, Ravasco P. Body composition evaluation in head and neck cancer patients: a review. *Front Oncol* (2019) 9:1112. doi: 10.3389/fonc.2019.01112

20. Pan Y, Chen Z, Yang L, Wang X, Yi Z, Zhou L, et al. Body composition parameters may be prognostic factors in upper urinary tract urothelial carcinoma treated by radical nephroureterectomy. *Front Oncol* (2021) 11:679158. doi: 10.3389/fonc.2021.679158

21. Prado CM, Lieffers JR, McCargar LJ, Reiman T, Sawyer MB, Martin L, et al. Prevalence and clinical implications of sarcopenic obesity in patients with solid tumours of the respiratory and gastrointestinal tracts: a population-based study. *Lancet Oncol* (2008) 9(7):629–35. doi: 10.1016/S1470-2045(08)70153-0

22. Bauer J, Morley JE, Schols AM, Ferrucci L, Cruz-Jentoft AJ, Dent E, et al. Sarcopenia: a time for action. an SCWD position paper. *J Cachexia Sarcopenia Muscle* (2019) 10(5):956–61. doi: 10.1002/jcsm.12483

23. Consultation WE. Appropriate body-mass index for Asian populations and its implications for policy and intervention strategies. *Lancet* (2004) 363 (9403):157–63. doi: 10.1016/S0140-6736(03)15268-3

24. Weir CB, Jan A. *BMI classification percentile and cut off points*. Treasure Island (FL): StatPearls Publishing (2019).

25. Jin SB, Tian ZB, Ding XL, Guo YJ, Mao T, Yu YN, et al. The impact of preoperative sarcopenia on survival prognosis in patients receiving neoadjuvant therapy for esophageal cancer: a systematic review and meta-analysis. *Front Oncol* (2021) 11:619592. doi: 10.3389/fonc.2021.619592

26. Mirkin KA, Luke FE, Gangi A, Pimiento JM, Jeong D, Hollenbeak CS, et al. Sarcopenia related to neoadjuvant chemotherapy and perioperative outcomes in resected gastric cancer: a multi-institutional analysis. *J Gastrointest Oncol* (2017) 8 (3):589. doi: 10.21037/jgo.2017.03.02

27. Shafiee G, Keshtkar A, Soltani A, Ahadi Z, Larijani B, Heshmat R. Prevalence of sarcopenia in the world: a systematic review and meta-analysis of general population studies. *J Diabetes Metab Disord* (2017) 16(1):1–10. doi: 10.1186/s40200-017-0302-x

28. Tamura T, Sakurai K, Nambara M, Miki Y, Toyokawa T, Kubo N, et al. Adverse effects of preoperative sarcopenia on postoperative complications of patients with gastric cancer. *Anticancer Res* (2019) 39(2):987–92. doi: 10.21873/anticanres.13203

29. Yang Z, Zhou X, Ma B, Xing Y, Jiang X, Wang Z. Predictive value of preoperative sarcopenia in patients with gastric cancer: a meta-analysis and systematic review. *J Gastroint Surg* (2018) 22(11):1890–902. doi: 10.1007/s11605-018-3856-0

30. Choi MH, Yoon SB, Lee K, Song M, Lee IS, Lee MA, et al. Preoperative sarcopenia and post-operative accelerated muscle loss negatively impact survival after resection of pancreatic cancer. *J Cachexia Sarcopenia Muscle* (2018) 9(2):326–34. doi: 10.1002/jcsm.12274

31. Deng HY, Zha P, Peng L, Hou L, Huang KL, Li XY. Preoperative sarcopenia is a predictor of poor prognosis of esophageal cancer after esophagectomy: a comprehensive systematic review and meta-analysis. *Dis Esophagus* (2019) 32(3): doy115. doi: 10.1093/dote/doy115

32. Chen F, Chi J, Liu Y, Fan L, Hu K. Impact of preoperative sarcopenia on postoperative complications and prognosis of gastric cancer resection: A meta-analysis of cohort studies. *Arch Geront Geriatr* (2022) 98:104534. doi: 10.1016/j.archger.2021.104534

33. Xie H, Wei L, Liu M, Yuan G, Tang S, Gan J. Preoperative computed tomography-assessed sarcopenia as a predictor of complications and long-term prognosis in patients with colorectal cancer: a systematic review and meta-analysis. *Langenbeck's Arch Surg* (2021) 406(6):1775–88. doi: 10.1007/s00423-021-02274-x

34. Wendrich AW, Swartz JE, Bril SI, Wegner I, de Graeff A, Smid EJ, et al. Low skeletal muscle mass is a predictive factor for chemotherapy dose-limiting toxicity in patients with locally advanced head and neck cancer. *Oral Oncol* (2017) 71:26–33. doi: 10.1016/j.oraloncology.2017.05.012

35. Sjøblom B, Grønberg BH, Benth JŠ, Baracos VE, Fløtten Ø, Hjermstad MJ, et al. Low muscle mass is associated with chemotherapy-induced haematological toxicity in advanced non-small cell lung cancer. *Lung Cancer* (2015) 90(1):85–91. doi: 10.1016/j.lungcan.2015.07.001

36. Kurk S, Peeters P, Stellato R, Dorresteijn B, de Jong P, Jourdan M, et al. Skeletal muscle mass loss and dose-limiting toxicities in metastatic colorectal cancer patients. *J Cachexia Sarcopenia Muscle* (2019) 10(4):803–13. doi: 10.1002/jcsm.12436

37. Xia L, Zhao R, Wan Q, Wu Y, Zhou Y, Wang Y, et al. Sarcopenia and adverse health-related outcomes: An umbrella review of meta-analyses of observational studies. *Cancer Med* (2020) 9(21):7964–78. doi: 10.1002/cam4.3428

38. Shachar SS, Williams GR, Muss HB, Nishijima TF. Prognostic value of sarcopenia in adults with solid tumours: a meta-analysis and systematic review. *Eur J Cancer* (2016) 57:58–67. doi: 10.1016/j.ejca.2015.12.030

frontiers | Frontiers in Oncology

TYPE Systematic Review
PUBLISHED 28 September 2022
DOI 10.3389/fonc.2022.894861

Check for updates

OPEN ACCESS

EDITED BY
Sonia Pernas,
Catalan Institute of Oncology, Spain

REVIEWED BY
Richard De Boer,
Peter MacCallum Cancer Centre, Australia
Samuel Ken-En Gan,
Kean University-Wenzhou, China
Simona Ruxandra Volovat,
Grigore T. Popa University of Medicine and Pharmacy, Romania

*CORRESPONDENCE
Xianghe Wang
wangxh@bjsjth.cn

SPECIALTY SECTION
This article was submitted to Breast Cancer, a section of the journal Frontiers in Oncology

RECEIVED 12 March 2022
ACCEPTED 22 August 2022
PUBLISHED 28 September 2022

CITATION
Liu X, Fang Y, Li Y, Li Y, Qi L and Wang X (2022) Pertuzumab combined with trastuzumab compared to trastuzumab in the treatment of HER2-positive breast cancer: A systematic review and meta-analysis of randomized controlled trials. *Front. Oncol.* 12:894861. doi: 10.3389/fonc.2022.894861

COPYRIGHT
© 2022 Liu, Fang, Li, Li, Qi and Wang. This is an open-access article distributed under the terms of the Creative Commons Attribution License (CC BY). The use, distribution or reproduction in other forums is permitted, provided the original author(s) and the copyright owner(s) are credited and that the original publication in this journal is cited, in accordance with accepted academic practice. No use, distribution or reproduction is permitted which does not comply with these terms.

Pertuzumab combined with trastuzumab compared to trastuzumab in the treatment of HER2-positive breast cancer: A systematic review and meta-analysis of randomized controlled trials

Xiaoyun Liu, Yingying Fang, Yinjuan Li, Yan Li, Lu Qi and Xinghe Wang*

Department of Phase I Clinical Trail Center, Beijing Shijitan Hospital, Capital Medical University, Beijing, China

Objective: Although dual anti-HER2 therapy, namely, pertuzumab plus trastuzumab, has shown promising results in patients with HER2-positive breast cancer (BC), it is still unclear whether dual therapy will increase adverse effects (AEs) while ensuring the efficacy compared with trastuzumab monotherapy. We conducted a systematic review and meta-analysis to compare the efficacy and safety of combined therapy with monotherapy.

Methods: A systematic search was performed to identify eligible randomized controlled trials (RCTs) that evaluated the administration of dual anti-HER2 therapy [pertuzumab plus trastuzumab or trastuzumab emtansine (T-DM1)] versus monotherapy (trastuzumab or T-DM1). The primary endpoints were overall survival (OS) and progression-free survival (PFS).

Results: Fourteen RCTs (8,378 patients) were identified. Compared to monotherapy, dual therapy significantly improved the OS (HR = 0.77, 95% CI: 0.59–0.99) and PFS (HR = 0.74, 95% CI: 0.63–0.86) in advanced BC. In neoadjuvant therapy, dual blockade has a higher ORR rate than monotherapy. Grade 3 or higher febrile neutropenia, diarrhea, and anemia as well as heart failure were more frequently reported in dual therapy compared to monotherapy. No significant difference in serious AEs was observed between the two groups. In the subgroup analysis, compared to single-target therapy, dual-target therapy has higher OS and PFS rates in Asian patients with advanced therapy; however, total grade ≥3 AEs and serious AEs were significantly higher in the dual group in Asian patients.

Conclusions: Our study confirms that the combination of pertuzumab and trastuzumab therapy could substantially improve the outcome of patients with HER2-positive breast cancer and was well tolerated compared to trastuzumab monotherapy.

KEYWORDS

breast cancer, HER2-positive, pertuzumab, trastuzumab, meta-analysis

Introduction

In 2020, breast cancer was the fourth leading cause of cancer-related deaths among women in China and ranked first in the incidence of female cancer (1). Approximately 20% of breast cancers strongly overexpressed human epidermal growth factor receptor 2 (HER2), which has historically been associated with a poor prognosis, an aggressive phenotype, and a shorter overall survival (OS) (2). Trastuzumab, a recombinant humanized monoclonal antibody targeting HER2, combined with chemotherapy increased response rates and time to progression. However, the majority of cancers that initially respond to trastuzumab begin to progress again within 1 year (3). Moreover, the cardiotoxicity rate in the trastuzumab arm (4.0%) was higher than in the non-trastuzumab arm (1.3%) (4).

Pertuzumab, another monoclonal HER2 antibody, binds to a different region of trastuzumab and blocks the dimerization of HER2 with other HER family members such as HER3. Previous studies proved that the combination of trastuzumab and pertuzumab demonstrated a strongly enhanced antitumor effect combined as compared with either agent alone in preclinical studies (5). Pertuzumab was approved by the FDA for use in combination with trastuzumab and chemotherapy for the advanced, neoadjuvant, and adjuvant treatment of patients with HER2-positive breast cancer (6, 7). Although they generally are well tolerated, HER2-targeted therapies are associated with cardiotoxicity such as an asymptomatic decrease in the left ventricular ejection fraction (LVEF) (8).

Therefore, it is still unclear whether the combination of pertuzumab and trastuzumab does not increase the incidence of adverse effects (AEs) while enhancing the antitumor effect, compared with trastuzumab single-agent therapy. We conducted an up-to-date systematic review and meta-analysis of randomized controlled trials (RCTs) on pertuzumab plus trastuzumab (or ado-trastuzumab emtansine, T-DM1) dual anti-HER2 therapy compared with trastuzumab or T-DM1 monotherapy in patients with HER2-positive breast cancer. Due to the effect of conjugated trastuzumab, i.e., T-DM1, which is expected to be greater than the original trastuzumab, we divided pertuzumab plus trastuzumab or T-DM1 into two groups.

Material and methods

Study design, patients, comparison, and outcome

We quantitatively summarized data on the efficacy and safety of pertuzumab from RCTs. Patients were diagnosed with HER2-positive breast cancer. The primary endpoints were progression-free survival (PFS) and OS. The secondary endpoints included pathologic complete response (pCR), partial response (PR), complete response (CR), and objective response rate (ORR). The safety endpoints were adverse events (AEs) including cardiotoxicities, serious AEs, any-grade AEs, and so on. The risk estimates were pooled by comparing the pertuzumab plus trastuzumab (or pertuzumab plus T-DM1) group with or without chemotherapy versus the trastuzumab (or T-DM1) monotherapy group with or without chemotherapy.

Search strategy and selection criteria

This systematic review adhered to the Preferred Reporting Items for Systematic Reviews and Meta-Analyses (PRISMA) statement (9). Relevant articles were identified by searching PubMed, Medline, Embase, Cochrane Library, Web of Science, ClinicalTrials.gov, CNKI, and Wanfang (the last two were Chinese literature databases) without year and language restrictions, by using the following keywords: pertuzumab or Perjeta or Rhumba 2C4; breast or mammary; randomized or randomised or randomly. The last search was updated on 17 February 2022. To identify additional articles, the reference lists of identified studies and relevant reviews were reviewed. When more than one publication was identified from the same clinical trial, we used the most recent or complete report of that trial.

We used the following selection criteria: 1) original articles reporting RCTs; 2) patients that had HER2-positive breast cancer; 3) studies that had at least two groups included: a dual anti-HER2 therapy group which is pertuzumab plus trastuzumab or T-DM1 with or without chemotherapy and a

monotherapy group which is trastuzumab or T-DM1 with or without chemotherapy; 4) studies that reported at least one of the above efficacy or safety indicators; and 5) studies published in English. Studies not matching the selection criteria were excluded. Other exclusion criteria included the following: 1) repeated publications or incomplete data, 2) conference abstracts and unpublished results, and 3) phase I clinical trials.

Data extraction and quality assessment

The following information was extracted from each included study: the first author's name, publication year, trial names, country of origin, study design, demographics of participants, diagnosis and grading of diseases, number of patients in each group, interventions (including type, dose, and duration of anti-HER2 therapy; type of chemotherapy), follow-up time, outcomes, and other important characteristics of the study population. Data extraction was conducted independently by two investigators, and any disagreement was resolved by consensus. Risk of bias assessment was carried out using the Cochrane risk of bias tool (10). Risk of bias was rated as high/low/unclear. The quality assessment was measured using RevMan Version 5.4 (The Cochrane Collaboration, the UK).

Statistical analysis

The pooled hazard ratio (HR) and 95% confidence interval (CI) on primary endpoints (PFS and OS) were used as the effect size of survival data. The pooled relative risk ratio (RR) and 95% CI were used to calculate the effect size of dichotomous data. Statistical heterogeneity was assessed using the I^2 and Q-statistic. In cases of no heterogeneity between results ($I^2 < 50\%$; $p > 0.1$), a fixed-effect model based on Mantel–Haenszel was used; otherwise, the random-effect model was used to estimate τ^2 using DerSimonian and Laird (11, 12). A sensitivity analysis was used to assess the influence of each study on the overall results by omitting one study at a time. Potential publication bias was assessed by Begg's test and Egger's test. A two-sided p-value <0.05 was considered statistically significant. All statistical analyses were performed with Stata 12.0 (StataCorp, America).

Results

Search results and trial characteristics

The study selection process is summarized in Figure 1. **A** total of 3,165 potentially relevant records were retrieved. After removing 608 duplicates, 2,557 remained for

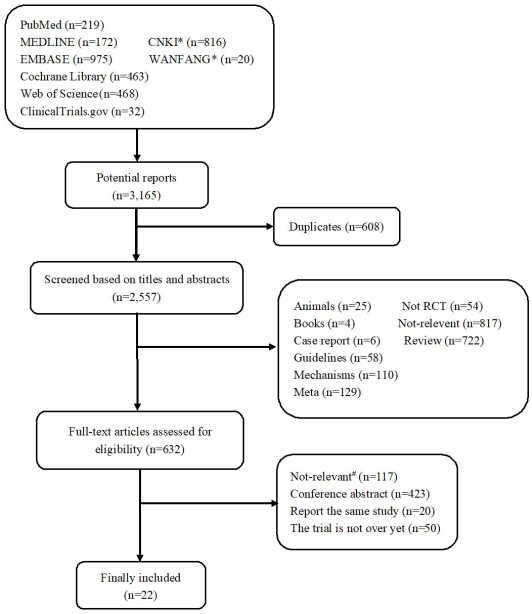

FIGURE 1
Flowchart diagram of the study selection. *CNKI and Wanfang were two Chinese literature databases. #Not-relevant, including non-breast cancer (n = 6); both the trial group and the control group used pertuzumab (n = 106); the control group did not use trastuzumab (n = 2); phase I clinical trial (n = 2) and without efficacy or safety indicators (n = 1).

evaluation. After screening titles and abstracts, 1,925 records were excluded, including non-original research, non-relevant studies, and so on. After screening the full text, 610 records were further excluded due to the following reasons: the patients included had no breast cancer, both experimental and control groups used pertuzumab, the control group did not use trastuzumab, the studies were conference abstracts, the studies did not complete or provide results, and studies reported the same study. Thus, a total of 22 records (13–33) reporting 15 RCTs were included.

In terms of efficacy, six, one, and eight RCTs were included in the neoadjuvant, adjuvant, and advanced breast cancer therapies. One trial (28) has compared the fixed-dose combination of pertuzumab and trastuzumab for subcutaneous (SC) administration with pertuzumab IV and trastuzumab IV formulations and, thus, was excluded from the meta-analysis. The characteristics of each trial are presented in Table 1. Finally, 14 RCTs (8,378 patients) were included for the meta-analysis, with 4,241 patients in the dual-targeted therapy group and 4,137 in the monotherapy group. Two trials had more than three arms, but we only extracted the data related to our purpose, that is, the comparison between pertuzumab plus trastuzumab and trastuzumab alone (14, 20).

TABLE 1 Characteristics of the included studies.

Authors, year	Trial name	Region	Phase	Experimental group			Control group			Duration[b]
				Treatment	Sample size	Age[a]	Treatment	Sample size	Age[a]	
Neoadjuvant setting										
Gianni, L., et al., 2012 (14, 18)	NeoSphere	International	2	T+P+D	107	–	T+D	107	50 (32–74)	12w
Buxton, M., et al., 2016 (33)	I-SPY 2 TRIAL	International	3	T+P+D-AC	150	–	T+D-AC	150	–	12w
Patel, T. A., et al., 2019 (24)	TEAL	International	2	T+P	16	57 (40–75)	T-DM1+L +/-nab-Pac	14	53 (28–70)	18w
Shao, Z., et al., 2020 (26)	PEONY	International	3	T+P+D	219	49 (24–72)	T+Placebo+D	110	49 (27–70)	12w
Tan, A. R., et al., 2021 (28)	FeDeriCa	International	3	T+P, IV	252	49 (42–58)	T+P, fdc sc	248	52 (44–59)	12w
Zhang, Q., et al., 2021 (29)	NA	China	NA	T+P+Pac	20	45.3 ± 1.3	T+Pac	20	45.3 ± 1.3	NA
Adjuvant setting										
Minckwitz, G., et al., 2017 (22)	APHINITY	International	3	T+P+FEC-D/Pac	2,400	51.7 ± 10.9	T+Placebo +FEC-D/Pac	2404	51.4 ± 10.7	52w
Metastatic setting (first line)										
Baselga, J., et al., 2012 (13, 15–17, 32)	CLEOPATRA	International	3	T+P+D	402	54.0 (27–89)	T+Placebo+D	406	54.0 (22–82)	Until[c]
Krop, I. E., et al., 2016 (19)	–	USA	2	T-DM1+P+Pac	22	54 (43–72)	T-DM1+Pac	22	50 (35–81)	Until[c]
Urruticoechea, A., et al., 2017 (21)	PHEREXA	International	3	T+P+Cap	228	54	T+Cap	224	55	Until[c]
Perez, E. A., et al., 2017 (20, 25)	MARIANNE	International	3	T-DM1+P	363	52 (27–86)	T-DM1 +Placebo	367	52 (27–82)	Until[c]
Rimawi, M., et al., 2018 (23)	PERTAIN	International	2	T+P+AI	129	59 (35–87)	T+AI	129	61 (31–89)	18–24w
Xu, B., et al., 2020 (27)	PUFFIN	China	3	T+P+D	122	51 (26–74)	T+Placebo+D	121	53 (25–71)	Until[c]
Jiang, Y., et al., 2021 (31)	NA	China	NA	T+P+D	40	56.4 ± 2.4	T+D	40	56.6 ± 2.5	18w
Ma, S. Y., et al., 2021 (30)	NA	China	NA	T+P+Pac+CBP	23	43.9 ± 21.8	T+Pac+CBP	23	45.8 ± 20.9	12w

T, trastuzumab; D, docetaxel; P, pertuzumab; T-DM1, trastuzumab emtansine; Pac, paclitaxel; Cap, capecitabine; A, doxorubicin; C, cyclophosphamide; FEC, fluorouracil+epirubicin +cyclophosphamide; AI, anastrozole or letrozole; L, lapatinib; nab-pac, nab-paclitaxel; CBP, carboplatin.

[a]Age was expressed as median (IQR) or mean ± SD.

[b]Duration of anti-HER2 therapy.

[c]Anti-HER2 therapy was given until disease progression or unacceptable toxicity.

Primary endpoints

In the treatment of advanced breast cancer, two RCTs (13, 21, 32) reported OS, including 630 patients in the pertuzumab plus trastuzumab group and 630 in the trastuzumab group. The pooled results showed that dual anti-HER2 therapy significantly prolonged OS compared with monotherapy (HR = 0.67, 95% CI: 0.57–0.79; Figure 2), with no evidence of publication bias (Begg's test, p = 1.000). We noted no evidence of heterogeneity across the included studies (I^2 = 0%, p = 0.933).

In advanced therapy, five RCTs (13, 21, 23, 27), including 881 patients of pertuzumab plus trastuzumab and 880 of trastuzumab, reported PFS data. The pooled PFS demonstrated a statistically significant improvement for patients in the dual therapy group compared to the monotherapy group (HR = 0.69, 95% CI: 0.61–0.78; Figure 2), with no heterogeneity across studies (I^2 = 16.2%, p = 0.310) and no publication bias (Egger's test, p = 0.904; Begg's test, p = 0.734).

Secondary endpoints

In neoadjuvant therapy, the pCR and ORR data were reported in four (14, 26, 29, 33) and two RCTs (14, 26), respectively (Supplementary Figure 2). The pooled pCR and ORR had a significant absolute improvement (RR = 1.61, 95% CI: 1.30–2.01; RR = 1.11, 95% CI: 1.02–1.21) in the dual blockade group (pertuzumab plus trastuzumab) compared to the monotherapy group. In advanced therapy of pertuzumab plus trastuzumab versus trastuzumab, in evaluating the CR, PR, and ORR rates, four (13, 27, 30, 31), four (13, 27, 30, 31), and five (13, 21, 27, 30, 31) RCTs were included, respectively. The pooled PR and ORR showed a substantial benefit in the dual HER2 blocking group compared to the monotherapy group (RR = 1.23, 95% CI: 1.11–1.36; RR = 1.21, 95% CI: 1.11–1.31, respectively) with no heterogeneity among studies. There was no statistical significance in the pooled CR (RR = 1.24, 95% CI: 0.76–2.03) (Supplementary Figure 3). However, in advanced therapy of pertuzumab plus T-DM1 versus T-DM1, there was no statistical significance in the pooled CR, PR, and ORR (Supplementary Figure 4).

Safety endpoints

Eight RCTs (13, 18, 20–22, 26, 27, 29) reported cardiotoxicities, including LVEF decline, asymptomatic left ventricular systolic dysfunction (LVSD), and heart failure (HF). The pooled HF was statistically significant in the dual HER2 blocking group compared with monotherapy (RR = 4.18, 95% CI: 1.07–16.30), whereas LVEF decline and asymptomatic LVSD did not show significant difference (Supplementary Table 1). We conducted an analysis of grade ≥3 AEs reported in the trials: neutropenia (eight trials), diarrhea (eight trials), febrile neutropenia (five trials), leukopenia (five trials), anemia (five trials), asthenia (four trials), fatigue (four trials), and so on (Supplementary Table 2). Patients receiving dual blockade of pertuzumab plus trastuzumab had a significant increase in the incidence of febrile neutropenia (RR = 1.17, 95% CI: 1.01–1.34), diarrhea (RR = 2.26, 95% CI: 1.87–2.74), and anemia (RR = 1.39, 95% CI: 1.11–1.73), whereas only diarrhea was significant in patients with pertuzumab plus T-DM1 dual therapy compared to T-DM1 monotherapy. There were no statistical differences in total grade ≥3 AEs and the other grade ≥3 AEs between the dual therapy group and the monotherapy group (Figure 4). The pooled analysis showed no substantial increase in the incidence of total serious AEs (RR = 1.12, 95% CI: 0.90–1.38) and death (RR = 0.83, 95% CI: 0.68–1.00) (Figure 4 and Supplementary Table 3). More than half of the trials reported all-grade AEs such as diarrhea (13 trials), nausea (11 trials), rash (9 trials), neutropenia (8 trials), and alopecia (7 trials). Compared with the monotherapy group, the incidence rates of

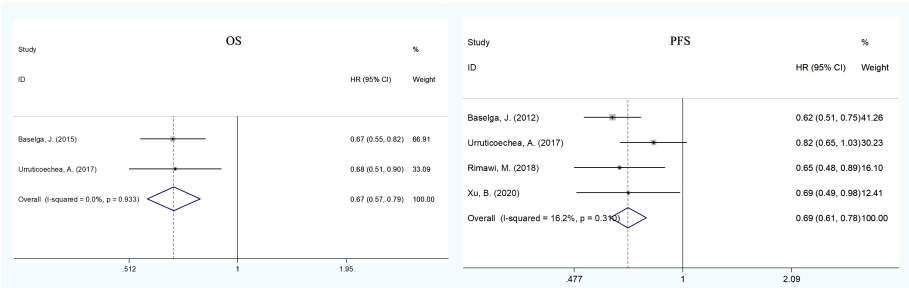

FIGURE 2
Meta-analysis of primary endpoints [overall (OS) and progression-free survival (PFS)] between the dual anti-HER2 therapy group (pertuzumabplus trastuzumab) and the monotherapy group in advanced breast cancer. The size of the squares indicates the weight of the study. Error barsrepresent 95% confidence intervals (CIs). The diamond indicates the summary odds ratio.

diarrhea (RR = 1.48, 95% CI: 1.30–1.69), rash (RR = 1.54, 95% CI: 1.29–1.83), and mucosal inflammation (RR = 1.45, 95% CI: 1.17–1.78) were significantly higher in the dual therapy (pertuzumab plus trastuzumab) group; however, only the incidence of rash (RR = 1.42, 95% CI: 1.07–1.87) was significant in the dual therapy of pertuzumab plus T-DM1. No other differences were observed in the other all-grade AEs (Supplementary Table 4).

Subgroup analysis

To explore the effect of pertuzumab in Asian patients, we conducted a subgroup analysis and extracted data from nine publications on the treatment of advanced breast cancer (17, 20, 21, 26, 27, 29–31, 34). The pooled analysis found that the dual treatment of pertuzumab and trastuzumab resulted in an improvement in both OS and PFS compared with trastuzumab alone (HR = 0.63, 95% CI: 0.42–0.94; HR = 0.65, 95% CI: 0.52–0.82) (Figure 3). The incidence rates of total grade ≥3 AEs (HR = 1.11, 95% CI: 1.03–1.21) and SAEs (HR = 1.39, 95% CI: 1.07–1.82) were statistically significant in the pertuzumab plus trastuzumab group compared with the monotherapy group (Figure 4 and Supplementary Tables 5, 6). For all-grade AEs, the incidence rates of diarrhea, mucosal inflammation, and infusion-related reactions were significantly higher in Asian patients treated with dual anti-HER2 therapy (Supplementary Table 7).

Quality assessment and publication bias

The risk of bias for the included trials is shown in Figure 5 (and Supplementary Figure 1). Overall, the quality of the studies was satisfactory. Six trials (14, 19, 21, 23, 24, 33) were open label, that is, no blinding of the study participants and personnel. One trial (31) used a list of random numbers, which could possibly foresee assignments and, thus, introduce selection bias. One trial (24) was closed early due to superiority, with 14 patients not completing the experimental group. No evidence of significant publication bias was detected for any of the measured outcomes by Egger's test and Begg's test.

Discussion

As we know, this is the first meta-analysis of RCTs focusing on the combination of pertuzumab and trastuzumab/T-DM1 therapy versus trastuzumab/T-DM1 single-agent therapy in patients with HER2-positive breast cancer. Most other studies discussed different combination regimens of dual anti-HER2 therapy (35, 36). This meta-analysis of RCTs observed the efficacy of pertuzumab plus trastuzumab with or without chemotherapy that was superior to trastuzumab monotherapy with or without chemotherapy in the treatment of advanced breast cancer, with a significant improvement in OS, PFS, PR, and ORR. In neoadjuvant therapy, the dual blockade of pertuzumab and trastuzumab has higher pCR and ORR rates than monotherapy (trastuzumab). Moreover, the total incidence of grade ≥3 AEs and SAEs did not increase in patients with dual therapy (pertuzumab plus trastuzumab) compared to monotherapy (trastuzumab). However, compared with trastuzumab, pertuzumab plus trastuzumab therapy has a higher incidence of heart failure and grade ≥3 febrile neutropenia, diarrhea, and anemia. Furthermore, in Asian patients in advanced therapy, compared to single-target therapy (trastuzumab), the double-target therapy (pertuzumab plus trastuzumab) also has a higher OS rate and PFS rate, which was consistent with the efficacy in global patients. However, the incidence of total grade ≥3 AEs and SAEs was increased significantly in Asian patients.

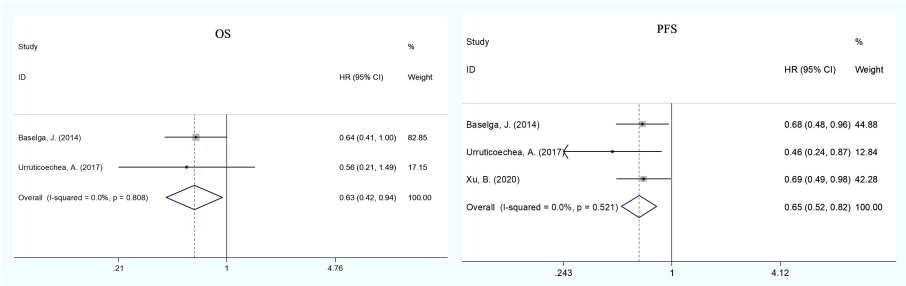

FIGURE 3
Subgroup analysis of OS and PFS between the dual anti-HER2 therapy group (pertuzumab plus trastuzumab) and the monotherapy group in advanced breast cancer in Asian patients. The size of the squares indicates the weight of the study. Error bars represent 95% confidence intervals (CIs). The diamond indicates the summary odds ratio. No evidence of publication bias was detected for OS (Begg's test: p = 1.000) and PFS (Egger's test: p = 0.752, Begg's test: p = 1.000).

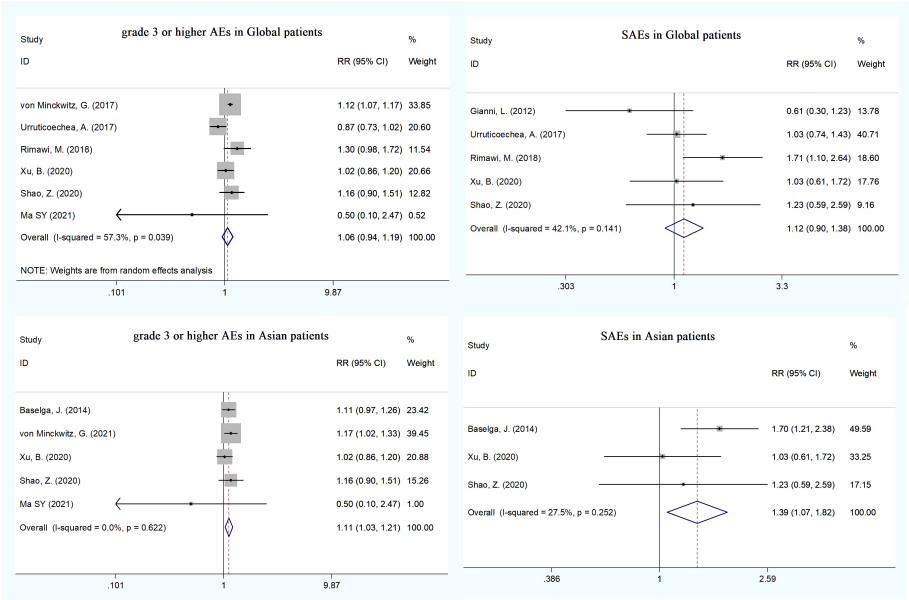

FIGURE 4
The incidence of total grade ≥3 AEs and SAEs between the dual anti-HER2 therapy group (pertuzumab plus trastuzumab) and the monotherapygroup in global and Asian patients.

The HER family plays an important role in cell survival and proliferation and is implicated in oncogenesis. Overexpression of HER2 is associated with aggressive disease and poor prognosis. Both pertuzumab and trastuzumab are humanized monoclonal antibodies targeting HER2 and have proven to offer survival benefit for women with HER2-positive breast cancer. Several mechanisms have been proposed to explain the synergism of pertuzumab and trastuzumab in treating HER2-positive breast cancer, the favored theory of which was the different functions of the two antibodies (5, 37–39). Trastuzumab and T-DM1 bind to domain IV of HER2 and inhibit the homodimerization of HER2 and the downstream signaling pathways activated by the HER2 homodimer. However, pertuzumab binds HER2 in domain II, a different domain than trastuzumab, and preferentially blocks the heterodimerization of HER2 with EGFR, HER3, and HER4, and the downstream signaling pathways activated by HER2 heterodimers, which activates several intracellular signaling cascades, including cell proliferation and survival (38, 39). Therefore, the combination of the two antibodies could synergistically enhance the blocking effect of the downstream signaling, resulting in greater antitumor activity than either agent alone in preclinical studies (5). However, the German Federal Joint Committee (G-BA) and the Institute for Quality and Efficiency in Health Care (IQWiG) did not conclude that there is any additional benefit of adding pertuzumab to the neoadjuvant combination treatment of chemotherapy and trastuzumab based on the prognostic benefit, which was at that time unconfirmed (40). The combination of pertuzumab with trastuzumab and chemotherapy has been approved both by the FDA and the European Medicines Agency in the metastatic, neoadjuvant, and adjuvant settings (6, 7). Therefore, we extracted and summarized RCT studies to explore the efficacy and safety of dual blockade compared with monotherapy.

In pivotal studies of breast cancer, PFS was widely used as a primary endpoint although the choice of PFS or OS remained the subject of debate. In the CLEOPATRA trial, PFS was significantly improved with pertuzumab plus trastuzumab plus docetaxel, which was first approved in June 2012 by the FDA for the first-line treatment of HER2-positive MBC (13). After one additional year of follow-up, the OS analysis also demonstrated statistically significant and clinically meaningful survival benefit with this combination compared with trastuzumab plus docetaxel (16), which was maintained after a median follow-up of more than 8 years (41). However, the PHEREXA study did not show this consistency between PFS and OS in advanced breast cancer. It was found that adding pertuzumab to trastuzumab and capecitabine modestly increased PFS, but there was no statistical significance. Although the median OS was increased by using two anti-HER2 regimens, the statistical significance of OS cannot be claimed as a result of the hierarchical testing of OS after the primary PFS endpoint (21). In this study, after the pooling analysis, we demonstrated that dual blocking therapy could significantly prolong OS and PFS in advanced and neoadjuvant therapy in patients with HER2-positive breast cancer compared with trastuzumab single-agent

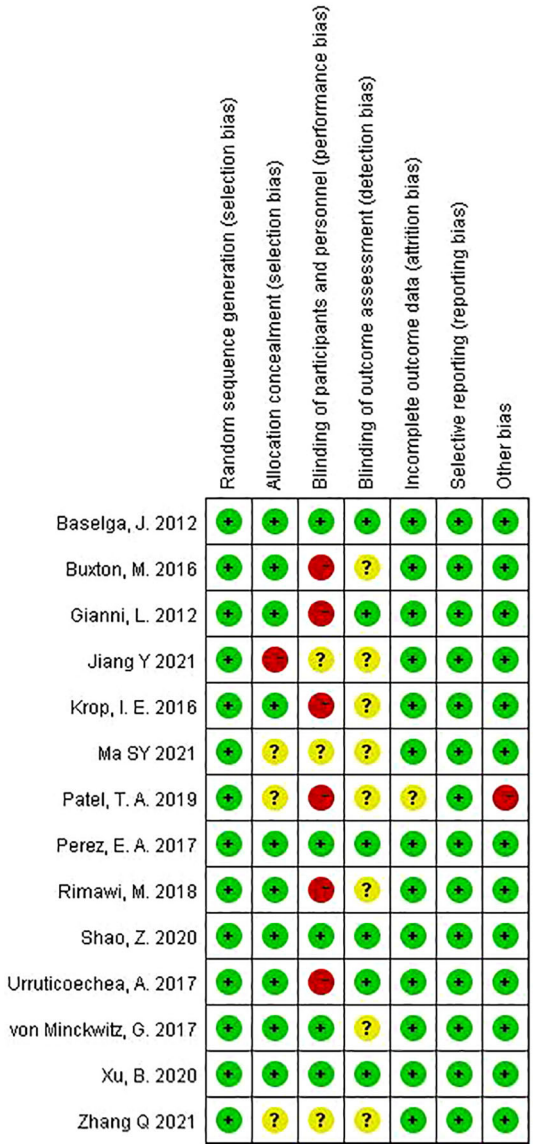

FIGURE 5
Risk of bias summary.

therapy with or without chemotherapy. Furthermore, a subgroup analysis of the CLEOPATRA trial showed that patients experienced PFS benefit with treatment in the pertuzumab plus trastuzumab arm compared with the placebo plus trastuzumab arm in both the <65-year (HR = 0.65; 95% CI: 0.53–0.80) and >65-year groups (HR = 0.52; 95% CI: 0.31–0.86) (42). They suggested that the combined use of pertuzumab and trastuzumab should not be limited by age, though proactive management of toxicities and regular cardiac monitoring should clearly be undertaken.

pCR is an established predictor of the prognosis, and improvements in pCR appear to be associated with improvements in the prognosis to some extent (40). Combining trastuzumab and pertuzumab in neoadjuvant therapy in the NeoSphere trial resulted in a pCR rate of 45.8% and was significantly superior to neoadjuvant chemotherapy plus trastuzumab alone (29%; $p = 0.014$) (14). However, a 5-year survival analysis of this trial did not show any significant differences between the two groups (HR = 0.69; 95% CI: 0.34–1.40) (18). Two further neoadjuvant treatment trials reported that the pCR rate in patients treated with dual blockade was approximately twice as high as that in patients with trastuzumab single-agent therapy (26, 29). In our study, however, the pooled pCR was significantly increased in the dual blockade group

compared to the monotherapy group in neoadjuvant therapy. A meta-analysis by Chen et al. confirmed that trastuzumab plus pertuzumab significantly improved the pCR compared to trastuzumab in neoadjuvant settings (OR = 1.33; 95% CI: 1.08–1.63; p = 0.006) (43). However, this study included non-RCTs, such as single-arm studies and retrospective studies, which might generate biases.

Although dual anti-HER2 therapies were associated with an efficacy benefit in HER2-positive breast cancer, they could increase the risk of cardiac toxicity in previous trials. The FDA recommendations for pertuzumab, trastuzumab, and T-DM1 limit their use to patients whose LVEF prior to treatment exceeds 50% or 55%, and the agency advises dose delay or discontinuation in the setting of LVEF decline during treatment (44). Our study showed that the combined anti-HER2 therapy increases the incidence of heart failure compared with single-agent therapy, which was not consistent with the findings from the meta-analysis, concluding that doubling up on anti-HER2 drugs did not increase cardiac toxicity compared with the use of anti-HER2 drugs individually (45). However, this study did not specify the administration of pertuzumab plus trastuzumab versus trastuzumab. Our results should be considered valid because of the included patients with an adequate cardiac function prior to therapy.

Furthermore, adverse events (any grade) such as diarrhea, rash, and mucosal inflammation which were mostly grade 1 or 2 were reported more frequently in the pertuzumab plus trastuzumab group than in the trastuzumab monotherapy group. Furthermore, a higher incidence of grade 3 or higher febrile neutropenia, diarrhea, and anemia was reported in the dual therapy group, which was consistent with the reports of the meta-analysis published by Chen et al. (43). The meta-analyses of Yu et al. (36) and Zhang et al. (46) only confirmed that dual therapy increased the incidence of grade 3–4 diarrhea because they did not collect the data of other AEs. Although our study demonstrated that dual HER2 blocking does not significantly increase the risk of total grade ≥3 AEs and total serious AEs, strict patients' selection criteria should be adopted in future trials, and patients receiving dual regimens should be closely monitored in clinical practice. However, in the subgroup analysis of Asian patients, we found that the incidence of total grade ≥3 AEs and serious AEs was significantly higher in the dual therapy group, suggesting that clinical monitoring should be given more to Asian patients with dual-targeted therapy.

In 2002, trastuzumab (Herceptin) was initially granted regular approval by the NMPA of China, and its safety and efficacy in Chinese patients have been fully verified. In December 2018, pertuzumab was initially approved by the NMPA, and on 1 January 2020, it was included in the Chinese national reimbursement drug list (NRDL) to reduce the burden of disease. However, the data of the application of pertuzumab in Chinese patients mostly came from a subgroup analysis of international trials or bridging studies. Due to the lack of RCTs in Chinese patients, we observed the use of the combination of pertuzumab and trastuzumab therapy in global studies. This meta-analysis provides the basis for clinical practice supporting the use of the combined therapy in China. However, this meta-analysis has several limitations. First, the number of studies included was relatively small. There are some ongoing trials investigating the dual anti-HER2 therapy compared to monotherapy, and the results are yet to be released. Moreover, some studies outlined in the included studies are still in progress, and follow-up results will be used in the future analysis. Second, clinical heterogeneity does exist among trials in terms of treatment setting. Third, the calculations were based on published positive study results, and many negative results may not be published, which might generate biases.

In summary, our findings provide robust information that the combination of pertuzumab and trastuzumab with or without chemotherapy in breast cancer is warranted. The combined therapy could substantially improve the outcome of patients with HER2-positive breast cancer in both advanced and neoadjuvant therapies and was well tolerated, with no increase in total grade ≥3 AEs and serious adverse events, compared with trastuzumab monotherapy. However, in Asian patients, the incidence of total grade ≥3 AEs and SAEs was more frequent in the dual therapy group, which needs to be more closely monitored in clinical practice. Additional large-scale randomized controlled trials should be designed to further confirm the efficacy and safety of dual blocking therapy in Chinese patients with HER2-positive breast cancer.

Data availability statement

The original contributions presented in the study are included in the article/Supplementary Material. Further inquiries can be directed to the corresponding author.

Author contributions

XL and XW conceived the idea, designed the study, defined the search strategy and inclusion/exclusion criteria, and were the major contributors in writing the manuscript. XL and YF performed the literature search and the analysis. YJL, YL, and LQ contributed to the writing and editing of the manuscript. All authors contributed to the manuscript and approved the submitted version.

Funding

The current analyses were supported by funding from Beijing Science and Technology Program (Project No. Z211100002521011).

Conflict of interest

The authors declare that the research was conducted in the absence of any commercial or financial relationships that could be construed as a potential conflict of interest.

Publisher's note

All claims expressed in this article are solely those of the authors and do not necessarily represent those of their affiliated organizations, or those of the publisher, the editors and the reviewers. Any product that may be evaluated in this article, or claim that may be made by its manufacturer, is not guaranteed or endorsed by the publisher.

Supplementary material

The Supplementary Material for this article can be found online at: https://www.frontiersin.org/articles/10.3389/fonc.2022.894861/full#supplementary-material

References

1. Jie H, Wanqing C, Mi L, Hongbing S, Jiang L, Yong W, et al. China Guideline for the screening and early detection of female breast Cancer(2021 Beijing. *China Cancer* (2021) 30(3):161–91. doi: 10.11735/j.issn.1004-0242.2021.03.A001

2. Mitri Z, Constantine T, O'Regan R. The HER2 receptor in breast cancer: Pathophysiology, clinical use, and new advances in therapy. *Chemother Res Pract* (2012) 2012:743193. doi: 10.1155/2012/743193

3. Goldhirsch A, Gelber RD, Piccart-Gebhart MJ, de Azambuja E, Procter M, Suter TM, et al. 2 years versus 1 year of adjuvant trastuzumab for HER2-positive breast cancer (HERA): An open-label, randomised controlled trial. *Lancet* (2013) 382(9897):1021–8. doi: 10.1016/s0140-6736(13)61094-6

4. Romond EH, Jeong JH, Rastogi P, Swain SM, Geyer CEJr., Ewer MS, et al. Seven-year follow-up assessment of cardiac function in NSABP b-31, a randomized trial comparing doxorubicin and cyclophosphamide followed by paclitaxel (ACP) with ACP plus trastuzumab as adjuvant therapy for patients with node-positive, human epidermal growth factor receptor 2-positive breast cancer. *J Clin Oncol Off J Am Soc Clin Oncol* (2012) 30(31):3792–9. doi: 10.1200/jco.2011.40.0010

5. Scheuer W, Friess T, Burtscher H, Bossenmaier B, Endl J, Hasmann M. Strongly enhanced antitumor activity of trastuzumab and pertuzumab combination treatment on HER2-positive human xenograft tumor models. *Cancer Res* (2009) 69(24):9330–6. doi: 10.1158/0008-5472.Can-08-4597

6. Blumenthal GM, Scher NS, Cortazar P, Chattopadhyay S, Tang S, Song P, et al. First FDA approval of dual anti-HER2 regimen: pertuzumab in combination with trastuzumab and docetaxel for HER2-positive metastatic breast cancer. *Clin Cancer Res* (2013) 19(18):4911–6. doi: 10.1158/1078-0432.CCR-13-1212

7. Howie LJ, Scher NS, Amiri-Kordestani L, Zhang L, King-Kallimanis BL, Choudhry Y, et al. FDA Approval summary: Pertuzumab for adjuvant treatment of HER2-positive early breast cancer. *Clin Cancer Res* (2018) 25(10):2949–55. doi: 10.1158/1078-0432.CCR-18-3003

8. Fiúza M. Cardiotoxicity associated with trastuzumab treatment of HER2+ breast cancer. *Adv Ther* (2009) 26 Suppl 1:S9–17. doi: 10.1007/s12325-009-0048-z

9. Liberati A, Altman DG, Tetzlaff J, Mulrow C, Gøtzsche PC, Ioannidis JP, et al. The PRISMA statement for reporting systematic reviews and meta-analyses of studies that evaluate health care interventions: explanation and elaboration. *J Clin Epidemiol* (2009) 62(10):e1–34. doi: 10.1016/j.jclinepi.2009.06.006

10. Higgins JPT, Altman DG. Assessing risk of bias in included studies. In: JPT Higgins, S Green, editors. *Cochrane handbook for systematic reviews of interventions*. (Hoboken, America: Wiley) (2008). p. 187–241.

11. DerSimonian R, Laird N. Meta-analysis in clinical trials. *Controlled Clin trials* (1986) 7(3):177–88. doi: 10.1016/0197-2456(86)90046-2

12. Normand SL. Meta-analysis: formulating, evaluating, combining, and reporting. *Stat Med* (1999) 18(3):321–59. doi: 10.1002/(sici)1097-0258(19990215)18:3<321::aid-sim28>3.0.co;2-p

13. Baselga J, Cortés J, Kim SB, Im SA, Hegg R, Im YH, et al. Pertuzumab plus trastuzumab plus docetaxel for metastatic breast cancer. *New Engl J Med* (2012) 366(2):109–19. doi: 10.1056/NEJMoa1113216

14. Gianni L, Pienkowski T, Im YH, Roman L, Tseng LM, Liu MC, et al. Efficacy and safety of neoadjuvant pertuzumab and trastuzumab in women with locally advanced, inflammatory, or early HER2-positive breast cancer (NeoSphere): A randomised multicentre, open-label, phase 2 trial. *Lancet Oncol* (2012) 13(1):25–32. doi: 10.1016/S1470-2045(11)70336-9

15. Swain SM, Ewer MS, Cortes J, Amadori D, Miles D, Knott A, et al. Cardiac tolerability of pertuzumab plus trastuzumab plus docetaxel in patients with HER2-positive metastatic breast cancer in CLEOPATRA: A randomized, double-blind, placebo-controlled phase III study. *oncologist* (2013) 18(3):257–64. doi: 10.1634/theoncologist.2012-0448

16. Swain SM, Kim SB, Cortes J, Ro J, Semiglazov V, Campone M, et al. Pertuzumab, trastuzumab, and docetaxel for HER2-positive metastatic breast cancer (CLEOPATRA study): overall survival results from a randomised, double-blind, placebo-controlled, phase 3 study. *Lancet Oncol* (2013) 14(6):461–71. doi: 10.1016/s1470-2045(13)70130-x

17. Swain SM, Im YH, Im SA, Chan V, Miles D, Knott A, et al. Safety profile of pertuzumab with trastuzumab and docetaxel in patients from Asia with human epidermal growth factor receptor 2-positive metastatic breast cancer: results from the phase III trial CLEOPATRA. *oncologist* (2014) 19(7):693–701. doi: 10.1634/theoncologist.2014-0033

18. Gianni L, Pienkowski T, Im YH, Tseng LM, Liu MC, Lluch A, et al. 5-year analysis of neoadjuvant pertuzumab and trastuzumab in patients with locally advanced, inflammatory, or early-stage HER2-positive breast cancer (NeoSphere): a multicentre, open-label, phase 2 randomised trial. *Lancet Oncol* (2016) 17(6):791–800. doi: 10.1016/S1470-2045(16)00163-7

19. Krop IE, Modi S, LoRusso PM, Pegram M, Guardino E, Althaus B, et al. Phase 1b/2a study of trastuzumab emtansine (T-DM1), paclitaxel, and pertuzumab in HER2-positive metastatic breast cancer. *Breast Cancer Res* (2016) 18(1):34. doi: 10.1186/s13058-016-0691-7

20. Perez EA, Barrios C, Eiermann W, Toi M, Im YH, Conte P, et al. Trastuzumab emtansine with or without pertuzumab versus trastuzumab plus taxane for human epidermal growth factor receptor 2-positive, advanced breast cancer: primary results from the phase III MARIANNE study. *J Clin Oncol* (2017) 35(2):141–8. doi: 10.1200/JCO.2016.67.4887

21. Urruticoechea A, Rizwanullah M, Im S-A, Sanchez Ruiz AC, Lang I, Tomasello G, et al. Randomized phase III trial of trastuzumab plus capecitabine with or without pertuzumab in patients with human epidermal growth factor receptor 2-positive metastatic breast cancer who experienced disease progression during or after trastuzumab-based therapy. *J Clin Oncol* (2017) 35(26):3030–+. doi: 10.1200/jco.2016.70.6267

22. von Minckwitz G, Procter M, de Azambuja E, Zardavas D, Benyunes M, Viale G, et al. Adjuvant pertuzumab and trastuzumab in early HER2-positive breast cancer. *New Engl J Med* (2017) 377(2):122–31. doi: 10.1056/NEJMoa1703643

23. Rimawi M, Ferrero JM, de la Haba-Rodriguez J, Poole C, De Placido S, Osborne CK, et al. First-line trastuzumab plus an aromatase inhibitor, with or without pertuzumab, in human epidermal growth factor receptor 2-positive and hormone receptor-positive metastatic or locally advanced breast cancer (PERTAIN): A randomized, open-label phase II trial. *J Clin Oncol Off J Am Soc Clin Oncol* (2018) 36(28):2826–35. doi: 10.1200/jco.2017.76.7863

24. Patel TA, Ensor JE, Creamer SL, Boone T, Rodriguez AA, Niravath PA, et al. A randomized, controlled phase II trial of neoadjuvantado-trastuzumab emtansine, lapatinib, and nab-paclitaxel versus trastuzumab, pertuzumab, and paclitaxel in HER2-positive breast cancer (TEAL study). *Breast Cancer Res* (2019) 21(1):100. doi: 10.1186/s13058-019-1186-0

25. Perez EA, Barrios C, Eiermann W, Toi M, Im YH, Conte P, et al. Trastuzumab emtansine with or without pertuzumab versus trastuzumab with taxane for human epidermal growth factor receptor 2-positive advanced breast

cancer: Final results from MARIANNE. *Cancer* (2019) 125(22):3974–84. doi: 10.1002/cncr.32392

26. Shao Z, Pang D, Yang H, Li W, Wang S, Cui S, et al. Efficacy, safety, and tolerability of pertuzumab, trastuzumab, and docetaxel for patients with early or locally advanced ERBB2-positive breast cancer in Asia: the PEONY phase 3 randomized clinical trial. *JAMA Oncol* (2020) 6(3):e193692. doi: 10.1001/jamaoncol.2019.3692

27. Xu B, Li W, Zhang Q, Shao Z, Li Q, Wang X, et al. Pertuzumab, trastuzumab, and docetaxel for Chinese patients with previously untreated HER2-positive locally recurrent or metastatic breast cancer (PUFFIN): a phase III, randomized, double-blind, placebo-controlled study. *Breast Cancer Res Treat* (2020) 182(3):689–97. doi: 10.1007/s10549-020-05728-w

28. Tan AR, Im SA, Mattar A, Colomer R, Stroyakovskii D, Nowecki Z, et al. Fixed-dose combination of pertuzumab and trastuzumab for subcutaneous injection plus chemotherapy in HER2-positive early breast cancer (FeDeriCa): a randomised, open-label, multicentre, non-inferiority, phase 3 study. *Lancet Oncol* (2021) 22(1):85–97. doi: 10.1016/s1470-2045(20)30536-2

29. Q Z, DH L, TY Q, ML C. PCR rate and safety of trastuzumab combined with pertuzumab in the treatment of HER-2 positive breast cancer. *J Chin Baby* (2021) 2:90.

30. SY M, J M, FF W, CY L, F Y, ZL S, et al. Application value of trastuzumab combined with pertuzumab in the treatment of HER2-overexpressed breast cancer. *Int J Pathol Clin Med* (2021) 41(07):1573–8. doi: 10.3978/j.issn.2095-6959.2021.07.017

31. Y J, HB Z, Z W. Effect of dual target regimen combined with docetaxel on prognosis of patients with her-2 positive metastatic breast. *J Med Innovation China* (2021) 18(2):72–5. doi: 10.3969/j.issn.1674-4985.2021.02.018

32. Swain SM, Baselga J, Kim SB, Ro J, Semiglazov V, Campone M, et al. Pertuzumab, trastuzumab, and docetaxel in HER2-positive metastatic breast cancer. *New Engl J Med* (2015) 372(8):724–34. doi: 10.1056/NEJMoa1413513

33. Buxton M, DeMichele AM, Chia S, Van't Veer L, Chien J, Wallace A, et al. Efficacy of pertuzumab/trastuzumab/paclitaxel over standard trastuzumab/paclitaxel therapy for HER2+ breast cancer: Results from the neoadjuvant I-SPY 2 TRIAL. *Cancer Res* (2016) 76(14):CT106. doi: 10.1158/1538-7445.AM2016-CT106

34. Piccart M, Procter M, Fumagalli D, de Azambuja E, Clark E, Ewer MS, et al. Adjuvant pertuzumab and trastuzumab in early HER2-positive breast cancer in the APHINITY trial: 6 years' follow-up. *J Clin Oncol Off J Am Soc Clin Oncol* (2021) 39 (13):1448–57. doi: 10.1200/JCO.20.01204

35. Wang C, Chen J, Xu X, Hu X, Kong D, Liang G, et al. Dual HER2 blockade in neoadjuvant treatment of HER2+ breast cancer: A meta-analysis and review. *Technol Cancer Res Treat* (2020) 19:1533033820960721. doi: 10.1177/1533033820960721

36. Yu L, Fu F, Li J, Huang M, Zeng B, Lin Y, et al. Dual HER2 blockade versus a single agent in trastuzumab-containing regimens for HER2-positive early breast cancer: A systematic review and meta-analysis of randomized controlled trials. *J Oncol Print* (2020) 2020:5169278. doi: 10.1155/2020/5169278

37. Nahta R, Hung MC, Esteva FJ. The HER-2-targeting antibodies trastuzumab and pertuzumab synergistically inhibit the survival of breast cancer cells. *Cancer Res* (2004) 64(7):2343–6. doi: 10.1158/0008-5472.can-03-3856

38. Nami B, Maadi H, Wang Z. Mechanisms underlying the action and synergism of trastuzumab and pertuzumab in targeting HER2-positive breast cancer. *Cancers (Basel)* (2018) 10(10):342. doi: 10.3390/cancers10100342

39. Pernas S, Barroso-Sousa R, Tolaney SM. Optimal treatment of early stage HER2-positive breast cancer. *Cancer* (2018) 124(23):4455–66. doi: 10.1002/cncr.31657

40. Fasching PA, Hartkopf AD, Gass P, Haeberle L, Akpolat-Basci L, Hein A, et al. Efficacy of neoadjuvant pertuzumab in addition to chemotherapy and trastuzumab in routine clinical treatment of patients with primary breast cancer: a multicentric analysis. *Breast Cancer Res Treat* (2019) 173(2):319–28. doi: 10.1007/s10549-018-5008-3

41. Swain SM, Miles D, Kim S-B, Im Y-H, Im S-A, Semiglazov V, et al. Pertuzumab, trastuzumab, and docetaxel for HER2-positive metastatic breast cancer (CLEOPATRA): end-of-study results from a double-blind, randomised, placebo-controlled, phase 3 study. *Lancet Oncol* (2020) 21(4):519–30. doi: 10.1016/s1470-2045(19)30863-0

42. Miles D, Baselga J, Amadori D, Sunpaweravong P, Semiglazov V, Knott A, et al. Treatment of older patients with HER2-positive metastatic breast cancer with pertuzumab, trastuzumab, and docetaxel: subgroup analyses from a randomized, double-blind, placebo-controlled phase III trial (CLEOPATRA). *Breast Cancer Res Treat* (2013) 142(1):89–99. doi: 10.1007/s10549-013-2710-z

43. Chen S, Liang Y, Feng Z, Wang M. Efficacy and safety of HER2 inhibitors in combination with or without pertuzumab for HER2-positive breast cancer: A systematic review and meta-analysis. *BMC Cancer* (2019) 19(1):973. doi: 10.1186/s12885-019-6132-0

44. Lynce F, Barac A, Geng X, Dang C, Yu AF, Smith KL, et al. Prospective evaluation of the cardiac safety of HER2-targeted therapies in patients with HER2-positive breast cancer and compromised heart function: the SAFE-HEaRt study. *Breast Cancer Res Treat* (2019) 175(3):595–603. doi: 10.1007/s10549-019-05191-2

45. Valachis A, Nearchou A, Polyzos NP, Lind P. Cardiac toxicity in breast cancer patients treated with dual HER2 blockade. *Int J Cancer* (2013) 133(9):2245–52. doi: 10.1002/ijc.28234

46. Zhang X, Zhang X-J, Zhang T-Y, Yu F-F, Wei X, Li Y-S, et al. Effect and safety of dual anti-human epidermal growth factor receptor 2 therapy compared to monotherapy in patients with human epidermal growth factor receptor 2-positive breast cancer: A systematic review. *BMC Cancer* (2014) 14:625. doi: 10.1186/1471-2407-14-625

frontiers | Frontiers in Oncology

TYPE Original Research
PUBLISHED 06 October 2022
DOI 10.3389/fonc.2022.1019925

Check for updates

OPEN ACCESS

EDITED BY
Raffaella Massafra,
Bari John Paul II Cancer Institute (IRCCS), Italy

REVIEWED BY
Shengchun Liu,
First Affiliated Hospital of Chongqing Medical University, China
Mauro Giuseppe Mastropasqua,
University of Bari Medical School, Italy

*CORRESPONDENCE
Pin Zhang
zppumc@163.com

SPECIALTY SECTION
This article was submitted to Breast Cancer, a section of the journal Frontiers in Oncology

RECEIVED 15 August 2022
ACCEPTED 20 September 2022
PUBLISHED 06 October 2022

CITATION
Qian X, Xiu M, Li Q, Wang J, Fan Y, Luo Y, Cai R, Li Q, Chen S, Yuan P, Ma F, Xu B and Zhang P (2022) Clinical N3 is an independent risk factor of recurrence for breast cancer patients achieving pathological complete response and near-pathological complete response after neoadjuvant chemotherapy. *Front. Oncol.* 12:1019925. doi: 10.3389/fonc.2022.1019925

COPYRIGHT
© 2022 Qian, Xiu, Li, Wang, Fan, Luo, Cai, Li, Chen, Yuan, Ma, Xu and Zhang. This is an open-access article distributed under the terms of the Creative Commons Attribution License (CC BY). The use, distribution or reproduction in other forums is permitted, provided the original author(s) and the copyright owner(s) are credited and that the original publication in this journal is cited, in accordance with accepted academic practice. No use, distribution or reproduction is permitted which does not comply with these terms.

Clinical N3 is an independent risk factor of recurrence for breast cancer patients achieving pathological complete response and near-pathological complete response after neoadjuvant chemotherapy

Xiaoyan Qian[1,2], Meng Xiu[1], Qing Li[1], Jiayu Wang[1], Ying Fan[1], Yang Luo[1], Ruigang Cai[1], Qiao Li[1], Shanshan Chen[1], Peng Yuan[3], Fei Ma[1], Binghe Xu[1] and Pin Zhang[1*]

[1]Department of Medical Oncology, National Cancer Center/National Clinical Research Center for Cancer/Cancer Hospital, Chinese Academy of Medical Sciences and Peking Union Medical College, Beijing, China, [2]Department of Oncology, Henan Provincial People's Hospital, People's Hospital of Zhengzhou University, Zhengzhou, China, [3]Department of VIP Medical Services, National Cancer Center/National Clinical Research Center for Cancer/Cancer Hospital, Chinese Academy of Medical Sciences and Peking Union Medical College, Beijing, China

Background: Although achieving pathological complete response (pCR) and near-pathological complete response (near-pCR) after neoadjuvant chemotherapy (NAC) in breast cancer predicts a better outcome, some patients still experience recurrence. The aim of our study was to investigate the predictive factors of recurrence in the pCR and near-pCR population.

Methods: We reviewed 1,209 breast cancer patients treated with NAC between January 2010 and April 2021 in the Cancer Hospital, Chinese Academy of Medical Sciences (CHCAMS). A total of 292 patients achieving pCR and near-pCR were included in our analysis. pCR was defined as ypT0N0/ypTisN0. Near-pCR was defined as ypT1mi/1a/1bN0 or ypT0/isN1mi. Clinical features and follow-up information were collected. Survival and predictive factors of recurrence were analyzed.

Results: Of the 292 patients, 173 were pCR and 119 were near-pCR. The median age was 46 years (range, 23–75 years). The predominant tumor subtypes were human epidermal growth factor receptor type 2 (HER2)-positive breast cancer (49.0%) and triple-negative breast cancer (TNBC) (30.8%). The median duration of follow-up was 53 months (range, 9–138 months). A total of 25 (8.6%) patients developed recurrence, with 9 (5.2%) in the pCR group and 16 (13.4%) in the near-pCR group. The vast majority of recurrence occurred within 36 months from onset of NAC. The 5-year recurrence-free survival (RFS) rate of patients achieving pCR was significantly

10.3389/fonc.2022.1019925

higher than that of patients achieving near-pCR (94.6% vs. 85.6%, p = 0.008). However, the 5-year overall survival (OS) rate between the two cohorts had no statistical difference (94.3% vs. 89.6%, p = 0.304). Clinical N3 (cN3) before NAC was an independent risk factor of recurrence in patients who achieved pCR (p = 0.003) and near-pCR (p = 0.036). Tumor size before NAC, subtypes of breast cancer, and chemotherapy regimens showed no significant association with RFS both for patients who achieved pCR and for those who achieved near-pCR (p > 0.05).

Conclusions: cN3 before NAC was an independent risk factor of recurrence in patients who achieved pCR and near-pCR. It is worthwhile to closely monitor patients with cN3, especially in the first 3 years.

KEYWORDS

breast cancer, pathological complete response, near-pathological complete response, survival, predictive factors

Introduction

Neoadjuvant chemotherapy (NAC) was widely used in patients with human epidermal growth receptor 2 (HER2)-positive breast cancer and triple-negative breast cancer (TNBC) (1–3). HER2-positive breast cancer and TNBC are relatively sensitive to NAC, and pathological reaction to NAC can provide prognostic information and guide the selection of postoperative treatment (4–9). Due to the rapid development of antineoplastic drugs in recent decades, the rate of pathological complete response (pCR) after NAC has significantly increased (10). Studies have demonstrated that patients achieving pCR had significantly better disease-free survival (DFS) and overall survival (OS) than patients with residual disease (11, 12). The assessment of obtaining a real pCR is of great importance and has been gradually standardized nowadays. The generally accepted definition of pCR is that there is no residual invasive carcinoma in the breast and in all sampled lymph nodes (ypT0/isN0) (13–15). More recently, the concept of near-pCR was gradually being proposed and has attracted more and more attention. Substantial research elucidated that patients who achieved near-pCR also had outstanding DFS and OS (13, 14). A variety of definitions of near-pCR have been used in neoadjuvant clinical trials in breast cancer. The most common consensus was that the residual disease ≤1 cm (9, 16).

In spite of the outstanding outcomes of patients achieving pCR and near-pCR, some of them may still experience recurrence. In order to identify clinical and pathological predictive factors of cancer recurrence, we performed this retrospective analysis among breast cancer patients who achieved pCR and near-pCR in the Cancer Hospital, Chinese Academy of Medical Sciences (CHCAMS). In this study, we aimed to explore the predictive factors associated with recurrence for the patients achieving pCR and near-pCR, and investigate whether the risk for recurrence and death of patients achieving near-pCR was comparable with those achieving pCR.

Methods

Study population

We reviewed 1,209 breast cancer patients that were treated with NAC between January 2010 and April 2021 in CHCAMS. The inclusion criteria in this study were as follows: (1) patients who were pathologically diagnosed with invasive breast cancer based on WHO criteria; (2) patients who have early-stage or locally advanced breast cancer (4, 13); (3) patients receiving surgery after NAC; (4) patients with complete clinical information; and (5) patients with follow-up data. Exclusion criteria were as follows: (1) patients with distant metastasis before or during NAC; (2) patients without detailed pathology after surgery; and (3) patients who withdraw active follow-up data. A final cohort of 292 patients who achieved pCR and near-pCR was incorporated in this study. Clinical and pathological data of these patients were collected: age, menstruation, tumor size, regional lymph node, estrogen receptor (ER), progesterone receptor (PR), HER2, Ki67 index, chemotherapy, radiation, endocrine, and surgery regimens.

Pathological assessment

pCR was defined as no residual invasive carcinoma in the breast and negative axillary lymph nodes, including ypT0N0 and

ypTisN0 (13–15). Near-pCR was defined as the residual tumor size ≤1 cm in the breast and negative axillary lymph nodes, or no residual invasive carcinoma in the breast yet existing micrometastasis in lymph node, including ypT1mi/a/bN0 and ypT0/isN1mi (9, 16). Pathologically, T and N were defined according to the AJCC Staging System of Breast Cancer, 8th edition (17).

The Miller–Payne grade system was used to evaluate breast cancer pathological responses to NAC (18). Grade 1: no significant reduction in tumor cells; Grade 2: a minor reduction in tumor cells (≤30%); Grade 3: reduction in tumor cells between 30% and 90%; Grade 4: disappearance of tumor cells > 90%; Grade 5: no invasive tumor cells identifiable, and DCIS may be present.

ER and PR status was assessed by immunohistochemistry (IHC) and categorized as positive when more than 1% of cancer cells were stained (19). HER2 positive was defined as 3+ by IHC or positive by fluorescence *in situ* hybridization (FISH) (20). Ki67 index was defined as the mean tumor cells with marker expression by IHC: low (<20%), intermediate (20%–49%), and high (≥50%) (21–23).

The molecular subtype classification was on the basis of IHC of ER, PR, HER2, and Ki67 (24). Luminal A: ER and PR positive (PR ≥ 20%), HER2 negative, and Ki67 low expression; Luminal B HER2-negative: ER and/or PR positive, HER2 negative; Luminal B HER2-positive: ER and/or PR positive, HER2 positive; HER2-positive (non-luminal): ER and PR negative, HER2 positive; Triple-negative: ER and PR negative, HER2 negative.

Recurrence-free survival (RFS) was calculated as the time from the onset of NAC to local or distant recurrence, or death due to any cause, whichever came first. OS was calculated as the time from the onset of NAC to death due to any cause.

Statistical analysis

All statistical analyses were conducted using SPSS 25.0 and R (version 3.5.1). The Kaplan–Meier method with the log-rank test was used for recurrence and survival analysis. The factors significant at the 20% level in the univariate analysis were considered for inclusion in the multivariate model. The Cox proportional hazards regression model was used to assess the association of clinical and pathological predictive factors with RFS. C-statistics was conducted to evaluate the predictive value of the factors. All tests were two tailed and a p-value less than 0.05 was considered to indicate a statistically significant difference.

Results

Patient characteristics

A total of 292 patients with pCR and near-pCR were included in this study. Their clinical and pathological characteristics are described in Table 1. The median age of patients was 46 years (range, 23–75 years); 62.3% were premenopausal. The median duration of follow-up for these patients was 53 months (range, 9–138 months). There were 173 patients achieving pCR and 119 achieving near-pCR. The predominant tumor subtypes were HER2 positive (49.0%) (including luminal B HER2+ and non-luminal HER2+) and TNBC (30.8%). Among the patients with HER2 positive, 63.6% received trastuzumab, while 24.4% received trastuzumab and pertuzumab. The majority of the tumors were T2+ (91.4%) and N+ (76.0%). Overall, 77.0% of the patients underwent mastectomy and 83.2% of the patients had axillary lymph node dissection.

Disease recurrence

As shown in Table 2, a total of 25 (8.6%) patients developed recurrence. Twenty-one (84.0%) recurrences occurred within 36 months. Among patients achieving pCR, 9 (5.2%) patients developed cancer recurrence, with 2 patients presenting with both local recurrence and distant metastasis, while 7 patients presented with distant metastasis. The median time to recurrence was 14 months (range, 8–62 months) from the onset of NAC. Four (44.4%) patients presented liver metastasis and 2 (22.2%) patients presented brain metastasis as the first event.

With regard to patients achieving near-pCR, 16 (13.4%) patients developed cancer recurrence, with 4 patients presenting with local recurrence only, 4 patients with both local recurrence and distant metastasis, while 8 patients presenting with distant metastasis only. The median time to recurrence was 18 months (range, 4–69 months). Three (18.8%) patients experienced lung metastasis and 6 (37.5%) patients presented bone metastasis as the first event.

RFS and OS

The 3-year RFS rates of patients achieving pCR and near-pCR were 95.6% and 85.6%, respectively. The 5-year RFS rates of patients achieving pCR and near-pCR were 94.6% and 85.6%, respectively. The risk of cancer recurrence was significantly higher in patients achieving near-pCR than that in patients achieving pCR (HR = 3.01, 95% CI: 1.34–7.01, p = 0.008, Figure 1A). A total of 15 (5.1%) patients died. The 3-year OS rates of the pCR group and the near-pCR group were 96.6% and 96.3%, respectively. The 5-year OS rates of the pCR and near-pCR groups were 94.3% and 89.6%, respectively. There was no statistical difference in OS between the two cohorts (HR = 1.69, 95% CI: 0.61–4.67, p = 0.304, Figure 1B).

Predictive factors of RFS in patients achieving pCR

Table 3 shows the results of the analyses for factors associated with RFS of patients achieving pCR. Clinical lymph node status

10.3389/fonc.2022.1019925

TABLE 1 Patient characteristics.

Characteristics	Total (n = 292)		pCR (n = 173)		Near-pCR (n = 119)	
	No.	%	No.	%	No.	%
Median age (range)	46 (23–75)		48 (23–73)		42 (24–75)	
Age						
<40	94	32.2	43	24.9	51	42.9
40–59	168	57.5	110	63.6	58	48.7
≥60	30	10.3	20	11.6	10	8.4
Menopausal status						
Premenopausal	182	62.3	101	58.4	81	68.1
Postmenopausal	110	37.7	72	41.6	38	31.9
cT						
T1	25	8.6	15	8.7	10	8.4
T2	168	57.5	108	62.4	60	50.4
T3	69	23.6	35	20.2	34	28.6
T4	30	10.3	15	8.7	15	12.6
cN						
N0	70	24.0	33	19.1	37	31.1
N1	69	23.6	35	20.2	34	28.6
N2	98	33.6	68	39.3	30	25.2
N3	55	18.8	37	21.4	18	15.1
cTNM						
I	4	1.4	1	0.6	3	2.5
IIA	49	16.8	23	13.3	26	21.8
IIB	51	17.5	29	16.8	22	18.5
IIIA	108	37.0	70	40.5	38	31.9
IIIB	25	8.6	13	7.5	12	10.1
IIIC	55	18.8	37	21.4	18	15.1
ER status						
Negative	203	69.5	128	74.0	75	63.0
Positive	89	30.5	45	26.0	44	37.0
PR status						
Negative	174	59.6	115	66.5	59	49.6
Positive	118	40.4	58	33.5	60	50.4
HER2 status						
Negative	149	51.0	86	49.7	63	52.9
Positive	143	49.0	87	50.3	56	47.1
Ki67						
<20	16	5.5	7	4.0	9	7.6
20-49	117	40.1	65	37.6	52	43.7
≥50	142	48.6	92	53.2	50	42.0
Unknown	17	5.8	9	5.2	8	6.7
Breast cancer subtype						
Luminal A	1	0.3	0	0.0	1	0.8
Luminal B HER2–	58	19.9	30	17.3	29	24.4
Luminal B HER2+	77	26.4	41	23.7	35	29.4
Non-luminal HER2+	66	22.6	45	26.0	21	17.6
Triple negative	90	30.8	57	32.9	33	27.7
Chemotherapy regimens of NAC						
Anthracycline and taxane	86	29.5	40	23.1	46	38.7

(Continued)

10.3389/fonc.2022.1019925

TABLE 1 Continued

Characteristics	Total (n = 292)		pCR (n = 173)		Near-pCR (n = 119)	
	No.	%	No.	%	No.	%
Taxane and platinum	175	59.9	117	67.6	58	48.7
Anthracycline and taxane and platinum	15	5.1	10	5.8	5	4.2
Anthracycline or taxane	13	4.5	6	3.5	7	5.9
Endocrine	3	1.0	0	0.0	3	2.5
Cycle number of NAC						
<4	10	3.4	2	1.2	8	6.7
4–6	248	84.9	153	88.4	95	79.8
>6	31	10.6	18	10.4	13	10.9
Other (Endocrine Therapy)	3	1.0	0	0.0	3	2.5
Surgery of breast cancer						
Breast-conserving surgery	67	23.0	41	23.7	26	21.8
Mastectomy	225	77.0	132	76.3	93	78.2
Surgery of lymph nodes						
Sentinel lymph node biopsies	49	16.8	28	16.2	21	17.6
Axillary lymph node dissection	243	83.2	145	83.8	98	82.4
Adjuvant radiation						
Yes	211	72.3	125	72.3	86	72.3
No	81	27.7	48	27.7	33	27.7
Adjuvant endocrine						
Yes	128	43.8	67	38.7	61	51.3
No	164	56.2	106	61.3	58	48.7
HER2 positive						
With trastuzumab	91	63.6	59	67.8	32	57.1
With trastuzumab and pertuzumab	35	24.4	23	26.4	12	21.4
With trastuzumab and TKI	1	0.7	0	0	1	1.8
Without HER2 targeted therapy	16	11.1	5	5.7	11	19.6

pCR, pathological complete response; Near-pCR, near-pathological complete response; cT, clinical tumor size; cN, clinical lymph node status; ER, estrogen receptor; PR, progesterone receptor; HER2, human epidermal growth factor receptor type 2; Ki67, Ki67 index; NAC, neoadjuvant chemotherapy; TKI, tyrosine kinase inhibitor.

(cN) before NAC was a significant covariate in the univariate analysis for RFS in patients achieving pCR ($p < 0.001$). The 5-year RFS rates for cN0–2 and cN3 patients who achieved pCR were 98.0% and 82.7%, respectively. cN3 was an independent factor of higher risk for recurrence on the multivariate analysis (Figure 2, HR = 9.8, 95% CI: 2.1–44.5, $p = 0.003$). The C-statistics was 0.77 (95% CI: 0.63–0.91) of cN3 for RFS prediction. Age at diagnosis, tumor size at diagnosis, subtypes of breast cancer, and other factors showed no significant association with RFS of patients who achieved pCR ($p > 0.05$).

Predictive factors of RFS in patients achieving near-pCR

Table 4 shows the results of the analyses for the factors associated with RFS of patients achieving near-pCR. cN before NAC was a significant covariate in the univariate analysis for RFS in patients achieving near-pCR (Figure 3, $p = 0.036$). The 5-year RFS rates for cN0–2 and cN3 patients who achieved near-pCR were 88.5% and 71.1%, respectively. The C-statistics was 0.63 (95% CI: 0.52–0.74) of cN3 for RFS prediction. There was no difference between ypT1miN0, ypT1aN0, and ypT1bN0 for RFS ($p = 0.942$). The Miller–Payne grade after NAC also showed no significant association with the RFS of patients who achieved near-pCR ($p > 0.05$). There were no other factors significant at the 20% level in the univariate analyses of RFS for patients achieving near-pCR; thus, we did not conduct multivariate analyses further.

Discussion

In this retrospective study of 292 patients achieving pCR and near-pCR after NAC, the recurrence pattern of patients was described, and the vast majority of recurrence occurred within

10.3389/fonc.2022.1019925

TABLE 2 Time and site of recurrence.

	pCR		Near-pCR	
	N	%	*N*	%
	9		16	
Median (range), months	14 (8–62)		18 (4–69)	
≤12 months	3	33.3	5	31.3
12–36 months	4	44.4	9	56.3
>36 months	2	22.2	2	12.5
Site of disease recurrence				
Local recurrence	2	22.2	8	50.0
Breast or chest wall	1	11.1	3	18.8
Regional lymph nodes	1	11.1	5	31.3
Distant metastasis	9	100	12	75.0
Liver	4	44.4	1	6.3
Lung	1	11.1	3	18.8
Brain	2	22.2	2	12.5
Bone	0	0	6	37.5
Other sites	2	22.2	2	12.5

pCR, pathological complete response; Near-pCR, near-pathological complete response.

36 months from onset of NAC. This study found that the risk for recurrence of patients achieving near-pCR after NAC was higher than those achieving pCR. Moreover, cN3 before NAC was identified as a robust predictive factor of RFS for patients achieving pCR and near-pCR.

The 5-year RFS rate of pCR was 94.6% in our study, which was consistent with previous studies (25–27). The sub-study of EORTC 10994/BIG 1-00 phase III trial including 283 patients found that clinical tumor size was the only predictor for distant recurrence-free interval (DRFI) after pCR (27). In the research from the Anderson group, the authors identified that clinical stage IIIB–C and inflammatory breast cancer, premenopausal status, and resection of fewer than 10 lymph nodes were associated with an increased risk of developing distant metastasis for patients achieving pCR (28). Since cN contributes to the clinical stage, our study was partly consistent with the Anderson research. The predictive value of cN3

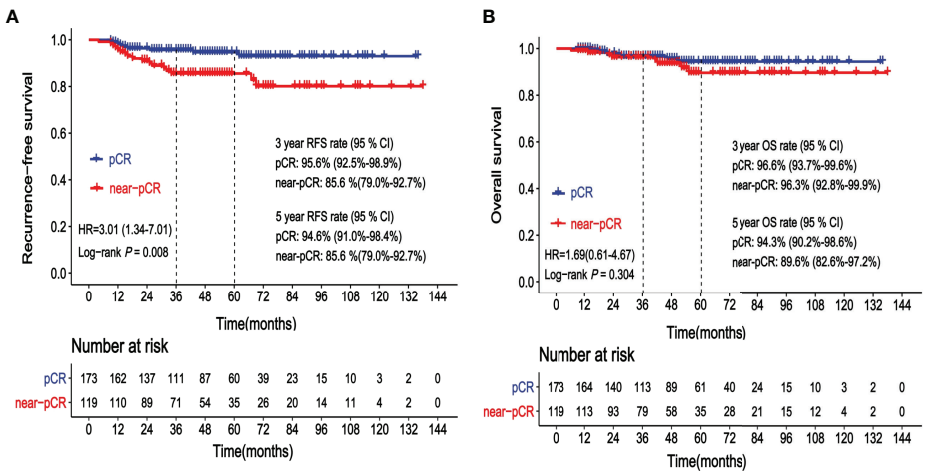

FIGURE 1
(A) Kaplan–Meier curve showing recurrence-free survival (RFS) according to the status after neoadjuvant chemotherapy (NAC): pathological complete response (pCR) vs. near-pathological complete response (near-pCR). **(B)** Kaplan–Meier curve showing overall survival (OS) according to the status after neoadjuvant chemotherapy (NAC): pathological complete response (pCR) vs. near-pathological complete response (near-pCR).

10.3389/fonc.2022.1019925

TABLE 3 Analysis of predictive factors for RFS in patients who achieved pCR.

	Univariate analysis				Multivariate analysis		
	N	Events	5-year RFS rate (%) (95% CI)	*P*-value	HR (95% CI)	*P*-value	C-statistics (95% CI)
Total	173	9					
Age				0.416			
<40	44	3	92.0 (83.7–100)				
≥40	129	6	95.5 (88.2–99.1)				
Menopausal status				0.919			
Premenopausal	101	5	95.8 (91.9–99.9)				
Postmenopausal	72	4	93.3 (87.0–100)				
cT				0.730			
T1–2	123	5	96.3 (92.8–99.9)				
T3–4	50	4	91.1 (83.0–100)				
cN				0.000			
N0–2	136	3	98.0 (95.1–100)		Reference		
N3	37	6	82.7 (70.9–96.3)		9.8 (2.1–44.5)	**0.003**	**0.77 (0.63–0.91)**
ER status				0.154			
Negative	128	5	96.2 (92.5–100)		Reference		
Positive	45	4	89.7 (80.5–99.9)		0.9 (0.2–4.2)	0.939	
PR status				0.151			
Negative	115	4	96.6 (92.8–100)		Reference		
Positive	58	5	90.7 (83.2–98.8)		2.2 (0.5–9.1)	0.296	
HER2 status				0.737			
Negative	86	4	95.0 (90.3–99.9)				
Positive	87	5	94.2 (88.6–100)				
Ki67				0.623			
<50	72	5	93.0 (86.5–100)				
≥50	92	4	95.5 (91.2–99.9)				
unknown	9	0	—				
Breast cancer subtype				0.750			
Luminal*	29	2	92.1 (82.3–100)				
HER2 positive**	87	5	94.2 (88.6–100)				
Triple negative	57	2	96.4 (91.6–100)				
Chemotherapy regimens of NAC				0.063			
Anthracycline and taxane	40	5	87.4 (77.7–98.4)		Reference		
Taxane and platinum	117	3	98.2 (95.9–100)		0.3 (0.1–1.4)	0.116	
Others	16	1	85.7 (63.3–100)		2.1 (0.2–22.7)	0.534	
Cycle number of NAC				0.591			
<4	2	0	—				
4–6	153	9	94.0 (90.0–98.2)				
>6	18	0	—				
Surgery of breast cancer				0.359			
Breast-conserving surgery	41	3	94.5 (87.4–100)				
Mastectomy	132	6	94.8 (90.7–99.0)				
Surgery of lymph nodes				0.873			
Sentinel lymph node biopsies	28	1	100				
Axillary lymph node dissection	145	8	93.8 (89.6–98.1)				
Adjuvant radiation				0.695			
Yes	125	7	94.2 (89.8–98.9)				
No	48	2	95.5 (89.5–100)				

(Continued)

TABLE 3 Continued

			Univariate analysis		Multivariate analysis		
	N	Events	5-year RFS rate (%) (95% CI)	*P*-value	HR (95% CI)	*P*-value	C-statistics (95% CI)
Adjuvant endocrine				0.234			
Yes	67	5	91.5 (84.6–99.0)				
No	106	4	96.5 (92.5–100)				

RFS, recurrence-free survival; pCR, pathological complete response; cT, clinical tumor size; cN, clinical lymph node status; ER, estrogen receptor; PR, progesterone receptor; HER2, human epidermal growth factor receptor type 2; Ki67, Ki67 index; NAC, neoadjuvant chemotherapy.
*Luminal included luminal A and luminal B HER2-.
**HER2 positive included luminal B HER2+ and non-luminal HER2+.
The bold value means having statistical difference.

was also confirmed by C-statistics (0.77, 95% CI: 0.63–0.91) and Cox proportional hazards regression (cN3 vs. cN0–2, HR = 9.8, 95% CI: 2.1–44.5, $p = 0.003$). Asaoka and colleagues' research also found that lymph node metastasis before NAC was the only predictor of cancer recurrence on multivariate analyses for patients achieving pCR (29).

The 5-year RFS rate of near-pCR was 85.6%, which was 9% lower than that of patients achieving pCR, but the OS of the two cohorts had no significant difference. The Spring et al. meta-analysis (30), which included 27,895 patients from 52 publications, showed that patients with residual disease after NAC had a 5-year DFS rate of 67%, which was much lower compared with the near-pCR population (85.6%) in our study. This illustrated the fact that it was necessary to distinguish the near-pCR population from the residual disease. There has been controversy regarding the definition of near-pCR in the past few years (31). In Cheng's study, near-pCR was defined as residual tumor volume <1 cm^3 (16). While residual tumor size ≤ 1 cm was excluded in KATHERINE, a clinical trial focused on intensive postoperative treatment (9). However, Lee and colleagues defined near-pCR as tumor size ≤ 0.5 cm (32). In our study, near-pCR was defined as the residual tumor size ≤1 cm in the breast (ypT1mi/1a/1bN0), or no residual invasive carcinoma in the breast yet existing micrometastasis in lymph node (ypT0/isN1mi).

To our best knowledge, this study is the first one to report the potential predictive factors of RFS for patients achieving near-pCR. We found that cN3 was an independent factor of higher risk for recurrence in the near-pCR subgroup, which was consistent with the pCR subgroup. The 5-year RFS rates for cN0–2 and cN3 patients who achieved near-pCR were 88.5% and 71.1%, respectively ($p = 0.036$). According to AJCC 8th edition staging system of breast cancer, cN3 is defined as metastasis to ipsilateral infraclavicular/supraclavicular lymph node(s), or metastasis to ipsilateral internal mammary lymph node(s) and axillary lymph node(s). There is controversy regarding the treatment of the local

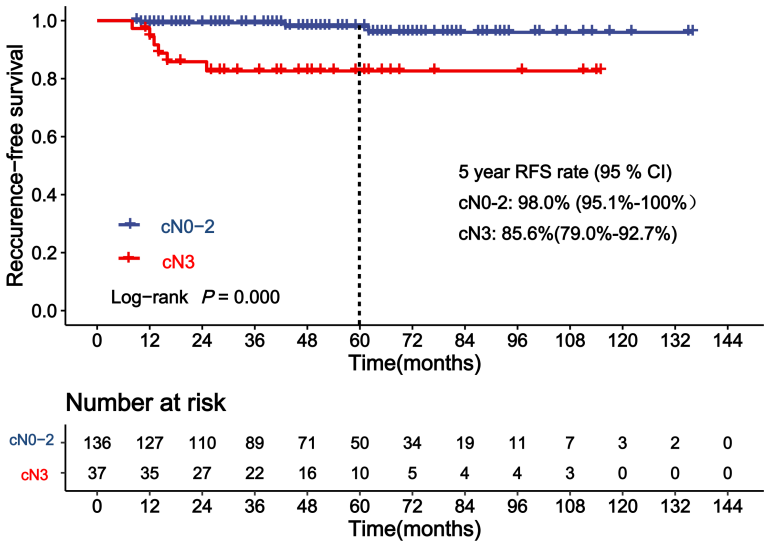

FIGURE 2
Kaplan–Meier curve showing recurrence-free survival (RFS) of patients achieving pathological complete response (pCR) according to clinical lymph node status (cN).

TABLE 4 Analyses of predictive factors for RFS in patients who achieved near-pCR.

	Univariate analyses				
	N	Events	5-year RFS rate (%) (95% CI)	*P*-value	C-statistics (95% CI)
Total	119	17			
Age				0.251	
<40	51	9	81.5 (70.6–94.1)		
≥40	68	8	88.5 (80.8–97.0)		
Menopausal status				0.467	
Premenopausal	81	13	84.7 (76.7–93.5)		
Postmenopausal	38	4	87.6 (76.7–100)		
cT				0.506	
T1–2	70	12	83.6 (74.6–93.6)		
T3–4	49	5	88.5 (79.4–98.6)		
cN				**0.036**	**0.63 (0.52–0.74)**
N0–2	101	12	88.5 (82.0–95.5)		
N3	18	5	71.1 (52.6–96.1)		
ER status				0.720	
Negative	75	10	86.5 (78.6–95.2)		
Positive	44	7	83.8 (72.7–96.7)		
PR status				0.411	
Negative	59	10	83.4 (74.1–94.0)		
Positive	60	7	87.2 (78.2–97.4)		
HER2 status				0.300	
Negative	56	6	90.8 (82.5–99.9)		
Positive	63	11	80.9 (71.3–91.8)		
Ki67				0.740	
<50	61	10	83.1 (73.5–93.9)		
≥50	50	6	85.9 (76.0–97.2)		
Unknown	8	1	—		
Breast cancer subtype				0.583	
Luminal*	30	5	80.3 (66.2–97.5)		
HER2 positive**	56	6	90.8 (82.5–99.9)		
Triple negative	33	6	81.4 (68.9–96.0)		
Treatment of NAC				0.476	
Anthracycline and taxane	46	5	90.5 (82.0–99.8)		
Taxane and platinum	58	10	83.0 (73.4–93.9)		
Others	15	2	77.1 (53.5–100)		
Cycle number of NAC				0.944	
<4	8	1	75.0 (42.6–100)		
4–6	95	14	86.0 (79.0–93.8)		
>6	13	2	81.5 (61.1–100)		
Surgery of breast cancer				0.610	
Breast-conserving surgery	26	3	87.8 (75.8–100)		
Mastectomy	93	14	84.6 (76.8–93.1)		
Surgery of lymph nodes				0.432	
Sentinel lymph node biopsies	21	4	76.3 (58.0–100)		
Axillary lymph node dissection	98	13	87.3 (80.5–94.7)		
ypTNM after NAC				0.942	
ypT1miN0M0	5	1	80.0 (51.6–100)		
ypT1aN0M0	73	11	86.1 (78.0–95.0)		

(Continued)

10.3389/fonc.2022.1019925

TABLE 4 Continued

	Univariate analyses				
	N	Events	5-year RFS rate (%) (95% CI)	*P*-value	C-statistics (95% CI)
ypT1bN0M0	39	5	85.0 (73.5–98.2)		
ypT0N1miM0	2	0	—		
Miller–Payne grade				0.334	
1–3	42	4	89.2 (79.8–99.8)		
4–5[#]	77	13	83.8 (75.5–93.1)		
Adjuvant radiation				0.545	
Yes	86	12	86.1 (78.7–94.1)		
No	33	5	83.8 (70.4–99.8)		
Adjuvant endocrine				0.925	
Yes	61	9	84.1 (74.5–95.9)		
No	58	8	86.9 (78.2–96.5)		

RFS, recurrence-free survival; near-pCR, near-pathological complete response; cT, clinical tumor size; cN, clinical lymph node status; ER, estrogen receptor; PR, progesterone receptor; HER2, human epidermal growth factor receptor type 2; Ki67, Ki67 index; NAC, neoadjuvant chemotherapy.
*Luminal included luminal A and luminal B HER2-.
**HER2 positive included luminal B HER2+ and non-luminal HER2+.
[#]Two patients with Miller–Payne grade 5 were ypT0N1miM0.
The bold value means having statistical difference.

supraclavicular and internal mammary lymph node(s). It is difficult to remove the supraclavicular lymph node(s) and internal mammary lymph node(s) during the surgery. Radiation therapy is usually applied to deal with the supraclavicular and internal mammary lymph node(s) involvement. However, it is difficult to evaluate whether the status of no evidence of disease (NED) is reached. In recent years, growing interest was focused on post-NAC treatment, and some trials noted that reinforcing the adjuvant treatment could improve prognosis for patients with residual disease. In the subset of CREATE-X, TNBC patients with residual invasive disease who received capecitabine had a 5-year DFS rate of 69.8%, 13.7% higher than the control group (HR = 0.58, 95% CI: 0.39–0.87) (8). In the KATHERINE clinical trial, the invasive DFS at 3 years of HER2-positive breast cancer patients with residual invasive disease who received T-DM1 was 88.3%, higher than patients receiving trastuzumab (HR = 0.5, $p < 0.001$) (9). However, numerous post-NAC clinical trials incorporated patients with a residual disease of at least 1.0 cm or node positive

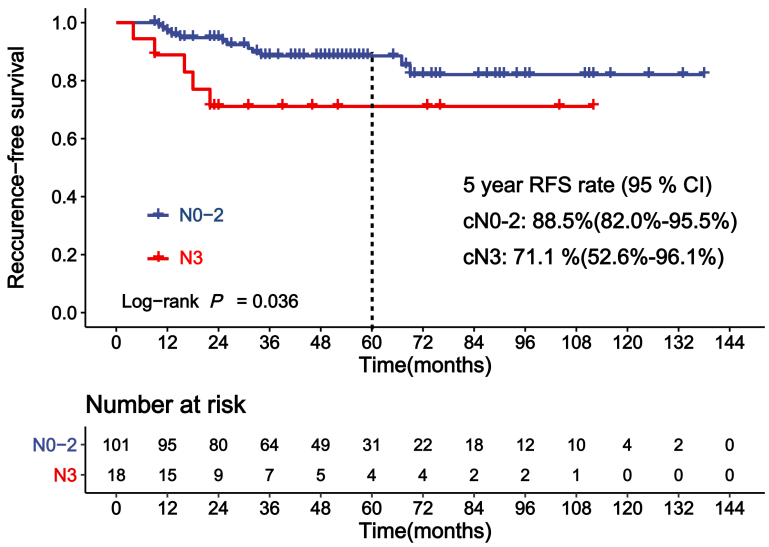

FIGURE 3
Kaplan–Meier curve showing recurrence-free survival (RFS) of patients achieving near-pCR according to clinical lymph node status (cN).

disease, excluding patients who achieved near-pCR. Our study showed that patients with near-pCR still had a certain risk of recurrence. Adjuvant therapy to minimize the risk of recurrence for patients with near-pCR is needed to be illuminated in further prospective research.

Our study also has several limitations. First, it was a retrospective study; therefore, selection bias was inevitable. Second, because the number of death events was small, we did not conduct analysis on the predictive factors of OS in patients achieving pCR and near-pCR.

Conclusions

Patients achieving pCR had excellent outcomes. The recurrence risk of patients achieving near-pCR after NAC was higher than that of patients achieving pCR. The vast majority of recurrence occurred within 3 years from onset of NAC. Patients with cN3 before NAC had a higher risk of developing local and distant metastasis, even achieving pCR or near-pCR after NAC. It is worthwhile to closely monitor patients with cN3, especially in the first 3 years.

Data availability statement

The raw data supporting the conclusions of this article will be made available by the authors, without undue reservation.

Ethics statement

The studies involving human participants were reviewed and approved by the National Cancer Center/National Clinical Research Center for Cancer/Cancer Hospital, Chinese Academy of Medical Sciences and Peking Union Medical College. Written informed consent for participation was not required for this study in accordance with the national legislation and the institutional requirements.

Author contributions

PZ contributed to the study concept, design, and patient management, and revised the manuscript. XQ contributed to data collection and data analysis, and drafted the manuscript. MX revised the manuscript. QinL, JW, YF, YL, RC, QiaL, SC, PY, FM, BX participated in patient management. All authors approved the final version of the manuscript.

Funding

This project was funded by Cancer Prevention and Research Fund of China Medical Foundation and the fund supported the follow-up and publication costs.

Acknowledgments

The authors wish to thank all the study participants and research staff who participated in this work.

Conflict of interest

The authors declare that the research was conducted in the absence of any commercial or financial relationships that could be construed as a potential conflict of interest.

Publisher's note

All claims expressed in this article are solely those of the authors and do not necessarily represent those of their affiliated organizations, or those of the publisher, the editors and the reviewers. Any product that may be evaluated in this article, or claim that may be made by its manufacturer, is not guaranteed or endorsed by the publisher.

References

1. Loibl S, Poortmans P, Morrow M, Denkert C, Curigliano G. Breast cancer. *Lancet* (2021) 397(10286):1750–69. doi: 10.1016/S0140-6736(20)32381-3

2. Loibl S, Gianni L. HER2-positive breast cancer. *Lancet* (2017) 389 (10087):2415–29. doi: 10.1016/S0140-6736(16)32417-5

3. Harbeck N, Gluz O. Neoadjuvant therapy for triple negative and HER2-positive early breast cancer. *Breast* (2017) 34 Suppl 1:S99–S103. doi: 10.1016/j.breast.2017.06.038

4. Korde LA, Somerfield MR, Carey LA, Crews JR, Denduluri N, Hwang ES, et al. Neoadjuvant chemotherapy, endocrine therapy, and targeted therapy for breast cancer: ASCO guideline. *J Clin Oncol* (2021) 39(13):1485–505. doi: 10.1200/JCO.20.03399

5. Zardavas D, Piccart M. Neoadjuvant therapy for breast cancer. *Annu Rev Med* (2015) 66:31–48. doi: 10.1146/annurev-med-051413-024741

6. Killelea BK, Yang VQ, Mougalian S, Horowitz NR, Pusztai L, Chagpar AB, et al. Neoadjuvant chemotherapy for breast cancer increases the rate of breast conservation: results from the national cancer database. *J Am Coll Surg* (2015) 220 (6):1063–9. doi: 10.1016/j.jamcollsurg.2015.02.011

7. Volders JH, Negenborn VL, Spronk PE, Krekel NMA, Schoonmade LJ, Meijer S, et al. Breast-conserving surgery following neoadjuvant therapy-a systematic review on surgical outcomes. *Breast Cancer Res Treat* (2018) 168(1):1–12. doi: 10.1007/s10549-017-4632-7

8. Masuda N, Lee SJ, Ohtani S, Im YH, Lee ES, Yokota I, et al. Adjuvant capecitabine for breast cancer after preoperative chemotherapy. *N Engl J Med* (2017) 376(22):2147–59. doi: 10.1056/NEJMoa1612645

9. von Minckwitz G, Huang CS, Mano MS, Loibl S, Mamounas EP, Untch M, et al. Trastuzumab emtansine for residual invasive HER2-positive breast cancer. *N Engl J Med* (2019) 380(7):617–28. doi: 10.1056/NEJMoa1814017

10. Funt SA, Chapman PB. The role of neoadjuvant trials in drug development for solid tumors. *Clin Cancer Res* (2016) 22(10):2323–8. doi: 10.1158/1078-0432.CCR-15-1961

11. Cortazar P, Zhang L, Untch M, Mehta K, Costantino JP, Wolmark N, et al. Pathological complete response and long-term clinical benefit in breast cancer: the CTNeoBC pooled analysis. *Lancet* (2014) 384(9938):164–72. doi: 10.1016/S0140-6736(13)62422-8

12. Berruti A, Amoroso V, Gallo F, Bertaglia V, Simoncini E, Pedersini R, et al. Pathologic complete response as a potential surrogate for the clinical outcome in patients with breast cancer after neoadjuvant therapy: a meta-regression of 29 randomized prospective studies. *J Clin Oncol* (2014) 32(34):3883–91. doi: 10.1200/JCO.2014.55.2836

13. Guerini-Rocco E, Botti G, Foschini MP, Marchio C, Mastropasqua MG, Perrone G, et al. Role and evaluation of pathologic response in early breast cancer specimens after neoadjuvant therapy: consensus statement. *Tumori* (2022) 108:196–203. doi: 10.1177/03008916211062642

14. Bossuyt V, Provenzano E, Symmans WF, Boughey JC, Coles C, Curigliano G, et al. And c. breast international group-north American breast cancer group, recommendations for standardized pathological characterization of residual disease for neoadjuvant clinical trials of breast cancer by the BIG-NABCG collaboration. *Ann Oncol* (2015) 26:1280–91. doi: 10.1093/annonc/mdv161

15. Bossuyt V, Symmans WF. Standardizing of pathology in patients receiving neoadjuvant chemotherapy. *Ann Surg Oncol* (2016) 23:3153–61. doi: 10.1245/s10434-016-5317-x

16. Cheng Q, Huang J, Liang J, Ma M, Ye K, Shi C, et al. The diagnostic performance of DCE-MRI in evaluating the pathological response to neoadjuvant chemotherapy in breast cancer: A meta-analysis. *Front Oncol* (2020) 10:93. doi: 10.3389/fonc.2020.00093

17. Amin MB, Edge SB, Greene FL, Byrd DR, Brookland RK, Washington MK, et al. *AJCC cancer staging manual[M]. 8th ed*. New York: Springer (2017). Available at: https://link.springer.com/book/10.1007/978-1-4757-3656-4

18. Ogston KN, Miller ID, Payne S, Hutcheon AW, Sarkar TK, Smith I, et al. A new histological grading system to assess response of breast cancers to primary chemotherapy: prognostic significance and survival. *Breast* (2003) 12:320–7. doi: 10.1016/s0960-9776(03)00106-1

19. Hammond ME, Hayes DF, Dowsett M, Allred DC, Hagerty KL, Badve S, et al. American Society of clinical Oncology/College of American pathologists guideline recommendations for immunohistochemical testing of estrogen and progesterone receptors in breast cancer. *J Clin Oncol* (2010) 28:2784–95. doi: 10.1200/JCO.2009.25.6529

20. Wolff AC, Hammond MEH, Allison KH, Harvey BE, Mangu PB, Bartlett JMS, et al. Human epidermal growth factor receptor 2 testing in breast cancer: American society of clinical Oncology/College of American pathologists clinical practice guideline focused update. *J Clin Oncol* (2018) 36:2105–22. doi: 10.1200/JCO.2018.77.8738

21. Li XR, Liu M, Zhang YJ, Wang JD, Zheng YQ, Li J, et al. Evaluation of ER, PgR, HER-2, ki-67, cyclin D1, and nm23-H1 as predictors of pathological complete response to neoadjuvant chemotherapy for locally advanced breast cancer. *Med Oncol (Northwood London England)* (2011) 28 Suppl 1:S31–8. doi: 10.1007/s12032-010-9676-z

22. Alba E, Lluch A, Ribelles N, Anton-Torres A, Sanchez-Rovira P, Albanell J, et al. High proliferation predicts pathological complete response to neoadjuvant chemotherapy in early breast cancer. *oncologist* (2016) 21:778. doi: 10.1634/theoncologist.2015-0312erratum

23. Chen X, He C, Han D, Zhou M, Wang Q, Tian J, et al. The predictive value of ki-67 before neoadjuvant chemotherapy for breast cancer: a systematic review and meta-analysis. *Future Oncol* (2017) 13:843–57. doi: 10.2217/fon-2016-0420

24. Goldhirsch A, Wood WC, Coates AS, Gelber RD, Thurlimann B, Senn HJ. And m. panel, strategies for subtypes–dealing with the diversity of breast cancer: highlights of the st. gallen international expert consensus on the primary therapy of early breast cancer 2011. *Ann Oncol* (2011) 22:1736–47. doi: 10.1093/annonc/mdr304

25. Mittendorf EA, Vila J, Tucker SL, Chavez-MacGregor M, Smith BD, Symmans WF, et al. The neo-bioscore update for staging breast cancer treated with neoadjuvant chemotherapy: Incorporation of prognostic biologic factors into staging after treatment. *JAMA Oncol* (2016) 2(7):929–36. doi: 10.1001/jamaoncol.2015.6478

26. Symmans WF, Wei C, Gould R, Yu X, Zhang Y, Liu M, et al. Long-term prognostic risk after neoadjuvant chemotherapy associated with residual cancer burden and breast cancer subtype. *J Clin Oncol* (2017) 35(10):1049–60. doi: 10.1200/JCO.2015.63.1010

27. Fei F, Messina C, Slaets L, Chakiba C, Cameron D, Bogaerts J, et al. Tumor size is the only predictive factor of distant recurrence after pathological complete response to neoadjuvant chemotherapy in patients with large operable or locally advanced breast cancers: a sub-study of EORTC 10994/BIG 1-00 phase III trial. *Eur J Cancer* (2015) 51(3):301–9. doi: 10.1016/j.ejca.2014.11.023

28. Gonzalez-Angulo AM, McGuire SE, Buchholz TA, Tucker SL, Kuerer HM, Rouzier R, et al. Factors predictive of distant metastases in patients with breast cancer who have a pathologic complete response after neoadjuvant chemotherapy. *J Clin Oncol* (2005) 23(28):7098–104. doi: 10.1200/JCO.2005.11.124

29. Asaoka M, Narui K, Suganuma N, Chishima T, Yamada A, Sugae S, et al. Clinical and pathological predictors of recurrence in breast cancer patients achieving pathological complete response to neoadjuvant chemotherapy. *Eur J Surg Oncol* (2019) 45(12):2289–94. doi: 10.1016/j.ejso.2019.08.001

30. Spring LM, Fell G, Arfe A, Sharma C, Greenup R, Reynolds KL, et al. Pathologic complete response after neoadjuvant chemotherapy and impact on breast cancer recurrence and survival: A comprehensive meta-analysis. *Clin Cancer Res* (2020) 26(12):2838–48. doi: 10.1158/1078-0432.CCR-19-3492

31. Cortazar P, Geyer CEJr. Pathological complete response in neoadjuvant treatment of breast cancer. *Ann Surg Oncol* (2015) 22(5):1441–6. doi: 10.1245/s10434-015-4404-8

32. Lee HB, Han W, Kim SY, Cho N, Kim KE, Park JH, et al. Prediction of pathologic complete response using image-guided biopsy after neoadjuvant chemotherapy in breast cancer patients selected based on MRI findings: a prospective feasibility trial. *Breast Cancer Res Treat* (2020) 182(1):97–105. doi: 10.1007/s10549-020-05678-3

frontiers | Frontiers in Oncology

TYPE Original Research
PUBLISHED 21 October 2022
DOI 10.3389/fonc.2022.956167

Check for updates

OPEN ACCESS

EDITED BY
Annarita Fanizzi,
National Cancer Institute Foundation (IRCCS), Italy

REVIEWED BY
Diana Resendez-Perez,
Universidad Autónoma de Nuevo León, Mexico
Inese Cakstina-Dzerve,
Riga Stradins University, Latvia

*CORRESPONDENCE
Xiaodong Zheng
zxd0052005@163.com
Xiaohua Zeng
qq-zxh@126.com

†These authors have contributed equally to this work and share first authorship

SPECIALTY SECTION
This article was submitted to Breast Cancer, a section of the journal Frontiers in Oncology

RECEIVED 30 May 2022
ACCEPTED 05 October 2022
PUBLISHED 21 October 2022

CITATION
Gu Z, Yin H, Zhang H, Zhang H, Liu X, Zeng X and Zheng X (2022) Optimization of a method for the clinical detection of serum exosomal miR-940 as a potential biomarker of breast cancer.
Front. Oncol. 12:956167.
doi: 10.3389/fonc.2022.956167

COPYRIGHT
© 2022 Gu, Yin, Zhang, Zhang, Liu, Zeng and Zheng. This is an open-access article distributed under the terms of the Creative Commons Attribution License (CC BY). The use, distribution or reproduction in other forums is permitted, provided the original author (s) and the copyright owner(s) are credited and that the original publication in this journal is cited, in accordance with accepted academic practice. No use, distribution or reproduction is permitted which does not comply with these terms.

Optimization of a method for the clinical detection of serum exosomal miR-940 as a potential biomarker of breast cancer

Zhiyun Gu[1,2†], Haojie Yin[3†], Haiwei Zhang[1,2], Hui Zhang[1,2], Xiaoyu Liu[1,2], Xiaohua Zeng[1,2*] and Xiaodong Zheng[1,2,4*]

[1]Department of Oncology Laboratory, Chongqing University Cancer Hospital, Chongqing, China, [2]Chongqing Key Laboratory of Translational Research for Cancer Metastasis and Individualized Treatment, Chongqing University Cancer Hospital, Chongqing, China, [3]Bioengineering College, Chongqing University, Chongqing, China, [4]Medical College of Chongqing University, Chongqing University, Chongqing, China

Serum exosomal microRNAs (miRNAs) are potential biomarkers for tumor diagnosis. Clinically, reverse transcription-quantitative polymerase chain reaction (RT–qPCR) can be used to determine the expression of exosomal miRNAs in the serum of breast cancer patients. The prerequisites for obtaining meaningful serum exosomal miRNA data of breast cancer patients include a suitable extraction method for exosomes and RT–qPCR data standardized by internal reference genes. However, the appropriate methods for the extraction of exosomes and the applicability of reference genes for analyzing exosomal miRNAs in breast cancer patients remain to be studied. This study compared the effects of three exosome extraction methods as well as the expression of exosomal miRNA in different initial serum amounts and at different serum states to identify the selection of the best method for serum exosome extraction. Five candidate reference genes including miR-16, miR-484, miR-1228, miR-191 and miR-423 for standardizing serum exosomal miRNAs were screened using five algorithms and were used for the quantification of serum exosomal miR-940. Significant downregulation of serum exosomal miR-940 expression in breast cancer was detected using miR-191 and miR-1228, whereas no significant down or up regulation was observed with miR-484, miR-423 and miR-16. Previous studies have shown that the expression level of miR-940 is downregulated in breast cancer tissues. The absolute quantitative results showed that miR-940 was significantly downregulated in breast cancer serum exosomes, which was consistent with the results from the analysis using miR-191 or miR-1228 as reference genes. Therefore, miR-191 and miR-1228 could serve as reference genes for the relative quantification of serum exosomal miRNAs. This finding indicated the importance of rigorously evaluating the stability of reference genes and standardization for serum exosomal miRNA expression. Moreover, the level of serum exosomal

miR-940 in breast cancer could reflect the presence of lymph node metastasis and the status of HER2/neu, which indicates its potential as a biomarker for breast cancer metastasis. In summary, an optimized protocol for the detection of serum exosomal miR-940 as a breast cancer marker was preliminarily established.

KEYWORDS

exosomes, reference genes, miR-940, RT-qPCR, breast cancer

Introduction

MicroRNAs (miRNAs) are short noncoding RNA molecules that can participate in the regulation of posttranscriptional gene expression (1). Such regulation is essential for embryonic development, tumor initiation, immune modulation, and other biological processes. Exosomes are 40-100-nm disc-shaped vesicles. Various types of cells can release exosomes under normal and pathological conditions (2). Exosomes are involved in cell–cell communication and are released from donor cells into the microenvironment to affect target cells. This biological process exerts important biological functions (1). To date, exosomes have been found in various body fluids, such as human blood, urine, tears, breast milk, and semen (3).

An et al. verified that exosomes contain many proteins, cytokines, DNA, mRNAs, miRNAs, lncRNAs, and other nutritional elements (4). A previous study showed that exosomal miRNAs play an important role in communication between breast cancer cells (4, 5). A cohort study compared the serum levels of exosomal miRNAs between healthy women and breast cancer patients with different molecular subtypes and found that exosomal miRNAs can be regarded as blood-specific biomarkers for more aggressive tumors, such as triple-negative and hormone receptor-negative breast cancer (6). Another study noted that exosomes are potential biomarkers for ovarian cancer and breast cancer (7). Zhou et al. proved that the content level of miRNAs is significantly altered in serum exosomes from breast cancer patients, which indicates that exosomal miRNAs can be used as biomarkers for the identification of breast cancer (8). Additionally, Rodriguez et al. proved that the expression of exosomal miRNAs found at high levels in serum can be used as a biomarker of breast cancer (9).

Several different histological subtypes of breast cancer have been identified, and each subtype has different levels of invasiveness, clinical presentations, treatment programs, and prognoses (10). The diagnosis of breast cancer must be made as soon as possible such that treatment can be started in time. The difference in the expression level of exosomal miRNAs between healthy people and breast cancer patients can be used as a biomarker for the prediction of breast cancer.

Accurately measuring the level of miRNA in exosomes is the first step for its detection as a biomarker (11). RT–qPCR is a precise method for detecting and quantifying circulating miRNAs. To ensure that the measurements are comparable across different samples, the same volume of each body fluid is needed for RNA extraction. Despite using the same initial biofluid volume for each sample, the total RNA levels will not be consistent between samples due to different upstream procedures for RT–qPCR, such as sample preparation, exosome isolation, and miRNA extraction. Hemolysis may occur in clinically collected blood samples, and the effect on exosomal RNA is unknown (12). Therefore, standardized sample collection must be performed to address these problems. Notably, stable internal reference genes are essential for qPCR standardization and accurate miRNA quantification. Differences in expression results may not be caused by the disease itself but may instead be caused by differences in the processes used for sample acquisition, sample preservation, RNA extraction, and target gene quantification (13).

Therefore, appropriate methods for exosome extraction and optimal reference genes with stable expression must be determined to accurately normalize the quantitative data of exosomal miRNA (14). To date, in the RT–qPCR analysis of breast cancer exosomal miRNA, a consensus has not been reached regarding appropriate exosome extraction methods and appropriate internal reference genes.

MicroRNA-940 (miR-940) is a recently identified miRNA family member that is abnormally expressed in cardiovascular and neoplastic diseases. This miRNA has different expression levels in different diseases; in gastric cancer, the expression level of miR-940 is increased, whereas in cardiovascular disease, the expression level of miR-940 is decreased (15–17), which indicates its important regulatory role. Previous studies found that triple-negative breast cancer tissues express lower levels of miR-940 compared with normal tissues and that proliferation and migration in triple-negative breast cancer are affected by miR-940 (18). However, the clinicopathological relationship between serum exosomal miR-940 and breast cancer patients is unclear.

To select a suitable methods for serum exosome extraction that can be used in clinical practice, we extracted exosomes from the same sample using three extraction methods, analyzed the expression differences of serum exosomal miRNAs among different methods, analyzed the effect of differences in the initial serum volume on the RT–qPCR results, and finally analyzed the changes in hemolytic blood sample exosomal miRNAs in blood samples and normal blood samples.

Based on previous studies, various candidate reference genes were used to normalize the expression levels of exosomal miRNAs in breast cancer patients and healthy controls to screen the reference genes. A total of 5 candidate internal reference genes were selected based on previous reports of their suitability for RT–qPCR analyses of cancer using tissues or serum. Two of these genes were previously described as reference genes for exosome miRNA analysis: miR-16 and miR-484 (6). The remaining genes, miR-1228, miR-191, and miR-423, were obtained from other studies (19, 20). Five genes were initially screened as internal reference genes of serum exosomal miRNA, and the expression levels of the five candidate genes were then detected. The expression stability of these five genes was evaluated to determine suitable reference genes. The screened internal reference genes were used to evaluate the expression level of miR-940 and verified that the results of the screened internal reference genes were stable and reproducible.

Moreover, the applicable clinical exosomes extraction method identified from our comparison of breast cancer serum and normal serum was used to explore the differential expression of exosomal miR-940 using the selected stable reference genes. The serum exosomal miR-940 copy number and clinical data for breast cancer patients were analyzed by absolute quantification, and the results confirmed that serum exosomal miR-940 could serve as a metastatic marker for breast cancer.

This study provided the first identification of suitable reference genes for the clinical study of serum exosomal miRNA expression in breast cancer while screening pretreatment methods suitable for the clinical extraction of serum exosomes; moreover, this study demonstrated that serum exosomal miR-940 could serve as a potential metastatic marker for breast cancer.

Materials and methods

Patient and control sample collection

This study was approved by the Ethics Committee of the Chongqing University Cancer Hospital. Blood samples were donated by the Chongqing University Cancer Hospital. The blood sample set was composed of 118 breast cancer patients and 40 healthy controls. The all blood samples collected from patients were collected before treatment (including radiotherapy, chemotherapy, and surgery). The blood samples from patients without any treatment were drawn on an empty stomach, whereas those from healthy controls were also drawn early in the morning. A total of 5 mL of whole blood was drawn from each donor. Peripheral blood was collected into a tube containing heparin sodium and centrifuged at 3000×g for 10 min. The upper part of the serum was collected into a brand new centrifuge tube and centrifuged at 12000×g for 10 min to remove a cellular component. All centrifugation operations were performed at 4 °C. The separated serum was stored at -80 °C. To standardize the treatment of different serum samples, exosomal RNA was extracted from 1000 μL of serum, and the samples were preliminarily standardized according to a uniform volume. We randomly selected 59 of them to verify the stability of the candidate genes. The remaining 59 cases were used to investigated the relationship between serum exosomal miR-940 expression level and patient physiological indicators, so we looked up the clinicopathological reports of these patients. The clinicopathological were provided by the Department of Pathology and specific clinical data were presented in Schedules 1 and 2 (Supplementary Table 1, Supplementary Table 2).

Serum exosome isolation

Exosomes were extracted by ultracentrifugation, membrane affinity, and precipitation. Equal portions of the collected serum were removed from the -80 °C refrigerator, thawed on ice, and centrifuged at 12000×g and 4 °C for 10 min, and 1 mL of serum was then collected. Ultracentrifugation was performed using a 10-mL sample consisting of 1 mL of serum sample and 9 mL of PBS, and the sample was centrifuged by ultracentrifuge (Optima L-100XP, Beckman, USA) at 4°C and 100000×g for 70 min. The supernatant was carefully removed from the ultracentrifugation tube, and the remaining 2 mL of liquid containing exosomes was mixed with 8 mL of PBS. The supernatant was centrifuged again at 100000×g and 4°C for 70 min. Exosomes were resuspended in 200 μL of PBS and stored at -80 °C. Precipitation was performed with ExoQuick exosome precipitation solution (SBIS, System Biosciences, USA). The reagents were added to 1 mL of serum, and the mixture was shaken thoroughly. The flocculent precipitate appeared and was allowed to rest overnight at 4°C. The supernatant was then centrifuged at 12000×g for 10 min, and the precipitate contained exosomes. The exosomes were resuspended in 200 μL of PBS and stored in a -80°C refrigerator. The membrane affinity method was performed by collecting exosomes using an exoEasy Maxi Kit (QIAGEN GmbH, Hilden, Germany). Briefly, buffer XBP and serum were mixed in equal volumes, 2 mL of the mixture of each sample was then added to the exoEasy spin column and centrifuged at 4200×g for 1 min, and the waste after centrifugation was discarded. Ten milliliters of buffer XWP was added to the spin column and centrifuged at

5000×g for 5 min to remove the buffer XWP. Next, 200 μL of Buffer XE was added to the spin column and incubated for 1 min. The XE buffer was collected after centrifugation at 5000×g for 5 min. Exosomes were resuspended in XE buffer and stored at -80 °C.

Characteristic analysis of exosomes

The extracted exosomes were characterized using different methods. The characteristics of the exosomes were determined by transmission electron microscopy (TEM) (Tecnai G2 F30S-TWIN, FEI, USA). The exosomal particle size was measured using a nanoparticle tracking analysis (NTA) instrument (ZetaView, Particle Metrix, Meerbusch, Germany) according to the experimental requirements. The characteristic proteins of exosomes, such as CD9, CD63, and TSG101, were analyzed by Western blotting.

Monoclonal anti-CD63 (#98327) antibodies, anti-CD9 (#52090) antibodies, and anti-TSG101 antibodies (#72312) were obtained from Cell Signaling Technology (Denver, MA, USA).

Reference genes and primer design

The sequence of the target gene was obtained from the NCBI and miRBase databases, and the primers were designed according to the requirements of the SYBR Green method for RT–qPCR and were synthesized by Biotechnology (Biotechnology, Shanghai, China). The primer information of each gene designed is shown in Table 1.

RNA extraction and RT–qPCR

The exosomes extracted from each sample were lysed with 1 mL of QIAzol® (Qiagen GmbH, Hilden, Germany). The quality of the RNA was assessed by measuring the A260/A280 value of the extracted RNA using a NanoDrop™ One/OneC (Thermo Scientific, China). These cDNAs were obtained by reverse transcription of 1 ng of the extracted exosomal RNA using a miRcute Plus miRNA first-strand cDNA kit (TianGen, Beijing, China). The thermal cycling parameters for reverse transcription were 60 min at 42 °C and 3 min at 95 °C. The cDNA samples were diluted 10-fold in nuclease-free water and stored at −20 °C.

The expression levels of candidate internal reference genes in the serum exosomes were analyzed by RT–qPCR, which was performed with 384-well reaction plates using a LightCycler 480 II (Roche, Germany). The qPCR conditions are shown in Table 2. The data were analyzed using the software provided for the fluorescence quantitative PCR system. When the Ct value is greater than 35, the data have no meaning and are regarded as unexpressed, and this type of data is removed. Moreover, the arithmetic average of the Ct values of the three wells was used as the final Ct value of the miRNA PCR amplification.

Determination of the miR-940 copy number

The method used for copy number determination was described in the literature (21). Briefly, standard curves for miR-940 expression in serum exosomes were constructed by a serial dilution series of standard miR-940 ranging from 100 to 10^6 copies/μL. The plasmid copy number was calculated using the following equation:

$$\frac{6.02 \times 10^{23}(\text{copy/mol}) \times \text{DNA amount(g)}}{\text{DNA length(bp)} \times 660(\text{g/mol/bp})}$$

The corresponding logarithm template copy number was then plotted against the Ct values obtained by real-time qPCR. Statistical analyses were performed using Student's t test (two-tailed) to analyze the differences between groups. All values are expressed as the means ± S.E.Ms. A value of $P< 0.05$ was regarded as statistically significant.

Statistical analysis

First, the standard deviation (SD) and coefficient of variation (CoV) of each sample were calculated. In addition, four commonly used methods were applied to more comprehensively assess the stability of the candidate genes:

TABLE 1 Primer information of each gene.

Accession number	Gene	Primer
MIMAT0004983	hsa-miR-940	5'-ATAAGGCAGGGCCCCCGCT-3'
MIMAT0000069	hsa-miR-16-5p	5'-TAGCAGCACGTAAATATTGGCG-3'
MIMAT0002174	hsa-miR-484	5'-TCAGGCTCAGTCCCCTCCCGAT-3'
MIMAT0001340	hsa-miR-423-3p	5'-AGCTCGGTCTGAGGCCCCTCAGT-3'
MIMAT0000440	hsa-miR-191-5p	5'-CAACGGAATCCCAAAAGCAGCTG-3'
MIMAT0005583	hsa-miR-1228-3p	5'-TCACACCTGCCTCGCCCCCC-3'

TABLE 2 RT–qPCR procedure.

Cycle	Temperature	Time
1X	95°C	15 min
5X	94°C	20 sec
	63~65°C	30 sec
	72°C	34 sec
1X	94°C	20 sec
	60°C	34 sec

geNorm (22), NormFinder (23), BestKeeper (24), and the comparative ΔCt method (25). These four methods use online tools to evaluate reference gene expression (26). Moreover, statistical analyses were performed with the paired t test using SPSS Statistics 21 software, and a P value less than 0.05 indicated significant differences.

Results

Characterization of serum exosomes

The first step in the evaluation of exosomal miRNAs is the successful isolation of exosomes from serum. Ultracentrifugation, membrane affinity, and precipitation were used to isolate exosomes from serum, and a physical examination by transmission electron microscopy (TEM) showed a spherical structure of 30~150 nm and a typical doughnut-like shape (Figure 1A). The characteristics of the exosomes were consistent with those previously reported (27). Nanoparticle tracking assessment (NTA) analysis showed that the average particle size of exosomes ranged from 110 nm to 140 nm (Figure 1B). A Western blot analysis of the characteristic proteins of serum exosomes (3), i.e., CD63, CD9, and TSG101, was performed (Figure 1C).

The selection of the best method for serum exosome extraction

Twenty serum samples were randomly selected from our collected serum samples and divided into two groups to screen the best method for the clinical serum exosome extraction. We analyzed the effects of various exosome extraction methods and the starting amount of serum samples on the expression levels of three serum exosomal miRNAs, analyzed the expression levels of three serum exosomal miRNAs under hemolytic conditions, and established a pretreatment method suitable for the clinical detection of serum exosomal miRNAs.

The results from the literature and our experiments confirmed that all three extraction methods could extract exosomes. Therefore, through the detection of miRNA expression levels in exosomes using three different extraction methods, the influence of different extraction methods on the serum exosomal miRNA levels was analyzed. miR-16, miR-1228 and miR-940 were selected: the first two represent internal reference genes, and the last one represents the target gene of this study.

Among the three extraction methods, the exosomes extracted by ultrasonication had the lowest content of the three miRNAs tested. No significant differences in the contents of the three miRNAs were identified between exosomes extracted using the membrane affinity method and exosomes obtained using the precipitation method (Figure 2A). However, the coefficient of variation (CoV) of miRNA expression in exosomes extracted using precipitation was higher than the coefficient of variation (CoV) obtained for exosomes extracted

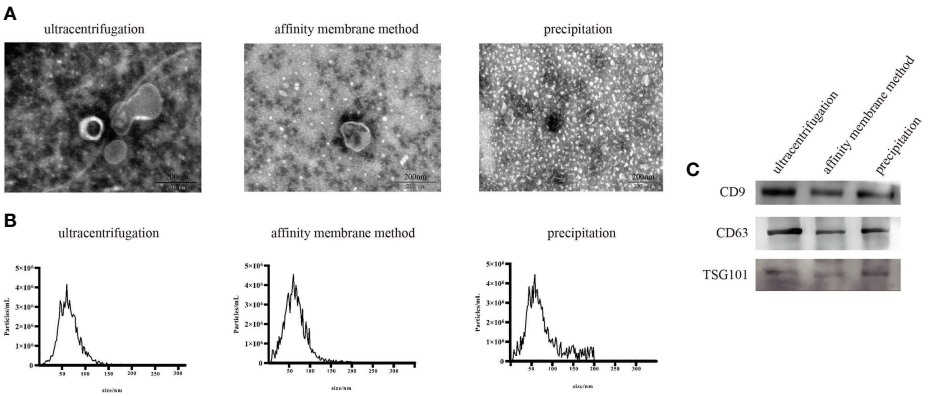

FIGURE 1
Characterization of exosomes extracted using three exosome extraction methods. **(A)** Physical examination of the isolated exosomes. **(B)** NTA of the isolated exosomes. **(C)** Western blot results of the isolated exosomes.

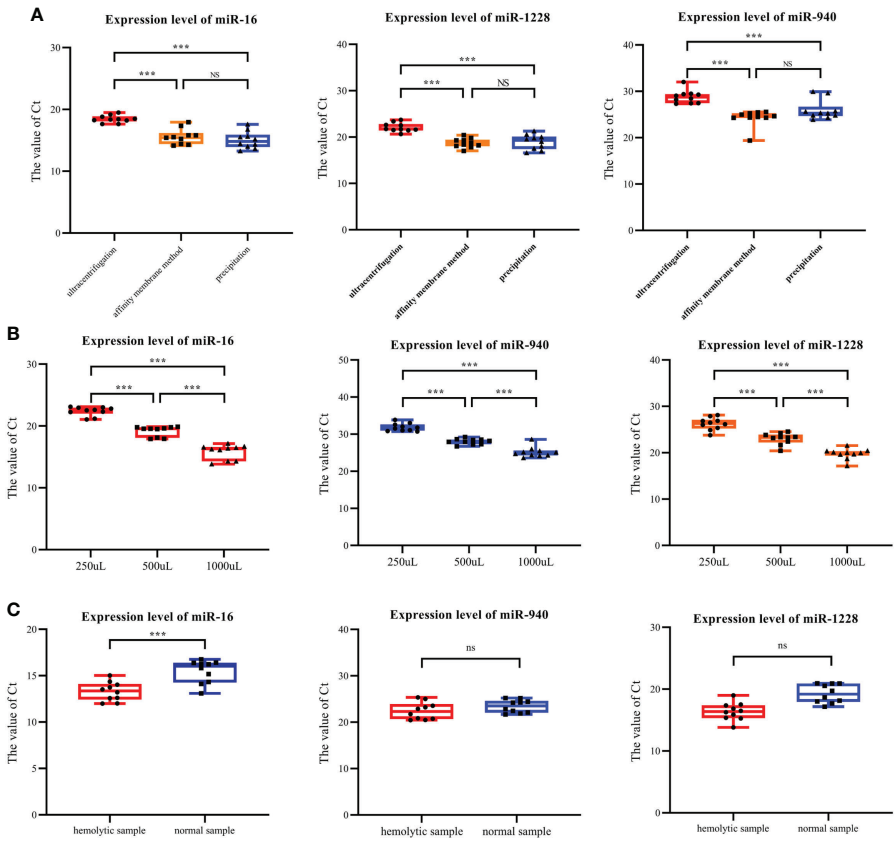

FIGURE 2
Expression levels of exosomal miR-940, miR-1228 and miR-16 under various conditions. **(A)** The three types of miRNAs were found at the lowest levels in the exosomes isolated by ultracentrifugation. **(B)** Three miRNAs were expressed in serum exosomes obtained with initial serum levels of 250, 500 and 1000 µL. **(C)** Expression of three exosome miRNAs in hemolysis and normal blood samples. (*p<0.05, **p<0.01, ***p<0.001, no significance, ns p>0.05).

using membrane affinity (Table 3). Therefore, membrane affinity was selected for exosome extraction in all subsequent experiments.

RT–qPCR was used to detect the expression levels of miR-16, miR-1228 and miR-940 in the exosomes extracted from the different initial volumes of serum from breast cancer patients. The initial serum levels were 250, 500 and 1000 µL. When the serum volume of breast cancer patients doubled, the Ct values of all miRNAs decreased over three cycles (Figure 2B). Therefore, for small blood samples, a serum volume lower than that detailed in the instructions could also be used for exosome extraction.

In the process of preserving samples, hemolysis occurred in 10 samples, and we subsequently collected normal blood samples from these patients. Therefore, we studied the influence of hemolysis on the content of miRNA in the exosomes of the samples. Exosomal RNA was extracted from both hemolytic and normal blood samples, and the same method was used for the extraction of exosomal miRNA from hemolysis samples. The levels of miR-16, miR-1228 and miR-940 were detected. The RT–qPCR results showed that in hemolyzed blood, the expression levels of miR-16, miR-940 and miR-1228 in the extracted exosomes were significantly higher than those in serum exosomes without hemolysis (Figure 2C). This finding is likely because blood cells release exosomes during blood storage, which alters the amount of exosomes that will be collected through plasma/serum. In plasma or serum samples, the quantification of exosomal miRNAs may be impaired due to contamination with erythrocyte-derived miRNA caused by hemolysis. Therefore, in clinical serum exosome experiments, hemolysis may increase the expression level of target genes.

Screening of candidate reference genes and analysis of their applicability

Because the primary requirement of internal reference genes is to present similar expression levels under diseased and healthy conditions, we compared the expression of candidate internal reference genes in serum exosomes under breast cancer and healthy conditions. We read out the Ct values of different

TABLE 3 Coefficient of variation (CoV) of miRNA expression in exosomes extracted using different methods.

	Ultracentrifugation	Affinity membrane method	Precipitation
miR-16	0.031891952	0.079909031	0.091907362
miR-1228	0.04270173	0.054146769	0.083191199
miR-940	0.048764364	0.073463689	0.081203994

candidate genes in each serum sample (Figure 3A). Among them, the serial numbers 1-20 correspond to samples from the controls, whereas the numbers 21-79 correspond to samples from breast cancer patients. The picture shows the Ct value of different candidate genes obtained for each serum sample. The Ct values ranged from 12.01 (miR-16) to 24.78 (miR-432).

Subsequently, the expression levels of miR-16, miR-1228, miR-484, miR-191, and miR-423 in the serum exosomes of breast cancer patients and normal human serum exosomes were compared (Figure 3B). The results showed that the Ct value of each candidate gene was not significantly different between the serum exosomes from the breast cancer patients and those from the controls. We also showed the dispersion of the Ct values (Table 4).

The stability of the five candidate internal genes was analyzed and sorted using four algorithms, namely, BestKeeper, NormFinder, GeNorm, and ΔCT; however, the four methods used to analyze the stability of the internal genes were not the same (Figure 3C).

BestKeeper compared the correlation coefficient (r), standard deviation (SD), and coefficient of variation (CV) generated by the pairing of each gene and ultimately determined a relatively stable internal reference gene. The principle was that a more stable internal reference gene would have a smaller standard deviation and coefficient of variation and a larger correlation coefficient. Gene stability was also judged according to the SD value. At SD>1, the expression of the internal reference gene was unstable. The results obtained with BestKeeper are shown in Figure 3C, which indicates high SD variation among miR-1228, miR-16, and miR-484. In this study, miR-423 was the most stable gene (std dev=1.012), followed by miR-16 (std dev=1.275).

NormFinder software was designed by Claus et al. to screen out internal reference genes suitable for RT–qPCR. A linear scale was used for quantification of the raw data, analyze the stability of candidate genes and provide the stability value of each gene: a higher stability value indicates lower stability of the gene as an internal control and thus indicates that the gene is not suitable as an internal control in this experiment. Among the five candidate genes tested in this study, the results obtained using NormFinder showed that miR-1228 has the lowest stability value of 0.778, which indicates that this gene was the most stable internal reference gene in this experiment, followed by miR-423 (1.056) and miR-191 (1.139), and the least stable gene was miR-484.

The standard for using GeNorm to evaluate the stability of the internal reference genes was to calculate the average coefficient of variation M value of the logarithmic conversion value of the ratio of the first gene to the remaining genes. The M value must be less than 1.5, and a smaller M value corresponds to greater stability of the gene as an internal reference. The final result obtained by calculation was two or more candidate combinations. The results obtained using GeNorm showed that the M values of miR-484, miR-423 and miR-16 in the sample were higher than 1.5, indicating that these candidate genes are unreliable and cannot be used as internal reference genes for the standardization of breast cancer serum exosomal RNA. The most stable gene combination was the combination of miR-1228 and miR-191, which had an expression stability M value of 1.391.

The comparative ΔCt method was used to analyze the stability of the internal reference gene, and the result was a combination of two genes. The ΔCT method could eliminate the influence of coordinated regulation and evaluate the reference genes from various aspects. The results obtained using the ΔCt method indicated that miR-1228 and miR-423 constituted the most stable group.

Because the four analysis methods use different algorithms, the results obtained were also different; thus, normalization and integration of the data were performed when necessary. RefFinder is a web tool that can synthesize the results from the four software programs to generate the final overall ranking of reference genes. According to the output, the most stable reference gene was miR-1228, and the lowest and most unstable reference gene was miR-484 (Figure 3D). These results indicated that miR-1228 may be used as the most stable reference gene in breast cancer research.

Impact of reference genes on the expression levels of target genes

RT–qPCR analysis was applied to further evaluate the stability of each candidate reference gene in the sample. miR-940 exhibits low expression levels in the serum of breast cancer patients (28, 29).

The expression level data of miR-940 were normalized (Figure 4) using the RefFinder program recommended for miR-1228, miR-191, and miR-423 and the geNorm program recommended for miR-484. Although miR-16 was not

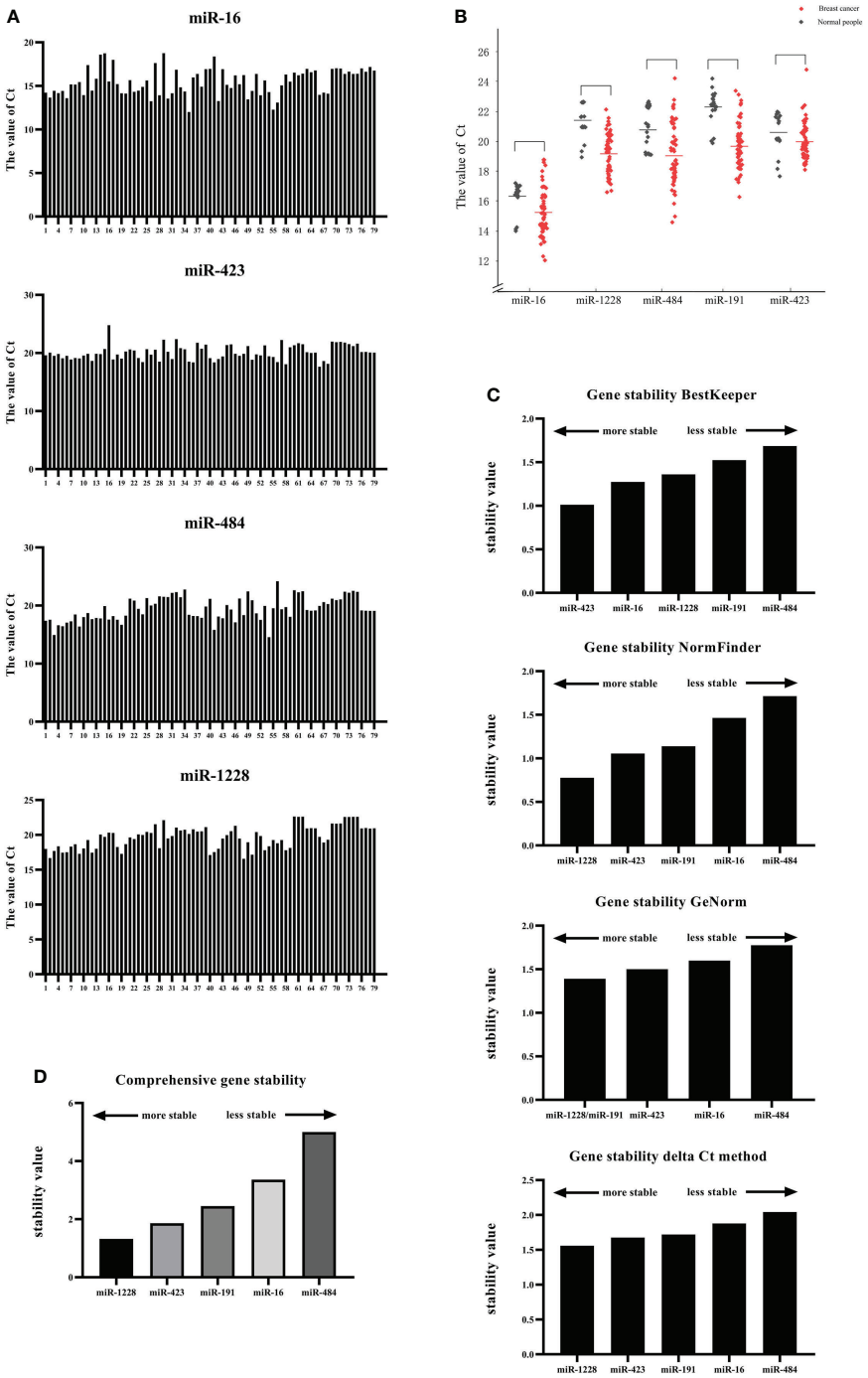

FIGURE 3
Screening of candidate reference genes and analysis of their applicability. **(A)** Expression of candidate internal reference genes in serum exosomes under breast cancer and healthy conditions. **(B)** The expression levels of miR-16, miR-1228, miR-484, miR-191, and miR-423 in the serum exosomes of breast cancer patients and normal human serum exosomes were compared. **(C)** The stability of the five candidate internal genes was analyzed and sorted using four algorithms, namely, GeNorm, NormFinder, BestKeeper, and ΔCT. **(D)** The stability of the five candidate internal genes was analyzed and sorted using RefFinder.

TABLE 4 Dispersion of the Ct values.

Gene	miR-16	miR-1228	miR-484	miR-191	miR-423
STDEV	1.511947796	1.632827144	2.035326422	2.035326422	1.275306533

recommended as a suitable reference gene by BestKeeper and geNorm, we used miR-16 to normalize the content of miR-940 because this gene has often been used for expression studies (30, 31). When using different internal reference genes, the fold change in serum exosomal miR-940 in each group was calculated (Figure 4). The results from the normalization of miR-940 were used. miR-191 and miR-1228 showed that the serum exosomal miR-940 levels in breast cancer patients were significantly downregulated, whereas the results obtained by normalization using other candidate genes did not show the same result. This analysis showed that different normalization schemes may affect the quantitative expression of data. However, miR-940 should be assessed in a large sample study to confirm the reliability of the reference gene.

Standard quantification of exosomal miR-940

For the quantification of miR-940, a standard linear regression curve of the Ct values against the copy numbers was derived from serially diluted known amounts of miR-940 cDNA (Figure 5A). Based on the curve, the copy number of miR-940 transcripts per nanogram of exosomal RNA isolated from each cancer patient was determined. The copy number of miR-940 in serum exosomes of breast cancer patients was significantly lower than that of normal controls, which is similar to the results from the relative quantification of miR-940 using miR-191 and miR-1228 (Figure 5B), and this finding demonstrated that miR-191 and miR-1228 were appropriate reference genes. However, miR-16, miR-484 and miR-423 could not be used as reference genes for breast cancer exosomal miRNAs. These results indicated that the expression level of miR-940 in the serum exosomes of breast cancer patients was significantly downregulated.

To investigate the potential physiological significance of circulatory exosomal miR-940, the correlation of the levels of exosomal miR-940 with a spectrum of pathophysiological parameters in cancer patients was tested (Figure 5C). The patients were grouped according to various pathological indicators, and the grouping results are shown in Table 5. Among the 59 samples, we found that one of the breast cancer patients was male and the youngest, but we did not find any special pathological information, so we analyzed it in the same way. The patients were divided into two groups according to different parameters, and the corresponding miR-940 copy numbers were averaged within groups and compared with each other using a t test. The correlations between exosomal miR-940 and pathophysiological parameters in breast cancer patients are shown in Figure 5C, which showed that exosomal miR-940 levels were significantly lower in HER2/neu-positive patients than in HER2/neu-negative patients (median copy number: 9.43×10^{11} vs. 1.46×10^{12}, P=0.017). The serum exosomal miR-940 levels were significantly higher in breast

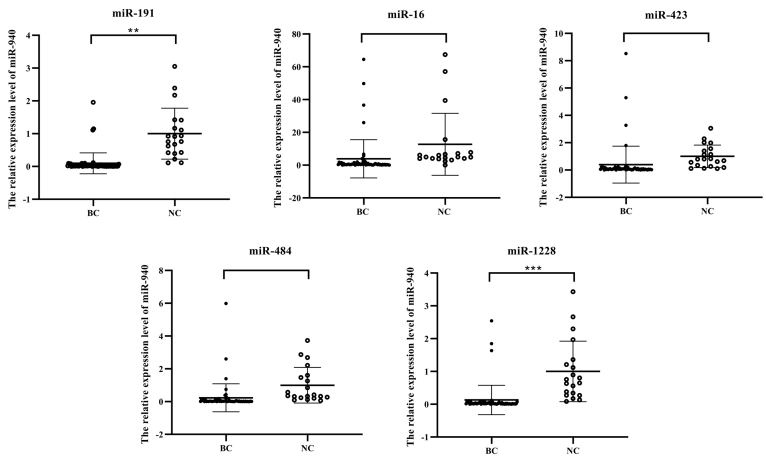

FIGURE 4
Results from normalization using the candidate internal reference miR-940. (*p<0.05, **p<0.01, ***p<0.001, no significance, ns p>0.05).

10.3389/fonc.2022.956167

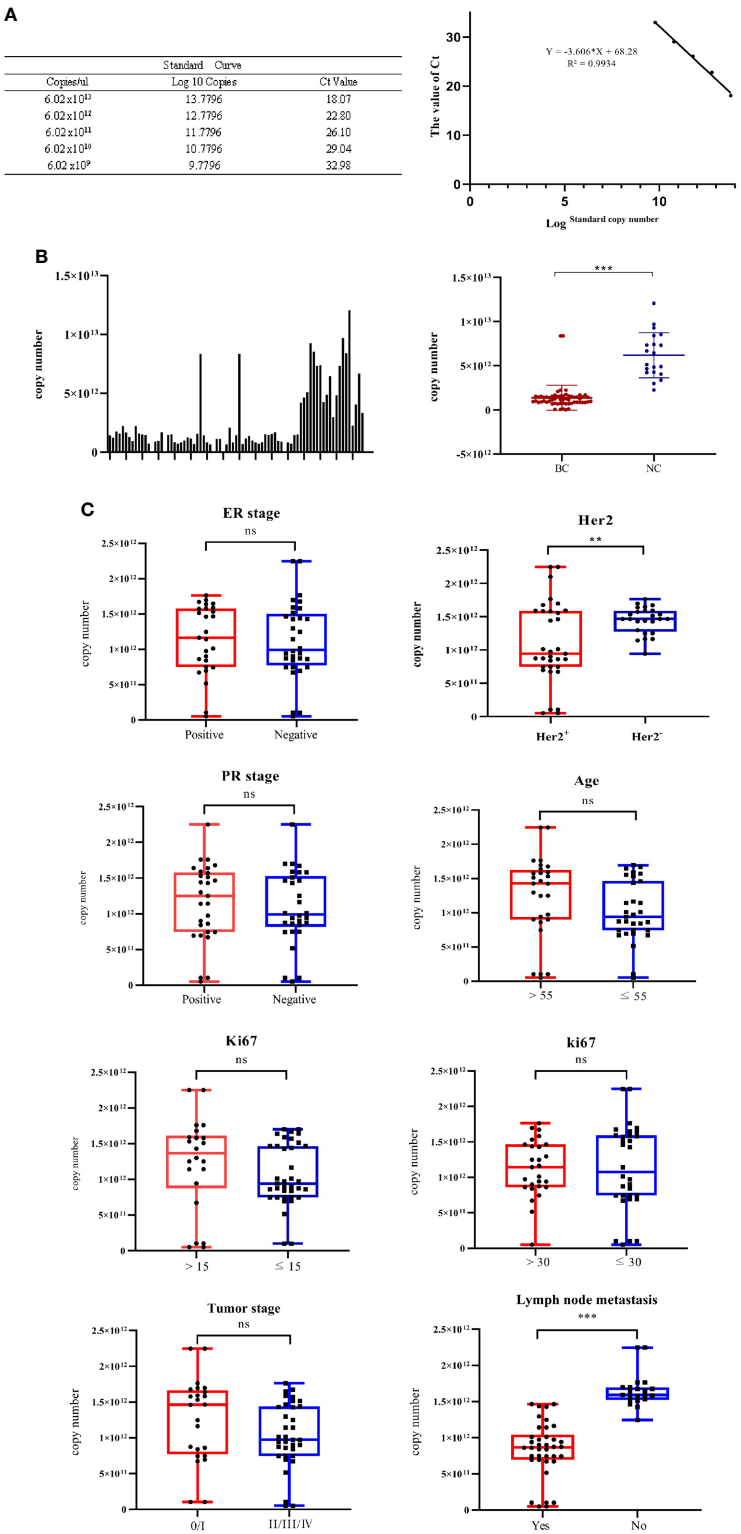

FIGURE 5
The correlations of the levels of exosomal miR-940 with a spectrum of pathophysiological parameters in cancer patients were tested. **(A)** Standard linear regression curve of miR-940. **(B)** The copy number of miR-940 transcripts per nanogram of exosomal RNA in each column sample, and the copy number of miR-940 in serum exosomes of breast cancer patients was significantly lower than that of normal controls. **(C)** Correlations of the levels of exosomal miR-940 with a spectrum of pathophysiological parameters in cancer patients. (*p<0.05, **p<0.01, ***p<0.001, no significance, ns p>0.05).

TABLE 5 Pathological grouping of blood samples.

Variable	Number	Variable	Number
age		ER	
≤55	28	(+)	27
>55	31	(-)	32
Lymph node metastasis		PR	
Negative	38	(+)	30
Positive	21	(-)	29
TNM stage		Ki67	
0/I	24	>15	32
II/III/IV	35	≤15	27
HER2		Ki67	
(+)	33	<30	37
(-)	26	≥30	22

cancer patients without lymph node metastasis than in those with lymph node metastasis (median copy number: 8.7×10^{11} vs. 1.59×10^{12}, $P=1.110^{-11}$). However, the level of serum exosomal miR-940 was not related to the age, degree of differentiation, ER/PR status, Ki67 or TNM stage of the breast cancer patients ($P>0.05$). These results showed that the content of miR-940 in the serum exosomes of breast cancer patients was related to lymph node metastasis and HER2/neu expression status.

Discussion

With the development of precise tumor therapy and the continuous improvement of liquid biopsy technology, extracellular vesicles that can be secreted by various cells, such as exosomes, have attracted increasing attention. Exosomal miRNAs are not as degraded as free miRNAs in human fluids, and this type of RNA may be more suitable for the detection of tumor markers (32). Breast cancer is the leading cause of cancer death among women. Differences in the expression levels of circulating exosomal miRNAs between healthy people and breast cancer patients could identify molecular markers for the diagnosis and prediction of breast cancer (33). However, the detection methods of serum exosomal miRNAs in breast cancer patients have not been unified in clinical practice. Based on previous experiments, we first analyzed the effects of various exosome extraction methods and the starting amount of serum sample on miR-940, miR-16, miR-16 and miR-1228, analyzed the expression levels of three serum exosome miRNAs under hemolysis, and established a preprocessing method suitable for the clinical detection of serum exosomal miRNAs. To clinically detect the expression level of exosomal miRNA in breast cancer, an appropriate volume of insoluble blood samples should be used for serum exosomal RNA extraction using the membrane affinity method. We then demonstrated that miR-1228 and miR-191 could be used as reference genes for breast cancer serum exosomal miRNA, whereas miR-16, miR-484 and miR-423 were not suitable as reference genes. We also found that the expression level of serum exosomal miR-940 could reflect the presence of lymph node metastasis in breast cancer patients and the expression level of serum exosomal HER2/neu in breast cancer patients, indicating its potential as a metastasis marker.

As a novel diagnostic marker, exosomes have many advantages, such as their rapid, efficient and economic isolation and their important potential application value in clinical diagnosis and treatment (34). However, due to the complex formation environment and small diameter of exosomes, an ideal separation technology is key to limiting the research and application of exosomes. Among these, the preservation and pretreatment of samples is crucial. Ultracentrifugation was the first technique used for exosome isolation and remains the most common technique in articles (35). However, this method is time-consuming and complicated and requires a high amount of serum. Although precipitation can yield exosomes (36), the separated exosomes have very low purity because almost all soluble granules can settle, which is not conducive to downstream analysis. This study was used to extract exosomes using the membrane affinity column method with high efficiency and low loss obtained outside secreted RNA, which is suitable for clinical laboratory work and advantageous for downstream analysis (37). In addition, the storage state of serum samples is also very important in clinical testing, and hemolysis may occur. Studies have shown that the levels of various proteins, RNAs and DNAs in whole blood are greatly changed after hemolysis, whereas previous studies have shown that exosomal miRNAs are not as degraded as free miRNAs in body fluids. This study experimentally verified that hemolytic samples also have a great impact on the extraction of serum exosomal miRNA, which fills the gap in this aspect. Moreover, due to limited clinical serum resources, our study conducted a

preliminary exploration of whether a sample size lower than that recommended by the protocol could achieve the same experimental effect.

Among the many techniques for the analysis of miRNA transcription levels, RT–qPCR is considered the most accurate technique due to its high sensitivity and easy reproducibility (38). Although relative quantification is a common method, it needs a reference gene for the normalization of different samples to ensure high sensitivity because the expression differences in the data results may not be due to the disease itself but rather to differences in the processes used for sample collection, stabilization, RNA extraction and target quantification. Therefore, identification of the best reference genes suitable for study is necessary for the accurate standardization of exosomal miRNA data. However, suitable reference genes for serum exosomal miRNAs in clinical breast cancer patients have not been reported to date. Based on previous reports, five candidate internal reference genes were selected for RT–qPCR studies of breast cancer using tissue, serum or plasma. Among them, miR-484, miR-423 and miR-1228 were used in the study of serum miRNA, and miR-16 and miR-191 were used in the study of breast tissue. Due to differences in the environment of exosomes, tissues and body fluids, the effect of these genes in standardizing breast cancer serum exosomes has been questioned. Therefore, we selected five genes as candidate genes to study their applicability as internal references for serum exosomal miRNAs in breast cancer patients. The results demonstrate that both miR-1228 and miR-191 could be used as reference genes for breast cancer serum exosomal miRNA. Although the results from the software analysis showed that miR-191 was not suitable as a reference gene for breast cancer serum exosomes, the relative quantification of the target genes using miR-191 also yielded the same results as those obtained with miR-1228. Similarly, high differences were observed when different miRNAs were used under the differentiation conditions described by Roulex-Bonin and Coste, which suggested that miR-191-5p was the most stable reference gene (39). Therefore, we believe that miR-191 could also serve as a suitable reference gene.

Previous studies have confirmed that the expression level of miR-940 in breast cancer tissues was significantly lower than that in adjacent tissues. Further studies found that miR-940 could inhibit the proliferation, invasion and migration of breast cancer cells by targeting and regulating CXC chemokine 2 (CXCR2) or ZNF24 (18, 40). Zhang et al. indicated that miR-940 induces malignant progression of breast cancer by regulating FOXO3 (41). In addition, the serum miR-940 levels in breast cancer patients predicted the efficacy of trastuzumab in patients with HER2-positive metastatic breast cancer (29). The downregulation of miR-940 levels in breast cancer tissues also led to the low content of free miR-940 in patient serum, and the stability of free miR-940 in serum was susceptible to environmental influences, which limited the ability of free miR-940 as a prognostic marker.

To verify whether breast cancer serum exosomal miR-940 has potential as a tumor marker of breast cancer, the copy number of miR-940 in the serum exosomes of each patient was calculated by an absolute quantitative method, and the results demonstrated that the content of miR-940 in the serum exosomes of breast cancer patients was significantly lower than that in normal human serum exosomes. The relationship between the copy number of serum exosomal miR-940 and the clinical data of breast cancer patients was analyzed.

The results showed that the expression level of miR-940 in the serum exosomes of breast cancer patients with lymph node metastasis was significantly downregulated. Therefore, the expression level of miR-940 in serum exosomes of patients can be used to judge whether a patient has lymph node metastasis. Similarly, we found that the expression level of miR-940 in the serum exosomes of HER2/neu-positive patients was significantly lower than that in those of HER2/neu-negative patients. However, as shown in Figure 5C, the differences were not as distinct due to the high dispersion of data points in both groups. Exosomal miR-940 alone may not be sufficiently accurate to judge the HER2/neu status of patients. We also demonstrated that serum exosomal miR-940 is a potential metastatic marker for breast cancer patients.

Li et al. found that exosomal miR-940 was mainly secreted by tumor cells *in vivo* through an analysis of exosomes and exosome-free supernatant from primary breast cancer cells and peripheral immune cells and revealed that miR-940 expression is increased in trastuzumab-sensitive HER2-positive metastatic breast cancer patients and further increased in trastuzumab-resistant patients (29). Therefore, they speculated that serum exosomal miR-940 has the potential to be used as an indicator of trastuzumab sensitivity in HER2/neu-positive metastatic breast cancer. Wang et al. found that the expression level of exosomal lncRNA-HOTAIR is able to reflect the HER2/neu status (21). Therefore, we hypothesized that the expression levels of exosomal miR-940 and lncRNA-HOTAIR may be used to judge the HER2/neu status of breast cancer patients. Of course, further experiments are needed to verify our hypothesis. In conclusion, serum exosomal miR-940 can be used as a minimally invasive liquid biopsy for monitoring disease progression.

In this study, we only selected some of the most frequently used reference genes in the literature and screened out the most stable reference genes. We did not sequence the RNA in the serum exosomes of breast cancer patients and normal people, and thus, more accurate reference genes may be obtained. When comparing clinical exosome extraction methods, the number of samples is small. If the sample size can be increased, the results may be more convincing. In addition, this paper describes one gene selected for miR-940, which shows that it can be used as a metastasis marker of breast cancer. We should test multiple miRNAs to increase its efficacy as a biomarker. Only one gene

was selected. If multiple miRNAs are selected for combined detection with existing tumor markers, the reliability will be higher.

Data availability statement

The raw data supporting the conclusions of this article will be made available by the authors, without undue reservation.

Ethics statement

The studies involving human participants were reviewed and approved by The Ethics Committee of the Chongqing University Cancer Hospital. The patients/participants provided their written informed consent to participate in this study.

Author contributions

ZG and HY performed and analyzed the experiments and wrote the manuscript. HWZ, HZ, and XHZ helped to perform the experiments. XDZ designed and supervised the study. All authors have read and approved the final manuscript.

Funding

The present study was supported by a grant from the Fundamental Research Funds for the Central Universities (2019CDYGZD006).

Acknowledgments

The authors of the present study are grateful for the valuable comments from members of the department of Breast Cancer, Chongqing University Cancer Hospital. The authors of this study also thank JunLi Huang from Chongqing University for valuable comments.

Conflict of interest

The authors declare that the research was conducted in the absence of any commercial or financial relationships that could be construed as a potential conflict of interest.

Publisher's note

All claims expressed in this article are solely those of the authors and do not necessarily represent those of their affiliated organizations, or those of the publisher, the editors and the reviewers. Any product that may be evaluated in this article, or claim that may be made by its manufacturer, is not guaranteed or endorsed by the publisher.

Supplementary material

The Supplementary Material for this article can be found online at: https://www.frontiersin.org/articles/10.3389/fonc.2022.956167/full#supplementary-material

References

1. Kalluri R, LeBleu VS. The biology, function, and biomedical applications of exosomes. *Science* (2020) 367:1–15. doi: 10.1126/science.aau6977

2. Barile L, Moccetti T, Marban E, Vassalli G. Roles of exosomes in cardioprotection. *Eur Heart J* (2017) 38:1372–9. doi: 10.1093/eurheartj/ehw304

3. Doyle LM, Wang MZ. Overview of extracellular vesicles, their origin, composition, purpose, and methods for exosome isolation and analysis. *Cells-Basel* (2019) 8(7):727. doi: 10.3390/cells8070727

4. An T, Qin S, Xu Y, Tang Y, Huang Y, Situ B, et al. Exosomes serve as tumour markers for personalized diagnostics owing to their important role in cancer metastasis. *J Extracell Vesicles* (2015) 4:27522. doi: 10.3402/jev.v4.27522

5. Groza M, Zimta A, Irimie A, Achimas-Cadariu P, Cenariu D, Stanta G, et al. Recent advancements in the study of breast cancer exosomes as mediators of intratumoral communication. *J Cell Physiol* (2020) 235:691–705. doi: 10.1002/jcp.29096

6. Eichelser C, Stuckrath I, Muller V, Milde-Langosch K, Wikman H, Pantel K, et al. Increased serum levels of circulating exosomal microRNA-373 in receptor-negative breast cancer patients. *Oncotarget* (2014) 5:9650–63. doi: 10.18632/oncotarget.2520

7. Norouzi-Barough L, Shahi AAK, Mohebzadeh F, Masoumi L, Haddadi MR, Shirian S. Early diagnosis of breast and ovarian cancers by body fluids circulating tumor-derived exosomes. *Cancer Cell Int* (2020) 20:1–10. doi: 10.1186/s12935-020-01276-x

8. Zhou W, Fong MY, Min Y, Somlo G, Liu L, Palomares MR, et al. Cancer-secreted miR-105 destroys vascular endothelial barriers to promote metastasis. *Cancer Cell* (2014) 25:501–15. doi: 10.1016/j.ccr.2014.03.007

9. Rodriguez M, Silva J, Herrera A, Herrera M, Pena C, Martin P, et al. Exosomes enriched in stemness/metastatic-related mRNAS promote oncogenic potential in breast cancer. *Oncotarget* (2015) 6:40575–87. doi: 10.18632/oncotarget.5818

10. Tsang JYS, Tse GM. Molecular classification of breast cancer. *Adv Anat Pathol* (2020) 27:27–35. doi: 10.1097/PAP.0000000000000232

11. Chakraborty C, Das S. Profiling cell-free and circulating miRNA: a clinical diagnostic tool for different cancers. *Tumor Biol* (2016) 37:5705–14. doi: 10.1007/s13277-016-4907-3

12. Pritchard CC, Kroh E, Wood B, Arroyo JD, Dougherty KJ, Miyaji MM, et al. Blood cell origin of circulating MicroRNAs: A cautionary note for cancer biomarker studies. *Cancer Prev Res* (2012) 5:492–7. doi: 10.1158/1940-6207.CAPR-11-0370

13. Occhipinti G, Giulietti M, Principato G, Piva F. The choice of endogenous controls in exosomal microRNA assessments from biofluids. *Tumour Biol* (2016) 37:11657–65. doi: 10.1007/s13277-016-5164-1

14. Crossland RE, Norden J, Bibby LA, Davis J, Dickinson AM. Evaluation of optimal extracellular vesicle small RNA isolation and qRT-PCR normalisation for serum and urine. *J Immunol Methods* (2016) 429:39–49. doi: 10.1016/j.jim.2015.12.011

15. Liang S, Zhang X, Li J. Zinc finger asp-His-His-Cys palmitoyl-acyltransferase 19 accelerates tumor progression through wnt/beta-catenin pathway and is upregulated by miR-940 in osteosarcoma. *Bioengineered* (2022) 13:7367–79. doi: 10.1080/21655979.2022.2040827

16. Xu R, Zhou F, Yu T, Xu G, Zhang J, Wang Y, et al. MicroRNA-940 inhibits epithelial-mesenchymal transition of glioma cells *via* targeting ZEB2. *Am J Transl Res* (2019) 11:7351–63.

17. Wang R, Wu Y, Huang W, Chen W. MicroRNA-940 targets INPP4A or GSK3 beta and activates the wnt/beta-catenin pathway to regulate the malignant behavior of bladder cancer cells. *Oncol Res* (2018) 26:145–55. doi: 10.3727/096504017X14902261600566

18. Hou L, Chen M, Yang H, Xing T, Li J, Li G, et al. MiR-940 inhibited cell growth and migration in triple-negative breast cancer. *Med Sci Monit* (2016) 22:3666–72. doi: 10.12659/MSM.897731

19. Babion I, Snoek BC, van de Wiel MA, Wilting SM, Steenbergen R. A strategy to find suitable reference genes for miRNA quantitative PCR analysis and its application to cervical specimens. *J Mol Diagn* (2017) 19:625–37. doi: 10.1016/j.jmoldx.2017.04.010

20. Hu J, Wang Z, Liao BY, Yu L, Gao X, Lu S, et al. Human miR-1228 as a stable endogenous control for the quantification of circulating microRNAs in cancer patients. *Int J Cancer* (2014) 135:1187–94. doi: 10.1002/ijc.28757

21. Wang YL, Liu LC, Hung Y, Chen CJ, Lin YZ, Wu WR, et al. Long non-coding RNA HOTAIR in circulatory exosomes is correlated with ErbB2/HER2 positivity in breast cancer. *Breast* (2019) 46:64–9. doi: 10.1016/j.breast.2019.05.003

22. Vandesompele J, De Preter K, Pattyn F, Poppe B, Van Roy N, De Paepe A, et al. Accurate normalization of real-time quantitative RT-PCR data by geometric averaging of multiple internal control genes. *Genome Biol* (2002) 3:H34. doi: 10.1186/gb-2002-3-7-research0034

23. Andersen CL, Jensen JL, Orntoft TF. Normalization of real-time quantitative reverse transcription-PCR data: A model-based variance estimation approach to identify genes suited for normalization, applied to bladder and colon cancer data sets. *Cancer Res* (2004) 64:5245–50. doi: 10.1158/0008-5472.CAN-04-0496

24. Pfaffl MW, Tichopad A, Prgomet C, Neuvians TP. Determination of stable housekeeping genes, differentially regulated target genes and sample integrity: BestKeeper - excel-based tool using pair-wise correlations. *Biotechnol Lett* (2004) 26:509–15. doi: 10.1023/B:BILE.0000019559.84305.47

25. Silver N, Best S, Jiang J, Thein SL. Selection of housekeeping genes for gene expression studies in human reticulocytes using real-time PCR. *BMC Mol Biol* (2006) 7:33. doi: 10.1186/1471-2199-7-33

26. Xie F, Xiao P, Chen D, Xu L, Zhang B. miRDeepFinder: a miRNA analysis tool for deep sequencing of plant small RNAs. *Plant Mol Biol* (2012) 80:75–84. doi: 10.1007/s11103-012-9885-2

27. Silverman JM, Reiner NE. Exosomes and other microvesicles in infection biology: organelles with unanticipated phenotypes. *Cell Microbiol* (2011) 13:1–9. doi: 10.1111/j.1462-5822.2010.01537.x

28. Liu W, Xu Y, Guan H, Meng H. Clinical potential of miR-940 as a diagnostic and prognostic biomarker in breast cancer patients. *Cancer Biomark* (2018) 22:487–93. doi: 10.3233/CBM-171124

29. Li H, Liu J, Chen J, Wang H, Yang L, Chen F, et al. A serum microRNA signature predicts trastuzumab benefit in HER2-positive metastatic breast cancer patients. *Nat Commun* (2018) 9:1614. doi: 10.1038/s41467-018-03537-w

30. Song J, Bai Z, Han W, Zhang J, Meng H, Bi J, et al. Identification of suitable reference genes for qPCR analysis of serum microRNA in gastric cancer patients. *Dig Dis Sci* (2012) 57:897–904. doi: 10.1007/s10620-011-1981-7

31. Li J, Wei H, Li Y, Li Q, Li N. Identification of a suitable endogenous control gene in porcine blastocysts for use in quantitative PCR analysis of microRNAs. *Sci China Life Sci* (2012) 55:126–31. doi: 10.1007/s11427-012-4289-8

32. Moller A, Lobb RJ. The evolving translational potential of small extracellular vesicles in cancer. *Nat Rev Cancer* (2020) 20:697–709. doi: 10.1038/s41568-020-00299-w

33. Min L, Zhu S, Chen L, Liu X, Wei R, Zhao L, et al. Evaluation of circulating small extracellular vesicles derived miRNAs as biomarkers of early colon cancer: a comparison with plasma total miRNAs. *J Extracell Vesicles* (2019) 8:1643670. doi: 10.1080/20013078.2019.1643670

34. Michael A, Bajracharya SD, Yuen PS, Zhou H, Star RA, Illei GG, et al. Exosomes from human saliva as a source of microRNA biomarkers. *Oral Dis* (2010) 16:34–8. doi: 10.1111/j.1601-0825.2009.01604.x

35. Zeringer E, Barta T, Li M, Vlassov AV. Strategies for isolation of exosomes. *Cold Spring Harb Protoc* (2015) 2015:319–23. doi: 10.1101/pdb.top074476

36. Szabo G, Momen-Heravi F. Extracellular vesicles in liver disease and potential as biomarkers and therapeutic targets. *Nat Rev Gastroenterol Hepatol* (2017) 14:455–66. doi: 10.1038/nrgastro.2017.71

37. Sugimachi K, Matsumura T, Hirata H, Uchi R, Ueda M, Ueo H, et al. Identification of a bona fide microRNA biomarker in serum exosomes that predicts hepatocellular carcinoma recurrence after liver transplantation. *Br J Cancer* (2015) 112:532–8. doi: 10.1038/bjc.2014.621

38. Tang YT, Huang YY, Zheng L, Qin SH, Xu XP, An TX, et al. Comparison of isolation methods of exosomes and exosomal RNA from cell culture medium and serum. *Int J Mol Med* (2017) 40:834–44. doi: 10.3892/ijmm.2017.3080

39. Coste E, Rouleux-Bonnin F. The crucial choice of reference genes: identification of miR-191-5p for normalization of miRNAs expression in bone marrow mesenchymal stromal cell and HS27a/HS5 cell lines. *Sci Rep* (2020) 10:17728. doi: 10.1038/s41598-020-74685-7

40. Chen JY, Lai YS, Chu PY, Chan SH, Wang LH, Hung WC. Cancer-derived VEGF-c increases chemokine production in lymphatic endothelial cells to promote CXCR2-dependent cancer invasion and MDSC recruitment. *Cancers (Basel)* (2019) 11:1120. doi: 10.3390/cancers11081120

41. Zhang H, Peng J, Lai J, Liu H, Zhang Z, Li X, et al. MiR-940 promotes malignant progression of breast cancer by regulating FOXO3. *Biosci Rep* (2020) 40 (9):9. doi: 10.1042/BSR20201337

frontiers | Frontiers in Oncology

TYPE Original Research
PUBLISHED 01 November 2022
DOI 10.3389/fonc.2022.995196

Check for updates

OPEN ACCESS

EDITED BY
Nicola Amoroso,
University of Bari Aldo Moro, Italy

REVIEWED BY
Tianfu Li,
Goethe University Frankfurt, Germany
Wancun Zhang,
Zhengzhou University, China
Célio Junior da Costa Fernandes,
State University of Campinas, Brazil

*CORRESPONDENCE
Yunjiang Liu
lyj818326@outlook.com
Yixin Qi
13932153600@139.cn

†These authors have contributed equally to this work

SPECIALTY SECTION
This article was submitted to Breast Cancer, a section of the journal Frontiers in Oncology

RECEIVED 15 July 2022
ACCEPTED 04 October 2022
PUBLISHED 01 November 2022

CITATION
Liu J, Peng X, Yang Y, Zhang Y, Han M, Shi X, Zheng J, Li T, Chen J, Lv W, Liu Y, Qi Y, Zhang L and Liu Q (2022) The value of hsa_circ_0058514 in plasma extracellular vesicles for breast cancer.
Front. Oncol. 12:995196.
doi: 10.3389/fonc.2022.995196

COPYRIGHT
© 2022 Liu, Peng, Yang, Zhang, Han, Shi, Zheng, Li, Chen, Lv, Liu, Qi, Zhang and Liu. This is an open-access article distributed under the terms of the Creative Commons Attribution License (CC BY). The use, distribution or reproduction in other forums is permitted, provided the original author(s) and the copyright owner(s) are credited and that the original publication in this journal is cited, in accordance with accepted academic practice. No use, distribution or reproduction is permitted which does not comply with these terms.

The value of hsa_circ_0058514 in plasma extracellular vesicles for breast cancer

Jiani Liu[1†], Xinyu Peng[2†], Yang Yang[3†], Yao Zhang[4†], Meng Han[1], Xiaohui Shi[5], Jie Zheng[1], Tong Li[6], Jinxia Chen[7], Weihua Lv[7], Yunjiang Liu[5*], Yixin Qi[5*], Lei Zhang[8] and Qi Liu[8]

[1]Department of Breast Surgery, The First Hospital of Qinhuangdao, Qinhuangdao, China, [2]Department of Gastrointestinal Surgery, Affiliated Hospital of Hebei University, Baoding, China, [3]Department of Oncology, Affiliated Hospital of Hebei University, Baoding, China, [4]Department of Plastic Surgery, Hangzhou Xiaoshan Yaoran Medical Cosmetology Clinic Co. Ltd, Hangzhou, China, [5]Department of Breast Surgery, The Fourth Hospital of Hebei Medical University, Shijiazhuang, China, [6]Graduate school of Chengde Medical University, Chengde, China, [7]Clinical Laboratory of the Fourth Hospital of Hebei Medical University, Shijiazhuang, China, [8]School of Nursing, Hebei Medical University, Shijiazhuang, China

The aim of this study was to investigate the diagnostic value of hsa_circ_0058514 in plasma extracellular vesicles (EVs) in BC patients and its predictive value for neoadjuvant chemotherapy. The expression of hsa_circ_0058514 in a large sample of BC plasma and healthy subjects' plasma was detected by qPCR, and the ROC curve was drawn to verify its diagnostic value as a plasma tumor marker. Furthermore, the association between the expression of hsa_circ_0058514 and clinicopathological characteristics before and after treatment was detected in the plasma of 40 pairs of BC patients undergoing neoadjuvant therapy. The expression level of hsa_circ_0058514 in the plasma of BC patients was significantly higher than that of healthy subjects. The ROC curve showed that plasma hsa_circ_0058514 ROC in differentiating non-metastatic BC and healthy people had better diagnostic efficiency than conventional tumor markers CA153, CA125, and CEA. In patients with neoadjuvant therapy, the decrease in plasma hsa_circ_0058514 value before and after treatment correlated with pathological MP grade (r = 0.444, p = 0.004) and imaging tumor regression value (r = 0.43, p = 0.005) positive correlation. The detection of hsa_circ_0058514 in both extracellular vesicles of BC cell culture medium and human plasma was demonstrated. Hsa_circ_0058514 is detected in the plasma from BC cells secreted in the form of vesicles. Hsa_circ_0058514 can be used as an early plasma biological indicator for the diagnosis of BC in clinical applications, with a higher risk of recurrence and metastasis, and as a predictor of the effect of neoadjuvant therapy to guide the clinical use of neoadjuvant therapy.

KEYWORDS

hsa_circ_0058514, EVS, biomarker, plasma, extracellular vesicles

Introduction

According to the reported Global Cancer Statistics 2020 (GLOBOCAN) estimates of incidence and mortality worldwide by the International Agency for Research on Cancer, female BC has surpassed lung cancer as the most common cancer, and the estimated data of the morbidity and mortality showed that there were 2.3 million new cases annually, accounting for 11.7% of all new cancers (1). About 70%–80% of patients with early-stage non-metastatic BC are curable, but advanced BC with distant organ metastasis is considered to be incurable by current treatments, due to the poor prognosis, with a 26% 5-year survival rate (2). Based on the presence or absence of progesterone receptors, estrogen receptors, and human epidermal growth factor receptor-2 (HER-2), BC can be roughly divided into three different subtypes, namely, intraluminal (luminal A/B) type (positive hormone receptor), HER-2 type (overexpression of HER-2), and triple-negative BC (TNBC) (the loss of all three receptors) (3). Compared with luminal and HER2 subtypes, TNBC manifests more aggression, with a poorer prognosis and higher metastatic potential (3).

Because of the improvement in people's health awareness and the advancement of diagnosis level, more and more BCs can be detected and treated early, but due to the systemic and complex nature of cancer, there are still many challenges in diagnosis. Traditional cancer detection methods, such as tissue biopsy, are not comprehensive enough to capture the entire genomic landscape of breast tumors. However, with the introduction of new technologies, the use of liquid biopsy has been more popular, resulting from the improvements in all aspects of BC management, including early screening and diagnosis, prognosis prediction, early detection of recurrence, and assessment of disease progression and response to treatment by continuous sampling and effective longitudinal monitoring (4). Compared with tissue biopsy, blood biopsy sampling as a liquid biopsy has the following advantages: low trauma, repeatability, easy operation, and dynamic monitoring during treatment (5). *Via* liquid biopsy sampling, various components of tumor cells released into the blood circulation can be analyzed, including circulating tumor cells (CTCs), circulating tumor DNA (ctDNA), cell-free RNA, tumor-induced platelets, and outer vesicles (5). However, nonspecific tumor markers can be used to achieve early diagnosis, treatment, and monitoring of treatment effects for improving the disease-free survival outcome of patients.

Circular RNA (circRNA) is a kind of non-coding RNA (ncRNA) that has been recently rediscovered. Different from linear RNA with a 5' cap and a 3' tail, circRNA is a single-stranded covalently closed circular transcript, only a few of which have been discovered in different organisms in the past 30 years (6). At present, many circRNAs are also found in human body fluids, such as plasma, urine, and saliva (6). Therefore, circRNAs have attracted interest as potential novel diagnostic and prognostic biomarkers for BC. At present, serum biomarkers used in the diagnosis and monitoring of BC include CEA, CAl53, and CA125, which have low sensitivity and specificity for the diagnosis of intermediate and early BC without recurrence and metastasis (7). There are no current data available that recommend the use of CA153, CEA, and CA125 to monitor treatment effectiveness.

Previous literature showed that circAGFG1, one of the circRNAs, is highly expressed in TNBC and associated with the poor prognosis outcome of TNBC, with a circBase ID of hsa_circ_0058514, located in chr2: 228356262-228389631 (8). This gene is highly expressed in cancer tissues and is a cancer-promoting gene (8). This study was the first to verify the expression of hsa_cir c_0058514 in BC plasma and to verify its clinical value and secretion mechanism as a tumor marker.

Materials and methods

The enrollment of subjects and the collection of plasma and tissue samples

Fasting venous blood was collected from BC patients admitted to the Fourth Hospital of Hebei Medical University from September 2019 to November 2020. Those who had received chemotherapy, radiotherapy, or targeted or interventional therapy in the past, and those with hypertension, diabetes, coronary heart disease, and other cancer histories were excluded. A total of 135 cases were excluded from our study. Intraoperative tumors and adjacent tumor tissues were collected from 38 cases without preoperative adjuvant therapy. Preoperative fasting venous blood were collected from 40 patients had after neoadjuvant treatment. Fasting venous blood was collected from healthy people who underwent a physical examination at the Fourth Hospital of Hebei Medical University from September 2020 to November 2020, and 95 cases were matched according to age. This study was approved by the Medical Ethics Committee of the Fourth Hospital of Hebei Medical University, and all subjects signed the informed consent.

Miller Payne pathology evaluation system after neoadjuvant BC

Evaluation of residual invasive tumor cell abundance in primary breast foci after neoadjuvant therapy was performed by comparing hollow needle aspiration specimens with surgical specimens after treatment. MP grade 1: no change in invasive cancer cells or only individual cancer cells changed, and the overall number of cancer cells did not decrease. MP grade 2: invasive cancer cells were slightly reduced, but the total number was still high, and the reduction of cancer cells did not exceed 30%. MP grade 3: 30%–90% reduction in invasive cancer cells; MP grade 4: invasive cancer cells are significantly reduced by more than 90%,

with only scattered small clusters of cancer cells or single cancer cells remaining. MP grade 5: the original tumor bed has not been infiltrated with cancer cells; there may be ductal carcinoma *in situ*.

Quantitative real-time polymerase chain reaction

Plasma samples were isolated from 4 ml of peripheral blood using BD Vacutainer tubes (EDTA-K2 acted as anticoagulation) (BD, New Jersey, USA), and 4 ml of fasting venous blood was collected from healthy subjects and BC patients. Samples were centrifuged within 1 h (centrifugation condition: 4°C, 1,500 rpm for 10 min), and plasma was sucked with a 1-ml de-enzyme pipette tip, transported to the laboratory on ice, and centrifuged in low-temperature high-speed centrifuge within 6 h (centrifugation condition: 4°C, 15,000 rpm for 10 min). The supernatant was carefully aspirated with a de-enzyme pipette tip, aliquoted into 1.5-ml de-enzymatic EP tubes (AXYGEN, JIANGSU, China), 300 µl per tube, and stored in a −80°C refrigerator for later use. Postoperative plasma samples were collected about 2 weeks after curative resection for breast cancer. Plasma was collected preoperatively after neoadjuvant chemotherapy.

Total RNA in the plasma of BC patients and healthy volunteers was extracted by the TIANamp Virus RNA Kit (TIANGEN, Beijing) according to the instructions of the manufacturer. The purity and concentration of total RNA samples were detected by a NanoDrop 1000 instrument spectrophotometer (Thermo Scientific, Waltham, MA, USA). The average concentration of plasma-extracted RNA was 130–150 ng/µl; A260/280 was nearly 2.0. Total RNAs were reversely transcribed into cDNA using First-Strand cDNA Synthesis Super Mix (Beijing Quanshijin Biotechnology Co., Ltd.), and qRT-PCR was carried out using Top Green qPCR Super Mix (Beijing Quanshijin Biotechnology Co., Ltd.) and the Applied Biosystems Real-Time PCR System. The expression level of hsa_circ_0058514 in the plasma was determined by qRT-PCR assay using the sequences of the primers as listed in Table S1. Thermal cycling conditions were as follows: an initial 5-min step at 95°C followed by 45 cycles of 10 s denaturing at 95°C, 35 s annealing at 55°C, and 15 s extension at 95°C. The final step was conducted at 55°C for 1 min. Each sample was tested in triplicate for the last calculation and run with a non-template control (NTC) composed of sterile water instead of cDNA. The results of qRT-PCR analysis were presented using the $2^{-\Delta\Delta CT}$ method, and the relative expression level of hsa_circ_0058514 was normalized to the GAPDH expression. To verify the qRT-PCR products of the plasma circRNAs, 5 µl of the product mixture was subjected to 2% agarose gel electrophoresis. The qRT-PCR product of each circRNA was sent for DNA sequencing at Sangon Biotech Co, Ltd. (Sangon, Shanghai, China).

Enzyme-linked immunosorbent assay

The concentrations of serum tumor biomarkers (including CEA, CA125, and CA153) in BC patients and healthy controls were measured by the Cobas e602 system with the Elecsys CEA Assay kit (Roche Diagnostics, Basel, Switzerland) according to the manufacturer's instructions. The cutoff values of CEA, CA153, and CA125 were 5 ng/ml, 37 U/ml, and 24 U/ml, respectively.

Cell culture and exosome extraction

All the BC cells were obtained from the National Biomedical Laboratory Cell Resource Bank. MCF-10a cells were donated by the Department of Pharmacology, China Medical University. Before extracting exosomes from the cell culture medium, the medium was changed to a serum-free medium and cultured for 24 h, following the instructions of the TransExo Cell Media Exosome Kit (Transgen, Beijing). Human plasma exosome extraction followed the instructions of the Plasma Exosome Total RNA Extraction Kit (Transgen, Beijing). The exosome downstream isolated from 1 ml of cell supernatant was used for transmission electron microscopy and that from 6 ml of cell supernatant was used for Western blot and qPCR experiments. The extracted RNA was stored at −80°C for later use.

Identification of extracellular vesicles of BC cells by transmission electron microscopy

The extracted EVs were resuspended in 30 µl of phosphate-buffered saline (PBS) and stored at 4°C. Excess liquid was removed from the edges of the beads with filter paper and stained with 1% uranyl acetate dye solution for 1 min. After drying at room temperature, EVs were observed with a transmission electron microscope (Hitachi ht7800).

Western blotting

Protein was prepared with SDS-PAGE loading buffer. Equal amounts (30 µl) of protein samples were separated by a 12% gel using sodium dodecyl sulfate-polyacrylamide gel electrophoresis (SDS-PAGE) and transferred onto PVDF membranes (Millipore, Billerica, MA, USA). Monoclonal rabbit anti-CD9 (ET1601-9, Huaan Bio) and monoclonal rabbit anti-CD81 (ET1611-87, Huaan Bio) were incubated overnight at 4°C with the membranes. Immune complexes were detected by enhanced chemiluminescence (Cell Signaling Technology).

Statistical analysis

Receiver operating characteristic (ROC) curves and the area under the ROC curve (AUC) were used to assess the diagnostic performance of hsa_circ_0058514. Differences in the values for plasma hsa_circ_0058514 between groups were determined by using the *t*-test and analysis of variance (ANOVA). Wilcoxon rank sum test and Pearson correlation analysis were used to determine correlations between expression levels of plasma hsa_circ_0058514 and clinical indexes. Statistical analysis was performed with SPSS (Version 22.0, IBM, USA) and presented graphically in GraphPad Prism 8.0. A *p*-value of 0.05 was statistically significant.

Results

Expression of plasma hsa_circ_0058514 in BC patients

Hsa_circ_0058514 molecules showed an upregulated molecule in various cancer tissues, including triple-negative BC tissues. In the present study, in order to verify the expression of hsa_circ_0058514 in plasma samples of BC patients, a reverse primer spanning the circRNA cleavage point was used to amplify circRNA by qRT-PCR. The results of agarose gel electrophoresis showed that the fragment size of hsa_circ_0058514 was 166 kb (Figure 1A). The amplified product was sequenced, and it was further found that the hsa_circ_0058514 sequence had a reverse splicing structure, consistent with the structure in the circRNA database Circbase (Figure 1B). The specific detection of qRT-PCR indicated that the expression of hsa_circ_0058514 was in the peripheral blood of BC patients.

The expression level of plasma hsa_circ_0058514 in BC patients and the association with clinicopathological features

To further determine the expression level of hsa_circ_0058514, the comparison between plasma samples from 135 non-metastatic BC patients and 95 age- and sex-matched healthy volunteers showed a higher expression in patients, which was three times that of the control group ($p < 0.001$) (Figure 2A). On this basis, we analyzed the correlation between the expression of plasma hsa_circ_0058514 and the clinicopathological characteristics of BC patients. Results indicated that the higher expression was associated with lymph node metastasis ($p < 0.001$), high tumor stage ($p < 0.05$), high risk of BC recurrence after surgery ($p < 0.001$), and non-luminal molecular type ($p < 0.05$), but was not associated with age, tumor diameter, and high expression of Ki-67 correlation (Table 1). Meanwhile, we also detected the expression level of hsa_circ_0058514 in 38 pairs of BC samples and adjacent tissues. The expression level of hsa_circ_0058514 in BC tissues was consistent with the expression level in plasma. The expression level of normal breast tissue was four times that of normal breast tissue, and the difference was statistically significant ($p < 0.001$) (Figure 2B). The stability experiment of hsa_circ_0058514 showed that the fresh plasma of the same patient was placed at room temperature for 24 h to extract RNA, and the expression of hsa_circ_0058514 was not significantly different ($p = 0.771$), compared with 0 h directly (Figure 2C). At the optimal cutoff value of 0.509 with the value of sensitivity and specificity considered to be maximal for hsa_circ_0058514, the sensitivity and specificity were 84.70% and 66.70%, and the AUC value was 0.828 with a 95% CI of 0.776–0.880 (Figure 2D).

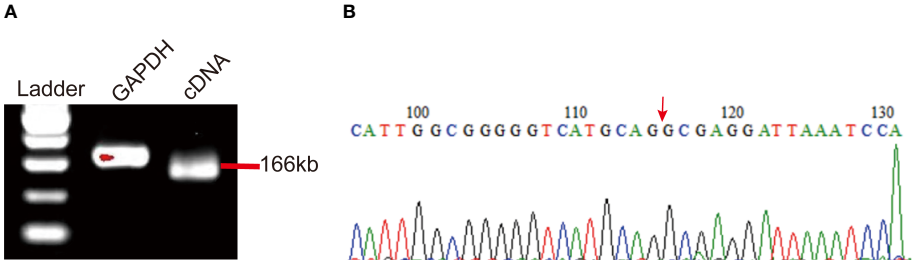

FIGURE 1
The identification and detection of hsa_circ_0058514 in BC patients' plasma. **(A)** PCR product of hsa_circ_0058514 in agarose gel electrophoresis. **(B)** The structure of hsa_circ_0058514 searched in Circbase.

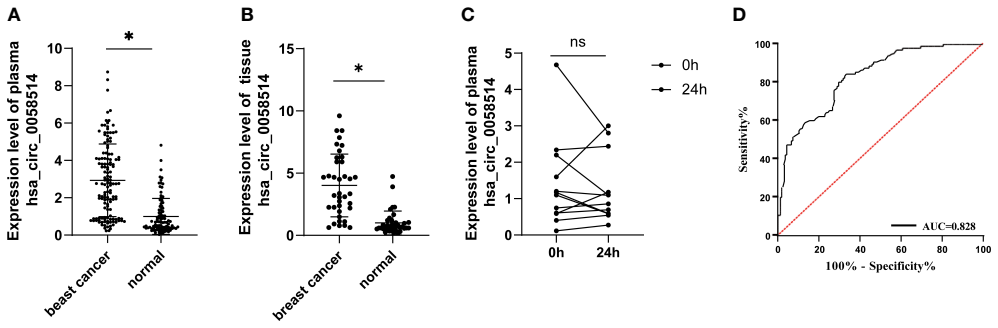

FIGURE 2
The expression level of hsa_circ_0058514 was higher in both plasma and cancer tissues of BC patients than healthy subjects. **(A)** The expression level of hsa_circ_0058514 detected in plasma and cancer tissues. **(B)** The stability experiment of hsa_circ_0058514 in plasma. **(C)** The stability experiment of hsa_circ_0058514. **(D)** The ROC curve of hsa_circ_0058514. *P < 0.05; ns, nonsignificant.

The superior diagnostic value of plasma hsa_circ_0058514 in BC patients without distant metastasis and early BC patients (stage 0 and stage 1)

In order to clarify the value of hsa_circ_0058514 expression in the diagnosis of BC patients without metastasis, we performed ROC curve analysis for its plasma expression level, and the results showed that hsa_circ_0058514 expression had better sensitivity (66.7%) and specificity (84.2%), and AUC was 0.828 with a 95% CI of 0.776–0.898. The sensitivity and specificity of CA153 were 21.5% and 92.6%, respectively, and AUC was 0.512 with a 95% CI of 0.437–0.586. CA125 was demonstrated with 42.2% sensitivity and 70.5% specificity, and AUC was 0.527 with

TABLE 1 The difference in hsa_circ_0058514 expression level associated with the clinical characteristics of BC patients.

	N (%)	△△CtM (IQR)	z/χ^2	*p*
Age (years)				
<50	75 (55.6)	2.902 (3.414)	−1.275	0.202
≥50	60 (44.4)	2.358 (3.217)		
Tumor size (cm)				
≤2	69 (51.1)	2.154 (2.981)	−1.919	0.055
>2	66 (48.9)	3.111 (4.039)		
Lymphatic metastasis				
With	68 (50.4)	1.915 (1.943)	−4.791	<0.001
Without	67 (49.6)	3.777 (2.378)		
Stage				
0–1	51 (37.8)	1.969 (1.921)	−3.443	<0.05
2–4	84 (62.2)	3.452 (3.628)		
Ki-67 expression				
Lower	59 (43.7)	2.671 (3.185)	−1.251	0.211
Higher	76 (56.3)	2.843 (3.735)		
Risk of BC recurrence after surgery				
Low	23 (17.0)	1.786 (2.124)*	37.017	<0.001
Medium	72 (53.3)	2.052 (2.795)*		
High	40 (29.7)	4.590 (2.075)		
Subtype				
Luminal type	79 (58.5)	2.066 (2.934)*	13.426	<0.05
HER-2 positive	37 (27.4)	2.765 (2.660)		
Triple negative	19 (14.1)	4.949 (1.726)		

*, P < 0.05.

a 95% CI of 0.453–0.602. CEA had 26.7% sensitivity and 89.5% specificity, and AUC was 0.573 with a 95% CI of 0.499–0.647 (Figure 3A). In early-stage (stage 0 and 1) BC patients, hsa_circ_0058514 showed a higher sensitivity than CA153, CA125, and CEA, which was 64.7% *vs.* 13.7%, 43.1%, and 51.0%. The specificity was also not much lower, 80.0% *vs.* 92.6%, 69.5%, and 55.8%. A higher AUC was also shown in hsa_circ_0058514, which was 0.776 *vs.* 0.463, 0.532, and 0.522; 95% CI was 0.700–0.852, 0.362–0.564, 0.431–0.634, and 0.424–0.621, respectively (Figure 3B), which suggested that plasma hsa_circ_0058514 might be used as a good biomarker for the diagnosis of BC.

Plasma hsa_circ_0058514 can dynamically monitor the effect of neoadjuvant therapy for BC

Among 40 pairs of BC plasma samples collected before and after neoadjuvant therapy, the expression of hsa_circ_0058514 in plasma significantly decreased ($p < 0.001$) (Figure 4). According to the pathological MP grading of neoadjuvant chemotherapy, RESIST grading of imaging target lesions before and after treatment, and histological grading, molecular type, age, tumor stage before treatment, and Ki-67 expression levels were stratified, and the association between the changes of these clinical indicators and

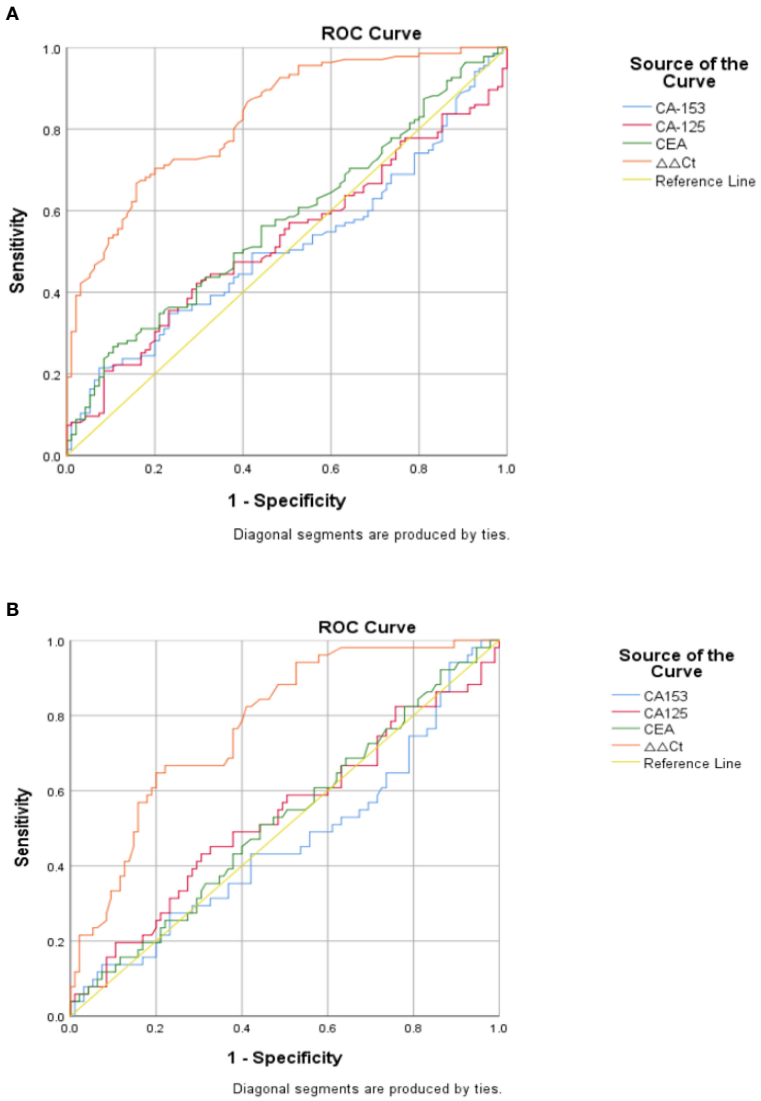

FIGURE 3
Diagnostic value of hsa_circ_0058514 for BC was evaluated by ROC curve. **(A)** In BC patients without metastasis. **(B)** In early BC patients (stages 0 and 1).

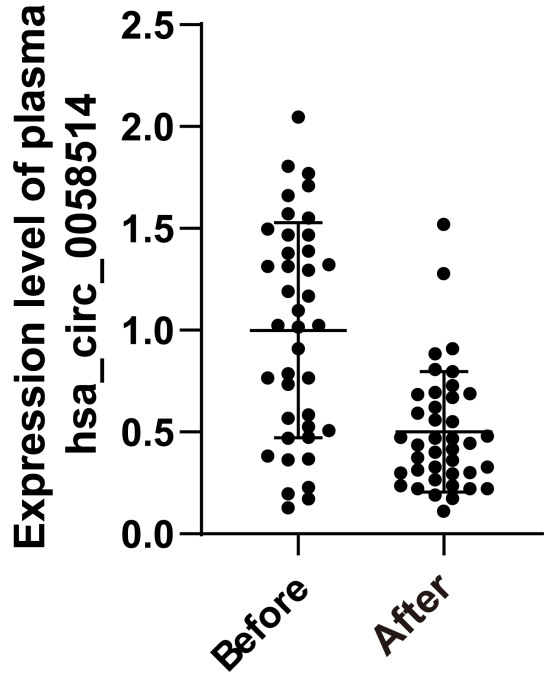

FIGURE 4
The dynamic monitoring effect of hsa_circ_0058514. The expression level of hsa_circ_0058514 plasma detected in samples of 40 pairs of BC patients before and after neoadjuvant therapy.

the difference of hsa_circ_0058514 before and after treatment was analyzed. The results showed that the decreased expression level of hsa_circ_0058514 was associated with a higher pathological MP grade ($p = 0.004$) and a greater degree of regression of the imaging target lesions ($p = 0.005$), but was not significantly correlated with histological grade, molecular type, age, tumor stage before treatment, and Ki-67 expression (Table 2). It is suggested that plasma hsa_circ_0058514 can be used as a predictor of the efficacy of BC treatment.

TABLE 2 The correlation analysis between expression level of hsa_circ_0058514 and clinicopathological features.

Clinicopathological features	*r* value	*p*-value
Subtypes	0.168	0.299
MP grade	0.444	0.004*
RESIST	0.433	0.005*
Histological grade	−0.002	0.993
Age	0.010	0.952
Stage	0.284	0.075
Ki-67 expression level	0.195	0.227

*P < 0.05.

BC intracellular and EVs encapsulate hsa_circ_0058514 and the detection in plasma

Via transmission electron microscopy, we observed ectosomes in the serum-free culture medium of BC cells, which were disc-like vesicle-like structures with a diameter of 100–500 nm (Figure 5A). The vesicle membrane marker proteins CD9 and CD81 were also proved by Western blotting (Figure 5B). The expression of hsa_circ_0058514 from extracellular vesicles was also detected in EVs extracted from the serum-free culture medium of normal breast ductal epithelial MCF-10a cells, and three different BC cell lines including hormone receptor-positive MCF-7 cells, SK-BR-3 cells with Her-2 overexpression, and triple-negative BT-549 cells (Figure 5C). Moreover, the expression level of normal mammary duct epithelial cells was significantly lower than that of various BC cells, and the difference was statistically significant ($p < 0.001$) (Figure 5D). We further examined the correlation between plasma and plasma extracellular vesicle expression levels in 16 patients with BC, and the qPCR results showed no significant difference between the two groups (Figure 5E).

Discussion

In the present study, it was demonstrated that hsa_circ_0058514 exists in BC patients' plasma and tumor tissue, and the expression level was associated with lymphatic metastasis, higher tumor stages, recurrence, and non-luminal subtypes. The diagnostic value of plasma hsa_circ_0058514 in early BC patients without distant metastasis was better than CA125, CEA, and CA153, which can also be used to dynamically monitor the effect of neoadjuvant therapy for BC. We also found hsa_circ_0058514 enriched in EVs of plasma and BC tissue.

With the development and widespread application of high-throughput RNA sequencing technology, more evidence suggests that circRNAs might play an important role in the pathogenesis of a variety of diseases, especially the occurrence, development, invasion, metastasis, and drug resistance of cancer (9). Through circRNA chip analysis, it was demonstrated that there were 41 circRNAs with more than two times expression in the plasma of BC patients, of which 19 were upregulated and 22 were downregulated (10). Researchers developed a circular RNA high-throughput workflow to identify unique circular RNAs in breast tumor samples and classify them according to the three BC subtypes (11). An increasing amount of evidence suggests that circRNAs participate in carcinogenesis and the progression of TNBC, which, in turn, can be used as a potential diagnostic and prognostic biomarkers or therapeutic targets for TNBC (12). For example, several upregulated circRNAs like SEPT9, circGNB1, circPGAP3, and hsa_circ_0058514 promote tumor cell proliferation both *in vitro* and *in vivo*, and are associated with larger tumor sizes and shorter survival times for TNBC patients (12, 13). It was also demonstrated that they also

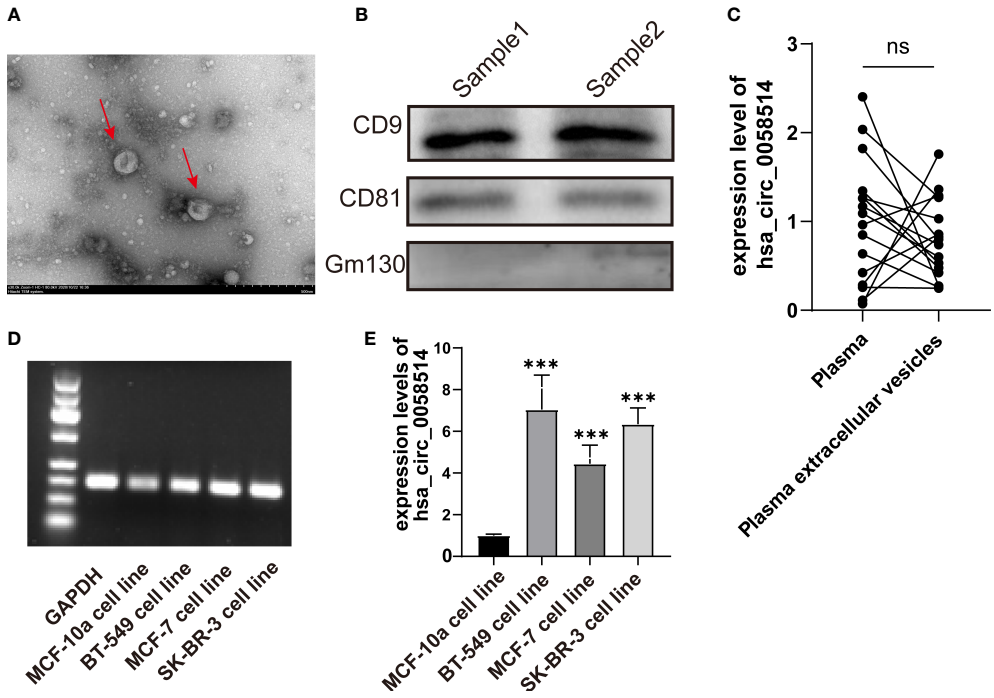

FIGURE 5
The detection of EVs in BC patients. **(A)** EVs with a diameter of 100–500 nm observed by transmission electron microscopy. **(B)**. Membrane marker proteins CD9 and CD81 detected by Western blotting. **(C)** The detection and **(D)** the quantitative results of hsa_circ_0058514 in EVs of four BC cell lines; the size was 166 bp. **(E)** The expression level of hsa_circ_0058514 in plasma and plasma extracellular vesicle of 16 BC patients. ***P < 0.001; ns, nonsignificant.

contributed to the invasion and metastasis of TNBC cells both *in vitro* and *in vivo*, which might be correlated with advanced TNM stage and poor prognosis of TNBC patients, like circSEPT9, circGNB1, and hsa_circ_0058514 (12, 13). Hsa_circ_0005320 and hsa_circ_0058514 were also associated with decreased cell apoptosis rates of TNBC cells (12, 13). Meanwhile, it was proved that hsa_circ_0058514 significantly promoted tumor angiogenesis *via* CCNEI, associated with positive lymph node metastasis (13). The above-mentioned studies reported the roles of hsa_circ_0058514 in BC, and our study also demonstrated a higher level of expression of hsa_circ_0058514 in BC patients than in healthy subjects.

Notably, hsa_circ_0058514 was detected not only in TNBC, but also in two other subtypes of BC, Her-2 positive and luminal, which revealed its profound clinical application for BC diagnosis. We also compare its diagnostic effect and power with other identified biomarkers, CA153, CA125, and CEA. In addition, we also demonstrate its dynamic monitoring effect for early BC without metastasis. A previous study put forward overexpressed linc-ROR, which might be used as a potential biomarker for BC diagnosis and dynamic monitoring (14). However, this non-coding RNA was also identified in multiple types of cancers, including pancreatic cancer, hepatocellular cancer, bladder cancer, and nasopharyngeal carcinoma (14). Distinct from the above cancer types, hsa_circ_0058514 can be detected in cervical cancer (15), lung cancer (16), colorectal cancer (17), and esophageal cancer (18). Upregulated hsa_circ_0058514 is expressed in cervical cancer tissues and promotes RAF1 expression through the activation of miR-370-3p, which further regulates ovarian cancer progression *via* the RAF/MEK/ERK pathway (15). The hsa_circ_0058514 sponge miR-203 promotes EMT and metastasis of non-small cell lung cancer by upregulating the expression of ZNF28 (16). Hsa_circ_0058514 acts as a sponge of miR-4306 to stimulate the progression of esophageal cancer by regulating the expression of MAPRE2 (18). Hence, the combination of the two biomarkers can be useful for the differential diagnosis of various possible cancers from BC.

In recent years, EVs have received extensive attention as a novel structure vital for intercellular communication mechanism (19). Especially in the field of cancer, there is increasing evidence that EVs play an important role in tumor metastasis and dissemination, for example, the establishment of pre-metastatic niche, angiogenesis, and the formation of cancer-associated fibroblast heterogeneity (20). According to the size and origin of EVs, they can be roughly classified as follows: exosomes (50–200 nm), microvesicles (100–1,000 nm), apoptotic bodies (50–4,000 nm), and prostatic corpuscles (40–

500 nm) (19). Furthermore, EVs have been reported to carry a variety of molecules, such as nucleic acids, that reflect the phenotype of their parental cells (19, 21). Since EVs circulate stably in almost all body fluids, they also have great potential as tumor biomarkers (20, 22), even as drug delivery administration systems transferring miRNAs or therapeutic agents to target cells (21). A total of 439 circRNAs detected in plasma EVs with significantly different levels between BC patients and healthy subjects indicated the potential clinical application (23). Moreover, the circRNAs showed temporospatial characteristics that were exhibited in a patient-specific and stage-specific manner, which also implied the relatively more prominent advantage of its specificity (23). It was demonstrated in our preliminary results that hsa_circ_0058514 was encapsulated in EVs, which provided us with a potential mechanism that needs to be investigated as an alternative treatment for BC.

Although this study is limited by its small sample size, our results suggest that upregulation of hsa_circ_0058514 plays an important role in breast cancer development and progression. Large-scale prospective studies should be carried out in the future to verify the accuracy and validity of hsa_circ_0058514 as a representative biomarker for BC. We will further follow up on the prognosis of BC patients to observe the prognostic value of hsa_circ_0058514. In addition, we hope to carry out further animal experiments to further elucidate the secretion mode of exovesicle hsa_circ_0058514 *in vivo*.

Data availability statement

The original contributions presented in the study are included in the article/Supplementary Material. Further inquiries can be directed to the corresponding authors.

Ethics statement

This study was reviewed and approved by This study was approved by the Ethics Committee of The First Hospital of Qinhuangdao (No. 2022A011 and 2022DW004), and written informed consents were obtained from each study subject. The patients/participants provided their written informed consent to participate in this study.

Author contributions

YJL, YXQ and MH designed the study. JNL, XYP, XHS and LZ performed the experiments. JXC and WHL collated the data. JZ, TL and QL carried out the data analyses. YY and YZ contributed to drafting the manuscript. All authors have read and approved the final submitted manuscript.

Acknowledgments

The relevant work of transmission electron microscope imaging was completed in the Electron Microscope Experimental Center of Hebei Medical University. We thank Professor Zhou Chenming for his help in sample preparation and image collection.

Conflict of interest

Author YZ was employed by Hangzhou Xiaoshan Yaoran Medical Cosmetology Clinic Co. Ltd.

The remaining authors declare that the research was conducted in the absence of any commercial or financial relationships that could be construed as a potential conflict of interest.

Publisher's note

All claims expressed in this article are solely those of the authors and do not necessarily represent those of their affiliated organizations, or those of the publisher, the editors and the reviewers. Any product that may be evaluated in this article, or claim that may be made by its manufacturer, is not guaranteed or endorsed by the publisher.

Supplementary material

The Supplementary Material for this article can be found online at: https://www.frontiersin.org/articles/10.3389/fonc.2022.995196/full#supplementary-material

References

1. Sung H, Ferlay J, Siegel RL, Laversanne M, Soerjomataram I, Jemal A, et al. Global cancer statistics 2020: Globocan estimates of incidence and mortality worldwide for 36 cancers in 185 countries. *CA Cancer J Clin* (2021) 71(3):209–49. doi: 10.3322/caac.21660

2. Harbeck N, Penault-Llorca F, Cortes J, Gnant M, Houssami N, Poortmans P, et al. Breast cancer. *Nat Rev Dis Primers* (2019) 5(1):66. doi: 10.1038/s41572-019-0111-2

3. Sadeghalvad M, Mohammadi-Motlagh HR, Rezaei N. Immune microenvironment in different molecular subtypes of ductal breast carcinoma. *Breast Cancer Res Treat* (2021) 185(2):261–79. doi: 10.1007/s10549-020-05954-2

4. Pesapane F, Suter MB, Rotili A, Penco S, Nigro O, Cremonesi M, et al. Will traditional biopsy be substituted by radiomics and liquid biopsy for breast cancer diagnosis and characterisation? *Med Oncol* (2020) 37(4):29. doi: 10.1007/s12032-020-01353-1

5. Tay TKY, Tan PH. Liquid biopsy in breast cancer: A focused review. *Arch Pathol Lab Med* (2021) 145(6):678–86. doi: 10.5858/arpa.2019-0559-RA

6. Qu S, Yang X, Li X, Wang J, Gao Y, Shang R, et al. Circular rna: A new star of noncoding rnas. *Cancer Lett* (2015) 365(2):141–8. doi: 10.1016/j.canlet.2015.06.003

7. Li HF, Xie Q, Nie QW, Ye X. Prostate specific antigen as a biomarker for breast cancer: A meta-analysis study. *Eur Rev Med Pharmacol Sci* (2018) 22 (13):4188–95. doi: 10.26355/eurrev_201807_15412

8. Maass PG, Glažar P, Memczak S, Dittmar G, Hollfinger I, Schreyer L, et al. A map of human circular rnas in clinically relevant tissues. *J Mol Med (Berl)* (2017) 95 (11):1179–89. doi: 10.1007/s00109-017-1582-9

9. Patop IL, Kadener S. Circrnas in cancer. *Curr Opin Genet Dev* (2018) 48:121–7. doi: 10.1016/j.gde.2017.11.007

10. Xu Z, Yan Y, Zeng S, Dai S, Chen X, Wei J, et al. Circular rnas: Clinical relevance in cancer. *Oncotarget* (2018) 9(1):1444–60. doi: 10.18632/oncotarget.22846

11. Nair AA, Niu N, Tang X, Thompson KJ, Wang L, Kocher JP, et al. Circular rnas and their associations with breast cancer subtypes. *Oncotarget* (2016) 7 (49):80967–79. doi: 10.18632/oncotarget.13134

12. Lyu L, Zhang S, Deng Y, Wang M, Deng X, Yang S, et al. Regulatory mechanisms, functions, and clinical significance of circrnas in triple-negative breast cancer. *J Hematol Oncol* (2021) 14(1):41. doi: 10.1186/s13045-021-01052-y

13. Yang R, Xing L, Zheng X, Sun Y, Wang X, Chen J. The circrna Circagfg1 acts as a sponge of mir-195-5p to promote triple-negative breast cancer progression through regulating Ccne1 expression. *Mol Cancer* (2019) 18(1):4. doi: 10.1186/s12943-018-0933-7

14. Zhao T, Wu L, Li X, Dai H, Zhang Z. Large Intergenic non-coding rna-ror as a potential biomarker for the diagnosis and dynamic monitoring of breast cancer. *Cancer biomark* (2017) 20(2):165–73. doi: 10.3233/cbm-170064

15. Wu F, Zhou J. Circagfg1 promotes cervical cancer progression *Via* mir-370-3p/Raf1 signaling. *BMC Cancer* (2019) 19(1):1067. doi: 10.1186/s12885-019-6269-x

16. Xue YB, Ding MQ, Xue L, Luo JH. Circagfg1 sponges mir-203 to promote emt and metastasis of non-Small-Cell lung cancer by upregulating Znf281 expression. *Thorac Cancer* (2019) 10(8):1692–701. doi: 10.1111/1759-7714.13131

17. Zhang L, Dong X, Yan B, Yu W, Shan L. Circagfg1 drives metastasis and stemness in colorectal cancer by modulating Yy1/Ctnnb1. *Cell Death Dis* (2020) 11 (7):542. doi: 10.1038/s41419-020-2707-6

18. Zhang D, Li C, Cheng N, Sun L, Zhou X, Pan G, et al. Circagfg1 acts as a sponge of mir-4306 to stimulate esophageal cancer progression by modulating Mapre2 expression. *Acta Histochem* (2021) 123(7):151776. doi: 10.1016/j.acthis.2021.151776

19. Raposo G, Stahl PD. Extracellular vesicles: A new communication paradigm? *Nat Rev Mol Cell Biol* (2019) 20(9):509–10. doi: 10.1038/s41580-019-0158-7

20. Naito Y, Yamamoto Y, Sakamoto N, Shimomura I, Kogure A, Kumazaki M, et al. Cancer extracellular vesicles contribute to stromal heterogeneity by inducing chemokines in cancer-associated fibroblasts. *Oncogene* (2019) 38(28):5566–79. doi: 10.1038/s41388-019-0832-4

21. Rahbarghazi R, Jabbari N, Sani NA, Asghari R, Salimi L, Kalashani SA, et al. Tumor-derived extracellular vesicles: Reliable tools for cancer diagnosis and clinical applications. *Cell Commun Signaling CCS* (2019) 17(1):73. doi: 10.1186/s12964-019-0390-y

22. Verma M, Lam TK, Hebert E, Divi RL. Extracellular vesicles: Potential applications in cancer diagnosis, prognosis, and epidemiology. *BMC Clin Pathol* (2015) 15:6. doi: 10.1186/s12907-015-0005-5

23. Lin L, Cai GX, Zhai XM, Yang XX, Li M, Li K, et al. Plasma-derived extracellular vesicles circular rnas serve as biomarkers for breast cancer diagnosis. *Front Oncol* (2021) 11:752651. doi: 10.3389/fonc.2021.752651

frontiers | Frontiers in Oncology

TYPE Original Research
PUBLISHED 10 November 2022
DOI 10.3389/fonc.2022.982011

Check for updates

OPEN ACCESS

EDITED BY
Annarita Fanizzi,
National Cancer Institute Foundation (IRCCS), Italy

REVIEWED BY
Marco Materazzo,
Policlinico Tor Vergata, Italy
Hung-Yin Lin,
National University of Kaohsiung, Taiwan

*CORRESPONDENCE
Zhao-Peng Zhang
happy110@126.com
Yong-Sheng Wang
wangysh2008@aliyun.com

SPECIALTY SECTION
This article was submitted to Breast Cancer, a section of the journal Frontiers in Oncology

RECEIVED 30 June 2022
ACCEPTED 20 October 2022
PUBLISHED 10 November 2022

CITATION
Bi Z, Qiu P-F, Yang T, Chen P, Song X-R, Zhao T, Zhang Z-P and Wang Y-S (2022) The modified shrinkage classification modes could help to guide breast conserving surgery after neoadjuvant therapy in breast cancer. *Front. Oncol.* 12:982011. doi: 10.3389/fonc.2022.982011

COPYRIGHT
© 2022 Bi, Qiu, Yang, Chen, Song, Zhao, Zhang and Wang. This is an open-access article distributed under the terms of the Creative Commons Attribution License (CC BY). The use, distribution or reproduction in other forums is permitted, provided the original author(s) and the copyright owner(s) are credited and that the original publication in this journal is cited, in accordance with accepted academic practice. No use, distribution or reproduction is permitted which does not comply with these terms.

The modified shrinkage classification modes could help to guide breast conserving surgery after neoadjuvant therapy in breast cancer

Zhao Bi[1], Peng-Fei Qiu[1], Tao Yang[2], Peng Chen[1], Xian-Rang Song[1], Tong Zhao[1], Zhao-Peng Zhang[1*] and Yong-Sheng Wang[1*]

[1]Shandong Cancer Hospital and Institute, Shandong First Medical University and Shandong Academy of Medical Sciences, Jinan, Shandong, People's Republic of China, [2]The First People's Hospital of Lian Yun Gang, Radiotherapy Department, Xuzhou, Jiangsu, China

Purpose: The traditional shrinkage classification modes might not suitable for guiding breast conserving surgery (BCS) after neoadjuvant therapy (NAT). Aim was to explore the modified shrinkage classification modes to guide BCS after NAT.

Methods: From April 2010 to 2018, 104 patients were included. All patients underwent MRI examinations before and after NAT. Residual tumors were removed and divided into more than 30 tissue blocks at 5-mm intervals. After performing routine procedures for paraffin-embedded histology, we made semiserial sections (6-μm thick). The MRI and pathology 3D models were reconstructed with 3D-DOCTOR software. Combined with traditional shrinkage modes and efficacy of NAT, we derived modified shrinkage classification modes which oriented by BCS purpose: modified concentric shrinkage modes (MCSM) and modified non concentric shrinkage modes (MNCSM). The MCSM means the longest diameter of residual tumor was less than 50% and ≤2cm in comparison with the primary tumor before NAT. Other shrinkage modes were classified as MNCSM.

Results: According to traditional shrinkage modes, 50 (48.1%) cases were suitable for BCS;while 70 (67.3%) cases were suitable for BCS according to the modified shrinkage modes (p=0.007). The consistency of MRI 3D reconstruction in assessing modified shrinkage classification modes was 93.2%, while it was 61.5% when assessing traditional shrinkage modes. Multivariate analysis showed that primary tumor stage, mammographic malignant calcification, molecular subtypes and nodal down-staging after NAT were independent predictors of modified shrinkage modes (all p<0.05). A nomogram was created based on these four predictors. With a median follow-up time of 77 months, the recurrence/metastasis rate in the MCSM and MNCSM group was 7.1% and 29.4%, respectively.

Conclusion: Modified shrinkage classification modes could help to guide the individualized selection of BCS candidates and scope of resection after NAT. MRI 3D reconstruction after NAT could accurately predict modified shrinkage modes and extent of residual tumor.

KEYWORDS

breast cancer, neoadjuvant therapy, shrinkage, breast conserving surgery, prognosis

Introduction

Neoadjuvant therapy (NAT) is currently administered to patients with locally advanced breast cancers, to breast cancer of poor prognosis (triple-negative and HER2-positive tumors, or with nodal involvement and/or high proliferation rates), or to early-stage breast cancer having an indication of systemic therapy (1–4). A major clinical benefit of NAT is downstaging of the tumor. As a result, inoperable tumors may become operable and patients with large tumors could receive breast conserving surgery (BCS) to facilitate better cosmetic outcomes (2, 5, 6).

For patients who plan to receive BCS after NAT, the 5-year local-regional reference (LRR) rate was 2~7% in patients with tumor-free margins, but the risk increased to as high as 22% if the margin was positive (7, 8). Three strategies to mitigate the increased LRR after BCS in tumors downsized by NAT should be considered: careful tumor localization (including place marker clip, tumor range, and shrinkage modes), detailed pathological assessment, and appropriate radiotherapy (8). After NAT, tumor extent assessment can be difficult and shrinkage modes can be heterogeneous, making surgery technically more difficult than without NAT. So, for patients who plan to receive BCS after NAT, it is important to accurately assess residual tumor extent and shrinkage modes after NAT to ensure negative margins and reduce LRR as well as resection rate (9). The traditional view believed that patients with multinodular lesions, solitary lesion with adjacent spotty lesions and diffuse lesions were not suitable for BCS. In cases of multifocal residual tumor and/or cases of "scattered" residual tumor, the 2017 St. Gallen consensus conference expressed an opinion to favor more "generous" margins (10). However, the 2019 St. Gallen consensus conference recommended that the optimal resection remains removal of all known residual as opposed to original tumor lesions with a margin goal of "no ink on tumor" regardless of the presence of unifocal or multi-focal disease (11). That is to say, the traditional shrinkage classification modes would not sufficient as an indication for BCS.

Therefore, the aim of the present study is to explore and definite the modified shrinkage classification modes which oriented by BCS purpose after NAT.

Patients and methods

Patients

Between April 2010 to 2018, patients who treated at Shandong Cancer Hospital Breast Cancer Center were enrolled in this study. The study was approved by the Shandong Cancer Hospital Ethics Committee (No. SDTHEC20110324). Written informed consent was obtained from all patients before participation in the study, and all procedures were in accordance with the ethical standards of the responsible institutional committee on human experimentation and with the Helsinki Declaration. Adult women were included in this study if they 1) had histologically confirmed invasive breast carcinoma; 2) were clinical staging $T_{1\text{-}4}N_{0\text{-}3}M_0$; 3) agreed to undergone NAT for the primary breast cancer. Patients were excluded according to the pre-established exclusion criteria if they had undergone therapy prior to NAT, concurrent cancer, bilateral breast cancer, or distant metastases.

In this study, we constructed the MRI and pathology three-dimensional (3D) reconstruction model of residual tumor. All patients underwent MRI examinations before and after NAT. The MRI and pathology 3D models of residual tumors were reconstructed with 3D-DOCTOR software. Then we explored and definite the modified shrinkage classification modes which oriented by BCS purpose after NAT, and assessed the advantage of modified shrinkage classification modes in guiding BCS after NAT. In addition, we assessed the accuracy of MRI 3D reconstruction in predicting the extent of residual tumor and modified shrinkage classification modes. Next, we analyzed the predictors of modified shrinkage classification modes, and generated a nomogram in predicting the modified shrinkage classification modes after NAT. The consort diagram of the study was illustrated in Figure 1.

Treatment

Each patient underwent MRI examination twice, that is, before core biopsy and within 3 weeks after the last cycle of

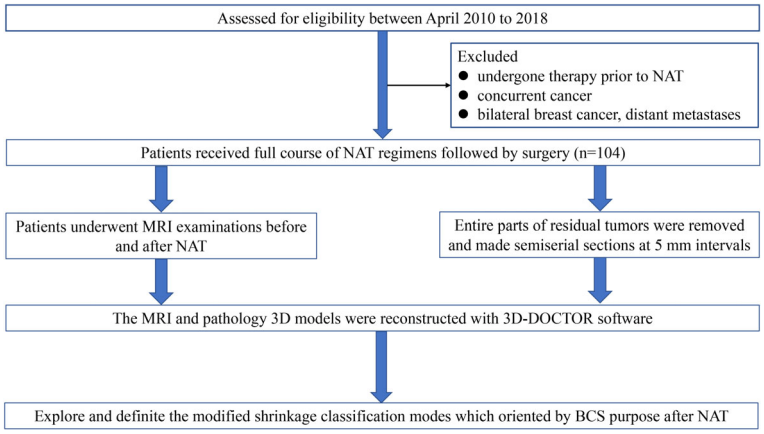

FIGURE 1
The consort diagram of the study.

NAT. The mean interval time between the preoperative MRI examination and final surgery was 3 days (range 1~5 days).

Before NAT, all patients received core biopsy of the breast tumor and fine-needle aspiration of the clinical/image positive/suspicious axillary nodes guided by ultrasound. Hormone receptor (HR) was defined as positive with more than one percent expression rate. HER-2 receptor was considered as positive with immune-histochemical staining of 3+, or fluorescence *in situ* hybridization that was amplified (12). After these evaluations, molecular subtypes could be classified into Luminal A subtype, Luminal B HER2 negative (Luminal B HER2-) subtype, HER-2 positive (HER2+) and Tripe negative (TN) subtypes to precisely evaluate the biomarker effect.

All patients received standard dose four cycles of anthracycline and cyclophosphamide followed by four cycles of paclitaxel before surgery. HER2+ patients received anti-HER-2 targeted therapy.

MRI acquisition and MRI 3D reconstruction

MRI was performed using 3.0T scanners (Philips Medical Systems, Best, The Netherlands) with a dedicated 7 elements sense breast coil. Patients underwent imaging in the prone position with breast immobilized. Our imaging protocol included a localizing sequence followed by unilateral fast spin-echo T2-weighted imaging. The breast MRI imaging of all patients were independently assessed by one radiologist with 15 years of experience in reading breast MRI. He was unaware of the pathological outcomes and used the same measurement standard to measure the tumor size. In cases of rim enhancement, the necrotic core was included in measurement of the largest diameter. In cases of multifocal or diffuse tumor growth, the complete enhancing area, including intermediate (non-enhancing) tissue around the tumor, was measured on maximum intensity projection images. After scanning of the whole breast, bidimensional MRI images were transferred to 3D-DOCTOR software workstation to create and analysis 3D image of the breast (Figure 2A).

After delineating the extent of residual tumors in each MRI image, we chosen the command "3D Rendering/Surface Rendering/Simple surface", then the MRI 3D model could be reconstructed (Figure 2B) (13). The shape and location of tumors in the breast and their relation to the adjacent tissues were examined. Using 3D images of MRI reconstruction model, the extent of each tumor was assessed by its largest diameter in three reformatted planes (sagittal, axial, and coronal) at initial and late enhancements. When there was no discernible contrast enhancement or a faint enhancement equal to the background normal tissue in previous tumor bed, this case was determined as radio complete response on MRI (14).

Sub-serial sections of breast specimens and pathology 3D reconstruction

After mastectomy, according to the blue dye labeled extent of tumors before surgery, the tumor specimens were excised with a distance of 3.0 cm from the tumor boundary. After BCS, entire excised specimens were prepared for sub-serial sections.

The upper margins of specimens were marked with black ink, double-needle dyeing method to mark anchor points. Then the specimens were stored in a -20°C refrigerator. Then the specimen was cut into several blocks at 5-mm intervals based on the markers (Figure 2C). The tissue blocks were marked with continuous numbers and were immersed in 10% formalin solution for 48h. After performing routine procedures for dehydration and paraffin-embedded histology, we made one

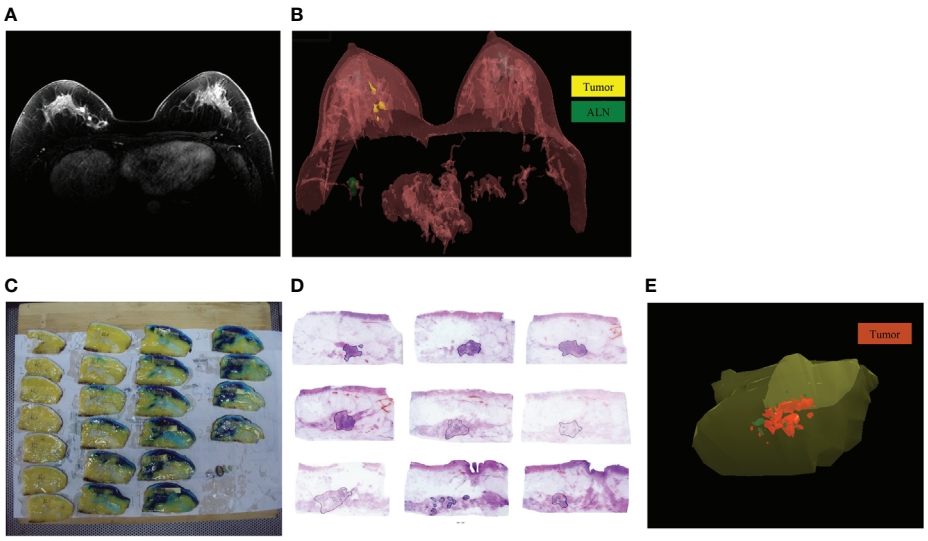

FIGURE 2
The MRI and pathology 3D reconstruction. **(A)**: The MRI imaging of residual tumor after NAT; **(B)**: The MRI 3D reconstruction model of residual tumor after NAT; **(C)**: The specimen was cut into several blocks at 5-mm intervals based on the markers; **(D)**: The extent of residual tumors was delineated under microscope; **(E)**: The pathology 3D reconstruction model of residual tumor after NAT.

section of 4~6-μm thick in each block. The sections were cut using a Leica RM2010 slicer (Leica Biosystems, Nussloch, Germany) and stained with hematoxylin and eosin (13, 14).

Invasive tumors, calcification and ductal carcinoma *in situ* (DCIS) were delineated and recorded under microscope respectively (Figure 2D). The sections' images were collected with the Epson V600 scanner (resolution 360 bpi) and stored as JPG format. The JPG data were integrated and calibrated based on anchor points using Photoshop software, then the sections' images were imported into the 3D-DOCTOR software. With the "3D Rendering/Surface Rendering/Simple surface" command, the pathology 3D reconstruction model of residual tumor after NAT was presented (Figure 2E). The residual invasive tumor and calcification were marked with different colors in the pathology 3D reconstruction.

The measurement of residual tumor

The longest diameter, maximum cross-sectional area and volume of residual tumors were measured according to the MRI and pathology 3D reconstruction models. The longest diameter refers to the longest distance in the 3D planes of residual tumors. Using the 3D-DOCTOR software, we select the "Boundaries in All Planes" command to project all the outlined tumor boundaries into the same plane. Then we measure the longest diameter and the longest vertical diameter of each plane. The maximum cross-sectional area would be calculated (the longest diameter × the longest vertical diameter). The volume could be automatically calculated by selecting the "Tools/Calculate Volumes" command from the 3D-DOCTOR software.

After surgery, the histopathological diagnosis of residual tumors was interpreted by two experienced pathologists. The tumor was evaluated using the Miller-Payne grading system. Surgical pCR was defined as no residual invasive tumor or DCIS within all slices (15).

Shrinkage classification modes after NAT

The traditional shrinkage classification modes of residual tumors after NAT were divided into five categories: surgical pCR, solitary lesion without surrounding lesions, multinodular lesions, solitary lesion with adjacent spotty lesions and diffuse lesions (Figure 3A) (16–19).

The BCS indications after NAT of MD Anderson Cancer Center (MDACC) include: ypT<2 cm, no vascular lymphatic invasion, single-focal lesions, and negative margins (20). Combined with the BCS indications of MDACC and traditional shrinkage classification modes, we derived and definite the modified shrinkage classification modes which oriented by BCS purpose: modified concentric shrinkage modes (MCSM) and modified non concentric shrinkage modes (MNCSM) (9). As the BCS indications after NAT of MDACC include diameter of residual tumor <2 cm, so we chose 2 cm as tumor size cutoffs. The MCSM means the longest diameter of residual tumor was less than 50% and ≤2cm in comparison with the primary tumor before NAT, including surgical pCR, solitary lesion without surrounding lesions, multinodular

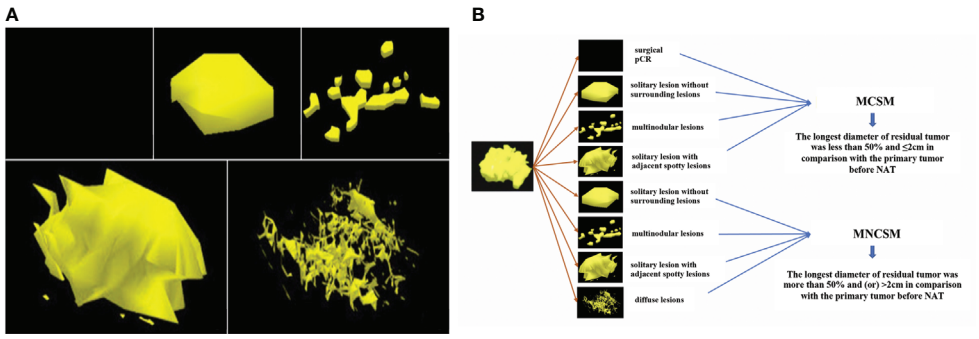

FIGURE 3
The shrinkage modes of residual tumors after NAT. **(A)**: The traditional shrinkage classification modes, including surgical pCR, solitary lesion without surrounding lesions, multinodular lesions, solitary lesion with adjacent spotty lesions and diffuse lesions. **(B)**: The modified shrinkage classification modes, including MCSM and MNCSM.

lesions and solitary lesion with adjacent spotty lesions. The longest diameter of residual tumor was more than 50% and (or) >2cm in comparison with the primary tumor before NAT were classified as MNCSM, including solitary lesion without surrounding lesions, multinodular lesions, solitary lesion with adjacent spotty lesions and diffuse lesions (Figure 3B). The modified shrinkage classification modes dismissed the shape, and focuses on efficacy and tumor extent, and our purpose was to guide BCS according to efficacy and tumor extent.

Statistical analysis

For diagnostic accuracy based on the measurement of residual tumor size, the gold standard was defined as the pathology 3D reconstruction model-measured tumor size. Spearman rank correlation test and Bland-Altman method were used to evaluate the correlation and consistency between MRI and pathology 3D reconstruction measurement of residual tumor.

The association of different clinicopathological variables with modified shrinkage classification modes was analyzed. Pearson chi-square test or Fisher exact test was used to perform univariate analysis on categorical variables. Multivariable logistic regression analysis was conducted to identify the independent predictive factors of MCSM by using backward stepwise analysis.

A nomogram was developed based on variables in the final model with $p<0.05$ using "rms" package for R. Calibration of the nomogram was carried out by internal validation using the bootstrap resampling approach and was displayed using a calibration curve. The discrimination of the model was evaluated using the area under the curve (AUC) value of the ROC curve. Statistical analyses were performed using SPSS Statistics 22.0 software (IBM Corporation, Armonk, NY, USA) and R version 3.3.3 software (The R Foundation for Statistical Computing, Austria, Vienna). A $p<0.05$ was considered statistically significant.

Results

Patients' characteristics

Between April 2010 to 2018, 104 patients received full course of NAT regimens followed by surgery in Breast Cancer Center. The median age of patients was 49 years old (rang 25 to 70 years). The clinical characteristics of the patients are summarized in Table 1.

The different shrinkage classification modes after NAT

The traditional shrinkage classification modes presented by pathology 3D reconstruction were 34, 16, 19, 25, 10 cases among surgical pCR, solitary lesion without surrounding lesions, multinodular lesions, solitary lesion with adjacent spotty lesions and diffuse lesions, respectively (Table 2; Figure 3A). The modified shrinkage classification modes presented by pathology 3D reconstruction were 70 and 34 cases among MCSM and MNCSM, respectively.

The modified shrinkage classification modes were more suitable for guiding BCS

According to the traditional shrinkage classification modes, 50 (48.1%) cases in this study were suitable for BCS;while 70 (67.3%) cases were suitable for BCS according to the modified shrinkage classification modes ($p=0.007$, Table 3). According to the traditional shrinkage classification modes, patients with multinodular lesions and solitary lesions with adjacent spotty lesions were not suitable for BCS; while there were 52.3% (23/44)

10.3389/fonc.2022.982011

TABLE 1 The clinical characteristics of 104 patients.

Characteristic		No.	%
Molecular subtypes			
	Luminal A subtype	23	22.1
	Luminal B HER-2 negative	21	20.2
	HER-2 positive	33	31.7
	Tripe negative	27	26.0
Clinical nodal stage			
	cN_0	18	17.3
	cN_1	41	39.4
	cN_2	32	30.8
	cN_3	13	12.5
Clinical tumor stage			
	cT_1	11	10.6
	cT_2	68	65.4
	cT_3	13	12.5
	cT_4	12	11.5
Breast surgery			
	Mastectomy	78	78.8
	BCS	22	21.2

of them present with MCSM, they were still suitable for BCS. Among patients with solitary lesions without surrounding lesions, there were 18.8% (3/16) of patients present with MNCSM, they were still not suitable for BCS (Table 2).

MRI 3D reconstruction could accurately assess modified shrinkage classification modes

The accuracy, sensitivity, specificity, positive predictive value and negative predictive value of MRI 3D reconstruction in assessing traditional shrinkage modes were 84.6%, 61.9%, 90.4%, 61.9% and 90.4%, respectively (the consistency rate was 61.5%) (Table 4).

The MRI and pathology 3D reconstruction had a high consistency in assessing modified shrinkage classification modes (the consistency rate was 93.2%). The accuracy, sensitivity, specificity, positive predictive value and negative predictive value of MRI 3D reconstruction in assessing the modified shrinkage classification modes were 93.3%, 97.0%, 86.5%, 92.9% and 94.1%, respectively (Table 5).

MRI 3D reconstruction could accurately assess residual tumor extent

For diagnostic accuracy based on the measurement of residual tumor size, the gold standard was defined as the pathology 3D reconstruction model-measured tumor size. The correlation

TABLE 2 Patients according to the different shrinkage classification modes.

Shrinkage modes	MCSM (%)	MNCSM (%)	Total (%)
Surgical pCR	34 (48.6%)	0 (0)	34 (32.7%)
Solitary lesion without surrounding lesions	13 (18.6%)	3 (8.9%)	16 (15.4%)
Multinodular lesions	12 (17.1%)	7 (20.6%)	19 (18.3%)
Solitary lesion with adjacent spotty lesions	11 (15.7%)	14 (41.1%)	25 (24.0%)
Diffuse lesions	0 (0)	10 (29.4%)	10 (9.6%)
Total	70 (100%)	34 (100%)	104 (100%)

MCSM, modified concentric shrinkage modes; MNCSM, modified non concentric shrinkage modes

TABLE 3 Candidates of BCS according to the different shrinkage classification modes.

Different shrinkage modes	Suitable for BCS (%)	Not suitable for BCS (%)	Total
Traditional shrinkage modes	50 (48.1%)	54 (51.9%)	104
Modified shrinkage modes	70 (67.3%)	34 (32.7%)	104

TABLE 4 The traditional shrinkage modes after NAT between MRI and pathology 3D reconstruction.

Traditional shrinkage modes	MRI 3D reconstruction	Pathology 3D reconstruction	
		+	-
Surgical pCR	+	26 (25.0%)	7 (6.7%)
	-	8 (7.7%)	63 (60.6%)
Solitary lesion without surrounding lesions	+	8 (7.7%)	19 (18.3%)
	-	8 (7.7%)	69 (66.3%)
Multinodular lesions	+	7 (6.7%)	6 (5.8%)
	-	12 (11.5%)	79 (76.0%)
Solitary lesion with adjacent spotty lesions	+	18 (17.3%)	8 (7.7%)
	-	7 (6.7%)	71 (68.3%)
Diffuse lesions	+	5 (4.8%)	0 (0)
	-	5 (4.8%)	94 (90.4%)

TABLE 5 The modified shrinkage classification modes after NAT between MRI and pathology 3D reconstruction.

Pathology 3D reconstruction	MRI 3D reconstruction		Total
	MCSM	MNCSM	
MCSM	65 (62.5%)	5 (4.8%)	70 (67.3%)
MNCSM	2 (1.9%)	32 (30.8%)	34 (32.7%)
Total	67 (64.4%)	37 (35.6%)	104 (100%)

among the longest diameter, maximum cross-sectional area and volume of residual tumors after NAT measured by MRI and pathology 3D reconstruction has statistically significance, respectively. And the *r* value was 0.942, 0.941 and 0.903, respectively (all $p<0.001$). In terms of the largest diameter and largest cross-sectional area of the residual tumor, the correlation between 3D pathology and 3D MRI was better than two-dimensional MRI measurement (Table 6).

Compared with pathology 3D reconstruction, MRI 3D reconstruction slightly underestimated the maximum diameter and maximum cross-sectional area of residual tumors, with a median disparity (*MD*) of -0.074cm (95% CI: -0.313~0.165cm) and -1.148cm^2 (95% CI: -2.146~ -0.148 cm^2). And it overestimated the volume of residual tumors compared with pathology 3D reconstruction, with *MD* of 0.433 cm^3 (95%CI: -9.55~12.34 cm^3).

The nomogram of modified shrinkage classification modes after NAT

The authors generated a unique, random number using a computer for each patient included. And authors sorted patients according to their random numbers. Finally, 71 patients with smaller numbers were assigned to the training set, and the other 33 patients were assigned to the validation set.

In the training set, although there was no important difference in year and menopausal status among the modified shrinkage classification modes after NAT, significant difference between modified shrinkage classification modes and primary tumor stage before NAT ($p=0.009$), clinical nodal stage after NAT ($p=0.013$), lymph nodes downstaging after NAT ($p<0.001$), mammographic malignant calcification ($p=0.002$) and molecular subtypes ($p<0.001$) were observed in univariate analysis. Variables with *p*-value<0.05 in the univariate analysis were assessed for multivariate analysis. The independent predictors of modified shrinkage classification modes were comprised of primary tumor stage (OR=2.059, 95%CI: 1.187-3.574, $p=0.001$), mammographic malignant calcification (OR=3.424, 95%CI: 1.437-8.161, $p=0.005$), molecular subtypes (OR=0.530, 95%CI: 0.364-0.772, $p=0.001$) and nodal down staging after NAT (OR=0.183, 95%CI: 0.067-0.497, $p=0.010$) (Table 7).

Based on the aforementioned multivariate analysis results, the authors built the nomogram to predict patients with MNCSM (Figure 4). To calculate the probability of MNCSM, the scores for the four factors were summed up. And the total scores and bottom risk scale were referenced (Figure 4A). The overall performance and discriminative performance of the model were assessed by the calibration curve and ROC curve analysis, respectively. The nomogram was internally validated using the bootstrap method. The nomogram had an AUC of 0.801 (95% CI: 0.781–0.822) in the training set, indicating that the multivariate logistic regression model had potentially promising predictive power (Figure 4B).

The external validation set of 33 patients also showed good discriminatory ability, with an AUC of 0.791 (95% CI: 0.765–0.818), indicating that use of a multivariate logistic regression model in an individual set had potentially promising predictive power (Figure 4C). The difference between the two AUCs was not statistically significant ($p=0.778$). The calibration curve showed a satisfactory fit between the actual and predicted probability of achieving MNCSM in the training (Figure 4D) and validation (Figure 4E) sets, indicating that the nomogram was well calibrated.

TABLE 6 Different examination methods to measure the largest diameter and cross-sectional area of residual tumor after NAT [M (95%CI)].

Methods	Largest diameter (cm)	Largest cross-sectional area (cm^2)
2D MRI	1.25 (0.785-1.955)	1.107 (0.655-1.817)
MRI 3D reconstruction	1.40 (0.810-2.010)	1.250 (0.750-1.850)
Pathology 3D reconstruction	1.45 (0.812-2.050)	1.312 (0.801-1.930)

Patients with MNCSM had higher recurrence/metastasis

The median follow-up was 77 months (40-134 months), with the last follow-up in May 2022. Twelve cases were lost to follow-up, and the effective follow-up rate was 88.5% (92/104). We observed 5 cases of recurrences/metastasis (7.1%) in the MCSM group and 10 cases (29.4%) in the MNCSM group ($p=0.002$). In MCSM group, one patient had chest wall recurrence and 4 patients had distant metastases. While in MNCSM group, 2 patients had chest wall recurrence, and 8 patients had distant metastasis. At the same time, the multivariate analysis also showed that modified shrinkage modes were the independent predictors of recurrence/metastasis.

TABLE 7 The predictive factors for modified shrinkage classification modes after NAT in the training cohorts.

Factors	MCSM	MNCSM	Univariable analysis	Multivariable analysis
			p value	*p* value
Clinical tumor stage			0.009	0.001
cT1	7	1		
cT2	33	14		
cT3	4	4		
cT4	3	5		
Clinical nodal stage			0.659	
cN0	8	4		
cN1	17	11		
cN2	16	6		
cN3	7	2		
Nodal stage after NAT			0.013	
ycN0	27	7		
ycN1	12	5		
ycN2	5	5		
ycN3	5	5		
Molecular subtypes			0.001	0.001
Luminal A	5	10		
Luminal B HER2-	9	5		
HER2+	18	5		
TN	16	3		
Lymph nodes downstaging			0.001	0.010
Yes	43	14		
No	6	8		
Malignant calcification			0.002	0.005
Yes	20	16		
No	29	6		

Patients with MCSM had better survival benefit

Previous studies had confirmed that pCR after NAT was associated with survival benefits. So, we want to exclude the effect of pCR on the survival benefit of MCSM group. We performed a subgroup analysis to assess survival benefit of patients who did not achieve pCR. The median overall survival (OS) in MCSM and MNCSM group was 108.5 months and 89.0 months, respectively (Figure 5A). The median disease-free survival (DFS) was 101.5 months and 60.5 months, respectively (Figure 5B) in patients with MCSM and MNCSM. Even patients with MCSM did not achieve pCR, they also had a better survival benefit compared to patients with MNCSM.

Discussion

The continuous optimization of local-regional control under the guidance of molecular subtype allows clinicians to make reasonable adjustments based on the efficacy of NAT to achieve the maximum treatment benefits. In this study, we constructed the MRI and pathology 3D reconstruction model of residual tumor after NAT. Then we explored and definite the modified shrinkage classification modes which oriented by BCS purpose after NAT, we found that modified shrinkage classification modes were more suitable for guiding BCS after NAT. At the same time, based on the gold standard of 3D pathology reconstruction model-measured tumor size, we also found that MRI 3D reconstruction after NAT could accurately predict the modified shrinkage classification modes and extent of residual tumor. In addition, a nomogram was developed based on the predictors of modified shrinkage classification modes that might aid clinicians in surgical decisions. The nomogram indicated that patients with large primary tumor, mammographic malignant calcification, Luminal A/Luminal B HER2- subtype, and high nodal burden after NAT were more likely to present with MNCSM. With an AUC of 0.801 and internal validation using the bootstrap resampling method, the model exhibited sufficient ability to predict modified shrinkage modes after NAT. Patients with MCSM had better survival benefit.

The main strength of the study was that we constructed the BCS-oriented modified shrinkage classification modes which combined traditional shrinkage modes with residual tumor extent. Compared with traditional shrinkage modes, modified shrinkage classification modes were more suitable to guide the individualized selection of BCS candidates and scope of resection. This mode could help to decrease the negative margins distance and simultaneously maintain the natural breast shape to facilitate better cosmetic outcomes. And it represents a transformation of treatment concept, which from maximum and tolerable treatment to the minimum and effective treatment (11).

The single-focal lesion was one of the BCS indications after NAT of MDACC (20). The traditional view believed that multinodular lesions and solitary lesion with adjacent spotty lesions were not suitable for BCS. However, in our study, for patients with a high probability of MCSM after NAT, even if they had multinodular lesion or solitary lesion with adjacent spotty lesion, BCS would also be safe if they had a negative margin. So, our study might partly expand the indications of BCS after NAT: patients might also accept BCS safely even if they had multi-focal disease after NAT. And for these patients, there would be no increase in LRR if they received BCS

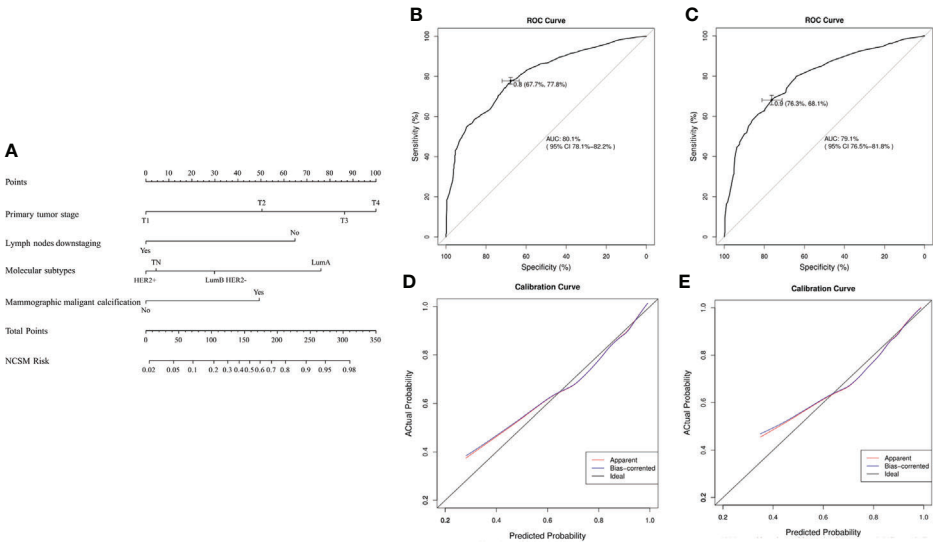

FIGURE 4
The nomogram to predict modified shrinkage classification modes after NAT. **(A)**: To calculate the probability of MNCSM, the scores for the four factors were summed up. And the total scores and bottom risk scale were referenced. **(B)**: The ROC curve in the training cohort indicates an AUC of 0.801. **(C)**: In the validation cohort, the ROC curve indicates an AUC of 0.791. The calibration curve showed a satisfactory fit between the actual and predicted probability of achieving MNCSM in the training **(D)** and validation **(E)** cohorts. The horizontal axis indicates the predicted probability measured by the nomogram, and the vertical axis indicates the actual probability.

successfully. For patients with a high probability of MNCSM, the basic goal of NAT (tumor downstage) had not been achieved. If satellite lesions were missed during surgery, LRR would increase due to "false negative margins". So, these patients need to be cautious when choosing BCS, at the same time, they also need a more "generous" resection extent. The 2019 St. Gallen consensus conference also recommended that patients with multi-focal disease could also accept BCS after NAT, but the scope of residual tumors need to be more accurately assessed.

The MRI 3D reconstruction model provides an intuitive image of tumor extent in the breast and is helpful for surgeons to plan surgery. Furthermore, it can display more precise information than routine bidimensional images, because 3D tumor images can be observed from various directions by rotation (20–24). Taking advantage of these characteristics, MRI 3D reconstruction has a high degree of accuracy in assessing the residual tumor extent after NAT. Several reports have demonstrated that MRI 3D reconstruction significantly and strongly correlated with pathology examination (25, 26). Chae YL et al. (25) evaluated the accuracy of 3D measurement by computer-aided program of breast MRI for the assessment of residual tumor extent. The result showed that there was no

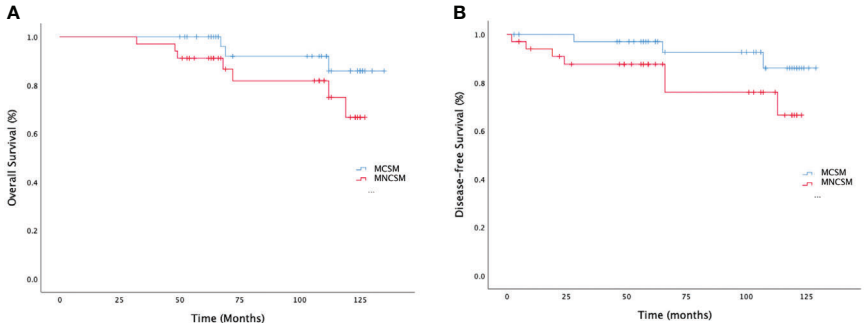

FIGURE 5
The survival analysis of modified shrinkage classification modes. **(A)**: The overall survival of MCSM and MNCSM among patients without pCR. **(B)**: The disease-free survival of MCSM and MNCSM among patients without pCR.

significant difference between the 3D measurement and histological diameter. Kenji et al. (26) also found that the tumor size determined by 3D MRI showed a strong correlation with that determined by pathologic examination (r=0.896). However, most of them compared the tumor extent which was assessed by its largest diameter at MRI 3D reconstruction model with the pathology examination of routine sliced images. The pathology 3D reconstruction has also been previously used in researches, and it could also provide more precise information about tumor extent than routine sliced images (13, 14, 27, 28). However, as far as we know, few studies compared the association and correlation between MRI 3D reconstruction and pathology 3D reconstruction in evaluation of residual tumor extent. In this study, taking pathology 3D reconstruction-measured tumor size as the gold standard, we further confirmed the accuracy of MRI 3D reconstruction in assessing residual tumor extent after NAT. At the same time, the MRI images were easy to obtain, and the 3D reconstruction technology was relatively mature. So, we recommend applying MRI 3D reconstruction techniques to evaluate residual tumor extent after NAT in clinical practice.

Our results also showed that molecular subtype was an independent predictor of the modified shrinkage classification modes. Patients with Luminal A and Luminal B HER2- subtypes had more chance to achieve MCSM. The correlation between molecular subtype and modified shrinkage modes might reflect tumor biologic characteristics. One possible reason might be the growth characteristic of Luminal A and Luminal B HER2- subtypes, tumor cells tend to grow slowly with low apoptosis rate and genetic instability (17). Simultaneously, tumor cells in these subtypes may be more resistant to preoperative therapy. However, tumor cells in TN and HER2+ subtypes had poor differentiation and strong proliferation ability, the aggressive tumor cells were more sensitive to therapy (29). After NAT, the tumor boundary of patients with MCSM was easy to judge, and the margins of these tumors were often negative after finishing tumor resection. But the tumor boundary of patients with MNCSM is difficult to determine accurately. For those patients, LRR might be increased due to "false negative margin" when performing BCS. Therefore, Luminal A and Luminal B HER2- patients with large primary tumor and/or high nodal burden after NAT should be cautious to receive BCS after NAT, and the negative margin distance might also need to be appropriately increased. Although some patients with TN and HER2+ subtypes had the poor prognosis, patients with these subtypes were more likely to present with MCSM after NAT, suggesting that BCS after NAT was also feasible for TN and HER2+ patients.

Shrinkage classification modes were reported to be associated with prognosis. Ippei et al. (17) found patients with concentric shrinkage pattern has an excellent DFS (p=0.007) and OS (p=0.037). Our study also found that the modified shrinkage classification modes might be related to the prognosis. Patients with MNCSM might have a worse prognosis. The reasons might be that the predictors associated with MNCSM indicated high tumor burden, and these predictors were associated with poor prognosis. Another reason might be that molecular subtype was associated with DFS and OS after NAT. The result of Orsaria et al. (30) showed that patients with pCR after NAT had better DFS, particularly for HER2+ and TN subtypes. Zarotti et al. (31) also found that clinicopathological factors and distinct therapy regiments especially in HER2+ and TN subtypes had prognostic impact on pCR, OS and DFS after NAT. In our study, patients with HER2+ and TN subtypes had more chance to achieve MCSM, these patients also had a better DFS and OS after NAT.

This study has certain limitations, and the most important of which is the small sample size. Additionally, lacking multi-center external data to verify the accuracy of the nomogram is another limitation in our study. Therefore, further prospective multi-center studies are required to confirm and assess the results of modified shrinkage classification modes.

Conclusion

The modified shrinkage classification modes could help to guide the individualized selection of BCS candidates and scope of resection after NAT. MRI 3D reconstruction after NAT could accurately predict the modified shrinkage classification modes and extent of residual tumor. The nomogram combined clinical factors, imaging, molecular subtypes and NAT efficacy showed sufficient predicting accuracy in predicting modified shrinkage classification modes. Patients with MNCSM after NAT might have a worse prognosis.

Data availability statement

The datasets presented in this study can be found in online repositories. The names of the repository/repositories and accession number(s) can be found in the article/supplementary material.

Ethics statement

Written informed consent was obtained from the minor(s)' legal guardian/next of kin for the publication of any potentially identifiable images or data included in this article.

Author contributions

All authors contributed to the study conception and design. Material preparation, data collection and analysis was performed by BZ, QPF, YT, and CP. The first draft of the manuscript was

written by BZ and ZZP, and all authors commented on previous versions of the manuscript. All authors contributed to the article and approved the submitted version.

Funding

This work was funded by National Natural Science Foundation of China (82172873, 81672104), Shandong Cancer Hospital and Institute Clinical Training Program (2020PYA08), National Natural Science Foundation of Shandong Province (ZR2021QH002), China Postdoctoral Science Foundation (2021M691334), Bethune Foundation Project (G-X-2019-0101-12), Shandong Province Medical and Health Science and Technology Development Plan Fund (2019WS201).

Conflict of interest

The authors declare that the research was conducted in the absence of any commercial or financial relationships that could be construed as a potential conflict of interest.

Publisher's note

All claims expressed in this article are solely those of the authors and do not necessarily represent those of their affiliated organizations, or those of the publisher, the editors and the reviewers. Any product that may be evaluated in this article, or claim that may be made by its manufacturer, is not guaranteed or endorsed by the publisher.

References

1. Gianni L, Pienkowski T, Imh H, Roman L, Tseng LM, Liu MC, et al. Efficacy and safety of neoadjuvant pertuzumab and trastuzumab in women with locally advanced, inflammatory, or early HER-2-positive breast cancer (NeoSphere): a randomised multicenter, open-label, phase 2 trial. *Lancet Oncol* (2012) 13(1):25–32. doi: 10.1016/S1470-2045(11)70336-9

2. Laas E, Labrosse J, Hamy AS, Benchimol G, de Croze D, Feron JG, et al. Determination of breast cancer prognosis after neoadjuvant chemotherapy: comparison of residual cancer burden (RCB) and neo-bioscore. *Br J Cancer* (2021) 124:1421–7. doi: 10.1038/s41416-020-01251-3

3. Bi Z, Cong BB, Wang YS, Chen P, Wang YS. Molecular subtypes and axillary downstaging surgery after neoadjuvant chemotherapy for breast cancer. *Chin J Clin Oncol* (2018) 45(8):390–3.doi: 10.1038/s41416-020-01251-3

4. Mamtani A, Andrea V, Tari A, Van Zee KJ, Plitas G, Pilewskie M, et al. How often does neoadjuvant chemotherapy avoid axillary dissection in patients with histologically confirmed nodal metastases? results of a prospective study. *Ann Surg Oncol* (2016) 23(11):3467–74. doi: 10.1245/s10434-016-5246-8

5. Jose HV, Vera LN, Pauline ES, Krekel NMA, Schoonmade LJ, Meijer S, et al. Breast-conserving surgery following neoadjuvant therapy-a systematic review on surgical outcomes. *Breast Cancer Res Treat* (2018) 168(1):13–5doi: 10.1007/s10549-017-4598-5.

6. Tasoulis MK, Lee HB, Yang W, Pope R, Krishnamurthy S, Kim SY, et al. Accuracy of post-neoadjuvant chemotherapy image-guided breast biopsy to predict residual cancer. *JAMA Surg* (2020) 155(12):e204103. doi: 10.1001/jamasurg.2020.4103

7. Kuerer HM, Rauch GM, Krishnamurthy S, Adrada BE, Caudle AS, DeSnyder SM, et al. A clinical feasibility trial for identification of exceptional responders in whom breast cancer surgery can be eliminated following neoadjuvant systemic therapy. *Ann Surg* (2018) 267(5):946–51. doi: 10.1097/SLA.0000000000002313

8. Early Breast Cancer Trialists' Collaborative Group (EBCTCG). Long-term outcomes for neoadjuvant versus adjuvant chemotherapy in early breast cancer: meta-analysis of individual patient data from ten randomized trials. *Lancet Oncol* (2018) 191(1):27–39doi: 10.1016/S1470-2045(17)30777-5.

9. Bi Z, Zhao T, Qiu PF, Qiu PF, Zhang ZP, Wang YS. Clinical-pathological shrinkage modes could help to guide breast-conserving surgery after neoadjuvant therapy. *Future Oncol* (2021) 18(10):1171–3doi: 10.2217/fon-2021-1526.

10. Curigliano G, Burstein HJ, Winer E, Gnant M, Dubsky P, Loibl S, et al. De-escalating and escalating treatments for early-stage breast cancer: the st. gallen international expert consensus conference on the primary therapy of early breast cancer 2017. *Ann Oncol* (2017) 28(8):1700–12doi: 10.1093/annonc/mdx308.

11. Burstein HJ, Curigliano G, Loibl S, Dubsky P, Gnant M, Poortmans P, et al. Estimating the benefits of therapy for early-stage breast cancer: the st. gallen international consensus guidelines for the primary therapy of early breast cancer 2019. *Ann Oncol* (2019) 30(8):1541–57doi: 10.1093/annonc/mdz235.

12. Ishitobi M, Ohsumi S, Inaji H, Ohno S, Shigematsu H, Akiyama F, et al. Ipsilateral breast tumor recurrence (IBTR) in patients with operable breast cancer who undergo breast-conserving treatment after receiving neoadjuvant chemotherapy: risk factors of IBTR and validation of the MD Anderson prognostic index. *Cancer* (2012) 118(18):4385–93. doi: 10.1002/cncr.27377

13. Yang T, Zhang ZP, Wang YS, Liu G, Mu DB, Wang YS. Shrinkage mode of the primary breast tumor after neoadjuvant chemotherapy analyzed with part-mount sub-serial sectioning and three-dimensional reconstruction technique. *Chin J Oncol* (2016) 38(4):1–7doi: 10.3760/cma.j.issn.0253-3766.2016.04.006.

14. Yang T, Zhang ZP, Wang YS, Mu D, Sun X, Chen Z, et al. Accuracy of MRI for estimating residual tum or size after neoadjuvant chemotherapy in breast cancer with three-dimension reconstruction technique. *Chin J Surg* (2015) 53 (4):280–2doi: 10.1080/02841860701373587.

15. Ogston KN, Miller ID, Payne S, Hutcheon AW, Sarkar TK, Smith I, et al. A new histological grading system to assess response of breast cancers to primary chemotherapy: prognostic significance and survival. *Breast* (2003) 12(5):320–7. doi: 10.1016/S0960-9776(03)00106-1

16. Wang S, Zhang Y, Yang X, Fan L, Qi X, Chen Q, et al. Shrink pattern of breast cancer after neoadjuvant chemotherapy and its correlation with clinical pathological factors. *World J Surg Oncol* (2013) 11(1):166–72. doi: 10.1186/1477-7819-11-166

17. Ippei F, Kazuhiro A, Kokoro K, Shibayama T, Takahashi S, Gomi N, et al. Pattern of tumor shrinkage during neoadjuvant chemotherapy is associated with prognosis in low-grade luminal early breast cancer. *Radiology* (2018) 286(1):49–57doi: 10.1148/radiol.2017161548.

18. Kim TH, Kang DK, Yim H, Jung YS, Kim KS, Kang SY. Magnetic resonance imaging patterns of tumor regression after neoadjuvant chemotherapy in breast cancer patients: correlation with pathological response grading system based on tumor cellularity. *J Comput Assist Tomogr* (2012) 36(2):200–6. doi: 10.1097/RCT.0b013e318246abf3

19. Wei J, Wang C, Xie X, Jiang DQ. Meta-analysis of quantitative dynamic contrast-enhanced MRI for the assessment of neoadjuvant chemotherapy in breast cancer. *Am Surg* (2019) 85(6):645–53.

20. Nakamura S. Image-guided breast conserving surgery based on 3D-MRI. *Nihon Geka Gakkai Zasshi* (2002) 103(11):794–8.

21. Nakamura R, Nagashima T, Sakakibara M, Sangai T, Fujimoto H, Arai M, et al. Breast-conserving surgery using supine magnetic resonance imaging in breast cancer patients receiving neoadjuvant chemotherapy. *Breast* (2008) 17(3):245–51. doi: 10.1016/j.breast.2007.10.007

22. Wang CB, Lee S, Kim T, Hong D, Kim GB, Yoon GY, et al. Breast tumor movements analysis using MRI scans in prone and supine positions. *Sci Rep* (2020) 10(1):4858. doi: 10.1038/s41598-020-61802-9

23. Beom SK, Namkug K, Jong WL, Kim HJ, Chung IY, Kim J, et al. MRI-Based 3D-printed surgical guides for breast cancer patients who received neoadjuvant chemotherapy. *Sci Rep* (2019) 9(1):11991. doi: 10.1038/s41598-019-46798-1

24. Tomida K, Ishida M, Umeda T, Sakai S, Kawai Y, Mori T, et al. Magnetic resonance imaging shrinkage patterns following neoadjuvant chemotherapy for breast carcinomas with an emphasis on the radiopathological correlations. *Mol Clin Oncol* (2014) 2:783–8. doi: 10.3892/mco.2014.333

25. Chae YL, Cho N, Kim SM, Jang M, Park JS, Baek SY, et al. Computer-aided evaluation of breast MRI for the residual tumor extent and response monitoring in breast cancer patients receiving neoadjuvant chemotherapy. *Korean J Radiol* (2011) 12(1):34–43. doi: 10.3348/kjr.2011.12.1.34

26. Kenji A, Yasuhiro T, Tetsuya T, Tanji Y, Miyoshi Y, Kim SJ, et al. Preoperative evaluation of residual tumor extent by three-dimensional magnetic resonance imaging in breast cancer patients treated with neoadjuvant chemotherapy. *Breast J* (2006) 12(2):130–7. doi: 10.1111/j.1075-122X.2006.00220.x

27. Zheng CH, Liu ZY, Yuan CX, Dong XY, Li HM, Wang JJ, et al. Mutant allele frequency-based intra-tumoral genetic heterogeneity related to the tumor shrinkage mode after neoadjuvant chemotherapy in breast cancer patients. *Front Med (Lausanne)* (2021) 8:651904. doi: 10.3389/fmed.2021.651904

28. Kazuaki U, Tosei O, Koichi H, Yoshiyuki N, Gen M. D2-40 positive lymphatic endothelial cell density is much higher in and along the mammary glandular tissues than in subcutaneous tissue: Case report of a 20-Year-Old donated female cadaver. *Breast Cancer* (2006) 13(4):340–3. doi: 10.2325/jbcs.13.340

29. Nakahara H, Yasuda Y, Machida E, Maeda Y, Furusawa H, Komaki K, et al. MR and US imaging for breast cancer patients who underwent conservation surgery after neoadjuvant chemotherapy: comparison of tripe negative breast cancer and other intrinsic subtypes. *Breast Cancer* (2011) 18(3):152–60. doi: 10.1007/s12282-010-0235-4

30. Orsaria P, Grasso A, Ippolito E, Pantano F, Sammarra M, Altomare C, et al. Clinical outcomes among major breast cancer subtypes after neoadjuvant chemotherapy: Impact on breast cancer recurrence and survival. *Anticancer Res* (2021) 41(5):2697–709. doi: 10.21873/anticanres.15051

31. Zarotti C, Papassotiropoulos B, Elfgen C, Dedes K, Vorburger D, Pestalozzi B, et al. Biomarker dynamics and prognosis in breast cancer after neoadjuvant chemotherapy. *Sci Rep* (2022) 12(1):91. doi: 10.1038/s41598-021-04032-x

frontiers | Frontiers in Oncology

TYPE Original Research
PUBLISHED 01 December 2022
DOI 10.3389/fonc.2022.1026647

Check for updates

OPEN ACCESS

EDITED BY
Nicola Amoroso,
University of Bari Aldo Moro, Italy

REVIEWED BY
Weiwei Zhan,
Shanghai Jiaotong University School of Medicine, China
Fajin Dong,
Jinan University, China

*CORRESPONDENCE
Tian'an Jiang
tiananjiang@zju.edu.cn

SPECIALTY SECTION
This article was submitted to Breast Cancer, a section of the journal Frontiers in Oncology

RECEIVED 24 August 2022
ACCEPTED 18 October 2022
PUBLISHED 01 December 2022

CITATION
Guo J, Wang B-H, He M, Fu P, Yao M and Jiang T (2022) Contrast-enhanced ultrasonography for early prediction of response of neoadjuvant chemotherapy in breast cancer. *Front. Oncol.* 12:1026647. doi: 10.3389/fonc.2022.1026647

COPYRIGHT
© 2022 Guo, Wang, He, Fu, Yao and Jiang. This is an open-access article distributed under the terms of the Creative Commons Attribution License (CC BY). The use, distribution or reproduction in other forums is permitted, provided the original author(s) and the copyright owner(s) are credited and that the original publication in this journal is cited, in accordance with accepted academic practice. No use, distribution or reproduction is permitted which does not comply with these terms.

Contrast-enhanced ultrasonography for early prediction of response of neoadjuvant chemotherapy in breast cancer

Jiabao Guo[1], Bao-Hua Wang[1], Mengna He[1], Peifen Fu[2], Minya Yao[2] and Tian'an Jiang[1*]

[1]Department of Ultrasound Medicine, The First Affiliated Hospital, School of Medicine, Zhejiang University, Hangzhou, Zhejiang, China, [2]Department of Breast Surgery, The First Affiliated Hospital, School of Medicine, Zhejiang University, Hangzhou, Zhejiang, China

Neoadjuvant chemotherapy (NAC) is widely accepted as a primary treatment for inoperable or locally advanced breast cancer before definitive surgery. However, not all advanced breast cancers are sensitive to NAC. Contrast-enhanced ultrasonography (CEUS) has been considered to assess tumor response to NAC as it can effectively reflect the condition of blood perfusion and lesion size. Therefore, this study aimed to evaluate the diagnostic performance of CEUS to predict early response in different regions of interest in breast tumors under NAC treatment. This prospective study included 82 patients with advanced breast cancer. Parameters of TIC (time-intensive curve) between baseline and after the first cycle of NAC were calculated for the rate of relative change (Δ), including Δpeak, ΔTTP (time to peak), ΔRBV (regional blood volume), ΔRBF (regional blood flow) and ΔMTT (mean transit time). The responders and non-responders were distinguished by the Miller-Payne Grading (MPG) system and parameters from different regions of tumors were compared in these two groups. For ROI 1(the greatest enhancement area in the central region of the tumor), there were significant differences in Δpeak1, ΔRBV1 and ΔRBF1 between responders and non-responders. For ROI 2 (the greatest enhancement area on edge of the tumor), there were significant differences in Δpeak2 and ΔRBF2 between the groups. The Δpeak1 and ΔRBF2 showed good prediction (AUC 0.798-0.820, $p \leq 0.02$) after the first cycle of NAC. When the cut-off value was 0.115, the ΔRBF2 had the highest diagnostic accuracy and the maximum NPV. Quantitative TIC parameters could be effectively used to evaluate early response to NAC in advanced breast cancer.

KEYWORDS

ultrasonography, neoadjuvant chemotherapy, breast cancer, response, vascular heterogeneity

Introduction

Neoadjuvant chemotherapy (NAC) is widely accepted as the primary treatment for inoperable or locally advanced breast cancer before definitive surgery. The benefits of NAC in terms of overall survival and improvement in quality of life have been verified in many clinical trials and studies and have been able seen turning inoperable tumors into operable tumors and providing the option of breast-conserving surgery instead of mastectomy (1). However, not all locally advanced breast cancers are sensitive to NAC. Studies have indicated that almost 10-35% of patients were insensitive to chemotherapy drugs, meaning that these patients experienced disease progression during the period of NAC (2–4). Therefore, the ability to predict early response to initial cycles and replace drugs with alternative agents in non-responders would be of considerable clinical significance (5).

Magnetic resonance imaging (MRI) is the best method for assessing the tumor response to NAC, for its performance was generally superior to that of mammography, ultrasonography (US), and clinical examination in a meta-analysis with 300 patients (6). Nevertheless, some studies suggest that MRI gadolinium-based contrast agents diffuse from the blood vessels into adjacent interstitial tissues, overestimating the extent of the residual tumor (7–10).

Changes in blood vessels in breast lesions are known to occur before morphological changes (11), and contrast-enhanced ultrasonography (CEUS) can effectively reflect the condition of blood perfusion and lesion size due to its ability to obtain macrovascular and microvascular information about the lesions (12, 13). CEUS is a quantitative kinetic imaging modality that offers the time-intensity curve (TIC) before and after NAC treatment to aid our understanding of the complexity of angiogenesis in breast tumors (14, 15).

Previous studies on breast cancer have explored changes in tumor size, that usually occur after the second cycle of NAC, so earlier predictors reflecting angiogenesis and metabolic activity may change before tumor shrinkage (16, 17). The viability of CEUS to predict tumor response after completing the first cycle of NAC is unknown (11). Several studies have suggested that CEUS could predict early response to NAC (18–22). However, the heterogeneity of tumor vessels has been ignored and the different regions of interest inside the tumor need to be discussed. The difference between the CEUS features of the marginal zone and central region in breast cancer deserves attention. Therefore, it was crucial to highlight the characteristics of CEUS in the marginal zone and central region of breast cancer in this study.

In this study, we performed a comparative analysis of the relative variation ratio of quantitative TIC parameters from different regions of tumors between responders and non-responders to investigate the potential role of CEUS in evaluating the early response to NAC in breast cancer patients.

Material and methods

Clinical materials

This prospective study was approved by the ethics committee of the First Affiliated Hospital of Zhejiang University (Hangzhou, China). All patients provided written informed consent. A total of 82 female patients diagnosed with stage II or III unilateral breast cancer and scheduled to receive NAC were recruited for this study at the First Affiliated Hospital of Zhejiang University (Hangzhou, China) between May 2019 and May 2022.

Chemotherapy regimen

Prior to surgery, there were two main NAC regimens for all patients in this study: (1) anthracycline-based regimens and (2) taxane regimens. Then the duration of NAC was mainly 6 or 8 cycles. In addition, HER2-positive patients were treated with trastuzumab. The treatment protocol and timeline followed the guidelines provided by NCCN and China Anti-Cancer Association (CACA). Drug treatment for 21 days was considered 1 cycle and an interval of 20 days occurred following before the initiation of the next round of chemotherapy. Image examinations were performed before the second NAC cycle. Surgical excision was performed within 20 days after 6 or 8 cycles of drug treatment.

CEUS examination

All patients underwent the CEUS before NAC, after the first cycle of NAC. An ESAOTE MyLab ClassC ultrasound diagnostic instrument (Esaote SpA, Genoa, Italy) was performed for CEUS. The ultrasound contrast agent SonoVue (59 μg; Bracco SpA, Milan, Italy) was added to 5 ml saline, and a milky microbubble suspension was generated by vigorous agitation. The breast was first scanned with B-mode and CDFI to identify the tumor location and detect its vascularity. Choosing the largest section of the tumor, a real-time contrast-enhanced US imaging using a low mechanical index ranging between 0.06 and 0.08 was

performed. A total of 4.8 ml SonoVue suspension was rapidly injected through an anterior elbow vein and then 5 ml of saline was injected to flush the tube. When the transducer was stabilized with minimal pressure, images were recorded with a clip function for 120 secs. Contrast observation continued until the lesion-enhanced image disappeared.

Image review and data analysis

The postprocessing analysis of the data was performed quantitatively by two senior physicians, with more than 5 years and 10 years of experience in breast imaging. The gold standard-postoperative pathological diagnosis was assessed by the Miller-Payne Grading (MPG) system (described in further detail below). TIC was generated from the region of interest (ROI), in which quantitative blood perfusion parameters, including peak percent (peak), time to peak (TTP), regional blood volume (RBV), regional blood flow (RBF) and mean transit time (MTT) were compared in responders and non-responders. The detailed explanations of above TIC parameters were described in Figure 1. The different regions of breast cancer are defined as follows: central region: the region with a diameter of 0.5 cm in the center of the lesion. If the lesion is small, the sampling frame can be appropriately reduced; marginal zone: the boundary of the enhanced range of lesions was taken as the external area. The relative variation ratio (Δ) in the parameters after the first cycle of NAC vs. baseline were calculated as follows: $\Delta = (\text{parameter}_{pre}\text{-parameter}_{1st})/\text{parameter}_{pre}$.

Pathological evaluation

The pathology was assessed by the Miller-Payne Grading (MPG) system, which compares the cancer cellularity of the core needle biopsy (before NAC) with the resected tumor (23–25). 1): no reduction in overall cellularity, 2): a minor loss of tumor cells (up to 30% loss), 3): 30-90% loss of malignant cells, 4): more than 90% loss of malignant cells, and 5): no identifiable malignant cells, although ductal carcinoma may be presented *in situ*. 1)-3) were defined as "non-response", while 4)-5) were defined as "response".

Statistical analysis

The data were analyzed by SPSS version 17.0 statistics software (IBM Corp., Armonk, NY, USA). The measurement data was checked by Student's t-test, which was expressed as $\bar{x}\pm s$. The count data were evaluated by the Chi-square test. To investigate inter-observer agreement and intra-observer reliability, we evaluated both Pearson correlation coefficients and Cronbach's Alpha. Receiver operating characteristic (ROC) curves and the area under the curve (AUC) were obtained to

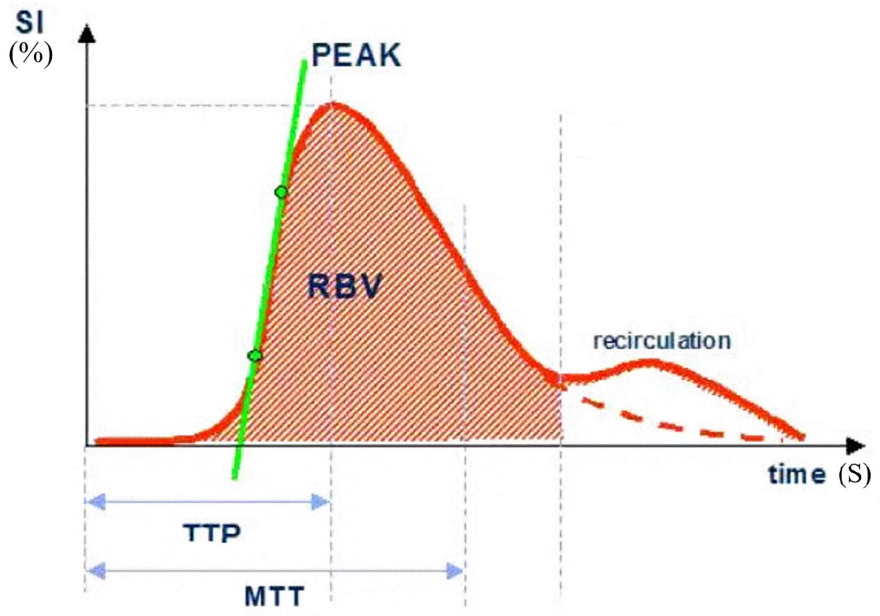

FIGURE 1
SI, signal intensity; TTP, time to peak; MTT, mean transit time; Peak, peak intensity (%); RBV, regional blood volume; RBF, regional blood flow (RBV/MTT).

evaluate the performance of perfusion parameters to predict early response after NAC. The range of 0.9–1.0 indicates an excellent predictor; 0.8–0.9, a good predictor; 0.7–0.8, a general predictor; and< 0.7, a poor predictor (25). The optimal threshold (cut-off) was chosen according to the Youden index. A p value<0.05 was considered to indicate a statistically significant difference.

Results

Clinical characteristics of the patients

Eighty-two female patients with a mean age 47.5±10.8 (30 to78) years who received NAC and surgery were recruited for this present study. The mean tumor diameter measured by ultrasound was 2.78±1.42cm (1.03 cm to 5.63 cm). All patients, including 45 cases (45 lesions) of infiltrating ductal carcinoma, 28 cases (28 lesions) of infiltrating lobular carcinoma and 9 case (9 lesion) of mucinous carcinoma were confirmed by postoperative pathology. 54 of the 82 patients showed a response (Miller-Payne score 4 or 5) and 28 showed non-response (Miller-Payne score 1, 2, or 3) (Figures 2, 3). There were no significant differences between the clinical characteristic parameters of these two groups (Table 1).

Agreement and reliability of perfusion parameters

The results were compared by independent analysis of two senior physicians. All perfusion parameters had high inter-observer and intra-observer repeatability (r>0.886, p<0.001, Cronbach's Alpha>0.936).

Comparison of the relative variation ratio of quantitative TIC parameters

The data in Table 2 were obtained by analysis of ROI 1, which represents the greatest enhancement area in the central region of the tumor, and ROI 2, which indicates the greatest enhancement area in the edge of the tumor. The data show us that there were significant differences in Δpeak1, ΔRBV1, and ΔRBF1 after the first cycle of NAC between responders and non-responders (p-values were 0.001, 0.012, and 0.002 respectively). No statistically significant difference was found for ΔTTP 1 and ΔMTT1 (p-values were 0.068, and 0.056 respectively). It was observed that Δpeak2 and ΔRBF2 after the first cycle of NAC in responders were higher than those of non-responders (p-values were 0.000 and 0.003 respectively). Other parameters, including ΔTTP2, ΔRBV2, and ΔMTT2, had no significant difference (Figures 4, 5).

Early predictors of tumor NAC response

Table 3 present the diagnostic performance of each statistically significant predictor for early response of NAC. After the first cycle of NAC, Δpeak1 and ΔRBF2 showed good prediction (AUC 0.806-0.820, p ≤ 0.02). ΔRBF1, ΔRBV1 and Δpeak2 showed general prediction (AUC 0.725-0.798, p ≤ 0.032). The sensitivity, specificity, PPV, NPV and accuracy of the cut-off value of each statistically significant predictor for early response of NAC were analyzed in Table 4. ΔRBF2 with a cut-off value of 0.115 had the highest diagnostic accuracy and the maximum NPV.

Discussion

Neoadjuvant chemotherapy has been recognized as a crucial method to decrease tumor cells and significantly increase the rate of breast-conserving and surgical resection (26). However, not every patient who underwent the NAC gets treatment benefits, because the effective rate of NAC ranges from 60-90%. Hence, assessing early response to treatment is key to ensure success in NAC.

A previous study revealed that there was an imbalance in the spatial distribution of tumor blood vessels (27). The microvascular density around the tumor was higher than that in the center, and the necrotic and cystic area was lower than the central areas. This is tumor vascular heterogeneity. CEUS features of breast cancer have regional distribution differences, which are due to the heterogeneity of the tumor. As the front of tumor invasion, the marginal zone of breast cancer has special biological characteristics and may be more sensitive to drugs than the central region. In this study, the perfusion parameters of the central region and the marginal zone were studied separately.

The multiple parameters, Δpeak1, ΔRBV1, and ΔRBF1, after the first cycle of NAC in ROI 1, were larger in responders than non-responders (p<0.05). The peak was an enhancement description index for blood perfusion assessment. That means when the tumor has more macrovascular inside, more contrast agents stay in the vessels, leading to a high peak value. Our study proved that the value of Δpeak1 increased significantly after the first cycle of NAC, especially in responders, which is consistent with the results of Amioka et al. (18). RBV is a quantitative parameter representing regional blood volume, which can reflect the blood supply inside the lesion. Before NAC, the vascularity of malignant lesions was rich, twisted, and easy to form arterio-venous fistula, which would present a higher enhancement in tumors. Effective NAC can shrink vessels providing nutrients to the tumor and reduce the number of new blood vessels. That might explain why ΔRBV1 increased significantly after the first cycle of NAC in responders. RBF was an index indicating regional blood flow, which was calculated by RBV/MTT, closely related to the patency of blood flow inside the tumor.

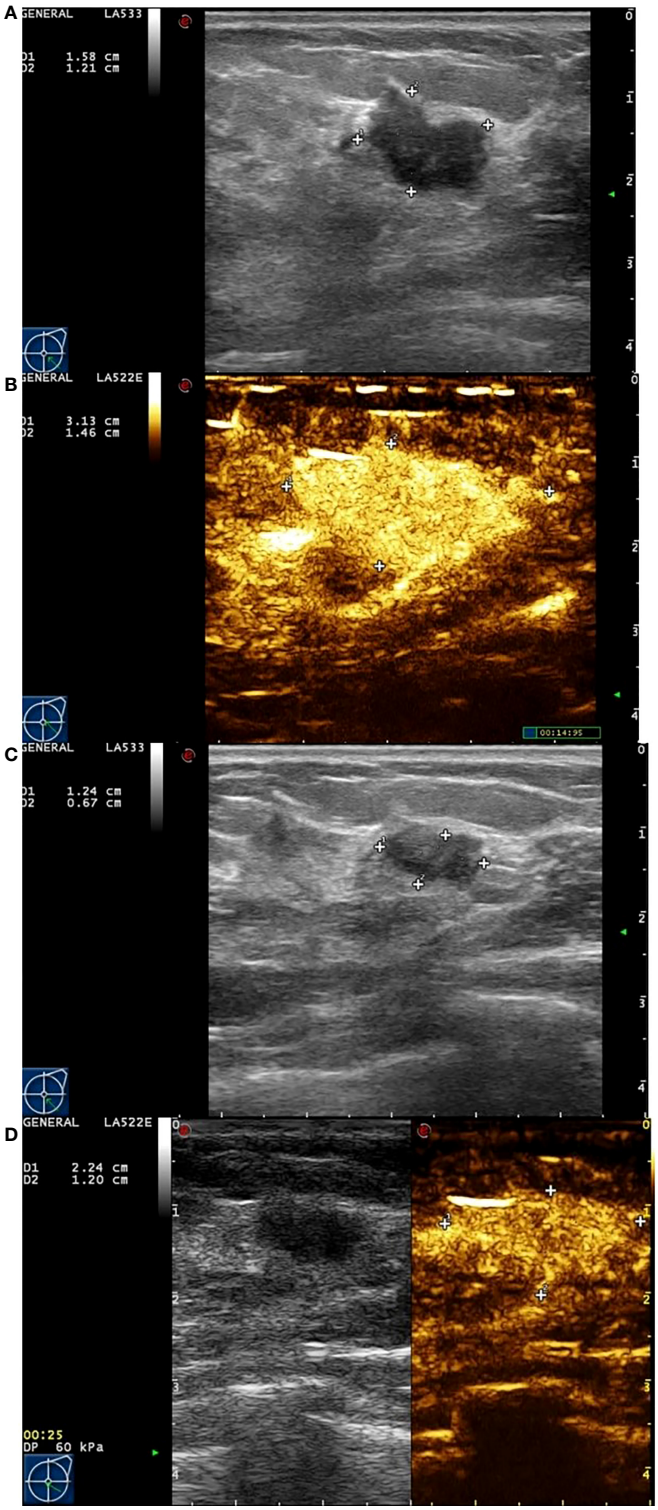

FIGURE 2
Images from a patient of non-response to NAC. **(A)** At baseline before NAC, the tumor size was measured by ultrasonography. **(B)** At baseline before NAC, the tumor size was measured by contrast-enhanced ultrasound. The extent of tumor was significantly larger than that of ultrasonography. **(C)** After the last cycle of NAC before surgery, the tumor size was measured by ultrasonography. **(D)** After the last cycle of NAC before surgery, the tumor size was measured by contrast-enhanced ultrasound. Although the extent of tumor has shrunken, there still have large number of contrast agents inside.

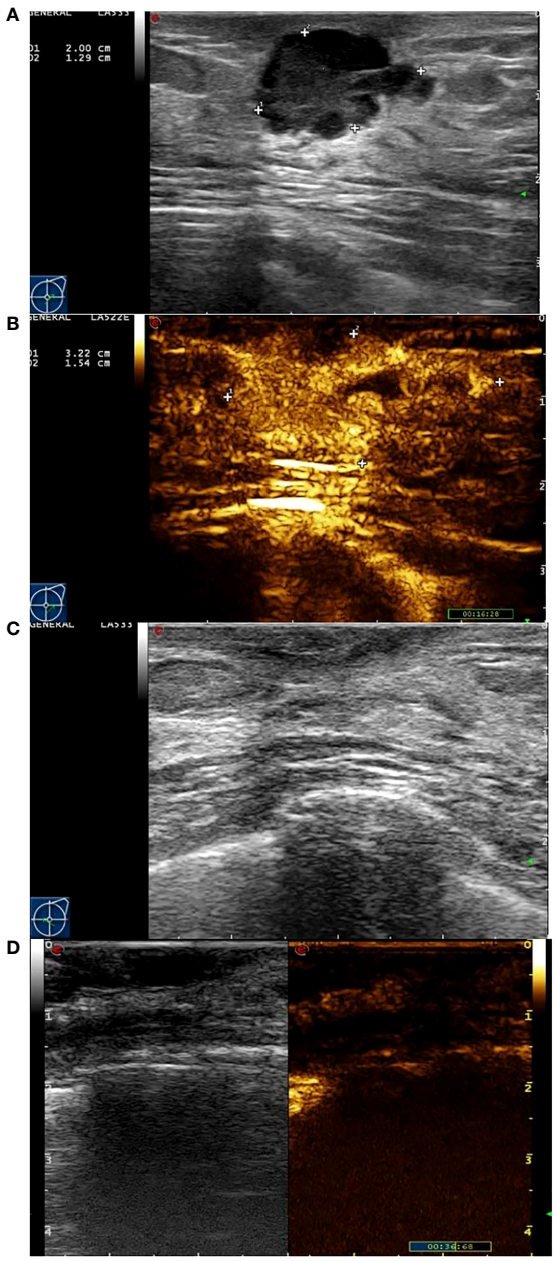

FIGURE 3
Images from a patient of response to NAC. **(A)** At baseline before NAC, the tumor size was measured by ultrasonography. **(B)** At baseline before NAC, the tumor size was measured by contrast-enhanced ultrasound. The extent of tumor was significantly larger than that of ultrasonography. **(C)** After the last cycle of NAC before surgery, the tumor has disappeared fundamentally by ultrasonography. **(D)** After the last cycle of NAC before surgery, there was not area of high enhancement fundamentally.

Chemotherapy-induced changes such as necrosis, sclerosis, or inflammation can obstruct contrast agents' flow in the original tumor site (28), which would lead to an increase in the ΔRBF1 value.

Δpeak2 and ΔRBF2, obtained from ROI 2 after the first cycle, were significantly higher in responders than non-responders ($p<0.05$). Some studies (11, 12, 29) have explained that different regions within the same malignant lesion can have different characteristics because of tumor heterogeneity. We know that large and rich nourishing vessels in the tumors provide nutrients, whereas tumor angiogenesis as well as new tumor tissue formation are often at the edge of the lesion to infiltrate

TABLE 1 Clinicopathological features of the patients at baseline.

characteristic	Response (54)	Non-response (28)	P-value
Age (years)	47.0±10.14	49.1±11.47	0.169
Tumor maximum diameter (cm)	3.15±1.21	2.96±1.53	0.456
histology			0.470
MC	7 (13.0%)	2 (7.1%)	
IDC	29 (53.7%)	16 (57.1%)	
ILC	18 (33.3%)	10 (35.7%)	
Tumor subtype			0.205
Luminal A	21 (30.6%)	11 (39.3%)	
Luminal B	17 (25%)	9 (32.1%)	
HER-2 positive	12 (38.9%)	5 (17.9%)	
TNBC	4 (5.6%)	3 (10.7%)	

MC, mucinous carcinoma; IDC, infiltrating ductal carcinoma; ILC, infiltrating lobular carcinoma; TNBC, triple negative breast carcinoma.

surrounding normal tissues. Unlike ROI 1, there are abundant new expansive microvascular with wall thin, lack of muscular layer, direction circuity, and formation of arteriovenous fistula in ROI 2, which lead to high concentration contrast agents in tumor vascular bed. With the marginal vein lymphatic tumor emboli in formation, however, interstitial edema became more serious, leading to slower perfusion of contrast agents relative to the central region and resulting in turbulence in blood flow (30–32). That might explain why ΔRBF2 increased after the first cycle of NAC in responders. These parameters from different ROI highlighted that the optimal ROI positioning would have brought more accurate predictors. The microbubble agents in the CEUS only stayed within blood vessels, and the new vessels at the edge were richer than those in the center. The loss of basement membrane resulted in increased vascular permeability, and formed abundant anastomosis, which led to the contrast agent turbulence in blood flow (30–32). Hence, ΔRBF2 was the most accurate indicator.

TTP is the time from zero intensity to the peak, and MTT is the mean transit time. Some researchers (20) observed longer TTP in responders compared to non-responders after two cycles of NAC. In our research, however, there was no significant difference in TTP and MTT between responders and non-responders. The reason may be that TTP and MTT will be changed effectively until after two cycles of NAC.

To our knowledge, this is the first study to assess the value of TIC at different ranges including the edge and central regions of the lesion for early prediction of the efficiency of NAC in breast cancer using CEUS. In this study, we observed some meaningful changes after the first cycle of NAC. Δpeak1 and ΔRBF2 were potential criteria to predict the early response of NAC on breast cancer. This study could be of great clinical significance and further in-depth research on different regions of lesions with TIC could help predict the early response in breast cancer tumors under NAC.

Our study had several limitations. First, the study population was too small. A large-scale study with a standardized method is still needed. Second, the histopathology and tumor subtype of these breast cancer recruited were heterogeneous. Third, even though the TIC parameters calculated by contrast software had excellent inter-observer and intra-observer repeatability and

TABLE 2 TIC parameters in ROI 1 and ROI 2 after 1st Cycle of NAC for Discrimination between Responders and Non-responders.

	n	Response 54	Non-response 28	P-value
ROI 1	Δpeak1	0.17±0.13	0.01±0.17	0.001
	ΔTTP1	-0.40±0.67	-0.01±0.52	0.068
	ΔRBV1	0.31±0.31	-0.07±0.60	0.012
	ΔRBF1	0.18±0.13	0.03±0.14	0.002
	ΔMTT1	0.19±0.31	0.10±0.50	0.056
ROI 2	Δpeak2	0.17±0.14	-0.01±0.12	0.000
	ΔTTP2	-0.26±0.53	-0.05±0.45	0.218
	ΔRBV2	0.10±0.52	-0.15±0.55	0.169
	ΔRBF2	0.16±0.18	-0.02±0.13	0.003
	ΔMTT2	0.01±0.51	-0.12±0.47	0.446

Δ, the relative variation ratio; ROI 1, the greatest enhancement area in central region of tumor; ROI 2, the greatest enhancement area in edge of tumor.

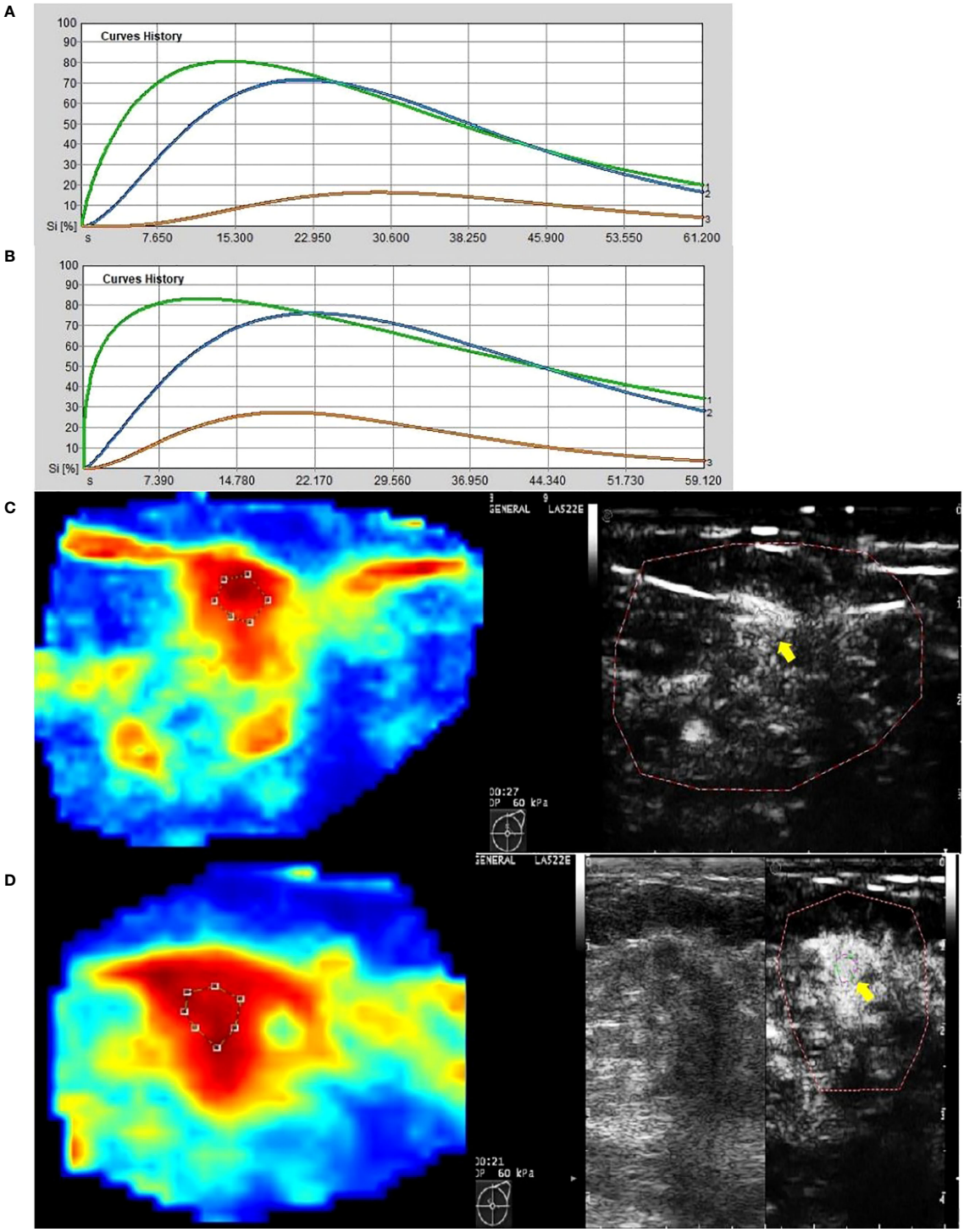

FIGURE 4
Images from a patient of non-response to NAC. **(A)** At baseline before NAC, contrast-enhanced ultrasound imaging showed a time-intensity curve generated according to regions of interest. The green line represents ROI 1 (the greatest enhancement area in central region of tumor), the blue line represents ROI 2 (the greatest enhancement area in edge of tumor), the yellow line represents normal breast tissue. **(B)** After the first cycle of NAC, neither ROI 1 nor ROI 2 declined significantly. **(C)** At baseline before NAC, the circle represents ROI 1, and the red area means rich blood supply; the right image was gray-scale which correspond to the left one, and the yellow arrow referred to ROI 1. **(D)** After the first cycle of NAC, the circle represents ROI 1, and the red area expanded, instead of shrunk; the right image was gray-scale which correspond to the left one, and the yellow arrow referred to ROI 1.

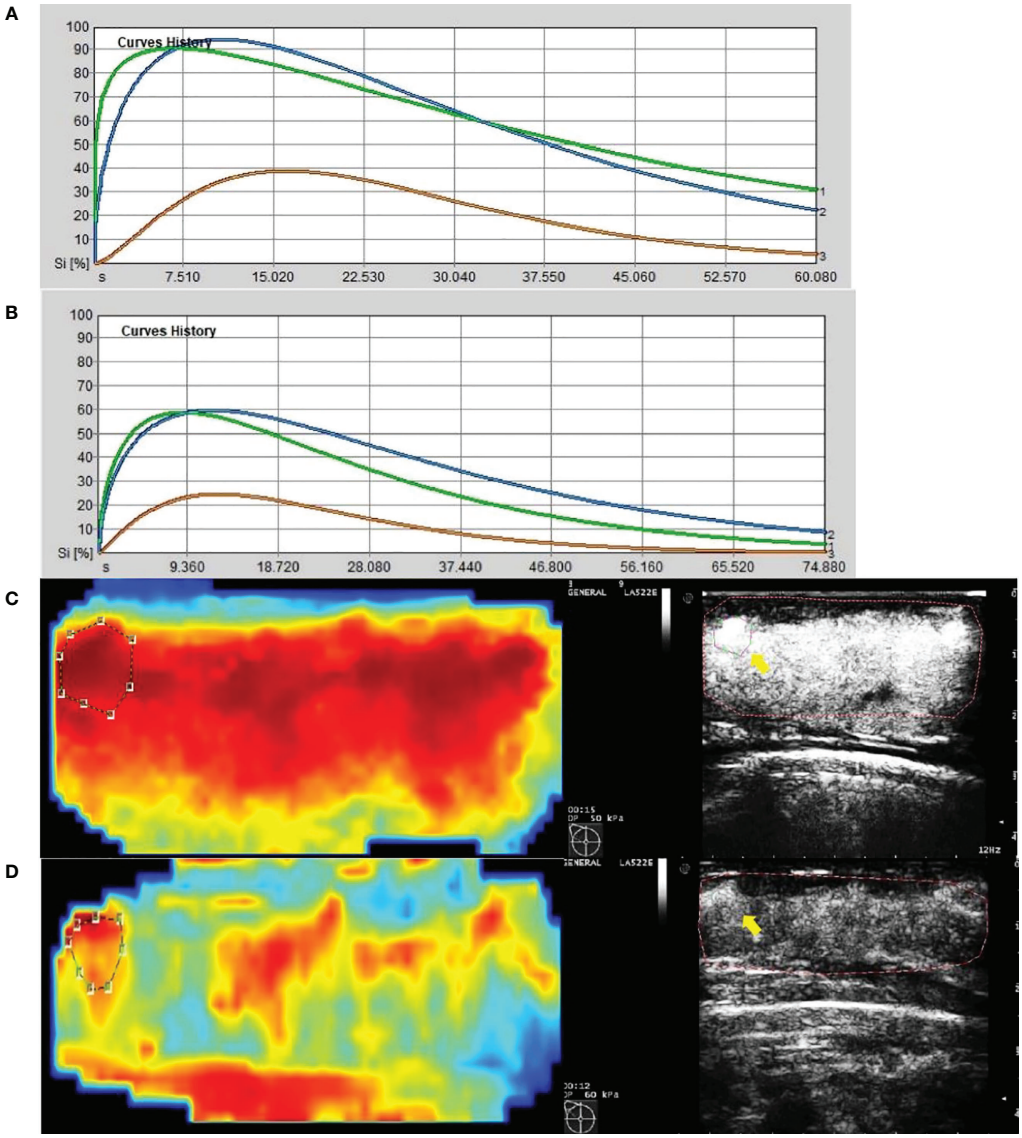

FIGURE 5
Images from a patient of response to NAC. **(A)** At baseline before NAC, contrast-enhanced ultrasound imaging showed a time-intensity curve generated according to regions of interest. The green line represents ROI 1(the greatest enhancement area in central region of tumor), the blue line represents ROI 2(the greatest enhancement area in edge of tumor), the yellow line represents normal breast tissue. **(B)** After the first cycle of NAC, both ROI 1 and ROI 2 declined significantly. **(C)** At baseline before NAC, the circle represents ROI 2, and the red area means rich blood supply; the right image was gray-scale which correspond to the left one, and the yellow arrow referred to ROI 2. **(D)** After the first cycle of NAC, the circle represents ROI 2, and the red area shrunk significantly; the right image was gray-scale which correspond to the left one, and the yellow arrow referred to ROI 2.

TABLE 3 Diagnostic Performance of TIC parameters in ROI 1 and ROI 2 to Predict Response after 1st cycle of NAC.

variable	Cut-off	AUC	SE	95%CI	P-value
Δpeak1	>0.075	0.806	0.071	(0.668, 0.945)	0.020
ΔRBV1	>0.412	0.725	0.081	(0.567, 0.884)	0.020
ΔRBF1	>0.065	0.798	0.076	(0.649, 0.947)	0.002
Δpeak2	>0.137	0.769	0.080	(0.612, 0.926)	0.005
ΔRBF2	>0.115	0.820	0.068	(0.687, 0.953)	0.001

Cut-off, the optimal threshold; AUC, area under ROC curve; SE, standard error; CI, confidence interval; ROC, receiver operating characteristic.

TABLE 4 Comparison of sensitivity, specificity, accuracy, PPV and NPV (%) of cut-off value of parameters between ROI 1 and ROI 2.

Cut-off	ROI 1			ROI 2	
	Δpeak1>0.075	ΔRBV1>0.412	ΔRBF1>0.065	Δpeak2>0.137	ΔRBF2>0.115
sensitivity	84.6%	61.5%	69.2%	61.5%	88.5%
specificity	78.6%	92.9%	92.9%	100%	78.6%
PPV	88%	94.1%	94.7%	100%	88.5%
NPV	73.3%	56.5%	61.9%	58.3%	78.6%
accuracy	82.5%	72.5%	77.5%	75%	85%

Cut-off, the optimal threshold; ROI 1, the greatest enhancement area in central region of tumor; ROI 2, the greatest enhancement area in edge of tumor.

reliability, the CEUS examination was performed only once before NAC and after the first cycle of NAC for each patient.

In conclusion, quantitative TIC parameters can be effectively used to evaluate early response to NAC in advanced breast cancer.

Data availability statement

The original contributions presented in the study are included in the article/supplementary material. Further inquiries can be directed to the corresponding author.

Ethics statement

Written informed consent was obtained from the individual(s) for the publication of any potentially identifiable images or data included in this article.

Author contributions

TJ designed the experiments. MH, PF, and MY collected the data. JG and B-HW conducted the experiments and analyzed the data. All authors contributed to the article and approved the submitted version.

Funding

This study was supported by the Foundation of Zhejiang Natural Science Committee, grant No LQ20H180013.

Conflict of interest

The authors declare that the research was conducted in the absence of any commercial or financial relationships that could be construed as a potential conflict of interest.

Publisher's note

All claims expressed in this article are solely those of the authors and do not necessarily represent those of their affiliated organizations, or those of the publisher, the editors and the reviewers. Any product that may be evaluated in this article, or claim that may be made by its manufacturer, is not guaranteed or endorsed by the publisher.

References

1. Lee SC, Grant E, Sheth P, Garcia AA, Desai B, Ji L, et al. Accuracy of contrast-enhanced ultrasound compared with magnetic resonance imaging in assessing the tumor response after neoadjuvant chemotherapy for breast cancer. *J Ultrasound Med* (2017) 36(5):901–11. doi: 10.7863/ultra.16.05060"10.7863/ultra.16.05060

2. Chu W, Jin W, Liu D, Wang J, Geng C, Chen L, et al. Diffusion-weighted imaging in identifying breast cancer pathological response to neoadjuvant chemotherapy: A meta-analysis. *Oncotarget* (2018) 9:7088–100. doi: 10.18632/oncotarget.23195

3. Wang BH, Jiang TA, Huang M, Wang J, Chu YH, Zhong LY, et al. Evaluation of the response of breast cancer patients to neoadjuvant chemotherapy by combined contrast-enhanced ultrasonography and ultrasound elastography. *Exp Ther Med* (2019) 17(5):3655–63. doi: 10.3892/etm.2019.7353

4. Galli G, Bregni G, Cavalieri S, Porcu L, Baili P, Hade A, et al. Neoadjuvant chemotherapy exerts selection pressure towards luminal phenotype breast cancer. *Breast Care (Basel)* (2017) 12:391–4. doi: 10.1159/000479582

5. Kaufmann M, von Minckwitz G, Mamounas EP, Cameron D, Carey LA, Cristofanilli M, et al. Recommendations from an international consensus conference on the current status and future of neoadjuvant systemic therapy in primary breast cancer. *Ann Surg Oncol* (2012) 19:1508–16. doi: 10.1245/s10434-011-2108-2

6. Marinovich ML, Macaskill P, Irwig L, Sardanelli F, Mamounas E, Von Minckwitz G, et al. Agreement between MRI and pathologic breast tumor size after neoadjuvant chemotherapy, and comparison with alternative tests: individual patient data meta-analysis. *BMC Cancer* (2015) 15:662. doi: 10.1186/s12885-015-1664-4

7. Kim HJ, Im YH, Han BK, Choi N, Lee J, Kim JH, et al. Accuracy of MRI for estimating residual tumor size after neoadjuvant chemotherapy in locally advanced breast cancer: relation to response patterns in MRI. *Acta Oncol* (2007) 26:996–1003. doi: 10.1080/02841860701373587

8. Denis F, Desbiez-Bourcier AV, Chapiron C, Arbion F, Body G, Brunereau L. Contrast enhanced magnetic resonance imaging underestimates residual disease

following neoadjuvant docetaxel-based chemotherapy for breast cancer. *Eur J Surg Oncol* (2004) 30:1069–76. doi: 10.1016/j.ejso.2004.07.024

9. Hieken TJ, Boughey JC, Jones KN, Shah SS, Glazebrook KN. Imaging response and residual metastatic axillary lymph node disease after neoadjuvant chemotherapy for primary breast cancer. *Ann Surg Oncol* (2013) 20(10):3199–204. doi: 10.1245/s10434-013-3118-z

10. Rosen EL, Blackwell KL, Baker JA, Soo MS, Bentley RC, Yu D, et al. Accuracy of MRI in the detection of residual breast cancer after neoadjuvant chemotherapy. *AJR Am J Roentgenol* (2003) 181(5):1275–82. doi: 10.2214/ajr.181.5.1811275

11. Lee YJ, Kim SH, Kang BJ, Kim YJ. Contrast-enhanced ultrasound for early prediction of response of breast cancer to neoadjuvant chemotherapy. *Ultraschall Med* (2019) 40(2):194–204. doi: 10.1055/a-0637-1601

12. Atri M, Hudson JM, Sinaei M, Williams R, Milot L, Moshonov H, et al. Impact of acquisition method and region of interest placement on inter-observer agreement and measurement of tumor response to targeted therapy using dynamic contrast-enhanced ultrasound. *Ultrasound Med Biol* (2016) 42:763–8. doi: 10.1016/j.ultrasmedbio.2015.11.005

13. Feng Y, Qin XC, Luo Y, Li YZ, Zhou X. Efficacy of contrast-enhanced ultrasound washout rate in predicting hepatocellular carcinoma differentiation. *Ultrasound Med Biol* (2015) 41:1553–60. doi: 10.1016/j.ultrasmedbio.2015.01.026

14. Wilson SR, Kim TK, Jang HJ, Burns PN. Enhancement patterns of focal liver masses: discordance between contrast-enhanced sonography and contrast-enhanced CT and MRI. *Am J Roentgenol* (2007) 189:W7–W12. doi: 10.2214/AJR.06.1060

15. Bhayana D, Kim TK, Jang HJ, Burns PN, Wilson SR. Hypervascular liver masses on contrast-enhanced ultrasound: the importance of washout. *Am J Roentgenol* (2010) 194:977–83. doi: 10.2214/AJR.09.3375

16. Rousseau C, Devillers A, Sagan C, Ferrer L, Bridji B, Campion L, et al. Monitoring of early response to neoadjuvant chemotherapy in stage II and III breast cancer by (18F) fluorodeoxyglucose positron emission tomography. *J Clin Oncol* (2006) 24:5366–72. doi: 10.1200/JCO.2006.05.7406

17. Schwarz-Dose J, Untch M, Tiling R, Sassen S, Mahner S, Kahlert S, et al. Monitoring primary systemic therapy of large and locally advanced breast cancer by using sequential positron emission tomography imaging with (18F) fluorodeoxyglucose. *J Clin Oncol* (2009) 27:535–41. doi: 10.1200/JCO.2008.17.2650

18. Amioka A, Masumoto N, Gouda N, Kajitani K, Shigematsu H, Emi A, et al. Ability of contrast-enhanced ultrasonography to determine clinical responses of breast cancer to neoadjuvant chemotherapy. *Jpn J Clin Oncol* (2016) 46:303–9. doi: 10.1093/jjco/hyv215

19. Wang JW, Zheng W, Liu JB, Chen Y, Cao LH, Luo RZ, et al. Assessment of early tumor response to cytotoxic chemotherapy with dynamic contrast-enhanced ultrasound in human breast cancer xenografts. *PloS One* (2013) 8:e58274. doi: 10.1371/journal.pone.0058274

20. Saracco A, Szabó BK, Tánczos E, Bergh J, Hatschek T. Contrast-enhanced ultrasound (CEUS) in assessing early response among patients with invasive breast cancer undergoing neoadjuvant chemotherapy. *Acta Radiol* (2017) 58:394–402. doi: 10.1177/0284185116658322

21. Dong T. Early response assessed by contrast-enhanced ultrasound in breast cancer patients undergoing neoadjuvant chemotherapy. *Ultrasound Q* (2018) 34 (2):84–7. doi: 10.1097/RUQ.0000000000000333

22. Ignee A, Jedrejczyk M, Schuessler G, Jakubowski W, Dietrich CF. Quantitative contrast enhanced ultrasound of the liver for time intensity curves–reliability and potential sources of errors. *Eur J Radiol* (2010) 73:153–8. doi: 10.1016/j.ejrad.2008.10.016

23. Ogston KN, Miller ID, Payne S, Hutcheon AW, Sarkar TK, Smith I, et al. A new histological grading system to assess response of breast cancers to primary chemotherapy: prognostic significance and survival. *Breast* (2003) 12:320–7. doi: 10.1016/s0960-9776(03)00106-1

24. Gu LS, Zhang R, Wang Y, Liu XM, Ma F, Wang JY, et al. Characteristics of contrast-enhanced ultrasonography and strain elastography of locally advanced breast cancer. *J Thorac Dis* (2019) 11(12):5274–89. doi: 10.21037/jtd.2019.11.52

25. Kim Y, Kim SH, Song BJ, Kang BJ, Yim KI, Lee A, et al. Early prediction of response to neoadjuvant chemotherapy using dynamic contrast-enhanced MRI and ultrasound in breast cancer. *Korean J Radiol* (2018) 19(4):682–91. doi: 10.3348/kjr.2018.19.4.682

26. Baulies S, Belin L, Mallon P, Senechal C, Pierga J-Y, Cottu P, et al. Time-varying effect and long-term survival analysis in breast cancer patients treated with neoadjuvant chemotherapy. *Br J Cancer* (2015) 113:30–6. doi: 10.1038/bjc.2015.174

27. Yang X., Knopp M. V. Quantifying tumor vascular heterogeneity with dynamic contrast-enhanced magnetic resonance imaging: a review. *J Biomed Biotechnol* (2011) 2011:732848. doi: 10.1155/2011/732848

28. Kim SY, Cho N, Shin SU, Lee HB, Han W, Park IA, et al. Contrast-enhanced MRI after neoadjuvant chemotherapy of breast cancer: lesion-to-background parenchymal signal enhancement ratio for discriminating pathological complete response from minimal residual tumor. *Eur Radiol* (2018) 9(11):1–10. doi: 10.1007/s00330-017-5251-8

29. Nakata N, Ohta T, Nishioka M, Takeyama H, Toriumi Y, Kato K, et al. Optimization of region of interest drawing for quantitative analysis. *J Ultrasound Med* (2015) 34:1969–76. doi: 10.7863/ultra.14.10042

30. Goddard LM, Iruela-Arispe ML. Cellular and molecular regulation of vascular permeability. *Thromb Haemost* (2013) 109(3):407–15. doi: 10.1160/TH12-09-0678

31. Jain RK, Martin JD, Stylianopoulos T. The role of mechanical forces in tumor growth and therapy. *Annu Rev BioMed Eng* (2014) 16:321–46. doi: 10.1146/annurev-bioeng-071813-105259

32. Wong PP, Demircioglu F, Ghazaly E, Alrawashdeh W, Stratford MRL, Scudamore C, et al. Dual-action combination therapy enhances angiogenesis while reducing tumor growth and spread. *Cancer Cell* (2015) 27(1):123–37. doi: 10.1016/j.ccell.2014.10.015

frontiers | Frontiers in Oncology

TYPE Original Research
PUBLISHED 19 December 2022
DOI 10.3389/fonc.2022.999716

Check for updates

OPEN ACCESS

EDITED BY
Raffaella Massafra,
National Cancer Institute Foundation (IRCCS), Italy

REVIEWED BY
Jiong Wu,
Fudan University, China
Takahiro Kogawa,
Cancer Institute Hospital of Japanese Foundation for Cancer Research, Japan
Luisa Carbognin,
Agostino Gemelli University Polyclinic (IRCCS), Italy

*CORRESPONDENCE
Shengchun Liu
liushengchun1968@163.com

†These authors have contributed equally to this work

SPECIALTY SECTION
This article was submitted to Breast Cancer, a section of the journal Frontiers in Oncology

RECEIVED 21 July 2022
ACCEPTED 05 December 2022
PUBLISHED 19 December 2022

CITATION
Tang L, Li Z, Jiang L, Shu X, Xu Y and Liu S (2022) Efficacy evaluation of neoadjuvant chemotherapy in patients with HER2-low expression breast cancer: A real-world retrospective study.
Front. Oncol. 12:999716.
doi: 10.3389/fonc.2022.999716

COPYRIGHT
© 2022 Tang, Li, Jiang, Shu, Xu and Liu. This is an open-access article distributed under the terms of the Creative Commons Attribution License (CC BY). The use, distribution or reproduction in other forums is permitted, provided the original author(s) and the copyright owner(s) are credited and that the original publication in this journal is cited, in accordance with accepted academic practice. No use, distribution or reproduction is permitted which does not comply with these terms.

Efficacy evaluation of neoadjuvant chemotherapy in patients with HER2-low expression breast cancer: A real-world retrospective study

Lingfeng Tang†, Zhenghang Li†, Linshan Jiang, Xiujie Shu, Yingkun Xu and Shengchun Liu*

Department of Breast and Thyroid Surgery, the First Affiliated Hospital of Chongqing Medical University, Chongqing, China

Background: To characterize the clinicopathological features and evaluate the neoadjuvant chemotherapy (NACT) efficacy of patients with human epidermal growth factor receptor 2 (HER2)-low breast cancer.

Methods: A total of 905 breast cancer patients who received 4 cycles of thrice-weekly standard NACT in the First Affiliated Hospital of Chongqing Medical University were retrospectively enrolled, including 685 cases with HER2-low expression and 220 cases with HER2-negative expression. Clinicopathological features were compared between patients with HER2-negative and HER2-low expression. Univariate and multivariate logistic regression analyses were used to find the independent factors of achieving a pathological complete response (pCR) after NACT.

Results: There were significant differences in stage_N (P = 0.014), histological grade (P = 0.001), estrogen receptor (ER) status (P < 0.001), progesterone receptor (PgR) status (P < 0.001), NACT regimens (P = 0.032) and NACT efficacy (P = 0.037) between patients with HER2-negative and HER2-low expression breast cancer. In subgroup analysis, histological grade (P = 0.032), ER (P = 0.002), Ki-67 (P < 0.001) and HER2 status (P = 0.025) were independent predictors of achieving a pCR in ER-positive breast cancer. And the nomogram for pCR in ER-positive breast cancer showed great discriminatory ability with an AUC of 0.795. The calibration curve also showed that the predictive ability of the nomogram was a good fit to actual observations. Then, in the analysis of ER-negative breast cancer, only stage_N (P = 0.001) and Ki-67 (P = 0.018) were independent influencing factors of achieving a pCR in ER-negative breast cancer.

Conclusion: HER2-low breast cancer was a different disease from HER2-negative breast cancer in clinicopathological features. Moreover, the NACT efficacy of HER2-low breast cancer patients was poorer.

KEYWORDS

HER2-low, neoadjuvant chemotherapy, pathologic complete response, nomogram, targeted therapy

Introduction

Breast cancer is recognized as a highly heterogeneous disease, which was distinguished distinct pathological subtypes through the expression of hormone receptors (HR) and human epidermal growth factor receptor 2 (HER2) (1). HER2-enriched breast cancer has been reported to be associated with aggressive clinical features and a poor prognosis, nevertheless, due to the development of anti-HER2 agents the outcomes of HER2-enriched breast cancer patients were significantly improved (2–5). But the remaining 85% of breast cancers patients with HER2-low expression (immunohistochemistry (IHC) 1+ or IHC 2+, fluorescence *in situ* hybridization (FISH) non-amplified) or HER2-negative expression (IHC 0) failed to derive no benefit from the currently available anti-HER2 treatments (6, 7).

Neoadjuvant chemotherapy (NACT), which is utilized before surgery, is mainly used for the management of patients with locally advanced breast cancer. By killing active cancer cells, NACT can effectively reduce the clinical stage of breast cancer, making inoperable breast cancer operable breast cancer or increasing the chances of breast conservation (8). Meanwhile, many studies have demonstrated that patients who achieve a pathological complete response (pCR) after NACT seem to have improved long-term outcomes (9, 10). However, chemoresistance has always been a clinical problem in the treatment of breast cancer. Some studies have shown that high HER2 expression indicated high viability, proliferation and invasive ability in tumor cells, in addition, increased drug resistance mediated by HER2 expression was an important factor for the tumor malignancy and poor patient prognosis (11). In HER2-positive breast cancer, HER2/HER3 can up-regulate survivin *via* the PI3K/Akt pathway and confer paclitaxel resistance to tumor cells (12–14). Moreover, it has been reported that HER2 can activate calmodulin dependent protein kinases and Raf/MEK/ERK signaling pathway in gastric cancer cells and induce drug resistance (15). Recently, a phase II study about a novel antibody-drug-conjugate (ADC) in HR-positive, HER2-low expression advanced breast cancer patients reported promising preliminary results in terms of clinical activity and safety (16). Besides, trastuzumab deruxtecan also showed the therapeutic potential for HER2-low expression breast cancer patients (17).

With the development of this novel therapeutic strategy, HER2-low expression breast cancer may be recognized as a distinct clinical entity. This study compared the clinicopathological characteristics of patients with HER2-low or HER2-negative expression and established a nomogram based on the influential factors of NACT for predicting the probability of achieving pCR. Such a model would be useful in evaluating sensitivity to chemotherapy, which can provide a reference for the use of novel anti-HER2 agents in neoadjuvant therapy.

Methods

Population

The database was reviewed to identify all patients diagnosed from the First Affiliated Hospital of Chongqing Medical University between 1 January 2012 and 31 December 2019. We used the following inclusion criteria: (I) female; (II) performed neoadjuvant chemotherapy; (III) invasive ductal breast cancer; and (IV) no anti-tumor treatment before NACT. The exclusion criteria were as follows: (I) inflammatory breast cancer; (II) HER2-enrich breast cancer (IHC 3+ or IHC 2+ with FISH amplified); (III) other primary tumors; (IV) bilateral breast cancer; and (V) incomplete data. A total of 905 eligible patients were ultimately included in this study. The database of patients diagnosed between 1 January 2020 and 31 June 2021 was collected according to the same standard, which would be used as the validation group of the nomogram (Figure 1).

All histological specimens were paraffin-embedded and evaluated by two skilled pathologists. This study was approved by the Ethics Committee of the First Affiliated Hospital of Chongqing Medical University (No. 2020-202). This article does not refer to the privacy of patients, so informed consent was exempted. All data were fully anonymized before we accessed them. The authors were not provided with information that could identify individual participants during or after data collection.

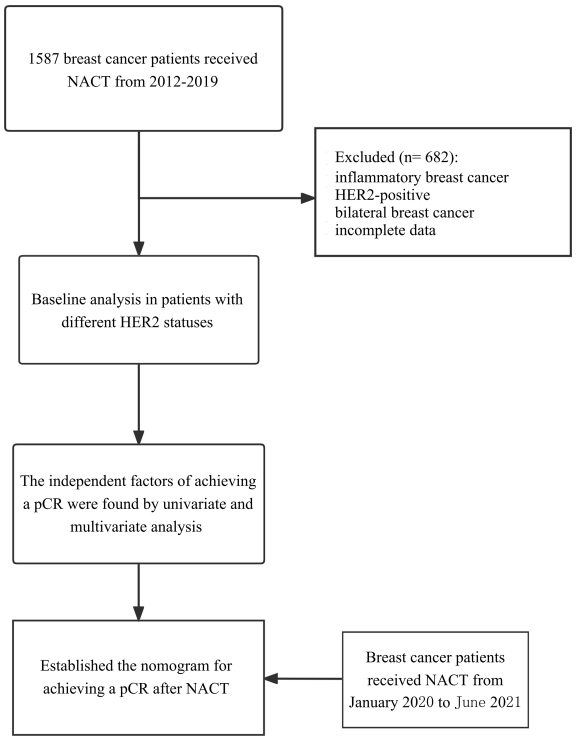

FIGURE 1
Study flowchart. Flow-chart shows the process of including patients in the study. NACT, neoadjuvant chemotherapy; pCR, pathologic complete response.

Clinicopathologic analysis

Data on the medical history, concurrent diseases, age, menopausal status, histological grade, tumor size, lymph node (LN) status, HR status, Ki-67 index, and NACT regimens were estimated before NACT. Clinical assessments of the breast, including preoperative LN status, tumor size depended on MRI or breast ultrasonography. RECIST criteria were used for the clinical response evaluation (18). The estrogen receptor (ER), progesterone receptor (PgR) and Ki-67 status were evaluated by IHC of the pretreatment core biopsy specimens. The HER2-negative group consisted of the breast cancer patients with a completely negative HER2 staining (IHC score of 0) and the HER2-low group consisted of the breast cancer patients with low level of HER2 expression (IHC scores of 1+ and 2+ with FISH non-amplified). Cancers with 1–100% of cells positive for ER/PgR expression were considered ER-positive/PgR-positive. The Ki-67 index was defined as the percentage of the total number of tumor cells (at least 1000) with nuclear staining over 10 high powered fields (× 40).

Treatment

The criteria for receiving neoadjuvant chemotherapy were as follows: patients the local stage of the disease was relatively late, such as patients with axillary lymph node metastasis or large mass or invasion of skin and chest wall, as well as patients who had a strong desire to do breast conserving surgery but did not meet the indication of breast conserving surgery when diagnosed.

NACT was given according to the local protocol and national guidelines. The treatments were predominantly anthracycline and taxane. The TEC (docetaxel 75 mg/m^2, epirubicin 75 mg/m^2, and cyclophosphamide 500 mg/m^2) or EC (epirubicin 75 mg/m^2, and cyclophosphamide 500 mg/m^2) NACT regimens were administered every 3 weeks. After diagnosis, all patients started the first cycle of NACT in a week and received four cycles of NACT regimens we evaluated the clinical response.

Objective

For all patients enrolled, mastectomy or breast conserving surgery (NACT for breast conservation) plus axillary lymphadenectomy was the basic surgical treatment after 4-cycle NACT. Two pathologists blindly and independently diagnosed all resected breast and lymph node specimens. Then, pCR was defined as no residual invasive cancer in the breast or evidence of disease in the axillary lymph nodes (ypT0ypN0) after NACT. In this study, we took pCR as our observation objective.

Statistical methods

Statistical analysis was performed by R software (Version 4.2.0) and SPSS (Version 25.0). Categorical variables were compared using the chi-squared test or Fisher's exact test. Then, univariate and multivariate logistic regression analyses were used to screen out the independent predictors. To quantify the discrimination performance of the nomogram, Harrell's C-index was measured. The intolerant abilities of the model were assessed by measuring the area under the receiver operating characteristic (ROC) curve. Calibration curves were plotted to assess the calibration of the nomogram (19). In this case, the calibration is the agreement between the frequencies of the observed outcomes and the probabilities predicted by the model. $P < 0.05$ was defined as statistically significance.

Results

Baseline patient characteristics based on HER2 status

A total of 905 patients with HER2-low expression or HER2-negative breast cancer who received NACT were identified (mean age 49.2 ± 9.5 years (range 20–75 years)) and 119 patients (13.1%) who achieved pCR after NACT. In addition, 685 (75.7%) cases with HER2-low expression and 220 (24.3%) HER2-negative cases. We compared the clinicopathological characteristics and NACT efficacy of patients with different HER2 status (HER2-low group vs. HER2-negative group), and the results are displayed in Table 1. There were significant differences in stage_N ($P = 0.014$), histological grade ($P = 0.001$), ER status ($P < 0.001$), PgR status ($P < 0.001$), NACT regimens ($P = 0.032$) and NACT efficacy ($P = 0.037$) between patients with HER2-negative and HER2-low breast cancer. The patients with HER2-low breast cancer had a lower percentage of pCR compared to those with HER2-negative tumors.

Analysis in different breast cancer subtypes

The results of chi-squared test found that HER2 status was significantly associated with ER status. The distribution of different HER2 status in ER-positive patients and ER-negative patients was shown in Figure 2. Therefore, we analyzed the relationship between clinicopathological features and HER2 status in different breast cancer subtypes. In ER-positive breast cancer, there were significant differences in NACT efficacy ($P = 0.014$) and stage_N ($P = 0.003$) were significantly among HER2-low and HER2-negative breast cancers. The patients with HER2-low breast cancer had a lower percentage of pCR. Nevertheless, in ER-negative breast cancer only stage_N ($P = 0.01$) are related to HER2 status (Table 2). A significant association was observed between HER2 status and the probability to achieve a pCR. Of note, HER2-low breast cancer was associated with the low rate of pCR, especially in ER-positive patients, as shown in Figure 3. Here we found that there may exist some relevance between HER2 and HR, so subsequent analysis was performed in ER-positive patients and ER-negative patients respectively.

Univariate and multivariate analysis on the factors of achieving a pCR after NACT

Based on univariate analysis, there were significant differences in stage_N ($P = 0.029$), histological grade ($P = 0.003$), ER ($P < 0.001$), PgR ($P = 0.047$), Ki-67 ($P < 0.001$) and HER2 status ($P = 0.015$) for achieving a pCR in patients with ER-positive breast cancer. Then, we included the factors ($P< 0.05$) in the multivariate analysis. We found that histological grade ($P = 0.032$), ER ($P = 0.002$), Ki-67 ($P < 0.001$) and HER2 status ($P = 0.025$) were independent predictors of achieving a pCR in ER-positive breast cancer (Table 3).

Next, through the same analysis strategies, we found that stage_N ($P = 0.001$) and Ki-67 ($P = 0.018$) were independent predictors of achieving a pCR in ER-negative breast cancer (Table 4).

Establish and validate the nomogram for NACT efficacy in ER-positive breast cancer

Through the univariate and multivariate logistic regression analysis, we established a nomogram to predict the probability of achieving a pCR after NACT in ER-positive breast cancer. The factors in the model included histological grade, ER expression, Ki-67 index and HER2 status (Figure 4).

According to this model, the ROC curve was drawn (Figure 5A), and the area under the curve (AUC) was 0.795 (95% CI: 0.735–0.855). The C-index of the prediction models was 0.787, which demonstrates good discriminative ability. The calibration plot revealed good agreement between the predictions and actual observations (Figure 5C).

Then, we took the data of patients diagnosed between 1 January 2020 and 31 June 2021 as external validation. There were no significant differences in age, menopausal status, stage_T, stage_N, histological grade, PgR status, HER2 status, Ki-67 index, NACT regimens and NACT efficacy between the derivation and validation groups (Table 5). Similarly, we established another nomogram through univariate and multivariate logistic regression analysis (Supplement Figure 1), these two models have good consistency. The ROC curve (AUC 0.802 (95% CI 0.785–0.819)) and calibration plot of validation group also indicated a good prediction ability(Figures 5B, D).

In summary, these results showed that this nomogram has good efficacy in predicting the probability of achieving a pCR in ER-positive breast cancer.

Discussion

HER2 is a prototype oncogene and its amplification represents a poor breast cancer subtype (17). Therapeutic interventions are focused on a small group of tumors that show an amplification of the HER2 gene with subsequent overexpression of the HER2 protein. High HER2 expression not only promotes the occurrence and development of tumors, but also is related to chemotherapy resistance (11). However, at present, in clinical the treatment strategy of patients with HER2-low breast cancer is the same as that of patients with HER2-negative breast cancer. In the present study, we retrospectively analyzed the clinicopathological features of patients with HER2-

10.3389/fonc.2022.999716

TABLE 1 Baseline clinicopathological characteristics of breast cancer patients with different HER2 status.

Characteristic	Total (n= 905)	HER2-low (n= 685)	HER2-negative (n= 220)	*P* value[a]
Age (years)				0.105
< 45	496(54.8%)	365(53.2%)	131(59.5%)	
≥ 45	409(45.2%)	320(46.7%)	89(40.5%)	
Menopausal status				0.385
Premenopausal	315(34.8%)	233(34.0%)	82(37.3%)	
Perimenopausal	353(39.0%)	265(38.7%)	88(40.0%)	
Postmenopausal	237(26.2%)	187(27.3%)	50(22.7%)	
Stage_T				0.386
T1	88(9.7%)	71(10.4%)	17(7.7%)	
T2	653(72.2%)	487(71.1%)	166(75.5%)	
T3/T4	164(18.1%)	127(18.5%)	37(16.8%)	
Stage_N				**0.014**
cN0	324(35.8%)	234(34.1%)	90(40.9%)	
cN1	451(49.8%)	360(52.6%)	91(41.4%)	
cN2/cN3	130(14.4%)	91(13.3%)	39(17.7%)	
Histological grade				**0.001**
I/II	532(58.8%)	424(61.9%)	108(49.1%)	
III	373(41.2%)	261(38.1%)	112(50.9%)	
ER status				< **0.001**
Negative	280(30.9%)	176(25.7%)	104(47.3%)	
Positive	625(69.1%)	509(74.3%)	116(52.7%)	
PgR status				< **0.001**
Negative	395(43.6%)	270(39.4%)	125(56.8%)	
Positive	510(56.4%)	415(60.6%)	95(43.2%)	
Ki-67(%)				0.071
≤ 20	421(46.5%)	332(48.5%)	89(40.5%)	
(20, 50]	323(35.7%)	240(35.0%)	83(37.7%)	
>50	161(17.8%)	113(16.5%)	48(21.8%)	
NACT regimens				**0.032**
TEC	808(89.3%)	603(88.0%)	205(93.2%)	
EC-T	97(10.7%)	82(12.0%)	15(6.8%)	
NACT efficacy				**0.037**
pCR	119(13.1%)	81(11.8%)	38(17.3%)	
Non-pCR	786(86.9%)	604(88.2%)	182(82.7%)	

pCR, pathologic complete response; ER, estrogen receptor; PgR, progesterone receptor; HER2, human epidermal growth factor receptor2; NACT, neoadjuvant chemotherapy.
[a]*P* values were determined by chi-square tests. Bold values indicate statistical significance ($P < 0.05$).

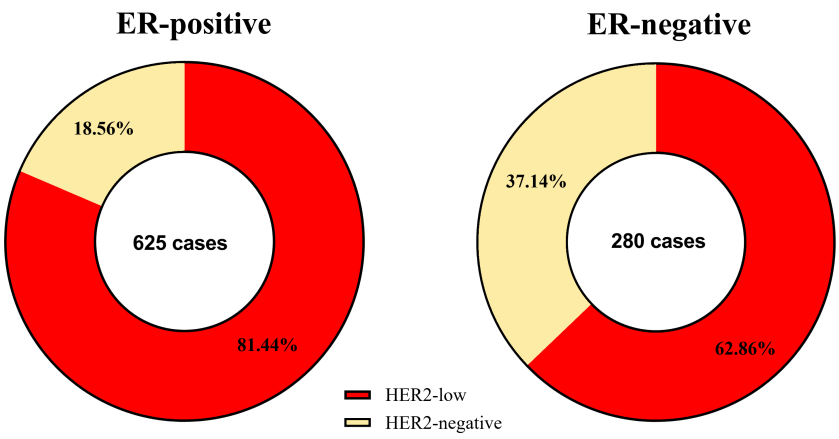

FIGURE 2
The compositions of different HER2 status by ER status.

TABLE 2 Patient characteristics by HER2 status in different breast cancer subtypes.

Characteristic	ER-positive			ER-negative		
	HER2-low (n = 509)	HER2-negative (n = 116)	*P* value	HER2-low (n = 176)	HER2-negative (n = 104)	*P* value
Age (years)			0.139			0.379
< 45	273(53.6%)	71(61.2%)		92(52.3%)	60(57.7%)	
≥ 45	236(46.4%)	45(38.8%)		84(47.7%)	44(42.3%)	
Menopausal status			0.518			0.738
Premenopausal	171(33.6%)	45(38.8%)		62(35.2%)	37(35.6%)	
Perimenopausal	195(38.3%)	43(37.1%)		70(39.8%)	45(43.3%)	
Postmenopausal	143(28.1%)	28(24.1%)		44(25.0%)	22(21.2%)	
T stage			0.195			0.927
T1	58(11.4%)	8(6.9%)		13(7.4%)	9(8.7%)	
T2	359(70.5%)	91(78.4%)		128(72.7%)	75(72.1%)	
T3/T4	92(18.1%)	17(14.7%)		35(19.9%)	20(19.2%)	
N stage			**0.042**			**0.010**
cN0	142(27.9%)	45(38.8%)		91(51.7%)	39(37.5%)	
cN1	294(57.8%)	53(45.7%)		67(38.1%)	42(40.4%)	
cN2/cN3	73(14.3%)	18(15.5%)		18(10.2%)	23(22.1%)	
Histological grade			0.260			0.227
I/II	348(68.4%)	73(62.9%)		72(40.9%)	35(33.7%)	
III	161(31.6%)	43(37.1%)		104(59.1%)	69(66.3%)	
ER status			0.832			
(0, 10]	36(7.1%)	9(7.8%)				
(10, 40]	48(9.4%)	14(12.1%)				

(Continued)

TABLE 2 Continued

Characteristic	ER-positive			ER-negative		
	HER2-low (n = 509)	HER2-negative (n = 116)	*P* value	HER2-low (n = 176)	HER2-negative (n = 104)	*P* value
(40, 70]	145(28.5%)	31(26.7%)				
>70	280(55.0%)	62(53.4%)				
PgR status			0.908			
Negative	103(20.0%)	27(23.3%)				
(0, 10]	75(14.7%)	16(13.8%)				
(10, 50]	98(19.3%)	22(19.0%)				
>50	233(45.8%)	51(44.0%)				
Ki-67(%)			0.715			0.072
≤ 20	273(53.6%)	67(57.8%)		57(32.4%)	21(20.2%)	
(20, 50]	176(34.6%)	36(31.0%)		62(35.2%)	47(45.2%)	
>50	60(11.8%)	13(11.2%)		57(32.4%)	36(34.6%)	
NACT regimens			0.098			0.102
TEC	452(88.8%)	109(94.0%)		151(85.5%)	96(92.3%)	
EC-T	57(11.2%)	7(6.0%)		25(14.2%)	8(7.7%)	
NACT efficacy			**0.014**			0.414
pCR	38(7.5%)	17(14.7%)		43(24.4%)	21(20.2%)	
Non-pCR	471(92.5%)	99(85.3%)		133(75.6%)	83(79.8%)	

Bold values indicate statistical significance (P < 0.05).

negative or HER2-low breast cancer and explored the influencing factors of achieving a pCR after NACT.

In our cohort of 905 breast cancer patients undergoing neoadjuvant chemotherapy, we found the intense association between HER2-low expression and HR-positive status ($P < 0.001$), and confirmed the possible role for ER in HER2-low expression biology (20, 21). Consequently, we performed a subgroup analysis of HER2 status in ER-positive and ER-negative breast cancer. Compared with ER-positive, HER2-negative breast cancer patients, a higher rate of axillary lymph node metastasis was found in patients with ER-positive, HER2-low breast cancer ($P = 0.042$). Analogous findings have been reported by previous studies, which consistently with our study have found a higher stage_N and lower histological grade in HER2-low breast cancer (22–24). In addition, it has also been found that HER2 status was related to age and stage_T in previous studies. Therefore, HER2-low breast cancer is different from HER2-negative breast cancer in clinicopathological features and may be recognized as a distinct diseases.

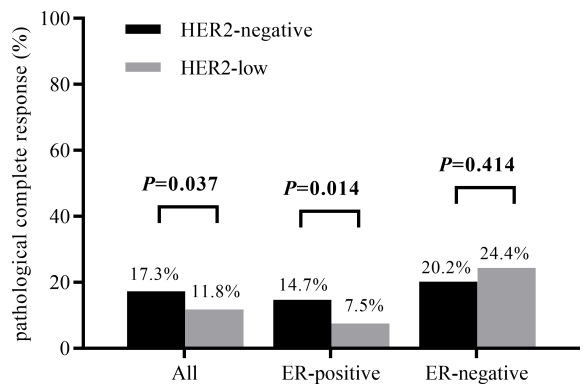

FIGURE 3
pCR rates according to HER2 status in different breast cancer subtypes (*P* value obtained by $\chi 2$ test).

In the last century, the expression of HER2 was observed to confer resistance in breast cancer cells to several chemotherapy agents (25, 26). In the previous understanding HER2-low breast cancer was less malignant than HER2-positive breast cancer, however, there was no strong evidence that low expression of HER2 did not impact the process of tumorigenesis and drug resistance. In our study, overall in neoadjuvant chemotherapy for breast cancer patients, pCR rates were lower in HER2-low

TABLE 3 Univariate and multivariate analysis of achieving a pCR in patients in ER-positive breast cancer.

Characteristics	Univariate analysis OR (95% CI)	*P* value	Multivariate analysis OR (95% CI)	*P* value
Age, years (≥ 45 vs < 45)	0.736 (0.417–1.300)	0.291		–
Menopausal status		0.207		–
Premenopausal	1 (reference)			–
Perimenopausal	0.625 (0.331–1.181)			–
Postmenopausal	0.577 (0.281–1.184)			–
T stage		0.229		–
T1	1 (reference)			–
T2	2.333 (0.704–7.735)			–
T3/T4	1.441 (0.360–5.777)			–
N stage		**0.029**		0.109
cN0	1 (reference)		1 (reference)	
cN1	0.579 (0.326–1.030)		0.668 (0.357–1.252)	
cN2/cN3	0.236 (0.069–0.803)		0.276 (0.076–1.000)	
Histological grade (III vs I/II)	2.322 (1.329–4.055)	**0.003**	1.952 (1.061–3.590)	**0.032**
ER status		**< 0.001**		**0.002**
(0, 10]	1 (reference)		1 (reference)	
(10, 40]	0.125 (0.033–0.472)		0.096 (0.023–0.411)	
(40, 70]	0.229 (0.100–0.528)		0.208 (0.076–0.571)	
>70	0.186 (0.086–0.400)		0.201 (0.076–0.532)	
PgR status		**0.047**		0.302
Negative	1 (reference)		1 (reference)	
(0, 10]	0.269 (0.088–0.818)		0.321 (0.096–1.071)	
(10, 50]	0.590 (0.268–1.297)		0.979 (0.393–2.440)	
>50	0.466 (0.241–0.902)		0.847 (0.370–1.937)	
Ki-67(%)		**< 0.001**		**< 0.001**
≤ 20	1 (reference)		1 (reference)	
(20, 50]	3.255 (1.659–6.388)		2.687 (1.317–5.484)	
>50	6.022 (2.760–13.138)		6.402 (2.804–14.617)	
NACT regimens (EC-T vs TEC)	0.481 (0.146–1.588)	0.230		–
HER2 status (HER2-low vs HER2-negative)	0.470 (0.255–0.866)	**0.015**	0.460 (0.233–0.906)	**0.025**

OR, odd ratio.
Bold values indicate statistical significance (P < 0.05).

breast cancer patients (11.8%) than in HER2-negative patients (17.3%). Federica Miglietta et al. performed a retrospective study of 488 cases and obtained a consistent result that a lower proportion of pCR in HER2-low breast cancer patients (21.4%) after NACT than HER2-negative ones (33.6%) (27). Furthermore, another study including four prospective neoadjuvant clinical trials have reported analogous findings (pCR rates: 29.2% (HER2-low) vs 39.0% (HER2-negative)), which also showed that the proportion of pCR was significantly lower in HER2-low tumors versus HER2-negative tumors in the ER-positive subgroup ($P = 0.024$) but not in the ER-negative subgroup ($P = 0.21$).

Recently, a phase II study about a novel ADC reported promising preliminary results in HR-positive, HER2-low expression advanced breast cancer patients (16). Besides, trastuzumab-deruxtecan (T-Dxd) with a cleavable linkage to a

TABLE 4 Univariate and multivariate analysis of achieving a pCR in patients in ER-negative breast cancer.

Characteristics	Univariate analysis OR (95% CI)	*P* value	Multivariate analysis OR (95% CI)	*P* value
Age, years (≥ 45 vs < 45)	1.152 (0.659–2.015)	0.619		
Menopausal status		0.353		
Premenopausal	1 (reference)			
Perimenopausal	0.861 (0.463–1.604)			
Postmenopausal	0.562 (0.256–1.234)			
T stage		0.261		
T1	1 (reference)			
T2	0.871 (0.323–2.348)			
T3/T4	0.454 (0.137–1.508)			
N stage		**< 0.001**		**0.001**
cN0	1 (reference)		1 (reference)	
cN1	0.312 (0.162–0.600)		0.319 (0.164–0.622)	
cN2/cN3	0.271 (0.100–0.740)		0.276 (0.099–0.765)	
Histological grade (III vs I/II)	1.791 (0.974–3.291)	0.061	1.581 (0.834–2.996)	0.160
Ki-67(%)		**0.023**		**0.018**
≤ 20	1 (reference)		1 (reference)	
(20, 50]	3.047 (1.356–6.848)		2.733 (1.186–6.302)	
>50	2.667 (1.156–6.150)		2.554 (1.079–6.046)	
NACT regimens (EC-T vs TEC)	1.091 (0.466–2.554)	0.840		
HER2 status (HER2-low vs HER2-negative)	1.278 (0.709–2.304)	0.415		

Bold values indicate statistical significance (P < 0.05).

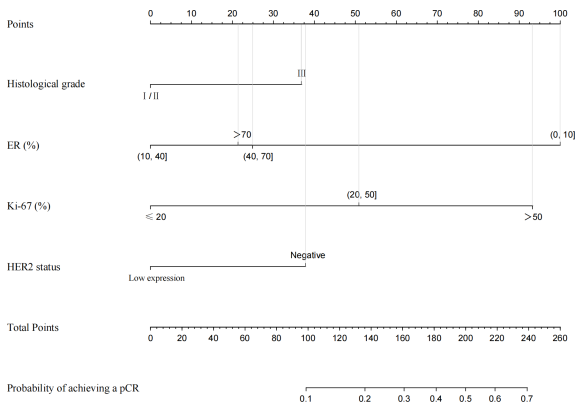

FIGURE 4
Nomogram for predicting pCR in ER–positive breast cancer patients after NACT. A line is drawn straight up to the point axis that corresponds with each patient variable to obtain the points. The sum of these points is located on the total score points axis. A line is drawn downwards to the risk axis to determine the possibility of achieving a pCR.

potent topoisomerase I inhibitor payload and excellent membrane permeability, which laid the foundation for the treatment of HER2-low breast cancer (28). For instance, T-Dxd has achieved an objective response rate (ORR) of 37% in advanced breast cancer patients with low HER2 expression in preliminary trail (17). Recently, some encouraging results have been reported from the critical phase III trial DESTINY-Breast 04, which showed that regardless of HR status PFS and OS were both improved in HER2-low breast cancer patients treated with T-Dxd (29). Based on these promising results, several additional trails were gradually promoted. Interestingly, previous findings reported similar prognosis between HER2-low and HER2-negative breast cancer, so the drug used for the HER-low patients can better improve the prognosis of most breast cancer patients in the future (21, 30).

In addition to HER2 status, histological grade ($P = 0.032$), Ki-67 ($P < 0.001$), and ER status ($P = 0.002$) were independent predictors of achieving a pCR in ER-positive breast cancer *via* univariate and multivariate analysis. Based on these factors we developed an easy-to-use nomogram to predict the probability of achieving a pCR after NACT in ER-positive breast cancer patients. With this model we can rapidly predict the possibility

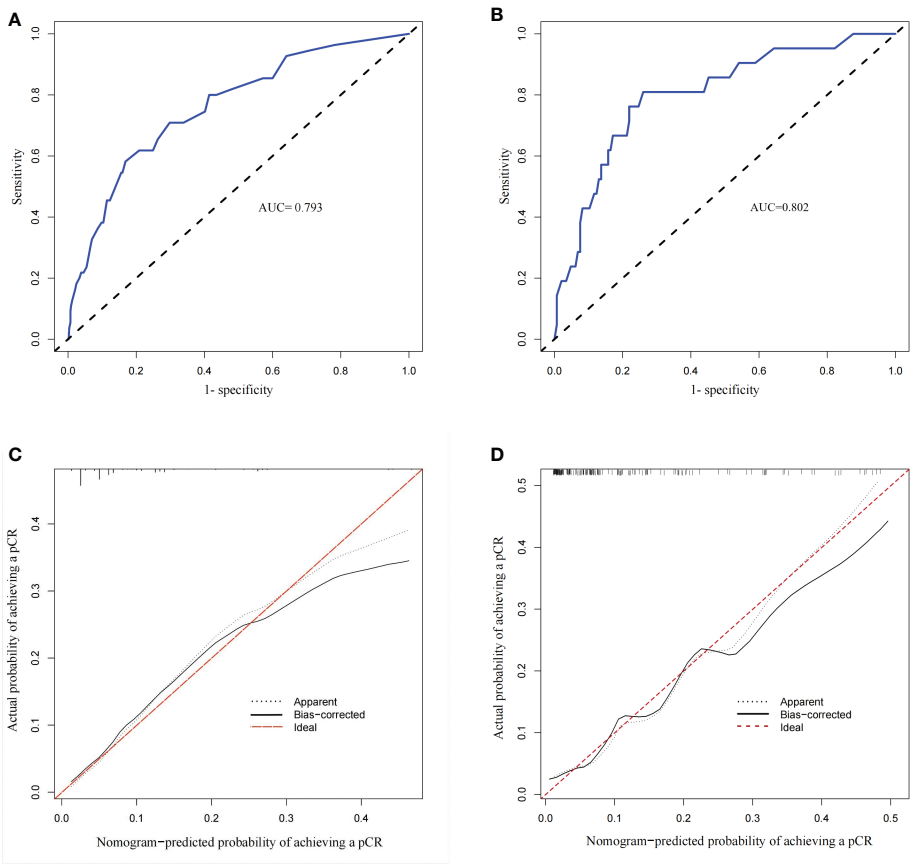

FIGURE 5
Calibration plots and Receiver operating characteristic (ROC) curves of the model. **(A)** ROC curve of the derivation group with an AUC of 0.795 (95% CI 0.735–0.855). **(B)** ROC curve of the validation group with an AUC of 0.802 (95% CI 0.785–0.819). **(C)** Calibration plot of the derivation group (The calibration plot depicts the calibration of the model in terms of the agreement between the predicted and the observed possibility of achieving a pCR in ER-positive breast cancer). **(D)** Calibration plot of the validation group.

of an ER-positive patient achieving a pCR after NACT. Then, similar analysis performed in patients with ER-negative breast cancer demonstrated that stage_N (P = 0.001) and Ki-67 (P < 0.018) were independent factors of achieving a pCR. The ER-negative breast cancer patient with earlier stage_N and higher Ki-67 index is more likely to achieving a pCR after NACT. Herein, patients with HER2-low breast cancers account for 75.7% of the total, thus, if the novel agents can be used in neoadjuvant therapy in the future, the pCR rate and the prognosis will be improved.

Our study has several limitations. Firstly, single institution and retrospective nature may responsible for both selection and information bias. Then, the lack of follow-up data has prevented us from conducting a deeper analysis of survival and recurrence rates in patients treated with neoadjuvant chemotherapy. However, our study collected detailed preoperative clinicopathological data and established a predictive model, which can better provide reference for clinical practice.

Conclusion

For a long time, HER2-negative breast cancer and HER2-low breast cancer were recognized as the same biological subtype. Here, our study provides new insight into the clinicopathological features and NACT efficacy of HER2-low tumors. We evaluated some important factors that affect chemotherapy efficacy in a large cohort of patients undergoing neoadjuvant chemotherapy, with HER2 status being an independent influencing factor of pCR. Whereas, HER2-low breast cancer patients with a low probability of achieving a pCR will be candidates for new ADC drugs in the future.

Data availability statement

The original contributions presented in the study are included in the article/Supplementary Material. Further inquiries can be directed to the corresponding author.

10.3389/fonc.2022.999716

TABLE 5 Difference between the derivation and validation data groups.

Characteristic	Derivation Group (n = 625)	Validation Group (n = 167)	*P* value
Age (years)			0.670
< 45	344(55.0%)	95(56.9%)	
≥ 45	281(45.0%)	72(43.1%)	
Menopausal status			0.673
Premenopausal	216(34.6%)	61(36.5%)	
Perimenopausal	238(38.1%)	66(39.5%)	
Postmenopausal	171(27.4%)	40(24.0%)	
Stage_T			0.408
T1	66(10.6%)	12(7.2%)	
T2	450(72.0%)	123(73.7%)	
T3/T4	109(17.4%)	32(19.1%)	
Stage_N			0.149
cN0	187(29.9%)	61(36.5%)	
cN1	347(55.5%)	89(53.3%)	
cN2/cN3	90(14.9%)	17(10.2%)	
Histological grade			0.276
I/II	421(67.4%)	105(62.9%)	
III	204(32.6%)	62(37.1%)	
ER status			**0.035**
(0, 10]	45(7.2%)	15(9.0%)	
(10, 40]	62(9.9%)	27(16.2%)	
(40, 70]	176(28.2%)	52(31.1%)	
>70	342(54.7%)	73(43.7%)	
PgR status			0.251
Negative	130(20.8%)	35(21.0%)	
(0, 10]	91(14.6%)	34(20.4%)	
(10, 50]	120(19.2%)	33(19.8%)	
>50	284(45.4%)	65(38.9%)	
HER2 status			0.371
Negative	116(18.6%)	26(15.6%)	
Low	509(81.4%)	141(84.4%)	
Ki-67(%)			0.086
≤ 20	340(54.4%)	88(52.7%)	
(20, 50]	212(33.9%)	49(29.3%)	
>50	73(11.7%)	30(18.0%)	
NACT regimens			0.982
TEC	561(89.8%)	150(89.8%)	

(Continued)

TABLE 5 Continued

Characteristic	Derivation Group (n = 625)	Validation Group (n = 167)	*P* value
EC-T	64(10.2%)	17(10.2%)	
NACT efficacy			0.141
pCR	55(8.8%)	21(12.6%)	
Non-pCR	570(91.2%)	146(87.4%)	

Bold values indicate statistical significance (P < 0.05).

Ethics statement

The studies involving human participants were reviewed and approved by Ethics Committee of the First Affiliated Hospital of Chongqing Medical University. Written informed consent for participation was not required for this study in accordance with the national legislation and the institutional requirements.

Author contributions

(I) Conception and design: LT, ZL, and SL; (II) Administrative support: LT, SL; (III) Collection and assembly of data: ZL and LJ; (IV) Data analysis and interpretation: LT, LJ and YX; (V) Manuscript writing: LT, XS and ZL. All authors contributed to the article and approved the submitted version.

Acknowledgments

The authors appreciate all of the staff involved in the preparation of the study.

Conflict of interest

The authors declare that the research was conducted in the absence of any commercial or financial relationships that could be construed as a potential conflict of interest.

Publisher's note

All claims expressed in this article are solely those of the authors and do not necessarily represent those of their affiliated organizations, or those of the publisher, the editors and the reviewers. Any product that may be evaluated in this article, or claim that may be made by its manufacturer, is not guaranteed or endorsed by the publisher.

Supplementary material

The Supplementary Material for this article can be found online at: https://www.frontiersin.org/articles/10.3389/fonc.2022.999716/full#supplementary-material

References

1. Cancer Genome Atlas N. Comprehensive molecular portraits of human breast tumours. *Nature* (2012) 490(7418):61–70. doi: 10.1038/nature11412

2. Cronin KA, Harlan LC, Dodd KW, Abrams JS, Ballard-Barbash R. Population-based estimate of the prevalence of HER-2 positive breast cancer tumors for early stage patients in the US. *Cancer Invest* (2010) 28(9):963–8. doi: 10.3109/07357907.2010.496759

3. Geyer CE, Forster J, Lindquist D, Chan S, Romieu CG, Pienkowski T, et al. Lapatinib plus capecitabine for HER2-positive advanced breast cancer. *N Engl J Med* (2006) 355(26):2733–43. doi: 10.1056/NEJMoa064320

4. Slamon DJ, Clark GM, Wong SG, Levin WJ, Ullrich A, McGuire WL. Human breast cancer: correlation of relapse and survival with amplification of the HER-2/neu oncogene. *Science* (1987) 235(4785):177–82. doi: 10.1126/science.3798106

5. Swain SM, Baselga J, Kim SB, Ro J, Semiglazov V, Campone M, et al. Pertuzumab, trastuzumab, and docetaxel in HER2-positive metastatic breast cancer. *N Engl J Med* (2015) 372(8):724–34. doi: 10.1056/NEJMoa1413513

6. Asif HM, Sultana S, Ahmed S, Akhtar N, Tariq M. HER-2 positive breast cancer - a mini-review. *Asian Pac J Cancer Prev* (2016) 17(4):1609–15. doi: 10.7314/apjcp.2016.17.4.1609

7. Fehrenbacher L, Cecchini RS, Geyer CE, Rastogi P, Costantino JP, Atkins JN, et al. NSABP b-47/NRG oncology phase III randomized trial comparing adjuvant chemotherapy with or without trastuzumab in high-risk invasive breast cancer negative for HER2 by FISH and with IHC 1+ or 2. *J Clin Oncol* (2020) 38(5):444–53. doi: 10.1200/JCO.19.01455

8. van der Hage JA, van de Velde CJ, Julien JP, Tubiana-Hulin M, Vandervelden C, Duchateau L. Preoperative chemotherapy in primary operable breast cancer: results from the European organization for research and treatment of cancer trial 10902. *J Clin Oncol* (2001) 19(22):4224–37. doi: 10.1200/JCO.2001.19.22.4224

9. Chollet P, Amat S, Cure H, Latour M, Bouedec GL, Mouret-Reynier MA, et al. Prognostic significance of a complete pathological response after induction chemotherapy in operable breast cancer. *Br J Cancer* (2002) 86(7):1041-6. doi: 10.1038/sj.bjc.6600210

10. Fisher ER, Wang J, Bryant J, Fisher B, Mamounas E, Wolmark NJC. Pathobiology of preoperative chemotherapy: Findings from the national surgical adjuvant breast and bowel (NSABP) protocol b-18. *Cancer* (2002) 95(4):681. doi: 10.1002/cncr.10741

11. Yu D, Hung MC. Overexpression of ErbB2 in cancer and ErbB2-targeting strategies. *Oncogene* (2000) 19(53):6115–21. doi: 10.1038/sj.onc.1203972

12. Chen J, Ren Q, Cai Y, Lin T, Zuo W, Wang J, et al. Mesenchymal stem cells drive paclitaxel resistance in ErbB2/ErbB3-coexpressing breast cancer cells via

paracrine of neuregulin 1. *Biochem Biophys Res Commun* (2018) 501(1):212–9. doi: 10.1016/j.bbrc.2018.04.218

13. Wang S, Huang X, Lee CK, Liu B. Elevated expression of erbB3 confers paclitaxel resistance in erbB2-overexpressing breast cancer cells via upregulation of survivin. *Oncogene* (2010) 29(29):4225–36. doi: 10.1038/onc.2010.180

14. Amin DN, Campbell MR, Moasser MM. The role of HER3, the unpretentious member of the HER family, in cancer biology and cancer therapeutics. *Semin Cell Dev Biol* (2010) 21(9):944–50. doi: 10.1016/j.semcdb.2010.08.007

15. Ji R, Zhang B, Zhang X, Xue J, Yuan X, Yan Y, et al. Exosomes derived from human mesenchymal stem cells confer drug resistance in gastric cancer. *Cell Cycle* (2015) 14(15):2473–83. doi: 10.1080/15384101.2015.1005530

16. Hamilton EP, Petit T, Pistilli B, Goncalves A, Ferreira AA, Dalenc F, et al. Clinical activity of MCLA-128 (zenocutuzumab), trastuzumab, and vinorelbine in HER2 amplified metastatic breast cancer (MBC) patients (pts) who had progressed on anti-HER2 ADCs. *J Clin Oncol* (2020) 38(15_suppl):3093–3093. doi: 10.1200/JCO.2020.38.15_suppl.3093

17. Modi S, Park H, Murthy RK, Iwata H, Tamura K, Tsurutani J, et al. Antitumor activity and safety of trastuzumab deruxtecan in patients with HER2-Low–expressing advanced breast cancer. *Results From Phase Ib Study* (2020) 38 (17):1887–96. doi: 10.1200/jco.19.02318

18. Eisenhauer EA, Therasse P, Bogaerts J, Schwartz LH, Sargent D, Ford R, et al. New response evaluation criteria in solid tumours: Revised RECIST guideline (version 1.1). *Eur J Cancer* (2009) 45(2):228–47. doi: 10.1016/j.ejca.2008.10.026

19. Kramer AA, Zimmerman JE. Assessing the calibration of mortality benchmarks in critical care: The hosmer-lemeshow test revisited. *Crit Care Med* (2007) 35(9):2052–6. doi: 10.1097/01.CCM.0000275267.64078.B0

20. Osborne CK, Shou J, Massarweh S, Schiff R. Crosstalk between estrogen receptor and growth factor receptor pathways as a cause for endocrine therapy resistance in breast cancer. *Clin Cancer Res* (2005) 11(2 Pt 2):865s. doi: 10.1158/1078-0432.865s.11.2

21. Schettini F, Chic N, Brasó-Maristany F, Paré L, Pascual T, Conte B, et al. Clinical, pathological, and PAM50 gene expression features of HER2-low breast cancer. *NPJ breast cancer* (2021) 7(1):1. doi: 1002/cncr.10741. :10.1038/s41523-020-00208-2

22. Rosso C, Voutsadakis IA. Characteristics, clinical differences and outcomes of breast cancer patients with negative or low HER2 expression. *Clin Breast Cancer* (2022) 22(4):391–7. doi: 10.1016/j.clbc.2022.02.008

23. Horisawa N, Adachi Y, Takatsuka D, Nozawa K, Endo Y, Ozaki Y, et al. The frequency of low HER2 expression in breast cancer and a comparison of prognosis between patients with HER2-low and HER2-negative breast cancer by HR status. *Breast Cancer* (2022) 29(2):234–41. doi: 10.1007/s12282-021-01303-3

24. Denkert C, Seither F, Schneeweiss A, Link T, Blohmer J-U, Just M, et al. Clinical and molecular characteristics of HER2-low-positive breast cancer: pooled analysis of individual patient data from four prospective, neoadjuvant clinical trials. *Lancet Oncol* (2021) 22(8):1151–61. doi: 10.1016/s1470-2045(21)00301-6

25. Jarvinen TA, Holli K, Kuukasjarvi T, Isola JJ. Predictive value of topoisomerase IIalpha and other prognostic factors for epirubicin chemotherapy in advanced breast cancer. *Br J Cancer* (1998) 77(12):2267–73. doi: 10.1038/bjc.1998.377

26. Muss HB, Thor AD, Berry DA, Kute T, Liu ET, Koerner F, et al. C-erbB-2 expression and response to adjuvant therapy in women with node-positive early breast cancer. *N Engl J Med* (1994) 330(18):1260. doi: 10.1056/NEJM199405053301802

27. Miglietta F, Griguolo G, Bottosso M, Giarratano T, Lo Mele M, Fassan M, et al. HER2-low-positive breast cancer: Evolution from primary tumor to residual disease after neoadjuvant treatment. *NPJ Breast Cancer* (2022) 8(1):66. doi: 10.1038/s41523-022-00434-w

28. Cortes J, Kim SB, Chung WP, Im SA, Park YH, Hegg R, et al. Trastuzumab deruxtecan versus trastuzumab emtansine for breast cancer. *N Engl J Med* (2022) 386(12):1143–54. doi: 10.1056/NEJMoa2115022

29. Modi S, Jacot W, Yamashita T, Sohn J, Vidal M, Tokunaga E, et al. Trastuzumab deruxtecan in previously treated HER2-low advanced breast cancer. *N Engl J Med* (2022) 387(1):9–20. doi: 10.1056/NEJMoa2203690

30. De Nonneville A,, Houvenaeghel G, Cohen M, Sabiani L, Bannier M, Viret F, et al. Pathological complete response rate and disease-free survivalafter neoadjuvant chemotherapy in patients with HER2-low and HER2-0breast cancers. *Eur J Cancer* (2022) 176:181–8. doi: 10.1016/j.ejca.2022.09.017

frontiers | Frontiers in Oncology

TYPE Original Research
PUBLISHED 04 January 2023
DOI 10.3389/fonc.2022.976823

Check for updates

OPEN ACCESS

EDITED BY
Raffaella Massafra,
National Cancer Institute Foundation (IRCCS), Italy

REVIEWED BY
Rajendra A. Badwe,
Tata Memorial Hospital, India
Simona Di Lascio,
Oncology Institute of Southern Switzerland (IOSI), Switzerland

*CORRESPONDENCE
Alessandro Inno
alessandro.inno@sacrocuore.it

SPECIALTY SECTION
This article was submitted to Breast Cancer, a section of the journal Frontiers in Oncology

RECEIVED 23 June 2022
ACCEPTED 08 December 2022
PUBLISHED 04 January 2023

CITATION
Inno A, Peri M, Turazza M, Bogina G, Modena A, Massocco A, Pezzella M, Valerio M, Mazzola R, Olivari L, Severi F, Foti G, Mazzi C, Marchetti F, Lunardi G, Salgarello M, Russo A and Gori S (2023) The predictive and prognostic role of metabolic and volume-based parameters of positron emission tomography/computed tomography as non-invasive dynamic biological markers in early breast cancer treated with preoperative systemic therapy.
Front. Oncol. 12:976823.
doi: 10.3389/fonc.2022.976823

COPYRIGHT
© 2023 Inno, Peri, Turazza, Bogina, Modena, Massocco, Pezzella, Valerio, Mazzola, Olivari, Severi, Foti, Mazzi, Marchetti, Lunardi, Salgarello, Russo and Gori. This is an open-access article distributed under the terms of the Creative Commons Attribution License (CC BY). The use, distribution or reproduction in other forums is permitted, provided the original author(s) and the copyright owner(s) are credited and that the original publication in this journal is cited, in accordance with accepted academic practice. No use, distribution or reproduction is permitted which does not comply with these terms.

The predictive and prognostic role of metabolic and volume-based parameters of positron emission tomography/computed tomography as non-invasive dynamic biological markers in early breast cancer treated with preoperative systemic therapy

Alessandro Inno[1*], Marta Peri[1,2], Monica Turazza[1], Giuseppe Bogina[3], Alessandra Modena[1], Alberto Massocco[4], Modestino Pezzella[4], Matteo Valerio[1], Rosario Mazzola[5], Laura Olivari[6], Fabrizia Severi[7], Giovanni Foti[8], Cristina Mazzi[9], Fabiana Marchetti[9], Gianluigi Lunardi[10], Matteo Salgarello[6], Antonio Russo[2] and Stefania Gori[1]

[1]Medical Oncology Unit, IRCCS Ospedale Sacro Cuore Don Calabria, Negrar di Valpolicella (VR), Italy, [2]Medical Oncology Unit, Department of Surgical, Oncological and Stomatological Sciences, University of Palermo, Palermo, Italy, [3]Pathology Unit, IRCCS Ospedale Sacro Cuore Don Calabria, Negrar di Valpolicella (VR), Italy, [4]Breast Surgery Unit, IRCCS Ospedale Sacro Cuore Don Calabria, Negrar di Valpolicella (VR), Italy, [5]Radiation Oncology Unit, IRCCS Ospedale Sacro Cuore Don Calabria, Negrar di Valpolicella (VR), Italy, [6]Nuclear Medicine Unit, IRCCS Ospedale Sacro Cuore Don Calabria, Negrar di Valpolicella (VR), Italy, [7]Medical Physics Unit, IRCCS Ospedale Sacro Cuore Don Calabria, Negrar di Valpolicella (VR), Italy, [8]Radiology Unit, IRCCS Ospedale Sacro Cuore Don Calabria, Negrar di Valpolicella (VR), Italy, [9]Clinical Research Unit, IRCCS Ospedale Sacro Cuore Don Calabria, Negrar di Valpolicella (VR), Italy, [10]Clinical Analysis Laboratory and Transfusional Medicine, IRCCS Ospedale Sacro Cuore Don Calabria, Negrar di Valpolicella (VR), Italy

Introduction: The role of fluorodeoxyglucose (FDG) positron emission tomography/computed tomography (PET/CT) in early breast cancer treated with preoperative systemic therapy (PST) is not yet established in clinical practice. PET parameters have aroused great interest in the recent years, as non-invasive dynamic biological markers for predicting response to PST.

Methods: In this retrospective study, we included 141 patients with stage II-III breast cancer who underwent surgery after PST. Using ROC analysis, we set optimal cutoff of FDG-PET/CT parameters predictive for pathological complete response (pCR). We investigated the correlation between FDG-PET/CT parameters and pCR, median disease-free survival (DFS), and median overall survival (mOS).

Results: At multivariable analysis, baseline SUVmax (high vs low: OR 9.00, CI 1.85 – 61.9, p=0.012) and Delta SUVmax (high vs low: OR 9.64, CI 1.84, 69.2, p=0.012) were significantly associated with pCR rates. Interestingly, we found that a combined analysis of the metabolic parameter Delta SUVmax with the volume-based parameter Delta MTV, may help to identify patients with pCR, especially in the subgroup of hormone receptor positive breast cancer. Delta SUVmax was also an independent predictive marker for both mDFS (high vs low: HR 0.17, 95%CI 0.05-0.58, p=0.004) and mOS (high vs. low: HR 0.19, 95% CI 0.04-0.95, p=0.029).

Discussion: Our results suggest that Delta SUVmax may predict survival of early BC patients treated with PST.

KEYWORDS

early breast cancer, PET CT scan, SUV, preoperative chemotherapy, predictive factors

1 Introduction

Breast cancer (BC) is the most common malignancy in women and represents a worldwide health problem. Therapy of early-stage disease includes local treatment with surgery, radiation therapy, or both, and systemic treatment with chemotherapy, endocrine therapy, biologic therapy, or combinations of the above. In general, chemotherapy regimens based on anthracyclines and taxanes reduce cancer-related mortality by about one-third in early-stage BC (1–3), by controlling undiscovered distant metastases. Among patients with HER2-positive early BC, the addition of anti-HER2 drugs to standard chemotherapy further improve the outcomes (4, 5).

Although the timing of chemotherapy in early-stage BC has not a demonstrated impact on survival (6–8), pre-operative systemic therapy (PST), also named neoadjuvant chemotherapy, is indicated in patients with locally advanced or inoperable breast cancer, desire of breast-conserving surgery, and operable tumors associated with a high likelihood of chemotherapy response, especially for tumors >2 cm (3, 9). The use of PST offers the advantage of downstaging the tumour and improving breast conservation rates, and provides an *in vivo* treatment response evaluation. Particularly, a pathological complete response (pCR) after PST is associated with favourable survival outcomes (10), especially for triple-negative breast cancer (TNBC) and with a lesser extent for HER2-positive BC. This does not apply to hormone receptor (HR)-positive, HER2-negative luminal subtypes, since pCR is rarely observed in these subtypes and patients maintain a good long-term prognosis independently of pCR (11). The administration of PST also represents an excellent research platform to test dynamic biological markers, such as metabolic parameters assessed through positron emission tomography (PET)/computed tomography (CT), or systemic inflammatory markers.

The role of PET/CT as non-invasive indicator of response has been recently established in early BC setting, since several meta-analyses showed that change of tumoral maximum standardized uptake value (Delta SUVmax) under therapy is significantly correlated with treatment response (12–14), and also with disease free-survival (DFS) and overall survival (OS) (15). More recently, PET/CT has been also used to optimize treatment in clinical trials, with the aim of discriminating good from poor responders to PST (16, 17).

Beyond Delta-SUVmax, other studies have focused on different metabolic parameters including tumor volume (MTV) and total lesion glycolysis (TLG), that evaluate not only metabolic activity but also the total tumor burden (18, 19). To date, however, the role of PET/CT for PST response evaluation is not fully established in clinical practice and no uptake cutoffs for pCR has been validated to classify the patients into metabolic responders and non-metabolic responders.

The aim of our study was to assess the predictive role of fluorodeoxyglucose (FDG) PET/CT indicators for pCR and survival outcomes, focusing on both metabolic and volume-based parameters.

2 Patients and methods

2.1 Patients

We included patients with histologically-proven, stage II-III breast cancer who underwent surgery after PST between January 2011 and May 2019 and performed FDG-PET/CT scan before

starting PST at IRCCS Ospedale Sacro Cuore Don Calabria Institution. Last updated follow-up data was August 13th, 2021. We excluded patients with <=6 months follow-up. Clinicopathological characteristics, hematologic tests, nuclear medicine data (before and after PST) and outcome information were retrospectively collected and included into an anonymized database. The study was conducted in accordance with the Declaration of Helsinki and the International Conference on Harmonization Guidelines on Good Clinical Practice.

2.2 Study design

We retrospectively reviewed medical records of consecutive patients selected according to inclusion criteria. Data for this retrospective analysis were extracted from several sources, including Oncology Unit, Nuclear Medicine Unit and Pathology Unit database.

Cancer staging was reported in accordance with the 8th edition of the Union for International Cancer Control/American Joint Committee on Cancer (UICC/AJCC) TNM staging system.

The molecular subtype was evaluated considering a value of 20% as ki67 cutoff for differentiating Luminal A (ki67<=20%) and Luminal B HER2-negative (ki 67 >20%) BC.

The pCR was defined as the absence of invasive BC both in the breast and in axillar lymph-nodes at surgical specimen. Disease-free survival (DFS) is defined as the time from histological diagnosis to local/distant recurrence of tumor or death.

Overall survival (OS) was defined as time from diagnosis to last follow-up or death from any cause. Cutoffs value for metabolic parameters were calculated based on their ability to discriminate between pathological complete response and no response.

2.3 Nuclear medicine imaging analyses

All FDG-PET/CT scans were performed at the same Institution. To quantify 18F-FDG uptake, the tumoral standardized uptake values (SUVs) were measured.

We set the volume of interest (VOI) as the area in which FDG accumulated in the breast. The maximum value of SUV in the VOI was defined as the SUVmax, and the volume of voxels of >= 40% of the SUVmax in the VOI was defined as the MTV. The average SUV value in the voxel that showed >= 40% was defined as the SUVmean and TLG was defined as MTV x SUVmean.

2.4 Statistical analysis

Continuous variables were summarized using descriptive statistics, including number of observations, mean, standard deviation, median, and interquartile range. Categorical values were summarized using the number of observations and percentages. Data distribution was first assessed, and non-parametric tests applied accordingly afterwards. Statistical comparisons were made using Kruskal Wallis for continuous variables and Chi-Square test with simulated p-value for binary variables. The Spearman correlation coefficient was used to evaluate the linear correlation between two continuous variables.

The percentage changes (Delta%) of PET data and systemic inflammatory biomarkers at baseline and after PST were calculated as follows: percentage change (Delta%) = (delayed parameter - baseline parameter)/baseline parameter x 100. The optimal cutoff point for the PET parameters (SUVmax, MTV, TLG, Delta SUVmax, Delta MTV, Delta TLG) was obtained using the maximum sum of sensitivity and specificity (Youden's J statistic) considering pCR outcome as reference standard. PET parameters were then dichotomized into "low" or "high" values based on the aforementioned threshold. Demographic and clinical characteristic along with PET parameters, were analysed by univariable logistic regression models to explore their association with the likelihood of reaching a pCR. Only variables significantly associated (p-value < 0.2) to a pCR were included in the full logistic regression model. Backward and forward elimination based on AIC was used for final model selection. The variable describing molecular subtypes was excluded from the logistic regression model because no pathological complete responses were observed in the luminal A and lumimal B (HER2+) subgroups. Model-building strategies included checking for convergence, correlation, and goodness-of-fit test. The Kaplan Meier method and log-rank test were performed to assess the difference in survival probabilities between type of pathological response and other covariates of interest. The multivariate Cox proportional hazards model was used to estimate the hazard ratios and 95% CIs for OS and DFS after checking for proportional hazard assumption.

All statistical tests were performed using two-sided 5% significance levels and P <.05 was considered statistically significant. Statistical analysis was performed using R statistical software version 4.1.1 (R Core Team 2021).

3 Results

3.1 Characteristics of the whole study population

The analysis included 141 patients with diagnosis of stage II-III breast cancer who underwent surgery after PST. Detailed demographics and clinical characteristics are reported in Table 1. Median age at diagnosis was 48 years, with an interquartile range (IQR) from 43 to 60 years. Prevalent histology was invasive ductal carcinoma (89.4%) and most cases were premenopausal (64.5%), cT2 (80.1%) and N1

(61.0%) at the diagnosis. Only 2.1% of tumors had a low grade (G1) and median Ki67 proliferation index was 30% (IQR 20-50) at diagnosis. Patients with HER2-enriched molecular subtype (i.e. HR-negative, HER2-positive) were 24.1%, Luminal B/HER2-negative were 23.4%, Luminal B/HER2-positive and triple-negative were 17.0% each, and Luminal A tumors were 16.3% of cases. One hundred and thirty-six patients (96.5%) received an anthracycline-based chemotherapy, and 41.1% received trastuzumab in combination with chemotherapy. After PST, 93 patients (66.4%) underwent a conservative surgical approach, while the remaining 47 (33.6%) were treated by mastectomy.

Thirty-two patients (23.2%) obtained a pCR after PST. At data cutoff, number of deaths from any cause were 23/141 and median OS was 57.3 months (interquartile range 41.9-83.0) for the whole population. Overall relapses were 39/141, of which 29 were distant and 10 were local, with a median DFS of 52 months (IQR 36.8-77.9 months).

Luminal-A, Luminal-B HER2-negative, Luminal-B HER2-positive, HER2 enriched and TNBC had a mDFS of 73.8 [48.0-96.5], 41.2 [32.6-59.5], 58.9 [41.9-82.4], 52.5 [35.9-74.7] and 45.9 [34.3–73.1] months, respectively.

Luminal-A, Luminal-B HER2-negative, Luminal-B HER2-positive, HER2 enriched and TNBC had a mOS of 81.4 [70.7-96.6], 47.7 [34.9-66.5], 61.0 [42.7-85.7], 54.7 [45.6-77.7] and 54.9 [41.2–73.2] months, respectively.

Time to relapse distribution according to molecular subtype showed a peak after primary resection between 36 and 47 months. Luminal A and HER2-positive patients experienced later relapse as compared with the other molecular subtypes. Bone (14.9%), liver (12.8%), extra-regional lymph nodes (7.4%), and lung (6.4%) were the most common sites of relapse.

3.2 Relationships between clinicopathological factors and pCR

Association between clinicopathological characteristics and pCR are reported in Table 1. The descriptive analysis showed that pCR rates were significantly associated with grading ($p<0.001$) and molecular subtype ($p<0.001$). In particular, none of the patients with Luminal A or Luminal B HER2-negative did achieve a pCR. The pCR rate was higher in HER2-enriched patients (53.1%), followed by Luminal B HER2-positive (25%) and triple-negative (21.9%).

We explored the association between systemic inflammatory indicators and pCR rate without discovering any relevant associations (Supplementary Table 1). Even correlations between inflammation biomarkers and metabolic parameters did not show any significant association (data not shown).

3.3 Relationships between metabolic parameters and pCR

Of the baseline metabolic parameters, only tumoral SUVmax as continuous variable showed a significant association with pCR ($p<0.001$). The pCR was significantly associated with higher Delta SUVmax, Delta MTV and Delta TLG ($p<0.001$), suggesting a predictive role for changes of both metabolic (SUV) and volume-based parameters (MTV and TLG) after treatment as compared with baseline.

3.4 Determination of the optimal metabolic parameters cutoff values for pCR

The cutoff values of baseline metabolic parameters and their reduction rate are shown in Table 2. We set the optimal cutoff values of baseline metabolic parameters for SUVmax, MTV, and TLG at 9.2, 1.5 and 16.9, respectively. For dynamic parameters the optimal cutoffs of Delta SUVmax, MTV, and TLG were -98.3%, -84.2%, and -94.4%, respectively.

3.5 Univariable and multivariable analyses of pCR

Among clinicopathological characteristics, logistic regression univariate model showed higher pCR rates for grade 3 compared to grade 2 ($p=0.002$) (Supplementary Table 2). Among metabolic parameters, baseline SUVmax (high *vs* low) ($p<0.001$) and MTV (high *vs* low) ($p=0.010$), Delta SUVmax (high *vs* low) ($p<0.001$), Delta TLG (high *vs* low) ($p<0.001$) and Delta MTV (high *vs* low) ($p<0.001$) were significantly associated to pCR. At multivariate analysis, baseline grading (3 *vs* 2) (OR 17.2, CI 2.39 - 372, $p=0.017$), baseline SUVmax (high *vs* low) (OR 9.00, CI 1.85 – 61.9, $p=0.012$) and Delta SUVmax (high *vs* low) (OR 9.64, CI 1.84, 69.2, $p=0.012$) were significantly associated to pCR (Table 3).

3.6 Predictive role of combined Delta SUVmax and Delta MTV for pCR

Three subgroups of patients were obtained by combining dichotomized Delta SUVmax and Delta MTV, respectively: “High-High”, “Low-Low” and “Low-High” subgroups. Very few patients had high Delta SUVmax associated with low Delta MTV.

TABLE 1 Demographics and clinical characteristics of whole population related to pCR.

			Pathological Response		
	N	Overall	No response or partial	Complete	
		(N=141)	***(N=106)***	***(N=32)***	
Age	141	48 [43 - 60]	48 [42 - 60]	48 [43 - 60]	P=0.742†
Post -menopausal	141	50 (35.5)	36 (34.0)	14 (43.8)	P=0.400§
Clinical T stage (cT)	141				P=0.587§
T0		0 (0.0)	0 (0.0)	0 (0.0)	
T1		8 (5.7)	6 (5.7)	2 (6.2)	
T2		113 (80.1)	85 (80.2)	26 (81.2)	
T3		14 (9.9)	9 (8.5)	4 (12.5)	
T4		6 (4.3)	6 (5.7)	0 (0.0)	
Clinical N stage (cN)	141				P=0.288§
N0		34 (24.1)	26 (24.5)	8 (25.0)	
N1		86 (61.0)	67 (63.2)	16 (50.0)	
N2		17 (12.1)	11 (10.4)	6 (18.8)	
N3		4 (2.8)	2 (1.9)	2 (6.2)	
Stage	141				P=0.679§
2A		29 (20.6)	22 (20.8)	7 (21.9)	
2B		77 (54.6)	60 (56.6)	15 (46.9)	
3A		13 (9.2)	8 (7.5)	5 (15.6)	
3B		12 (8.5)	8 (7.5)	3 (9.4)	
3C		10 (7.1)	8 (7.5)	2 (6.2)	
Baseline grading	140				P=0.003§
1		3 (2.1)	3 (2.8)	0 (0.0)	
2		49 (34.8)	45 (42.5)	3 (9.4)	
3		88 (62.4)	57 (53.8)	29 (90.6)	
Missing		1 (0.7)	1 (0.9)	0 (0.0)	
Hystotipe	139				P=0.262§
Ductal		126 (89.4)	92 (86.8)	31 (96.9)	
Lobular		9 (6.4)	9 (8.5)	0 (0.0)	
Others		4 (2.8)	3 (2.8)	1 (3.1)	
Missing		2 (1.4)	2 (1.9)	0 (0.0)	
Molecular subtype	138				P<0.001§
LUM-A		23 (16.3)	23 (21.7)	0 (0.0)	
LUM-B (HER2-)		33 (23.4)	31 (29.2)	0 (0.0)	
LUM-B (HER2+)		24 (17.0)	16 (15.1)	8 (25.0)	
HER2+		34 (24.1)	16 (15.1)	17 (53.1)	
TN		24 (17.0)	17 (16.0)	7 (21.9)	

(Continued)

TABLE 1 Continued

			Pathological Response		
	N	Overall	No response or partial	Complete	
Missing		3 (2.1)	3 (2.8)	0 (0.0)	
Baseline SUV_{max}	141	10.1 [5.9; 14.7]	8.8 [5.4; 12.8]	13.2 [9.9; 20.2]	P=0.002†
Delta SUV_{max} %	138	-68.2 [-100.0; -30.4]	-57.6 [-79.1; -22.9]	-100.0 [-100.0; -100.0]	P<0.001†
Baseline MTV	141	3.88 [2.13; 8.27]	4.12 [2.19; 8.57]	3.11 [1.64; 7.37]	P=0.244†
Delta MTV %	139	-89 [-100; -45]	-73 [-100; -36]	-100 [-100; -100]	P<0.001†
Baseline TLG	118	23.0 [11.6; 65.1]	26.8 [10.7; 61.4]	16.8 [11.6; 85.0]	P=0.793†
Delta TLG %	115	-88.0 [-100.0; -68.9]	-84.9 [-100.0; -56.6]	-100.0 [-100.0; -98.1]	P<0.001†

N is the number of non-missing value. Continuous variables are expressed as: median [Q1-Q3]. Categorical variables as n (%). †Wilcoxon-Mann-Whitney test. §Chi-square test.

Table 4 describes the relationship between combined Delta SUVmax/Delta MTV and pCR, highlighting that a low Delta SUVmax is related to a decreased pCR rate. Of interest, the intermediate subgroup "Low-High" showed a higher pCR rate compared to "Low-Low".

3.7 Relationships between clinicopathological factors, including metabolic parameters, and survival

Kaplan-Meier curves for DFS and OS are shown in Figures 1A, B, respectively. Kaplan-Meier curves for OS according to molecular subtype are shown in Supplementary Figures 1, 2. Detailed association between clinicopathological characteristics and metabolic parameters and clinical outcomes are reported in Figures 2–4 and Supplementary Tables 3, 4.

At multivariable analysis, clinical stage at diagnosis (III *vs* II: HR 1.98, 95%CI 1.01 – 3.87, p=0.046) and Delta SUVmax (high *vs* low: HR 0.17, 95%CI 0.05-0.58, p=0.004) were associated with DFS, whereas grading (Grade 3 *vs* 2: HR 2.81, 95%CI 1.06-8.07, p=0.038), age (HR 1.04, 95%CI 1.00-1.08, p=0.27) and Delta SUVmax (high *vs*. low: HR 0.19, 95%CI 0.04-0.95, p=0.029) to OS (Tables 5, 6). This final selected model did not include pCR, since this variable was excluded through the stepwise model selection.

TABLE 2 Optimal Metabolic Parameters Cutoff Values for pCR.

Variable	Cutoff	Sensibility(%)	Specificity(%)
Baseline SUV_{max}	9.2	81.2	53.8
Baseline MTV	1.5	25.0	92.5
Baseline TLG	16.9	52.0	60.0
Delta SUV_{max} %	-98.3	80.6	88.7
Delta MTV %	-84.2	90.6	57.5
Delta TLG %	-94.4	84.0	68.5

4 Discussion

Preoperative systemic therapy (PST) in breast cancer (BC) represents an intriguing research topic. Consistently with other reports, in the present study we observed at univariable analyses that pCR is significantly associated with DFS and OS among BC patients treated with PST.

Many efforts are ongoing to improve PST in order to obtain higher rates of pCR. Recent advances in PST include the use of dual anti-HER2 blockade with trastuzumab plus pertuzumab associated with chemotherapy in HER2-positive (Neosphere, TRYPHAENA and PEONY trial) (20–22) and the addition of platinum compounds in TNBC (23). The identification of patients with pCR after PST also provides the opportunity of tailoring postoperative treatments. At this regard, two randomized trials have recently changed the clinical practice, in TNBC (24) and in HER2-positive BC (25). Multiple trials are exploring the use of immune-checkpoints inhibitors in TNBC (A-brave, NCT02954874, KEYNOTE-522) and CDK4/6 inhibitors in hormone receptor-positive BC (Monarch-e). Poly (ADP-ribose) polymerase (PARP) inhibitors have recently emerged as a promising class of therapeutics in BC, and several clinical studies in early stage are ongoing (26).

Although pCR has a relevant prognostic impact at individual level, it seems to be not a surrogate endpoint for both DFS and OS at trial level (27). In our study, in fact, pCR was excluded from the final multivariable analysis during the stepwise elimination process because its association with survival outcomes was weak. Therefore, other predictive factors for survival should be investigated in the setting of PST in early BC (20–23).

In the last years, some retrospective studies have evaluated the predictive role of metabolic parameters in BC (18, 19, 28). In

10.3389/fonc.2022.976823

TABLE 3 Multivariable logistic regression model for pCR.

Characteristic	OR[1]	95% CI[1]	p-value
Baseline grading			
2	—	—	
3	17.2	2.39, 3.72	**0.017**
Baseline SUV_{max}			
Low	—	—	
High	9.00	1.85, 61.9	**0.012**
Baseline MTV			
Low	—	—	
High	0.15	0.02, 1.31	0.087
Delta SUV_{max}			
Low	—	—	
High	9.64	1.84, 69.2	**0.012**
Delta TLG			
Low	—	—	
High	4.84	0.73, 33.9	0.10
No. Obs.	111		

[1]OR, Odds Ratio, CI, Confidence Interval. Bold values indicate a p value of <.05.

the present study we focused on evaluation of the predictive role of PET/TC parameters as non-invasive dynamic biomarkers after PST. Although baseline SUVmax, baseline MTV, Delta SUVmax, Delta TLG and Delta MTV were significantly associated to pCR at univariable analysis, only baseline SUVmax and Delta SUVmax maintained an independent role for predicting pCR at multivariable analysis. This observation is consistent with other published studies (12–14).

In our study, patients with "low" Delta SUVmax achieved low pCR rates. Patients with "low" Delta SUVmax, however, were a heterogeneous population in terms of molecular subtype, mostly characterized by high HR expression, which is typically associated with chemoresistance. Since Delta SUVmax and Delta MTV were both significantly associated with pCR at univariable analysis, we further analyzed the role of a combination of these two metabolic parameters for predicting pCR. The combination of the two allows to assess metabolic and volume-based parameters together. Interestingly, we observed higher pCR rate in the "low" Delta SUVmax/"high" Delta MTV subgroup compared to "low" Delta SUVmax/"low" Delta MTV subgroup, suggesting that MTV together with SUVmax could be a useful dynamic biomarker for pCR in clinical practice, especially in heterogeneous breast cancer subtypes such as those HR-positive.

Recent reports described an interesting association between PET uptake and different biomarkers of inflammation (NLR, PLR, SIRS) (29–32), noting that patients with high SUVmax and

TABLE 4 Association between combined Delta SUVmax and Delta MTV evaluation and baseline clinicopathological characteristics and pCR.

Delta SUV_{max} x Delta MTV					
	N	High.High	Low.High	Low.Low	Test Statistic
		(N=36)	*(N=38)*	*(N=63)*	
Patological response after PST	138				P<0.001[$]
No response or partial		11 (30.6)	34 (89.5)	60 (95.2)	
Complete		25 (69.4)	3 (7.9)	3 (4.8)	
Missing		0 (0.0)	1 (2.6)	0 (0.0)	

[$]Chi-square test.

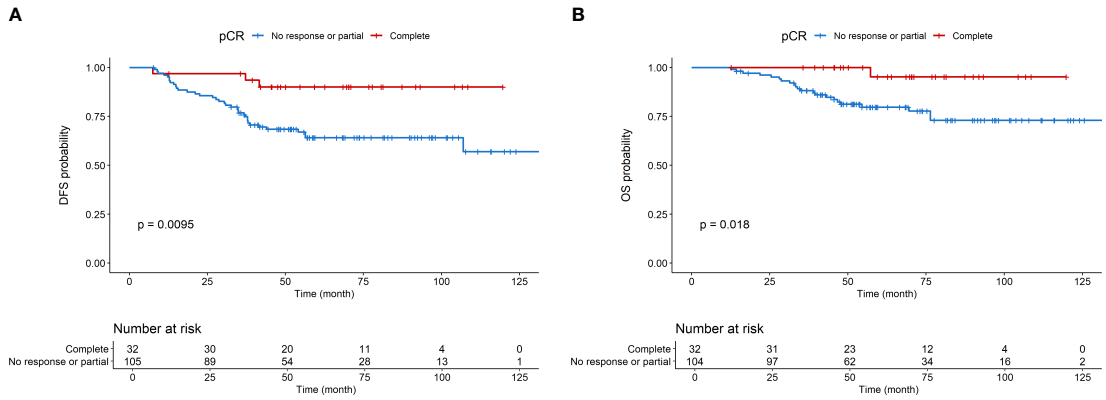

FIGURE 1
Disease-free survival **(A)** and overall survival **(B)** according to pCR.

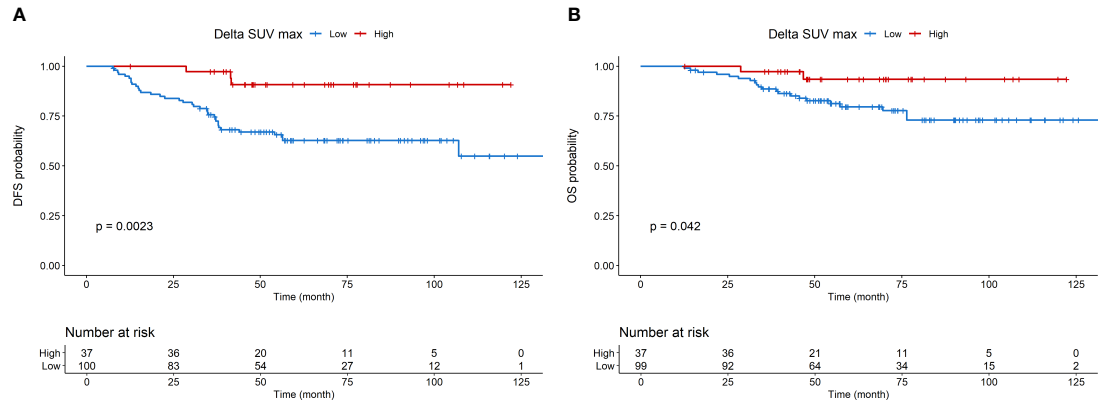

FIGURE 2
Disease-free survival **(A)** and overall survival **(B)** according to Delta SUVmax.

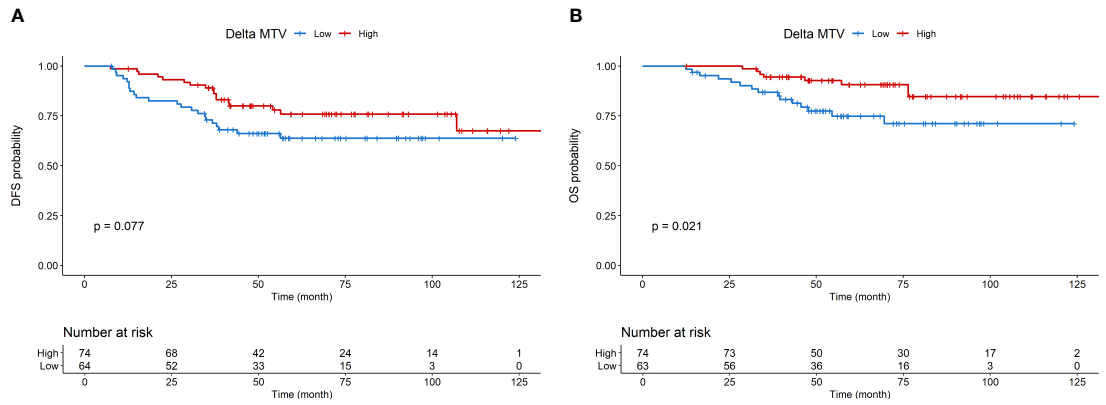

FIGURE 3
Disease-free survival **(A)** and overall survival **(B)** according to Delta MTV.

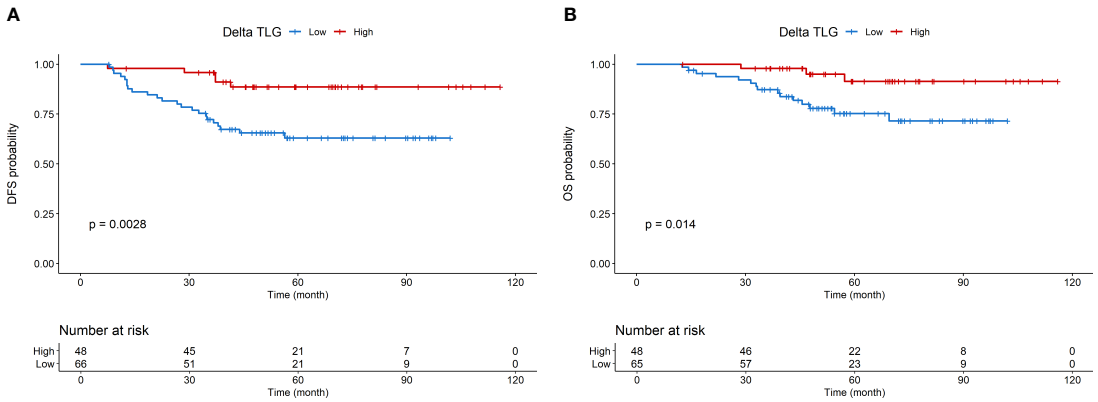

FIGURE 4
Disease-free survival **(A)** and overall survival **(B)** according to Delta TLG.

low NLR (indicating a status of immune system activation) had lower recurrent disease after surgery (30). In the present study, however, we did not find any correlation between PET parameters and systemic biomarkers of inflammation. An explanation for these conflicting results among studies could be that systemic inflammatory biomarkers could not reliably mirror the inflammatory status of tumor microenvironment, possibly related to metabolic parameters of the tumor detected through the PET/CT.

Interestingly, we reported a significant association at multivariable analysis between Delta SUVmax and survival outcomes, both in terms of DFS and OS, and this is consistent with the results of a meta-analysis that showed a significant predictive value of Delta SUVmax for disease recurrence and survival (12). Taken together, these data may support the rationale for including PET/CT assessment before, interim and after treatment in clinical trials on PST for early BC.

Our study has some limitations due to the retrospective design, the small sample size, and the heterogeneity of the study population in terms of molecular subtypes and treatment. Considering the prognosis of early BC, an extended follow-up period may provide additional information with the aim of identify patients that may need additional tailored treatments. Larger studies on single molecular subtypes may provide further

TABLE 5 Multivariable Cox proportional hazard model of the clinicopathological characteristics and metabolic parameters for DFS.

Characteristic	HR[1]	95% CI[1]	p-value
Stage			
2A 2B	—	—	
3A 3B 3C	1.98	1.01, 3.87	**0.046**
Baseline grading			
2	—	—	
3	2.78	1.30, 5.97	**0.009**
Baseline SUV_{max}			
Low	—	—	
High	0.57	0.29, 1.12	0.10
Delta SUV_{max}			
Low	—	—	
High	0.17	0.05, 0.58	**0.004**
No. Obs.	133		

[1] HR, Hazard Ratio, CI, Confidence Interval. Bold values indicate a p value of <.05.

TABLE 6 Multivariable Cox proportional hazard model of the clinicopathological characteristics and metabolic parameters for OS.

Characteristic	HR[1]	95% CI[1]	p-value
Baseline grading			
2	—	—	
3	2.93	1.06, 8.07	**0.038**
Age	1.04	1.00, 1.08	**0.027**
Delta SUV_{max}			
Low	—	—	
High	0.19	0.04, 0.84	**0.029**
No. Obs.	132		

[1] HR, Hazard Ratio, CI, Confidence Interval. Bold values indicate a p value of <.05.

information on the role of PET/CT among patients with early BC receiving PST.

5 Conclusion

The present study suggested a role for PET/TC imaging as non-invasive dynamic biomarker in early BC treated with PST. Particularly, Delta SUVmax was significantly associated with pCR, DFS and OS, and possibly deserve further investigation in prospective neoadjuvant trials as potential surrogate endpoint for survival.

Interestingly, this study is the first attempt to evaluate the prognostic role of volume-based parameters in BC neoadjuvant setting. Particularly, our results suggest that a combined evaluation of Delta SUV and Delta MTV could help to refine prognosis, especially among patients with HR-positive tumors.

Data availability statement

The raw data supporting the conclusions of this article will be made available by the authors, without undue reservation.

Ethics statement

The studies involving human participants were reviewed and approved by Ethics Committee (Comitato Etico per la sperimentazione clinica delle province di Verona e Rovigo). Written informed consent for participation was not required for this study in accordance with the national legislation and the institutional requirements.

Author contributions

SG designed the study. MT, AMo, GB, AMa, MPer, MPez, RM, LO, MS, FS and GF collected data. MV and CM analyzed data. MPer, CM and AI wrote the draft. AI, SG and AR critically revised the manuscript. All authors contributed to the article and approved the submitted version.

Conflict of interest

The authors declare that the research was conducted in the absence of any commercial or financial relationships that could be construed as a potential conflict of interest.

Publisher's note

All claims expressed in this article are solely those of the authors and do not necessarily represent those of their affiliated organizations, or those of the publisher, the editors and the reviewers. Any product that may be evaluated in this article, or claim that may be made by its manufacturer, is not guaranteed or endorsed by the publisher.

Supplementary material

The Supplementary Material for this article can be found online at: https://www.frontiersin.org/articles/10.3389/fonc.2022.976823/full#supplementary-material

References

1. Early Breast Cancer Trialists' Collaborative Group (EBCTCG). Effects of chemotherapy and hormonal therapy for early breast cancer on recurrence and 15-year survival: An overview of the randomised trials. *Lancet* (2005) 365(9472):1687–717. doi: 10.1016/S0140-6736(05)66544-0

2. Early Breast Cancer Trialists' Collaborative Group (EBCTCG). Comparisons between different polychemotherapy regimens for early breast cancer: Meta-analyses of long-term outcome among 100,000 women in 123 randomised trials. *Lancet* (2012) 379(9814):432–44. doi: 10.1016/S0140-6736(11)61625-5

3. Cardoso F, Kyriakides S, Ohno S, Penault-Llorca F, Poortmans P, Rubio IT, et al. Early breast cancer: ESMO clinical practice guidelines for diagnosis, treatment and follow-up. *Ann Oncol* (2019) 30(8):1194–220. doi: 10.1093/annonc/mdz173

4. Gianni L, Eiermann W, Semiglazov V, Manikhas A, Lluch A, Tjulandin S, et al. Neoadjuvant chemotherapy with trastuzumab followed by adjuvant trastuzumab versus neoadjuvant chemotherapy alone, in patients with HER2-positive locally advanced breast cancer (the NOAH trial): A randomised controlled superiority trial with a parallel HER2-negative cohort. *Lancet* (2010) 375 (9712):377–84. doi: 10.1016/S0140-6736(09)61964-4

5. Cameron D, Piccart-Gebhart MJ, Gelber RD, Procter M, Goldhirsch A, de Azambuja E, et al. 11 years' follow-up of trastuzumab after adjuvant chemotherapy in HER2-positive early breast cancer: final analysis of the HERceptin adjuvant (HERA) trial. *Lancet* (2017) 389(10075):1195–205. doi: 10.1016/S0140-6736(16) 32616-2

6. Mauri D, Pavlidis N, Ioannidis JP. Neoadjuvant versus adjuvant systemic treatment in breast cancer: A meta-analysis. *J Natl Cancer Inst* (2005) 97(3):188–94. doi: 10.1093/jnci/dji021

7. Rastogi P, Anderson SJ, Bear HD, Geyer CE, Kahlenberg MS, Robidoux A, et al. Preoperative chemotherapy: Updates of national surgical adjuvant breast and bowel project protocols b-18 and b-27. *J Clin Oncol* (2008) 26(5):778–85. doi: 10.1200/JCO.2007.15.0235

8. Early Breast Cancer Trialists' Collaborative Group (EBCTCG). Long-term outcomes for neoadjuvant versus adjuvant chemotherapy in early breast cancer: meta-analysis of individual patient data from ten randomised trials. *Lancet Oncol* (2018) 19(1):27–39. doi: 10.1016/S1470-2045(17)30777-5

9. Gradishar WJ, Moran MS, Abraham J, Aft R, Agnese D, Allison KH, et al. NCCN guidelines® insights: Breast cancer, version 4.2021. *J Natl Compr Canc Netw* (2021) 19(5):484–93. doi: 10.6004/jnccn.2021.0023

10. Cortazar P, Zhang L, Untch M, Mehta K, Costantino JP, Wolmark N, et al. Pathological complete response and long-term clinical benefit in breast cancer: The CTNeoBC pooled analysis. *Lancet* (2014) 384(9938):164–72. doi: 10.1016/S0140-6736(13)62422-8

11. Li X, Dai D, Chen B, Tang H, Wei W. Oncological outcome of complete response after neoadjuvant chemotherapy for breast conserving surgery: A systematic review and meta-analysis. *World J Surg Oncol* (2017) 15(1):210. doi: 10.1186/s12957-017-1273-6

12. Wang Y, Zhang C, Liu J, Huang G. Is 18F-FDG PET accurate to predict neoadjuvant therapy response in breast cancer? A meta-analysis. *Breast Cancer Res Treat* (2012) 131(2):357–69. doi: 10.1007/s10549-011-1780-z

13. Cheng X, Li Y, Liu B, Xu Z, Bao L, Wang J. 18F-FDG PET/CT and PET for evaluation of pathological response to neoadjuvant chemotherapy in breast cancer: a meta-analysis. *Acta Radiol* (2012) 53(6):615–27. doi: 10.1258/ar.2012.110603

14. Mghanga FP, Lan X, Bakari KH, Li C, Zhang Y. Fluorine-18 fluorodeoxyglucose positron emission tomography-computed tomography in monitoring the response of breast cancer to neoadjuvant chemotherapy: A meta-analysis. *Clin Breast Cancer* (2013) 13(4):271–9. doi: 10.1016/j.clbc.2013.02.003

15. Han S, Choi JY. Prognostic value of 18F-FDG PET and PET/CT for assessment of treatment response to neoadjuvant chemotherapy in breast cancer: A systematic review and meta-analysis. *Breast Cancer Res* (2020) 22(1):119. doi: 10.1186/s13058-020-01350-2

16. Coudert B, Pierga JY, Mouret-Reynier MA, Kerrou K, Ferrero JM, Petit T, et al. Use of [(18)F]-FDG PET to predict response to neoadjuvant trastuzumab and docetaxel in patients with HER2-positive breast cancer, and addition of bevacizumab to neoadjuvant trastuzumab and docetaxel in [(18)F]-FDG PET-predicted non-responders (AVATAXHER): an open-label, randomised phase 2 trial. *Lancet Oncol* (2014) 15(13):1493–502. doi: 10.1016/S1470-2045(14)70475-9

17. Pérez-García JM, Gebhart G, Ruiz Borrego M, Stradella A, Bermejo B, Schmid P, et al. Chemotherapy de-escalation using an 18F-FDG-PET-based pathological response-adapted strategy in patients with HER2-positive early breast cancer (PHERGain): A multicentre, randomised, open-label, non-comparative, phase 2 trial. *Lancet Oncol* (2021) 22(6):858–71. doi: 10.1016/S1470-2045(21)00122-4

18. Higuchi T, Fujimoto Y, Ozawa H, Bun A, Fukui R, Miyagawa Y, et al. Significance of metabolic tumor volume at baseline and reduction of mean standardized uptake value in 18F-FDG-PET/CT imaging for predicting pathological complete response in breast cancers treated with preoperative chemotherapy. *Ann Surg Oncol* (2019) 26(7):2175–83. doi: 10.1245/s10434-019-07325-8

19. Choi JH, Kim HA, Kim W, Lim I, Lee I, Byun BH, et al. Early prediction of neoadjuvant chemotherapy response for advanced breast cancer using PET/MRI image deep learning. *Sci Rep* (2020) 10(1):21149. doi: 10.1038/s41598-020-77875-5

20. Gianni L, Pienkowski T, Im YH, Tseng LM, Liu MC, Lluch A, et al. 5-year analysis of neoadjuvant pertuzumab and trastuzumab in patients with locally advanced, inflammatory, or early-stage HER2-positive breast cancer (NeoSphere): a multicentre, open-label, phase 2 randomised trial. *Lancet Oncol* (2016) 17 (6):791–800. doi: 10.1016/S1470-2045(16)00163-7

21. Schneeweiss A, Chia S, Hickish T, Harvey V, Eniu A, Waldron-Lynch M, et al. Long-term efficacy analysis of the randomised, phase II TRYPHAENA cardiac safety study: Evaluating pertuzumab and trastuzumab plus standard neoadjuvant anthracycline-containing and anthracycline-free chemotherapy regimens in patients with HER2-positive early breast cancer. *Eur J Cancer* (2018) 89:27–35. doi: 10.1016/j.ejca.2017.10.021

22. Shao Z, Pang D, Yang H, Li W, Wang S, Cui S, et al. Efficacy, safety, and tolerability of pertuzumab, trastuzumab, and docetaxel for patients with early or locally advanced ERBB2-positive breast cancer in Asia: The PEONY phase 3 randomized clinical trial. *JAMA Oncol* (2020) 6(3):e193692. doi: 10.1001/jamaoncol.2019.3692

23. Poggio F, Bruzzone M, Ceppi M, Pondé NF, La Valle G, Del Mastro L, et al. Platinum-based neoadjuvant chemotherapy in triple-negative breast cancer: a systematic review and meta-analysis. *Ann Oncol* (2018) 29(7):1497–508. doi: 10.1093/annonc/mdy127

24. Masuda N, Lee SJ, Ohtani S, Im YH, Lee ES, Yokota I, et al. Adjuvant capecitabine for breast cancer after preoperative chemotherapy. *N Engl J Med* (2017) 376(22):2147–59. doi: 10.1056/NEJMoa1612645

25. Mamounas EP, Untch M, Mano MS, Huang CS, Geyer CEJr, von Minckwitz G, et al. Adjuvant T-DM1 versus trastuzumab in patients with residual invasive disease after neoadjuvant therapy for HER2-positive breast cancer: subgroup analyses from KATHERINE. *Ann Oncol* (2021) 32(8):1005–14. doi: 10.1016/j.annonc.2021.04.011

26. Cortesi L, Rugo HS, Jackisch C. An overview of PARP inhibitors for the treatment of breast cancer. *Target Oncol* (2021) 16(3):255–82. doi: 10.1007/s11523-021-00796-4

27. Conforti F, Pala L, Sala I, Oriecuia C, De Pas T, Specchia C, et al. Evaluation of pathological complete response as surrogate endpoint in neoadjuvant randomised clinical trials of early stage breast cancer: systematic review and meta-analysis. *BMJ* (2021) 375:e066381. doi: 10.1136/bmj-2021-066381

28. Wen W, Xuan D, Hu Y, Li X, Liu L, Xu D. Prognostic value of maximum standard uptake value, metabolic tumor volume, and total lesion glycolysis of positron emission tomography/computed tomography in patients with breast cancer: A systematic review and meta-analysis. *PloS One* (2019) 14(12): e0225959. doi: 10.1371/journal.pone.0225959

29. Zhang K, Ping L, Ou X, Bazhabayi M, Xiao X. A systemic inflammation response score for prognostic prediction of breast cancer patients undergoing surgery. *J Pers Med* (2021) 11(5):413. doi: 10.3390/jpm11050413

30. Fujii T, Yanai K, Tokuda S, Nakazawa Y, Kurozumi S, Obayashi S, et al. Relationship between FDG uptake and Neutrophil/Lymphocyte ratio in patients with invasive ductal breast cancer. *Anticancer Res* (2018) 38(8):4927–31. doi: 10.21873/anticanres.12809

31. Can C, Komek H. Metabolic and volume-based parameters of (18F)FDG PET/CT for primary mass and axillary lymph node metastasis in patients with invasive ductal carcinoma: a retrospective analysis in relation to molecular subtype, axillary lymph node metastasis and immunohistochemistry and inflammatory markers. *Nucl Med Commun* (2019) 40(10):1051–9. doi: 10.1097/MNM.0000000000001074

32. Fujii T, Tokuda S, Nakazawa Y, Kurozumi S, Obayashi S, Yajima R, et al. Relationship between FDG uptake and the platelet/lymphocyte ratio in patients with breast invasive ductal cancer. *In Vivo* (2020) 34(3):1365–9. doi: 10.21873/invivo.11915

frontiers | Frontiers in Oncology

TYPE Original Research
PUBLISHED 31 January 2023
DOI 10.3389/fonc.2022.1028825

Check for updates

OPEN ACCESS

EDITED BY
Raffaella Massafra,
Bari John Paul II Cancer Institute, National Cancer Institute Foundation, Scientific Institute for Research, Hospitalization and Healthcare (IRCCS), Italy

REVIEWED BY
Yimin Cui,
Peking University, China
Claire Josse,
University Hospital of Liège, Belgium

*CORRESPONDENCE
Sara Pizzamiglio
sara.pizzamiglio@istitutotumori.mi.it

†These authors have contributed equally to this work and share first authorship

SPECIALTY SECTION
This article was submitted to Breast Cancer, a section of the journal Frontiers in Oncology

RECEIVED 26 August 2022
ACCEPTED 30 December 2022
PUBLISHED 31 January 2023

CITATION
Di Cosimo S, Ciniselli CM, Pizzamiglio S, Cappelletti V, Silvestri M, El-Abed S, Izquierdo M, Bajji M, Nuciforo P, Huober J, Cameron D, Chia S, Gomez HL, Iorio MV, Vingiani A, Pruneri G and Verderio P (2023) End-of-neoadjuvant treatment circulating microRNAs and HER2-positive breast cancer patient prognosis: An exploratory analysis from NeoALTTO. *Front. Oncol.* 12:1028825. doi: 10.3389/fonc.2022.1028825

COPYRIGHT
© 2023 Di Cosimo, Ciniselli, Pizzamiglio, Cappelletti, Silvestri, El-Abed, Izquierdo, Bajji, Nuciforo, Huober, Cameron, Chia, Gomez, Iorio, Vingiani, Pruneri and Verderio. This is an open-access article distributed under the terms of the Creative Commons Attribution License (CC BY). The use, distribution or reproduction in other forums is permitted, provided the original author(s) and the copyright owner(s) are credited and that the original publication in this journal is cited, in accordance with accepted academic practice. No use, distribution or reproduction is permitted which does not comply with these terms.

End-of-neoadjuvant treatment circulating microRNAs and HER2-positive breast cancer patient prognosis: An exploratory analysis from NeoALTTO

Serena Di Cosimo[1†], Chiara M. Ciniselli[2†], Sara Pizzamiglio[2*†], Vera Cappelletti[1], Marco Silvestri[1], Sarra El-Abed[3], Miguel Izquierdo[4], Mohammed Bajji[5], Paolo Nuciforo[6], Jens Huober[7,8], David Cameron[9], Stephen Chia[10], Henry L. Gomez[11,12], Marilena V. Iorio[13], Andrea Vingiani[1], Giancarlo Pruneri[1] and Paolo Verderio[2]

[1]Department of Advanced Diagnostics, Fondazione IRCCS Istituto Nazionale dei Tumori, Milan, Italy, [2]Unit of Bioinformatics and Biostatistics, Fondazione IRCCS Istituto Nazionale dei Tumori, Milan, Italy, [3]Breast International Group, Brussels, Belgium, [4]Novartis Pharmaceutical, Basel, Switzerland, [5]Institut Jules Bordet and l'Université Libre de Bruxelles (U.LB), Bruxelles, Belgium, [6]Molecular Oncology Group, Vall d'Hebron Institute of Oncology (VHIO), Barcelona, Spain, [7]Breast Center, University of Ulm, Ulm, Germany, [8]Breast Center, Cantonal Hospital St.Gallen, St. Gallen, Switzerland, [9]University of Leeds, Leeds, United Kingdom, [10]University of British Columbia, Vancouver, BC, Canada, [11]Department of Medical Oncology, Instituto Nacional de Enfermedades Neoplásicas, Lima, Peru, [12]Department of Medical Oncology, Universidad Ricardo Palma, Lima, Peru, [13]Department of Experimental Oncology, Fondazione IRCCS Istituto Nazionale dei Tumori, Milan, Italy

Background: The absence of breast cancer cells in surgical specimens, *i.e.*, pathological complete response (pCR), is widely recognized as a favorable prognostic factor after neoadjuvant therapy. In contrast, the presence of disease at surgery characterizes a prognostically heterogeneous group of patients. Here, we challenged circulating microRNAs (miRNAs) at the end of neoadjuvant therapy as potential prognostic biomarkers in the NeoALTTO study.

Methods: Patients treated within the trastuzumab arm (*i.e.*, pre-operative weekly trastuzumab for 6 weeks followed by the addition of weekly paclitaxel for 12 weeks; post-operative FEC for 3 cycles followed by trastuzumab up to complete 1 year of treatment) were randomized into a training (n= 54) and testing (n= 72) set. RT-PCR-based high-throughput miRNA profile was performed on plasma samples collected at the end of neoadjuvant treatment of both sets. After normalization, circulating miRNAs associated with event free survival (EFS) were identified by univariate and multivariate Cox regression model.

Results: Starting from 23 circulating miRNAs associated with EFS in the training set, we generated a 3-circulating miRNA prognostic signature consisting of miR-185-5p, miR-146a-5p, miR-22-3p, which was confirmed in the testing set. The 3-circulating miRNA signature showed a C-statistic of 0.62 (95% confidence interval [95%CI] 0.53-0.71) in the entire study cohort. By resorting to a multivariate Cox regression model we found a statistical significant interaction between the expression values of

miR-194-5p and pCR status (p.interaction =0.005) with an estimate Hazard Ratio (HR) of 1.83 (95%CI 1.14- 2.95) in patients with pCR, and 0.87 (95%CI 0.69-1.10) in those without pCR. Notably, the model including this interaction along with the abovementioned 3-circulating miRNA signature provided the highest discriminatory capability with a C-statistic of 0.67 (95%CI 0.58-0.76).

Conclusions: Circulating miRNAs are informative to identify patients with different prognosis among those with heterogeneous response after trastuzumab-based neoadjuvant treatment, and may be an exploitable tool to select candidates for salvage adjuvant therapy.

KEYWORDS

circulating microRNA, HER2-positive breast cancer, prognosis, MiR-194-5p, neoadjuvant treatment

Introduction

Neoadjuvant therapy is progressively replacing adjuvant therapy and is emerging as a new standard of care for early-stage HER2-positive and triple negative breast cancer (1). Primarily used to downstage locally advanced tumors (2), neoadjuvant therapy has the potential to enable breast cancer operability as well as to increase conservative surgery and to reduce the extent of axillary node dissection (3). Furthermore, individual response to neoadjuvant therapy provides prognostic information and assists treatment decisions after surgery in patients with human epidermal growth factor receptor 2 (HER2)-positive and triple-negative breast cancer. Indeed, while patients with a pathological complete response (pCR), defined by the absence of invasive tumor in excised breast tissue and nodes, have a favorable prognosis, those with persistent disease within the surgical specimens require adjuvant therapy escalation (4, 5).

The efficacy of additional treatments in HER2-positive breast cancer patients not achieving a pCR after neoadjuvant therapy is being investigated in several studies (6), and has been reported as beneficial by the KATHERINE trial (7). Noteworthy, not all patients with an incomplete tumor response to neoadjuvant therapy relapse - two third of them are indeed disease-free at five years from surgery (8) - while up to 20% of patients who achieve a pCR eventually recur (9). This creates uncertainty, and calls into question the prognostic relevance of pCR. However, a reliable tool to separate patients at risk of relapse from those already cured after neoadjuvant therapy is currently lacking, hindering appropriate selection of adjuvant therapy escalation candidates. Primary tumor gene expression, proteomics and mutational profiling represent promising biomarkers, but need repeated tissue sampling and high-profile technology which limit their use in daily practice (10, 11). A possible alternative is offered by the development of a non-invasive procedure such as liquid biopsy. In particular, circulating microRNAs (miRNAs) are promising biomarkers due to their storage stability, easy handling, and promising expression signatures associated with treatment response (12). Baseline levels of circulating miRNA-21, -4734 and -150-5p (13, 14), or "on treatment" levels of circulating miRNA-140-5p (15) have already been associated with treatment response to HER2-targeted therapies. As it is common practice to offer post-operative treatment to non-responding patients, and pCR is not always reliable, we aimed to challenge circulating miRNAs detected at the end of neoadjuvant therapy as prognostic biomarkers. To this end, and given that most patients with HER2-positive early-stage breast cancer, in the face of different strategies to increase or decrease systemic therapy, continue to receive only chemotherapy and trastuzumab, we decided to analyze the association between pre-operative circulating miRNAs and event-free survival (EFS) of patients treated in the NeoALTTO trial (16) with trastuzumab-based therapy.

Materials and methods

Patients

This is an exploratory analysis of the multicenter phase III NeoALTTO study (16), which randomized patients with HER2-positive primary breast cancer >2 cm to lapatinib (n = 154), trastuzumab (n= 149), or their combination (n= 152) for 6 weeks, followed by paclitaxel for 12 weeks. Surgery was performed within four weeks from the last paclitaxel dose. After surgery, patients received fluorouracil, epirubicin, and cyclophosphamide for 3 cycles and continued the same anti-HER2-targeted agent of the neoadjuvant phase to complete 52 weeks of treatment. NeoALTTO primary endpoint was pCR; secondary endpoints included EFS, defined as the time from randomization to first event. As reported (15, 16), all enrolled patients signed the main study consent form, which included a non-specific clause for using blood samples collected at baseline, during treatment, prior to surgery, and eventually at the time of relapse for future research. The current analysis was approved (INT 186-13) by the Ethics Committee of Fondazione IRCCS Istituto Nazionale dei Tumori, Milano.

Sample collection

Patients randomized to trastuzumab arm and with an available plasma sample collected prior to surgery were considered suitable for the purpose of this study, designed to address the prognostic value of

end-of-neoadjuvant treatment circulating miRNAs. A training-testing approach was used for model building and confirmation, respectively.

Circulating miRNA profiling data processing

Blood samples, collected in BDTM P-100 tubes (BD Bioscience), were separated within 2 hours of collection into plasma aliquots by centrifugation (2000-3000g for 15 minutes at room temperature) and stored at −80°C until assayed at the central biobank of Vall d'Hebron University Hospital (Barcelona, Spain). Plasma samples were shipped to Fondazione IRCCS Istituto Nazionale dei Tumori for RNA isolation as already reported (15). Briefly, reverse transcription and circulating miRNA profile was performed using the miRCURY LNA^{TM}Universal RT microRNA PCR system according to the Exiqon manufacturer's instructions. A total of 752 circulating miRNAs were profiled using microRNA Ready-to-Use PCR, Human panel I+II in each sample. The amplification curves were analyzed using the Roche LC software for determination of quantification cycle (Cq) values. Consistently with our previous report (15), we considered background filtered (BF) Cq data as processed by Exiqon (i.e., for assays that do not yield any signal on the negative control, the upper limit of detection was set to Cq = 37; otherwise, it was set to 3 Cq lower than the Cq value of a negative control, 17). The BF Cq values were then processed to calculate the relative quantity (RQ) of each miRNA by using the comparative threshold cycle method (18) following the formula $2^{-\Delta Cq}$ (where $\Delta Cq=Cq_{miRNA} - Cq_{reference}$). The $Cq_{reference}$ was computed according to the overall mean approach (19).

Statistical analysis

In the training set the association between circulating miRNAs levels (RQ considered on log2 scale) and event free survival (EFS) was assessed by resorting to a univariate Cox regression model. Event-free survival was defined as time from randomization to first event (i.e., events were defined as breast cancer relapse after surgery, second primary malignancy, death or failure to complete neoadjuvant therapy because of disease progression) (8). The relationship between each miRNA and clinical outcome was investigated by restricted cubic splines (20). In this selection step, according to the number of event per variable (EPV) (21), we considered as potentially relevant only those miRNAs detected in at least 10 patients experiencing the event of interest and in at least 85% of both training and testing sets (i.e. selected circulating miRNAs). Statistical significant circulating miRNAs at univariate analysis were included in multivariate Cox regression models following the all-subset approach (22) using penalized maximum likelihood estimations according to Firth method (23). For each model, the C-statistic (and its 95% Confidence Interval [CI]) computed according to Uno et al. (24) was used as pivotal measure for performance evaluation. Models with a statistically significant performance (i.e., with the lower 95%CI of the C-statistic >0.50) in the training set were then evaluated in the testing set. Those retaining a statistically significant performance in the testing set and including miRNAs with the same Hazard Ratio [HR] direction in both training and testing set were defined as promising prognostic signature(s). Noteworthy, models including miRNAs indicated in literature as haemolysis related (i.e., miR-16, miR-92a, miR-451 and miR-486) (25) were excluded as well as those with redundant circulating miRNAs according to the 95%CI of the Spearman correlation coefficient (i.e. upper limit of the 95%CI > 0.80 in absolute value). The "best" prognostic signature was eventually identified as that showing the highest prognostic performance in both the training and testing sets (Supplementary Figure S1). Next, by considering the whole study cohort (i.e., training and testing sets together), the prognostic performance of the "best" prognostic signature was evaluated with respect to clinico-pathological variables, i.e., estrogen receptor (ER) status (negative versus [vs] positive), nodal status (≥N1 vs N0), tumor size (>5cm vs ≤5cm), age (≥50 vs <50) and pCR (yes vs no). A 30-week landmark analysis was performed when pCR was considered as a covariate. Finally, a Cox regression model including each selected circulating miRNA the pCR status (main effects) together with their first order interaction term was implemented to highlight circulating miRNAs differently associated with EFS depending on pCR status. All statistical analyses were carried out with the SAS (version 9.4.; SAS Institute, Inc., Cary, NC) and R software (version 3.6.0; R Foundation for Statistical Computing) by adopting a significance alpha level of 5%. Prediction of target site of circulating miRNA(s) of interest was performed using miRWalk 3.0 (26). Functional enrichment of circulating miRNA targeted genes for Gene Ontology (GO) biological process terms and KEGG pathways was performed using the ClusterProfiler Bioconductor package, and a false discovery rate (FDR)< 0.05.

Results

Patient and tumor characteristics

Out of 149 patients treated within the NeoALTTO trastuzumab arm, 126 (85%) had evaluable circulating miRNA profile at the time of surgery (study cohort). The median age at breast cancer diagnosis was 48 years (interquartile range, 43-57). Most of the patients had clinical T2 (64%) and ≥N1 tumors (72%). Almost half (47%) had ER-positive tumors. pCR was observed in 31% of cases; a total of 40 events were reported at a median follow-up of 6.7 years (interquartile range, 6.1-6.9 years). Patients of the study cohort were randomized in a training (n= 54) and testing set (n= 72). No difference in clinico-pathological characteristics was observed between training and testing sets (Table 1), which were similar to the entire study cohort (Supplementary Table S1).

End-of-treatment circulating miRNA signature associated with EFS

In the training set, 23 circulating miRNAs were significantly associated with EFS by univariate analysis (Supplementary Table S2). For all these circulating miRNAs, a linear relationship between the EFS probability and their expression was found to be appropriate. By combining these 23 miRNAs into multivariate models following all-subset analysis approach (22), a total of 4 promising prognostic signatures were identified (Table 2). Among these 4 signatures, the model including miR-185-5p, miR-146a-5p, miR-22-3p, was selected as the "best" one. By using the regression coefficient of this model fitted on the whole study cohort, the 3-circulating miRNA signature was generated as following: (-0.062*miR-185-5p expression) +

10.3389/fonc.2022.1028825

TABLE 1 Clinico-pathological features of the training and testing sets.

Age	Traning set n= 54		Testing set n= 72	
	n	%	n	%
<50 years	28	*52*	39	*54*
≥50 years	26	*48*	33	*46*
ER status				
Negative	27	*50*	40	*56*
Positive	27	*50*	32	*44*
Nodal status				
N0	15	*28*	20	*28*
≥N1	39	*72*	52	*72*
Tumor size				
≤5 cm	35	*65*	46	*64*
>5 cm	19	*35*	26	*36*
pCR				
No	37	*69*	50	*69*
Yes	17	*31*	22	*31*
#Event	17	*31*	23	*32*

ER, estrogen receptor; N, clinical nodal status at baseline; pCR, pathological Complete Response; event (i.e. breast cancer relapse after surgery, second primary malignancy, patient death or failure to complete neoadjuvant therapy because of disease progression).

(-0.274*miR-146a-5p expression)+(0.105*miR-22-3p expression). Supplementary Figure 2 reports the EFS probability pattern of the 3-circulating miRNA signature.The results of multivariate Cox regression model including these circulating miRNAs are reported in Supplementary Table S3. Notably in the study cohort, the C-statistic of the 3-circulating miRNA signature was 0.62 (95%CI 0.53-0.71), against a C-statistic of 0.58 (95%CI 0.48-0.67) of the model including ER expression, nodal status, tumor size, age and pCR.

Circulating miRNA signature and clinico-pathological variables

Noteworthy, this 3-circulating miRNA signature was evenly distributed among clinico-pathological variables (Figure 1). Moreover, the 3-circulating miRNA signature retained its prognostic performance with respect to EFS even after adjusting for each of the considered clinico-pathological variables (Supplementary Table S4).

Prognostic value of circulating miRNAs by pCR status

As pCR is a driver of EFS in the NeoALTTO and other neoadjuvant studies, we next analyzed the prognostic value of miRNA according to pCR status. For this purpose, the expression levels of each of the 132 selected miRNAs detected in the study cohort was evaluated thought a multivariate Cox regression model with pCR status and the first-order interaction between miRNA and pCR. We found circulating miR-194-5p with a statistically significant interaction term at alpha level of 0.01 (p.interaction =0.005). The HR estimate in patients with pCR was 1.83 (95%CI 1.14-2.95), and 0.87 (95%CI 0.69-1.10) in those without pCR. Figure 2 reports the EFS probability plot for circulating miR-194-5p expression levels (Log2 RQ) according to pCR status.

End-of-treatment microRNA added prognostic value

For exploratory purposes, an analysis was performed by adding the interaction terms together with the corresponding main effects (circulating miR-194-5p and pCR) to the 3-circulating miRNA signature. The highest prognostic performance in terms of C-statistics was observed for the complete multivariate model (Table 3).

Discussion

Not all early-stage breast cancer patients with residual disease after neoadjuvant therapy have a poor prognosis; on the other hand, some patients achieving a pCR eventually relapse. Therefore, biomarkers are needed to properly identify patients at risk who are ideal candidates for additional post-surgical therapies. Using high-throughput analysis of plasma samples collected within a prospective randomized trial (16), we herein reported the first study investigating circulating microRNAs extensively, and not according to a pre-specified candidate panel, at the end of neoadjuvant therapy, and in association with prognosis. Several key findings with biological relevance and clinical potential were identified.

TABLE 2 Prognostic performance of the promising models.

Promising models	Training set*	Testing set*
	C-statistic (95% CI)	C-statistic (95% CI)
miR-185-5p, miR-146a-5p, miR-22-3p	0.705 (0.517; 0.894)	0.700 (0.519; 0.880)
miR-146a-5p, miR-15b-3p, miR-22-3p	0.688 (0.551; 0.825)	0.698 (0.534; 0.861)
miR-24-3p, miR-15b-3p, miR-22-3p	0.681 (0.541; 0.820)	0.697 (0.512; 0.882)
miR-185-5p, miR-23a-3p, miR-22-3p	0.683 (0.509; 0.857)	0.672 (0.520; 0.824)

*A penalized Cox regression model was implements according to the EPV in the training and testing set.

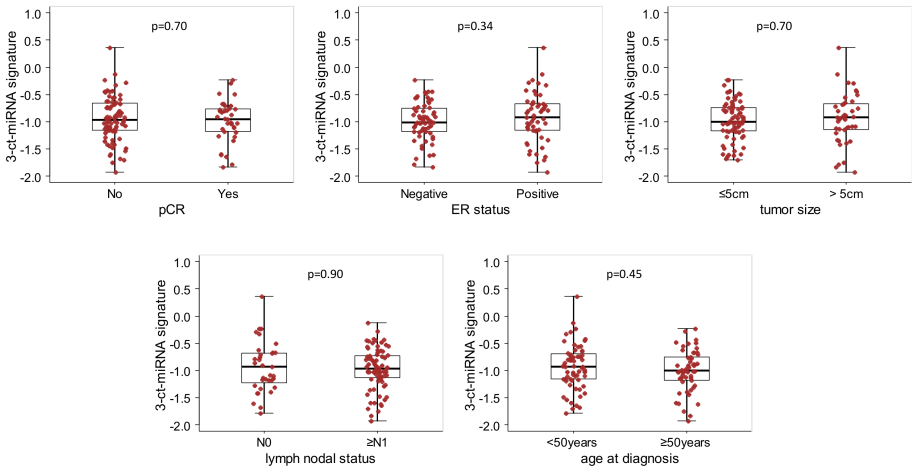

FIGURE 1
Box Plot of the 3-circulating miRNA signature according to clinical variables in the whole study cohort. Distribution of the 3-circulating miRNA signature expression levels according to pathological complete response (pCR), estrogen receptor (ER) status, primary tumor size, nodal status and age at diagnosis. Each box indicates the 25th and 75th percentiles. The horizontal lines inside the box indicate the median, and whiskers indicate the extreme measured values; individual value of the signatures are represented by dots. p=p.value of the Wilcoxon test.

Firstly, we identified a circulating signature composed of miR-185-5p, miR-146a-5p and miR-22-3p able to discriminate among patients treated with trastuzumab-based therapy with different prognosis. The functions of miRNAs composing our prognostic signature have been associated with tumor-related processes (proliferation, apoptosis, migration/invasion), and response to treatment. Specifically, miR-185-5p seems to act as a tumor suppressor in cancer progression and spreading, at least in central nervous system (27), and gastrointestinal malignancies (28). The precise effects and detailed mechanisms of miR-185-5p in breast cancer are yet to be defined. However, a recently reported pre-clinical study shows that over-expression of miR-185-5p is associated with reduced chemosensitivity (29). Iorio et al. first reported that miR145-5p acts as a tumor suppressor in a variety of tumors, including breast cancer (30); subsequently, miR-145-5p was shown to modulate immune response by targeting the 3'-untranslated region of Toll-like receptor 4 (31), and to increase epithelial-mesenchymal transition through the control of N-cadherin, vimentin and E-cadherin protein expression levels (32). Finally, miR-22 was found both as a tumor suppressor and a promoter in previous studies (33, 34). However, its serum expression levels have already been associated with poor prognosis in breast cancer patients (35). Consistent with these literature data, our analysis showed that both miR-185-5p and miR-146a-5p have a protective prognostic effect, as opposed to miR-22. Furthermore, an integrated analysis of miRNA target gene networks drew much attention because there are many common signaling pathways modulated by differentially expressed mRNAs and shared through GO and KEGG analysis (Supplementary Figure S3). Although circulating miRNAs are not necessarily expressed at the tumor tissue level, it is worthy to note that among the enriched terms, those related to growth factor signaling, metastatic spreading processes and immune response were shared by all dysregulated

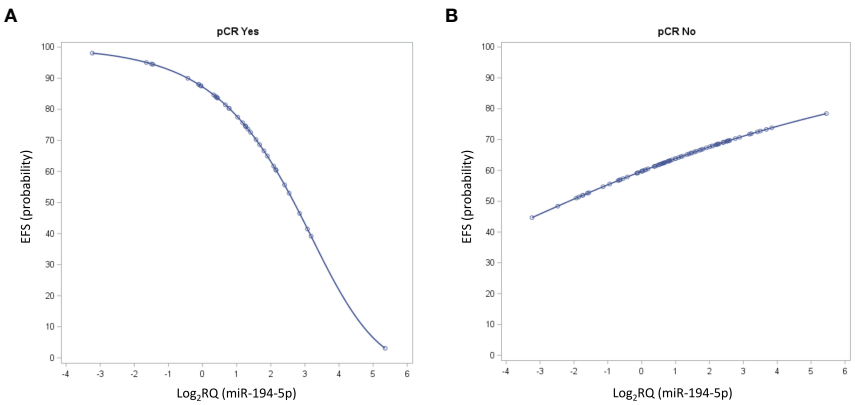

FIGURE 2
Seven-year Event Free Survival (EFS) probability curves for circulating miR-194-5p values according to pathological complete response (pCR) status. The curve depicts the predicted EFS probability of the circulating miR-194-5p expression levels considered on its continuous scale in patients **(A)** with pCR and **(B)** without pCR.

TABLE 3 Prognostic performance of multivariate Cox regression models in the study cohort.

Model	C-statistic	95% CI	
3-circulating miRNA signature + pCR (Yes *vs* No)[a]	0.62	0.53	0.71
miR-194-5p + pCR+ (miR-194-5p*pCR)[a]	0.62	0.54	0.71
3-circulating miRNA signature + pCR + miR-194-5p + (miR-194-5p*pCR)[a]	0.67	0.58	0.76

[a]30-week landmark analysis was performed when pCR was considered in the multivariate Cox regression model; CI, confidence interval.

circulating miRNAs after trastuzumab treatment. These findings are intriguing because development of predictors of recurrence after neoadjuvant therapy is still in its infancy, and presently the only established prognostic factors are stage and hormone receptor status (36). An attempt has been made with TILs (37). However, TILs assessment may be difficult after neoadjuvant therapy (38), so that Asano et al. proposed to combine their evaluation with residual cancer burden, which takes into account tumor dimension, cellularity of tumor bed, and axillary nodal burden (39). In addition TILs data in HER2-positive breast cancer are controversial (40), with several studies suggesting that high TILs values in residual disease after neoadjuvant therapy are associated with worse rather than improved prognosis (reviewed in 37).

Secondly, the 3 circulating miRNA signature ensures a C-statistic of 0.62 (0.53-0.7), instead of 0.58 (0.48-0.67) of the model including clinico-pathological variables, age, stage, estrogen receptor status and pCR. Thus, only three circulating markers assessed at a single time point offer a similar if not superior discriminatory capability of different variables assessed on patient, and primary tumor at baseline or after treatment. Furthermore, the discriminatory capability of the 3-circulating miRNA signature remained significant when clinico-pathological variables were included in multivariate analysis. All these findings support the development of our 3 circulating miRNA signature as a parsimonious and independent prognostic tool.

Thirdly, despite the favorable prognostic effect of invasive disease eradication, a few of patients with pCR eventually relapse (9, 10). Tumor recurrences are in the range of 10-15% at 5 years from surgery, as reported in the large pooled analysis of German Breast Group neoadjuvant studies on 2188 patients (41), and from a recent meta-analysis on 5748 patients (42). These findings are counterintuitive since complete eradication of cancer cells in breast and axilla has been proposed as a maximum effect reflecting the eradication of micrometastatic disease with no room for improvement. Yet, risk of relapse in patients with pCR increases with advanced stage at initial diagnosis, HER2-overexpression, younger age, and premenopausal status. Besides, patients who obtain pCR with the addition of trastuzumab have a better prognosis than patients who obtain pCR with chemotherapy alone (43). Recently, accumulating data suggest that patients who achieve pCR with HER2-dual blockade have a better prognosis than those who achieve pCR with single anti-HER2 agent (44). Although we cannot exclude that these results are due to the imbalance in the size of the subgroups, with fewer patients in the control arm achieving a pCR, these data challenge the idea that all pathological responses born equal and reinforce that of pCR quality. In this context, our data demonstrate for the first time that increased levels of circulating -miR-194–5p are associated with dismal prognosis exclusively in patients achieving a pCR following trastuzumab. miR-194-5p is a p53-responsive miRNA capable of inducing cell cycle arrest and inhibiting cell proliferation, migration, invasion and colony formation (45). These data are inconsistent with our results. However, it has recently been reported that the function miR-194 turns tumorigenic when treatment-sensitive cells promote stem cell survival during the so called "dying for surviving" phenomenon (46). Specifically, miR-194-5p is contained in the exosomes of dying cells and is released to residual ALDH- positive tumor-repopulating cells for their recovery. This finding is consistent with the enrichment of cells with stemness phenotype in occult metastatic lesion (47), and the overexpression of stemness signatures in triple negative breast cancer primary tumor of patients who eventually relapse regardless a pCR (10).

This study has some limitations. First, due to its retrospective nature, biological data were available in most but not all patients included in the NeoALTTO trastuzumab arm. Secondly, the analyzed sample size and the number of breast cancer events prevented subgroup analysis. Finally, the number of patients included in the analysis limits the impact of our findings. Therefore, the results of this study need a further confirmation in a much larger patient population, and with an extended follow-up period. Lastly, the prognostic value of TILs was not evaluated in this study. This would be interesting to be assessed in future studies. In addition, studied patients received additional adjuvant chemo-, ± endocrine- and trastuzumab-therapy and we are unaware of the impact of these treatments on miRNAs and *vice versa*. In view of developing a clinically usable assay, the identification of a limited number of reference miRNAs as well as assay-oriented step(s) should be considered, as described by Verderio et al. (22). As regards the selection of reference miRNAs, they should be properly chosen to resemble the overall mean (19), for example using the procedure we developed (48). The definition of operative procedures for miRs processing and detection as well as the evaluation of the assay performance and robustness, together with the clinical interpretability represent key aspects that should be opportunely addreesd during the assay-oriented step(s).

In conclusion, we have identified a 3 circulating miRNA signature able to differentiate among patients with distinct prognosis after trastuzumab-based neoadjuvant therapy, and the unique circulating-miR-194-5p associated with recurrence after pCR attainment, which warrant further investigation in additional studies. If confirmed, these miRNAs and their possible mechanisms of action could aid the development of new post-neoadjuvant strategies for high risk breast cancer patients. Furthermore, given the absence of tumor tissue in patients attaining a pCR, our results reinforce liquid biopsy as a promising tool to quantify and analyze

residual breast cancer burden beyond pathological findings and to predict tumor evolution for post-operative therapy personalization.

Data availability statement

The raw data supporting the conclusions of this article will be made available by the authors upon reasonable request.

Ethics statement

The studies involving human participants were reviewed and approved by Ethics Committee of Fondazione IRCCS Istituto Nazionale dei Tumori. The patients/participants provided their written informed consent to participate in this study.

Author contributions

SDC conceived of the presented idea. SDC, CMC, SP and PV contributed to the design and implementation of the research, to the analysis of the results and to the writing of the manuscript. VC and MS verified the analytical methods. All authors contributed to the article and approved the submitted version.

Funding

The NeoALTTO study was sponsored by GlaxoSmithKline; Lapatinib is an asset of Novartis AG as of March 2, 2015. This sub-study was supported by the Italian Ministry of Health to SC. No grant number is applicable, funds were obtained through a law that allows tax-payers to allocate the 5 × 1000 share of their payments to research.

Acknowledgments

These data were partially reported as oral presentation at Società Italiana di Cancerologia (SIC) Conference, Virtual Event, October 27-28, 2021.

Conflict of interest

SDC received fees for medical education from Novartis, Pierre-Fabre, and IQVIA; and the research grant IG 20774 from Fondazione Associazione Italiana Ricerca contro il Cancro AIRC; and served as "ad hoc" medical advisor for Medica Scientia Innovation Research MEDSIR, Barcelona Spain. SE-A received grants from Novartis during the conduct of the ALTTO study, and grants from Roche/Genentech and Pfizer outside of the submitted work. MI is employed at Novartis Pharma. HG received honoraria as speaker from AstraZeneca, Roche, BMS, and Novartis. PN received grants from Novartis, Roche/Genentech, MSD Oncology, Bayer, and Targos outside the submitted work. MB's institution received a research grant for the conduct of the NeoALTTO study. JH received advisory boards and honoraria from Roche and research grants from Novartis. DC received grant support, consulting fees, and fees for independent data monitoring committee work from Roche, grant support and consulting fees from Novartis, fees for independent data monitoring committee work from Synthon, and consulting fees from Daiichi Sankyo, Samsung BIOEPSIS, Puma Biotechnology, Seattle Genetics, and Zymeworks all support paid to his institution.

The remaining authors declare that the research was conducted in the absence of any commercial or financial relationships that could be construed as a potential conflict of interest.

Publisher's note

All claims expressed in this article are solely those of the authors and do not necessarily represent those of their affiliated organizations, or those of the publisher, the editors and the reviewers. Any product that may be evaluated in this article, or claim that may be made by its manufacturer, is not guaranteed or endorsed by the publisher.

Supplementary material

The Supplementary Material for this article can be found online at: https://www.frontiersin.org/articles/10.3389/fonc.2022.1028825/full#supplementary-material

References

1. Korde LA, Somerfield MR, Carey LA, Crews JR, Denduluri N, Hwang ES, et al. Neoadjuvant chemotherapy, endocrine therapy, and targeted therapy for breast cancer: ASCO guideline. *J Clin Oncol* (2021) 39:1485–505. doi: 10.1200/JCO.20.03399

2. Buchholz TA, Mittendorf EA, Hunt KK. Surgical considerations after neoadjuvant chemotherapy: Breast conservation therapy. *J Natl Cancer Inst Monogr* (2015) 51:11–4. doi: 10.1093/jncimonographs/lgv020

3. Classe JM, Loaec C, Gimbergues P, Alran S, de Lara CT, Dupre PF, et al. Sentinel lymph node biopsy without axillary lymphadenectomy after neoadjuvant chemotherapy is accurate and safe for selected patients: the GANEA 2 study. *Breast Cancer Res Treat* (2019) 173:343–52. doi: 10.1007/s10549-018-5004-7

4. Cortazar P, Zhang L, Untch M, Mehta K, Costantino JP, Wolmark N, et al. Pathological complete response and long-term clinical benefit in breast cancer: The CTNeoBC pooled analysis. *Lancet* (2014) 384:164–72. doi: 10.1016/S0140-6736(13)62422-8

5. Broglio KR, Quintana M, Foster M, Olinger M, McGlothlin A, Berry SM, et al. Association of pathologic complete response to neoadjuvant therapy in HER2-positive breast cancer with long-term outcomes: A meta-analysis. *JAMA Oncol* (2016) 2:751–60. doi: 10.1001/jamaoncol.2015.6113

6. Available at: https://clinicaltrials.gov (Accessed August 17, 2022).

7. von Minckwitz G, Huang CS, Mano MS, Loibl S, Mamounas EP, Untch M, et al. Trastuzumab emtansine for residual invasive HER2-positive breast cancer. *N Engl J Med* (2019) 380:617–28. doi: 10.1056/NEJMoa1814017

8. Huober J, Holmes E, Baselga J, de Azambuja E, Untch M, Fumagalli D, et al. Survival outcomes of the NeoALTTO study (BIG 1-06): updated results of a randomised multicenter phase III neoadjuvant clinical trial in patients with HER2-positive primary breast cancer. *Eur J Cancer* (2019) 118:169–77. doi: 10.1016/j.ejca.2019.04.038

9. Xie LY, Wang K, Chen HL, Shi YX, Zhang YQ, Lin HY, et al. Markers associated with tumor recurrence in patients with breast cancer achieving a pathologic complete response after neoadjuvant chemotherapy. *Front Oncol* (2022) 12:860475. doi: 10.3389/fonc.2022.860475

10. Bruzas S, Gluz O, Harbeck N, Schmid P, Cortes J, Blohmer J, et al. Gene signatures in patients with early breast cancer and relapse despite pathologic complete response. *NPJ Breast Cancer* (2022) 8:42. doi: 10.1038/s41523-022-00403-3

11. Afzal S, Hassan M, Ullah S, Abbas H, Tawakkal F, Khan MA. Breast cancer; discovery of novel diagnostic biomarkers, drug resistance, and therapeutic implication. *Front Mol Biosci* (2022) 9:783450. doi: 10.3389/fmolb.2022.783450

12. Müller V, Gade S, Steinbach B, Loibl S, von Minckwitz G, Untch M, et al. Changes in serum levels of miR-21, miR-210, and miR-373 in HER2-positive breast cancer patients undergoing neoadjuvant therapy: a translational research project within the geparquinto trial. *Breast Cancer Res Treat* (2014) 147:61–8. doi: 10.1007/s10549-014-3079-3

13. Du F, Yuan P, Zhao ZT, Yang Z, Wang T, Zhao JD, et al. A miRNA-based signature predicts development of disease recurrence in HER2 positive breast cancer after adjuvant trastuzumab-based treatment. *Sci Rep* (2016) 6:33825. doi: 10.1038/srep33825

14. Jung EJ, Santarpia L, Kim J, Esteva FJ, Moretti E, Buzdar AU, et al. Plasma microRNA 210 levels correlate with sensitivity to trastuzumab and tumor presence in breast cancer patients. *Cancer* (2012) 118:2603–14. doi: 10.1002/cncr.26565

15. Di Cosimo S, Appierto V, Pizzamiglio S, Tiberio P, Iorio MV, Hilbers F, et al. Plasma miRNA levels for predicting therapeutic response to neoadjuvant treatment in HER2-positive breast cancer: Results from the NeoALTTO trial. *Clin Cancer Res* (2019) 25:3887–95. doi: 10.1158/1078-0432.CCR-18-2507

16. Baselga J, Bradbury I, Eidtmann H, Di Cosimo S, de Azambuja E, Aura C, et al. Lapatinib with trastuzumab for HER2-positive early breast cancer (NeoALTTO): A randomised, open-label, multicentre, phase 3 trial. *Lancet* (2012) 379:633–40. doi: 10.1016/S0140-6736(11)61847-3

17. Blondal T, Jensby Nielsen S, Baker A, Andreasen D, Mouritzen P, Wrang Teilum M, et al. Assessing sample and miRNA profile quality in serum and plasma or other biofluids. *Methods* (2013) 59:S1–6. doi: 10.1016/j.ymeth.2012.09.015

18. Livak KJ andSchmittgen TD. Analysis of relative gene expression data using real-time quantitative PCR and the 2-ΔΔCt method. *Methods* (2001) 25:402–8. doi: 10.1006/meth.2001.1262

19. Mestdagh P, Hartmann N, Baeriswyl L, Andreasen D, Bernard N, Chen C, et al. Evaluation of quantitative miRNA expression platforms in the microRNA quality control (miRQC) study. *Nat Methods* (2014) 11:809–15. doi: 10.1038/nmeth.3014

20. Durrleman S, Simon R. Flexible regression models with cubic splines. *Stat Med* (1989) 8:551–61. doi: 10.1002/sim.4780080504

21. Concato J, Peduzzi P, Holford TR, Feinstein AR. Importance of events per independent variable in proportional hazards analysis. i. background, goals, and general strategy. *J Clin Epidemiol* (1995) 48:1495–501. doi: 10.1016/0895-4356(95)00510-2

22. Verderio P, Bottelli S, Pizzamiglio S, Ciniselli CM. Developing miRNA signatures: A multivariate prospective. *Br J Cancer* (2016) 115:1–4. doi: 10.1038/bjc.2016.164

23. Heinze G, Schemper M. A solution to the problem of monotone likelihood in cox regression. *Biometrics* (2001) 57:114–9. doi: 10.1111/j.0006-341X.2001.00114.x

24. Uno H, Cai T, Pencina MJ, D'Agostino RB, Wei LJ. On the c-statistics for evaluating overall adequacy of risk prediction procedures with censored survival data. *Stat Med* (2011) 30:1105–17. doi: 10.1002/sim.4154

25. Kirschner MB, Edelman JJB, Kao SCH, Vallely MP, van Zandwijk N, Reid G. The impact of hemolysis on cell-free microRNA biomarkers. *Front Genet* (2013) 4:94. doi: 10.3389/fgene.2013.00094

26. Sticht C, de la Torre C, Parveen A, Gretz N. miRWalk: An online resource for prediction of microRNA binding sites. *PLos One* (2018) 13:e0206239. doi: 10.1371/journal.pone.0206239

27. Wu W, Yu T, Wu Y, Tian W, Zhang J, Wang Y. The miR155HG/miR-185/ANXA2 loop contributes to glioblastoma growth and progression. *J Exp Clin Cancer Res* (2019) 38:133. doi: 10.1186/s13046-019-1132-0

28. Yuan M, Zhang X, Zhang J, Wang K, Zhang Y, Shang W, et al. DC-SIGN-LEF1/TCF1-miR-185 feedback loop promotes colorectal cancer invasion and metastasis. *Cell Death Differ* (2020) 27:379–95. doi: 10.1038/s41418-019-0361-2

29. Luo L, Zhang J, Tang H, Zhai D, Huang D, Ling L, et al. LncRNA SNORD3A specifically sensitizes breast cancer cells to 5-FU by sponging miR-185-5p to enhance UMPS expression. *Cell Death Dis* (2020) 11:329. doi: 10.1038/s41419-020-2557-2

30. Iorio MV, Ferracin M, Liu CG, Veronese A, Spizzo R, Sabbioni S, et al. MicroRNA gene expression deregulation in human breast cancer. *Cancer Res* (2005) 65:7065–70. doi: 10.1158/0008-5472.CAN-05-1783

31. Jin C, Wang A, Liu L, Wang G, Li G, Han Z. miR-145-5p inhibits tumor occurrence and metastasis through the NF-κB signaling pathway by targeting TLR4 in malignant melanoma. *J Cell Biochem* (2019) 120:11115–26. doi: 10.1002/jcb.28388

32. Liu Q, Chen J, Wang B, Zheng Y, Wan Y, Wang Y, et al. miR-145 modulates epithelial-mesenchymal transition and invasion by targeting ZEB2 in non-small cell lung cancer cell lines. *J Cell Biochem* (2019) 120:8409–18. doi: 10.1002/jcb.28126

33. Yang F, Hu Y, liu HX, Wan YJ. MiR-22-silenced cyclin a expression in colon and liver cancer cells is regulated by bile acid receptor. *J Biol Chem* (2015) 290:6507–15. doi: 10.1074/jbc.M114.620369

34. Lee JH, Park SJ, Jeong SY, Kim MJ, Jun S, Lee HS. MicroRNA-22 suppresses DNA repair and promotes genomic instability through targeting of MDC1. *Cancer Res* (2015) 75:1298–310. doi: 10.1158/0008-5472.can-14-2783

35. Shao Y, Yao Y, Xiao P, Yang X, Zhang D. Serum miR-22 could be a potential biomarker for the prognosis of breast cancer. *Clin Lab* (2019) 65:4. doi: 10.7754/clin.lab.2018.180825

36. Guarneri V, Broglio K, Kau SW, Cristofanilli M, Buzdar AU, Valero V, et al. Prognostic value of pathologic complete response after primary chemotherapy in relation to hormone receptor status and other factors. *J Clin Oncol* (2006) 24:1037–44. doi: 10.1200/JCO.2005.02.6914

37. Pelizzari G, Gerratana L, Basile D, Fanotto V, Bartoletti M, Liguori A, et al. Post-neoadjuvant strategies in breast cancer: From risk assessment to treatment escalation. *Cancer Treat Rev* (2019) 72:7–14. doi: 10.1016/j.ctrv.2018.10.014

38. Dieci MV, Radosevic-Robin N, Fineberg S, van den Eynden G, Ternes N, Penault-Llorca F, et al. Update on tumor-infiltrating lymphocytes (TILs) in breast cancer, including recommendations to assess TILs in residual disease after neoadjuvant therapy and in carcinoma in situ: A report of the international immuno-oncology biomarker working group on breast cancer. *Semin Cancer Biol* (2018) 52:16–25. doi: 10.1016/j.semcancer.2017.10.003

39. Asano Y, Kashiwagi S, Goto W, Takada K, Takahashi K, Hatano T, et al. Prediction of survival after neoadjuvant chemotherapy for breast cancer by evaluation of tumor-infiltrating lymphocytes and residual cancer burden. *BMC Cancer* (2017) 17:888. doi: 10.1186/s12885-017-3927-8

40. Hamy AS, Pierga JY, Sabaila A, Laas E, Bonsang-Kitzis H, Laurents C, et al. Stromal lymphocyte infiltration after neoadjuvant chemotherapy is associated with aggressive residual disease and lower disease-free survival in HER2-positive breast cancer. *Ann Oncol Off J Eur Soc Med Oncol* (2017) 28:2233–40. doi: 10.1093/annonc/mdx309

41. Huober J, Schneeweiss A, Blohmer JU, Denkert C, Tesch H, Hanusch CA, et al. Factors predicting relapse in early breast cancer patients with a pathological complete response after neoadjuvant therapy-results of a pooled analysis based on the GBG meta-database. *Cancer Res* (2019) 79:P2–08-01. doi: 10.1158/1538-7445.SABCS18-P2-08-01

42. Spring LM, Fell G, Arfe A, Sharma C, Greenup R, Reynolds KL, et al. Pathologic complete response after neoadjuvant chemotherapy and impact on breast cancer recurrence and survival: A comprehensive meta-analysis. *Clin Cancer Res* (2020) 26:2838–48. doi: 10.1158/1078-0432.CCR-19-3492

43. Gianni L, Eiermann W, Semiglazov V, Lluch A, Tjulandin S, Zambetti M, et al. Neoadjuvant and adjuvant trastuzumab in patients with HER2-positive locally advanced breast cancer (NOAH): Follow-up of a randomised controlled superiority trial with a parallel HER2-negative cohort. *Lancet Oncol* (2014) 15:640–7. doi: 10.1016/S1470-2045(14)70080-4

44. Swain SM, Macharia H, Cortes J, Dang C, Gianni L, Hurvitz S, et al. Risk of recurrence and death in patients with early HER2-positive breast cancer who achieve a pathological complete response after different types of HER2-targeted therapy: A retrospective exploratory analysis. 2019 San Antonio Breast Cancer Symposium. Abstract P1-18-01. *Cancer Res* (2020) 80(4_Supplement):P1-18-01.

45. Kurata JS, Lin RJ. MicroRNA-focused CRISPR-Cas9 library screen reveals fitness-associated miRNAs. *RNA* (2018) 24:966–81. doi: 10.1261/rna.066282.118

46. Obenauf AC, Zou Y, Ji AL, Vanharanta S, Shu W, Shi H, et al. Therapy-induced tumour secretomes promote resistance and tumour progression. *Nature* (2015) 520:368.72. doi: 10.1038/nature14336

47. Gooding AJ, Schiemann WP. Epithelial-mesenchymal transition programs and cancer stem cell phenotypes: Mediators of breast cancer therapy resistance. *Mol Cancer Res* (2020) 18:1257–70. doi: 10.1158/1541-7786.MCR-20-0067

48. Verderio P, Bottelli S, Ciniselli CM, Pierotti MA, Gariboldi M, Pizzamiglio S. NqA: An r-based algorithm for the normalization and analysis of microRNA quantitative real-time polymerase chain reaction data. *Anal Biochem* (2014) 46:7–9. doi: 10.1016/j.ab.2014.05.020

Frontiers in Oncology

Advances knowledge of carcinogenesis and tumor progression for better treatment and management

The third most-cited oncology journal, which highlights research in carcinogenesis and tumor progression, bridging the gap between basic research and applications to imrpove diagnosis, therapeutics and management strategies.

Discover the latest Research Topics

See more →

Frontiers

Avenue du Tribunal-Fédéral 34
1005 Lausanne, Switzerland
frontiersin.org

Contact us

+41 (0)21 510 17 00
frontiersin.org/about/contact